NASA Conference Publication 2345

Local Interstellar Medium

International Astronomical Union Colloquium Number 81

Proceedings of a colloquium held at
The University of Wisconsin
Madison, Wisconsin
June 4-6, 1984

NASA

NASA Conference Publication 2345

Local Interstellar Medium

International Astronomical Union Colloquium Number 81

Edited by
Y. Kondo
NASA Goddard Space Flight Center
Greenbelt, Maryland

F. C. Bruhweiler
The Catholic University of America
Washington, D.C.

B. D. Savage
The University of Wisconsin
Madison, Wisconsin

Proceedings of a colloquium held at
The University of Wisconsin
Madison, Wisconsin
June 4–6, 1984

NASA
National Aeronautics
and Space Administration

Scientific and Technical
Information Branch

1984

Editors' Comments

In order to enable timely publication of the proceedings, we have made no efforts to make any editorial changes or corrections on the camera-ready manuscripts that were submitted to us. About the only editorial work performed has been rearranging the sequence of papers from the order in which they were presented so that papers pertaining to similar themes may be placed more cogently in the proceedings.

We thank the contributors to this proceedings for submitting their manuscripts by the stringent deadline.

Frederick C. Bruhweiler Yoji Kondo Blair D. Savage

IAU Colloquium No. 81 on Local Interstellar Medium

Scientific Organizing Committee

A. Boksenberg (U.K.)
A.A. Boyarchuk (U.S.S.R.)
F.C. Bruhweiler (U.S.A.) - Co-Chairman
A.D. Code (U.S.A.)
M. Grewing (F.R.G.)
Y. Kondo (U.S.A.) - Chairman
W.L. Kraushaar (U.S.A.)
D.C. Morton (Australia)
M. Oda (Japan)
M. Peimbert (Mexico)
A. Vidal-Madjar (France)

Local Organizing Committee

R.C. Bless
J.S. Mathis
D. McCammon
B.D. Savage - Chairman

Colloquium Session Chairmen

R.C. Bless, F.C. Bruhweiler, G.W. Clark, D.P. Cox, J.V. Feitzinger, L.M. Hobbs, Y. Kondo, W.L. Kraushaar, J.S. Mathis, N. Panagia, B.D. Savage,

Foreword

There has recently been substantial improvement in our knowledge of the local interstellar medium due in no small part to the availability of X-ray and ultraviolet observations from space. At the time of the IAU General Assembly in Patras in 1982 we felt that a colloquium sponsored by the IAU would be timely and proposed it to the Executive Committee after receiving the endorsement of Commission 34 (Interstellar Matter) and Commission 44 (Astronomy from Space). At that time Art Code and Bob Bless of the University of Wisconsin graciously offered to host the meeting in Madison. The meeting that took place on 4 through 6 June 1984 at the University of Wisconsin has amply demonstrated that the subject field has come of age.

There still exist a number of knotty problems that must be addressed through future observational and theoretical work. In particular, the location and nature of the observed diffuse soft X-ray background remains an unresolved issue. The nature of radio Loop 1 and other loop structures and their relation to other observational data are among the intriguing problems yet to be clarified. The understanding of the interaction of the solar wind with the matter in the immediate environ of the solar system has made strides through such work as helium back-scattering observations but the interpretation of these results imply a wide range of uncertainties in temprature and ionization.

However, out of an apparent chaos has emerged a certain concensus, albeit one drawn with a very broad brush. It appears that the solar system is imbedded not far from the edge of a warm ($\sim 10^4$ K), relatively low density ($\sim 10^{-1}$ atom cm^{-3}) gas cloud with a radius of a few parsecs, which is surrounded by a pervasive hot ($\sim 10^{5 \text{ to } 6}$ K), low density ($\sim 10^{-2 \text{ to } -3}$ atom cm^{-3}) plasma that extends some fifty parsecs or more in all directions observed; the ubiquitous hot gas is most likely the result of past supernova events. The Sun appears to be moving in the general direction of the center of this warm gas cloud at a relative velocity of some 20 km s^{-1}. There is some evidence that the density is higher and the temperature lower at the core of this warm cloud but further verification is needed on this last issue.

The forthcoming launch of the Hubble Space Telescope in 1986 and the anticipated flight of extreme ultraviolet satellite Columbus later on, as well as other observational efforts in the X-ray, optical, infrared and radio regions, are expected to advance our understanding of the local interstellar medium significantly. Another such colloquium several years hence might witness the resolution of at least some of the current outstanding issues.

We thank the IAU, U.S. National Science Foundation, the University of Wisconsin and NASA for their various and much appreciated support. This meeting was also co-sponsored by the American Astronomical Society. The efficient support provided by the members of the Local Organizing Committee,

Bob Bless, John Mathis and Dan MaCammon, was much appreciated. We wish in particular to thank Bob and Dianne Bless for the generous hospitality extended to all participants at their home.

Yoji Kondo	Frederick C. Bruhweiler	Blair D. Savage
Chairman	Co-Chairman	Chairman
Scientific Organizing Committee		Local Organizing Committee

IAU COLLOQUIUM PARTICIPANTS

Ardeberg, A.
Arnaud, Monique
Beckman, J. E.
Bertaux, J.
Bless, Robert C.
Blitz, Leo
Bloch, Jeff
Bochkarev, Niklay
Bregman, Joel N.
Brinkmann, Jonathan
Bruhweiler, Fred C.
Burrows, David
Buscombe, Bill
Caplan, James
Cardelli, Jason A.
Chu, You-Hua
Churchwell, Edward B.
Clark, George W.
Clayton, Jeff
Code, Arthur D.
Costero, Rafael
Cowie, L.
Cox, Donald
Crutcher, Richard M.
Cugnon, P.
Dame, Thomas
Danly, Laura
de Boer, Klaas S.
Deguchi, Shuji
Dickey, John
Ducati, Jorge R.
Eastwood, Kathleen
Edgar, Richard
Fahr, H. J.
Feitzinger, J. V.
Ferlet, R.
Fich, Michel
Fitzpatrick, Edward L.
Franco, Jose
Frisch, Priscilla
Gautier, T. N.
Gilden, David
Gilra, Daya P.
Goulet, Thomas
Gry, Cecile
Guinn, Carl
Heiles, Carl
Hobbs, Lewis
Holberg, Jay B.
Jahoda, Keith
Jenkins, Edward
Juda, Michael
Judge, Darrell
Knude, Jens K.
Kondo, Yoji
Konigl, Arieh
Kraushaar, William
Kulkarni, Shrinivas
Kumar, Krisha
Labov, Simon
Lallement, Rosine
Landsman, Wayne
Lebrun, Francois
Linsky, Jeffrey
Lockman, Felix J.
Martin, Chris
Massa, Derck
Mathis, John S.
McCammon, Dan
Mebold, U.
Meier, Robert R.
Molaro, P.
Morrison, James
Nash, Ana
Nousek, John A.
Oegerle,William R.
Oliversen, Ron
Panagia, Nino
Paresce, Francesco
Perry, Charles
Raymond, John
Reynolds, R.
Ripken, Hartmut W.
Roueff, Evelyne
Sanders, Wilton
Savage, Blair D.
Scherb, Frank
Shuter, W. L. H.
Snowden, Steven
Tinbergen, J.
Vidal-Madjar
Weaver, Harold F.
Weller, Charles
Wolfire, Mark
York, Donald G.

TABLE OF CONTENTS

TABLE OF CONTENTS (Continued)

TABLE OF CONTENTS (Continued)

TABLE OF CONTENTS (Continued)

TABLE OF CONTENTS (Continued)

TABLE OF CONTENTS (Continued)

HELIUM AND HYDROGEN BACKSCATTERING RESULTS AND THE VERY LOCAL INTERSTELLAR MEDIUM

HELIUM AND HYDROGEN OF THE LOCAL INTERSTELLAR MEDIUM OBSERVED IN THE VICINITY OF THE SUN

Jean-Loup BERTAUX
Service d'Aéronomie du CNRS
BP 3 - 91370 Verrières-le-Buisson - France

ABSTRACT

The Sun is moving in respect to the nearby stars with a velocity of 20 $km.s^{-1}$ in the direction of the Apex, $\alpha = 271°$ and $\delta = 30°$ (celestial coordinates). As the lights of a car illuminate the water droplets when driving in the fog, the Sun illuminates the Hydrogen and helium atoms of the interstellar medium which it travels through. As a result, the sun and the whole solar system are imbedded in a glow of the resonance lines of hydrogen (H Lyman α ; 121.6 nm) and helium (58.4 nm), which have been studied by several space instruments in the last 14 years.

From the intensity distribution of the glow in the solar system, one can derive the density of H and He in the LISM and the direction of the relative motion $\vec{V}_W$ between the sun and the LISM in the very vicinity of the sun. The velocity module V_W and the LISM temperature T are more adequately found from a measurement of the Lyman α line shape, which is an image of the velocity distribution of H atoms.

A summary of results will be presented, together with a discussion of the methods of interpretation and their difficulties. The vector $\vec{V}_W$ is found to be 20 $\pm$ 1 $km.s^{-1}$ in the direction $\alpha = 254 \pm 3°$, $\delta = -17 \pm 3°$, quite different from the Apex direction. This means that the LISM is moving also in respect to the local frame of reference giving rise to the so-called Interstellar Wind. This wind blows in the galactic plane at 16 $km.s^{-1}$, in the direction $\ell_{II} = 124°$, significantly different from the direction $\ell_{II} = 169°$ found by interstellar absorption lines on stars within $\simeq$ 100 pc, pointing to a local significance of this flow. The temperature of the LISM is T = 8,000 $\pm$ 1,000 K, the density n (H) $\simeq$ 0.04 to 0.06 cm^{-3}, and the helium density n (He) $\simeq$ 0.015 to 0.020. The high helium/hydrogen ratio, in respect to the cosmological ratio, would imply that a substantial part of the hydrogen is ionized. Temperature, density and degree of ionization of the LISM are suggesting that the sun is now in an intermediate phase of the interstellar medium, at the interface between a hot and tenuous gas, and a dense and cold cloud of gas.

INTRODUCTION

A great deal of what we know today about the Local Interstellar Medium (LISM) comes from observations of stellar spectra, on which are "printed" absorption features from atomic, ionic, and molecular species. These spectral features correspond most often to strong resonance lines and some corresponding resonance emission lines would also be expected. In fact, this emission is concentrated in a small region around each star, which is surrounded by a glow of resonance lines. Though it would be very interesting to study this glow which contains a local information on the LISM, it would be extremely difficult to observe from one star to another star, since it will be re-absorbed by interstellar matter (except in a few particular cases).

We are still left with one particular star, the Sun, which illuminates the LISM in which it is embedded. It is only since the early seventies that it was realized that neutral Hydrogen and Helium atoms from the LISM would become detectable through emission in the resonance lines Lyman- α HI 121.566 nm and HeI 58.4 nm. Since 1969, a number of space experiments have studied this resonance glow of the LISM, which takes place right in the solar system within a few astronomical units (AU) from the Sun.

Interestingly enough, it is not the usual LISM scientific community which has provided most studies in this field, but rather scientists dealing with UV instruments, distributed in Earth's orbit, other planets' orbits, and even solar system escape trajectory (Pioneer and Voyager missions).

My purpose in the present paper is not to present an exhaustive review of the numerous work performed by active group of scientists from different countries. Rather, my paper is addressed to the LISM community, which may not be totally familiar with the following problem : how safely can we deduce the characteristics of the very local interstellar medium (VLISM ?) by the study of the resonance glow of H and He in the Solar system ? Therefore, I will try to discuss some difficulties associated with the experimental methods of diagnostic, and present the most recent results on the VLISM characteristics : temperature, H and He densities, direction of the VLISM flow (an alternate acronym is SLISM, Solar System Local Interstellar Meidum).

The situation of the resonance glow around the Sun is comparable to the glow produced by a thick fog around a gas light. If you are near the gas light and observing the glow in a direction opposite to the gas light, the brightest is the glow, the densest is the fog. If there is some wind, it will not modify the distribution of light, which makes impossible to detect such a wind. The same situation happens sometimes when you are on a pair of skies in a thick fog ; sometimes you do not even realize if you are moving or not, a particularly uncomfortable feeling.

ZERO DEGREE APPROXIMATION

As a first approach, let us consider the simple situation, similar to the fog case, in which the flow of interstellar gas is not modified by the Sun : the only interaction being that H and He atoms are illuminated by the solar resonance light.

For an observer at 1 AU looking opposite from the sun, the measured intensity is :

$$I = \frac{1}{4\pi} \quad \frac{\pi e^2}{m_e c} \; f. \; F_s \int_1^\infty n(r) \frac{dr}{r^2} \qquad (1)$$

in which F_s is the exciting solar flux (in photons /cm^2 s Å), $\frac{\pi e^2}{m_e c} f$ the integrated cross section of the resonance transition, and $n(r)$ is the density distribution of the gas at distance r from the sun, which is uniform in the simple case considered here, and equal to n_∞, the LISM gas density. Introducing the excitation rate at one AU, $g_o = \frac{\pi e^2}{m_e c} f. F_s$, we have the simple relationship between the density n_∞ and the scattered intensity :

$$4\pi I = g_o \, n_\infty \times 1 \text{ AU (in cm)} \qquad (2)$$

The intensity is measured with a photometer which has a certain sensitivity a, giving a signal S when the measured intensity is I.

$$S = a \, I$$

Since g_o contains the solar flux F_s, we finally arrive at the expression :

$$S = \gamma \, a \, F_s \, n_\infty \qquad (3)$$

where γ is a known coefficient. Such an expression would be valid for any direction of sight, the integral of (1) being modified, and its value integrated in the coefficient γ.

The diagnostic problem is to extract an estimate of n_∞ form a photometric measurement S. The solar flux suffers from some uncertainties, as well as the calibration factor ; the point to be made here is that the effect of a and the effect of F_s are not distinguishable from one another.

One possibility to overcome this problem is to use the same photometer to observe a known quantity of atoms, illuminated by the same solar flux F_s . This situation can happen in the upper atmosphere of planets, where other methods (like neutral mass spectrometers) can yield a value of the density. Therefore, a photometric observation of an upper atmosphere can provide the value of a F_s for the time of observation, which can then be used for the derivation of n_∞ with an improved accuracy.

The temperature and the flow velocity, both related to the velocity distribution of atoms, is accessible through high resolution spectrometric measurement. All atoms are re-emitting at the central wavelength λ_o in their frame of reference, but observed photons are at wavelengths shifted from λ_o through Doppler effect. With the provision that the solar flux F_s is constant over a reasonable wavelength interval, the observed line shape in a given direction is the exact velocity distribution of these atoms, projected on the line of sight and weighted according to the local excitation rate (r^{-2} decrease).

On Figure 1 are illustrated the various possible Doppler shift $\Delta\lambda$ in various directions, for an observer near the sun. It depends on the value of V_o (the wind velocity in respect to the sun) and on the angle α with the wind direction :

$$\Delta\lambda = \frac{\lambda_o}{c} \; V_o \cos \alpha \qquad (4)$$

Usually the vector $\vec{V}_o$ designates the velocity of the wind flow in respect to the sun, whereas $\vec{V}_w = - \vec{V}_o$ refers to the velocity of the sun relative to the local interstellar medium.

The temperature T of the LISM is related to the linewidth $\Delta\lambda_D$ (half width at 1/e) of the gaussian spectral profile :

$$\Delta\lambda_D = \frac{\lambda_o}{c} \quad \frac{2\ kT}{m} \qquad (5)$$

where m is the mass of the atom.

Therefore, if high resolution spectrometric measurements can be made over many points of the celestial sphere, it is possible to find where there is a maximum Doppler shift $\Delta\lambda_m$, which determines the direction of the wind flow, whereas the value of $\Delta\lambda_m$ gives immediately the modulus of V_o . At 90° from V_o , the Doppler shift is zero ; on the celestial sphere, there is a whole great circle with zero Doppler shift called the zero Doppler shift circle (ZDSC). Determining this ZDSC allows also to determine the direction of the flow.

Up to now, we have considered the very simple case of no interaction of the sun with the wind flow, and have described the physical ways to perform a diagnostic on the LISM characteristics. In such a case (zero degree approximation) the projected velocity distribution is a uniform gaussian. In reality, there are substantial interactions which modifies greatly the density and velocity distributions of H and He in the solar system as we will describe now. However, the physical ways to perform a diagnostic still remain valid : the density is still accessible through absolute photometric measurements, and the velocity distribution (connected to $\vec{V}_o$ and T) is still accessible to high resolution spectrometric measurements.

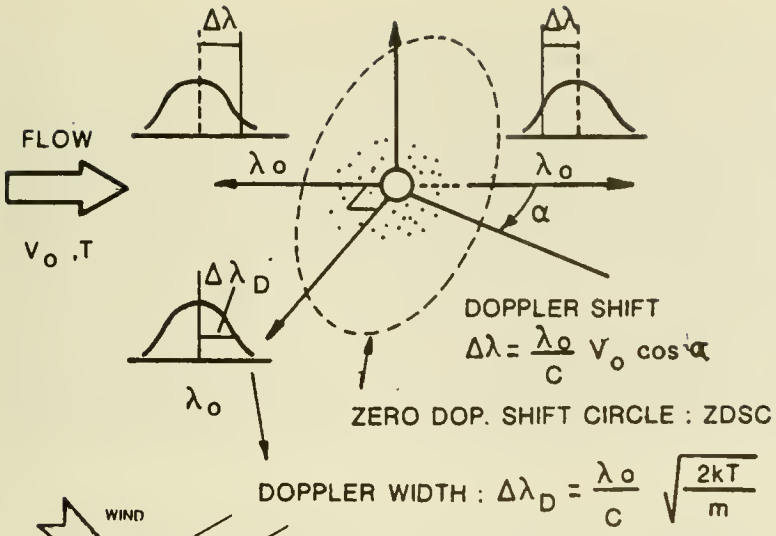

Figure 1. The Doppler width of the backscattered line profile is connected to the temperature ; the wavelength shift $\Delta\lambda$ depends on angle α between the line of sight and the flow direction.

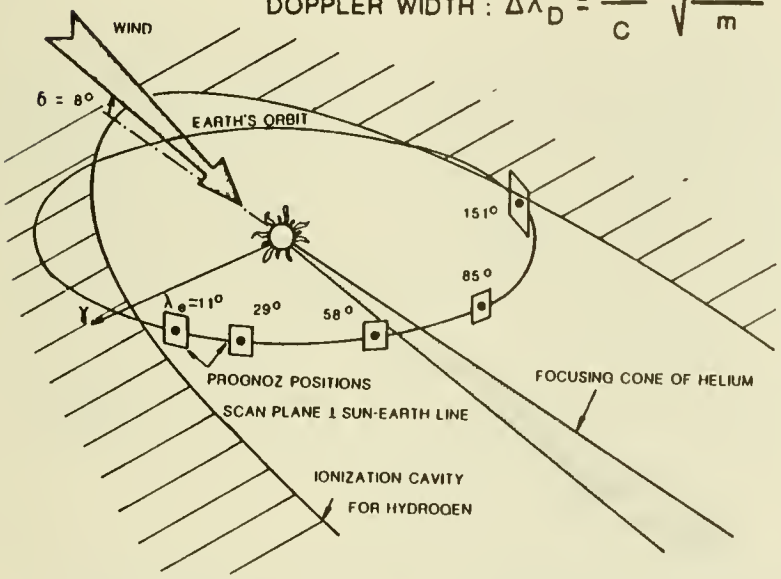

Figure 2. The main features of interstellar gas distribution in the solar system are i) a focusing cone of helium in the downwind direction ; ii) a cavity of ionization, void of atoms, elongated toward the downwind direction.

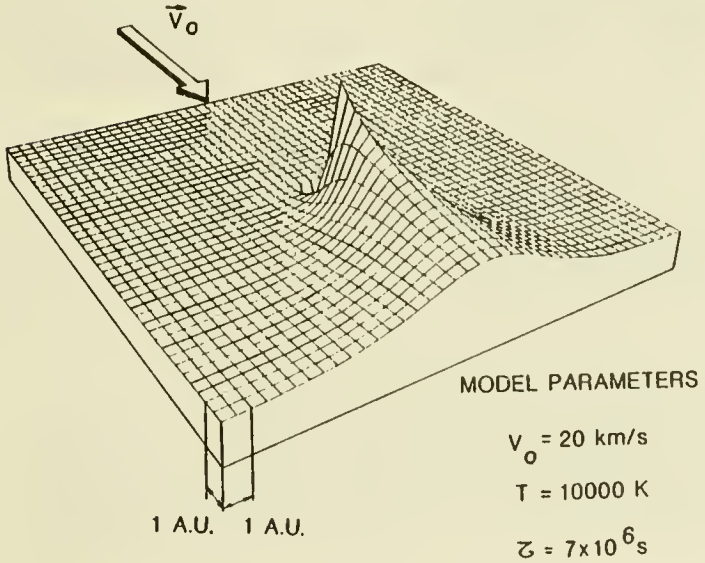

Figure 3. 3D representation of the density distribution in a plane containing the flow vector $\vec{V}_o$. The vertical coordinate is proportional to the He density in the horizontal plane (after Dalaudier et al., 1984).

MODIFIED DENSITY DISTRIBUTION AND PHOTOMETRIC DIAGNOSTIC

Even before it was realized that the observed extraterrestrial Lyman-α glow was due to an interstellar flow of H in the solar system, Blum and Fahr (1970) had pointed out the effect of solar gravity, which bends individual trajectories into hyperbolae, and the ionization of atoms by solar wind charge exchange and solar EUV photoionization. In the case of hydrogen, the continuous scattering of solar Lα photons is acting as a radiation pressure F_r, which is of the same order of magnitude as the gravitation force F_g, but of opposite direction. The ratio $\mu = F_r/F_g$ is negligible for helium, but can vary between $\simeq 0.5$ and 1.5, for hydrogen, depending on the solar Lα flux which varies with solar activity. The solar flux which corresponds to $\mu = 1$ is $F_s = 3.32 \times 10^{11}$ photons $(cm^2.s.\text{Å})^{-1}$.

The results of these effects on the H and He density distribution inside the solar system are illustrated on Figure 2. For helium atoms, if we assume that they are monocinetics (T = 0) all hyperbolae are crossing along a line determined by $\vec{V}_o$, in the downwind direction of the solar system, creating a density singularity on this line, and a region of greatly enhanced density around this line. If $T \neq 0$, the singularity disappears, but there is still a cone of gravitationnal focusing. A model computation by Dalaudier et al. (1984) illustrates this dramatic effect (Figure 3).

For hydrogen, ionization and Lα radiation pressure prevents H atoms to approach very near the sun, and there is a cavity of ionization "carved" into the H flow, elongated along the downwind direction, which would be void of H atoms if it were not for the filling in resulting from the velocity dispersion associated to the LISM temperature.

All these effects (which we call DEGREE ONE physical description) can be modeled on computer codes, basically with the use of Liouville's theorem and at the expense of a quadruple integration. Density distributions, emissivity distributions and spectral line shapes can be and have been predicted by several groups of research scientists.

Now we have to understand how these solar effects are going to modify the basic methods of diagnostic that were discussed above.

The purely photometric diagnostic method

1) Helium density distribution

The focusing effect allows to determine simply the downwind direction. The first attempt to observe this spectacular focusing cone of helium failed in 1972, when the french satellite D2-A polaire could not reach its orbit. Later, the Naval Research Laboratory group successfully mapped the Helium 58.4 nm emission distribution with an Earth orbiting spacecraft (STP-72) and determined the direction of the incoming flow $\vec{V}_w$ to be

[Weller and Meier, 1974] :

$\alpha = 252 \pm 3°$, $\delta = -15 \pm 3°$ (celestial coordinates)

which is slightly above the ecliptic plane.

The exact shape of the cone (its angular width about the downwind axis) depends slightly on the temperature T and on the bulk velocity V_o, and careful measurements compared to accurate modeling allows to determine an estimate of these parameters. A 58.4 nm photometer flown on soviet satellite PROGNOZ 6 in 1977 provided a series of swaths across the helium cone, compared to models at various temperatures. A summary of V_o and T determination from various space instruments performing purely photometric measurements is presented on Figure 4. The most recent PROGNOZ measurements [Dalaudier et al., 1984] indicates parameters in the range :

$T = 11{,}000 - 24{,}000$ K $\qquad V_w = 23 - 30$ km.s^{-1}

From the shape of the (V_w, T) domaine of Figure 4, it seems as if there is some coupling between parameters V_w and T ; in fact, it can be understood intuitively that the most important parameter is the ratio V_t/V_w of the thermal velocity V_t to the bulk velocity V_w.

One difficulty of the modeling is that the exciting solar line shape at 58.4 nm has to be taken into account, since its width is comparable to the velocity dispersion of He atoms (expressed in Doppler shifts). This line shape and its width are not very well known, but Dalaudier et al. (1984) showed that the derived parameters V_w and T did not change substantially when various spectral profiles were introduced in the modeling.

Besides the conspicuous focusing cone, the HeI 58.4 nm intensity distribution is very smooth in the other directions. The density n_∞(He) of helium atoms can be obtained with the help of equation (3), in which the coefficient γ includes a modeling of the He distribution in the solar system and the geometric conditions of observations. The difficulty of the absolute value of axF_s remains.

2) Lyman-alpha photometric observations of hydrogen distribution

For a typical set of LISM parameters and solar parameters, the resulting H density distribution has a cylindrical symmetry about the wind axis. The shape of the isodensity contours illustrates quite well the ionization cavity, elongated in the downwind direction. The corresponding emissivity distribution is obtained after multiplying by a r^{-2} factor and presents a broad region of maximum emissivity at 2 to 3 AU on the upwind axis.

An observer located at one 1 AU is well inside the ionization cavity. The resulting Lα photometric pattern is characterized by a broad region of maximum intensity not far from the upwind direction $\vec{V}_w$ of the incoming flow of hydrogen (opposite to the focusing cone direction V_o), and a gradual decrease toward the opposite downwind direction.

Therefore, a mapping of the Lα interplanetary emission gives immediately the general direction of the wind. However, since the maximum emission region is very broad, it can not give, as in the case of the helium cone, a very accurate determination. Besides, since the maximum **emissivity** region is not far from the sun, there is a parallax effect : the direction of the maximum **emission** depends on the location of the observer. Indeed, when the first global mappings of extraterrestrial Lα were made in 1969 with two Lα photometers, placed on board OGO-5 satellite [Bertaux and Blamont, 1971 ; Thomas and Krassa, 1971], two mappings made at 6 months intervall revealed clearly a $\simeq 40°$ displacement of the maximum region, definitely indicating that the source of Lα emission was right in the solar system, and was not of galactic origin as it was thought before. The direction of the wind $\vec{V}_w$ was found to be $\alpha = 265°$, $\delta = -15°$, with a rather large uncertainty margin ($\pm 15°$) [Bertaux and Blamont, 1971].

The filling of the ionization cavity depends on the temperature T, and one could hope that the shape of the ionization cavity (defined, for instance, by the ratio I_{max}/I_{min} of maximum to minimum measured intensities) would allow a measurement of this temperature from a purely photometric pattern. Unfortunately, the shape of the ionization cavity depends also on three other parameters : the flow velocity V_w, the ionization rate $\beta = T_D^{-1}$ and the solar Lα flux through $\mu = F_r/F_g$. Several sets of different parameters can yield nearly identical intensity distribution, as shown by Lallement and Bertaux (1984). Five different sets of parameters were selected to give approximately the same ratio I_{max}/I_{min}, and all model curves were normalized at the same value of I_{max}, since the density at infinity n_∞ (H) is an unknown free parameter which behaves linearly on the intensity.

All five curves are nearly identical. Since there are rather large uncertainties on the exact value of the solar parameters μ and β, this exercise clearly demonstrate that it is not possible to retrieve accurate LISM parameters V_w and T from only purely photometric measurements.

THE HIGH RESOLUTION SPECTROMETRIC METHOD OF DIAGNOSTIC

High resolution spectrometric measurements of line width, line shape and line position will yield, as explained in the first section, independent and crucial information on the LISM parameters, because through Doppler effect the line shape of the resonant emission is an image of the velocity distribution of atoms, projected on and integrated along the line of sight, and weighted by the resonance excitation rate.

However, gravitation, ionization and radiation pressure will modify the velocity distributions and corresponding line profiles.

For helium, two effects are playing an important role. First the velocity distribution of He atoms is strongly modified by the solar gravitation ; second, the solar line width is small enough that the resonant line

shape is modified in respect to the velocity distribution, since atoms with a large Doppler effect respective to the sun will be excited at a lower rate, and may even not be excited at all.

In the case of H Lyα , the solar line is wide enough that it may be considered as flat on the interval of sun radial velocities of H atoms, and the line shape is strictly the image of the projected velocity distribution (weighted by the excitation rate).

The velocity distribution of H atoms may be modified in theory by the following effects :

- The unbalance between solar gravitation F_g and the Lyα solar radiation pressure F_r, described by the parameter $\mu = F_r/F_g$ provides a mechanical effect which bends individual trajectories into hyperbolae, as in the case of Helium, but to a lesser degree.

- The solar ionization is more effective on slow atoms than on fast atoms [Wu and Judge, 1979 ; Lallement, 1983]. As a result, the bulk velocity and the velocity distribution are modified.

- Heating by solar corpuscular emissions should be only a minor effect [Holzer, 1977 ; Wu and Judge, 1978 ; Kunc, Wu and Judge, 1983].

All these effects can be taken into account in predictive spectrometric models of line shapes of H and He emission and can be implemented on expensive computer codes ; see for instance Meier (1977) and Wallis and Wallis for an approximate formulation (1979). The two first effects are included in the DEGREE ONE physical description.

It could be thought that, since the solar Lα radiation pressure is approximately in equilibrium with solar gravitation, the H velocity distribution would not be too much modified from its Maxwell-Boltzmann shape at infinity. In the case $\mu = 1$, all H atoms trajectories are straight lines, and the same gaussian shape could be seen in all directions.

However, even in the case $\mu = 0.75$, not very far from $\mu = 1$, Wu and Judge (1980) computed that the velocity distribution was substantially modified. Assuming that the LISM temperature was $T = 10^4$ K, they showed that, for directions of sight toward the upwind region, the "effective temperature" T_e of the modified velocity distribution was 9,500 K (slight cooling effect due to ionization), increasing up to T_e = 13,500 K when looking toward the downwind region.

We now turn our attention to the observations, made with different experimental methods, their interpretation and the LISM results.

HYDROGEN Lα HIGH RESOLUTION SPECTROMETRIC OBSERVATIONS

With the UV spectrometer of Copernicus observatory, Adams and Frisch (1977) obtained a weak line of the LISM H Lyα emission, in only one direction of sight after six days of integration. They found a Doppler shift of 22 ± 3 km.s^{-1} and a width corresponding to 20,000 K or less.

It would have been impossible to look in many directions, as would be required to detect different Doppler shifts in different directions to determine $\vec{V}_w$ independently of photometric measurements. The temperature diagnostic is not very accurate either.

The use of resonance absorption cells associated to photometers is much more powerful than the use of high resolution spectrometers, mainly because of the much larger instrumental throughput, and the theory of its use will be now briefly described, as well as the experimental results obtained in 1976 and 1977 with a french experiment on soviet PROGNOZ satellites.

The Lyman-α photometer flown on Prognoz 5 and Prognoz 6 consisted of a solar blind photomultiplier as the detector, placed behind a hydrogen absorption cell, which is a teflon coated glass vessel with two MgF_2 windows. The entrance window is a lens, which focus is between the cell and the PM tube. A rectangular hole at the focus defines a field of view of $1.3 \times 3°$. The exit window of the cell is covered with an evaporated thin film filter, which defines a total bandwidth of ~ 10 nm centered at Lyman-α. In the following, it will be assumed (unless otherwise specified) that the only radiation seen by the detector is resonance radiation from hydrogen atoms.

The cell is sealed and permanently filled with H_2 at a few mm Hg (a few hundreds Pascal) pressure. A tungsten filament placed inside the cell can be heated electrically, and H_2 molecules touching the filament are dissociated into atoms, creating an optical thickness τ of atomic hydrogen. When the filament is switched off, there is immediate (within $\simeq$ 0.05 seconds) recombination into molecules. Whereas H_2 is totally transparent to Lα, when the optical thickness $\tau = 10$ is created inside the cell, incoming photons lying near the resonance line center are scattered away from the direct beam and absorbed on the cell walls. The transmission function $T(\lambda)$ of the cell in its reference frame,looks like a rectangle with an equivalent width of absorption $W = 30$ mÅ or 7.4 km. s^{-1}. The cell may be regarded as a "negative" spectrometer with a bandwidth $W = 30$ mÅ ; the wavelength scanning is provided by varying the Doppler shift $\Delta\lambda_D$ between the interplanetary line and the cell. When the cell is not activated, the total Lα intensity I_0 is measured ; when it is activated, at the level $\tau = 10$, it is reduced to $I(\Delta\lambda_D)$ by a factor $R(\Delta\lambda_D)$ depending on the Doppler shift $\Delta\lambda_D$. The reduction factor $R = I(\Delta\lambda_D)/I_0$.

Looking in the sky at different directions of sight $\vec{u}$ a large wavelength exploration is obtained owing to the orbital velocity $\vec{V}_s$ of

the spacecraft in the solar system, combined with the wind velocity $\vec{V}_w$ of $\simeq 20 - 25$ km. s^{-1}. The total relative velocity between the spacecraft and the H interstellar flow is $\vec{V}_R = \vec{V}_s + \vec{V}_w$. For Prognoz satellites, which spend most of their time at large distances of the Earth, and have at apogee a low orbital velocity which can be neglected, $\vec{V}_s \simeq \vec{V}_E = 30$ km. s^{-1}, where $\vec{V}_E$ is the Earth's orbital velocity.

The Doppler effect in the line of sight $\vec{u}$ is :

$$\Delta \lambda_D = \frac{\lambda_o}{c} V_R \text{ Cos } (\vec{V}_R, \vec{u}) = \frac{\lambda_o}{c} V_R \text{ Cos } \alpha = \frac{\lambda_o}{c} V_D \qquad (6)$$

α being the angle between $\vec{u}$ and $\vec{V}_R$. Therefore, looking at various angles α provides a spectral scanning of the emission line through the variation of $\Delta \lambda_D$. A series of measurements $R (\Delta \lambda_D)$ can be deconvoluted to retrieve the spectral shape of $f (\lambda)$. This method can be described as the Doppler angular spectral scanning (DASS) method, and has been fully described by Bertaux and Lallement (1984). It should be noted that, since the reduction factor $R (\Delta \lambda_D)$ is a relative quantity, it is not required that the absolute intensity I_o be identical in all directions. It is only required that the **spectral shape** $f (\lambda)$ be the same in all directions, or in the sky region where it is applied.

The minimum reduction factor (maximum absorption effect of the cell) is obtained when the Doppler shift V_D is zero in the plane perpendicular to the vector $\vec{V}_R$, which intersects the celestial sphere along the zero Doppler shift circle ZDSC [Bertaux et al., 1976]. Therefore, a mapping of the R pattern allows to determine the position of the ZDSC circle, and the direction of vector $\vec{V}_R$.

From the study of Bertaux and Lallement (1984) we can summarize how the interstellar gas parameters can be determined from one single mapping of the R pattern of the complete celestial sphere with the Doppler angular spectral scanning (DASS) method, in the simple case of a uniform gaussian case (Figure 5) :

1. Minimum values of measured R are distributed alons a great circle of the celestial sphere (the ZDSC). The direction of $\vec{V}_R = \vec{V}_s + \vec{V}_w$ lies along the axis of this great circle (Figure 5).

2. The value of R_{min} directly determines the temperature T.

3. The module of V_R is determined from the angular width $\Delta\alpha$ of the absorption region along the ZDSC with the approximate relationship :

$$V_R \sin (\Delta\alpha) \simeq \frac{2 kT}{m} \qquad (7)$$

4. The vector $\vec{V}_R$ is determined ; since $\vec{V}_s$ is known, the vector $\vec{V}_w = \vec{V}_R - \vec{V}_s$ is therefore determined.

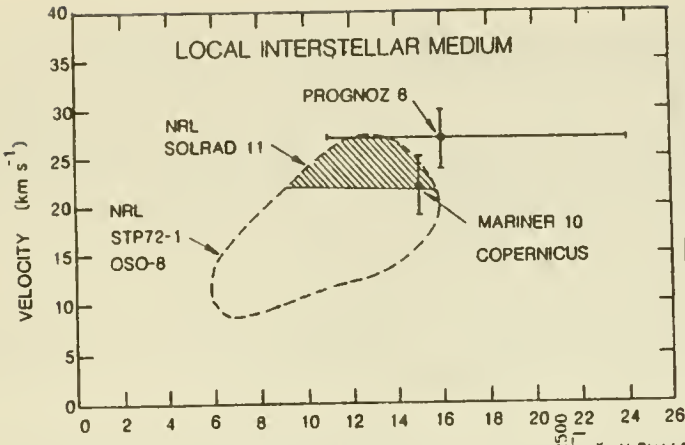

Fig.4

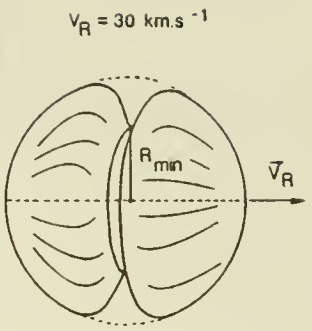

Fig.5

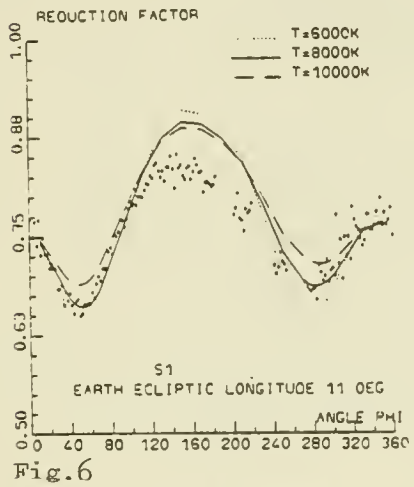

Fig.6

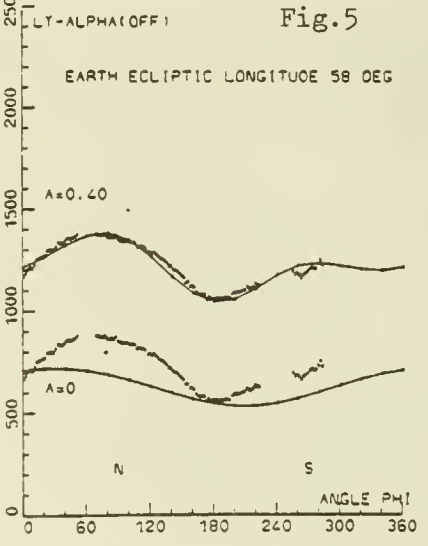

Fig.7

Figure 4. Determinations of V_o and T from photometric observations of the shape of the Helium focusing cone from various experiments. The spectrometric Lα observation of V_o by Copernicus was coupled to Helium observations by Mariner 10.

Figure 5. The pattern of the reduction factor R over the celestial sphere presents a "crunched-apple" shape. Along the plane perpendicular to the relative velocity vector $\vec{V}_R$, the reduction factor is at a constant minimum value R_{min}, linked to the temperature T. The width of the trough is linked both to T and the modulus V_R.

Figure 6. The distribution of the reduction factor R measured by PROGNOZ 6 in a plane perpendicular to the Earth Sun line is shown (data points) as a function of angle PHI with the Earth's velocity vector $-\vec{V}_E$ when the ecliptic longitude was 11°. Three curves are resulting from a model calculation at 3 different temperatures. The modulation of R is due to the variable Doppler shift. The fit with T = 8000 K is good everywhere except for $170 < PHI < 240$, which corresponds to downwind region. Other parameters were fixed at $\mu = 0.75$ and $V_o = 20$ km. s^{-1} (after Bertaux et al., 1984).

Figure 7. The Lα intensity distribution measured at an ecliptic longitude 58° (not far from the downwind axis) is compared to two models of the solar wind (solid lines). One is isotropic (A = 0) and the other (A = 0.40) corresponds to a decrease of 40 % of ionization rate at the solar pole (after Lallement et al., 1984). The intensity scale is in counts. s^{-1}. The lower curve has been displaced from the real curve by 500 counts. s^{-1}. The sensitivity is = 3.6 counts per Rayleigh.

Up to now it was assumed that the only source of Lα radiation is the interplanetary Lα from the LISM. If there is a Lα galactic background (which should be ≃ isotropic because of radiative transfer), Bertaux and Lallement (1984) have demonstrated that it is still possible to determine $\vec{V}_w$ with a purely geometric method (with three sets of observations at different places in the solar system). Once $\vec{V}_w$ is determined, the galactic Lα contribution can be derived and also the temperature.

This DASS method was successfully applied by Lallement et al. (1984) to a series of measurements made with the H-cell Lα photometer flown on Prognoz 5 and Prognoz 6, with the following results :

- an upper limit of 15 Rayleigh is found for the galactic background (whereas the interplanetary Lα ranges from 200 to 1,000 Rayleigh).

- both the bulk velocity $\vec{V}$ and the thermal velocity spread of H atoms are changing with position in the solar system.

This was the first experimental evidence that the real situation departs from the uniform gaussian case. However, one can still define, for each direction of observation, an effective temperature T_e , because a projected velocity distribution can still be approximated by a gaussian. With the DASS method, the value R_{min} of the minimum reduction factor obtained in a plane of scanning allows to assign an effective temperature T_e for the direction where R_{min} is found, since the Doppler shift is known to be zero in this case.

Wu and Judge (1980) concluded that the first spectrometric temperature measurement of the VLISM (T = 8,800 ± 1 000 K), published by Bertaux et al. (1977) form an early use of the DASS method with Prognoz 5 results, had to be re-interpreted because of the velocity distribution perturbations by gravitation, radiation pressure and ionization, and that the VLISM temperature was in reality T = 7,000 K ± 1 000 K. In order to arrive at this result, they had to assume in their model a certain value of the solar parameters μ and β, whereas, if enough measurements of the H absorption cell can be obtained, they can be compared to the result of the interaction model with β and μ as free parameters. This was done by Bertaux et al. (1984) in their final analysis of the Prognoz results, which could extract from such a comparison the following set of both solar and VLISM parameters :

μ = 0.75 ± 0.1	Ecliptic Coordinates
T = 8 000 ± 1 000 K	λ_w = 254 ± 3°
V_w = 20 ± 1 km s	β_w = + 6 ± 3°

In this global analysis, not only the values of R_{min} and the corresponding directions were used, but all measurements, many of them showing some absorption by the H cell.

The reduction factor measurements are compared for various models on Figure 6 from Bertaux et al. (1984). On each figure all parameters are fixed at their best final fit, except for T. Measured data were collected in scanning planes perpendicular to the Earth-Sun line at various places in the solar system, implying large differences for the relative vector $\vec{V}_R = \vec{V}_w + \vec{V}_E$, $\vec{V}_E$ being the Earth's orbital velocity. A visual estimate allowed to define the uncertainty bar for the various parameters. It can be noted that the fit is excellent for directions of sight probing upwind regions, but becomes poorer for downwind regions, corresponding to angle $120 \leq \phi \leq 240°$ for observations made when the Earth was on the right side of the wind flow (when $\vec{V}_E$ and $\vec{V}_w$ have opposite directions).

This is evidence that the observed heating effect is larger than predicted by DEGREE ONE approach. In particular, measurements toward the downwind region show still a significant absorption when the Doppler shift is large, which can be explained by a temperature of 20,000 K of the atomic hydrogen in the downwind region. This is probably the result of elastic collisions with the solar wind, as suggested by Lallement et al. (1984).

As Lallement and Bertaux (1984) pointed out, the ionization modifies substantially the line shape when the rate is changed from $\beta = 0$ to $\beta = 2.5 \times 10^{-7}\ s^{-1}$. Then, larger values (up to $10^{-6}\ s^{-1}$) do not modify substantially the line shape. Another effect is the convergence introduced by ionization.

In order to determine the ionization rate, the Lα photometric results were used. The shape of the cavity, once T, V_w and μ are determined by the DASS H cell method, indicated that the ionization rate (during 1975-1976 period) was $\beta = 4 \times 10^{-7}\ s^{-1}$ in the equatorial plane, and decreasing with latitude up to a value $\beta = 2.4 \times 10^{-7}\ s^{-1}$ at the solar pole. This solar anisotropy is attributed to a 50 % decrease of the solar wind mass flux at high solar latitudes [Lallement et al., 1984], and is imposed by the photometric observations, as it is clear on Figure 7.

Once the ionization rate is known, formula (3) can be used to determine the neutral density "at infinity" $n_\infty(H)$ (when it is not perturbed by the heliosphere interaction). The coefficient γ contains an integral which takes into account all DEGREE ONE physical assumptions. Since the absolute value of μ is determined (by the bending of the H flow under gravitation/ radiation pressure), the solar flux F_S is determined. For the Prognoz photometer, a stellar observation of several hot stars allowed to derive in addition an estimate of the calibration factor a = 3.6 counts $.s^{-1}$ per Rayleigh, and the value of $n_\infty(H)$ could be deduced :

$$n_\infty(H) = 0.04 \text{ to } 0.06 \text{ atom.cm}^{-3},$$

the range allowing mainly for the uncertainty of the stellar calibration procedure.

HIGH RESOLUTION SPECTROMETRIC MEASUREMENTS OF HELIUM 58.4 NM LINE

The best results in this field were obtained with a helium absorption cell with a fixed value $\tau = 10^5$ during the Apollo Soyouz Test Project by Freeman et al. (1980). Their results are reproduced on Figure 8, where their measurements are compared with model calculations of the DEGREE ONE type. Though they clearly measured a substantial absorption, varying with the Doppler shift, their model calculations indicated an absorption very little sensitive to the temperature, and the comparison of the observed absorption to their model yielded a wide range of temperature from 5,000 to 20,000 K.

As discussed by Bertaux and Lallement (1984), this is mainly due to their choice of a large optical thickness $\tau = 10^5$. When the DASS method is used for $\tau = 10^5$, the absorption convolution profile ressembles very much the transmission curve $T(\lambda)$ of the helium cell, which is larger than the interplanetary He line. There are some experimental difficulties to use a low optical thickness within a Helium cell, because as it is a monoatomic gas, the corresponding pressure would be very small and quite difficult to measure and control. The use of a buffer gas is therefore recommended in such a case [Bertaux and Lallement, 1984] for a future space experiment.

The photometric measurements of the helium cone shape remain up to now the ones yielding the narrower temperature range of interstellar helium.

COMPARISON OF HYDROGEN AND HELIUM LISM PARAMETERS

The **direction** of the wind as determined from the helium cone or from H cell analysis are identical, within the $\pm$ 3° error boxes. At variance, there is a major discrepancy between Hydrogen and Helium for the module velocity V_w and the temperature T :

	Hydrogen	Helium
T (°K)	8,000 $\pm$ 500	16,000 $\pm$ 5,000
V_w (km. s^{-1})	20 $\pm$ 1 km.s^{-1}	27 $\pm$ 3
density $n_\infty(cm^{-3})$	4 to 6 $\times 10^{-2}$	1.5 to 2 $\times 10^{-2}$

It is quite difficult to admit that the temperature difference is intrinsic to the VLISM, since the local mean free path of atoms between collisions is 0.04 pc only. Collisions would also tend to equalize the velocity modulus.

In order to have the same direction of $\vec{V}_w$ but different velocity modulus it would require an extraordinary coïncidence, as pointed out by Lallement (1983). As explained on Figure 9, the velocity $\vec{V}_w$ of the solar

system in respect to the VLISM is the composition of the solar motion $\vec{V}_a$ toward the Apex ($\alpha = 271°$, $\delta = 30°$) and the motion of the VLISM respective to the nearby stars forming the local frame of reference, the interstellar wind $\vec{V}_t = \vec{V}_a - \vec{V}_w$.

Applying this relationship for H and He separately and subtracting will yield :

$$\vec{V}_t \text{ (He)} - \vec{V}_t \text{ (H)} = \vec{V}_w \text{ (H)} - \vec{V}_w \text{ (He)}$$

The difference of intrinsic velocity vector is parallel to $\vec{V}_w$ (H) - $\vec{V}_w$ (He), which is parallel to both V_w (H) and V_w (He), which are found to be in the same direction. But this direction is imposed by the solar vector $\vec{V}_a$, a random vector which is completely independent from the intrinsic difference between H and He interstellar flow.

Therefore, it is likely that the difference of modulus is an artefact of our diagnostic methods. Since high resolution spectrometric measurements are quite sensitive to the Doppler shift, I believe that the hydrogen determination is more accurate for the modulus than the photometric determination of the helium velocity.

Returning to Figure 4 representing the (V_w, T) parameters giving a good fit to the helium cone shape, it was remarked a certain coupling between V_w and T. If a lower velocity $V_w = 20$ km. s^{-1} was imposed, perhaps a lower temperature for helium would also result in the fitting process, which would alleviate somewhat the H-He temperature discrepancy too.

The celestial and galactic coordinates of the intrinsic interstellar wind $\vec{V}_t$ can be computed. Assuming the hydrogen determination to be correct, the motion of the VLISM in respect to the local standard frame of reference (LSR) is characterized by a velocity $\vec{V}_t$ of 16 ± 1 km. s^{-1}, which direction coordinates are :

Celestial	Galactic
$\alpha = 14 \pm 3°$	$\ell_{II} = 124 \pm 3°$
$\delta = 66.5 \pm 3°$	$b_{II} = 4 \pm 3°$

The ratio of neutral densities n_∞ (H) / n_∞ (He) is ≃ 3, whereas one would expect a cosmological ratio 10. This is easily explained by a substantial ionization of the VLISM. If x is the fraction of ionized hydrogen, (we drop ∞ in the following)

$$x = n(H^+) / (n(H) + n(H^+)) = 1 - n(H) / 10\, n(He)$$

it indicates that f ≃ 0.7 in the VLISM, the total density being
$n(H^+) + n(H) + n(He) = 0.11$ cm^3.

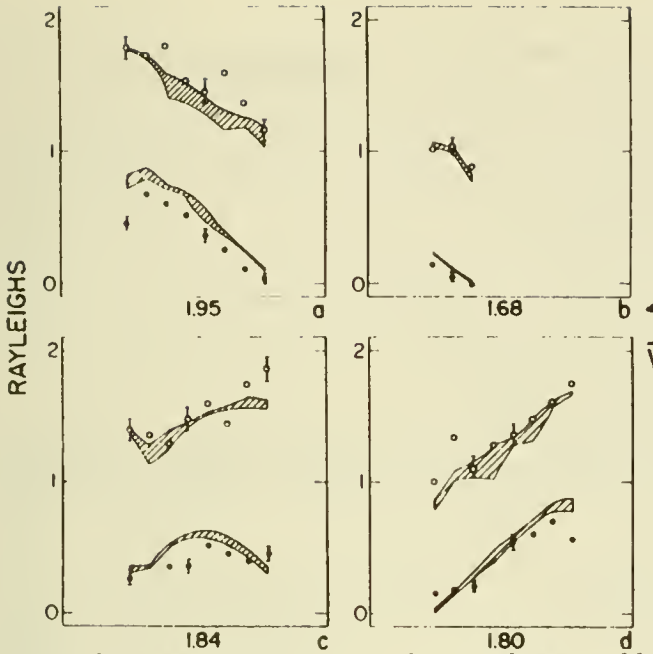

Fig. 8. Measurements with a Helium cell photometer on ASTP mission are compared with models. Open circle are with the cell empty. Black circle are with the cell filled with an optical thickness $\tau = 10^5$. The absorption of the cell is quite efficient and depends on the direction of sight because of variable Doppler shift (after Freeman et al., 1980). However, model predictions for a wide range of temperatures show little dependance on the temperature, because the optical thickness was too high.

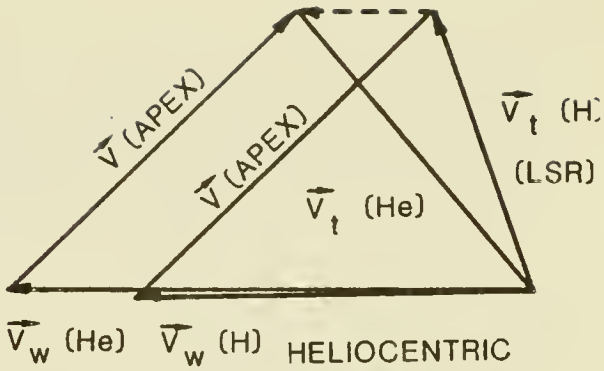

Fig.9 In the solar system, the vectors V_w (H) and V_w (He) have the same direction, but seems to have different modulus. Therefore, the difference $\vec{V}_w$ (H) - $\vec{V}_w$ (He), which is independant of the coordinates system, is parallel to V_w (H), which includes the particular motion of the Sun. This suggests an artefact in the determination of the modulus of V_w (He).

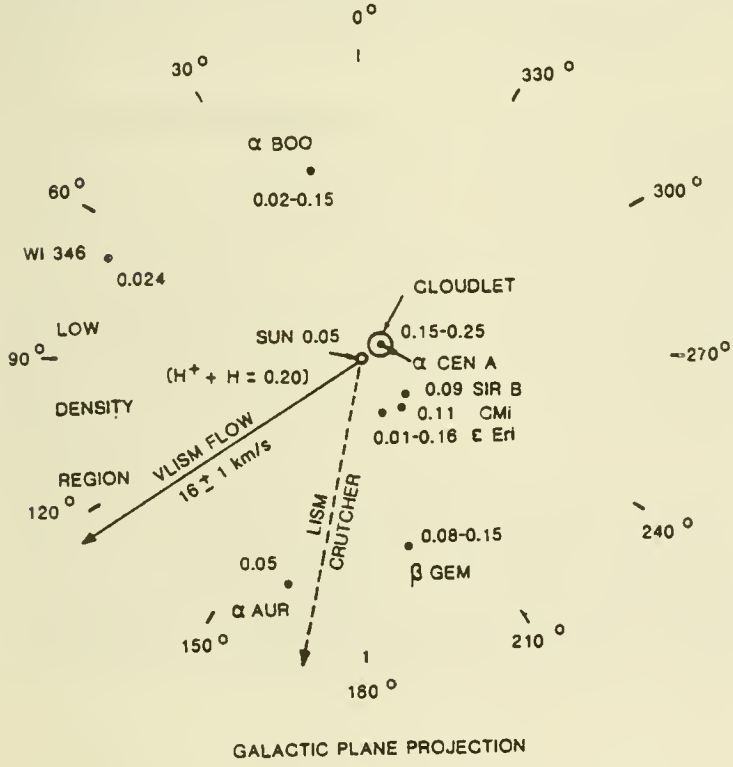

Figure 10 Some nearby stars (projected on the ecliptic plane) are shown, together with the average H density. A possible cloudlet of enhanced density is drawn around α Cen, toward the region of highest density. The VLISM vector, at $\ell_{II} = 124°$, is exactly opposite to the direction of α Cen, and is significantly different from the LISM vector, as determined by Crutcher (1982) for interstellar absorption within ≃ 100 pc.

Of course, neither H^+ nor He^+ are accessible to studies in the solar system, since they are prevented to enter through the heliosphere.

We will discuss these VLISM results in the next concluding section, in the frame of the other LISM studies.

CONCLUSIONS

The study of H and He back-scattered resonance emissions in the solar system provides information on three different topics, which are of interest to three different scientific communities :

- The very local characteristics of the LISM.
- The interaction processes between the solar environment and the interstellar medium in which it is embedded, which is of broader interest than just solar system studies, since similar interactions can be encountered in other astrophysical conditions (i.e., Stellar wind expansions).
- Some basic solar parameters concerning the solar wind and the Lα output at line center.

1. Solar parameters

The bending of the H atoms trajectories is determined with **relative** measurements with the H cell. It needs no calibrated instrument, and still yield a quite important **absolute** value of a solar parameter : with $\mu = 0.755 \pm 0.11$, the solar Lα flux at line center is :

$$F_s = 2.5 \pm 0.25 \times 10^{11} \text{ phot } (\text{cm}^2 \text{ Å s})^{-1}$$

This value is an average over a $\simeq$ one year period (the typical time for one H atom to travel through the solar system), and holds for a period of minimum solar activity (1975-1976).

The decrease of H density along the VLISM flow, which can be measured with an uncalibrated Lα photometer, allows to measure the **absolute** value of the ionization rate β. With weakly demanding physical assumptions,this ionization rate can be transformed into an **absolute** determination of the solar wind mass flux at **all latitudes** by remote sensing. The solar wind flux of protons F_p, averaged over one year, and for the 1975-1976 period (minimum solar activity), is :
$F_p = 1.87 \times 10^8$ protons $\text{cm}^{-2}\ \text{s}^{-1}$ in the equatorial plane and a strong anisotropy is found, with a 30 % decrease toward the solar poles. Large scale properties of the solar wind flux, averaged over $\simeq$ one year, can be monitored through Lyman-alpha mapping. A correct interpretation of the results needs, however, the accurate knowledge of $\vec{V}_w$ and T which is now in our hands. In a near future, the study of other data (VOYAGER) will allow to check if this anisotropy persists during a maximum of solar activity.

2. Interaction processes

The DEGREE ONE physical assumptions are clearly verified in the data. however, the H cell spectral data on the H velocity distribution, together with the photometric mapping of the helium cone give slightly inconsistant VLISM results. It seems more and more obvious that some interaction between the sun and the neutral gas, not included in the DEGREE ONE approach, is of importance to describe completely the data and reconcile H and He results.

Mainly two kind of effects have been considered by various authors.

One is located at the boundary of the heliosphere (at several hundreds AU), where the solar wind plasma and the VLISM neutral-ionized matter are interacting. As a possible consequence, Ripken and Fahr (1983) predict a decrease of density of H by a factor of $\simeq 2$.

The second kind includes elastic collisions with the solar wind plasma. One difficulty is that these effects, if they are of importance, would have a tendency to heat more hydrogen atoms than helium atoms, whereas what is observed is that T (He) > T (H).

However, PROGNOZ observations toward the downwind region do indicate very hot hydrogen ($\simeq 20\ 000$ K), after interaction with the solar environment. Together with the helium cone shape, both discrepancies are found in the downwind region, which is in my opinion a strong indication that deviations to the DEGREE ONE approach are more related to an interaction near the sun (i.e., elastic collisions with solar wind ions) than at the large distance of the heliosphere boundary.

3. The VLISM parameters

In the ISM description of Mc Kee and Ostriker (1977) small clouds of dense and cold neutral H (T = 80 K, n = 42 cm^{-3}) are embedded in a hot (10^5 - 10^6 K) low density (10^{-2} cm^{-3}) and totally ionized medium.

According to this model, there is an intermediate phase of the ISM at the interface between the cold and hot phase, composed of two distincts parts, both at 8,000 K (warm). The one on the side of the dense cloud is only weakly ionized (x = 0.15), and the one on the side of the hot ISM is substantially ionized, with x = 0.68, and a total number density of n = 0.25 cm^{-3} .

Though there is some discussion about the number of such cloudlets in the LISM (within $\simeq$ 100 pc) [Bruhweiler and Kondo, 1982], the characteristics found for the VLISM : T = 8,000 $\pm$ 1000 K, n = 0.11 cm^{-3} and x = 0.70 are strikingly reminiscent of the ionized part of this last interface phase as described by Mc Kee and Ostriker.

Therefore, it would mean that the Sun is presently within ≃ 2 pc from a dense cloud. The possibility that such a cloud is moving rapidly in our direction was discussed by Vidal-Madjar et al. (1978), on the ground of Copernicus LISM soundings, D/H distributions and EUV anisotropic radiation pattern. The estimated distance of the dense cloud was 0.03 pc, however, which seems uncompatible with the ≃ 1 pc thickness of the weakly ionized medium immediately surrounding the cold cloud in the description of Mc Kee and Ostriker (1977), and the strongly ionized medium in which the Sun is moving presently.

Figure 10 is an attempt to compare the characteristics of the VLISM, namely the density and the direction of the VLISM flow, with LISM densities measured on a few nearby stars, either with **Copernicus** or with IUE taken from Vidal-Madjar et al. (1977), and Bruhweiler and Kondo (1982).

If there is a dense cloudlet in the vicinity of the Sun, then it could very well be toward α CEN A, which is the nearest star (1.33 pc) and shows the largest averaged H neutral density of 0.20 ± 0.05 cm^{-3} [Dupree et al., 1977]. This neutral density is larger than the VLISM by a factor of ≃ 4, but is not very different from the total VLISM density (0.22 cm^{-3}).

One striking feature in that the VLISM flow is exactly opposite to the direction of this enhanced density, and is suggestive of an evaporation mechanism from the cold and dense cloudlet toward the hot and tenuous ISM. It should have therefore a quite local significance. However, accurate positionning of optical absorption lines on a number of stars in a range of 100 pc [Crutcher, 1982] shows a coherently moving piece of ISM of this scale around Sun. Suggesting that the ≃ 100 pc ISM around the Sun could be material which has been shocked and accelerated by stellar winds and supernovae associated with the Scorpio-Ophiucus OB stars, which lies approximately at the opposite of the VLISM flow. But, as indicated on Figure 10, the VLISM flow is near the galactic plane, at longitude $\ell_{II} = 124°$, whereas the Crutcher's vector (in respect to LSR) lies at $\ell_{II} = 169°$. This ≃ 45° difference points again to a local significance for the VLISM flow. In this respect, the recent detection of a dust cloud in the far infra-red around $\ell_{II} \simeq 315°$, extended over several tens of degrees [Caux et al., 1984], may confirm the proximity of a moderately dense cloud in the near vicinity of the solar system.

REFERENCES

ADAMS T.F., FRISCH P.C., 1977 - Astrophys. J., 212, 300.

BERTAUX J.L., BLAMONT J.E., 1971 - Astron. Astrophys., 11, 200.

BERTAUX J.L., BLAMONT J.E., TABARIE N., KURT V.G., BOURGIN M.C., SMIRNOV A.S., DEMENTEVA N.N., 1976 - Astron. Astrophys., 46, 19-29.

BERTAUX J.L., BLAMONT J.E., MIRONOVA E.N., KURT V.G., BOURGIN M.C., 1977 - Nature, 270, 156.

BERTAUX J.L., LALLEMENT R., 1984 - Astron. Astrophys., in press.

BERTAUX J.L., LALLEMENT R., KURT V.G., MIRONOVA E.N., 1984 - Astron. Astrophys., Submitted.

BLUM P.W., FAHR M.J., 1970 - Astron. Astrophys., 4, 280.
BRUHWEILER F.C., KONDO Y., 1982 - Astrophys. J., 259, 232.
CRUTCHER R.M., 1982 - Astrophys. J., 254, 82.
DALAUDIER F., BERTAUX J.L., KURT V.G., MIRONOVA E.N., 1984 - Astron. Astrophys., 134, 171-184.
CAUX et al., 1984 - Submitted to Astron. Astrophys.
FREEMAN J., PARESCE F., BOWYER S., LAMPTON L., 1980 - Astron. Astrophys., 83, 58-64.
HOLZER T.E., 1977 - Rev. Geophys. Space Phys., 15, 467.
KUNC J.A., WU F.M., JUDGE D.L., 1983 - Planet. Space Sci., 31, 1157.
LALLEMENT R., BERTAUX J.L., KURT V.G., MIRONOVA N.N., 1984 - Astron. Astrophys., In press.
LALLEMENT R., 1983 - Thèse de 3ème Cycle, Université P. et M. Curie.
LALLEMENT R., BERTAUX J.L., 1984 - Astron. Astrophys., Submitted.
MEIER R.R., 1977 - Astron. Astrophys., 55, 211.
McKEE C.F., OSTRIKER J.P., 1977 - Astrophys. J., 218, 148.
RIPKEN H.W., FAHR H.J., 1983 - Astron. Astrophys., 122, 181-192.
THOMAS G.E., KRASSA R.F., 1971 - Astron. Astrophys., 11, 218.
VIDAL-MADJAR A., LAURENT C., BRUSTON P., AUDOUZE J., 1978 - Astrophys. J., 223, 589.
WALLIS M.K. and WALLIS J., 1979 - Astron. Astrophys., 78, 41-45.
WELLER C.S., MEIER R.R., 1974 - Astrophys. J., 193, 471.
WELLER C.S., MEIER R.R., 1981 - Astrophys. J., 246, 386.
WU F.M., JUDGE D.L., 1978 - Astrophys. J., 225, 1045.
WU F.M., JUDGE D.L., 1979 - Astrophys. J., 231, 594-605.
WU F.M., JUDGE D.L., 1980 - Astrophys. J., 239, 389.

PIONEER 10 AND VOYAGER OBSERVATIONS OF THE INTERSTELLAR MEDIUM IN SCATTERED EMISSION OF THE He 584 A AND H Lyα 1216 A LINES

D. E. Shemansky, D. L. Judge, and J. M. Jessen
Center for Space Sciences, University of Southern California

ABSTRACT

The combination of Pioneer photometric and Voyager spectrometric observations of EUV interstellar-interplanetary emissions in the region beyond 5 AU have been applied to a determination of atomic hydrogen and helium densities. These density estimates obtained from direct measurement of scattered radiation depend on absolute calibration of the instruments, in the same way as other earlier determinations based on the same method. However, we have combined the spacecraft data with daily full sun averages of the H Lyα 1216 A line obtained by the Solar Mesospheric Explorer (SME) satellite, to obtain a measure of atomic hydrogen density independent of instrument absolute calibration. The method depends on observations of long and short term temporal variability of the solar line over a 1 year period, and the fact that the ISM is optically thick. The density estimates from preliminary work on these observations are [H] = 0.12 cm^{-3} and [He] = .016 cm^{-3}, giving a density ratio close to the cosmic abundance value, in contrast to some earlier results indicating a depletion of atomic hydrogen. We have obtained estimates of galactic background emissions in the signals of both spacecraft.

Introduction

The estimation of neutral densities in the LISM through observations of resonance scattered solar radiation is simplified somewhat if the observations are made beyond 5 AU, where local perturbation by the sun is not a serious consideration in the analysis. We have combined the data obtained by Pioneer 10 (P10), Voyager 2 (V2) and SME to produce estimates of hydrogen and helium densities using two basically different methods. The first method is the conventional one in which the H and He densities are estimated using instrument calibration and solar emission intensities to calculate densities from the scattered He 584 A and H 1216 A and 1025 A lines. The second method depends on comparing the daily average variation of the 1216 A line as measured by P10 and V2 with the directly measured solar emission line from the SME satellite. The time variations measured by the three instruments during the year 1982 are interpreted in terms of optical thickness of the LSIM to the solar 1216 A line. The measure of optical thickness then reduces to an estimate of H density through multiple scattering calculations. The present work obtains a rough density estimate on the basis of multiple scattering characteristics calculated by Keller, Richter and Thomas (1981). The results are preliminary in nature because we require more specific multiple scattering calculations. We suggest that the data is of sufficient quality that further detailed multiple scattering calculations specific to the observational data be pursued. In addition to ISM densities we have obtained estimates of galactic background emissions in the signals of the two spacecraft.

SUMMARY

Pioneer 10 and Voyager 2 observations of the ISM in the >5 AU region have been used to estimate hydrogen and helium densities. The spacecraft data has also been combined with SME 1216 A solar observations to obtain an H density independent of absolute instrument calibration, and to set a limit on galactic

background at 1216 A in the upstream direction.

1) The helium density based on the calibrations of both the P10 and V2 instruments is estimated to be [He] = 0.016 cm^{-3}. This density is based on a benchmark He 584 A flux of 1.3 x 10^9 Ph cm^{-3} s^{-1} measured by Heroux and Higgins (1977) in 1973. The P10 data for this estimate is taken from DOY 104/73 and DOY 163/74. The line width is assumed constant at 29.3 cm^{-1}. Using this benchmark at solar minimum the P10 data on DOY 278/79 imply a solar flux of 4. x 10^9 Ph cm^{-2} s^{-1} at 1 AU. With this value of F0 and the V2 data obtained on the same day, we obtain the same density [He] = 0.016 cm^{-3}. The two instruments are thus on the same calibration scale at 584 A.

2) Comparison of the two instruments at 1216 A on DOY 278/79 indicates a calibration difference of a factor of 4.4, where

$$I_{V2}(1216) = 4.4 I_{P10}(1216). \qquad (1)$$

Using P10 data and an SME reference in 1982, we estimate F_0 = 4.3 x 10^{11} Ph cm^{-2} s^{-1} on DOY 278/79. This yields [H] = 0.14 cm^{-3}, based on optically thin model and the V2 calibration. With equation 1, the two instruments give the same implied solar fluxes from 1979 to the present, within esimated temporal-spatial uncertainties. Correction for optical thickness using Keller Richter and Thomas (1981), gives [H] = 0.12 cm^{-3}. The most recent estimate of solar flux predicted by the two instruments on DOY 35-37/84 are F_0 = 4.0 x 10^{11} Ph cm^{-2} s^{-1}, for V2 and F_0 = 3.5 x 10^{11} Ph cm^{-2} s^{-1} for P10. Line shapes are based on Lemaire et al. (1978)

3) The I(1216)/I(1025) ratio measured by V2 in the ISM is constant over time and spacecraft position from 1977-1981, 1.5 AU - 10 AU. Assuming that relative line shapes do not change, this result is in accord with multiple scattering theory. The measured mean ratio is I(1216)/I(1025) = 485 ± 37. The mean solar source ratio using Heroux and Higgins (1977) and Hinteregger (1979) data is $I_0(1216)/I_0(1025)$ = 79.7 and 63.7 respectively. Using Lemaire et al line shapes we then have $I_0n(1216)/I_0n(1025)$ = 84.1 and 67.2 The predicted ratio from solar line intensities is then I(1216)/I(1025) = 503 and 402, for the optically thin model. For the optically thick model of Keller et al. (1981) we correct to obtain I(1216)/I(1025) = 600 and 480, which is to be compared to the measured value above of 485. On this basis the V2 1025 A measurement gives [H] = 0.10 and 0.12 cm^{-3} for the two cases.

4) Another method for calculating the H density independent of instrument calibration has been applied through comparing daily averages of the 1216 A signal of P10 and V2 with the solar emission line flux measured by SME, during 1982. During the last half of 1982 a strong 26 day cycle shows good stability for 7 cycles. Although the long term variation of V2 and SME during 1982 is the same, the 26 day period variation is depressed in the V2 data. This is also the case for P10, but the 26 day modulation is depressed still further. We interpret this to be caused primarily by multiple scattering, and using Keller et al. (1981) we obtain, [H] = 0.16 cm^{-3}, from the modulation of V2 observationa at 10 AU and, [H] = 0.11 cm^{-3}, from observation by P10 at 30 AU. This calculation assumes there is no additional contribution caused by line center intensity amplification relative to the integrated line. If there is line center amplification according to the formula obtainced here, we have [H] = 0.17 cm^{-3} and [H] = 0.12 cm^{-3}, in the two cases. According to these calculations only 20% of the P10 signal is zero order scattering. For V2, 50% of the observed signal is zero order scattering.We emphasize that spacecraft background signals have been carefully assessed using three independent means, in applying this method.

5) According to Keller et al. (1981), observations made at different radial distance should follow a 1/r curve whether the line is optically thick or not. This is borne out by the V2 I(1216)/I(1025) ratio measurements. On this basis we can use the continuous data of P10 to establish long term variation of solar flux line center. If we use the integrated 1216 A line full sun plot for solar cycle 21 estimated by Lean and Skumanich (1983), we obtain a slightly lower variation over the 1973-1982 period. If this is attributed to line center variation we obtain the relation $f_0 = C (F_0)^n$ Ph cm^{-2} a^{-1} A^{-1} where $C = 4.18 \times 10^{-6}$ and $n = 1.46$, following the relation developed by Vidal-Madjar. However, it is not clear this relation would improve the fit of the variations, F_0 from the above formula and P10 data vs. F_0 from Lean and Skumanich, over the whole 1973-1982 period.

6) Galactic background
Cross-correlation of the V2 and SME data at 1216 A in the first half of 1982 where there is a slow variation in solar intensity, indicates that there is no measureable galactic component. That is, <10 R of the 800 R total intensity can be attributed to a galactic 1216 A component. V2 is looking upstream and falling off proportional to 1/r from 1979 onward and there is no detectable bow shock component. P10 contains a galactic component in its field, detected by V2 in 1977. This emission accounts for the clock angle variation of the P10 1216 A signal at 30 AU.

Acknowledgements

This work is supported by NASA, Division of Planetary Sciences grants NAGW-163 and NAGW-106, to the University of Southern California.

REFERENCES

Heroux, L., and Higgins, J.E. 1977, J. Geophys. Res., 82, 3307.

Keller, H.U., Richter, K., and Thomas, G.E. 1981, Ast. Ap., 102, 415.

Lean, J.L., and Skumanich, A. 1983, J. Geophys. Res., 88, 5751.

FIGURES

Figures 1 and 2 show the daily average data of P10 and V2 plotted against the phase shifted SME direct observations of the solar 1216 A line in 1982. Although both sets of ISM data follow the long term trend in solar line intensity during 1982, the 26 day cycle modulation is depressed progressively in each spacecraft; V2 is at ~12 AU and P10 is near 30 AU observing approximately radially outward. The spacecraft data are shown as heavy lines.

Figure 3 shows the inferred solar flux at 1216 A from 1973 to 1983 using P10 data, compared to Lean and Skumanich (1983) calculations. We assume a constant line shape in the calculation. The P10 data is shown as a heavy line.

Figure 4 shows Voyager 2 spectrum in the direction of the galactic pole (RA 194.8°, Dec 28.18°) compared to the spectrum in the direction of the P10 line of sight (RA 73.64°, Dec 18.12°). The latter spectrum (light plotted line) shows a relatively strong spatially diffuse galactic emission longward of 912 A, and a substantially weaker 1216 A line due both to a lower solar source emission rate and observation across the downstream depletion cavity.

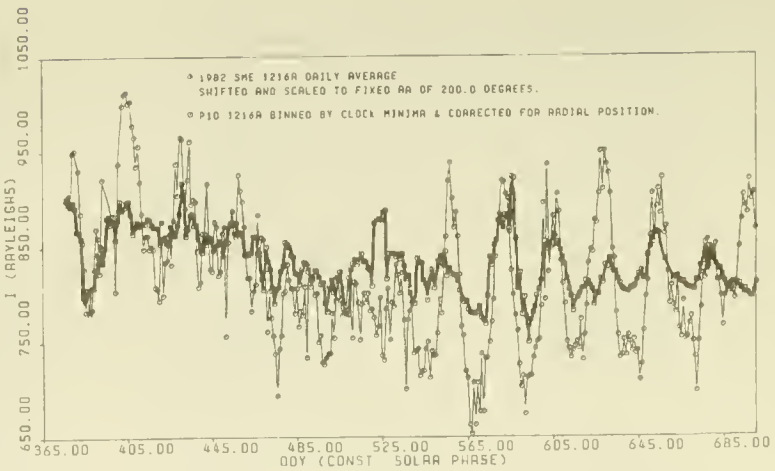

Figure 1

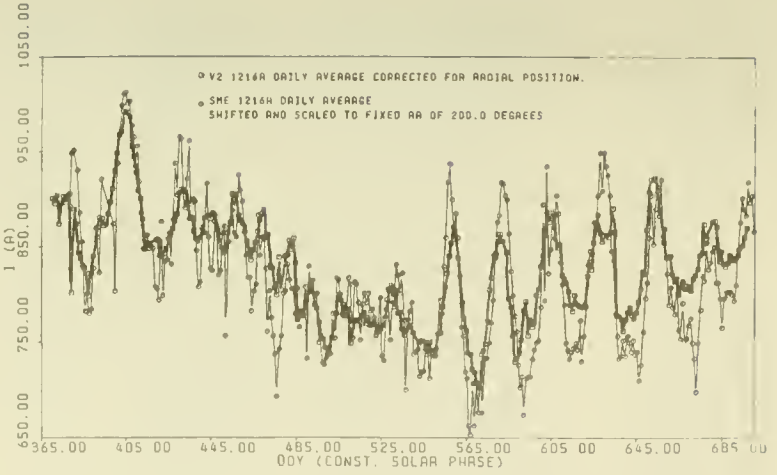

Figure 2

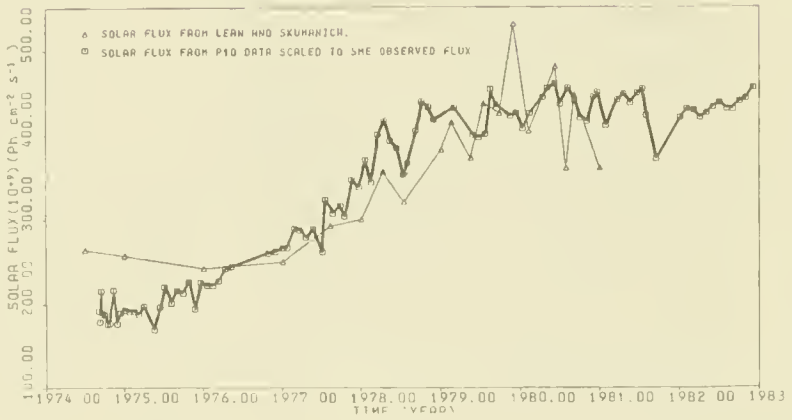

Figure 3

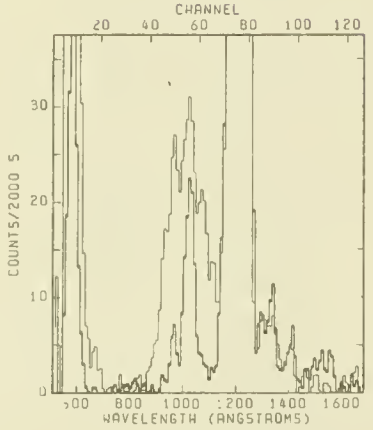

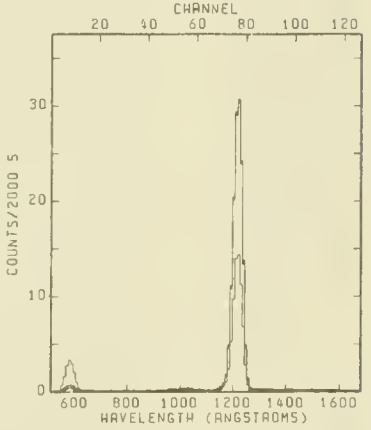

Figure 4

CHANGES OF LISM CHARACTERISTICS IN THE HELIOSPHERIC INTERFACE

Hartmut W. Ripken and Hans J. Fahr
Institut für Astrophysik, Universität Bonn, F.R. Germany

ABSTRACT

It is possible to deduce LISM properties from observations of interstellar neutral gases in the inner solar system. Parameters accessible by this method are the interstellar wind vector and the densities and temperatures of hydrogen and helium, implying also the deduction of the relative abundance ratios and the degree of ionization in the LISM. Direct inference from observations, for example resonance luminescence measurements of Ly-alpha and He-58.4 nm radiation, yields values appropriate only for the inner solar system, i.e. for the regions within the heliopause dominated by the solar wind plasma.

Particularly the subsonic LISM plasma interface ahead of the heliopause causes profound changes in the properties of the neutral LISM gas traversing this region. Mainly p-H charge exchange processes give rise to the destruction of primary hydrogen and the production of secondary hydrogen atoms, the net effect being a depletion of the neutral hydrogen component of the LISM by about 50%.

Details on the depletion mechanisms, the hydrogen and oxygen extinctions, and the consequences for the Ly-alpha resonance luminescence intensity interpretations are presented.

INTRODUCTION

Neutrals penetrating the region of a perturbed interstellar plasma flow along individual dynamical trajectories cannot be treated as moving under conservation of total energy and angular momentum, since their collisional mean free paths in most cases are smaller than the interface dimensions. Due to large charge exchange cross sections, especially H and O atoms effectively undergo charge exchange collisions with interstellar protons. This leads to both destruction of one sort of neutrals and production of another sort of neutrals with different dynamical trajectories. Thus the flow of neutrals along a specific trajectory s through the interface is not carried exclusively by those primary particles that have originally entered the perturbed region from the unperturbed one. Instead, primary particles are effectively removed from the trajectory s via charge exchange processes, and neutrals belonging to other trajectories undergo charge exchange reactions with ions moving along s at the instant of interaction, thus causing a repopulation of the trajectory s. In this respect, the primary neutrals on s are gradually, and in an extended subsonic interface entirely, replaced by secondary particles.

THE BOLTZMANN FORMULATION

The local change of the velocity distribution function f_n of the neutrals is thus defined by the local balance between destruction and production rates. This is adequately formulated in the characteristics form of

Boltzmann's integro-differential equation for charge exchange collisions (see Ripken and Fahr (1983), Eqs. (2), (3), and (5)),

$$v\frac{d}{ds}(f_n) = f_i(\underline{r},\underline{v}) \int^3 f_n\,(\underline{r},\underline{v}_n)\; v_{rel}\;(\underline{v},\underline{v}_n)\;\sigma_{ex}\;(v_{rel})\;d^3\,\underline{v}_n\;- \qquad (1)$$

$$- f_n\,(\underline{r},\underline{v}) \int^3 f_i\,(\underline{r},\underline{v}_i)\; v_{rel}\;(\underline{v},\underline{v}_i)\;\sigma_{ex}\;(v_{rel})\;d^3\,\underline{v}_i \quad ,$$

where f_i is the ion velocity distribution function, v_{rel} is the relative velocity between the collision partners, and σ_{ex} is the velocity-dependent charge exchange cross section. The differential line element ds is measured along the specific dynamical trajectory s that belongs to the particles with a velocity $\underline{v}$ at a place $\underline{r}$. The integrations are carried out over the entire velocity space. It needs to be stressed that in this form Eq. (1) fully incorporates the multiple collision concept and thus represents a complete treatment of the underlying redistribution effects.

The relative importanceof loss and gain terms critically depends on the type of species treated, the relevant individual particle velocity $\underline{v}$ along s, and the current position $\underline{r}$ in the interface. Due to the very small cross sections for charge exchange collisions between He atoms and protons ($2\ 10^{-17}$ cm^{-2}), charge exchange interactions of interstellar helium atoms in the pre-heliospheric plasma interface can be neglected. Other helium losses due to electron impact ionizations and critical velocity effect ionizations (Petelski et al., 1980) can be disregarded also since sufficient ionization energies are not available.

This is different for O and H atoms that traverse the interface. In these cases the relevant cross sections for charge exchange ($O\text{-}H^+$, $H\text{-}H^+$) are much larger (i.e. of the order of 10^{-15} cm^2). For O atoms the charge exchange collisions with protons only represent a loss process, whereas O atom gains only result from charge exchange collisions between O^+ interface-ions and H or O atoms. Assuming a cosmic abundance of O atoms and a degree of ionization comparable to that of interstellar hydrogen, $(N_p/N_H)_\infty \sim (N_{O^+}/N_O)_\infty$, and realizing that production processes are predominantly proportional to N_p, one can only expect loss processes for O atoms. Therefore the depletion of O atoms during the traversal of the heliospheric interface region is much larger than that of H atoms. The different elemental depletions can qualitatively be extracted from Fig. 1 (O atom depletion: corresponding to curve B, H atom depletion: curve A). In addition, at any given specific position in the O atom velocity space the local production and loss rates are greatly disbalanced, thus causing pronounced changes in the strongly depleted O atom velocity distribution function f_O.

Changes of the H atom velocity distribution function f_H are predominantly caused by charge exchange collisions between H atoms and protons. The resulting changes of f_H lead to a H atom depletion factor of 0.45. Thus, for boundary values of $N_{p\infty} = 0.0135$ cm^{-3} and $N_{H\infty} = 0.1105$ cm^{-3}, at the solar wind shock $N_H = 0.05$ cm^{-3} is realized, with a corresponding hydrogen temperature increase of 10%.

PRODUCTION AND LOSS PROCESSES

Under thermodynamic equilibrium conditions a detailed balance exists between collisional losses and gains for each cell in velocity space, i.e.

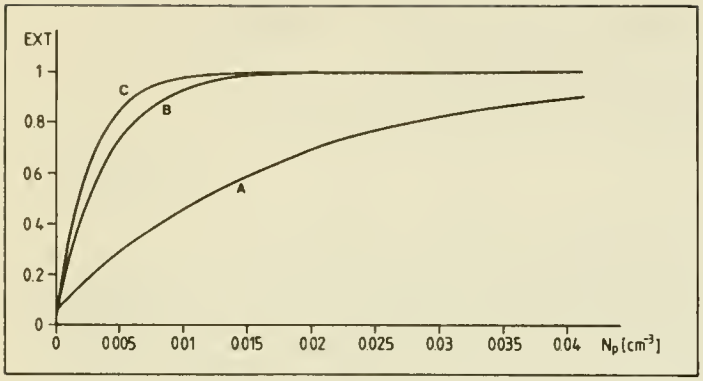

Figure 1: Hydrogen extinction EXT as a function of the asymptotic LISM proton density $N_{p\infty}$ Curve A: calculated including both production and loss terms; curve B: calculated using only loss terms, with $\sigma_{ex} = \sigma_{ex}(v_{rel})$; curve C: same as B, but with $\sigma_{ex} = 6\ 10^{-15}$ cm^2.

$df/ds = 0$. Such an equilibrium state can be adopted between ions and neutrals in the unperturbed interstellar medium far ahead of the heliosphere. However, in the region where the interstellar plasma flow approaches the heliosphere and becomes hydrodynamically perturbed and deflected around the impermeable heliospheric obstacle, a non-equilibrium between neutrals and ions is built up because the dynamical coupling of the two species is only very weak. The ion distribution function f_i, due to the action of electromagnetic forces and plasma waves, drastically changes over the last 10^2 to 10^3 AU ahead of the heliosphere, whereas the neutral distribution function cannot fully adapt to these rapidly varying ion conditions and attains an intermediate state.

A note concerning the balance of H atom production and loss terms and the method of calculation is in order here. For an extended subsonic interface like that proposed by Parker (1963) a solution of the form

$$f_n(s) = f_n(s_\infty) \exp\left(- \int_{s_\infty}^{s} \frac{v_{rel}}{v} \sigma_{ex} N_p \, ds \right) \qquad (2)$$

obtained from Eq. (1) when neglecting the production term is entirely unrealistic since no reasonable upper limit for s_∞ can be defined. Thus for $s_\infty \to \infty$ the function f_n and thus also N_H would systematically tend towards zero. This is due to the fact that even in the unperturbed plasma regions the loss processes do not drop to zero. Nevertheless, in the unperturbed region these loss processes are completely compensated by gain processes, and f_n remains unchanged.

The importance of treating the production term in Eq. (1) properly is further emphasized when considering Fig. 1. Curve B shows the extinction $EXT = 1 - N_H/N_{H\infty}$ versus proton density N_p in the interface, calculated under neglect of the production term (i.e. using a formula of the type $N \sim 1 - \exp(-\tau)$). This yields absolutely unrealistic values of the extinction. In contrast, inclusion of particle gain processes leads to the realistic curve A. This curve is not derivable under "forward scattering" or "destruction" concepts employing depletion factor expressions of $(1 + \langle 1-x \rangle \tau)^{-1}$ (Wallis, 1984) or $\exp(-\tau)$.

An interesting consequence of the interface-related H-atoms depletion is a revised form of how the unperturbed interstellar hydrogen densities $N_{H\infty}$ correlate with the interplanetary Ly-alpha resonance luminescence intensities. In the earlier theory, reviewed for instance by Thomas (1978), a

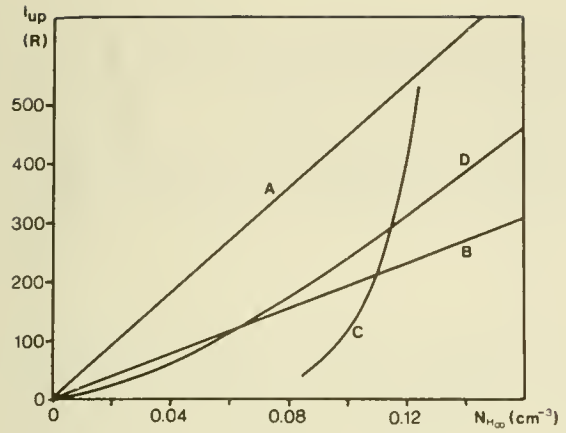

Figure 2: Upwind Ly-alpha resonance luminescence intensities versus asymptotic hydrogen density $N_{H\infty}$. Curve A: "Classical" dependence without interface extinction; curve B: with interface extinction, and constant $N_{p\infty}$; curve C: with interface extinction, using $(N_{H\infty}+N_{p\infty})$ = const; curve D: self-consistent interface of Baranov (1981), using only loss processes. Curves A, B, and C use as a reference point the interplanetary Ly-alpha observations of Bertaux et al. (1976).

linear relation between the upwind Ly-alpha intensity I_{up} and the unperturbed hydrogen density $N_{H\infty}$ was expected (curve A in Fig. 2). In the model of Ripken and Fahr (1983), a strongly varying nonlinear relation is found (curve C) due to the boundary value $(N_{H\infty} + N_{p\infty}) = 10\ N_{He\infty}$ employed in the model. Baranov (1981), though only treating loss processes, has calculated the resulting interface configuration in the two-shock approach self-consistently. In this case a different nonlinear relation of I_{up} and $N_{H\infty}$, shown in curve D, was obtained.

A rigorous treatment of both loss and gain processes, leading to the "luminosity-hydrogen density" relationship characterized by curve C, suggests that observed upwind Ly-alpha intensities strongly depend on the actual interstellar hydrogen density $N_{H\infty}$, and that the possible range of the densities $N_{H\infty}$ is narrowed down considerably as compared to the conventional solution in curve A. On the other hand, due to the steepness of curve C, an observational inaccuracy in I_{up} (e.g. by about $\pm$ 50 R) only leads to small differences in the derived interstellar hydrogen densities $N_{H\infty}$ (e.g. by about $\pm$ 0.002 cm^{-3}).

REFERENCES

Baranov, V.B.: 1981, private communication

Bertaux, J.L., J.E. Blamont, N. Tabarie, W.G. Kurt, M.C. Bourgin, A.S. Smirnov, and N.N. Dementeva: 1976, Astron. Astrophys. 46, 19-22

Parker, E.N.: 1963, Interplanetary Dynamical Processes, Interscience, New York

Petelski, E.F., Fahr, H.J., Ripken, H.W., Brenning, N., Axnäs, I.: 1980, Astron. Astrophys. 87, 20

Ripken, H.W., and Fahr, H.J.: 1983, Astron. Astrophys. 122, 181

Thomas, G.E.: 1978, Ann. Rev. Earth Planetary Sci. 6, 173

Wallis, M.K.: 1984, Astron. Astrophys. 130, 200

BROADENING OF THE INTERPLANETARY HELIUM CONE STRUCTURE DUE TO ELASTIC COLLISIONS OF LISM HELIUM ATOMS WITH SOLAR WIND IONS.

Hans J. Fahr, Hans U. Nass and Daniel Rucinski[+]
Institut für Astrophysik der Universität Bonn and
[+] Space Research Center of Polish Academy of Sciences, Warsaw

ABSTRACT

Neutral interstellar particles penetrating into the heliosphere, besides being subject there to specific loss processes, suffer elastic collisions with KeV-solar wind ions. The momentum transfer to the neutrals connected with these collisions leads to a loss of angular momentum with respect to the sun and to a fractional compensation of the effective solar gravity. The dynamical particle trajectories hence are changed into non-Keplerians leading to density and temperature distributions differing from those calculated in the past. This is found from a solution of the Boltzmann equation that linearizes the effect of this additional force. It is shown here that the HeI-584A resonance glow of the heliospheric helium cone lead to substantially lower interstellar helium temperatures if re-interpreted on the basis of this revised theory. These temperatures now seem to be in accordance with the derived temperatures for interstellar hydrogen.

INTRODUCTION

The problem of an LISM diagnostics based on interplanetary resonance glow interpretations is closely connected with the modelling of the penetration of neutral interstellar gases into the inner regions of the heliosphere, where they are resonantly excited by the solar radiation field. This modelling was done up to now taking into account only the effects of the net solar gravity and specific loss processes. There is, however, a definite need to consider also the effect of elastic collisions between interstellar neutrals and solar wind ion species, because, as shown by Fahr, Nass, Rucinski (1984), these substantially modify the LISM density structure in the heliosphere.

The virtue of elastic collisions to transfer specific amounts of energy to the neutrals, and thus to increase the mean velocity dispersion of their local velocity distribution function, had already been appreciated in a series of papers in the past (Fahr, 1974, Fahr and Lay, 1974, Wallis, 1975, Holzer, 1977, Fahr, 1978, Wu and Judge, 1978, Hassan and Wallis, 1983, Kunc et al., 1983). However, it was noticed only recently (Fahr, Nass, Rucinski, 1984) that due to these collisions also a linear momentum transfer to the neutrals takes place which results in a "drag-like" force of non-negligible magnitude operating into the direction of the relative velocity $\vec{v}_{rel}$ between a neutral and the solar wind bulk flow. The individual interaction is connected with the Coulomb field of the ion and the electric multipole field of the polarized atomic shell of the neutral.

In this context the "drag-like" force results from the averaging effect of many distant elastic collisions that one neutral undergoes simultaneously with a statistically relevant sample of solar wind ions passing over it per

unit of time. Each individual collision, when considered as a separate event, would turn the relative velocity $\underline{v}_{rel}$ of the collision partners around their center-of-mass-velocity $\underline{V}$ by specific angles χ, ϕ as illustrated in Figure 1. Due to the homogeneity of the solar wind flow over a Debye length l_D (10^3 cm!) this results in a cancellation of velocity changes perpendicular to $\underline{v}_{rel}$, but leads to a systematic change of the neutral particle velocity, equivalent with the action of a force in the direction $\underline{v}_{rel}$.

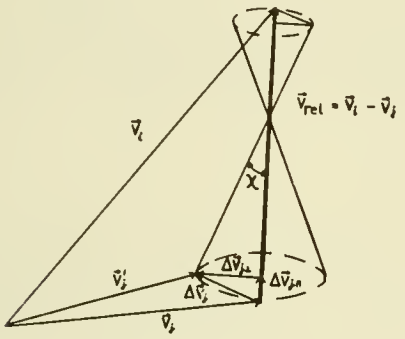

Fig. 1: Schematic illustration in velocity space of velocity changes $\Delta\vec{V}_j$ of the neutral species j elastically colliding with solar wind ion species of velocity $\vec{V}_i$.

This force can be calculated from the following formula (Fahr, Nass, Rucinski, 1984):

$$(1)\quad \underline{F}_v(\underline{r},\underline{v}) = n_i v_{rel}\, \mu_{ij}\, \underline{v}_{rel} \int_0^{l_D} (1-\cos\chi)\, 2\pi\, p_{el}(\chi) dp_{el}(\chi)$$

where n_i is the density of the solar wind ion species, μ_{ij} is the reduced mass of the collision partners, and p_{el} is the collisional impact parameter. The two components of the above force, the radial component, $\underline{F}_{v,r}$, and the latitudinal one, $\underline{F}_{v,\rho}$, yield the following ratio:

$$(2)\quad F_{v,\rho}/F_{v,r} = v_{rel,\rho}/v_{rel,r} \approx 10^{-1}$$

It turns out that for helium 30 percent of the gravity is compensated by $\underline{F}_{v,r}$, whereas for hydrogen even a full compensation of gravity can be established.

The joint influence of these two drag force components on the neutral atom velocity distribution function cannot be disentangled. Nevertheless, for clarifying purposes, their pinciple effects may be described separately:
1) The component $\underline{F}_{v,r}$ partly compensates solar gravity leading to particle trajectories that are less curved towards the sun. This would cause smaller helium cone densities, but no change of the half angle of the density cone, as is made evident in the Feldman-formula for this angle (Feldman et al., 1972).
2) The component $\underline{F}_{v,\rho}$ leads to an angular momentum loss of neutrals with

respect to the sun. Hence neutrals would be forced to move along trajectories with a stronger inclination towards the sun. A continuous change from a hyperbolic into elliptic Keplerians is occuring, even enabling a capture of interstellar neutrals into bound orbits. In an isolated consideration of this latter effect on LISM helium, an increase of the helium cone densities is obtained, even overcompensating the density decrease due to the first effect. Furthermore a broadening of the density structure of the helium cone, i.e. an increase of the cone angle, is caused.

It is clear that only the combined influence of the two drag force components on the velocity distribution function is worthwhile to be treated. This kinetic theory for particles moving under gravity- and drag-forces has been developed by Fahr, Nass, Rucinski (1984) as solutions of an appropriate Boltzmann equation, where use had been made of the solution $f_o(\underline{r},\underline{v})$ known for the simpler problem of sole gravitational forces. The local neutral atom density then is represented by

$$(3) \quad n(\underline{r}) = n_o(\underline{r}) \; (1 + \delta n(\underline{r}))$$

where $\delta n(\underline{r})$ is the relative change of the local density with respect to the density $n_o(\underline{r})$, obtained from $f_o(\underline{r},\underline{v})$ as the first velocity moment. The density $n_o(\underline{r})$ has to be considered as the conventional LISM model density in the heliosphere used in the up-to-now model fits for the observed interplanetary EUV resonance glow intensities. In the following we shall give results of an application of our theory to interstellar helium.

In Figure 2 we have given a contour plot of $\delta n(\underline{r})$ in a plane containing the sun and the interstellar wind vector $\underline{V}_\infty$. It can be seen that the relative helium density changes with respect to $n_o(\underline{r})$ are of inferior importance on the upwind side, whereas appreciable values are attained on the downwind side, especially pronounced at regions $\pm 40^o$ apart of the downwind axis, i.e. at regions flanking the conventional helium density cone. This is especially evident from Figure 3 where $\delta n(r=3AU)$ is shown for different interstellar helium temperatures.

Figure 4 now displays the total helium density n(r) obtained with formula (3) at a constant solar distance of r = 3AU versus the angle θ from the downwind axis. The lower curve in this figure gives, for comparison, conventional model densities $n_o(\underline{r})$ that would have been obtained for the same LISM helium temperature $T_{He}=10^4$ K. As is evident in a comparison of these two curves the n_o-density structure yields lower helium densities at the downwind axis and a smaller cone angle. In order to fit the helium density profile, a 10 percent increase of the LISM helium density and an increase of the LISM helium temperatures by 4000 K had to be applied to the conventional theory. This effectively means that the realistic density structure described by the formula (3) would give rise to the deduction of substantially too high helium temperatures T_{He} if interpreted with the help of the conventional model approaches. Since the effect raised here is of importance only for neutrals that reach the downwind side at relatively small solar distances r < 3AU, we believe that this leads to a mis-derivation of temperatures only for helium, but not for hydrogen. Therefore we conclude that the up-to-now outstanding problem of helium and hydrogen showing up in the heliosphere as gases of drastically different temperatures is brought to a satisfactory solution.

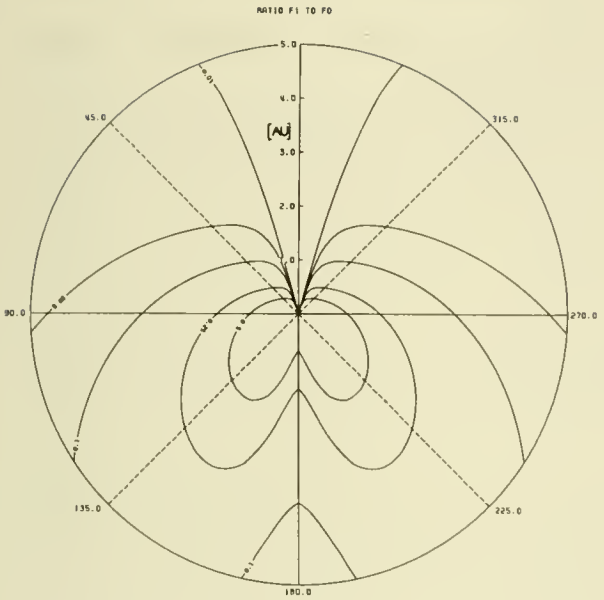

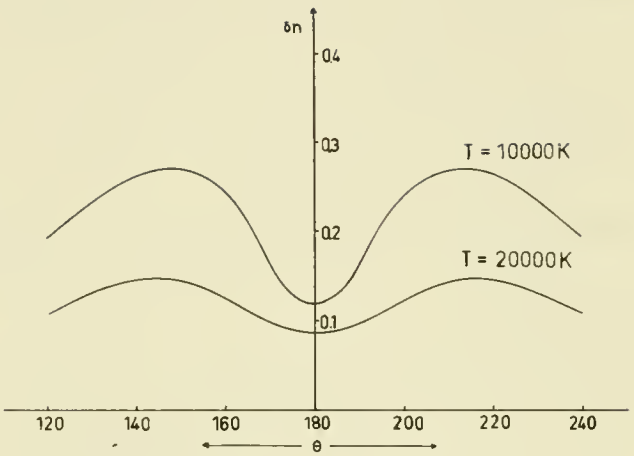

Fig. 2: Contour plot $\delta n(\underline{r})$=const showing curves of equal relative helium density enhancement in a circumsolar plane containing the interstellar wind vector $\underline{V}_\infty$. The solar distance r and the angle θ have been used as coordinates in this plane. The unperturbed interstellar helium temperature is taken to be $T_\infty = 1 \cdot 10^4$ K. (For solar data used, see: Fahr, Nass, Rucinski, 1984).-

Fig. 3: The relative helium density enhancement $\delta n(r=3AU, \theta)$ for both $T_\infty = 1 \cdot 10^4$ K and $T_\infty = 2 \cdot 10^4$ K is shown versus the angle θ at a constant solar distance of 3 AU.

REFERENCES

Fahr, H.J. (1974). The extraterrestrial UV-background and the neerby interstellar medium. Space Sci. Rev. 15, 483

Fahr, H.J. (1978). Change of interstellar gas parameters interstellar-wind-dominated astropheres. Astron. Astrophys.66, 103

Fahr, H.J., Lay G. (1974). Solar radiation asymmetries and heliospheric gas heating influencing extraterrestrial UVdata. Space Research XIV, 567

Fahr, H.J., Nass, H.U., Rucinski, D. (1984). Draglike effects on heliospheric neutrals due to elastic collisions with solar wind ions. Astron. Astrophys. (in press)

Feldman, W.C., Lange, J.J. Scherb, F., (1972). Interstellar helium in interplanetary space. Solar Wind IV, NASA special publ. 308, ed: Sonnett, C.P. et. al., 684

Hassan, M.H.A., Wallis, M.K. (1983) stochastic diffusion in inverse square fields: general formulation for interplanetary gas. Planet. Space Sci. 31, 1

Holzer, T.E. (1977). Neutral hydrogen in interplanetary space. Rev. Geophys. Space Phys. 15, 467

Kunc, J.A., Wu, F.M., Judge, D.C. (1983). Heating of the interstellar medium by the solar wind. Planet. Space Sci. 31, 1157

Wallis, M.K. (1975). Collisional heating of interplanetary gas: Fokker-Planck treatment. Planet. Space Sci. 23, 419

Wu, F.M., Judge, D.L. (1978). Elektron heating of inflowing interstellar gas. Ap.J. 225, 1045

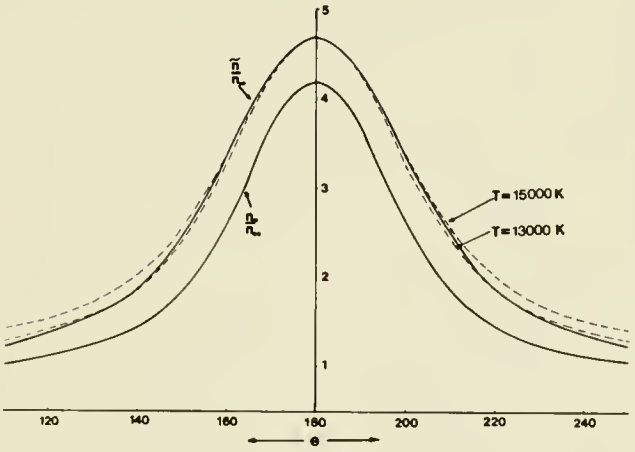

Fig. 4: The unperturbed densities $n_o(\underline{r})$ and perturbed densities $\tilde{n}(\underline{r})$ in the downwind cone region are shown versus the angle-θ at a constant solar distance of 3 AU. All densities are normalized with the helium density at large solar distances, n_∞. For comparison, the dashed curves give solutions for unperturbed densities n'_o which yield on the downwind axis a density that is identical to $\tilde{n}(r=3AU, \theta=\pi)$, but which belong to elevated interstellar helium temperatures T'_∞. The solid lines are calculated for $T_\infty = 1 \cdot 10^4$ K.

ULTRAVIOLET AND EUV ABSORPTION STUDIES

ABSORPTION LINE STUDIES AND THE DISTRIBUTION OF NEUTRAL GAS IN THE LOCAL INTERSTELLAR MEDIUM

Frederick C. Bruhweiler
Department of Physics
Catholic University of America

ABSTRACT

Previous published absorption line studies performed at ultraviolet and visual wavelengths are combined with new ultraviolet data in order to map out the distribution of HI within 150 pc of the Sun. Newly presented data for distances less than 50 pc further support the local cloud model as presented by Bruhweiler (1982). The Sun is embedded, near the edge of a diffuse cloud with total column density of 2 x 10^{19} cm^{-2}. Most observed directions within 50 pc away from the cloud body reveal trace amounts of gas (N)HI) $\sim 10^{18}$ cm-2) presumably arising in the outer skin of the local cloud. At greater distances ($50 \lesssim d \lesssim 150$ pc) most directions show significant absorption with $N(HI)>10^{19}$ cm^{-2}. Two directions, one toward the northern galactic pole (NGP), the other toward β CMa exhibit unusually low HI column densities out to distances of 150-200 pc. However, substantial amounts of gas, $N(HI) > 10^{19}$ cm^{-2}, are seen toward the NGP at greater distances. The implications of these results on astronomy at wavelengths shortward of 912Å are discussed.

1. INTRODUCTION

We shall here concentrate upon reviewing interstellar absorption line data for lines-of-sight $\lesssim$ 150 pc in the local interstellar medium (LISM) acquired at both visual and ultraviolet wavelengths. We will, first, develop a coherent picture for the distribution of neutral hydrogen within the proximity of the Sun, then we will expand this picture, as revealed through interstellar absorption line studies to larger distances. Our principal goal is to sketch out a "broad brush stroke" picture of the distribution of neutral H I. By including new ultraviolet results, some of which are still preliminary, and visual interstellar line data, a more detailed morphology of neutral hydrogen is presented than that presented previously for the local cloud by Bruhweiler (1982) and by Frisch and York (1983) for longer distances.

One of the initial principal reasons for studying the LISM was to probe the so-called "intercloud medium" (ICM). Naturally, only by sampling short lines-of-sight can we hope to examine the typical volume element of the ICM and avoid the unwanted contamination of cloud complexes and H II regions.

Our preceptions of the ICM changed dramatically when ultraviolet observations using the Copernicus satellite revealed the ubiquitous presence of interstellar O VI toward O and B stars (Jenkins and Meloy 1974). Instead of a warm ICM with T $\sim$ 10,000 K and n~0.1 cm^{-3}, these observations were strong evidence for pervasive, hot ($T\sim10^5$ - 10^6K), low density ($n\sim10^{-2}$-$10^{-3}$$cm^{-3}$) component (or substrate) to the ISM. This conclusion is valid and regardless of whether the OVI predominately arises in cloud interfaces (McKee and Cowie 1977) or in the pervasive hot substrate. Positive O VI detections in four

that N I column densities correlate extremely well with those of H I and is typically deleted by only 0.15 dex where log $(N(NI)/N(HI + 2H_2)) = -4.21$.

Of five white dwarfs sampled with parallaxes indicating distances less than 50 pc, all yield $N(H\ I) \sim 10^{18}$ cm^{-2} and clearly indicate a dropoff in $\bar{n}_{HI}$ for longer lines-of-sight. The values of n(H I) ranged from 0.087 for Sirius B (2.7 pc), the closest white dwarf studied, to 6×10^{-3} cm^{-3} for G191-B2B (48 pc), the most distant. These results mesh well with previous Copernicus studies of Lα in late-type stars, EUV results (Holberg et al. 1981a, 1981b), and backscattering data. The dropoff in H I number density at larger distances implies that the Sun is embedded in a cloud with a spatial extent of 3-4 pc in the directions studied.

B. Mg II toward nearby A and B stars.

Ultraviolet observations of interstellar Mg II in nearby A and B stars has also been used to trace out the distribution of neutral gas about the Sun. Both Copernicus and the IUE have been used to observe the interstellar lines of the Mg II resonance doublet at 2800 A as seen superimposed upon rotationally broadened corresponding stellar features in these stars (Kondo et al. 1978; Morgan et al. 1978; Frisch 1981; Bruhweiler and Kondo 1982b; Bruhweiler et al. 1984). Analysis of high quality Mg II data, where the doublet ratios can adequately define the Mg II curve of growth, provide important constraints on the distribution of this ion. We emphasize that high quality data are essential since Mg II lines in some lines-of-sight are approaching saturation. The Mg II distribution about the Sun is definitely not uniform. In particular, Mg II lines toward α Leo (25 pc) lie close to the linear portion of the curve of growth, while α Gru (20 pc) in the opposite direction in the sky yields $N(Mg\ II) = 6 \times 10^{+13}$ cm^{-2}, a column density an order of magnitude larger (Bruhweiler et al. 1984; also elsewhere in these proceedings).

Estimates of neutral hydrogen column densities based upon Copernicus data (York 1976) are available for two early-type B stars within 50 pc. From the lines of S II, which is like N I and relatively undepleted in the ISM, York found $N(H\ I) = 7 \times 10^{+17}$ cm^{-2} for η UMa (50 pc) and $(0.8\text{-}1.6) \times 10^{+19}$ cm^{-2} for α Gru (20 pc). Since these stars also have measured Mg II column densities, we can combine these results with the H I column densities for white dwarfs, which are toward other nearby stars with well-measured Mg II column densities, to determine the depletion of magnesium in the gas of the local cloud. We, then, infer that magnesium is depleted by only 0.7 ± 0.2 dex in the gas of the local cloud (Bruhweiler et al. 1984). Based upon this Mg depletion we find that the Mg II results of other A and B stars, within 50 pc, in the general direction of $l^{II} = 0°$ imply $N(H\ I) = (1\text{-}2) \times 10^{19}$ cm^{-2}. Directions away from the galactic center indicate $N(H\ I) \leq 10^{18} cm^{-2}$.

The above combined data indicate that the Sun is embedded in, and near the edge of, a rather diffuse cloud with a total column density of $2 \times 10^{+19}$ cm^{-2}. Interstellar polarization data are also interpreted as supporting this conclusion. A study of stars within 35 pc by Tinbergen (1982) shows detectable polarization only for stars within 20 pc in small "patch" with 30 - 60° total extent located near l = 5°, b = -20°. This patch coincides remarkably well with the bulk of the local cloud as delineated by the

stars with distances $\lesssim$ 100 pc also shows that this component is quite local. This suggested that the typical volume element in the LISM was representative of the hot interstellar substrate.

Studies of the LISM have been elevated to new levels of importance with current plans and discussions about spaceborne observatories with capabilities of sampling wavelength regions shortward of the Lyman limit ($\lambda \lesssim$ 912A). Even trace amounts of absorbing gas could greatly attentuate the radiation from any potential source at these wavelengths. For example, a H I column density of only 10^{18} cm^{-2} corresponds to optical depths of 6.7 and 1 at the Lyman limit and just longward of the ionization edge of He I (504 A), respectively.

II. Distribution of Gas within 5 pc.

Interstellar absorption line studies for lines-of-sight within 5 pc have been, for the most part, limited to studying H I Lα absorption superimposed upon chromospheric emission profiles in late-type stars (Anderson et al. 1978; McClintock et al. 1978; and references therein). There is a large degree of uncertainty in the derived H I column density estimates, since these results are very sensitive to profile modeling and the broadening parameter (b). Yet, these results, as a whole, are in relatively good agreement with the H I Lα and He I backscattering results (Bertaux et al. 1976; Weller and Meier 1981) and these combined results indicate that the immediate vicinity of the Sun has a average neutral hydrogen number density, $\overline{n(H\ I)}$ $\sim$ 0.04-0.1 cm^{-3}. It is important to mention that the most distant late-type star studied, HR 1099 (33 pc), yielded a very low $\overline{n(H\ I)} = 0.005$ cm^{-3} (Anderson and Weiler 1978), possibly signifying a dropoff in $\overline{n(H\ I)}$ at larger distances.

III. The LISM within 50 pc

A. Ultraviolet observations of nearby hot white dwarfs.

The almost featureless spectra of hot white dwarfs make them ideal backdrops to probe the LISM. Indeed, a serious attempt, within the last few years, has been made to utilize the International Ultraviolet Explorer (IUE) to investigate the interstellar lines in these objects. So far, results on five white dwarfs have appeared in the literature (Bruhweiler and Kondo 1981, 1982; Dupree and Raymond 1982), and further detailed results of other nearby white dwarfs should soon follow. The interstellar species detected in the IUE spectra of these white dwarfs include C II, N I, O I, Si II, Fe II, Mg II, and possibly Si III in one line of sight. Interstellar H I is superimposed upon the white dwarf stellar profiles and is unuseable for a direct determination of the H I column density. Thus, we must rely on estimates derived from lines of heavier atomic species.

A good estimate of N(H I) can be derived using the IUE from the N I triplet near 1200 A. Like H I, N I is neutral with an ionization potential (14.5 eV) not too different from that of hydrogen. More importantly, nitrogen appears to exhibit little or no depletion in the interstellar medium. A review of N I and H I Copernicus data by Ferlet (1981) shows

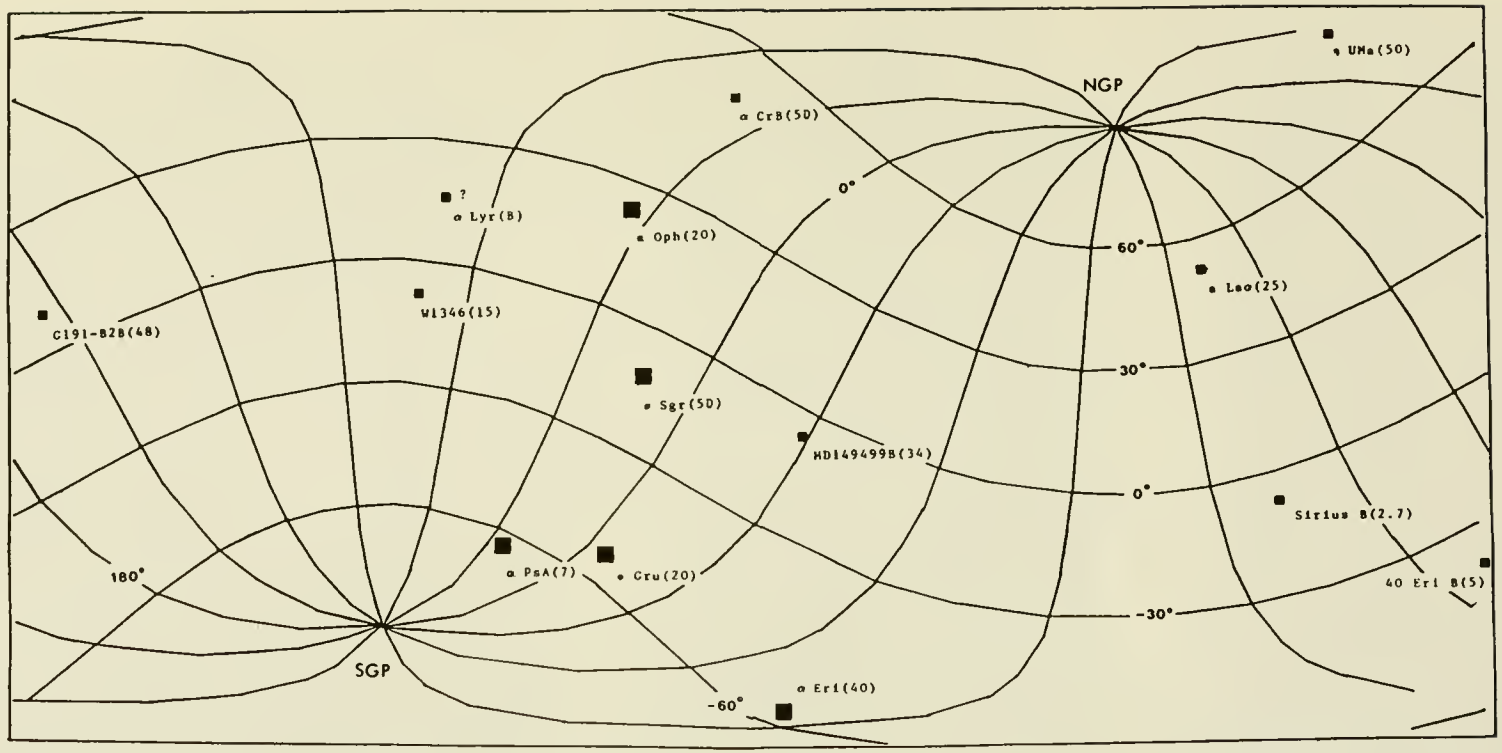

BRUHWEILER 1984

LEGEND

LOG N(H I):	≤19	19-20	20-21	≥21
DIRECT H I MEASUREMENT(COPERNICUS)	•	●	●	●
DIRECT H I MEASUREMENT(OAO-2)		⊙	⊙	
INFERRED H I(UV DATA)	■	■		
INFERRED H I (VISUAL DATA)		□	□	

Figure 1. H I Column Densities Toward Stars with d ≲ 50 pc. The stars with derived H I column densities are displayed in galactic coordinates. The star names are given, and their distances in parsecs are indicated in parentheses. Most stars with small symbols have N(H I)~10^{18} cm^{-2}. The stars, η UMa and 40 Eri B, have N(H I)<10^{18} cm^{-2}. The white dwarf, HD149499B, has N(H I)~4×10^{18}cm^{-2}. The stars delineating the local cloud have N(H I)~$1\text{-}2\times10^{19}$cm^{-2}, although the path to α Oph may be higher. (Note: The column density estimates come from references cited in text, Results different from published results, such as HD149499B, reflect more complete data. Additional data come from Bruhweiler and Kondo(to be published).

ultraviolet absorption line studies (See Figure 1).

IV. The LISM At Greater Distances: 50 pc< d≲ 150 pc.

At ultraviolet wavelengths, perhaps the most extensively analyzed lines-of sight in the LISM, are thos toward α Vir (88 pc; l = 316° b = 51°) and λ Sco (105 pc; l = 352°, b = -2°) (York and Kinahan 1979; York 1983). The Copernicus data for α Vir indicate N(H I) = 10^{+19} cm^{-2} with probably an equal amount in H II. Both the neutral and ionized regions have the same velocity within 2 km s^{-1}, and could be in the proximity of α Vir. Although we can not rule out the possibility that the local cloud intersects the path to α Vir, thereby giving rise to the observed 10^{+19} cm^{-2} of H I.

Detailed profile fitting of Copernicus data reveal possibly five different interstellar velocity components toward λ Sco. Yet, the overwhelming bulk of the H I (1.7 x 10^{+19} cm^{-2}) is in a component at -32 km s^{-1}. Since λ Sco lies behind the body of the local cloud and the -32 km s^{-1} radial velocity is in accord with what is expected from the local interstellar wind, this component, most assuredly, arises in the local cloud. Comparison of the b-values for various ions indicates that this component is warm, with T ∿ 10^{+4} K. Indeed, recent observations of Mg I and Mg II in the local cloud also supports this conclusion (Bruhweiler et al. 1984). All the other velocity components appear to be significantly ionized and only one has significant column density (log N(H II) = 18.5-19.3). These components must lie beyond the local cloud.

Interstellar O VI is seen in both α Vir and λ Sco and is most likely formed in thermal conduction fronts associated with the larger column density velocity components.

The Copernicus survey of Bohlin, Savage, and Drake (1978) has proved to be an important source of direct measurements of H I column density toward stars in the distance interval 50-150 pc. These H I measurements were supplemented with those determined from OAO-2 data (Savage and Jenkins 1972). Of the 35 stars in common in these two data, the derived H I column densities were in good agreement, generall well within a factor of two. We have combined these UV data with preliminary inferred H I column densities for several hot white dwarfs by Bruhweiler and Kondo in order to more fully map out the H I distribution away from the galactic plane (See Figure 2).

Up to this point, we have not made use of interstellar line studies undertaken at visual wavelengths. The reason for this is that many lines-of-sight within 50 pc exhibit only small traces of absorbing gas with N(H I) < 2x 10^{+19} cm $^{-2}$, which has gone undetected in published studies at visual wavelengths. The IUE and Copernicus have demonstrated the ability to detect interstellar features of species of abundant, relatively undepleted elements corresponding to H I column densities of a few times 10^{+17} cm^{-2}. Published results for studies undertaken at visual wavelengths indicate detectable amounts of Ca II, Ti II, K I, and Na I in directions where the H I column density is a few times 10^{+19} cm^{-2} (Stokes 1978). Although improved detectors mated with large ground-based telescopes should, in the future, provide smaller detection limits for these species, and more information on directions with lower column density.

Despite the problems for the directions displaying the lowest H I

column densities, very high-signal-to-noise, high-resolution data exist for the visual interstellar lines seen toward many of the early-type stars in the LISM (Stokes1978; Albert 1983; Hobbs 1978 ; Marshall and Hobbs 1972; Hobbs 1969; and references cited therin). These high quality data often show multiple velocity components in the interstellar gas in the same line-of-sight.

We wish to use the present high signal-to-noise and high-resolution visual data to again, further supplement the ultraviolet data in deriving a more complete map for the H I distribution in the LISM. First, however, we need to calibrate these data with the derived H I column densities obtained at ultraviolet wavelengths. All the visually observed interstellar species in the LISM show some depletion. Moreover, the elemental depletions appear to be variable and seem to be much lower in the low column density clouds of the LISM than in the much longer, higher column density lines-of-sight (York and Kinahan 1979; Hobbs 1978; Bruhweiler and Kondo 1982; York 1983). Therefore, we have taken the average of the relative abundance of Ca II/H I toward σ Sgr and α Vir along with the N(NaI)-N(H I) relation inferred from Hobbs (1978) to obtain estimates or the H I column densities when visual data are only available. We notice a possible tendency for the Na I to give a too high H I column density for stars near to α Vir in the sky and also toward α Oph (20 pc). The Ca II and Na I data indicate N(H I) = $6 \times 10^{+19}$ cm^{-2} toward α Oph. (See also Frisch 1981). However, we consider this as an upper limit based upon the non-detection of cloud shadows with $N(H) > 5 \times 10^{+19}$ cm^{-2} in the soft X-ray background in this direction (Fried et al. 1980). We emphasize that it has been long known that the N(Ca II)/N(Na I) ratio can vary dramatically in the ISM. Higher ratios are usually associated with higher velocity gas (shocks), although lower depletions in lower column density clouds might also be expected for both species. In short, our approximation of the H I column densities, based upon Ca II, may be lower limits for higher column density lines-of-sight.

The nearest substantial amount of gas not associated with the local cloud may lie toward δ Cyg (50 pc) where the Na I column density given by Stokes (1978) implies log N(H)=20.3. On the other hand, the observed Ca II features imply $N(H) = 1.1 \times 10^{19}$ cm^{-2}. The foreground white dwarf, W1346 (15 pc), in this direction exhibits an extremely low column density, log N(H I) = 18.0, which probably arises entirely from the outer skin of the local cloud in which the Sun is embedded. We conclude that the bulk of the observed gas toward δ Cyg must reside at greater distances than W1346.

We now turn our discussion to the regions of high column density revealed by the interstellar lines studies as displayed in figure 2.

We, first, point out a region of large column density with $N(H) = 10^{+21}$ cm^{-2} in the constellations Scorpius and Ophiucus ($340° < l < 30°$; $0 < d < 30)°$. This region is behind the local cloud. Both the Copernicus data for λ Sco and soft X-ray indicate this complex is not near, but is at distances greater than 100 pc.

Ultraviolet and visual data indicate absorbing gas with $N(H) = 10^{19} - 10^{20}$ cm^{-2} to higher galactic longitudes and latitudes from the gas complex seen in Scorpus and Ophicus. The stars, 85 Vir, 69 Leo, and α Vir, all with distances on the order of 85 pc show evidence of this gas. This gas may also be linked to that seen in Centaurus as delineated by OAO-2 data in Figure 2.

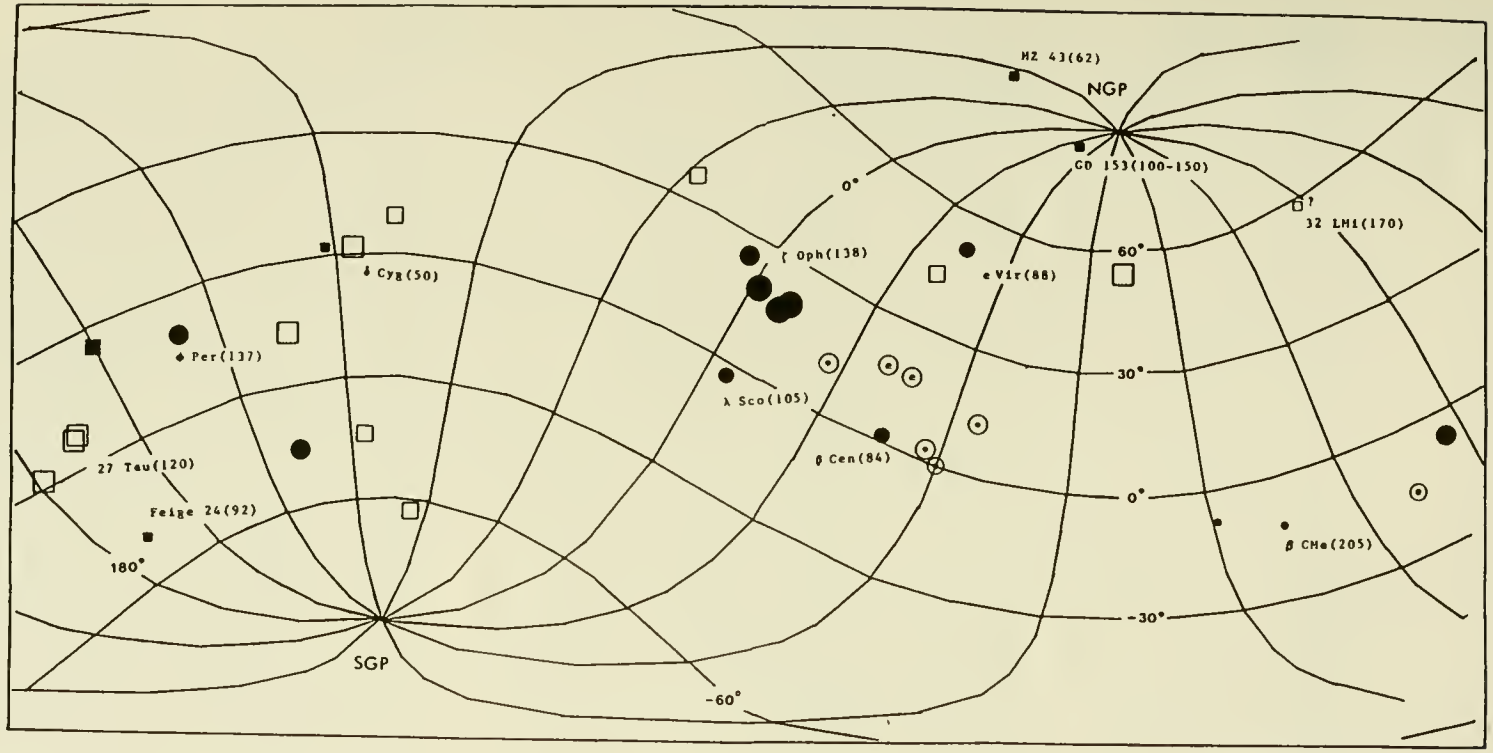

LEGEND

LOG N(N I):	<19	19-20	20-21	>21
DIRECT N I MEASUREMENT(COPERNICUS)	•	●	●	●
DIRECT H I MEASUREMENT(OAO-2)		⊙	⊙	
INFERRED H I(UV DATA)	■	■		
INFERRED H I (VISUAL DATA)		□	□	

Figure 2. H I Column Densities Toward Stars with $50 \leq d \leq 150$ pc. (See caption for Fig.1) Most directions exhibit $N(H\ I) > 10^{19}$ cm^{-2}. Two regions, with N(H I) on the order of 10^{18} cm^{-2} (β CMa) or less (GD 153 and HZ 43 toward the NGP), are indicated. Stars at greater distances toward the NGP reveal significant amounts, $N(H\ I) > 10^{19}$ cm^{-2} (See text.). A low column density measurement for the white dwarf, 2111+49, seems in conflict with that of δ Cyg, a few degrees away in the sky. Yet, uncertianties in distances may make 2111+49 like W1346(Fig. 1), a foreground object to δ Cyg. The column density measured for λ Sco is probably mostly due to the local cloud, which extends no further than 20 pc from the Sun.(Again, see Fig.1.)

Currently, there is no information for stars with shorter pathlengths in this general direction. Thus, we also can not rule out the possibility that some of the observed H I originated in the local cloud. Yet, the absence of soft X-ray cloud shadows in this direction indicates that this gas is at much larger distances.

The Copernicus data reveal what appears to be a low column density hole where N(H I)< a few times 10^{18} cm^{-2} extending to distances of at least 200 pc in the direction of β CMA and ε CMa (Bohlin et al. 1978; Bruhweiler and Kondo 1981; Frisch and York 1983). The IUE and EUV data also indicate another hole where N(H I) < 10^{18} cm^{-2} up to distances of 100-150 pc toward the north galactic pole (NGP). Evidences for this hole comes from the ultraviolet and EUV data for HZ 43(62 pc), ηUMa (50 pc), GD 153 (100-150 pc) and possibly the visual data for 32 LMi (170 pc).

Near 105° <l<200° and -30°<d< 0°, stars in Taurus, including the Pleadies, and in Perseus indicate a large complex of gas with hydrogen column densities of 10^{21} cm^{-2}.

Another patch of significant absorption can be found in Pegasus (l=90°, d=50°). Both γ Peg and 58 Peg at distances of 160 pc indicate N(H)= 10^{20} cm^{-2}. This gas could be an extension of the complex seen in Taurus and Perseus. Weak or non-detectable features in ψ Aqr (140 pc) could indicate that this gas complex does not extend to more southerly galactic latitudes.

Comparisons with the interstellar reddening results within 100 pc of Perry, Johnston, and Crawford (1982) based upon Strömgren photometry of stars accessible from the northern hemisphere, show good agreement. Notable reddening is only seen in stars with distances greater than 75 pc. This implies that gas complexes with column densities greater than 10^{20} cm^{-2} must lie at distances > 75 pc. The Perry et al. results delineate two distinct regions. One is a narrow concentrated arc perpendicular to the galactic plane (30° < l < 45°, -20° < d < 45°). The other is a broad diffuse band near the Milky Way extending from Cepheus through Taurus and Perseus to Orion (90° < l < 205°, - 45 < d < 20°).

V. Other Interstellar Absorption Line Results Relevant to the LISM

Some astronomers have voiced hopes of studying the EUV spectra of nearby extragalactic sources through holes in the neutral hydrogen distribution near the galactic poles. At first glance, the region of unusually low hydrogen column density near the NGP in Figure 2 (i.e. toward HZ 43, GD 153, η UMA) might provide a possible window for extragalactic EUV astronomy. However, observations of objects at greater distances (d $\gtrsim$ 300 pc) at b > 60° reveal significant column densities of neutral hydrogen. Galactic absorption due to hydrogen at 21-cm has been seen against the continuum of extragalactic radio sources indicating N(H I) ~ 10^{20} cm^{-2}. Also, IUE data for hot stars, especially Feige 86 (l=48°, b=79° and HZ 44 (l=88°, b=79°) show that neutral hydrogen column densities are at least 10^{19} cm^{-2} in these directions. We can not completely rule out the possibility of a substantial hole in the H I distribution toward the NGP. Nonetheless, if a hole exists, its angular size must be quite small. Initial inspection of the 21-cm maps for the polar regions (Burnstein and Heiles 1982) indicate that the chances of finding a hole toward the SGP seems less promising than toward the NGP. Further

studies of the ISM especially toward the SGP are needed to determine the feasibility of doing EUV extragalactic astronomy.

VI. Summary

We have attempted from the ultraviolet and visual interstellar absorption data, to present a picture of the distribution of the neutral hydrogen within 150 pc of the Sun. We will briefly summarize these results for the two distance intervals, $d \lesssim 50$ pc and $50 \lesssim d \lesssim 150$ pc.

A. Distances less than 50 pc.

i. The Sun is embedded in and near the edge of a rather diffuse cloud with a total column density of (1-2) x 10^{+19} cm^{-2} where the H I particle density near the Sun is 0.04 - 0.1 cm^{-3}

ii. The bulk of the cloud can be found toward the galactic center direction over the galactic latitude interval 25° >d >-70°. (Figure 1) Yet the actual spatial extent of the cloud still needs to be better defined.

iii. The backscattering data for H I Lα and He I 584, the observed N(Mg II)/N(mg I) ratios, and derived b-values indicate that the local cloud is warm with T ~ 10^4 K. Although, cooler regions seem to exist (i.e. toward α PsA; Bruhweiler and Kondo 1982b, Bruhweiler et al. 1984).

iv. Most directions away from the body of the cloud, which sample only the outer skin of the cloud, indicate rather low H I column densities, on the order of 10^{18} cm^{-2}.

v. The dropoff in H I particle density toward larger distances and the lack of shadows in the soft X-ray background indicate that the local is surrounded by the pervasive, hot 10^6 K, substrate.

B. The interval $50 \lesssim d \lesssim 150$ pc.

i. Significant amounts, N(H I) > 10^{19} cm^{-2}, of gas are found in most directions toward stars with distances greater than 75 pc.

ii. There are two regions, one in the direction of the NGP extending at least 100 - 150 pc, the other in the plane in the direction of β CMa, which have very low H I column density with N(H I) $\lesssim 10^{18}$ cm^{-2}.

iii. The presence of extended regions exhibiting very low H I column density indicate very long mean pathlengths between clouds, much longer than the 12 pc between cloudlets as in the model of McKee and Ostriker (1977). The general picture outlined by McKee and Ostriker may still be valid, but the interstellar absorption line studies of the LISM imply larger, more sparsely spaced clouds.

If the evolution of supershells (Bruhweiler et al. 1980; Tomisaka et al.

1980) play a significant role in the ISM, then stellar winds and the supernovae from massive stars in OB associations could efficiently evaporate away small clouds and also sweep away the clouds from the central regions of the supershells. This could account for the observed sparse distribution of cloudlets in the LISM.

It is worthwhile to compare these results with the H I 21-cm maps of Colomb et al. (1979). The two large predominant structures, Loop I and the Loop II-III complex, which are centered at galactic longitude 15° and 195°, are found within 150 pc (Spoelstra 1973). These structures could have been formed by supernovae and/or stellar winds (Develaar 1981; Weaver 1978). Estimates indicate that the Sun lies within 130 pc of the center of the 115 pc radius Loop I. This position along with the general direction of the interstellar wind (Weller and Meier 1981; Crutcher 1982) suggests that the local cloud to be a possible shell fragment of the Loop I structure.

In the future, high-resolution, high signal-to-noise observations with the Hubble Space Telescope and ground-based telescopes should not only provide a clearer picture of the morphology of the LISM, but also a better understanding of the physical processes occurring in both the local and general ISM.

References

Albert, C.E. 1983, Ap.J., 272, 509.
Anderson, R.C., Henry, R.C., Moos, H.W., and Linsky, J.L. 1978, Ap.J., 226, 883.
Anderson, R.C., and Weiler, E.J. 1978, Ap.J., 224, 143.
Bertaux, J.L., Blamont, J.E., Tabarie, N., Kurt, W.G., Bowgin, M.D., Smirnov, A.S., and Dementeva, N.N., 1976, Astr. Ap., 46, 16.
Bohlin, R., Savage, B., Drake, J. 1978, Ap.J., 224, 132.
Bruhweiler, F. 1982, Advances in Ultraviolet Astronomy: Four Years of IUE Research, Ed. Y. Kondo, R. Chapman, J. Mead, p. 125.
Bruhweiler, F., Gull, T., Kafateos, M., and Sofia, S. 1980, Ap.J. (Letters), 238, L27.
Bruhweiler, F.C. and Kondo, Y. 1982a, Ap.J., 259, 232.
Bruhweiler, F.C. and Kondo, Y. 1982b, Ap.J., (Letters), 260, L91.
Bruhweiler, F.C. and Kondo, Y. 1981, Ap.J., (Letters), 248, L123.
Bruhweiler, F., Oegerle, W., Weiler, E., Stencel, and Kondo, Y. 1984, Preprint
Burnstein, D. and Heiles, C. 1982, Ap.J., 87, 1165.
Colomb, F.R., Poppel, W.G.L., and Heiles, C. 1979, Astr. Ap., 40, 47.
Crutcher, R.M. 1982, Ap.J., 254, 82.
Davelaar, J.A., Bleeker, J., and Deerenberg, A. 1980, Astr. Ap., 92, 231.
Dickey, J.M., Salpeter, E.E., and Terzian, Y. 1978, Ap.J. Suppl., 36, 77.
Dupree, A.K. and Raymond, J. 1983, Ap.J. (Letters), 263, 63.
Ferlet, R. 1981, Astr. Ap., 98, L1.
Fried, P.M., Nousek, J.A., Sanders, W.T., and Kraushaar, W.L. 1980, Ap.J., 242, 987.
Frisch, P. 1981, Nature, 293, 377.
Frisch, P., and York, D.G. 1983, Ap.J. (Letters).
Hobbs, L.M. 1969, Ap.J., 157, 137.
Hobbs, L.M. 1976, Ap.J., 203, 143.
Holberg, J.B., Sandel, B.R., Forrester, W.T., Broadfoot, A.L., Chipman, H.L., and Barry, D.C. 1981a, Ap.J., 242, L119.
Holberg, J.B. 1981b, Bull. A.A.S., 12, 872.
Jenkins, E.B. and Meloy, D.A. 1974, Ap.J (Letters), 193, L121.
Kondo, Y., Talent, D.L., Barker, E.S., Dufour, R.J., and Modisette, J.L. 1978, Ap.J., 220, L97.
Marshall, L.A., and Hobbs, L.M. 1972, Ap.J., 173, 43.
Martin, E.R., and York, D.G. 1982, Ap.J., 257, 135.
McClintock, W., Henry, R.C., Linsky, J.L., and Moos, H.W. 1978, Ap.J., 225, 465.
McKee, C.F., and Ostriker, J.P. 1977, Ap.J., 218, 148.

Perry, C.L., Johnston, L., and Crawford, D.L. 1982, A.J., 87, 1751.
Savage, B.D. and Jenkins, E.B. 1972, Ap.J., 172, 491.
Spoelstra, T.A.Th. 1973, Astr.Ap., 24, 149.
Stokes, G.M. 1978, Ap.J. Suppl., 36, 115.
Tinbergen, J. 1982, Astr. Ap. 105, 53.
Weller, C.S. and Meier, R.R. 1981, Ap.J., 246, 386.
York, D.G. 1976, Ap.J., 204, 750.
York, D.G. 1983, Ap.J., 264, 172.
York, D.G. and Kinahan 1979, Ap.J., 228, 127.

Synthesis of Data on the Local Interstellar Medium

Donald G. York* and Priscilla C. Frisch
Department of Astronomy and Astrophysics
University of Chicago

I. Introduction

During this workshop, a considerable amount of data was presented, some refined versions of earlier results and some entirely new. While no completely definite picture of the local interstellar medium can be presented yet, some general conclusions can be drawn. We attempt to draw together the most relevant data in Section III. Some new UV results are collated with published results to help state the physical properties of the gas. A morphological view of the local medium is given in Section III. We confine ourselves to the region within 100 pc with the caveat that the distance of much of the material under discussion is poorly known.

II. Data on the Local Interstellar Medium

A) Neutral Hydrogen ($T<10^4$ °K)

Two views of the distribution of neutral hydrogen near the Sun can be derived from observations. First, large scale features in 21 cm all sky maps show high latitude loops and extensions above the galactic plane (Cleary et al. 1979). These loops form one or two "shells" roughly centered on the sight-line to the Sco-Oph association and known as "Loop I" or the "Sco-Oph Bubble" (Berkhuijsen et al. 1971, Weaver 1979). From 21 cm line widths, the shell gas material has T<400 °K (Heiles 1982) and it is observed when $N(HI) > 5 \times 10^{19}$ cm^{-2}. Studies of NaI absorption at the known velocity of specific filaments show that much of the material in Loop I is within 100 pc of the Sun (Frisch and York, this volume). Polarization studies (Mathewson and Ford 1970) confirm that interstellar dust with polarization vectors aligned along the Loop I shell is evident in stars from 50-100 pc from the Sun. This dust also shows up directly on 100 μ IRAS maps as elongated dust structures (or "cirrus") along the shell. The observations of nearby dust by Knude (this volume) and Perry and Johnson (1982), as well as nearby small CO clouds (Blitz this volume), may also sample some of this shell material. The magnetic field threading the shell has B~6μG (Heiles et al. 1980, Vallee preprint).

A second view based on UV observations sensitive to neutral gas with $N(HI) \gtrsim 10^{17}$ cm^{-2} was formulated by Frisch and York 1983. Figure 1 shows a view of a 500 pc region looking down on the plane. Figure 2 shows a 100 pc region looking at the Sun from l=270°, b=0°. Gas within the shaded contours is generally cool (T<200 °K), from observations of molecular hydrogen and its rotational excitation structure (Savage et al. 1977), Spitzer and Morton

*Also a member of the Enrico Fermi Institute

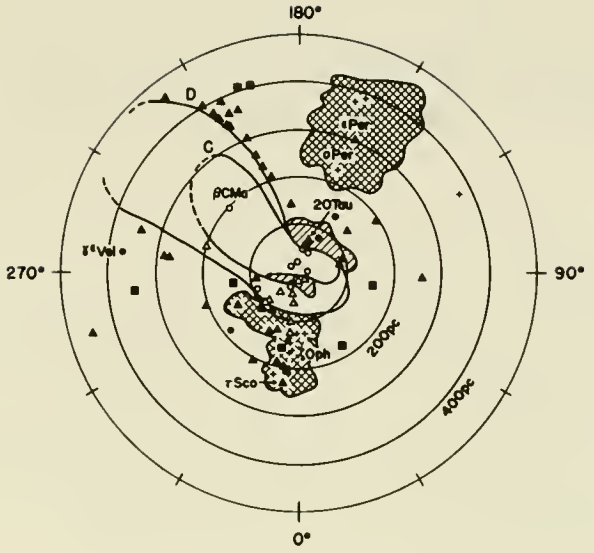

Figure 1: Nearby neutral hydrogen distribution as viewed looking down on the galactic plane. Contours A, B, C and D correspond to N(H)=0.05, 0.25, 0.5 and 5 x 10^{19} cm^{-2}, respectively. See Frisch and York (1983) for details.

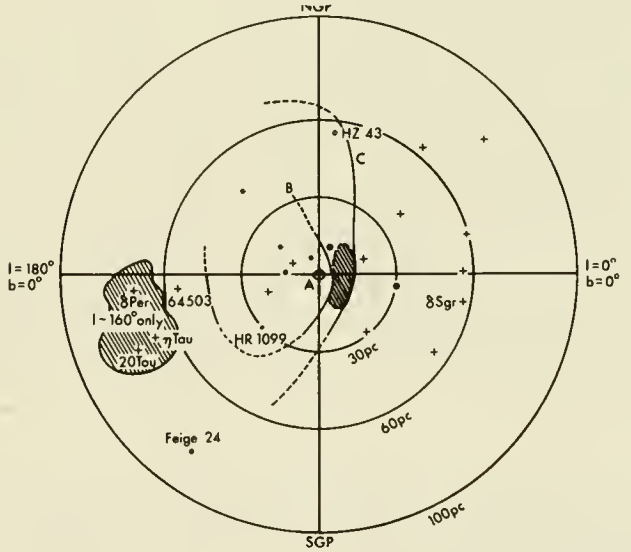

Figure 2: Same as Figure 1, but viewed from l=270°, b=0°.

1976), observations of 21 cm line widths (Crutcher, this volume), and observations of the hyperfine splitting of NaI D lines (Blades et al. 1980).

A warm component of HI is, however, evident in the UV data. Table 1 gives b-values for neutral species in the main neutral velocity components toward four stars, all of which lie in quadrants III (180° to 270°) and IV (270° to 360°) in Figure 1. The components have $N(HI)<3 \times 10^{19}$ cm^{-2}, and, according to the apparent decrease of line width with nuclear mass T>6000 °K. The small cloud near the center of Figure 1 may cover a large enough solid angle to explain these warm components toward α Vir, λ Sco, and β Cen (all at distances ~100 pc). The Lyα and HeI λ584 backscattered solar radiation discussed by several authors in this volume may also be related to this feature. Table 2 gives some constraints on the size of the HI regions toward the four stars used in Table 1.

Crutcher (1982) summarizes the local NaI observations that show a preferential direction of motion for gas seen in nearby stars. He concludes all the data are consistent with a V_{HC}=-28 km s^{-1} flow from the "apparent" upwind direction l=25°, b=+10°, corresponding to V_{LSR}=-15 km s^{-1} from the "true" (or LSR) upwind direction l=345°, b=-10°. Table 3 gives, for stars within 100 pc (or further for low column density paths), the velocity data for UV components where V_{HI} is the velocity of the dominant HI component and V_{HII} is the velocity of the dominant HII component. Additional components are readily discerned from profiles of strong UV lines (York 1983). These are, in general of mixed ionization, with N(HI + HII) between 10^{16} cm^{-2} and 10^{18} cm^{-2}. The number of such components and the minimum and maximum velocity found in each direction are also given. It is apparent that there is a tendency for all gas components to have more negative velocities in the direction toward the galactic center, more positive velocities away from it. On the other hand the values V_{HI} suggest more negative velocities than either Crutcher's NaI analysis or the Lyα backscatter of solar radiation from neutral interstellar material within the solar system (e.g., Adams and Frisch 1977, Weller and Meier 1981, and several papers in this volume) although several star positions are very close to the true upwind direction. We conclude that there is a general flow of nearby material, including regions with different physical properties, originating from a direction near the center of Loop I.

Much more information is potentially available on the details of motions of neutral gas near the Sun using MgI and MgII observations (Bruhweiler et al., Beckman et al., de Boer and Lenhart, all in this volume, Vidal Madjar private communication). However, MgII is formed in both neutral and ionized gas and the necessary detailed breakdown into HI/HII components has not yet been done for these data.

B) Ionized Gas ($T<10^5$ °K)

Observations of nearby stars often show regions with SII and other ions in absorption, but are accompanied by neutral nitrogen, argon, and oxygen with $N(XI)/N(SII)<\sim 0.1(N(X)/N(S))$, where X is nitrogen, argon, or oxygen and N is the column density in units of cm^{-2}. These are apparently HII regions.

Table 1: b Values in Neutral Components

	α Vir[1]	λ Sco[2]	β Cen[3]	β CMa[4]
HI	11(+1,-1)	11(+1,-1)	12(+1,-1)	14.0(+0.5,-0.5)
DI	6(+2,-2)	8(+3,-2)	8(+2,-2)	9-12
OI	4(+0.5,-1.0)	2.4(+.1,-0.1)	2(+1,-1)	6-8:
NI	4.7(+0.3,-0.2)	2.5(+.1,-.1)	3(+1,-1)	3-7
ArI	2.7(+0.3,-0.2)	1.7(+0.2,-0.2)	3(+0.5,-1.0)	---

[1]York and Kinahan 1979; [2]York 1983; [3]York, in preparation; [4]Gry, Vidal-Madjar, and York in preparation.

Table 2: HI Regions Near the Sun

Star	Size	Method
α Vir[1]	<5 pc	Some CII* in HI since HII region observed[2] is larger than CII*/CII implies
λ Sco	<5 pc	CII* at HI vel.
β CMa	<5 pc	Same N(HI) to α CMa 0.3 pc away from line of sight
β Cen	<10 pc	CII* seen at HI vel.

[1]References are as in Table 1; [2]Reynolds, this volume

Table 3: Velocities of Dominant Interstellar Components in Nearby Stars (LSR velocities given)

Star	l	b	d	V_{HI} (dom)	V_{HII} (dom)	No.>10^{16}	V_{min}	V_{max}	N(OVI)[7]
η UMa	100	65	29	---	---	---	---	---	<12.4
o And[2]	102	-16	90	0	-16	6	-16	+24	---
δ Per[3]	150	-6	82	-5	+4	6	-9	+27	<13.7
20 Tau[2]	166	-24	78	1,9	---	5	+1	+27	---
η Tau[2]	167	-23	59	8,16	-1	4	-1	+16	---
α Leo	226	49	22	---	---	---	---	---	<13.4
β CMa[4]	226	-14	214	(-1)	+9	6	-10	+26	<11.4
α Eri[2]	291	-59	22	0	---	5	-15	+17	13.1
β Cen[3]	312	1	100	-13	-5	6	-30	+12	13.0
α Vir[1]	316	51	87	-7	-15	4	-23	+2	13.4
α Gru[2,4]	350	-52	29	-9	---	3	-17	-1	<12.9
λ Sco[5]	352	-2	100	-32	-23	5(+1?)	-40	-8	13.3
υ Sco[6]	351	-2	134	-32	-22	4	-39	-12	---

[1]Same reference as Table 1; [2]Martin (1981); [3]Martin and York (1982); [4]York (unpublished); [5]York (1983); [6]Eder (1983); [7]Jenkins (1978).

Observations of excited CII from these regions allows derivation of electron densities. Doppler broadening of the lines from these regions may occur, but $T_{HII}<12000$ °K in all cases except β CMa, where $T_{HII}<10^5$ °K from considerations of b-values alone. Table 4 lists known HII regions from UV absorption data which are or may be near the Sun (the case of β CMa is ambiguous).

In several lines of sight, SiIII and CII absorption lines require the presence of material at velocities not seen in other species (α Vir, λ Sco). From considerations of ionization equilibrium, such gas has T>50000 °K, and it consists only of low column densities, $N(HI + HII)<10^{17}$ cm^{-2}.

From all sky studies of Hα emission maps Reynolds (this volume) concludes that Hα emission often comes from regions with radii>10 pc and $n_e>0.1$. A particular region likely to be near the Sun is centered on α Vir at d=100 pc.

Table 4: HII Regions Near the Sun[1]

Star	CII*/CII[2]	n_e	2r	Near Star?
α Vir	<0.04	<0.5	>6 pc	Yes (Hα)
λ Sco	0.006	0.2	30 pc	Yes(Eders 1982)
β CMa	0.003	0.1	60 pc	?
β Cen	0.1	1	6 pc	?

[1]References as for Table 1.; [2]The entry is $N(CII^*)/N(CII)=N(CII^*)/[N(CII)^*(C/S)|_0]$

Studies of MgII with Copernicus and IUE (several papers this volume) trace HI and HII gas indiscriminately. Every derivation from N(MgII) of N(H)=N(HI)+N(HII) in any given direction requires an assumption about the abundance of magnesium in interstellar gas. Magnesium may have a solar abundance (Dufton et al. 1984) or less (de Boer et al. this volume). However for all nearby stars studied so far in MgII, $N(H)<10^{20}$ cm^{-2} and $N(HII)<10^{20}$ cm^{-2}, in particular. Observations, in fewer stars (Table 4), of SII indicate $N(HII)<3 \times 10^{19}$ cm^{-2} within 100 pc of the Sun. It is noteworthy that N(HII)>N(HI) toward (190°, 0°) over a 200 pc path length to β CMa.

C) Hot Gas ($T>10^5$ °K)

Jenkins (this volume) reviews the fact that observations of absorption lines of OVI are consistent with the existence of gas within 100 pc with $T\sim4 \times 10^5$ °K. Theoretically, the ratio $N(OVI)/N(O_{total})$ drops dramatically with either an increase or decrease of temperature, so the absence of indications of gas at hotter or cooler temperatures in OVI is probably misleading. Some material at 10^5 °K may be present, but CIV and NV, the prime indicators of 10^5 °K gas, are weak (corresponding to $N(HII)<10^{17.5}$ at 10^5 °K) and may come entirely from the OVI producing regions. Small pockets of such gas may exist near white dwarfs within 100 pc (Raymond this volume).

X-ray emission over the entire sky has been observed near 78 Å (M-band), 56 Å (C-band), and 16 Å (B-band) (various papers in this volume by McCammon et al., Sanders et al., Clark). It is argued that at $b<60°$, the observed emission in the low energy B-band must be local because dark shadows from clouds are not seen toward any direction. The HI regions outside 100 pc (Figure 1) have $N(HI)>5 \times 10^{19}$ cm^{-2} and would certainly absorb X-rays from beyond. Since cloud shadows are not seen, the emission must be foreground to the HI. In the higher energy M-band, the region interior to Loop I and the North Polar Spur are bright, with a spectral softening towards the edge of the emitting region caused by the Loop I HI shell (Iwan 1980).

For $b>60°$, large regions of enhanced X-ray emissions are seen. In this case, a strong anticorrelation of HI emission and X-ray emission is seen (Clark, this volume) but the expected decrease in the ratio of B band X-rays to C band X-rays as HI emission increases is not seen (McCammon this volume). Several authors (this volume) concluded that very small high column density H I clouds not delineated in broad beam 21 cm surveys could offer a solution to this dilemma, since they would be opaque to both of the two lowest energy bands yet allow some radiation to come through unattenuated. On the other hand, small scale 21 cm structure that would allow this is ruled out based on several studies (this volume).

III. Synthesis

The above data can be fitted together in the following way, as pictured in Figure 3. A three dimensional model of local stars and interstellar gas has been constructed treating H I associated with Loop I and the more distant Sco-Oph filaments as a single giant bubble of radius roughly 90 pc. This model was photographed from a position corresponding to $l=180°$. The cotton represents HI from the Heiles maps and the dust clouds around the Pleiades (left foreground). In this model, the Sun is located in the shell of the bubble. The tight clump of stars at center left represents the Sun, α Cen AB, and α CMaAB. White dwarfs are small, stars hotter than F are blue, cooler stars are yellow (in reference to the color slide used at the conference - copies may be obtained from the authors). Ionized gas seen in CII* with Copernicus and/or in Hα emission (Reynolds this volume) fills large sections of the empty space (perhaps 10-30% of the volume). The large holes at $l=230°$ and $l=100°$ are probably filled by HII regions seen toward γ Cas (Ferlet et al. 1980) and toward β CMa (Gry et al., this volume).

The remainder of the void must be filled by the X-ray emitting gas. The brightening at the poles may be caused by shocks induced by blast waves from high latitude supernova (Pop I) that travel unimpeded through low density hot gas above the disk, but are slowed and emit X-rays on encountering HI gas in the plane. If higher density clouds lead to greater slowing and softer X-ray emission, the details of the X-ray flux discussed above may find a natural explanation.

Both interpretations of the soft X-ray data and theoretical discussions at this meeting have indicated the possibility of a supernova event possibly

10^5 years ago that reheated an already hot cavity (Iwan 1980, Cowie this volume, Edgar and Cox this volume, Rocchia et al. this volume). The models place the X-ray emission primarily in an idealized shell of HI, so the sky is uniform at b<60° in X-ray emission even if the Sun is off center. The high velocity CII and SiII components (Table 1) may be a consequence of the blast wave.

Detailed observation of OVI profiles for stars at d<100 pc are available (see Table 3). OVI may come from interfaces between the hot X-ray emitting gas and the clouds (HI or HII) at $T<10^5$ °K (Cowie et al. 1979). These lines are narrow and well defined in α Vir, but broad in λ Sco and β Cen. The stars γ Cas and β CMa show no OVI to very high limits. Considerations of projected velocities of the nearby cloud of warm HI (Figure 2) and the HII region velocities towards nearby stars (Table 3) offer a potential explanation of these results. Toward λ Sco and β Cen we may be seeing evaporation from the far side of the nearby cloud and from the near side of HII regions around these stars. Evaporation from the warm cloud near the Sun toward 1~0° at a higher velocity than the HII regions could cause the broadening of OVI profiles toward these two stars. Toward α Vir, the HI and HII regions have (accidentally) similar velocities, so evaporation from interfaces with both could produce profiles of nominal thermal width because they coincide closely in velocity space. (See York 1977, Cowie et al., 1979 for details of the data and the evaporation possibility). The absence of OVI towards the stars γ Cas (Jenkins 1978) and β CMa (Table 3), where both T<20000 °K clouds and X-ray emission are seen, is yet to be explained. The many different types of gas and their distribution in space would seem to indicate that the relatively smooth B-band X-ray emission around the Sun masks a rather complex irregular distribution of X-ray emitting gas.

The warm HI toward α Vir and λ Sco may well be within 20 pc of the sun (Ferlet et al. this volume). The various evidences of gas near the sun indicate there may be a single close cloud containing warm HI with a minimum extension of 25 pc parallel to the plane of the sky. If this cloud is a fragment of the Loop I shell it is probably much larger and may have a magnetic field of B~6μG threading it. Interstellar polarization is seen in stars in this direction as close as 5 pc (Tinbergen this volume). The Lyα backscatter suggests parts of this cloud are within a few AU of the Sun. So far, we have no good indication of what lies in the wake of the Sun if it is actually moving through this cloud. This cloud has mean neutral density $n_H<5$ cm^{-3}, but backscattering data implies a lower density, n_H~0.1 cm^{-3}, near the Sun. Refractory trace elements in this cloud show relatively high abundances indicating it may have been shocked (Frisch 1981, York 1983). The similar column densities of HI toward α CMa and β CMa, in spite of the great distance to the latter, suggest an extension of the warm cloud into Quadrant III consistent with the view that the Sun is in the shell of the Loop I bubble.

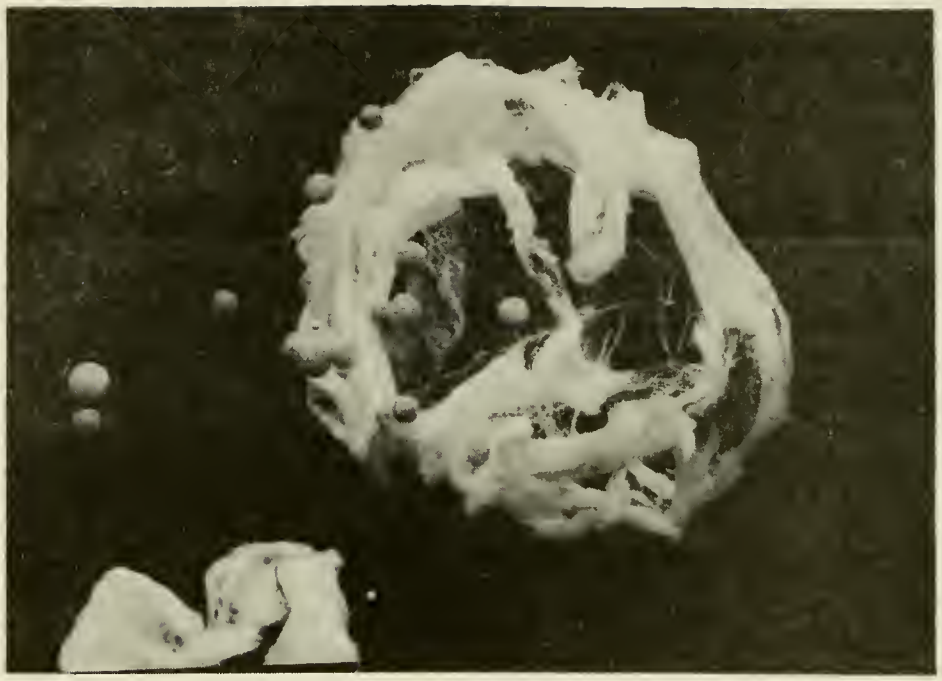

Figure 3: Three dimensional model of nearby interstellar gas with Loop I and the Sco-Oph bubble treated as a single giant bubble. Picture taken from the position corresponding to l=180° and b=0°.

References

Adams, T.F., and Frisch, P.C. 1977, Ap. J., 212, 300.

Berkhuijsen, E.M., Haslem, C.G.T., and Salter, C.J. 1971, Astr. Ap., 14, 252.

Blades, J.C., Wynne-Jones, I., and Wayte, R.C. 1980, M.N.R.A.S., 193, 849.

Bohlin, R.C., Hill, J.K., Jenkins, E.B., Savage, B. D., Snow, T.P., Spitzer, L. and York, D.G. 1983, Ap. J. Suppl. Ser., 51, 277.

Cleary, M.N., Heiles, C., and Haslam, C.G.T. 1979, Astr. Ap. Suppl. Ser., 36, 95.

Cowie, L.L., Jenkins, E.B., Songaila, A., and York, D.G. 1979, Ap. J., 232, 467.

Crovisier, J., Kazes, I., and Aubry, D. 1978, Astr. Ap. Suppl. Ser., 32, 205.

Crutcher, R.M. 1982, Ap. J., 254, 82.

Dufton, P.L., Hibbert, A., Murray, M.J., and York, D.G. 1984, Ap. J., to be published.

Eders, D.C. 1983, Ph.D. Thesis, Princeton University Observatory.

Ferlet, R., Vidal-Madjar, A., Laurent, C., and York, D.G. 1980, Ap. J., 242, 576.

Frisch, P.C. 1981, Nature, 293, 377.

Frisch, P.C., and York, D.G. 1983, Ap. J. (Letters), 271, L59.

Heiles, C. 1982, Ap. J., 262, 135.

Heiles, C., Chu, Y.H., Reynolds, R.J., Yegingil, I., and Troland, T.H. 1980, Ap. J., 242, 533.

Iwan, D. 1980, Ap. J., 239, 316.
Jenkins, E.B. 1978, Ap. J., 219, 845.
Martin, E.R. 1981, Ph.D. Thesis, Princeton University Observatory.
Martin, E.R., and York, D.G. 1982, Ap. J., 257, 135.
Mathewson, D.S., and Ford, V.L. 1970, Mem. R. Astr. Soc., 74, 139.
Perry, C.L., Johnston, L. and Crawford, P.L. 1982, Ap. J., Suppl. Ser., 50, 451.
Savage, B.D., Bohlin, R.C., Drake, J.F., and Budich, W. 1977, Ap. J., 216, 291.
Spitzer, L., and Morton, W.A. 1976, Ap. J., 204, 731.
Weaver, H. 1979, Proc. IAU Symp. No. 84, ed. W.B. Burton (Dordrecht & Reidel), 295.
Weller, C.S., and Meier, R.R. 1981, Ap. J., 246, 386.
York, D.G. 1977, Ap. J., 213, 43.
York, D.G. 1983, Ap. J., 264, 172.
York, D.G., and Kinahan, B.F. 1979, Ap. J., 228, 127.

OBSERVATIONS OF INTERSTELLAR HI TOWARD NEARBY LATE-TYPE STARS

Wayne B. Landsman[1]
NASA/Goddard Space Flight Center

Richard C. Henry and H. Warren Moos
Johns Hopkins University

Jeffrey L. Linsky[2]
JILA, Universtiy of Colorado, and NBS

ABSTRACT

High-dispersion Copernicus and IUE observations of chromospheric Ly α emission are used to study the distribution of HI in the local interstellar medium. Interstellar parameters are derived toward 3 stars within 5 pc of the sun, and upper limits are given for the Ly α flux from 9 other stars within 10 pc.

INTRODUCTION

Interstellar HI may be detected as an absorption feature cutting into the chromospheric Ly α emission of nearby late-type stars. McClintock et al. (1978) have detailed methods for deriving interstellar parameters from Copernicus Ly α data. Landsman et al. (1984) have applied these methods to high-dispersion IUE observations of α Cen A. Further discussion of the results in this paper is given by Landsman (1984).

RESULTS

Copernicus Upper Limits

The Copernicus data consist of repeated scans with the high-resolution U1 tube of the central 1.2Å of the Ly α emission. Listed in Table 1 are those observations for which the hypothesis of a featureless spectrum cannot be rejected at a confidence level greater than 90%. Upper limits have been expressed in terms of a typical solar flux of $F_{\odot} = 4.3 \times 10^{11}$ ph cm^{-2} s^{-1} $Å^{-1}$ at 1 A. U..

70 Oph A (KOV, d=5.0 pc, $l^{II}=30°$, $b^{II}=11°$, $V_r=-7$ km s^{-1})

Reduced spectra from Copernicus observations of 70 Oph A in 1976 and 1978 are shown in Figure 1 along with typical error bars. Definite structure is seen longward of the expected emission center at 1215.67 Å. The asymmetric emission is not

[1] NRC-NASA Research Associate
[2] Staff Member, Quantum Physics Division, National Bureau of Standards

unexpected, since 70 Oph is only 5° from the direction of the incoming gas as defined by Crutcher (1982). To further model this low signal-to-noise data, the following assumptions were made; (1) a gaussian intrinsic stellar profile with a total flux less than 100 times solar, (2) a fixed ratio D/H = 2.0×10^{-5}, and (3) a velocity dispersion $b_{HI} < 20$ km s^{-1}. With these constraints, and acceptable fit to the data can be made if the intervening gas has a volume density 0.04 $cm^{-3} \leq n_{HI} < 0.45$ cm^{-3}, and a heliocentric bulk velocity $v_{HI} < -14$ km s^{-1}.

Altair (=α Aql, A7IV, d=5.0 pc, $l^{II}=48°$, $b^{II}=-9°$, $V_r=-26$ km s^{-1})

The solid line in Figure 2 is from a large-aperture IUE observation (SWP 3427) of Altair, originally discussed from a chromospheric perspective by Blanco et al. (1980). Points contaminated by geocoronal emission have been deleted. The signal-to-noise is poor due to the existence of spectrograph scattered light. The dashed line in Figure 2 shows a Copernicus spectrum obtained on 20 Aug 1976, with the absolute flux level divided by a factor of two. After this scaling of the absolute flux, there is reasonable agreement between the two data sets. If the intrinsic stellar emission is modeled with a gaussian profile, then an upper limit can be set on the interstellar HI volume density of $n_{HI} < 0.11$ cm^{-3}.

Procyon (=α CMi F5IV-V, d=5.0 pc, $l^{II}=214°$, $b^{II}=13°$, $V_r=-3$ km s^{-1})

Figure 3 shows a Ly α spectrum of Procyon derived from a large-aperture IUE observation (SWP6660). The removal of the substantial geocoronal contribution and the estimation of uncertainties followed the procedure in Landsman et al. (1984). Modeling of the data yielded 90% confidence limits of 0.07 $cm^{-3} < n_{HI} < 0.2$, D/H > 0.8×10^{-5}, and $b_{HI} < 14$ km s^{-1}. These values are consistent with determinations using Copernicus data by Anderson et al. (1978). It is expected that substantially improved limits on interstellar parameters may be derived using small-aperture observations and co-addition of IUE spectra.

References

Anderson, R.C., Henry, R.C., Moos, H.W., and Linsky, J.L. 1978, Ap. J., 226, 883.
Blanco, C., Catalano, S., Marilli, E. 1980, in Proceedings of the Second European IUE Conference, (ESA SP-157), p.63.
Crutcher, R.M. 1982, Ap. J., 254, 82.
Landsman, W.B. 1984, Ph.D. Thesis, Johns Hopkins University.
Landsman, W.B., Henry, R.C., Moos, H.W., and Linsky, J.L. 1984, to be published in Ap. J.
McClintock, W. Henry, R.C., Linsky, J.L. and Moos, H.W. 1978, Ap. J., 202, 733.

Table 1
Copernicus Ly α Upper Limits

Star	Sp.T.	dis (pc)	Day	Year	Upper Limit Cts $(14\ s)^{-1}$	$F/F_{\odot}$
β Hyi	G2IV	6.3	197	1976	2.1	2.8
δ Eri	K0IV	8.8	300	1976	1.6	4.3
δ Pav	G8V	5.7	199	1976	1.3	1.4
η Boo	G0IV	9.3	110	1976	1.3	1.4
ζ Her	G0IV	9.8	174	1976	1.0	3.3
η Cas	G0V	5.7	304	1976	1.5	1.6
			299	1978	1.0	3.5
μ Her	G5IV	7.5	213	1976	1.3	2.4
			197	1978	1.3	5.4
τ Cet	G8V	3.5	264	1976	1.4	0.6
			267	1977	1.3	0.7
40 Eri	K1V	4.8	198	1976	1.6	1.2
			297	1978	1.4	3.5

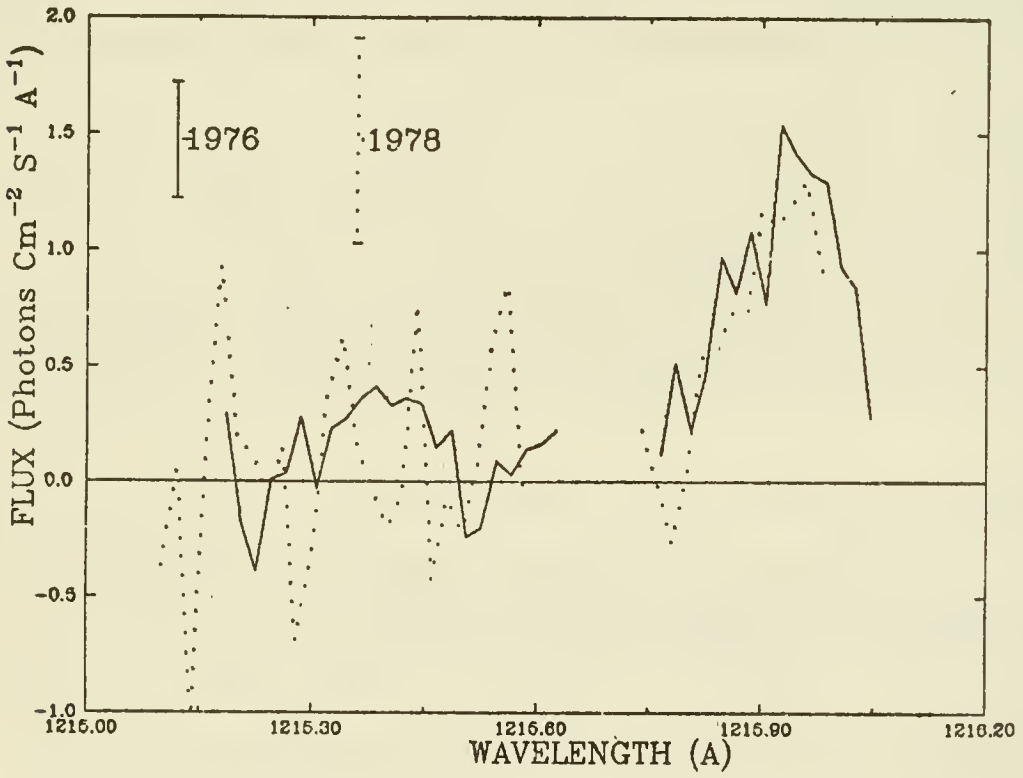

Figure 1: Copernicus spectra of 70 Oph A in 1976 and 1978.

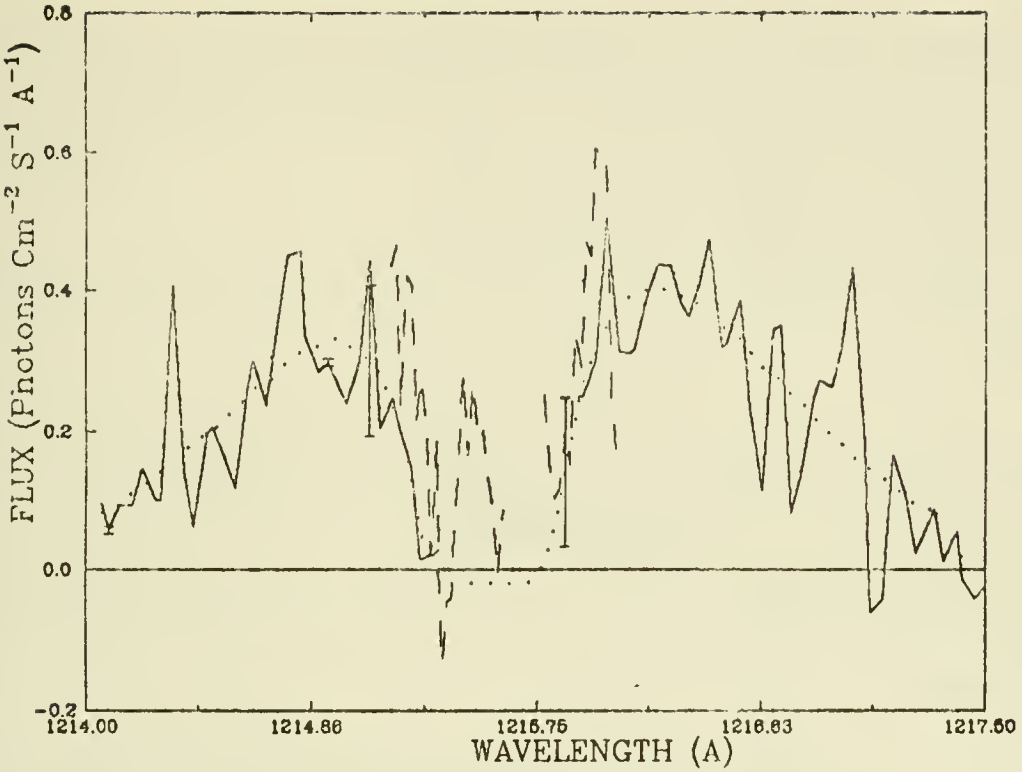

Figure 2: IUE (solid line) and Copernicus (dashed line) spectra of Altair with a best model fit (dotted line)

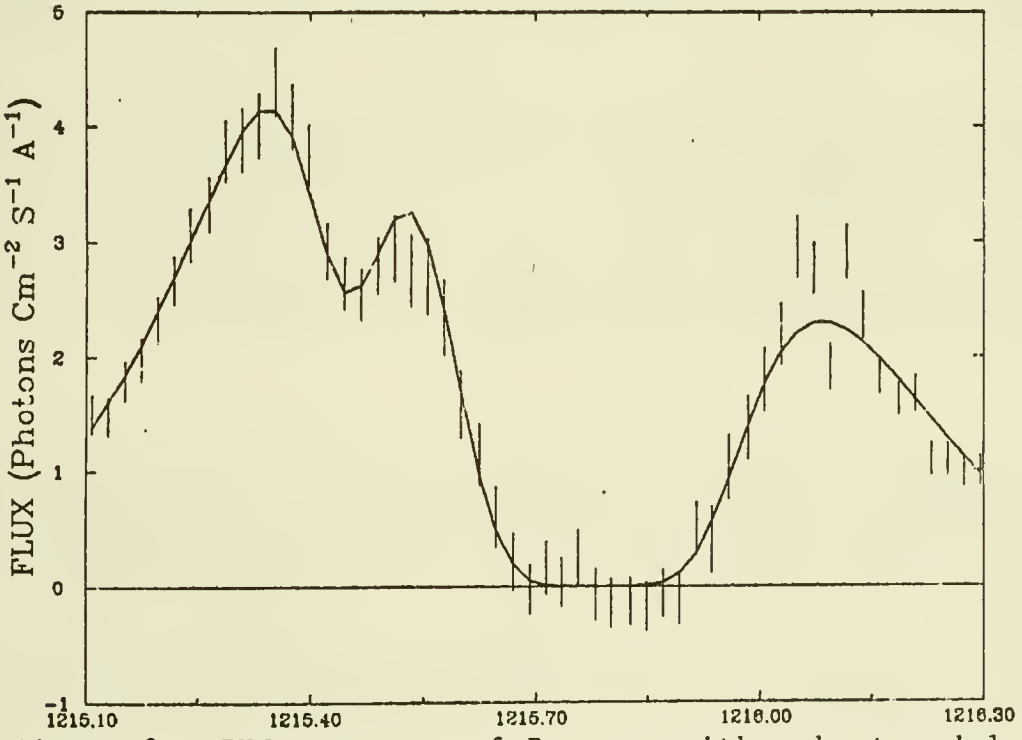

Figure 3: IUE spectrum of Procyon with a best model fit

OBSERVATIONS OF LOCAL INTERSTELLAR Mg I and Mg II

F. Bruhweiler, *Department of Physics, Catholic University of America*
W. Oegerle, *Space Telescope Science Institute*
E. Weiler and R. Stencel, *NASA Headquarters*
Y. Kondo, *NASA, Goddard Space Flight Center*

ABSTRACT

We have combined *Copernicus* and *IUE* observations of 5 stars within 50 pc of the Sun to study the ionization of magnesium in the local interstellar medium (LISM). The high resolution *Copernicus* spectrometer was used to detect interstellar Mg I 2852 in the spectra of α Gru, α Eri, and α Lyr, while placing upper limits on Mg I in the spectra of α CMa and α PsA. Observations of Mg II 2795, 2802 for these stars were also obtained with *IUE* and *Copernicus*. The column densities of Mg I and Mg II are used to place constraints on the temperature of the LISM.

INTRODUCTION

Recent studies of the LISM indicate that the Sun is embedded in a cloud with a hydrogen density of $n_H \sim 0.1 - 0.15$ cm^{-3} (McClintock et al.,1978; Cash, Bowyer, and Lampton 1979; Frisch 1981; Bruhweiler and Kondo 1982a,b; and Bruhweiler 1982). Bruhweiler and Kondo (1982a) have also presented some evidence that the Sun is near the edge of this local cloud.

In the McKee and Ostriker (1977) model of the ISM, small clouds of dimension 2-3 pc are distributed in a hot ($10^5 - 10^6$K) coronal gas. The edges of the clouds are partially ionized by evaporation and the diffuse UV and X-ray background and are predicted to have temperatures of $\sim$ 8000K and densities of $\sim$ 0.25 cm^{-3}. In this warm, partially ionized gas, detectable amounts of Mg I should be present due to dielectronic recombination, which is the principal means of recombination at temperatures of $\sim 10^4$K (York and Kinahan 1979). Consequently, studies of the Mg II/Mg I ionization balance in the LISM can be used to place constraints on the physical properties of this local cloud.

DATA

In Table 1, we present the equivalent widths of interstellar Mg I 2852 and Mg II 2795, 2802 in the spectra of α CMa (A1V, d=2.67 pc), α Gru (B5V, d=19.6 pc), α Eri (B5IV, d=40 pc), α Lyr (A0V, d=8.12 pc), and α PsA (A3V, d=6.94 pc). The corresponding column densities for the two ions are also listed. All the Mg I data was obtained with the *Copernicus* spectrometer. The Mg II data presented here was obtained by both the *IUE* and *Copernicus*.

The *Copernicus* near-UV photomultiplier tubes were subject to large particle backgrounds. In obtaining the Mg I data used here, special background measurements (off-source) were taken and were used in reducing the data. The *Copernicus* data for the Mg II lines in

Table 1 were obtained by Kondo et al. (1978), except for the α Eri data. The special techniques used to reduce the *IUE* data will be presented elsewhere along with figures displaying the spectra.

DISCUSSION

The Mg II lines in the spectra of α CMa are fairly weak, and the Mg I line was not detected. Based on the geometry of the local cloud (Bruhweiler and Kondo 1982a), the line of sight to α CMa is away from the cloud core. This could possibly explain the low column densities in this direction. The Mg I 2852 line was also not detected in the direction of α PsA (to be discussed further below).

Assuming that the LISM is in ionization equilibrium, we have

$$\frac{\mathrm{N(Mg\,II)}}{\mathrm{N(Mg\,I)}} = \frac{\Gamma}{n_e \alpha_t(T)} \ ,$$

where $\alpha_t(T)$ is the total recombination rate (radiative plus dielectronic) and Γ is the photoionization rate for Mg I. The total recombination rate is a fairly strong function of temperature, thereby making it possible to define the temperature of the absorbing gas if values of N(Mg II)/N(Mg I), Γ and n_e are known. The value of the recombination rate used here was obtained from Shull and Van Steenberg (1982).

Based on the data for the 3 stars in Table 1 for which a Mg I line was detected, we adopt N(Mg II)/N(Mg I)=500 for the LISM. The photoionization rate is a function of the local interstellar radiation field. Models for the radiation field have been calculated based on observations made with OAO (Witt and Johnson, 1973) and TD-1 (Gondhalekar, Phillips and Wilson (GPW), 1980). The radiation field in the wavelength region 1000-2000A calculated by Witt and Johnson (1973) was much larger than previous calulations (Habing 1968) and is larger than the more recent calculations of GPW. Using the radiation field from Witt and Johnson, we find $\Gamma = 7.9 \times 10^{-11}$ s^{-1} in agreement with the value calculated by de Boer, Koppenaal, and Pottasch (1973). Using the radiation field calculated by GPW, however, gives $\Gamma = 3.8 \times 10^{-11}$ s^{-1}, about a factor of two smaller.

Weller and Meier (1981) have recently calculated the density and ionization level of H and He in the LISM, based on EUV observations of backscattered He I 584 in the solar neighborhood combined with similar observations of H I Lyα. These authors find $0.06 \leq n_e \leq 0.09$ cm^{-3} and $n_e/n(HI) = 1.5$. This value of $n_H = 0.1 - 0.15$ cm^{-3} is in good agreement with other determinations of the density of the LISM (McClintock et al. 1978; Frisch 1981; Oegerle et al. 1982; and Bruhweiler and Kondo 1982a,b). The range in possible values of n_e and Γ, therefore, results in a range of possible values for the temperature of the LISM. Consequently, we find $7500 \leq T \leq 10{,}000$K. The ratio N(Mg II)/N(Mg I) increases rapidly with decreasing temperature below 7500K, making it extremely difficult to detect Mg I lines formed in a cool gas with low column density. The non-detection of Mg I in the spectrum of α PsA, when combined with the limits on the density of the ISM in this line-of-sight (Bruhweiler and Kondo (1982b), indicates temperatures below 7500K in this direction.

The temperature of the LISM derived here overlaps the lower end of the temperature range found by Weller and Meier (1981) for the very local ISM (9000-15000K). It is also in

good agreement with the temperature of 8000K predicted for the warm, ionized material (WIM) in the cloudlet model of McKee and Ostriker (1977). More detailed results of this work will appear elsehere.

REFERENCES

de Boer, K. S., Koppenaal, K. and Pottasch, S. R. 1973, *Astr. Ap.*, **28**, 145.
Bruhweiler, F. 1982, "Advances in Ultraviolet Astronomy: Four Years of *IUE*Research", ed. Y. Kondo, J.M. Mead and R. Chapman, NASA publication CP-2238, p. 125.
Bruhweiler, F. and Kondo, Y. 1982*a*, *Ap. J.*, **259**, 232.
_____. 1982*b*, *Ap. J. (Letters)*, **260**, L91.
Cash, W., Bowyer, S. and Lampton, M. 1979, *Astr. Ap.*, **80**, 67.
Frisch, P. 1981, *Nature* **293**, 377.
Gondhalekar, P.M., Phillips, A.P. and Wilson R. 1980, *Astr. Ap.*, **85**, 272.
Habing, H. 1968, *B.A.N.* **19**, 421.
Kondo, Y., Talent, D.L.,Barker, E.S. Dufour, R. and Modisette, J.L. 1978, *Ap. J. (Letters)*, **220**, L97.
McClintock, W., Henry, R.C., Linsky, J.L. and Moos, H.W. 1978, *Ap. J.*, **225**, 465.
McKee, C.F. and Ostriker, J.P. 1977, *Ap. J.*, **218**, 148.
Oegerle, W., Kondo, Y., Stencel, R. and Weiler, E. 1982, *Ap. J.*, **252**, 302.
Shull,J.M. and Van Steenberg, M. 1982, *Ap. J. Suppl.*, **48**,95.
Weller, C.S. and Meier, R. 1981, *Ap. J.*, **246**, 386.
Witt, A.N. and Johnson, M.W. 1973, *Ap. J.*, **181**, 363.
York, D.G. and Kinahan, B.F. 1979, *Ap. J.*, **228**, 127.

TABLE 1. Mg DATA

Star	Equivalent Width(mA)			Column Density(cm^{-2})	
	Mg II 2795	Mg II 2802	Mg I 2852	N(Mg II)	N(Mg I)
α CMa	71	47	≤ 1.5	3.3×10^{12}	$\leq 1.1 \times 10^{10}$
α Gru	162 ± 3 (3)	147 ± 3 (3)	-	6.1×10^{13}	-
	170 ± 14	153 ± 11	12.5	5.4×10^{13}	9.8×10^{10}
α Eri	312 (1)	297 (1)	-	-	-
	292	266	29.5	1.35×10^{14}	2.4×10^{11}
α Lyr	105 (2)	102 (3)	-	-	-
	120 ± 22	100 ± 31	22	8.1×10^{13}	1.9×10^{11}
α PsA	183 (4)	162,157 (4)	-	-	-
	133:	127:	≤ 2.5	4.0×10^{13}	$\leq 1.8 \times 10^{10}$

Notes: For each star (except α CMa) there are two rows of data. The top row contains measurements from the *IUE* spectra, while the lower row is from *Copernicus*. The number in parenthesis for the *IUE* data is the number of spectra that were combined to get the result. The α CMa data is from *Copernicus*. The photospheric and interstellar features are probably not resolved in the spectra of α Lyr, which has vsini=17 km s^{-1}.

MgII SPECTRA OF LATE TYPE STARS USED TO PROBE THE LISM

J.E. Beckman (1), L. Crivellari (2), M.L. Franco (3)
P. Molaro (2,4) and G. Vladilo (2)
1) Queen Mary College, Univ. of London, England; 2) Osservatorio Astronomico di Trieste, Italy; 3) I.A.F.E., Buenos Aires, Argentina; 4) I.S.A.S., Miramare, Trieste, Italy.

ABSTRACT

IUE spectra of Mg II **h** and **k** in late type dwarfs and giants have been used to detect and measure absorption components due to the LISM. This technique gives a method of probing the awkward range from **d** = 3 pc to **d** = 80 pc from the sun . In spite of interpretational uncertainties we can plot the HI component of the LISM well enough to confirm it as a cloud some 20-30 pc in extent, peaking sharply in density towards ℓ^{II}= 25°, moving towards the sun from ℓ^{II}= 25°, b^{II}= +10°, at 28 Km/sec. The "hole" towards ℓ^{II}= 150° is confirmed, suggesting a solar position close to the cloud's edge in this direction.

OBSERVATIONS

In order to explore the LISM using MgII absorptions at **h** and **k** we employed high resolution IUE spectra of late-type stars, some from our own programme on chromospheres, some from the IUE archive, and some taken specifically by ourselves for LISM measurements. The observational parameters are summarized in Table 1: col. 6 gives the radial velocity of the stars (RV), col.7 gives the predicted heliocentric velocity of the LISM according to Crutcher (1982) (V_{cR}) and col.8 the velocity of any interstellar feature with respect to the photospheric rest frame (Vis=V_{cR} -RV). Detection of a feature at Vis implies its origin in the LISM.

Table 1

Star	Type	**d** (pc)	ℓ^{II}(°)	b^{II}(°)	RV(km/s)	V_{cR}(km/s)	Vis(km/s)
τCet	G8 V	3.6	173	-63	-16	+15	+31
δPav	G5/8 V	5.9	338	-32	-22	-11	+11
βHyi	G1 IV	6.3	305	-40	+23	- 1	-24
ζTuc	G0 V	7.5	308	-52	+ 9	0	- 9
βTrA	F2 V	12.8	322	- 8	0	-12	-12
αHyi	F0 V	24.4	298	-54	+ 1v	+ 6	+ 5v
24UMa	G2 III	25.6	143	+39	-27	+ 7	+34
γMic	G6 III	29.4	12	-40	+18	-17	-35
δDra	G9 III	31.3	99	+23	+25	- 9	-34
20Mon	K0 III	33.3	219	+ 2	+79	+27	-52
ζVol	K0 III	58.8	285	-22	+48	+ 6	-42

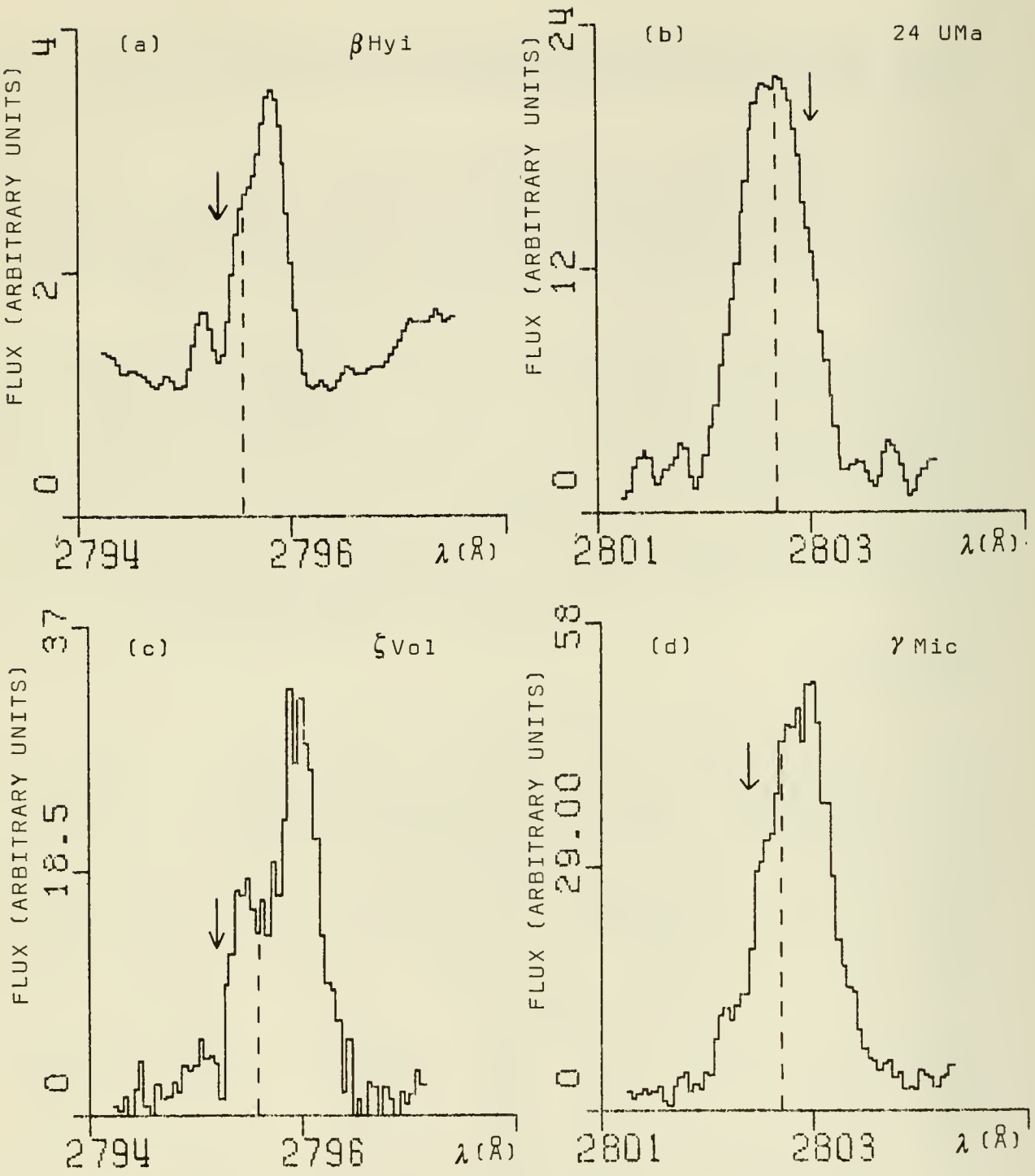

Figure 1. Profiles of MgII **h** ((a) and (c)) and **k** ((b) and (d)) in four late-type stars within 60 pc of the sun. Dashed lines show photospheric **h** or **k** rest wavelengths. Arrows show IS wavelengths predicted by the Crutcher (1982) relation.

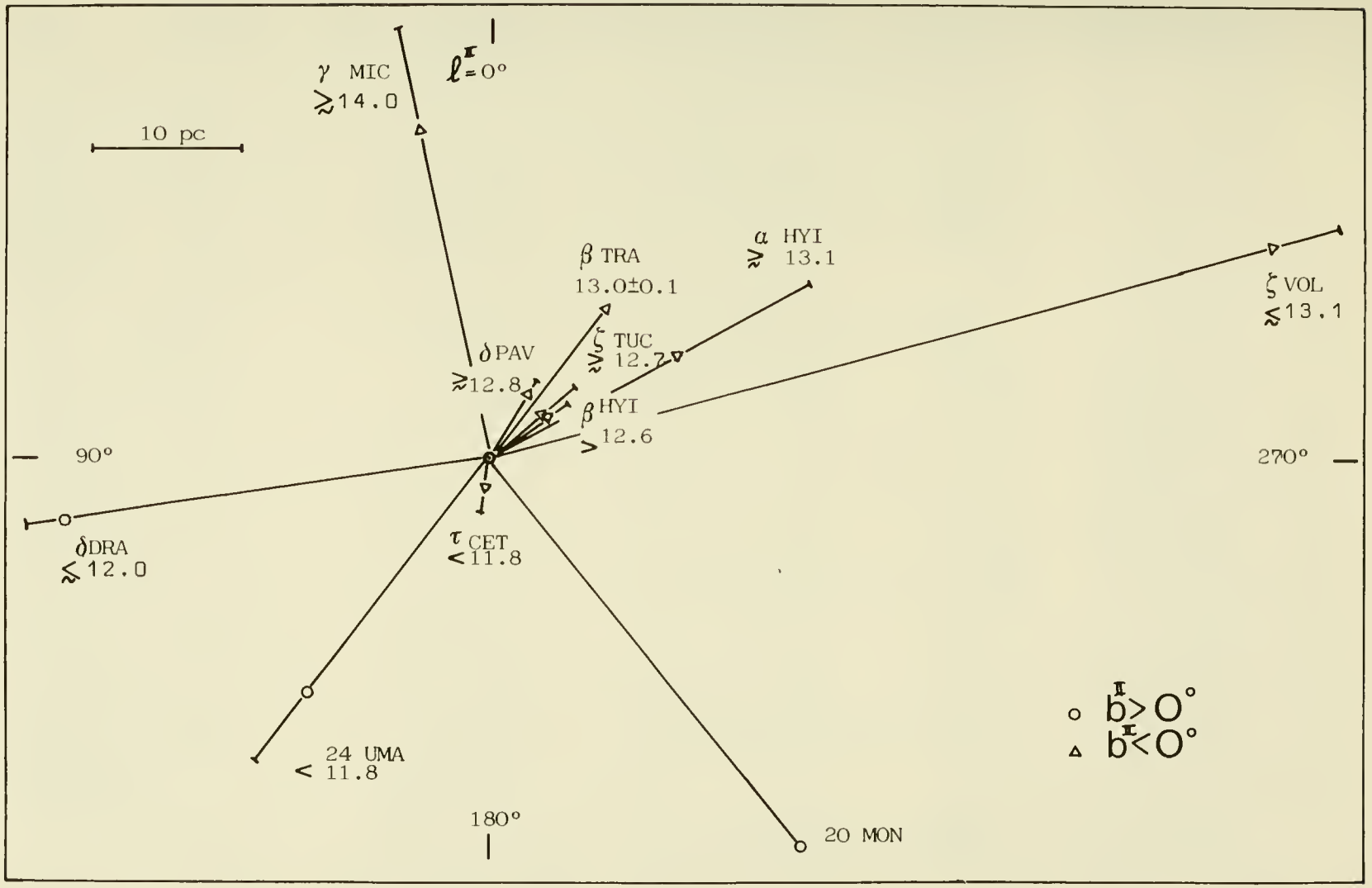

Figure 2. Log column densities of MgII towards late-type stars within 60 pc of the sun. Linear distances **d** to stars are solid lines. Projected distances d cos**b** in the galactic plane are indicated by triangles and circles.

RESULTS

Table 2 shows the results under the following headings: cols. 2 and 3, equivalent widths of IS k and h features; col. 4, MgII column densities (derived using doublet ratio method (Spitzer,1968)); col. 5, IS turbulence parameter (km/s); col. 6, HI column densities (assuming cosmic abundance and Mg depletion factor of 10 (Paresce,1984)); col. 7, mean MgII number density along line of sight (cm^{-3} $x10^{-7}$); col. 8, mean HI number density (cm^{-3}).

Table 2

Star	Wk(mÅ)	Wh(mÅ)	LogN(MgII)	b	LogN(HI)	n(MgII)	n(HI)
τ Cet	$<$ 30	$<$ 30	$<$ 11.8	--	$<$ 17.4	$<$ 0.6	$<$ 0.02
δ Pav	$\gtrsim$ 98	$\gtrsim$ 74	$\gtrsim$ 12.8	$\gtrsim$3.9	$\gtrsim$ 18.4	$\gtrsim$ 3.5	$\gtrsim$ 0.13
β Hyi	$>$ 77	$>$ 55	$>$ 12.6	$>$3.4	$>$ 18.2	$>$ 2.2	$>$ 0.08
	$<$165	$<$137	$<$ 13.2	$<$5.6	$<$ 18.8	$<$ 8.9	$<$ 0.34
ζ Tuc	$\gtrsim$ 92	$\gtrsim$ 67	$\gtrsim$ 12.7	$\gtrsim$3.8	$\gtrsim$ 18.3	$\gtrsim$ 2.3	$\gtrsim$ 0.09
β TrA	158±30	117±20	13.0±0.1	6.5	18.6±0.1	2.5	0.1
α Hyi	$>$135	$>$135	$>$ 13.1	--	$>$ 18.7	$>$ 1.7	$>$ 0.07
24UMa	$<$ 30	$<$ 30	$<$ 11.8	--	$<$ 17.4	$<$ 0.1	$<$ 0.003
γ Mic $\star$	$\approx$230	$\approx$220	$\gtrsim$ 14.0	--	$\gtrsim$ 19.5	$\gtrsim$10.2	$\gtrsim$ 0.39
δ Dra $\star$	$<$ 50	$<$ 50	$<$ 12.0	--	$<$ 17.6	$<$ 0.1	$<$ 0.004
20Mon $\star$	$<$100	$<$100	----	--	----	---	----
ζ Vol $\star$	$\lesssim$340	$\lesssim$205	$\lesssim$ 13.1	$\approx$25(?)	$\lesssim$ 18.6	$\lesssim$ 0.04	$\lesssim$ 0.02

$\star$ Preliminary reduction only: very recent data.

CONCLUSIONS

We have demonstrated the value of using late-type stars for MgII LISM measurements and have augmented the sum of reported MgII column densities within 80 pc by a factor two. We confirm the observations by, i.a., Bruhweiler (1982) of a "hole" in the neutral LISM centred on $\ell^{II}=150^{\circ}$, and by, i.a., Paresce (1984) of a strong density peak towards $\ell^{II}=10^{\circ}$. Detailed treatment of this work will appear elsewhere (Vladilo et al. 1984, Molaro et al. 1984).

REFERENCES

Bruhweiler,F.C.:1982,"Adv. in UV Astronomy",NASA CP-2238,p.125.
Crutcher,R.M.: 1982, Astrophys. J., 254,88.
Molaro,P.,Beckman,J.E., Crivellari,L.,Franco,M.L. and Vladilo, G.: 4th European IUE Conference, Rome 1984 (in press).
Paresce,F.: 1984, Astron. J. (in press).
Spitzer,L.:1968,Diffuse Matter in Space (Interscience),p.19.
Vladilo,G., Beckman,J.E., Crivellari,L., Franco,M.L. and Molaro,P.: 1984, submitted to Astron. Astrophys.

FeII AND MgII IN THE NEARBY INTERSTELLAR MEDIUM

Klaas S. de Boer and Heinz Lenhart
Astronomical Institute, University of Tübingen
D-7400 Tübingen, West Germany

ABSTRACT

UV spectra with 15 km s^{-1} resolution of bright stars have been searched for FeII and MgII interstellar lines. We present equivalent widths of absorption for 8 stars and find average line-of-sight densities $n(FeII) = 4\ 10^{-8}$ and $n(MgII) = 2\ 10^{-7}$ cm^{-3}. This represents approximately $n(H) = 0.03$ cm^{-3}.

INTRODUCTION

High-resolution echelle spectra have been obtained between 2000 and 3000A with the Balloon Borne Stellar Spectrograph (BUSS) in flights in 1976 and 1978. BUSS echellography is similar to that with the International Ultraviolet Explorer (IUE) satellite, but with the echelle orders crowding towards the longer wavelengths. The BUSS spectral resolution is about $3\ 10^4$ (better than that of the IUE). Full details about the instrument are given by Kondo et al (1979) and Kamperman et al (1979). The BUSS data base, made available by the Space Research Laboratory in Utrecht on tape as wavelength calibrated spectra, consists of some 80 spectra of 55 stars brighter than V= 5 and with spectral types ranging from O9 to K5 of all luminosity classes. The BUSS spectra have a large range in quality (perfect spectra, some with very low signal, overexposed ones, reduced signal between 2500 and 2700A due to stratospheric Ozone absorption). For stars later than B0 stellar lines may appear. Only in stars of later type with large rotation or with large radial velocity can interstellar lines be separated from the stellar features. Examples of spectra are shown in Fig. 1. There are about 25 stars nearer than 100 pc in the data base of which 8 show unambiguously recognizable interstellar lines.

RESULTS

We have plotted the relevant portions of BUSS spectra with velocity scale (Fig. 2.) and assessed the presence of interstellar absorption. The FeII 2373.73 A line is in BUSS spectra near an instrumental flaw and is not useable. The zero-point of the BUSS velocity scale is known to about 50 km s^{-1}, but relative velocities to an accuracy of 5 km s^{-1}. The two interstellar components detected in the spectrum of κ Dra are separated by 37 km s^{-1}.

The equivalent widths of the lines detected were determined and the data are collected in Table 1. The accuracy of each determination was derived from the noise locally in the spectrum. The BUSS line strengths can be compared with those from other observations. For ζ Oph the agreement of our data with those from the Copernicus (Lugger et al 1982) is fair, while for α Vir the

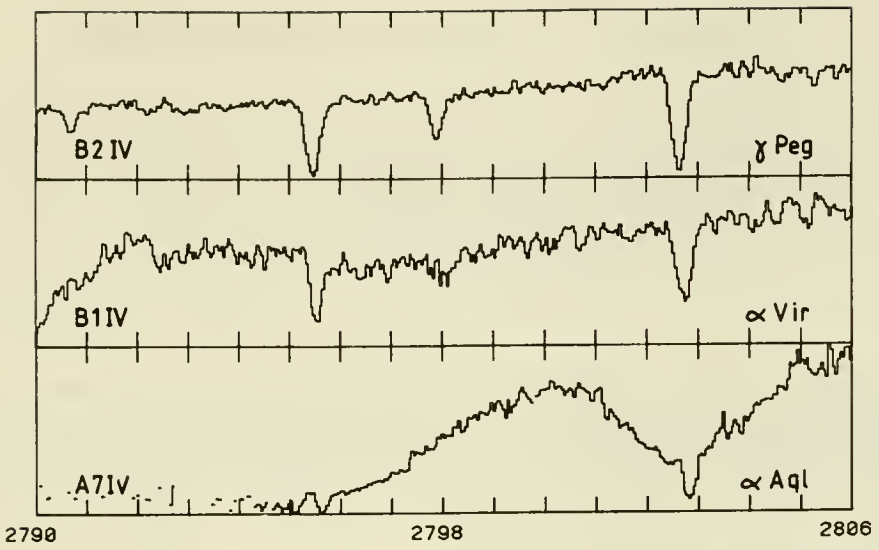

Fig. 1. The MgII region in BUSS spectra (linear intensity scale; echelle function not removed) showing the resonance lines near 2795.6 and 2802.7Å and the subsidiary lines near 2790.7 and 2798.0A. In γ Peg all MgII are essentially stellar, in α Vir essentially interstellar, in α Aql the narrow interstellar absorption is seen near the bottom of the stellar lines which are wide due to stellar rotation.

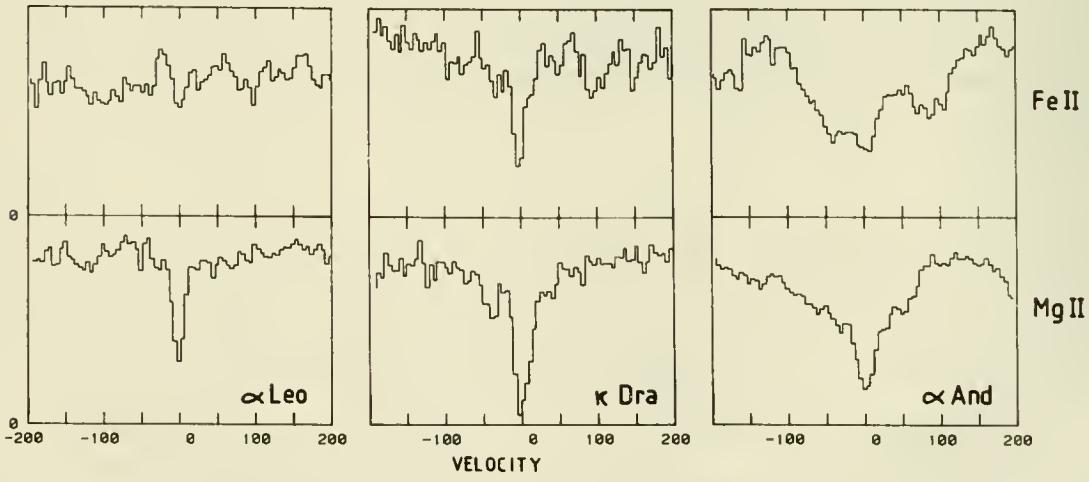

Fig. 2. For 3 stars the FeII 2382.03Å and the MgII 2802.70Å spectra are displayed showing the narrow interstellar absorption (shifted to 0 km s^{-1}).

Table 1. Eqivalent widths (mÅ) of interstellar FeII, MgII and MgI in nearby stars observed with the BUSS

		α And	α Leo	κ Dra	κ Dra	α Com	α Vir	δ Aql	α Aql	29 Cyg
	HD	358	87901	109387		114378	116658	182640	187642	192640
	V	2.06	1.35	3.87		5.22	0.98	3.36	0.76	4.97
	Sp.T.	B8IVp	B7V	B6IIIp		F5V	B1IV	F0IV	A7IV	A2V
	v sin i	56	329	249		28	159	85	242	37
	BUSS image	VII132	IX04	IX05	IX05	IX11	VIII1	VIII12	VIII04 VIII16	X05
FeII	2382.03	40 (5)	< 20	80	< 10	--	175 (20)	--	76 (20)	--
	2599.40	55 (20)	--	--	--	--	--	100 (50)	63 (10)	--
	2343.50	< 15	< 10	70 (20)	< 10	--	80 (10)	--	--	--
	2585.88	--	--	--	--	--	--	80 (50)	34 (10)	--
MgII	2795.53	155 (20)	125 (10)	255 (15)	140 (15)	70 (20)	180 (30)	190 (20)	>185 (40)	present
	2802.70	145 (20)	95 (5)	235 (20)	70 (15)	40 (20)	215 (10)	165 (40)	185 (15)	420 (100)
Mg I	2852.13	--	< 10	50 (10)	< 10	70 (20)	60 (10)	45 (10)	--	85 (20)

--= no continuum; ( )= estimated uncertainty; MgII 2795A less accurate in poor part of BUSS image
f-values for the listed FeII and MgII lines: log fλ= 2.98, 2.88, 2.55, 2.34, 3.22, 2.92 respectively.
BUSS flights were on: VII May 16, 1976; VIII Sep 19, 1976; IX May 8, 1978; X May 30, 1978.

BUSS line strengths are larger by 50% than those from Copernicus (Lugger et al 1982). For α Aql the BUSS Mg equivalent widths are 2 times the very uncertain ones reported from Copernicus (Kondo et al 1978). Toward α Leo the BUSS Mg lines are 30% stronger than those from Copernicus (Kondo et al 1978), but these in turn were 2 times as strong as those from other balloon payloads (Boksenberg et al 1975, Morgan et al 1978). For the moment we must leave these differences for what they are, even though they may have considerable effect on the derivation of interstellar gas densities.

Column densities (Table 2) were derived from plots of log fλ vs log Wλ/λ and comparison with standard single-cloud curves of growth. We assumed that MgII and FeII follow optical-depth relations with the same (effective) velocity dispersion b, and used FeII f-values from Nussbaumer et al (1981). Stellar distances are derived from the parallaxes as given by Uesugi and Fukuda (1982). For α And, α Leo and κ Dra a reliable Mg/Fe ratio is found, which averages at N(Mg)/N(Fe) = 10.

GAS DENSITIES

From the column densities and distances the ion densities can be calculated. In order to get to gas densities the abundances of free Fe and Mg have to be known. For Fe Savage and Bohlin (1979) found [Fe/H] = -6.0 in gas with little reddening; Mg has little depletion in such gas, was, however, never studied in detail, and we therefore assume [Mg/H] = -5.0 from our Mg/Fe column densities above. The gas densities so found are given with Table 2.

Table 2. Column densities of FeII and MgII derived from BUSS spectra

Name	δ Aql	α Aql	29Cyg	α And	κ Dra	α Leo	α Vir	α Com
l°	39.6	47.7	74.4	111.7	125.2	226.4	316.1	328.0
b°	- 6.1	- 8.9	1.2	-32.8	47.3	48.9	50.8	79.5
d(pc)	15	5	53	39	90	26	80	18
log N(FeII)	---	12.9	---	12.4	12.8	<12.1	13.1	---
log N(MgII)	13.3	>14.0	>14.3	13.3	13.8:	13.0	13.0	12.4
log n(H)	-1.3:	-0.3	>-0.9:	-1.8	-1.6	-1.9	-1.3	-2.3:

Gas densities are based on N(FeII), [Fe/H] =-6.0, and the distance; for δ Aql, 29 Cyg and α Com N(MgII) was used with [Mg/H] =-5.0

The average is n(H)= 0.03 cm^{-3}, while the number of determinations is too small to discriminate large scale directional differences.

When collecting from the literature all determinations of N(MgII) in the ISM within 100 pc, we find the average n(MgII)= 8 10^{-8} cm^{-3} for $90° < l < 270°$, and n(MgII)= 2 10^{-7} cm^{-3} for the directions toward the galactic center. These numbers convert (with [Mg/H] = -5) into n(H) = 0.014 cm^{-3}.

An account of all interstellar lines in the BUSS data base is in preparation. We thank the Space Lab in Utrecht, in particular Karel van der Hucht and Theo Kamperman, for so generously making available all information regarding the BUSS data. KSdB is supported through the grant Gr438/14a from the DFG. He also acknowledges a travel grant from the Deutsche Forschungsgemeinschaft which enabled participation in this IAU Colloquium.

REFERENCES

Boksenberg, A., Kirkham, B., Pettini, M., Bates, B., Carson, P.P.D., Dufton, P.L., McKeith, C.D. 1975, Astrophys. J. 202, L 91

Kamperman, T.M., et 7 alii. 1979, in "High Resolution Spectrometry" p.662, 4th Intern. Coll. Astrophys. Trieste, Ed. M. Hack, Osserv. Trieste

Kondo, Y., Talent, D.L., Barker, E.S., Dufour, R.J., Modisette, J.L. 1978, Astrophys. J. 220, L 97

Kondo, Y., et 7 alii. 1979, Astrophys. J. 230, 526

Lugger, P., Barker, E., York, D.G., Oegerle, W. 1982, Astrophys. J. 259, 67

Morgan, T.H., McDonnold, J.N., Modisette, J.L., Kondo, Y. 1978, Pub. Astron. Soc. Pacific 90, 89

Nussbaumer, H., Pettini, M., Storey, P.J. 1981, Astron. Astrophys. 102, 351

Savage, B.D., Bohlin, R.C. 1979, Astrophys. J. 229, 136

Uesugi, A., Fukuda, I. 1982, "Revised Cat. Stellar Rotational Vel.", in Centre des Données Stellaires, Strasbourg

A TYPE STARS AS PROBES OF THE LOCAL INTERSTELLAR MEDIUM

R. Freire Ferrero[1], R.Ferlet[2] and A.Vidal-Madjar[2]

1. Observatoire Astronomique,11 Rue de l'Université,67000-Strasbourg,FRANCE.
2. Institut d'Astrophysique de Paris,98 bis Bd.Arago,75014-Paris, FRANCE.

ABSTRACT.-

With the aim to sample well the Local Interstellar Medium (LISM),we propose to use A stars as targets. The Mg II UV lines seems to be the best interstellar absorption candidates. Several hundreths of A stars can be reached within 100 pc. First preliminary results (20 lines of sight) are presented, based on previous Copernicus and actual IUE observations.

I. INTRODUCTION.-

Typically, in order to study the gas in the interstellar medium (ISM), one uses rapidly rotating early type stars as background sources. For instance,UV observations with the Copernicus satellite have evidenced,through O VI sharp absorption lines, the existence of a pervasive,extremely low density ($n \sim 10^{-2.5}$ cm^{-3}) and high temperature ($T \sim 10^{5.5}$ °K) interstellar (IS)component which is quite local ($\lesssim$ 100 pc;Jenkins and Meloy 1974).This picture has been confirmed through diffuse X-ray observations.

Independent observational evidences have led several authors (e.g.Vidal-Madjar et al 1978;Bruhweiler and Kondo 1982;Tinbergen 1982;Crutcher 1982;Paresce 1983;Frisch and York 1983) to the conclusion that the Sun could be imbedded near the edge of small cold neutral IS cloud,which itself might be immersed in the observed hot component.

Nevertheless,O and B stars are distant and their lines of sight generally intercept several clouds with very different properties, making any analysis somewhat complex. Therefore,IS absorption has been observed with Copernicus and IUE toward much nearer late type stars but superimposed over stellar features. Despite the uncertainties due to the unknown intrinsic shape of the stellar profile, these results consistently pointed out a sharp drop-off in the hydrogen density ($\overline{n}_{HI} \sim 0.1$ cm^{-3}) beyond 3.5 pc of the Sun (see e.g. Mc Clintock et al,1978;Andersen and Weiler 1978). Furthermore,more recent IUE data on Mg II toward nearby white dwarfs (Bruhweiler and Kondo,1982) further support the above overall picture of the LISM.

However, all of these recent results appear to conflict with the model of Mc Kee and Ostriker (1977) in its present form (Bruhweiler and Kondo 1981) and much more additional lines of sight are needed before claiming that the current theoretical models have been adequately tested and in order to construct a detailed map of the LISM at a small scale length.

II. OBSERVATIONAL STRATEGY.-

To refine our knowledge of the ISM in the immediate vicinity of the Sun, one must study many sight-lines toward stars closer than the O B type ones. Because the visual IS lines are limited to species of low abundances and/or low oscillator strenghts,the UV resonance lines are much more sensitive and thus better candidates to the study of the low column densities expected in the LISM.

We are thus facing the following alternative: to sample well the LISM we need cooler stars (presenting less emission in the UV) and strong UV resonance lines (more and more numerous when going toward the far UV). The best choice is thus to select the strongest UV line present at the largest possible wavelength: the Mg II doublet near 2800 A is obviously the best candidate.

Having selected this line, we simultaneously define the observatory to be used (IUE) and the target stars that should be selected. The observatory having a spectral resolution of $\sim$20 Km/s at 2800 A, this constraint imposes to use fast rotating background stars in order to avoid stellar feature contamination extremely difficult to resolve with this instrument. These condition leads clearly to the A stars and the hotter coolFstars as ideal target stars. In effet, from Allen (1982) one can easily show that within 100 pc from the Sun,several hundred target stars of that type could be found.

Another advantage of this approach is that a large sample of sight lines could be explored with a unique observational technique.This should thus lead to an extremely homogeneous observational set of data sampling in detail the LISM.

III. STARTING THE Mg II, A STAR SURVEY.-

Such an approach was performed first by Kondo et al (1978) who derived Mg II column densities toward 2 late B and 4 A stars (α Gru, α Leo and α CMa, α Lyr, α PsA and α Aql) observed with Copernicus. In that type of stars,the IS lines appear superimposed on the photospheric absorption profile of the stellar Mg II lines. Therefore,both will be more easily delineated when observing A stars with high rotational velocities. In general, rotation washes out the small differences in the computed line cores for different upper stellar atmospheric models and with the same abundances, giving convolved profiles that are more or less similar. But in the case of slow rotators,one can only measure crude limits on equivalent widths (W). Even if a detailed theoretical stellar profile can be computed in the frame of non LTE,with the assumptions of complete or partial redistribution Freire Ferrero,Gouttebroze and Kondo (1983) have shown that in the case of α Lyr (v.sin i = 17 Km/s) the previous determination of Kondo et al (1978) may be decreased by a large factor.On the contrary,preliminary computations by Freire Ferrero et al (1984) for Altair (α Aql,v.sin i = 220 Km/s) give IS Mg II equivalent width similar to the previous ones reported by Kondo et al (1978).

The present paper is a first step to sinificantly increase the sample of Kondo et al (1978): 14 A stars were observed in October 1982 and February 1983 with the long wavelenth camera of IUE (Freire Ferrero 1984;Freire Ferrero et al 1984a) out of which 10 are rapid rotators. Relevant stellar parameters

along with Mg II equivalent widths are given in Table 1. More details can be found in Freire Ferrero (1984) and Freire Ferrero et al (1984).

We present here the first step toward a complete map of the LISM as seen through the Mg II lines in front of fast rotating A stars (Fig. 1).This study is still preliminary and for that reason only the quantity "equivalent width par parsec" (W/d) is presented.These values can underline quite clearly inhomogeneities in the LISM.

IV. DISCUSSION AND CONCLUSION.-

From this map,we can already underline the following main characteristics:

- the size of the sample is still too small to properly cover the LISM ;
- the general tendency found by other techniques is confirmed here,i.e. more matter seem to be present in the general direction of the galactic center,a drop in density beeing visible in the opposite direction.

This approach also shows fluctuation from line of sight to line of sight underlining the probable patchiness of the LISM. Before reaching such conclusions it is clear that a much larger sample of stars should be observed.This will be done by selecting properly target stars that will fill the large gaps present in the map, as well as stars which will allow a proper estimation of the precision of this approach. We think that when more than 100 A stars will be observed,a more detailed view of the LISM should arise.

V. REFERENCES.-

Allen C W 1981,Astrophysical Quantities,3rd ed,The Athlone Press,Univ London.

Anderson R C,Weiler E J 1978,Ap J 224,143.

Bruhweiler F C,Kondo Y 1981,Ap J Lett 248,L123.

Bruhweiler F C,Kondo Y 1982,Ap J 259,232.

Crutcher R M 1982,Ap J 254,82.

Freire Ferrero R,1984,in 4th European IUE Conf,Rome.

Freire Ferrero R,Gouttebroze P,Kondo Y,1983 Astron Astrophys 121,59.

Freire Ferrero R,Talavera A,Gouttebroze P,1984a,in 4th Europ IUE Conf,Rome.

Freire Ferrero R,Gouttebroze P,Catalano S,Talavera A,1984b,in preparation.

Frisch P C,York D G 1983,Ap J Lett 271,L59.

Jenkins E B,Meloy D A 1974,Ap J Lett 193,L121.

Kondo Y,Talent D L,Barker E S,Dufour R J,Modisette J L,1978,ApJ Lett 220,L97.

Mc Clintock W,Henry R C,Linsky J L,Moos H W,1978,ApJ 225,L65.

Mc Kee C F,Ostriker J B,1977,ApJ 218,148.

Paresce F 1983,Nature 302,806.

Tinbergen J 1982,Astron Astrophys 105,53.

Vidal-Madjar A,Laurent C,Bruston P,Audouze J 1978,ApJ 223,589.

TABLE 1

H D	name	Sp T	l	b	d(pc)	v.sin i	W_k(mA)	W/d	Fig.1 N°
48915	α CMa	A 1 V	227.22	- 8.88	2.67	11	71	26.6	1*
87901	α Leo	B 7 V	226.43	48.94	25.6	330	95	3.7	6*
172167	α Lyr	A 0 V	67.44	19.24	8.13	17	70	8.6	4*
187642	α Aql	A 7 IV-V	47.74	- 8.91	5.05	220	142	28.1	2*
209952	α Gru	B 7 IV	350.	-52.47	19.6	240	170	8.7	5*
216956	α PsA	A 3 V	20.49	-64.90	6.94	100	133	19.2	3*
19832	56 Ari	B 9 p Si	157.68	-25.95	140.**	115	300	2.1	15
28910	ρ Tau	A 8 V	182.05	-21.67	38.5	125	65	1.7	10
91312	- -	A 8 IV	178.93	58.62	32.3	135	<50	<1.	19
95934	51 Uma	A 3 III-IV	179.75	65.03	70.**	100	150	2.1	12
106661	6 Com	A 3 V	267.16	75.25	38.5	175	80	2.1	9
127762	γ Boo	A 7 IIIvar	67.26	66.17	40	145	<50	<1.	20
135382	γ Tra	A 1 V p	315.71	- 9.55	100.	225	255	2.6	14
139006	α Crb	A 0 V	41.87	53.77	22.2	135	95	4.3	8
159561	α Oph	A 5 III	35.90	22.57	14.9	230	160	11.	16
205767	ξ Aqr	A 7 V	46.45	-40.34	83.3	165	135	1.6	13
11753	φ Phe	A 3 V	267.17	-69.99	64.**	15	<50	<1.	17
28978	- -	A 2 V	190.32	-27.08	78.**	15	<50	<1.	18
155125	η Oph	A 2 V	6.72	14.01	19.2	<10	150	7.8	7
214994	o Peg	A 1 IV	91.71	-25.59	41.7	10	150	3.6	11

* Kondo et al (1978) observations.

** distances deduced photometrically.

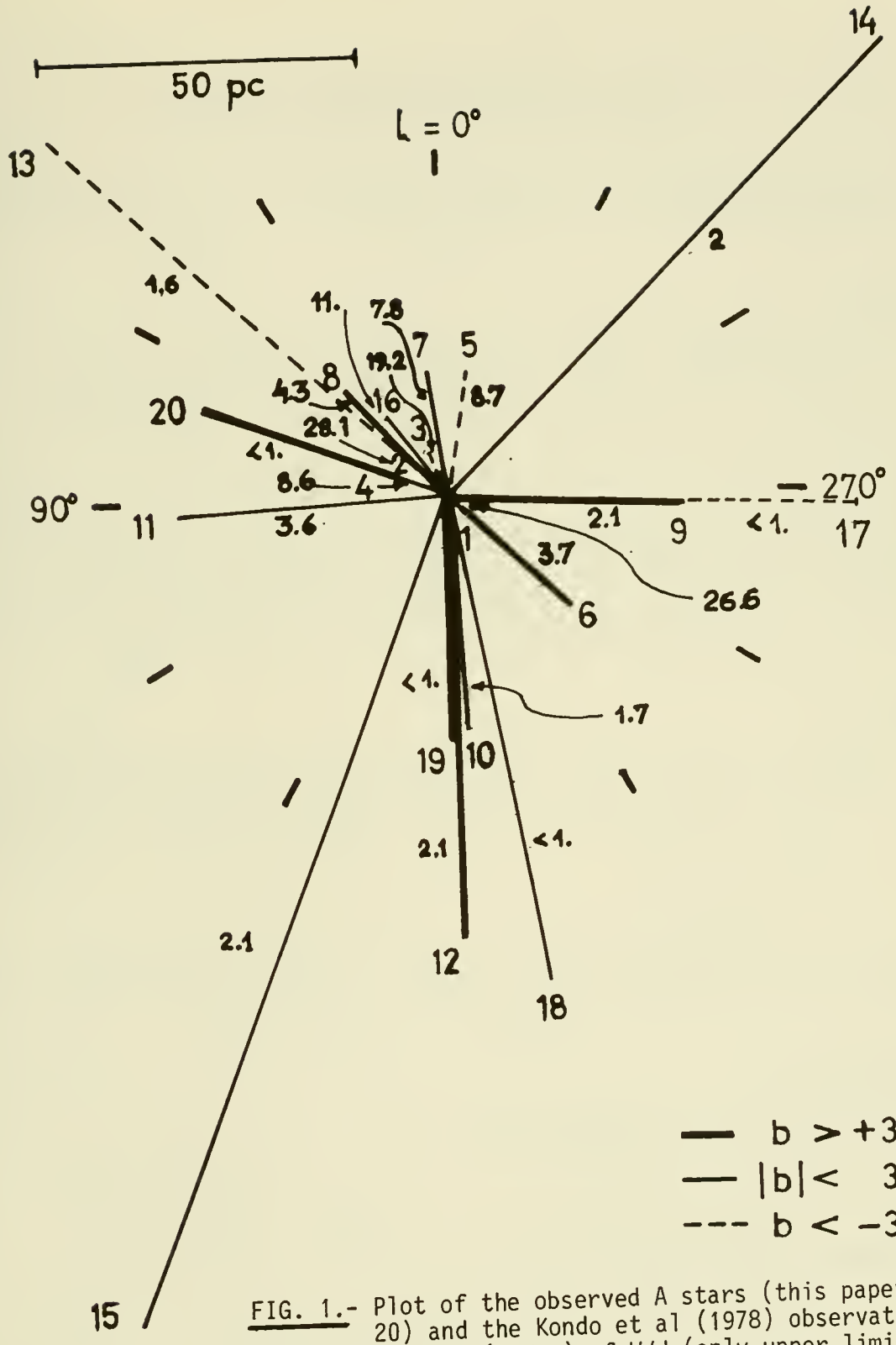

FIG. 1.- Plot of the observed A stars (this paper N°7 to 20) and the Kondo et al (1978) observations(N°1 to 6).The values (mA/pc) of W/d (only upper limits for slow rotators) are also indicated beside each sight-line.

PROBE OF THE NEARBY INTERSTELLAR MEDIUM BY THE VACANT LINE OF SIGHT TO β CMa

C. Gry
ESA Satellite Tracking Station, Madrid

D.G. York
University of Chicago
U.S.A.

A. Vidal-Madjar
Institut d'Astrophysique
Paris

ABSTRACT

The line of sight to βCMa has been probed by Copernicus observations. This particular line of sight is remarkable for the low mean densities. We find $\bar{n}_H \sim .002$ cm^{-3}. However we can distinguish two separate regions:

1) A local nearby HI region extends over a few parsecs from the sun with a density of the order of 0.1 cm^{-3} and a temperature of 11000 to 12500 K.

2) An HII region lies somewhere beyond the HI region and is spread over about 60pc. Its total hydrogen mean density is of the same order as the HI region, i.e. of $\sim$0.1 cm^{-3} and it contains only elements in low ionization state. All the data are coherent with the picture of a cloud in ionization equilibrium at T $\sim$ 23 000° K.

INTRODUCTION

Interstellar lines in all bright unreddened B stars within 150-200 pc have been observed with Copernicus to study the distribution of the various phases of the warm interstellar gas. This paper presents the results for βCMa, the line of sight to which is remarkable for the low mean densities ($\bar{n}_{HI} \sim 0.002$ cm^{-3}).

THE STAR AND ITS LOCATION

βCMa is a 1.98 magnitude star, of type B1 II-III. It is situated at a distance of 200pc, with galactic coordinates of $l \sim 226°$, $b \sim -14°$. Figure 1 shows its position on the galactic plane together with a few nearby stars to the direction of which the neutral hydrogen abundance is known.

THE OBSERVATIONS

Measurements of UV resonance lines of 10 elements (listed in Table 1) were made with the Copernicus spectrograph at high resolution (0.045 Å). The analysis of the UV lines was performed through line profile fitting (method described in Vidal-Madjar et al., 1977).

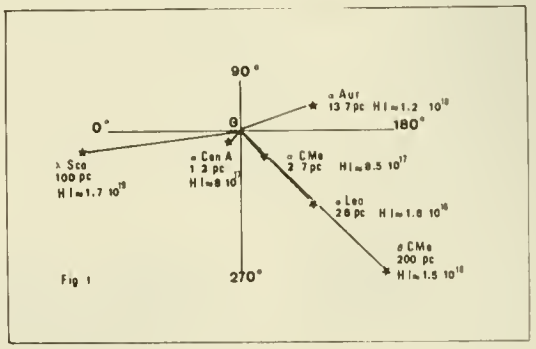

Fig 1

Velocity analysis

The fitting program can include a large number of velocity components but in the case of this line of sight the best fits were obtained for a unique component. There is however a systematic shift of about 5 km/s in velocity between the neutral and the ionised species with an intermediate velocity for the strongest NI line, suggesting the presence of 2 components: one containing almost all the neutral gas at about 1.5 km/s, the other one being almost entirely ionised and moving at a slightly different velocity of 6.5 km/s.

Abundances

HI and DI: The low hydrogen abundance is evidenced by the shape of the Lyman β line which shows no damping wings (see Figure 2). Independently of the assumed stellar line, the acceptable fits imply N(HI) to be in the range 1 to 2.2 10^{18} cm^{-2}, with a b-value of 13.5 to 14.3 km/s.
The deuterium line was fitted together with the hydrogen line, leading to the ratio D/H = 0.7-2.310^{-5}.

Other species: Examples of fits of the different lines are shown on Figure 3. The results of the fits are summarized in the first columns of Table 1. More precise abundances are obtained for NI and SII which were derived with 4 and 3 lines, respectively. OVI was not detected but an upper limit could be set.

DISCUSSION: STRUCTURE OF THE LINE OF SIGHT

Neutral region

Considering that the neutral hydrogen absorption comes from a unique component, the data give directly its column density (1 to 2.2 10^{18} cm^{-2}) and its temperature (11000 to 12500K). This latter is derived from the b-value which, being much higher than those found for the heavier species (see Table 1), indicates thermal broadening. On the other hand, the comparison with shorter lines of sight containing approximately the same amount of neutral matter shows that the neutral region can not be much extended. In particular, the line of sight to βCMa passes as close as 0.3 pc to the star αCMa in the direction of which the interstellar gas density is about 0.1 cm^{-3} (UV observations; Bruhweiler and Kondo 1982).

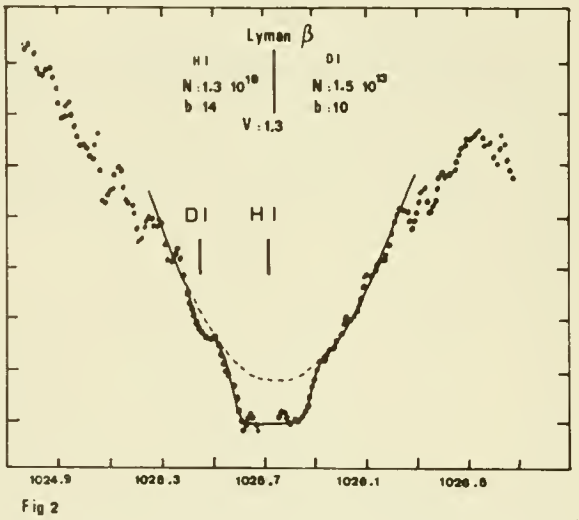

Fig 2

H and D Lyman profiles(...)observed, (—):theoretical. The IS absorption is superimposed on the stellar line(---).

The HI contribution in the spectrum of βCMa thus evidences the existence of a nearby neutral cloud of density 0.1 cm^{-3}, temperature 12000 K, extending over a few parsecs (less than 8 pc), the density of neutral gas dropping off by at least a factor of 100 beyond this cloud.
The contribution of this neutral region to the absorption profiles of other elements have been calculated on the assumptions of mean interstellar abundances (as given by Spitzer and Jenkins 1975; Ferlet, 1981; York et al.,

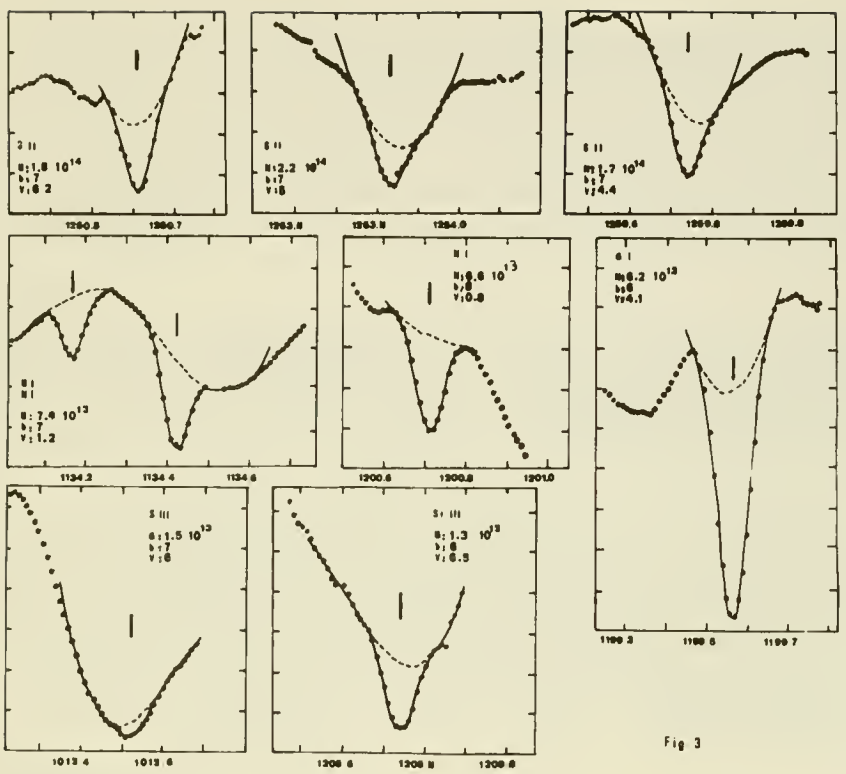

Fig 3

Figure 3: Observed (dots) and theoretical (continuous line) profiles of some of the lines studied here. The fits are performed with only one component having the characteristics indicated on each plot.

SPECIES	observations N (cm^{-2})	b (km/s)	V (km/s)	N (cm^{-2}) as expected in the HI region
HI	1 - 2.2 10^{18}	13.5 - 14.3	0.5 - 2.5	—
DI	1.5 - 2.3 10^{13}	9 - 12	0.5 - 2.5	—
NI	6 - 8.2 10^{13}	6.5 - 8	0.6 - 4.3	5 - 14 10^{13}
SII	1.7 - 2.2 10^{14}	6 - 8	4.4 - 6.2	< 2.9 10^{13}
SIII	0.9 - 1.6 10^{13}	7 - 8	5 - 8	< 7 10^{7}
SiIII	1.2 - 1.7 10^{12}	7 - 8	5 - 8	< 4 10^{10}
NII	1 - 50 10^{14}	7 - 8	5 - 8	
OI	3.8 -16.8 10^{14}	6 - 8	3.2 - 4.5	5.7 - 14.5 10^{14}
CII*	0.8 - 1.3 10^{13}	7 - 8	5 - 7	
OVI	< 5 10^{11}			

Table 1: Column 1,2,3 : column densities, b-values and velocities derived by fitting the profiles. column 4 : predicted abundances in the HI region deduced from the HI column density, a temperature of 11000 to 12500 K and the asumption of solar abundances.

1983) and thermal equilibrium ionisation fractions (as calculated by Shull and Van Steenberg, 1982), and are displayed also in Table 1.
From the comparison of the 1st and 4th columns of Table 1, it is clear that the neutral region contributes to part or all of the neutral species (NI and OI) column densities, but can not account for the abundances of the ionised species as SII, SIII, SiIII: an ionised region must lies beyond the HI cloud.

Ionised region

Since H/S and C/S can be assumed to be solar for this unreddened line of sight, we find $N(H^+) \sim 1.6 - 2\ 10^{19}$ cm^{-2} and $N(CII) \sim 3.7 - 5\ 10^{15}$ cm^{-2}. From Table 1, $N(CII^*) \sim 0.8 - 1.3\ 10^{13}$, thus $N(CII^*)/N(CII) = 1.6\ 10^{-3} - 3.5\ 10^{-3}$. From Table 4 of York and Kinahan (1979), this implies collisional excitation of the ground term of CII by electron in a medium with density $n_{H+} = n_e = 0.07 - 0.14$ cm^{-3}. Thus, the HII region is density bounded and extended over 40 to 90 pc.
It is unlikely that the ionisation is due to the UV flux of βCMa, as to get rise to such an abundance of H^+, the density in the Stromgren sphere of this star should be higher than 0.7 cm^{-3}.
Alternatively, a unique temperature (T = 22500 - 25000 K) can account for all observed line intensities ratios in the asumption of collisional ionisation equilibrium (again the ionisation ratios given by Shull and van Steenberg (1982) were used).
Finally two more remarks can be made after this study: First the non-detection of OVI shows that there is no coronal gas in this direction within 200 pc . Second, the presence in the distant line of sight to λSco (see Figure 1) of a component presenting abundances and characteristics very similar to those of the HII component discussed here (York, 1983), could suggest that these 2 components arise from a same hot (22500K-25000K), diffuse ($N_H \sim 0.1$ cm^{-3}) cloud surrounding the nearby HI regions.

REFERENCES

Bruhweiler,F.C.,Kondo,Y.,1982, Ap.J. 259, 232
Ferlet,R., 1981, A.and A.,,98, L1
Spitzer,L., Jenkins,E.B., 1975, Ann.Rev.Astron.Astrophys.13, 133
Vidal-Madjar, A., Laurent,C., Bonnet,R.M., York,D.G., 1977, Ap.J.,211, 91
York,D.G., 1983, Ap.J.,264, 172
York,D.G.,Kinahan,B.F., 1979,Ap.J.,264, 172
York,D.G., Spitzer,L., Bohlin,R.C., Hill,J., Jenkins,E.B., Savage,B.D.,Snow, T.P., 1983, Ap.J., 266, L55

DEUTERIUM ABUNDANCE IN THE LOCAL INTERSTELLAR MEDIUM

by Ferlet[1], R., Gry, C[2]., and Vidal-Madjar, A[1].

[1]. Institut d'Astrophysique de Paris
98bis Bd Arago - 75014 - Paris - France
[2]. IUE Observatory
Villafranca del Castillo - Appartado 54065 - Madrid - Spain

ABSTRACT

We underline the present situation of deuterium abundance evaluation in interstellar space and show that it should be $\leq 10^{-5}$. Studiing in more detail the λ Sco line of sight and having observed two NaI interstellar components toward that star, we can show that the D/H evaluation made toward λ Sco is in fact related to the local interstellar medium (less than 10 pc from the sun). Because this evaluation is also $\leq 10^{-5}$ it is in stricking contrast with the one made toward α Aur ($D/H > 1.8\ 10^{-5}$) confirming the fact that the deuterium abundance in the local interstellar medium varies by at least a factor of two over few parsecs.

I INTRODUCTION

The most likely source of formation of light elements is during the first few minutes of the Universe, according to the so-called generally accepted Big Bang theory (Wagoner, 1973). They represent thus extraordinary cosmological probes, the primordial deuterium abundance in particular being probably one of the best tracers of the present baryon density of the Universe. On the other side, deuterium is almost always destroyed in stars and therefore should be also a probe of the chemical galactic evolution.

In that frame, one should expect a constant deuterium abundance in the nearby interstellar medium and until recently it was accepted that the measurements were in good agreement with the standard Big Bang predictions (see e.g. Austin, 1980). However, the question has now arised about the real cosmological significance of the deuterium observations and of the validity of the many assumptions made either in the Big Bang model or in the chemical evolution calculations (Vidal-Madjar and Gry 1984).

In effect, Vidal-Madjar et al (1983) showed that in the case of ε Per, the DI line is blended by an HI component present in the stellar wind, changing in column-density and moving away from the star at approximately 80 km s^{-1}. Although this study could not give a significant D/H ratio, it clearly showed that a stellar wind phenomenon can lead to an apparent overestimation of the deuterium abundance and may have influenced the previous D/H evaluations.

To check this possibility Gry, Laurent and Vidal-Madjar (1983) carefully re-analysed the ε Per Copernicus deuterium spectra and they pointed out that definite time-variations were present. More recently, Gry,

Lamers and Vidal-Madjar (1984) have found similar variations in the Copernicus data toward three stars whose D/H have been measured by York and Rogerson (1976) through the curve of growth technique : γ^2 Vel, α Cru and α Vir. Therefore, one may suspect that the interstellar D/H ratio toward these stars could be lower than previously evaluated (though probably still within the originally quoted errors) and thus more in agreement with the low D/H values found toward the three Orion stars studied by Laurent, Vidal-Madjar and York (1979). Note that these Orion values already represented a strong constraint since they correspond to an average over three components detected on these sight-lines analysed with the profile fitting method. Note also that it is still possible to invoke a particularly strong astration toward the Orion region.

As a preliminary conclusion and in view of the possible stellar contamination of the interstellar DI absorption line, we suggest that the D/H interstellar ratio (within 1 kpc of the Sun) as measured toward early type stars with the profile fitting analysis should be more likely of the order or less than 10^{-5}, whereas the average of currently published values for hot stars is 1.45×10^{-5}.

II The λ Sco line of sight

Recently, York (1983) analysed the nearby B 1.5 IV star λ Sco, also through the use of the profile fitting method in many lines of different species observed with Copernicus. He has detected five components in that line of sight. The main one (2) seems to be essentially neutral, while all the others are partly or strongly ionised. The D/H evaluation was possible with precision only in this component and led to the range $6 \times 10^{-6} \leq D/H \leq 10^{-5}$ deduced from the quoted H and D column densities and error bars. This result per-se confirms our previous conclusion and seems to show that in the nearby interstellar medium the D/H abundance is in fact smaller than 10^{-5}.

Since λ Sco is only at about 120 pc from the Sun, one could question the fact that this evaluation is not only representative of the nearby ISM (~ 100 pc) but even of the local ISM (~ 10 pc ; LISM).

It could be therefore interesting to show that this main component observed toward λ Sco is in effect related to the immediate viccinity of the Solar system. Several studies have shown (see e.g. Vidal-Madjar et al, 1978 ; Mc Clintock et al, 1978 ; Bruhweiler and Kondo, 1982 ; Crutcher, 1982) that the LISM seems to contain a small neutral cloud in the general direction of the Sco-Cen association. Following the most recent compilation of observational information, Frisch and York (1983) showed that in the general direction of λ Sco one should expect a neutral hydrogen column density $N(HI) \sim 5.10^{18}$ cm^{-2} located over the first 10 pc away from the sun. This value is only a factor of 3 away from the total HI column density observed toward λ Sco ($N(HI) \sim 1.7\ 10^{19}$ cm^{-2}), 90% of which being locked in component 2. The HI cloud observed toward λ Sco thus must be related to the local interstellar cloud (LIC). York (1983) gave evidences that this HI component is probably quite compact and should spread over less than 5 pc. This is in very good agreement with the infered size of the LIC.

To be further convinced of the component 2 identification with the LIC, one should check two other physical parameters observed in this component :

temperature and velocity. From the b-values evaluated in absorption lines corresponding to elements presenting very different masses, York (1983) has derived b (HI) > b(DI) > b(OI) > b(ArI), concluding that component 2 cannot be cold and that the observed b-values are compatible with a medium at $T \simeq 10^4$ K. This result is in very good agreement with other studies and in particular with the observed temperature of the interstellar medium flowing inside interplanetary space (see e.g. Bertaux, 1984).

The component 2 velocity also could be compared to the LISM velocities as predicted and studied by Crutcher (1982). Unfortunately, the Copernicus velocity information are not precise enough to clearly identify through velocity component 2 with the LISM since furthermore York (1983) found five components separated by about 10 km/s, a value in the range of the maximum absolute velocity error to be expected with the Copernicus instrument.

Since no optical observations of the quality required to obviously detect faint interstellar absorption lines and to have a precise velocity scale were available, we decided to reobserve the D-lines of the interstellar neutral sodium toward λ Sco with a spectral resolution of 3 km s^{-1} and a signal to noise ratio high enough to be able to clearly detect equivalent width of the order of 1 mÅ. Performed at the ESO - La Silla Observatory in Chile with a Reticon detector, the details of the instrumentation, observational procedure and data reduction can be found in Ferlet and Dennefeld (1984). For the present purpose, let just recall that the wavelength calibration is based on more than 13 thorium-argon lines emitted by a hollow-cathode lamp over the 50 Å of the spectrum length giving an internal accuracy of 0.002 Å or 0.1 km s^{-1}. By comparing spectra taken at different epochs to be able to separate interstellar absorptions from telluric water vapor ones very numerous in the NaI D region, we have undoubtedly detected two interstellar components at V_0 = -26 km s^{-1} and at V_0 = - 17 km s^{-1} (see Figure 1).

From the study of York (1983) it is clear that one should expect some NaI counterpart (although weak) only from component 2 (the main HI component) and component 3, a component in which there is in fact a similar total hydrogen content as in component 2, but in which hydrogen is at about 90% ionised. Nevertheless this component is still weakly ionised and NaI could be significantly present in it. All other components are much too weak or too ionized to show any NaI.

Component 2 and 3 have a velocity separation of 9 km s^{-1} in remarkable agreement with the observed velocity separation of the two NaI components which is also observed to be of 9 km s^{-1}.

From Crutcher (1982) analysis, one should observe in the direction of the star λ Sco an heliocentric velocity for the LISM of -23 km s^{-1}. This result thus shows independently that component 2 is the more likely to be related to the LISM since as indicated by Crutcher (1982) most of the interstellar components observed toward nearby stars seem to fall within ± 3 km s^{-1} from the predicted values.

In conclusion, from that study, we have showed that all parameters related to component 2 observed by York (1983) toward λ Sco are in excellent agreement with the LISM parameters (column density, velocity, temperature) and thus seem to be clearly related to the LIC located at the edge of the solar system.

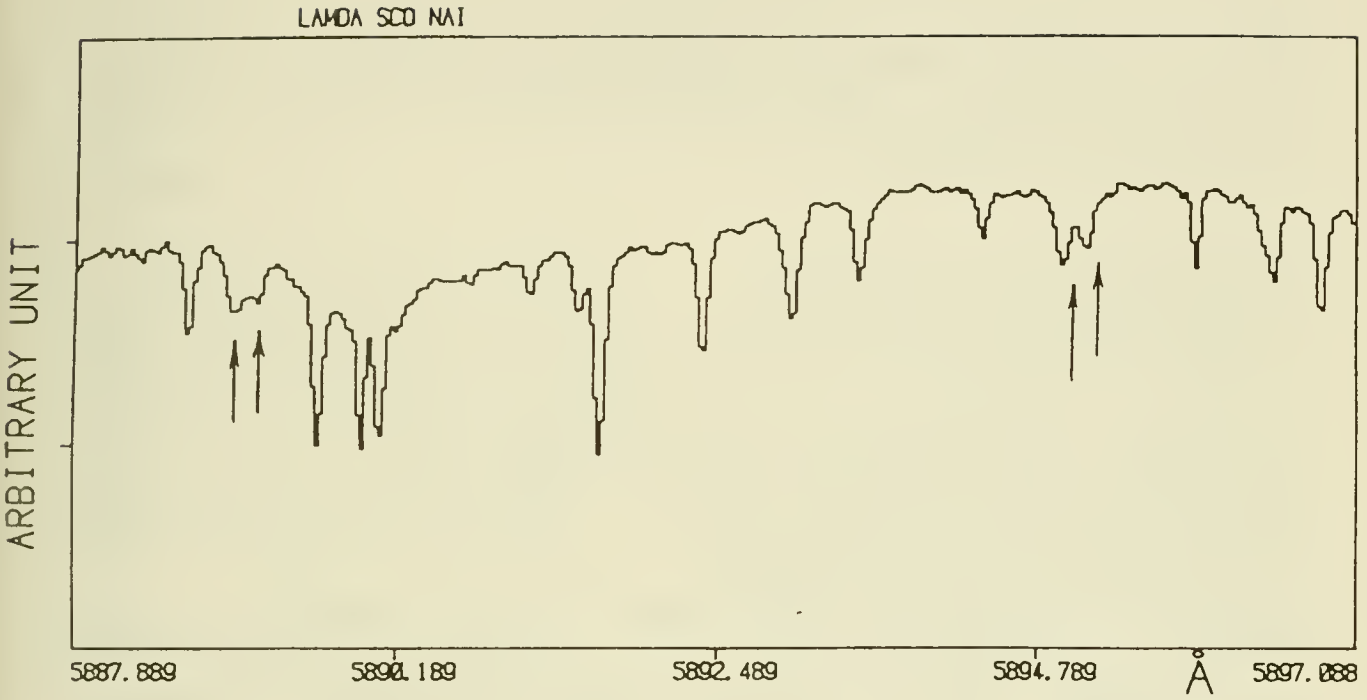

Figure 1 : Reticon spectrum of the interstellar D-lines of neutral sodium toward λ Sco, after corrections for the read-out noise and pixel to pixel sensitivity. The positions of the detected NaI absorptions are indicated. All other lines are telluric water vapor absorptions, superposed on broad stellar lines. The two interstellar lines near 5889 Å are almost uncontaminated by water vapor lines while the two corresponding ones near 5895 Å are heavily blended with two telluric lines.

III Discussion and Conclusion

Coming back to the deuterium evaluation, we now see that the λ Sco evaluation is not only related to the nearby interstellar medium but also to the LISM. It could be thus interesting to compare this value with the previous estimations of D/H in the LISM.

These estimations are very difficult due to the unknown stellar Lyman α profile of the target cool stars. Nevertheless, in the direction of α Aur, the Copernicus data are of very high quality and the conclusion of two independant groups (Dupree, Baliunas and Shipman, 1977 ; and Mc Clintock et al, 1978) are very similar, showing that at least in that direction the D/H value should be larger than $1.8\ 10^{-5}$, a more probable value beeing around $2.5\ 10^{-5}$. This result is in stricking disagreement with the λ Sco one, showing that the D/H ratio in the LISM varies by at least a factor of 2 (and more probably by a factor of 4) over a few parsecs.

Although this peculiar behaviour of the deuterium abundance in the LISM is clearly shown in at least two lines of sight, it is still difficult to

try to explain it by precise mechanisms due to lack of observational material (see some possibilities suggested by Vidal-Madjar et al, 1978). To improve the situation, more lines of sight toward nearby stars observed with Copernicus should be analysed with the profile fitting approach in order to give the component by component characteristics of the line of sight. Certainly also, one will have to wait for ST - HRS data which should improve considerably the situation.

References :

Anderson, R.C., Henry, R.C., Moos, H.W., and Linsky, J.L., 1978, Ap.J., 226, 883

Anderson, R.C., and Weiler, E.J., 1978, Ap.J., 224, 143

Austin, S.M., 1980, Prog. in Part. and Nucl. Phys.

Baliunas, S.L., and Dupree, A.K., 1979, Ap.J., 227, 870

Bertaux, J.L., 1984, these proceedings.

Bruhweiler, F.C. and Kondo, Y., 1982, Ap.J., 259, 232

Crutcher, R.M., 1982, Ap.J., 254, 82

Dupree, A.K., Baliunas, S.L., and Shipman, H.L., Ap.J., 218, 361

Ferlet, R. and Dennefeld, M., 1984, Astron. Astrophys., in press

Frisch, P.C., and York, D.G., 1983, Ap.J. Letters, 271, L59.

Gry, C., Lamers, H.J.G.L.M., and Vidal-Madjar, A., 1984, Astron. Astrophys., in press

Gry, C., Laurent, C. and Vidal-Madjar, A., 1983, Astron. Astrophys., 124, 99

Laurent, C., Vidal-Madjar, A. and York, D.G., 1979, Ap.J., 229, 923

Mc Clintock, W., Henry, R.C., Linsky, J.L., and Moos, H.W., 1978, Ap.J., 225, 465

Stokes, G.M., 1978, Ap.J. Suppl., 36, 115

Vidal-Madjar, A. and Gry, C., 1984, Astron. Astrophys., in press

Vidal-Madjar, A., Laurent, C., Bruston, P., and Audouze, J., 1978, Ap.J., 223, 589

Vidal-Madjar, A., Laurent, C., Gry, C., Bruston, P., Ferlet, R. and York, D.G., 1983, Astron. Astrophys., 120, 58

Wagoner, R.V., 1973, Ap.J., 179, 343

York, D.G., 1983, Ap.J., 264, 172

York, D.G. and Rogerson, J.B., 1976, Ap.J., 203, 378

IUE OBSERVATIONS OF THE GASEOUS COMPONENT OF THE LOCAL INTERSTELLAR MEDIUM

Daya P. Gilra
S M Systems and Research Corporation
Lanham, Md. 20706, U.S.A.

ABSTRACT

Discovery of interstellar Ge, Ga, and Kr is reported. Several intercombination lines of Fe II are detected. The depletion is most pronounced in Ca, Ti, and V. The highly ionized gas C IV and Si IV is not coextensive with the Si II and C II gas nor with the O VI gas. The molecular gas (CO) shows very small velocity dispersion (b~1 km/sec).

INTRODUCTION

About 350 high resolution IUE spectra of about 40 stars (mostly in C Ma, Ara, Scorpius and Orion Nebula) were obtained from the IUE VILSPA data bank to study interstellar absorption lines. To handle such large amounts of data, several computer programs were developed and preliminary scientific results were reported (Gilra et al. 1982a,b). In the present work a modified version of the programs was used.

RESULTS

Averaging of several spectra has helped in detecting weak lines. However, the final limitation is due to the fixed pattern noise. Highlights of the results are given below:

1. Several intercombination lines of Fe II and several Ni II have been detected. With the observations of the intercombination lines, the column densities can be easily derived since the lines are on the linear part of the curve of growth (Gilra 1982, Gilra et al. 1982b).

2. Depletion - Ca, Ti, V (and probably Sc) are the most depleted elements, the second place being taken by Cr, Mn, Fe, Co and Ni. Discovery of Ge, Ga, and Kr shows that elements with atomic number greater than 29 are very little depleted (atomic number of Zinc is 30). Elements occupying neighboring places in the periodic table show similar depletion.

3. Higher ionized species - The lines of C IV, Si IV are broad and show multiple components, often with no corresponding components in C II, Si II etc. Even in neighboring stars the C IV and Si IV lines show components at different velocities. N V lines have proved elusive with a probable detection in just one case. The C IV and Si IV gas is not coextensive with the C II and Si II gas, nor with the O VI gas.

4. Neutrals - There is a probable detection of one Fe I line. On the other hand, 6 Mg I lines have been detected (many for the first time). Apart from the much higher depletion of Fe,

the ratio [Fe I] / [Fe II] is much lower than the [Mg I] / [Mg II] ratio.

5. Recombination - An apparently unsuccessful attempt was made to detect interstellar lines from highly metastable levels of excited terms. Specifically, no line was detected from the Mg I ^3P_o level (life time = 10^{12} seconds). This fact combined with the strength of the lines from the ground level of Mg I has important bearing on the ionization, recombination and collision processes in interstellar space.

6. Molecules - A specific search for molecules other than CO was apparently unsuccessful. However, in the IUE spectrum of Zeta Oph there is an unidentified interstellar line which is almost certainly of molecular origin. Two "forbidden" $C^{12}O$ bands were also observed.

CONCLUDING REMARKS

HD 149404 has the richest interstellar spectrum (except molecules) of all the stars in this study. Ground-based work will be very useful. In particular, one should look for Zr II, Sc II, Y II, Rb I, and Fe I resonance lines, and, Mg I metastable lines near 3850 Å.

HD 147889, the heavily obscured star in the Rho Oph cloud, has the strongest interstellar CO spectrum. Noisy nature of the spectra precludes detection of other molecules. Space Telescope (ST) observations will be very useful.

Space Telescope high resolution spectrograph observations will resolve many blends, even of C IV and Si IV lines.

Interstellar CO line observations, e.g., in HD 147889, will be very useful in determining the instrumental profile of the ST high resolution spectrograph.

REFERENCES

Gilra, D.P., Pwa, T.H., Arnal, E.M., and Vries, J.de 1982a, in Proceedings of the Third European IUE Conference, Madrid, ESA Special Publication, ESA SP 176. pp 385-390.

Gilra, D.P., Pwa, T.H., and Arnal, E.M. 1982b, in ibid, pp 391-397.

Gilra, D.P. 1982, in ibid, pp 139-141.

VOYAGER EUV AND FUV OBSERVATIONS

J.B. Holberg
Lunar and Planetary Laboratory, University of Arizona

ABSTRACT

The Voyager 1 and 2 ultraviolet spectrometers are sensitive over the wavelength range 500 to 1700 A. In the EUV, at wavelengths shortward of the Lyman limit (912 A), Voyager observations have detected emission from three out of a sample of 11 nearby hot DA white dwarfs. These observations imply very low HI column densities in the directions of the three stars detected. In the FUV, at wavelengths between 912 and 1200 A, Voyager observations of O and B stars can be used to study interstellar reddening at the shortest wavelengths and to provide useful estimates of interstellar H_2 column densities.

INTRODUCTION

The ultraviolet spectrometers aboard the two Voyager spacecraft provide several unique means of exploring the local interstellar medium. Routine access to the 500 to 912 A region of the extreme ultraviolet (EUV) allows the use of nearby hot stellar sources as a probe of local neutral hydrogen column densities. A comprehensive set of observations of luminous O and B stars in the far UV (FUV) between 912 and 1200 A offers the possibility of systematically studying reddening at the shortest observable wavelengths. Because of the strong and characteristic band absorption from the H_2 molecule at these wavelengths, these same observations hold the promise of measuring interstellar H_2 column densities.

EUV OBSERVATIONS.

Observations of hot nearby subluminous stars in the EUV can be used to obtain local HI column densities. Meaningful results however, require the existence of lines of sight having very low HI column densities ($N_{HI} \lesssim 5 \times 10^{18}$ cm^{-2}). In this regard observations of hot white dwarfs have been especially important. Of the four sources initially detected with the Apollo-Soyuz EUV telescope two, HZ 43 (Margon et al. 1976a) and Feige 24 (Margon et al. 1976b), were determined to be hot DA white dwarfs.

The 500 to 912 A EUV capabilities of the Voyager 1 and 2 spacecraft have been used to survey a sample of nearby hot white dwarfs. A list of the DA white dwarfs surveyed along with their temperatures, distances and galactic coordinates is contained in Table 1. Of these eleven objects, three exhibit detectable continua shortward of 912 A (Fig. 1). Voyager 2 EUV observations of HZ 43 (Holberg et al. 1980a) indicate a column density of $N_{HI} = 3.9 \times 10^{17}$ cm^{-2} for this white dwarf. An interesting comparsion of HZ 43 with a nearly identical white dwarf GD 246 is shown in Figure 2. Here the FUV count rate spectra of both stars are virtually indistinguishable while only HZ 43 shows a measurable EUV continuum. Since there is no detectable EUV emission from GD 246 it is only possible to place a lower limit on the HI column density ($N_{HI} > 1.5 \times 10^{18}$). It is interesting to note however that GD 246 was detected as an Einstein soft X-ray source (Petre et al. 1983). The HI column density along its line of sight therefore cannot be much in excess of the above quantity,

and in fact could be easily determined by simple comparison with the HZ 43 soft X-ray flux.

Voyager observations have yielded two new EUV sources, G191 B2B (Holberg et al. 1980b) and GD 153. For G191 B2B the estimated N_{HI} column density is 10^{18} cm^{-2}. The corresponding preliminary value for GD 153 is 6 x 10^{17} cm^{-2}. Two interesting comments can be made concerning GD 153. First, GD 153 is separated from HZ 43 by only 8.3 of arc and lies at approximately the same distance so that it almost certainly is within the same low HI window in the ISM. Second, this star has also been identified as an Einstein soft X-ray source (Kahn et al. 1983) so that its entire EUV spectrum is potentially observable with future EUV instrumentation.

A survey of over 50 of the brighter subluminous objects has been conducted with Voyager. These observations include DO white dwarfs (PG 1034+001, HD 149499B, etc.), hot central stars of planetary nebulae (NGC 246, NGC 7293, etc.), and hot O and B subdwarfs (BD +28 4211, Feige 34, etc.). No EUV emission has been detected from any of these objects. Of particular interest are Voyager observations of cataclysmic variables in outburst. On the basis of soft X-ray and UV observations, it has been proposed (Córdova and Mason 1982) that the bulk of the outburst energy from cataclysmic variables such as SS Cyg and U Gem could be emitted in the EUV. This, in conjunction with the Apollo-Soyuz detection of SS Cyg at ~100 A (Margon et al. 1978) has led to the expectation that cataclysmic variables might represent a large class of EUV sources. Voyager has observed three cataclysmic variables in outburst, SS Cyg, U Gem and VW Hyi. No EUV emission (integrated flux < 2 x 10^{-11} ergs cm^{-2} s^{-1}, between 540 and 740 A) is detected. Descriptions of the SS Cyg and U Gem observations are contained in Polidan and Holberg (1984). In the case of U Gem this EUV upper limit can be translated into a highly model dependent lower limits on the HI column of 10^{17} to 10^{18} cm^{-2} compared with an upper limit of N_H < 5 x 10^{18} cm^{-2} derived from soft X-ray observations (Córdova et al. 1984). The failure to detect any of the cataclysmic variables in the EUV with Voyager is significant but perhaps even more important are the Voyager FUV observations (Polidan and Holberg 1984) which indicate a substantial flattening of the outburst energy distributions of all three objects below 1200 A. The clear implication of these observations is that little intrinsic EUV flux is actually emitted and that the FUV and soft X-ray fluxes arise from separate regions. Thus while cataclysmic variables may represent significant sources at 100 or 200 A, they have a diminished prospect for detection at longer wavelengths.

FUV OBSERVATIONS.

In addition to the Voyager observations of the subluminous stars discussed in the previous sections there exists a large body of observational data on luminous O and B stars. While none of these objects exhibits any detectable EUV emissions, the ability to observe down to the Lyman limit represents a unique opportunity to explore the effects of interstellar extinction below 1200 A. The only data currently available at these wavelengths is a study involving four, reddened-unreddened, pairs of stars observed with Copernicus (York et al. 1973). In Figure 3 we show an extinction curve derived from Voyager 2 of one pair of the stars observed by Copernicus (ξ Per and 15 Mon). Compared with this observation are the extinction data of York et al. and older OAO-2 data. Over most of the wavelength range agreement is good, as might be expected. Shortward of 1140 A however, the results diverge with Voyager extinctions lying higher than the Copernicus measurements. The simple explanation for this divergence is that at the spectral resolution of Voyager (~25 A) it is not possible to

distinguish narrow bands of continuum which are free from absorption due to interstellar H_2 bands. In effect extinction, as measured by Voyager, has two components, absorption due to interstellar dust and interstellar H_2. In spite of the fact that what is being measured is a low resolution convolution of absorption due to both dust and H_2, initial analysis has shown that a separation of these two components is practical through modeling. This separation is aided by the fact that, at Voyager resolution, H_2 absorption has a characteristic wavelength dependence which manifests itself in a broad 'absorption trough' centered on 1000 A.

REFERENCES

Córdova, F.A., and Mason, K.O. 1982, in Accretion Driven Stellar X-ray Sources, (ed. Levin, W.H.G. and van den Heuvel, E.D.J.).
Córdova, F.A., et al. 1984, Ap. J. (in press).
Holberg, J.B. et al. 1980a, Ap. J. (Letters), 242, L119.
Holberg, J.B., Forrester, W.T., and Broadfoot, A.L. 1980b, Bull. AAS, 12, 872.
Holberg, J.B., and Wesemael, F. 1984, Future of Ultraviolet Astronomy (NASA CP) (in press).
Holberg, J.B., Wesemael, F., and Hubený, I. 1983, Ap. J. (in press).
Kahn, S.M. et al. 1983, Ap. J., 278, 255.
Koester, D., Schultz, H., and Weidemann, V. 1979b, Astron. Ap., 76, 262.
Margon, B., et al. 1976a, Ap. J. (Letters), 203, L25.
Margon, B., et al. 1976b, Ap. J., 210, L79.
Margon, B., et al. 1978, Ap. J., 224, 167.
McCook, G.P., and Sion, E.M. 1984, Villanova Univ. Obs. Contribution No. 3.
Petre, R., Shipman, H.L., and Canizares, C.R. 1983, Bull. AAS, 15, 655.
Polidan, R.S., and Holberg, J.B. 1984, Nature (in press).
York, D.G., et al. 1973, Ap. J. (Letters), 182, L1.

TABLE 1

Voyager Observations of DA White Dwarfs

	Object	Type	T_{eff} (K)[1]	V	ℓ^{II}, b^{II}	D (pc)[2]	S/C[3]	EUV[4]	Ref.
1.	CoD–38°10980	DA2	24,700	11.00	342,7	15	2	--	
2.	Sirius B	DA2	27,000	8.30	227,-9	2.7	1,2	<2.6	Holberg, Wesemael, Hubený (1984)
3.	EG 118	DA2	31,400	13.45	359,24	40	2	--	
4.	GD 394	DA2	33,000	13.09	91,1	30	1	--	
5.	GD 71	DA1	34,800	13.06	192,-5	45	1	--	
6.	GD 659	DA1	38,500	13.36	299,-84	40	1,2	--	Holberg and Wesemael 1984
7.	GD 153	DA1	50,000	13.42	317,85	40	1,2	0.8	
8.	HZ 43	DA0	55,000	12.86	54,84	63	1,2	3.8	Holberg et al. 1980a
9.	GD 246	DA0	55,000	13.11	87,-45	40	1,2	<0.3	
10.	G191 B2B	DA0	62,500	11.78	156,7	48	1,2	3.5	Holberg et al. 1980b
11.	Feige 24	DA0	70,000	12.25	166,-50	90	1,2	?	

Notes
1. Temperatures determined from either Koester, Schultz and Weidemann (1979) or Voyager FUV fluxes.
2. Distances are from either measured parallaxes or absolute magnitudes (McCook and Sion, 1984).
3. Voyager 1 or 2.
4. Measured integrated EUV flux in the 540 to 740 Å band in units of 10^{-10} ergs cm^{-2} s^{-1}. No entry implies a preliminary upper limit of 5×10^{-11} erg cm^{-2} s^{-1}.

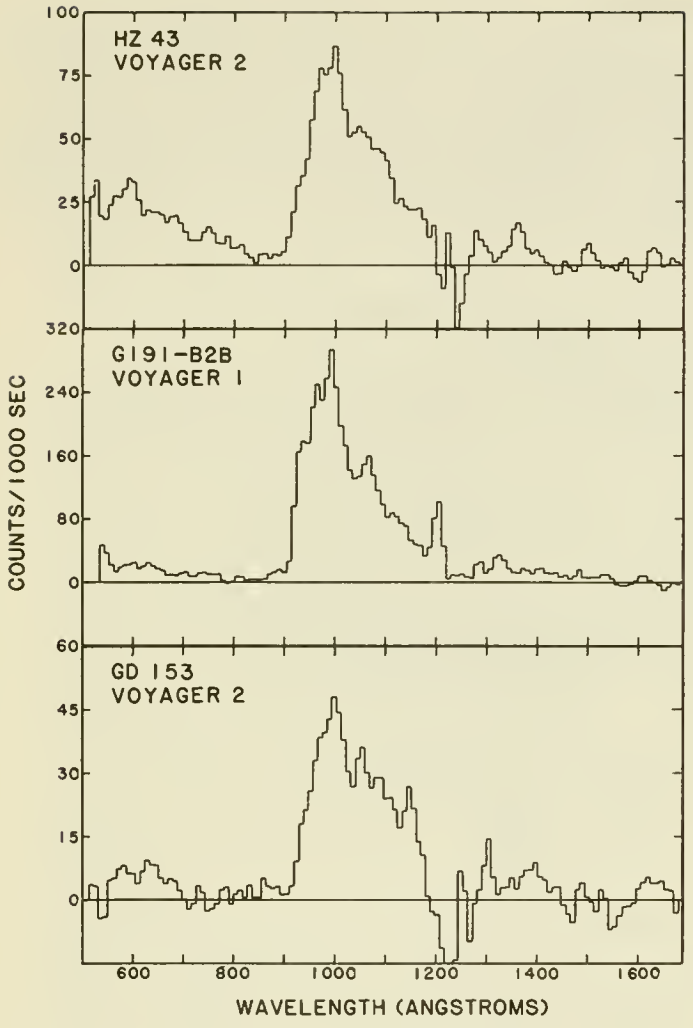

Fig. 1.--A comparison of the count rate spectra for the three hot white dwarfs which have been detected between 500 and 912 A by Voyager.

Fig. 2.--A comparison of two very similar hot white dwarfs, HZ 43 and GD 246, as observed with Voyager 2. Longward of 912 A the two stars are virtually identical. Shortward of 912 A HZ 43 shows strong EUV emission, which is due to the low HI column density in the direction of HZ 43 ($N_{HI} = 3.9 \times 10^{17}$ cm^{-2}). For GD 246 the corresponding HI column must be greater than 2.8×10^{18} cm^{-2}.

Fig. 3.--The interstellar extinction curve determined for a reddened (ξ Per) and unreddened (15 Mon) pair. Here a Voyager based determination (histogram) is compared with the data of York et al. (1973) (light dots) from Copernicus. The heavy dots correspond to earlier OAO-2 data. The Voyager data is in agreement with that of Copernicus down to ~1140 Å where the effects of absorption of the H_2 bands become significant. The Copernicus reddening determination was derived from high resolution data obtained between the H_2 band features. Voyager data include H_2 absorption blended with the effects of reddening from interstellar dust. Through modeling these two components can be separated in Voyager data and the interstellar reddening curve extended out to the Lyman limit and useful measurements of H_2 columns obtained.

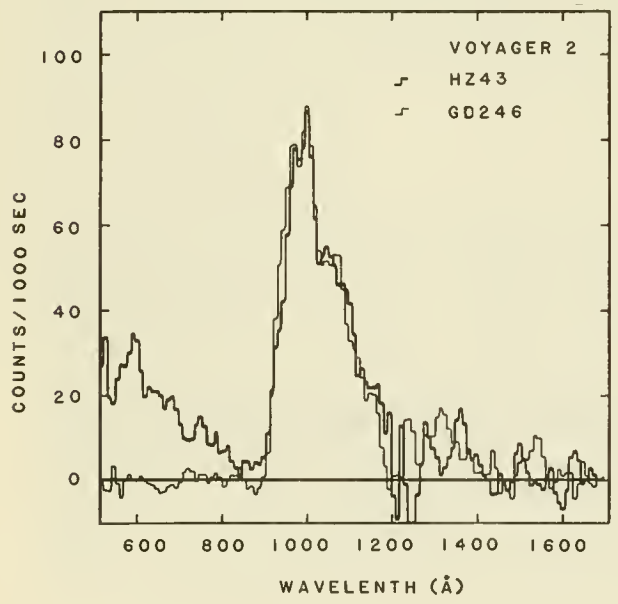

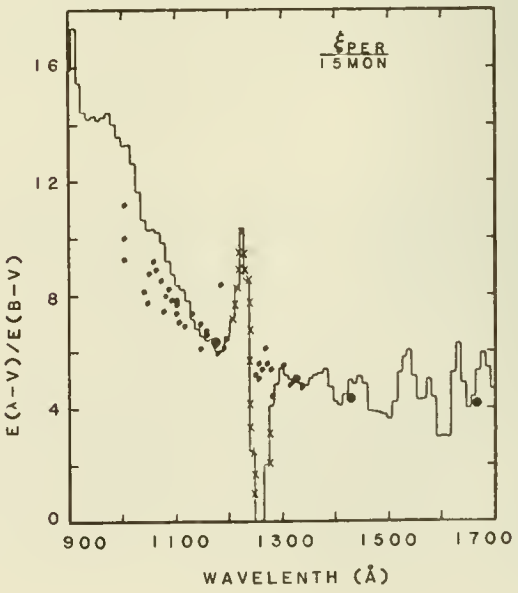

THE LISM AT OPTICAL WAVELENGTHS: SPECTRAL LINE STUDIES

OPTICAL EMISSION LINE STUDIES

AND

THE WARM, IONIZED COMPONENT OF THE LOCAL INTERSTELLAR MEDIUM

R. J. Reynolds

Physics Department, University of Wisconsin-Madison

Abstract

Observations of diffuse, galactic Hα, [NII]λ6583, and [SII]λ6716 emission lines provide evidence for a warm ($\sim 10^4$ K), primarily ionized component of the interstellar medium distributed throughout the galactic disk. This component of the interstellar gas has an electron density $\approx$ 0.1-0.2 cm^{-3} and occupies about 10-30% of the interstellar volume. Interstellar Hα emission near the galactic poles, the dispersion measure of a nearby pulsar, and observations of interstellar gas flowing into the solar system indicate that this ionized component is an important constituent of the interstellar medium in the solar neighborhood. The intensity of the Hα background at high galactic latitudes implies that this component is maintained by an average hydrogen ionization rate in the vicinity of the Sun of (2-4) x 10^6 s^{-1} per cm^2 of galactic disk. The emission measure is 1.3-2.3 cm^{-6} pc toward the galactic poles. The sources of this ionization have not yet been identified but may include escaping Lyman continuum radiation from planetary nebulae, hot white dwarfs, and early type stars. Investigations of the regions surrounding ζ Oph (O9V), the nearest (d ≈ 140 pc) O star, and α Vir (B1 IV), one of the nearest (d ≈ 87 pc) early B stars, have revealed areas of enhanced Hα emission extending 6°-12° from each star. However, it appears that these stars do not contribute significantly to the more diffuse ionization within the local interstellar medium.

I. INTRODUCTION

Diverse observations of the interstellar medium have provided evidence for significant ionization of the interstellar gas outside bright, localized HII regions. These observations include pulsar dispersion measures (e.g., Taylor and Manchester 1977), free-free absorption of low frequency galactic radio emission (Ellis 1982), ultraviolet absorption lines (e.g., York 1983), and faint, optical interstellar emission lines (Reynolds, 1980). The development of the large aperture Fabry-Perot spectrometer (Roesler et al. 1978) has made it possible to

detect and study very faint Hα, [NII], and [SII] emission from the diffuse interstellar medium. These emission lines have provided strong evidence for widespread regions of warm ($\simeq 10^4$ K), nearly fully ionized hydrogen distributed throughout the galactic disk.

Observations near the galactic equator (e.g., Reynolds 1983) reveal emission in every direction with a typical intensity (between the relatively bright, discrete emission regions) of about 1.3×10^{-6} ergs cm^{-2} s^{-1} sr^{-1}, while observations at higher latitudes (Reynolds 1984a) suggest that galactic Hα emission extends over the entire sky with an intensity that falls to $1.2\text{-}2.4 \times 10^{-7}$ ergs cm^{-2} s^{-1} sr^{-1} near the galactic poles. Although interstellar grains may scatter Hα photons from bright HII regions located near the galactic plane (Jura 1979), Hα observations toward high latitude reflection nebulae indicate that the intensity of this scattered component is small compared to the total background Hα intensity that is observed (Reynolds, Scherb, and Roesler 1973). Additional strong evidence that such scattered light is not a dominant source of background emission has been provided by the recent discovery that the [SII]λ6716/Hα intensity ratios in the diffuse background are approximately three to four times higher than the ratios found in the classical bright HII regions (Reynolds and Shih 1983).

The detection of the collisionally excited [NII]λ6583 and [SII]λ6716 emission in the galactic background places a lower limit of about 3000 K on the temperature of the emitting gas. If the H^+, N^+, and S^+ ions are well mixed within the ionized regions, then the observed widths of the emission lines indicate a temperature $\sim 10^4$ K (Reynolds, Roesler, Scherb 1977; Reynolds 1984b, in preparation). The absence of detectable [OI]λ6300 and [NI]λ5200 (Reynolds 1981; Reynolds, Roesler, and Scherb 1977) suggests a high fractional ionization of hydrogen (i.e., $H^+/H \gtrsim 0.75$). A typical electron density of 0.1-0.2 cm^{-3} within an ionized region has been derived from a comparison of emission measures and pulsar dispersion measures (Reynolds 1977). This analysis also indicates that the ionized component occupies about 10-30% of the interstellar volume.

II. THE Hα BACKGROUND AT HIGH GALACTIC LATITUDES

a) The Hα Intensity Distribution and The Emission Measure of the Galactic Disk Near the Sun

The Hα background near the galactic equator appears to originate from gas within the galactic disk that is distributed out to 3 kpc or more from the Sun (Reynolds 1983). On the other hand, observations at high galactic latitudes sample interstellar material that is more local to the Sun. A study of galactic Hα intensities at high latitudes has recently been carried out (Reynolds 1984a), and a summary of the results as they relate to the local Solar neighborhood are discussed below (Sections IIa, b).

Scans of the Hα were obtained toward 72 high galactic latitude pulsars as part of a program to compare emission measures and dispersion measures along lines of sight through the interstellar medium (in preparation). These observations include all of the pulsar directions listed by Manchester and Taylor (1981) that have galactic latitudes $|b| > 5°$ and declinations between -10° and +74°. (The siderostat which feeds the spectrometer cannot access declinations greater than +74°). Two additional scans that are not toward known pulsars were obtained near the north galactic pole. Figure 1 shows the distribution of observation directions in galactic coordinates. The galactic Hα intensity I_α for each of the 74 directions is plotted versus galactic latitude in Figure 2. The intensities are in rayleighs (R), where 1 R = 2.4×10^{-7} ergs cm^{-2} s^{-1} sr^{-1} at Hα. The open symbols in Figure 2 denote directions toward or within 5° of emission nebulosity that is visible on the Palomar Sky Survey red prints or on the photographic surveys of Sivan (1976) and Parker, Gull, and Kirshner (1979), and thus indicate directions that may not be sampling truly "background" Hα. The very large scatter in intensity within this subset of the data is evidence for significant contamination by discrete HII regions along some of the lines of sight. All except two of these potentially contaminated directions have galactic latitudes < 15°. The remaining "background" directions have Hα intensities that range from about 4-8 R for $|b| < 10°$ to about 1 R or a little less at $|b| > 50°$.

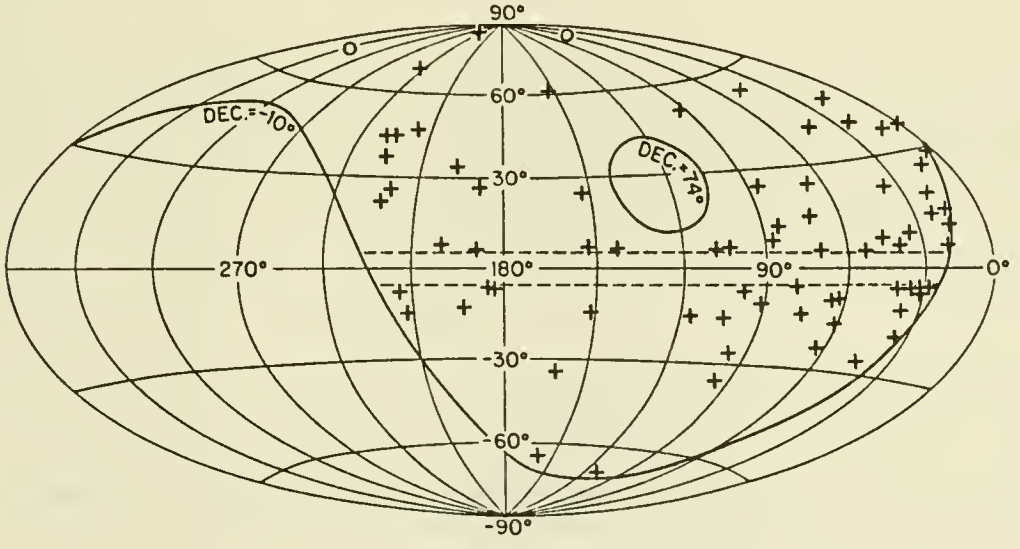

Fig. 1 - Directions of the high galactic latitude Hα scans. The map is in galactic coordinates centered on $\ell = 180°$, $b = 0°$. The crosses represent directions toward pulsars and the two open circles represent additional very high latitude Hα observations which are not part of the pulsar survey.

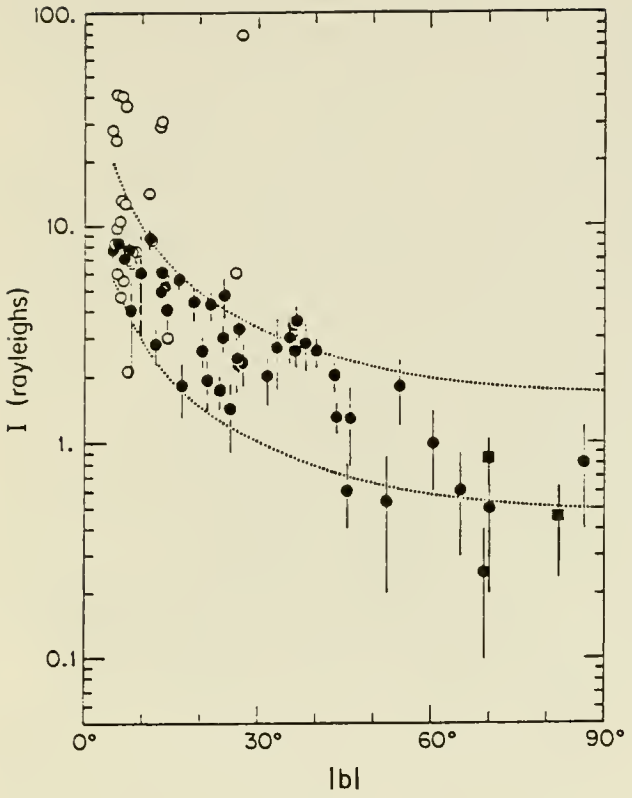

Fig. 2 - The Hα intensity in rayleighs (R) plotted versus the galactic latitude of the observation direction. The open circles represent directions toward or within 5° of emission nebulosity visible on photographic surveys. The squares represent the two additional very high latitude observations that are not part of the pulsar survey. The two dashed curves indicate the expected variation of intensity with galactic latitude for a uniformly emitting galactic disk with $I_\alpha \times \sin|b|$ = 0.5 R and 1.7 R and no extinction. 1 R = 2.42×10^{-7} erg cm^{-2} s^{-1} sr^{-1} at Hα or $10^6/4\pi$ photons cm^{-2} s^{-1} sr^{-1}.

The general decrease in Hα intensity with increasing latitude for $|b| > 10°$ is consistent with a disk-like distribution of the emitting gas, although the considerable scatter in intensities at any one value of $|b|$ suggests that the distribution is not entirely uniform. The two dashed curves in Figure 2 represent the expected variation of Hα intensity with galactic latitude for a uniformly emitting disk with values for $I_\alpha \times \sin|b|$ of 0.5 R and 1.7 R (and no extinction). These curves appear to bracket the data well. The clumping of data points near $I_\alpha \times \sin|b| \simeq 1.7$ R for $30° < |b| < 40°$ and near $I_\alpha \times \sin|b| \simeq 0.6$ R for $|b| > 60°$ could be merely statistical fluctuations in the small sample, or it may be an indication of large-scale features in the galactic Hα intensity distribution at high latitudes. Systematically lower values for $I_\alpha \times \sin|b|$ at $|b| > 60°$, for example, would occur if the Sun were located in a region of the interstellar medium with a lower than average Hα emissivity. More detailed information about the smaller scale distribution of diffuse emission at high latitudes will have to await a more intensive Hα mapping program.

The radius of the region surrounding the Sun within which the Hα emission at a given latitude originates depends upon the scale height of the emitting gas. Pulsar observations indicate a scale height of

500-1000 pc for the density n_e of free electrons (Bridle and Venugopal 1969; Readhead and Duffett-Smith 1975). These electrons appear to be closely associated with the Hα emitting regions (Reynolds 1984a). If n_e decreases exponentially with increasing height z above the galactic plane, then the Hα emission from this gas would originate from a region with a scale height of H/2, since the Hα emissivity is proportional to n_e^2. This suggests that the emission at galactic latitude $|b| \gtrsim 60° - 70°$ is from gas located primarily within a cylinder of radius 150 pc centered on the Sun. Therefore, the mean value of $I_\alpha * \sin|b|$ from all the data in Figure 2 appears to be $\approx$ 1 R with some evidence that the value decreases to $\approx$ 0.6 R within the more local 150 pc radius region surrounding the Sun. These values correspond to emission measures EM along a line of sight perpendicular to the galactic disk of 4.5 cm^{-6} pc and 2.7 cm^{-6} pc, respectively. A comparison of the emission measure with the estimated column density of electrons $N_e \approx 1.5 \times 10^{20}$ cm^{-2} through the galactic disk in the Solar neighborhood (e.g., Harding and Harding 1982) indicates a mean electron density $n_e \approx 0.11\text{-}0.18$ cm^{-3} within the ionized regions near the galactic plane.

b) The Hydrogen Recombination Rate and Possible Sources of Ionizing Radiation in the Local Interstellar Medium

The Hα intensity near the galactic poles provides a direct estimate of the hydrogen recombination rate r_g per cm^2 of galactic disk in the vicinity of the Sun. Specifically,

$$r_g = \frac{8\pi I_\alpha}{\varepsilon} ,$$

where I_α is the galactic Hα intensity (in photons cm^{-2} s^{-1} sr^{-1}), and ε is the average number of Hα photons produced per hydrogen recombination. The value of ε changes slowly with electron temperature and ranges from about 0.57 to 0.37 for temperature between 1250 K and 80,000 K, respectively (case B, Pengelly 1964). Therefore, the results presented in Section IIa indicate that $r_g \approx (2.4\text{-}4.0) \times 10^6$ s^{-1} cm^{-2} for the region of the galactic disk within 150 pc of the Sun. In steady state r_g must equal the hydrogen ionization rate.

This rate places an important constraint on the possible sources of ionizing radiation in the Solar neighborhood. Table 1 lists the ionizing fluxes per cm^2 of galactic disk of known sources of ionizing radiation averaged over a region within about 3 kpc of the Sun. The fluxes listed in Table 1 are upper limits on the amount of radiation that is actually available to ionize the diffuse interstellar medium, since some radiation may be absorbed by gas in the immediate vicinity of the source (e.g., to form a classical HII region) or may escape the galaxy entirely (X-rays). Each absorbed photon will produce approximately one hydrogen ionization in a nearly fully-ionized gas (Shull 1979). Only O-stars and perhaps planetary nebula nuclei have ionizing photon fluxes equal to or greater

TABLE 1

SOURCES OF IONIZING RADIATION

Source	Lyman Continuum Flux (10^6 photons s^{-1} per cm^2 of disk)	Reference
O stars	10–29	1, 2, 3
W-R stars	1.6	3
B stars	0.5–1	1, 2, 3
PN nuclei and white dwarfs	0.4–4	1, 4, 5
Supernovae	0.7	6, 7
QSOs	0.2	8, 9
Cosmic rays	0.008–0.08 [a]	10
X-rays ($h\nu \geq 0.1$ keV)	0.002	11

[a] Estimated number of hydrogen ionizations s^{-1} per cm^2 by cosmic rays ($\times 10^{-6}$).

REFERENCES.—(1) Terzian 1974. (2) Torres-Peimbert, Lazcano-Araujo, and Peimbert 1974. (3) Abbott 1982. (4) Salpeter 1978. (5) Hills 1973. (6) Chevalier 1974. (7) McKee and Ostriker 1977. (8) York 1982. (9) Paresce and Jakobsen 1980. (10) Spitzer and Jenkins 1975. (11) McCammon *et al.* 1983.

than the observed recombination rate. If O-stars are the primary source of the ionization, it remains to be determined how a significant fraction ($\gtrsim$ 10%) of the hydrogen ionizing radiation from these stars can escape the immediate vicinity of the stars and travel long distances through the interstellar medium. For example a line of sight through the galactic poles passes no closer than about 140 pc from the nearest O-star, ζ Oph (see Section IV). On the other hand, if the Lyman continuum flux from the central stars of planetary nebulae and hot white dwarf stars is near the high end of the range listed in Table 1 and if most of this radiation escapes the nebulae as has been suggested by Terzian (1974), then these older stars could be the primary source of the ionization for gas in the Solar neighborhood. Although B-stars, supernovae, and QSO's may not be able individually to account for the ionization rate, their combined effect ($< 2 \times 10^6$ s^{-1} cm^{-2}) could be significant if a large fraction of the ionizing radiation from each of these sources were absorbed in the diffuse interstellar medium. High resolution maps of the Hα background in regions which contain nearby planetary nebulae, hot white dwarfs, O and B stars may reveal surrounding ionization and thus may help to determine the importance of such sources for the ionization of the local interstellar gas (see Section IV).

III. EVIDENCE FOR WARM, IONIZED GAS IN THE LOCAL INTERSTELLAR MEDIUM FROM PULSAR AND UV BACKSCATTER OBSERVATIONS

While optical emission line observations supply useful information about the temperature, fractional ionization, emission measure, and ionization rate within the diffuse, ionized component, they provide very little information about the precise location of the ionized gas. For example, all of the Hα background near the galactic poles could originate from gas at z-distances > 100 pc. It is even tempting to speculate that a possible decrease in the value of $I_\alpha \times \sin|b|$ for $|b| > 60°$ (Section IIa) could be explained by a deficiency of ionized gas within about 150 pc of the Sun, displaced perhaps by the hot, x-ray emitting gas. However, the dispersion measure of a nearby pulsar and backscattered solar UV radiation in the interplanetary medium provide strong evidence that a substantial amount of ionized gas is present within the local interstellar medium.

A distance of 127 ± 13 pc has been determined for PSR 0950+08 by Gwinn et al. (1984) using the parallax method. This pulsar has galactic coordinates $\ell = 228°.9$, $b = +43°.7$ and a dispersion measure of 2.97 cm^{-3} pc. Therefore, along the line of sight to the pulsar the mean electron density $\langle n_e \rangle \simeq 0.023$ cm^{-3}, which is comparable to the mean electron density in the galactic disk (0.025 - 0.03 cm^{-3}) derived from much more distant pulsars (Weisberg, Rankin, and Borakoff 1980). It should also be noted that PSR 0950+08 is located in a quadrant in which the mean neutral hydrogen density appears to be < 0.01 cm^{-3} (Paresce 1984; Frisch and York 1983). If the ionized regions have an electron density $n_e \gtrsim 0.1$ cm^{-3} (see below), then they occupy $\gtrsim 30$ pc or $\gtrsim 24\%$ of the line of sight to PSR 0950+08. This suggests that a significant fraction of the local interstellar medium may be occupied by ionized hydrogen and that for some lines of sight the column density of H^+ may exceed that of H°. Salter, Lyne, and Anderson (1979) derived a distance of about 50 pc for PSR 1929+10, which has a dispersion measure of 3.2 cm^{-3} pc. If this distance is correct, then $\langle n_e \rangle \gtrsim 0.064$ cm^{-3} along the line to this pulsar ($\ell = 47°.4, b = -3°.9$). However, the validity of this distance is in some doubt (Backer and Sramek 1982).

Evidence that warm, ionized interstellar gas is present in the immediate vicinity of the Sun is provided by the hydrogen and helium Solar Lα backscatter results on gas flowing into the solar system. An analysis by Weller and Meier (1981) indicates that immediately outside the Solar system this interstellar gas has a temperature near 10^4 K, a neutral hydrogen density of 0.05 ± 0.01 cm^{-3} and a neutral helium density of 0.019 ± 0.008 cm^{-3}. They have suggested that the departure of the H° : H°_e ratio from its cosmic value can be explained if most (∼ 75%) of the hydrogen is ionized. This interpretation is supported by the results of Bobroff, Nousek, and Garmire (1984), who concluded that the failure to detect HeII 304 Å emission from Capella could be explained if the hydrogen ionization fraction is greater than 40% along the line to the star (distance ≃ 14 pc). These results indicate that in the immediate vicinity

of the Sun there exists a region of ionized gas with $n_e \gtrsim 0.1$ cm^{-3} and $T \gtrsim 10^4$ K. This gas therefore appears to be part of the same widespread, ionized component that is revealed by the Hα and pulsar data.

IV. O and B STAR HII REGIONS IN THE LOCAL ISM

In order to investigate the effect of O and B stars on the ionization of the local interstellar gas, Hα scans were obtained in the regions surrounding α Vir(B1 IV+B2 V), one of the nearest (d = 87 pc) early B stars, and ζ Oph (O9 V), the nearest (d = 140 pc) O star. The observations reveal significant Hα intensity enhancements in the vicinity of each star. The ζ Oph HII region extends over an 8° x 12° region and has an emission measure of about 400 cm^{-6} pc and an electron density of 3.8 cm^{-3} near the star (Reynolds and Ogden 1982). The H^+ column density through the region is expected to be approximately 3 x 10^{20} cm^{-2}. The total hydrogen recombination rate within the region is estimated to be 1.8 x 10^{48} s^{-1}, which is close to the predicted Lyman continuum flux of an O9 V star (Panagia 1973). Thus most of the ionizing flux appears to be absorbed in the immediate vicinity (within 15 pc) of the star.

Twenty-nine Hα scans were obtained in the region surrounding α Vir. The resulting Hα intensities are displayed as a contour map in Figure 3. The HII region has an extent of 14° x 18° and an emission of about 8 cm^{-6} pc near

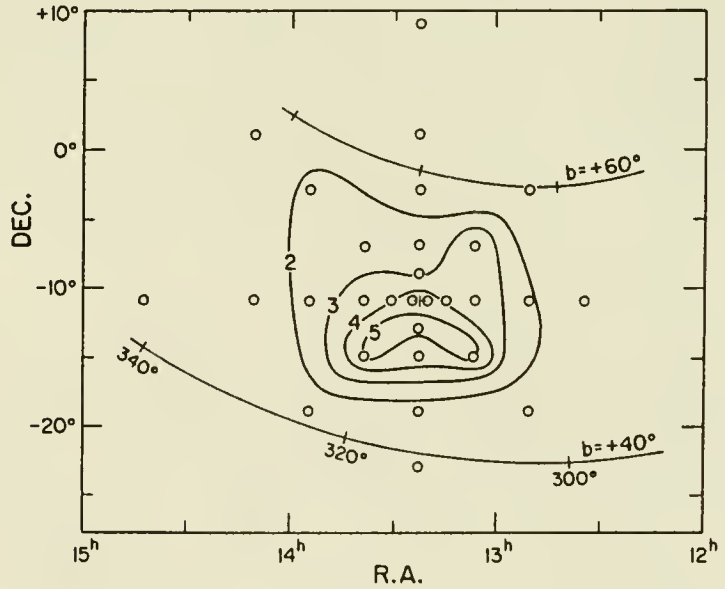

Fig. 3 - An Hα intensity contour map of the region surrounding α Vir. The open circles represent the location and field of view of the Hα scans. The contour values are in rayleighs (R). A galactic background Hα intensity of about 1.3 R near α Vir is indicated from the scans located outside the 2 R contour.

the star (above a background emission measure of about 3 cm^{-6} pc). The region appears asymmetric with the brightest emission toward and south of α Vir. The radial velocity of the region is -6.1 ± 1.0 km s^{-1} with respect to the LSR (-9.8 ± 1.0 heliocentric), and the width of the Hα emission component is 21.2 ± 1.5 km s^{-1}. The electron density within this 25 pc diameter region is $\gtrsim$ 0.58$f^{-1/2}$ cm^{-3} (where f is the fraction of the HII region's volume occupied by ionized gas), and the H^+ column density through the region is thus $\gtrsim$ 4 x $10^{19}f^{1/2}$ cm^{-2}. The total hydrogen recombination rate within the HII region is estimated to be 2.0 ± 0.7 x 10^{46} s^{-1}, which is larger than the total Lyman continuum flux ($\simeq$ 5.8 x 10^{45} s^{-1}) expected from a B1 IV + B2 V system (Panagia 1973). The factor of 3.5 discrepancy could be accounted for if α Vir had a slightly earlier spectral type (e.g., BO.7 IV instead of B1 IV) and/or its distance were less than 87 pc. In any case it appears that nearly all of the star's ionizing radiation is absorbed within its HII region and thus is not available to contribute to the ionization of the more diffuse component of the local interstellar medium.

The outer Hα intensity contour in Figure 3 is nearly coincident with a hole on the Berkeley 21-cm emission survey maps at radial velocities near 0 km s^{-1} (LSR). Also, the 21-cm maps centered near -6 km s^{-1} show the edge of a large HI feature just south of α Vir, where the Hα emission from the HII region is brightest. These coincidences suggest that the HII region surrounding α Vir is associated with the large, arch-like HI complex which extends up from the galactic plane at 0° to 20° longitude. The distance of this complex is therefore about 87 pc.

The Gum nebula, a 250 pc diameter region ionized by ζ Pup and γ Vel (Reynolds 1976a,b), and the equally large Orion-Eridanus shell ionized by the I Ori O-association (Reynolds and Ogden 1979) are two HII regions which may influence the local interstellar medium even though they are outside the arbitrarily defined 150 pc distance limit. Both regions have outer boundaries that appear to extend to within 300 pc of the Sun in the longitude interval 190° to 275°. This is the quadrant in which extremely low H° column densities (< 5 x 10^{18} cm^{-2}) are observed out to distances of at least 200 pc (e.g., Paresce 1984, and Figure 4 below). These two regions could be partially responsible for these low H° column densities if the boundaries of the regions extend somewhat closer to the Sun than their projection on the sky suggests, or if the regions are density bounded with a significant Lyman continuum flux escaping into the surrounding low density medium.

V. SUMMARY AND CONCLUSIONS

Observations of faint optical emission lines and pulsar dispersion measures provide evidence for a warm (10^4 K), ionized component of the interstellar medium which has an electron density of 0.1-0.2 cm^{-3}, and occupies $\gtrsim$ 10% - 30% of the interstellar volume. The dispersion measure of a nearby pulsar, the observations of interstellar hydrogen and helium

in the interplanetary medium, and UV observations toward Capella indicate that this ionized component is an important constituent of the local interstellar medium.

The source of this ionization has not yet been identified. However, the intensity of diffuse, galactic Hα emission at high galactic latitudes implies a hydrogen ionization rate in the vicinity of the Sun of $(2.4 - 4) \times 10^6$ s^{-1} per cm^2 of galactic disk. This places an important constraint on the possible sources of ionization. For example, this rate requires the equivalent Lyman continuum luminosity of one O9 V star or about 15 planetary nebula nuclei within a cylindrical region through the galactic disk of radius 150 pc centered on the Sun. The presence of an ionization

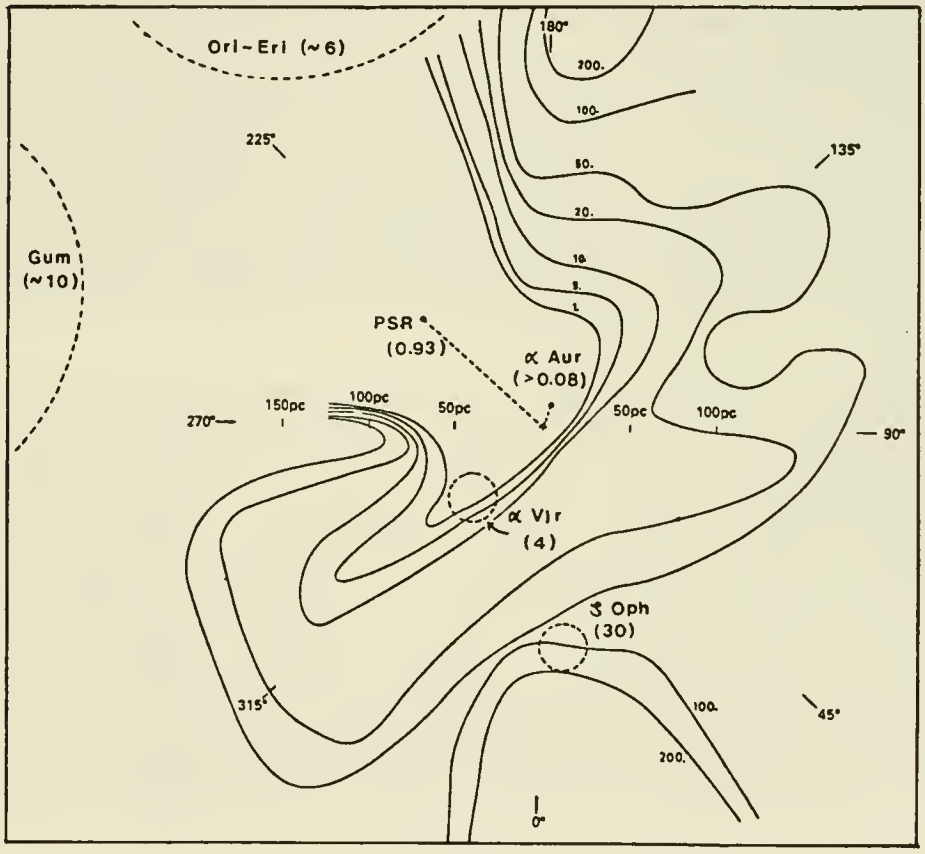

Fig. 4 - Observed regions of ionized gas in the local interstellar medium projected onto the galactic plane and superposed on a contour map of H° column densities by Paresce (1984). The lines of sight to PSR0950+08 and Capella (α Aur) are indicated by straight dotted lines. The size and location of HII regions are indicated by dotted circles. The number in parentheses denotes the H^+ column density in units of 10^{19} cm^{-2} along the line of sight to the star or pulsar or through the center of the HII region. The contours of H° column density (solid curves) are labeled from 1 to 200 units of 10^{19} cm^{-2}.

bounded HII region surrounding ζ Oph, appears to eliminate this nearest O-star as an important source of ionization for the local gas. The combined ionizing flux from B-stars, supernova remnants, hot white dwarfs, and planetary nebula nuclei may account for the ionization provided that the Lyman continuum fluxes from these sources are near the upper end of the ranges listed in Table 1 and provided that a significant portion of the flux is not absorbed by gas immediately surrounding the sources. For example, the one local (distance of 87 pc) early B star that was investigated, α Vir, has an ionization bounded HII region which appears to be immersed in a large HI complex. The ionizing radiation extends no further than about 18 pc from α Vir. Figure 4 summarizes the locations (projected onto the galactic plane) and H^+ column densities of the regions of ionized gas revealed by the Hα, pulsar, and UV data. The regions are denoted by dashed lines and are superposed on a contour map of H° column densities in the local interstellar medium prepared by Paresce (1984). The number associated with each ionized region is the estimated H^+ column density through the region in units of 10^{19} cm^{-2}. Understanding the relationship between these warm, ionized regions and the neutral and the X-ray emitting regions should lead to a better understanding of the morphology and physics of the local interstellar medium.

REFERENCES

Abbott, D. C. 1982, Ap. J., 263, 723.
Backer, D. C., and Sramek, R. A. 1982, Ap. J., 260, 512.
Bobroff, N., Nousek, J., and Garmire, G. 1984, Ap. J., 277, 678.
Bridle, A. H., and Venugopal, V. R. 1969, Nature, 224, 545.
Chevalier, R. A. 1974, Ap. J., 188, 501.
Ellis, G. R. A. 1982, Aust. J. Phys., 35, 91.
Frisch, P. C., and York, D. G. 1983, Ap. J.(Letters), 271, L59.
Gwinn, C. R., Taylor, J. H., Weisberg, J. M., and Rawley, L. A. 1984, IAU Colloquium No. 81.
Harding, D. S., and Harding, A. K. 1982, Ap. J., 257, 603.
Hills, J. G. 1972, Astr. Ap., 17, 155.
Jura, M. 1979, Ap. J., 227, 798.
Manchester, R. N., and Taylor, J. H. 1981, Ap. J., 86, 1953.
McCammon, D., Burrows, D. N., Sanders, W. T., and Kraushaar, W. L. 1983, Ap. J., 269, 107.
McKee, C. F., and Ostriker, J. P. 1977, Ap. J., 218, 148.
Panagia, N. 1973, A. J., 78, 929.
Paresce, F. 1984, preprint No. 15, Space Telescope Science Institute.
Paresce, F., and Jakobsen, P. 1980, Nature, 288, 119.
Parker, R. A. R., Gull, T. R., and Kirshner, R. P. 1979, An Emission Line Survey of the Milky Way (NASA SP-434).
Pengelly, R. M. 1964, MNRAS, 127, 145.
Readhead, A. C. S., and Duffett-Smith, P. J. 1975, Astr. Ap., 42, 151.

Reynolds, R. J. 1976a, Ap. J., 203, 151.
Reynolds, R. J. 1976b, Ap. J., 206, 679.
Reynolds, R. J. 1977, Ap. J., 216, 433.
Reynolds, R. J. 1980, Ap. J., 236, 153.
Reynolds, R. J. 1981, in The Phases of the Interstellar Medium: Proceedings of a Workshop held at the National Radio Astronomy Observatory, Green Bank, West Virginia, May 10-13, 1981, ed. J. M. Dickey, p. 109.
Reynolds, R. J. 1983, Ap. J., 268, 698.
Reynolds, R. J. 1984a, Ap. J. (July 1).
Reynolds, R. J., and Ogden, P. M. 1979, Ap. J., 229, 942.
Reynolds, R. J., and Ogden, P. M. 1982, A. J., 87, 306.
Reynolds, R. J., Roesler, F. L., and Scherb, F. 1977, Ap. J., 211, 115.
Reynolds, R. J., Scherb, F., and Roesler, F. L. 1973, Ap. J., 185, 869.
Reynolds, R. J., and Shih, P. 1983, B.A.A.S., 14, 892; in preparation.
Roesler, F. L., Reynolds, R. J., Scherb, F., and Ogden, P. M. 1978, High Resolution Spectroscopy: Proceedings of the Fourth Colloquium on Astrophysics of the Trieste Observatory, ed. M. Hack, p. 600.
Salpeter, E. E. 1978, in IAU Symposium No. 76, Planetary Nebulae, ed. Y. Terzian (Dordrecht: Reidel), p. 333.
Salter, M. J., Lyne, A. G., and Anderson, B. 1979, Nature, 280, 477.
Shull, J. M. 1979, Ap. J., 234, 761.
Sivan, J. P. 1974, Astr. Ap. Suppl., 16, 163.
Spitzer, L., and Jenkins, E. B. 1975, Ann. Rev. Astr. Ap., 13, 133.
Taylor, J. H., and Manchester, R. N. 1977, Ap. J., 215, 885.
Terzian, Y. 1974, Ap. J., 193, 93.
Torres-Peimbert, S., Lazcano-Araujo, A., and Peimbert, M. 1974, Ap. J., 191, 401.
Weller, C. S., and Meier, R. R. 1981, Ap. J., 246, 386.
Weisberg, J. M., Rankin, J., and Boriakoff, V. 1980, Astr. Ap., 88, 84.
York, D. G. 1982, Ann. Rev. Astr. Ap., 20, 221.
York, D. G. 1983, Ap. J., 264, 172.

A HIGH-RESOLUTION STUDY OF LOCAL INTERSTELLAR SODIUM

A. Ardeberg, H. Lindgren, E. Maurice
European Southern Observatory
Lund and Marseille Observatories

ABSTRACT

A high-resolution spectroscopic investigation has been made of interstellar lines of sodium. From identifications of D_1 and D_2 line components concentrations of interstellar sodium gas have been studied. Some preliminary data are provided on the spatial distribution of stronger sodium concentrations.

INTRODUCTION

For investigations of stronger concentrations of interstellar sodium gas spectroscopic identification of line components is a standard method. For the weak line components to be expected from local gas, identifications are more difficult than normally due to influence of stellar and atmospheric lines and, in case of more distant background stars, also due to blending by stronger sodium components from richer concentrations of interstellar sodium along the line of sight. Finally, the signal-to-noise ratios necessary for identification of faint lines require special observing techniques.

OBSERVATIONS

With the ESO Coudé Echelle Spectrometer at a resolution of 10^5 we have observed the interstellar lines of sodium at 5890/5896 Å. A total of around 250 observations have been made for 200 stars. With the Reticon array detector very high signal-to-noise ratios can be obtained. This means that at least for brighter stars we can avoid line-identification difficulties due to the limitations in the observing technique.

IDENTIFICATION OF CONCENTRATIONS OF INTERSTELLAR SODIUM

There are several features aiding us in our survey for faint line components of interstellar sodium. First, our spectral resolution is very high. Second, the signal-to-noise ratio of our spectrograms is very favourable, for brighter stars often well above 10^3. Third, the fact that both D_1 and D_2 are included is of high importance.

For a first analysis we have inspected our spectrograms visually and identified the stronger line components of interstellar sodium gas. Especially

for the line components resulting from local gas concentrations this provides only a lower limit to the number of interstellar sodium components really available.

Following the visual survey, a more detailed analysis is now in progress. A most important feature in this analysis is a careful mapping of the lines of atmospheric water vapour present in the spectral range of interest. From spectrograms of early-type stars and without interstellar sodium lines the relative atmospheric water-vapour spectrum is obtained. Measurements of the strengths of selected water-vapour lines in the programme spectrograms then transforms the relative atmospheric water-vapour spectrum into an absolute one. Correction for these lines provides programme spectrograms of considerable purity. Also very faint sodium-line components can then be identified.

For our detailed analysis of lines of interstellar sodium detailed account has to be taken also of the influence of stellar lines. Mapping of such lines for all spectral classes concerned is therefore very important.

Mutual blending of sodium lines from interstellar gas is another problem which needs careful attention. The problem is especially serious when distant stars are used and the line of sight crosses more massive sodium clouds outside the local solar neighbourhood. Spatial line mapping is the most direct approach. Still, blending can be rather serious, demanding facilities for powerful disentangling procedures. A special deconvolution programme has been developed for our purpose. The use of this programme is greatly facilitated by the presence of the two sets of sodium lines.

DISTANCES OF STARS

From available spectral classifications on the MK system and from UBV photometry distance moduli, corrected for influence of interstellar absorption, have been determined. They should be of an accuracy relevant for our present preliminary analysis.

PRELIMINARY RESULTS

In Figures 1-3 we present our preliminary estimate of the spatial distribution of interstellar sodium gas. For three intervals in galactic latitude we have noted the number of (stronger) interstellar lines in plots of distance modulus versus galactic longitude.

As could be expected, the stars most nearby do not display many stronger line components of interstellar sodium. However, there are examples of components of significant strength obviously resulting from gas clouds quite close to the sun. It is interesting to note that this is true also for stars situated outside the galactic plane.

The data presented indicate a number of nearby concentrations of interstellar sodium gas. It is our intention to follow this up in two ways. First, detailed analysis of our present spectrograms should provide increased accuracy and resolution for the local interstellar lines. Particularly,

fainter lines can be studied and thereby more components be identified. Second, more observations are planned for the nearby clouds indicated in the present work as well as for parts of the sky so far less well covered by our observations.

A programme is under way to determine radial velocities for all components of interstellar sodium from the observing material discussed in the present paper. We expect an accuracy of the order of 1 kms^{-1}. At the same time, line intensities will be measured for all components of interstellar sodium. Combination of radial velocities and line intensities will provide useful data on the distribution and kinematics of local sodium gas. Moreover, it means that much better use can be made also of more distant stars for the study of local gas clouds.

In this presentation we have excluded results from a relatively extensive study of interstellar sodium in the direction of IC 2944. This study clearly indicates at least two local gas components. The agreement with the present work is good.

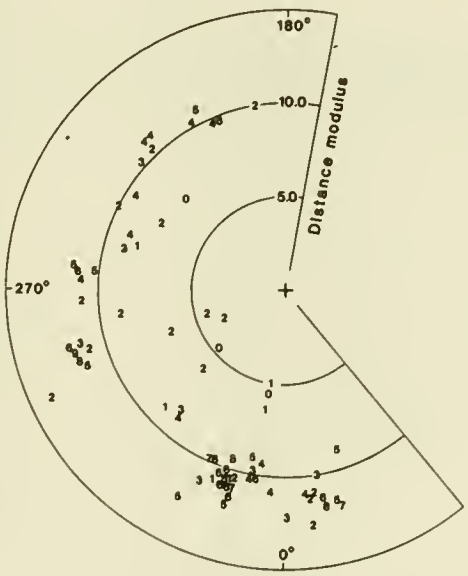

Fig. 1: Our estimated lower limits to the number of interstellar line components given in a diagram with distance modulus versus galactic longitude. Interval in galactic latitude, b, is $-5^{o} < b < +5^{o}$.

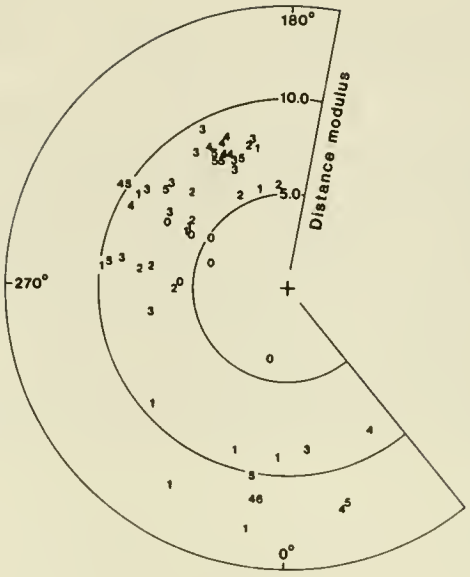

Fig. 2: Same as Figure 1 but for the latitude interval $-25^{o} < b < -5^{o}$.

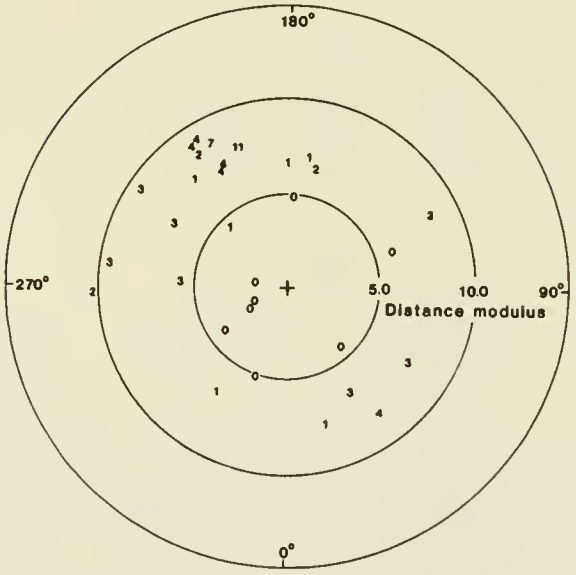

Fig. 3: Same as Figure 1 but for the latitude interval $b < -25^{o}$.

OPTICAL OBSERVATIONS OF NEARBY INTERSTELLAR GAS

P.C. Frisch and D.G. York
Astronomy and Astrophysics Center, University of Chicago

The yellow D lines from neutral sodium are some of the most useful interstellar absorption features for tracing out low density optically thin interstellar material. Hobbs (1978) compared column densities of NaI as determined from the D lines with HI column densities derived from ultraviolet observations and found values of $N(NaI)/N(H)<6.3\times10^{-9}$ in 18 sight-lines with very low reddening, with the exact value of the ratio apparently a function of temperature. If this ratio limit holds for diffuse clouds in nearby space, we expect that observations of the NaI D_2 lines at the 3 mA level can be used to trace out nearby clouds with column densities in the range of $\gtrsim 2.5\times10^{18}$ cm^{-2}. Thus sensitive measurements of the NaI D lines are a useful way of observing nearby neutral cloud material. With this in mind, we have chosen high-resolution observations of the yellow sodium lines as a means of locating and mapping nearby low density interstellar clouds.

In the past, most interstellar line observations have relied on O and B stars as target objects. Since these stars generally fall in associations that lie outside of the nearest 100 parsecs, there is no a priori way of identifying those interstellar absorption features which are formed in clouds within the nearest 100 parsecs. In order to determine the distance of nearby clouds, we have singled out relatively abundant nearby cool stars as target objects. The distance of the interstellar cloud is then determined by observing a sequence of stars spaced in distance along one line of sight. The distance of the nearest stars in which the interstellar absorption feature is seen provides an estimate of the distance of the cloud. Most of the distances we have used so far are based on the spectra of the target stars, and are therefore not known accurately. However, the upcoming astrometric Hipparcos satellite combined with the next generation of ground-based astrometric telescopes should allow the determination of stellar distances out to 100 parsecs more accurately.

The results of applying this technique to the clouds in the sight-line towards ζ Oph are shown in Figure 1. This star is located 170 parsecs from the Sun with probably the most well-studied interstellar spectrum of any star. We searched for, and found, surprisingly strong interstellar NaI D_1 and D_2 absorption lines in three stars within two degrees or less from the sight line to ζ Oph, and with distances less than 100 parsecs from the Sun. A fourth star with a slightly greater separation from the ζ Oph sight-line, but within 56 parsecs of the Sun, produced no detection of interstellar material. These NaI D_1 absorption features are shown in Fig. 1 where intensity is plotted versus heliocentric velocity. These data were taken using the McDonald Observatory coude Digicon detector at a resolution of 3 km/s. Information about the stars are given in the Table. The stellar distances listed in the Table are all spectral

distances and taken from Sky Catalogue 2000.0. Interstellar absorption features are seen in all but the nearest of these stars, 20 Oph. The broad absorption feature seen in that star is stellar. Broad, very shallow, stellar NaI absorption features are also found for the stars HD149662 and HD149807 on tracings of a larger velocity interval of the spectral continua. Also note that the weak absorption features seen between +15 and +40 km/s in all of the stars are telluric features from the earth's atmosphere.

In the 2x3 degree region of the sky defined by the four stars showing NaI absorption, two distinct cloud complexes are present centered near -14 km/s and -28 km/s (heliocentric velocity). Ultraviolet observations of ζ Oph show that each of these two NaI features is actually made up of several individual velocity features with distinct ionization properties (Morton 1975). Maps of 21-cm emission at 0 km/s and -14 km/s in the local standard of rest (corresponding to the two NaI clouds) in this 2x3 degree region do not show pronounced patchiness that could explain the variations in the line profiles seen in the Figure. (Cleary et. al. 1979) Based on the fact that one star, HD149108, shows only the -28 km/s cloud, while the other stars show both clouds, we thus conclude that the spectral star distances listed in the Table may not be correct, since the interstellar line strengths should increase in strength with star distance. The relative star positions implied by the interstellar lines, starting with the nearest stars, are 20 Oph, HD149108, HD149807, HD149662 and ζ Oph.

This narrow unsaturated Na D_1 feature in HD149108 has a column density of $N(NaI) \sim 3 \times 10^{11}$ cm^{-2}, corresponding to a hydrogren column density of $N(HI) \geq 5 \times 10^{19}$ cm^{-2}, providing the ratio limit quoted above from Hobbs (1978) encompasses the value for this cloud. According to the stellar distances entered in the Table, this cloud is certainly within 80 parsecs of the Sun, and within 55 parsecs if the distance to HD149662 is correct, in agreement with previous conclusions that this -28 km/s feature is near the Sun (Frisch 1981, Crutcher 1982).

Another point to note from these data is that material associated with some portion of the main interstellar absorption feature at ~-14 km/s found in ζ Oph must also lie within the nearest 100 parsecs. This strong feature has substantial amounts of H_2 as well as other interstellar molecules associated with it and is the prototypical diffuse cloud (Herbig 1968, Morton 1975). Based on the two stars HD149807 and HD149108, at estimated distances of about 80 parsecs and which both show distinct absorption from this -14 km/s gas, we conclude that this main feature is actually a cloud complex and that part(s) of this complex are within 100 parsecs.

A third thing to note from these data is that the variation in the strength of the -28 km/s cloud between the different stars indicates some patchiness is present within diffuse clouds on scales of the order of a parsec or less.

In summary, these observations indicate that a cloud with a heliocentric velocity of ~-28 km/s and a hydrogen column density that possibly could be on the order of, or greater than, 5×10^{19} cm^{-2} is located within the nearest 50-80 parsecs in the direction of Ophiuchus. This is a surprisingly large column density of material for this distance range. The patchy nature of the absorption from the cloud indicates that it may not be a feature with uniform properties, but rather one with small scale structure which includes local enhancements in the column density. This cloud is probably associated with the interstellar cloud at about the same velocity in front of the 20 parsec distant star α Oph (Frisch 1981, Crutcher 1982), and the weak interstellar polarization found in stars as near as 35 parsecs in this general region (Tinbergen 1982). These data also indicate that some portion of the -14 km/s cloud also must lie within the 100 parsec region.

Similar observations of both NaI and CaII interstellar absorption features have been performed in other lines of sight. We find similar interstellar absorption features in a dozen stars between 20 and 100 parsecs of the Sun, and located in Quadrants IV, I and II of the galaxy. A number of these stars also show surprisingly strong NaI absorption lines in light of their reported distances.

References

Cleary, M.N., Heiles, C., and Haslam, C.G.T. 1979, Astr. Ap. Sup., 36, 95.

Crutcher, R.M. 1982, Ap. J. 254, 82.

Frisch, P.C. 1981, Nature, 293, 377.

Herbig, G.H. 1968, Zs. F. Ap., 68, 243.

Hirshfeld, A., and Sinnott, R.W.(ed.) 1982, Sky Catalogue 2000.0 (Cambridge University Press and Sky Publishing Corporation)

Hobbs, L.M. 1978, Ap. J., 222, 491.

Morton, D.C. 1975, Ap. J., 197, 85.

Tinbergen, J. 1982, Astro. Ap., 105, 53.

Table: Stellar Data

Star	l^{II}	b^{II}	Sp	V (mag)	r (pc)	vsini (km/s)	RV_{star} (km/s)
ζ Oph	6.3	+23.6	09.5Vn	2.6	170	379	-15
HD149807	5.2	+22.8	F2V	7.9	87	—	—
HD149108	5.6	+24.4	A5V	6.8	81	—	—
HD149662	7.7	+24.7	F2V	6.8	55	—	—
20 Oph	8.0	+20.9	F7IV	4.7	<56	13	-1

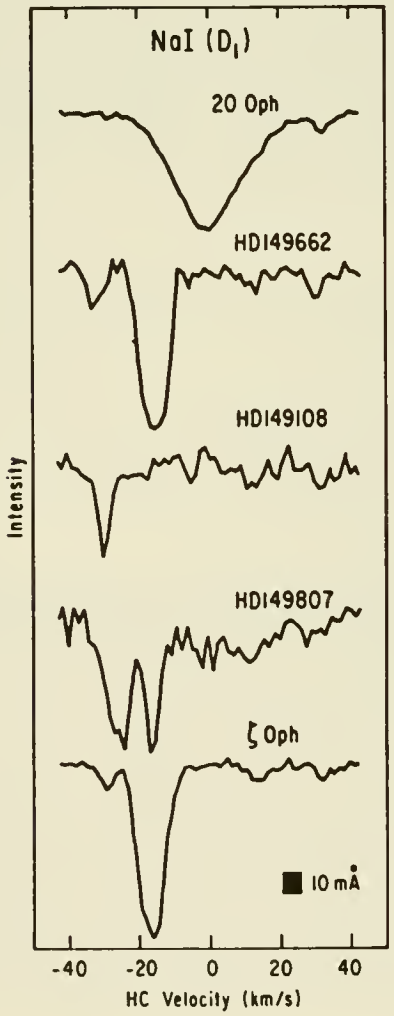

DISTANCES OF LOCAL CLOUDS FROM OPTICAL LINE OBSERVATIONS

Richard M. Crutcher and David J. Lien
Astronomy Department, University of Illinois

ABSTRACT

We observed the interstellar D-lines of Na I toward 49 stars in order to determine the distance (125 ± 25 pc) to a cold H I cloud. This sheet of gas may be part of the back side of the shell formed by the Loop I supernova.

INTRODUCTION

Riegel and Crutcher (1972) and Crutcher and Riegel (1974) studied the angular extent and physical properties of an H I cloud detected as a narrow self-absorption feature in 21-cm line profiles. It is seen in self-absorption over $345^{\circ} < l < 385^{\circ}$, $|b| < 7^{\circ}$ and apparently also in emission at higher galactic latitude and lower longitude. Its typical properties are T_k = 30 K, n(H I) = 100 cm^{-3}, N(H I) = 3 x 10^{20} cm^{-2}. Two separate velocity components are seen, at LSR velocities of +4 and +7 km s^{-1}. Narrow molecular lines of OH and CO are sometimes observed at the same velocites, and the cold H I seems to be spatially correlated with the distribution of local dust clouds.

OBSERVATIONS

In order to better define the distance of this cloud, observations of the optical interstellar Na I D-lines were made toward early-type stars in the direction of the cold cloud. The Na I lines are better tracers of denser gas than either the Ca II lines or color excess. The Varo-reticon detector on the coude spectrograph of the Mt. Wilson 2.5-m telescope was used. The velocity resolution was about 10 km s^{-1}, which was sufficient to exclude the possibility of stellar Na I lines with a high degree of confidence. The rms error in measured equivalent widths and the minimum detectable equivalent width were typically 10 mA and 20 mA, respectively. New observations of the 21-cm line of H I were also made at the position of each star with the 43-m telescope of the NRAO. The velocity resolution was 0.4 km s^{-1} and the beamsize was 20 arcmin. A strong optical interstellar line at the velocity of H I self-absorption was taken as evidence that the stellar distance was an upper limit to the distance of the cold cloud. Velocity differences of 4-5 km s^{-1} between Na I and H I are not significant because of the low spectral resolution of the optical data, the complexity of the background H I emission profiles, and the presence of multiple velocity components. Using a curve of growth with a velocity parameter b = 2.5 km s^{-1}, we estimated column densities of Na I from the weaker D-line which was observed. Because of line saturation, these estimates are not particularly accurate; and any column density greater than 10^{13} cm^{-2} is given as a lower limit only. For the relative comparison purposes of this paper, this procedure is adequate.

Our results are given in the Table. Column headings are the HD number of the star, the galactic coordinates in degrees, the spectral type, the visual

magnitude and color, the color excess, the photometric distance derived from the preceeding data, the equivalent widths in milliangstroms of the Na I D_1 and D_2 lines, the column density of Na I in units of 10^{12} cm^{-2}, the LSR radial velocity of the Na I and of the H I, and an index p which specifies the nature of the H I line. Figure 1 shows the H I profiles which are the prototypes of the H I classification index p. The very strong self-absorption feature toward HD163955 is p = 1, and the progressively weaker features as one moves clockwise in the Figure are of types 2 and 3. The lack of self-absorption seen toward HD154481 is p = 4; in these cases the H I emission velocity is given. Some of the stars had missing luminosity type or photometric data. Although such stars are included in the Table, they are not used in the subsequent analysis.

DISCUSSION

Figure 2 shows the Na I column densities plotted against stellar distance. The points begin to rise significantly at about 100 pc, and by 150 pc virtually all stars have strongly saturated interstellar Na I lines. Hence, our distance estimate for the cold cloud is 125 ± 25 pc. Figure 3 shows the stellar distances plotted against galactic longitude. There is no clear evidence for part of the cloud being closer than other parts. However, at longitudes near 20° a distance near 100 pc seems most appropriate. For $l < 360^{\circ}$ the distance is less well defined and may be up to 200 pc. There is therefore a fairly dense cloud of cold H I, dust, and molecules about 125 pc from the sun with an extent of at least 90 pc along the galactic plane. Since the thickness is 1-5 pc, the morphology is that of a sheet.

Berkhuijsen (1973) found a distance of 130 ± 75 for the center of the Loop I supernova remnant; the corresponding radius of the remnant is 115 pc. The morphology of a cold sheet of gas lying within Loop I and oriented radially with respect to the center is rather unlikely. The observations of x-rays from this direction argue against the cold sheet being in front of Loop I. We suggest that the cold sheet forms part of the back side of the compressed shell of gas swept up by Loop I. If the distance of the sheet were 100 pc for $l > 20^{\circ}$ and 150-200 pc for $l < 0^{\circ}$, which is perfectly compatible with our data, the morphology would fit this hypothesis very well.

Crutcher (1982) analyzed the velocities of published optical interstellar line data and showed that the sun is immersed in a coherently moving local interstellar medium which he identified with the solar system's interstellar wind. The velocity vector is consistent with this gas being the front side of the Loop I shell. The center of Loop I would then have a radial velocity with respect to the LSR of about -5 km s^{-1} and an expansion velocity of about 10 km s^{-1}; hence, the age would be $< 10^7$ yr.

REFERENCES

Berkhuijsen, E.M. 1973, Astron.Ap., 24, 143.
Crutcher, R.M. and Riegel, K.W. 1974, Ap.J., 188, 481.
Crutcher, R.M. 1982, Ap.J., 254, 82.
Riegel, K.W. and Crutcher, R.M. 1972, Astron.Ap., 18, 55.

HD	l	b	Sp	V	B-V	E_{B-V}	dist	W_{D1}	W_{D2}	$N(10^{12})$	V_{Na}	V_H	p
148898	356.3	17.8	A7p	4.46	.12	.00	30	–	–	<0.2	–	2	3
149438	351.5	12.8	B0V	2.83	-.25	.05	260	87	45	0.6	6	5	3
150366	355.3	14.2	F0V	6.06	.22	.00	50	–	–	<0.2	–	4	1
150638	349.6	9.0	B9	6.46	-.08	.00	>240	62	–	0.4	3	4	2
150768	353.4	11.8	A0	6.38	–	–	>140	–	–	<0.2	–	4	3
150894	352.6	11.1	A2	5.96	–	–	>90	74	–	0.4	4	4	4
151527	4.3	18.8	A0V	6.03	.20	.20	90	254	214	>10	-2	4	1
152909	1.6	14.4	B6V	6.28	.07	.21	180	286	216	>10	-4	5	2
153613	352.0	6.0	B8V	5.03	-.10	.00	110	–	–	<0.2	–	4	1
154204	1.9	12.4	B6IV	6.30	-.02	.12	320	179	142	4.6	9	4	3
154481	357.3	8.5	A3IV	6.28	.02	.00	110	261	116	2.5	11	5	4
155379	359.0	8.3	A0	6.52	-.01	–	>150	83	64	0.9	0	5	4
155401	356.9	6.7	B9	6.11	.02	–	>180	–	–	<0.2	–	4	1
156247	22.7	21.6	B5V	5.70	.07	.23	160	219	164	9.5	2	1	4
156325	353.8	2.9	B6IV	6.37	.14	.28	270	241	192	>10	5	5	3
156717	6.3	11.0	A2V	6.02	.04	.00	90	–	–	<0.2	–	7	2
156928	10.6	13.5	A1V	4.33	.03	.02	50	–	–	<0.2	–	2	2
157056	0.5	6.6	B2IV	3.28	-.21	.03	200	89	51	0.7	0	4	1
157546	6.3	9.7	A0V	6.37	.00	.00	140	201	147	5.4	2	5	4
157792	1.7	6.2	A9V	4.17	.28	.02	20	–	–	<0.2	–	4	1
158643	2.5	5.4	B9.5V	4.81	.00	.03	70	–	–	<0.2	–	4	1
158704	0.6	4.0	B9p	6.08	-.06	–	>200	–	–	<0.2	–	4,7	1,2
159877	10.5	8.6	A5V	5.94	.37	.22	180	514	509	>10	0	3	3
159975	17.0	12.3	B8II	4.62	.11	.20	140	319	250	>10	7	4	1
161056	18.7	11.6	B3V	6.28	.38	.58	180	483	440	>10	10	4	2
161701	12.4	6.9	B9III	5.95	.01	.07	170	167	93	1.6	7	3	1
161840	358.0	-2.1	B8V	4.82	-.04	.05	100	156	88	1.5	6	5,7	1,2
163318	2.0	-1.6	A3	5.72	.21	–	>70	–	–	<0.2	–	6	1
163336	12.5	4.6	A1V	5.89	.05	.04	90	–	–	<0.2	–	6	1
163955	6.0	-0.1	B9V	4.75	-.05	.01	80	–	–	<0.2	–	7	1
164536	6.0	-0.9	O9III	7.11	-.03	.28	2500	228	174	>10	6	7	1
165402	20.3	6.1	B8IV	5.84	.20	.29	140	202	181	>10	-1	4	1
165814	5.6	-2.7	B4V	6.66	.04	.22	300	229	173	>10	4	7	1
166393	10.8	0.5	A4V	6.36	.16	.04	80	126	51	0.7	10	7	1
166937	10.0	-1.6	B8Ia	3.85	.22	.24	1100	253	180	>10	9	6	1
167666	3.7	-5.9	A4	6.12	.16	–	>70	233	162	9.0	7	6	4
167833	20.3	3.0	A5III	6.30	.38	.23	130	150	132	3.6	8	4	3
169033	19.0	0.7	B8V	5.73	.01	.10	150	190	168	>10	6	5	1
169990	14.5	-3.0	B8V	6.03	.01	.10	150	189	148	5.6	-2	7	2
170296	17.5	-1.8	A3V	4.70	.06	.00	40	116	93	1.6	1	3	4
170680	14.3	-4.0	A0V	5.14	.00	.00	80	–	–	<0.2	–	7	3
170740	21.1	-0.5	B2V	5.91	.27	.51	240	234	189	>10	5	4,8	1,1
170902	17.7	-2.5	A4V	6.37	.22	.10	80	87	74	1.1	4	4	3
171130	17.7	-2.9	A2V	5.76	.04	.00	80	–	–	<0.2	–	4	4
171957	18.9	-3.5	B9IV	6.40	.21	.27	140	346	346	>10	9	4	3
171961	10.5	-7.8	B9	5.75	.02	–	>170	179	129	3.4	5	5	4
175156	19.3	-7.7	B5III	5.08	.17	.33	150	351	279	>10	6	6	2
175623	20.2	-7.9	B9	7.15	.22	–	>320	351	304	>10	3	6	3
176162	22.3	-7.6	B5IV	5.53	-.04	.12	170	201	171	>10	-1	3	4

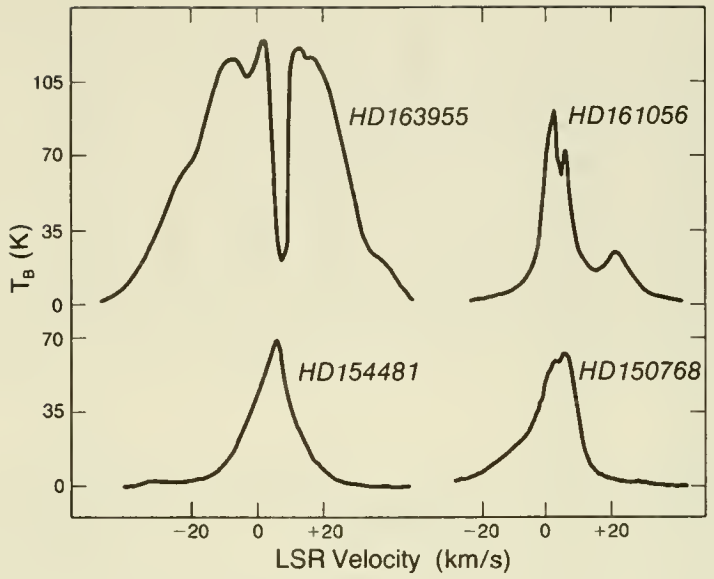

Figure 1 - Examples of the H I line profiles.

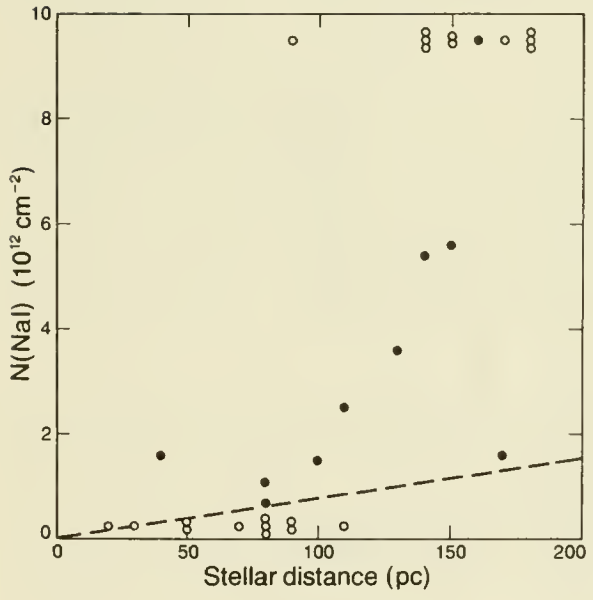

Figure 2 - Na I column density versus stellar distance. The open circles represent lower and upper limits on N(Na I).

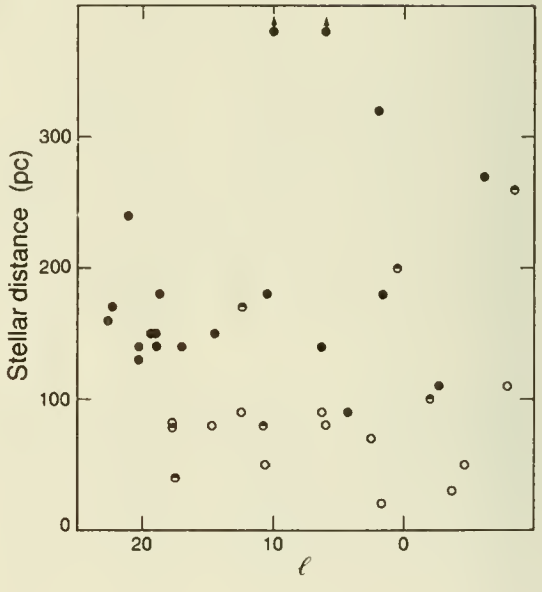

Figure 3 - The open and filled circles represent N(Na I) < 0.2 and > 2 x 10^{12} cm^{-2}, respectively. The intermediate cases are half-filled.

OPTICAL EXTINCTION AND POLARIZATION STUDIES

LOCAL INTERSTELLAR EXTINCTION WITH AN EMPHASIS ON uvbyβ RESULTS

Jens Knude

Copenhagen University Observatory

Introduction

Despite only a few percentages of the interstellar mass are contained in solid dust grains knowledge of its distribution is of importance per se,for dereddening purposes and because it probably correlates with the interstellar gas.General information on the bulk of the interstellar mass is thus obtainable from continuum absorption studies. Compared to diffuse emission data interstellar reddenings have the additional advantage by including an upper distance to the material observed.

Three dimensional mapping of the local dust has been attempted since the calibration of the uvbyβ system,Strömgren(1966),for B,A and F stars was completed by Crawford (1975,1978,1979). Being the primary calibrating sources makes local field F stars particularly useful as background sources in the search for interstellar reddening matter. Computed distances and color excesses for A and F stars are thought to be more accurate than 15% and 0.01 mag respectively.

Two interpretations of the color excess observations have been suggested. Either is the solar vicinity virtually free from dust within 75 - 100 pc or 4.4 10**-4 clouds/pc**3 filling about 2 % of the volume are distributed randomly in a low density medium.

Average reddenings and the distribution of local dust

Several comprehensive surveys for local dust by means of uvbyβ photometry have been published recently.

Perry and Johnston (1982) obtained data for 3458 northern A and early F stars. Spectral types and limiting magnitudes were selected in order to sound a volume with inner and outer radius 100 and 300 pc respectively. This sample has later been supplemented with data for 305 late F stars within 100 pc, Perry,Johnston and Crawford (1982).

If the scale height of the dust density distribution is about 200 pc the distribution of the dust concentrations in the galactic pole directions, where they are studied most conviniently,may be typical for the solar vicinity. The existence and abundance of matter perpendicular to the galactic have important consequences in galactic as well as in extra galactic studies. Hill,Barnes and Hilditch (1982) have presented uvbyβ data for about 1000 stars

within 15 deg of the NGP. Program stars were taken from the literature and may lack spectral completeness and a systematic limiting magnitude. This may complicate the interpretation of their results. An identical invesigation comprising 572 HD stars with b< -70 deg has been conducted by McFadzean,Hilditch and Hill (1983).

Knude (1977,1981,1982) has taken a different observational approach by observing magnitude limited,"complete", samples of B,A and F stars in small areas. The three published lists contain data for about 1200 stars.

The distribution of color excesses calculated from published photometric and spectroscopic data,Lucke (1978) leaves the impression that the sun might be located in a dust free region enclosed by more or less coherent large scale structures. But it must be noticed that the lowest reddening contour presented within 500 pc is E(B-V)=0.1 mag ,a rather large excess in the present context. Local excesses are thought to be much smaller. An important parameter in the search for local extinction is the angular spacing of the lines of sight and it is essential for the detection of small dust features how the spacing compares to the projected sizes of the dust structures. Unless the dust distribution is continuous the applied angular separation determines the linear sizes which may be detected. Cloud dimensions were expected smaller than about 10 pc. Within a few hundred pc this requires an angular resolution better than one degree. To be manageable such inverstigations are restricted to smaller areas. The survey of the complete northern hemisphere by Perry and Johnston op.cit. has one star per six square degree,whereas the Hill et.al. and the McFadzean et.al. mappings have 1.4 and 0.5 line of sight per square degree on the average. Knude´s observations have an average ranging from 1 to about 10.

Concerning the existence of local dust,average reddenings may not be representative if the matter happens to have a clumped distribution. A significant amount of material may be concentrated in a small part of space but only covering a minor fraction of the local sky. With an irregular dust distribution within a certain distance the fraction of the sky covered by diffuse dust clouds must be estimated before any average reddening value can be accepted as valid for the volume sounded. Closer than 150 pc less than 50 % of the sky is expected to be covered by diffuse clouds and for galactic latitudes above 70 deg less than 20 % of the area is thought to be reddened, Knude (1983). But dust <u>is</u> present.

The selection of the stellar samples used for probing the dust in a certain volume is most important. If some upper distance limit is chosen a priori the amount of absorption expected must be added to the magnitude of the unreddened sampel stars at this distance. If this is not done the lines of sight observed have a tendency to avoid the reddened directions present,Perry and Johnston op.cit. This point is also illustrated by the observation that in magnitude limited samples the most distant stars are always among the less reddened ones.

The problems of the local dust distribution are closely connected to the questions of the spatial distribution of the various

gas phases of the ISM as typified by e.g. McKee and Ostriker(1977) and Fried et al.(1980). Three principal conclusions drawn from Perry et al. op.cit. favor the local void: (a) the sun is located in a reddening free region extending at least 75 pc in all directions.(b) the galactic pole zones have negigibel reddening.(c) the local dust,distances larger than 75 pc, is concentrated in coherent large scale structures,displaying density variations.

Detailed observations in many small areas, Knude (1979) do not corroborate the conclusion (a). A substantial amount of clouds do show up in the reddening data even within 75 pc in an area totaling 5 % of the sky. These clouds have color excesses E(b-y) in the range from 0.014 to 0.1 mag. From statistical considerations,Knude (1981a),a maximum of 750 clouds is estimated to be present within 75 pc, but they will only be seen to cover about 20 % of the complete sky. Tinbergen (1982) finds indications of a very local,D<20 pc, dust patch in the direction (l,b)~(0,-20). In this part of the sky color excess data, Knude (1978), also show that some stars closer than 50 pc have color excesses larger than 0.020 mag. In the distance range from 50 to 75 pc some even have E(b-y): 0.03 - 0.04 mag. This is in the general direction of the proposed large Sco - Cen bubble, Weaver (1977). So in some directions very local, significant amounts of reddening seem present.

Of the published photometric data samples none are well suited to locate any small dust concentrations within 50 pc. The spatial density of the F stars is too small,so the clouds may slip through the network. Background sources more frequent by an order of magnitude is required,but as the column densities of such structures are unknown photometry may prove too inaccurate for a search.

Neither is there any perfect agreement on the existence of local dust in the pole directions. McFadzean et al.(1982) confirm the conclusion that the average reddening at the SGP is about zero, whreas Hilditch et al. (1983) find significant reddening in part of the zone b>75 deg. Knude (1977b,1978) also finds substantial amounts of dust in some regions at both polar caps. On Figure 1 is shown a histogram of color excesses resulting from uvbyβ observations of all stars earlier than G1 and brighter than V~12 mag in SA 141,b~-85.8 deg. The distribution displays a positive tail and the average excess is not zero but 0.02. Figure 2 is a compilation of such data for 50 square degrees with b<-45 deg, and comprises data for about 450 lines of sight. Figure 3 is a similar diagram based on data drawn from Perry and Johnston (1982), Table 1. There is a noticeable difference particularly in the low excess parts of these diagrams. Such a difference is not easy to explain but it is strange tc note that the distribution of theβ index observed by Perry and Johnston has a narrow maximum at 2.735 just where other investigations of field stars and galactic cluster find a gap in the distribution and just where the calibrations by Crawford may not be the most accurate.

Perry,Johnston and Crawford op.cit. do not find any variation of color excess with distance (projected) from the galactic plane. The reason for this may be that the observed distance range,200 pc,

is too small to pick up any significant changes. Averages excesses in 50 pc bins for the stars in SA 141 within 650 pc are shown on Figure 4. These excesses do show an increasing trend with distance. Assuming an exponential density variation a linear regression of the averages on exp(-z/h) results in a scale height h=160 pc and in an equivalent average gas density in the galactic plane of 0.37 atoms cm** -3. With the patchy dust distribution observed cloud and inter cloud dust need not have identical scale heights. Figure 5 shows a color excess distance diagram for a small area at latitude +25 deg. There may be several explanations of the origin a the lover envelope seen,one that it is a specimen of the effect of intercloud dust exclusively.

Figure 1 of Hilditch,Hill and Barnes (1983) shows that about half the area above B=75 deg has an average reddening 0.001 mag, the remaining half 0.008 mag but also the existence of a patch with E(b-y) = 0.024 mag.

Another investigation of the distribution of the dust at the NGP presently being conducted. T.Oja (1981) has performed a spectral survey at the NGP, b>70 deg, to a limiting magnitude V~11mag finding ~5500 candidates in the spectral range from A2 to G0. Knude,Winther and Strömgren have prepared positions for these stars for subsequent uvbyβ observations. The observations are complete for about 50 % of the sample and some preliminary results for the north pole are presented. As the survey has four stars per square degree these new data are expected to result in a more detailed understanding of the dust distribution at the NGP. Table 1 contains the variation of average excesses in 25 pc bins with distance (not z) as based on color excess and distance for about 2000 stars. The average starts out with a value E(b-y) = 0.011 mag within the first 50 pc and rises to 0.014 mag in the next 25 pc and then remains constant out to 300 pc. This behaviour very much resembles the variation encountered within the first few hundred pc in SA 144 at the SGP,Figure 4. In Table 2 a coarse representation of the reddening variation across the north pole region and within 100 pc is given. The average reddening is doubled from 0.009 to 0.018 mag when the pole is crossed from the center to the anticenter direction. Note that the observations so far is not complete to the same magnitude in the three sections, the final values may therefor change a little. At the north pole a most interesting result is the very small distance within which significant reddening is found. Figure 6a and 6b show the distribution of E(b-y) for the few stars closer than 50 pc and how the excesses vary with distance respectively. For the 18 stars with D< 50 pc E(b-y) = 0.011±0.013 mag and the distribution does show a positive tail. Only two of the stars have photometric distances smaller than 35 pc and have no reddening but between 35 and 50 pc reddenings as large as 0.030 show up. If the matter along these lines of sight is representative one may tentatively conclude that within 35 pc no reddening material is present but in the range from 35 to 50 pc reddening free as well as rather heavily regions do exist. Similar data pertaining to the distances 75 < D < 100 pc ,b>70 deg are shown in Figure 7a,c.

In order to indicate the preference of positive reddenings for stars at these latitudes Figure 7 b demonstrates the E(b-y) distribution with the entire symmetric counterpart of the E(b-y)<0 part of Figure 7a removed. Figure 7b may be a crude first approximation to the dust column distribution to be expected in the high latitude dust features. Figure 7c displays the considerable scatter of color excesses for a sample of stars with almost the same distance. As Table 1 shows the scatter is nearly constant when moving out to large distances contrary to what is the case in the galactic plane, where the excess distribution is seen to flatten at the larger distances. This is probably an effect of scale height, only in rare cases a high latitude line of sight will penetrate more than one cloud.As a final example of a reddening histogram, the distribution reddenings within 100 pc and with b>70 deg,δ<20 deg is shown in Figure 8. This area covers the northern part of the Virgo cluster parts of which apparently have absorptions as large as A_v=0.2 mag.

As to whether the local diffuse dust clouds exclusively are located in larger coherent features Figure 9 shows the resulting spatial distribution of clouds for which upper and lower distance limits could be determined from a survey of 63 small areas with |b|<30 deg. The cloud distances are not projected in the galactic plane in order not to overstate their nearness. No clouds are indicated in the immediate solar vicinity ; this does not necessarily imply that no clouds are present but may be caused by the scarcity of very local background sources,most of which are more distant than 50 pc. Apparently diffuse clouds are omnipresent localy with a constant spatial density. There may be a weak tendency that there are fewer clouds for the longtudes l: 340-0-30 deg and those present are concentrated in a smaller volume. This is however not born out by the results on Figure 10, where the clouds with only upper distance limits are pictured. They show much the same distribution as in Figure 9, but some clouds are present even within 50 pc. On basis of Figure 9 and 10 one would rather suggest a homogeneous distribution of the local diffuse dust clouds than that they only exist in large scale features. There is thus only little support from the discrete cloud data to conclude that sun is located in a cavity more or less void of dust, not even a cavity as small as 100 pc across. Within 35 pc 75 clouds are expected, but they are estimated to cover only a mere 10 % of the whole sky.

Some properties of local diffuse dust clouds

From observations of suitable stars in fine but irregular networks and subsequent statistical correction for the sensitivity of the observations to detect various dimensions at different distances the distributions of dust column densities,linear dimensions,spatial density and volume filling factor have been possible, Knude (1981 a,b). It is found that for the distance range from 50 to 150 pc the diffuse clouds in the dimension range from

1.5 to 10 pc occupy 1.8% of space, have a spatial density 4.4 10**-4 pc**-3. Their linear dimensions obey a power law (2R)**-2.62. Their one-dimesional frequncy is 4.3 clouds/kpc . By using the method of moments an average inter cloud density 0.001 mag/100 pc or 0.02 H atoms cm**-3 is estimated, Knude (1979 b). Note how well the local average density derived from cloud statistics n(H) = 0.5 cm**-3 compares to the estimate from the scale height considerations 0.37 cm**-3. The average cloud density is about 20 H atoms cm**-3. The distribution functions of the cloud parameters must of course reflect the physical conditions of the diffuse medium of which the constitute the most massive part. As an example the variation of linear dimension with distance from the galactic plane is shown in Figure 11. For $|z| < 20$ pc there is a remarkable absence of clouds with $(2R) > 5$ pc, whereas clouds in the range $20 < |z| < 40$ pc shown a tendency of being larger on the average. Figure 12 displays the variation of the clouds equivalent density with z-distance. Apparently the high |z| clouds have a lower density than those in the plane. No temperature information is presently available for these specific clouds, but the variation could indicate that the clouds expand in low pressure regions away from the plane?

Little is presently known on shapes and density gradients in the clouds. The clouds used for statistical studies were identified from spatialy confined identical color excesses delineated by lines of sight with negligibel excesses. The clouds were assumed spherical, though only 20 % show equal radial and lateral dimensions. The constancy of the excesses used to identify a cloud may indicate either that the clouds are part of stratified structures or that only the dominating cores have been detected. So far clouds with dimensions as small as 1.5 pc have been identified. An extremely interesting problem is whether the distribution of smaller dimensions follows an extrapolation of the power law or it shows an extremum somewhere below 2 pc. If the distribution shows a maximum its location may be used as an indicator of the ISM pressure. A search for local subparsec structures has been initiated by observing a few areas with approximately 10 stars/ square deg and one area with almost 100 stars/ square deg. Figure 13 is an example of a dust feature within 100 pc and with linear size less than 0.8 pc. At the SGP the elongated feature shown on Figure 14 was found. It has a western extension only 0.2 pc across. The higher resolution data may also be used addressing the unsolved problems on the shapes of the diffuse dust clouds, on there internal structure and whether they generaly posses low density outer envelopes.

As an indication of what may be obtained from the high resolution data a diffuse cloud in SA 141 is discussed. Reddenings along 13 lines of sight within 0.5 square degrees are shown on Figure 15a as they appear on the sky and with stellar distances indicated. A certain systematics is noticed. There are two iso-excess curves: $E(b-y) = 0.0085 \pm 0.0015$ mag and $E(b-y) = 0.0335 \pm 0.0013$ mag, two close, nearly identical reddening directions with $E(b-y) = 0.049$ and 0.054 respectively and an apparently deviating reddening not fitting any pattern.

Two interpretations are possible:
a. The 0.0085 mag contour represents intercloud lines of sight and consequently delineates a cloud with E(b-y) ≥ 0.017 mag. The excesses 0.049 and 0.054 are the result of a superposition of two clouds with E(b-y)=0.017 and 0.0335 respectively. Figure 15b visualizes this suggestion. The probability of having two clouds within a distance of 300 pc is 0.2 .
b. The angular distribution of these 13 color excesses offers another interesting interpretation in terms of only one cloud displaying a change of column density nearly one order of magnitude from its center to its outer portions. Figure 15 c shows what the column density contours could be like. The cloud appears a little elongated, but for computational convinience it is anyhow assumed spherical. The clouds center is taken between the two largest excesses. The radial dependence of the dust column density is seen on figure 15d, where also is shown a power law fitted to the data: $E(b-y) \propto \varrho^{-0.785}$,r=-0.68. The low correlation coefficient and the largely deviating point are caused by assuming sphericity. Outer low density parts of diffuse clouds may not survive for long if the clouds are overtaken by supernovae blast waves too frequently, Heathcote and Brand (1983). The occurence of clouds with density gradients would accordingly be interesting to evaluate. Unfortunately no unreddened stars have been observed in front of this feature wherefor only an upper distance limit are available,D<300 pc. The clouds equivalent density scales with 1/D. Figure 15e is finally a display of the clouds radial density dependence, assuming a spherical structure. A maximum radius is assumed. The density $E(\varrho)/21(\varrho)$ translates to n(H) = 7958 (E/21)/D(pc) atoms cm^{-3}. At 100 pc the density will vary from 40 cm^{-3} at the center to 10 at the outskirts. At 300 pc the envelope density approximates the WNM density suggested by McKee and Ostriker(1977).

References

Crawford,D.L. 1975,A.J.80,955.
————.1978,A.J.83,48.
————.1979,A.J.84,1858.
Fried,P.M.,Nousek,J.A.,Sanders,W.T.,Kraushaar,W.L. 1980,Ap.J., 242, 987.
Heathcote,S.R.,Brand,P.W.J.L. 1983,M.N.R.A.S.,203, 67.
Hilditch,R.W.,Hill,G.,Barnes,J. 1983,M.N.R.A.S.,204, 241.
Hill,G.,Barnes,J.V.,Hilditch,R.W. 1982,Publ.D.A.O. 16, 111.
Knude,J. 1977a,Astr.Ap.Suppl.,30, 297.
———.1977b,Ap.Letters,18, 115.
———.1978a,in "Astronomical Papers Dedicated to Bengt Strömgren", ed. A.Reiz and T.Andersen,CUO 1978, p.273.
———.1978b,Astr.Ap.Suppl.33,247.
———.1979a,Astr.Ap.Suppl.38,407.
———.1979b,Astr.Ap.77, 198 .
———.1981,Astr.Ap.Suppl.44, 225 .

Knude,J. 1981a Astr.Ap. 97, 380 .
———. 1981b, Astr.Ap. 98,74 .
———. 1982, Astr.Ap.Suppl. 49, 148 .
———. 1983, Astr.Ap. 126, 89 .
Lucke,P.B. ,1978,Astr.Ap. 64, 367 .
McFadzean,A.D. ,Hilditch,R.W.,Hill, G. 1983, M.N.R.A.S.205,525 .
McKee,C.F.,Ostriker,J.P. 1977,Ap.J.218, 148 .
Oja, T. 1981, personal communication to Bengt Strömgren .
Perry,C.L.,Johnston,L. 1982,Ap.J.Suppl.50, 451 .
Perry,C.L.,Johnston,L.,Crawford,D.L. 1982, A.J.87, 1751 .
Strömgren,B. 1966,Ann.Rev.Astr.Ap. 4, 433 .
Tinbergen,J. 1982,Astr.Ap. 105, 53 .
Weaver,H. 1977, IAU Symposium No 84,ed.W.B. Burton,p. 295 .

Table 1

Average color excesses E(b-y) for A and F stars at the NGP, b>70 deg.Only 40 % of the final sample is presented

Distance range pc		N los	E(b-y) mmag	σ(E(b-y)) mmag
20	50	18	11.15	12.75
51	75	102	13.58	14.07
76	100	206	13.52	16.80
101	125	222	13.19	20.61
126	150	286	12.93	19.13
151	175	305	12.94	18.79
176	200	264	13.11	19.43
201	225	210	12.62	19.88
226	250	191	13.57	19.97
251	275	144	15.64	19.38
276	300	108	14.28	17.68

Table 2

Color excess variation across the NGP, b>70 deg, only stars within 100 pc. The three cross sections are defined by the range of BD numbers observed.

BD range	N los	E(b-y) mmag	σ(E(b-y)) mmag
+ 7 2586 +20 2779	112	9.39	17.48
+20 2786 +27 2034	112	13.99	16.59
+27 2037 +44 2289	108	18.41	15.56

Figure Captions

Figure 1. E(b-y) histogram for ~150 stars in 15 square deg at the South Galactic Pole.

Figure 2. E(b-y) histogram for ~450 stars in 50 sq.deg below -45 deg.

Figure 3. E(b-y) histogram for 158 stars with b < -45 deg from Perry & Johnston (1982).

Figure 4. Average E(b-y) in 50 pc bins versus distance for the stars in SA 141.

Figure 5. An example of a lower envelope thought due to inter cloud dust.

Figure 6a. Histogram for E(b-y) of stars with b>70 deg and closer than 50 pc.

Figure 6b. Variation of E(b-y) with distance for the stars described in Fig. 6a.

Figure 7a. Caption as for Fig.6a, but for stars with 75 < D < 100 pc .

Figure 7b. As Fig.7a but with the symmetric counterpart to E(b-y) < 0 removed.

Figure 7c. Caption as for Fig 6b, but for stars with 75 < D < 100 pc.

Figure 8. Distribution of dust columns for stars with D 100 pc and b>70 deg, δ<20 deg. This region covers part of the Virgo cluster.

Figure 9. Location of diffuse dust clouds with known distance.

Figure 10. As Fig. 9, but only upper distance limits are available.

Figure 11. Variation of clouds linear dimensions 2R (pc) with their distance from the galactic plane.

Figure 12. Cloud density n(H) cm-3 versus z(pc).

Figure 13. Example of a $\lesssim$0.8 pc structure in SA 162.

Figure 14. Example of small elongated feature in SA 141.

Figure 15a. Reddening and distance of 13 stars within 0.5 sq.deg in SA 141, projected on the sky.

Figure 15b. Reddening distribution explained in terms of a superposition of two clouds.

Figure 15c. Reddening angular distribution interpreted as a density gradient in only one feature.

Figure 15d. Column density versus radial distance. A power is adopted to the data assuming a spherical cloud: $E \propto \rho^{-0.785}$.

Figure 15e. Radial variation of equivalent gas density n(H).
n(H) = 7958 E(b-y)(ϱ)/2l / D(pc) atoms cm-3. A maximim cloud radius of 50 arc min is assumed. E/2l is measured in mmag/arc min .

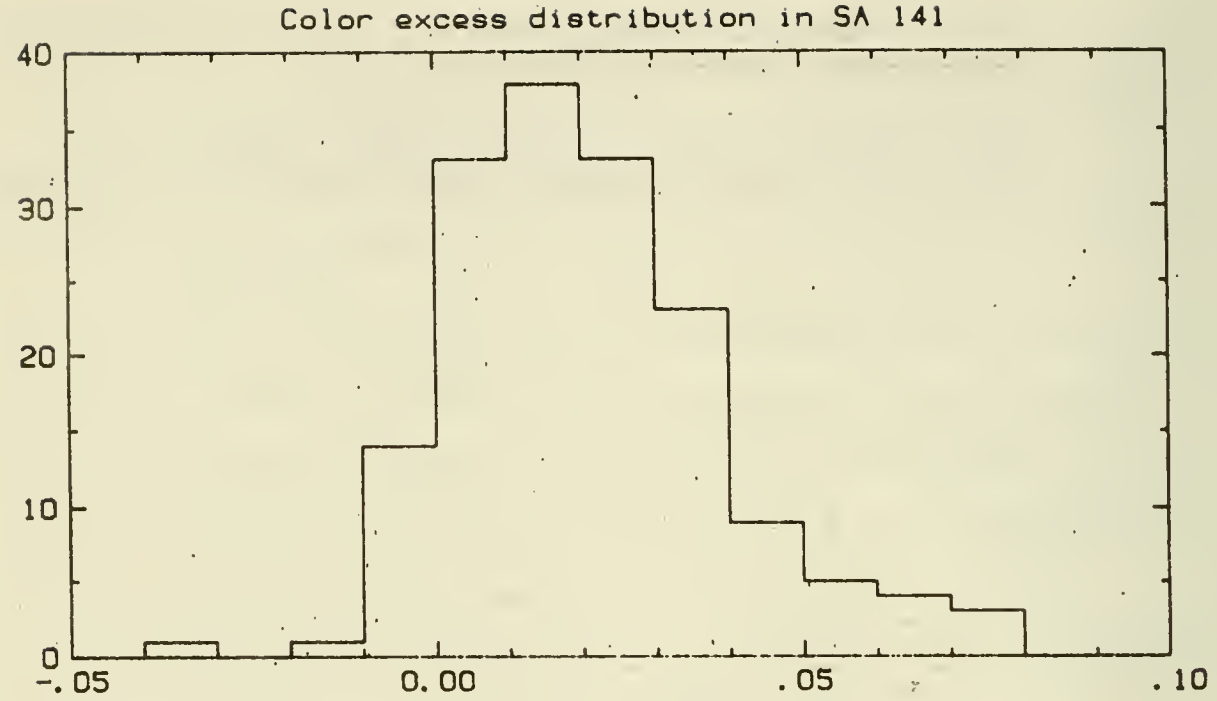

Figure 1

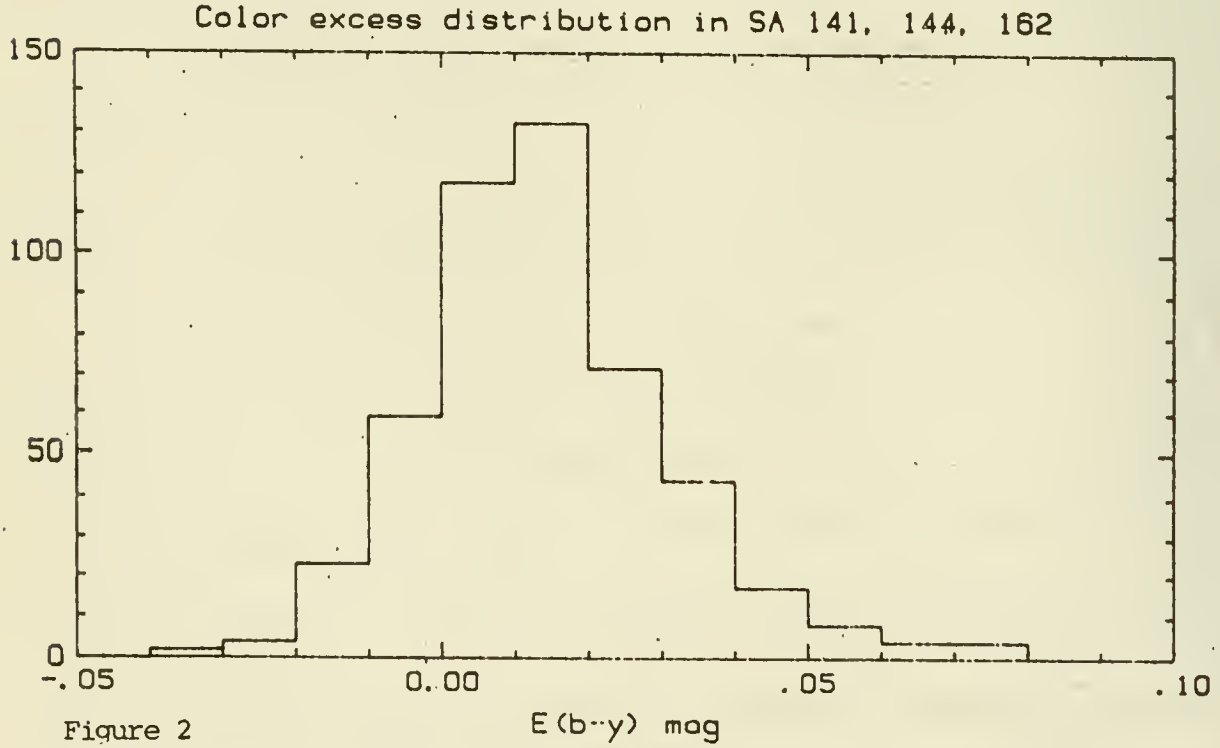

Figure 2

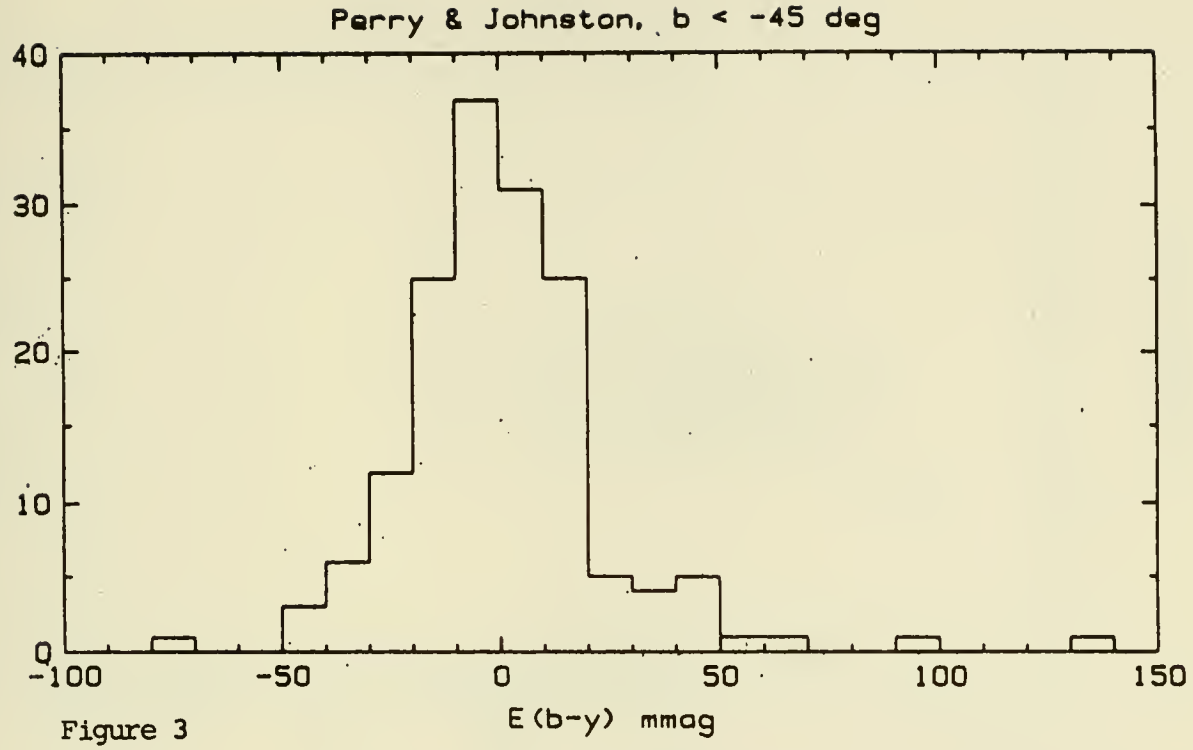

Figure 3

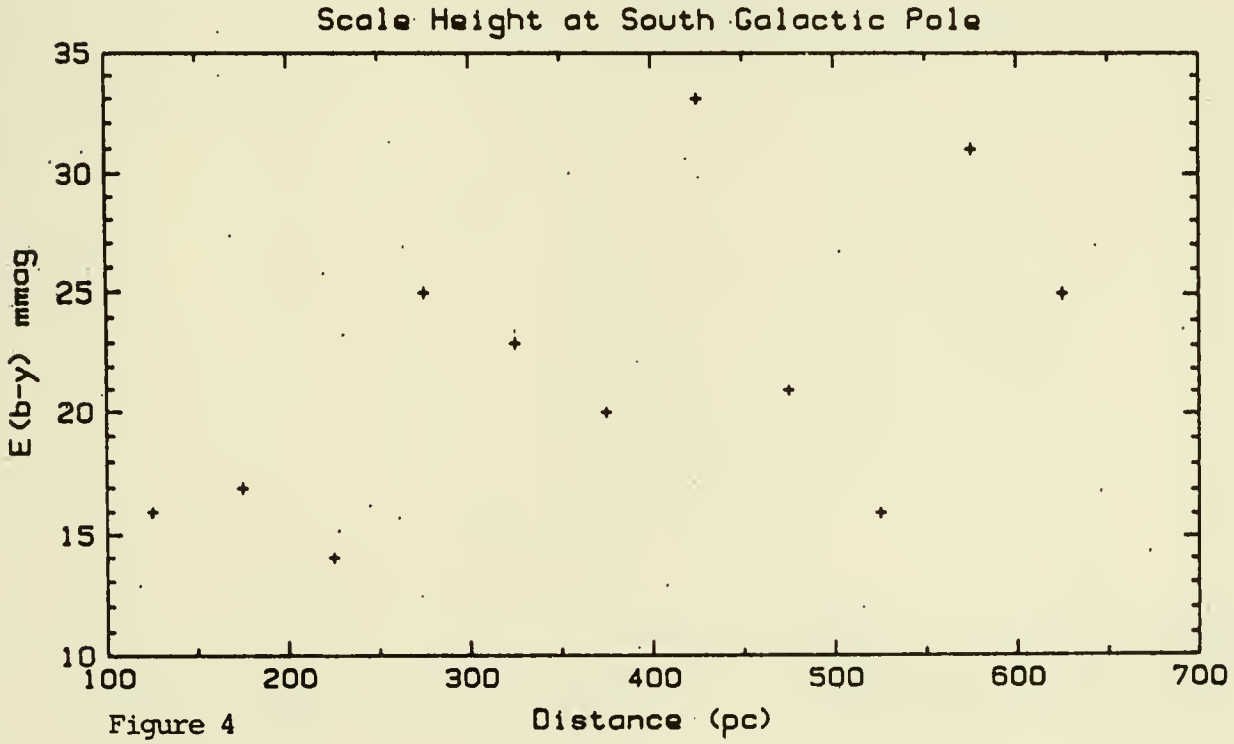

Figure 4

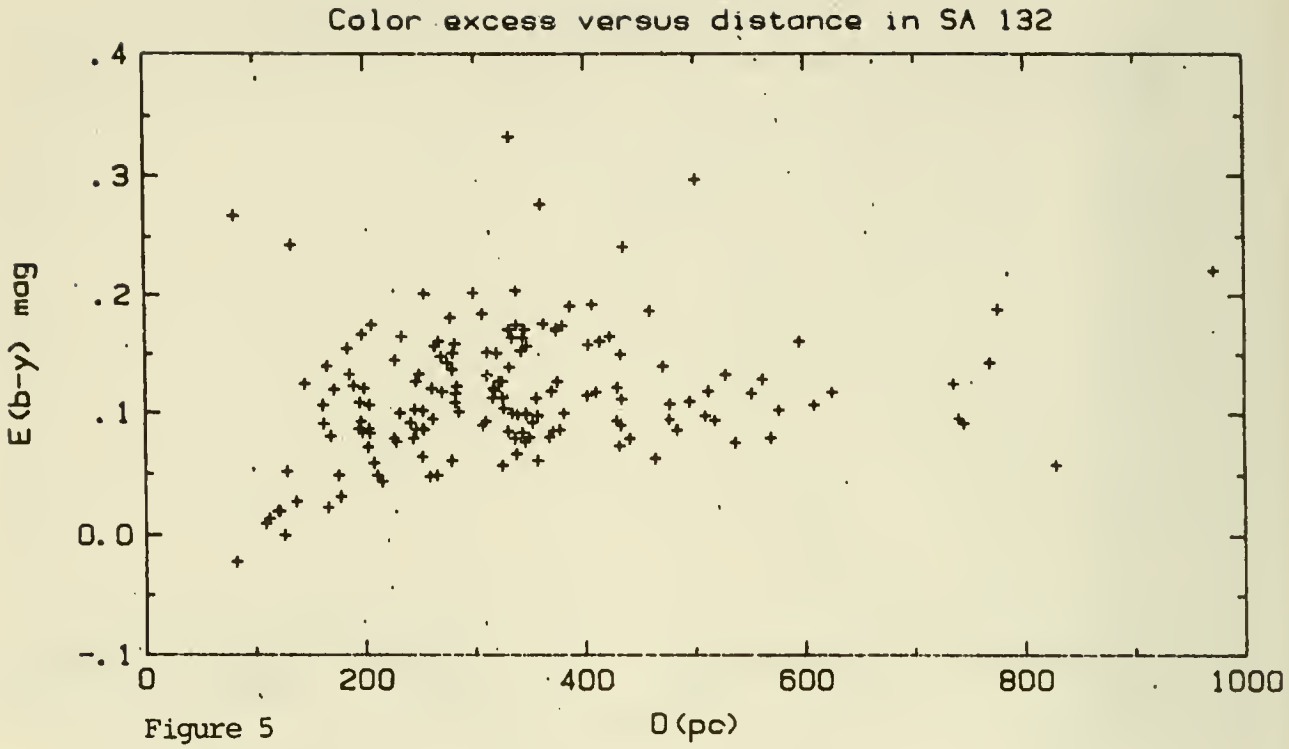

Figure 5

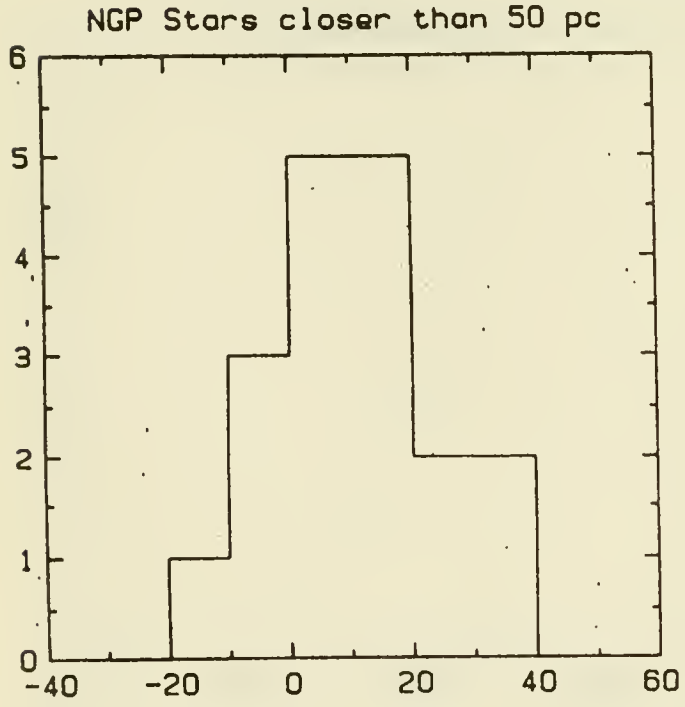

Figure 6a

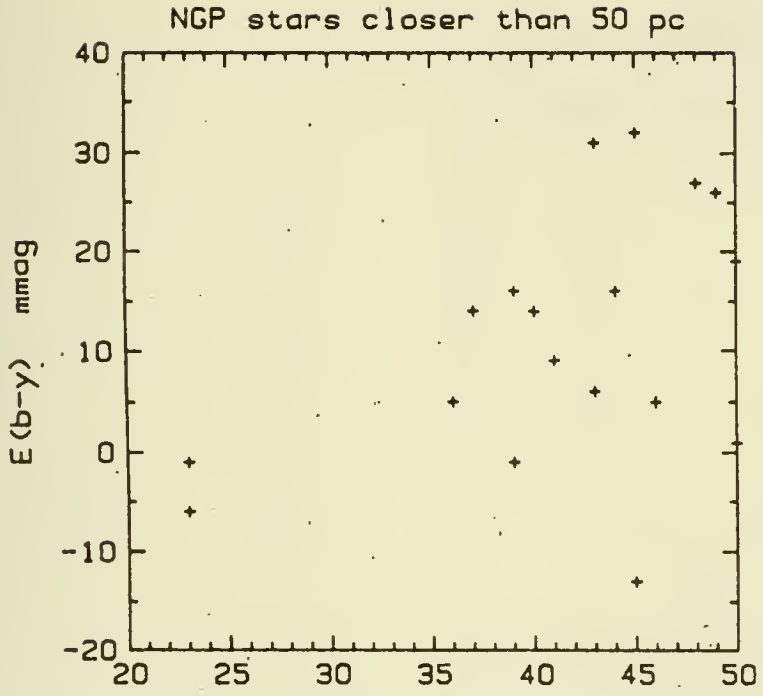

Figure 6b

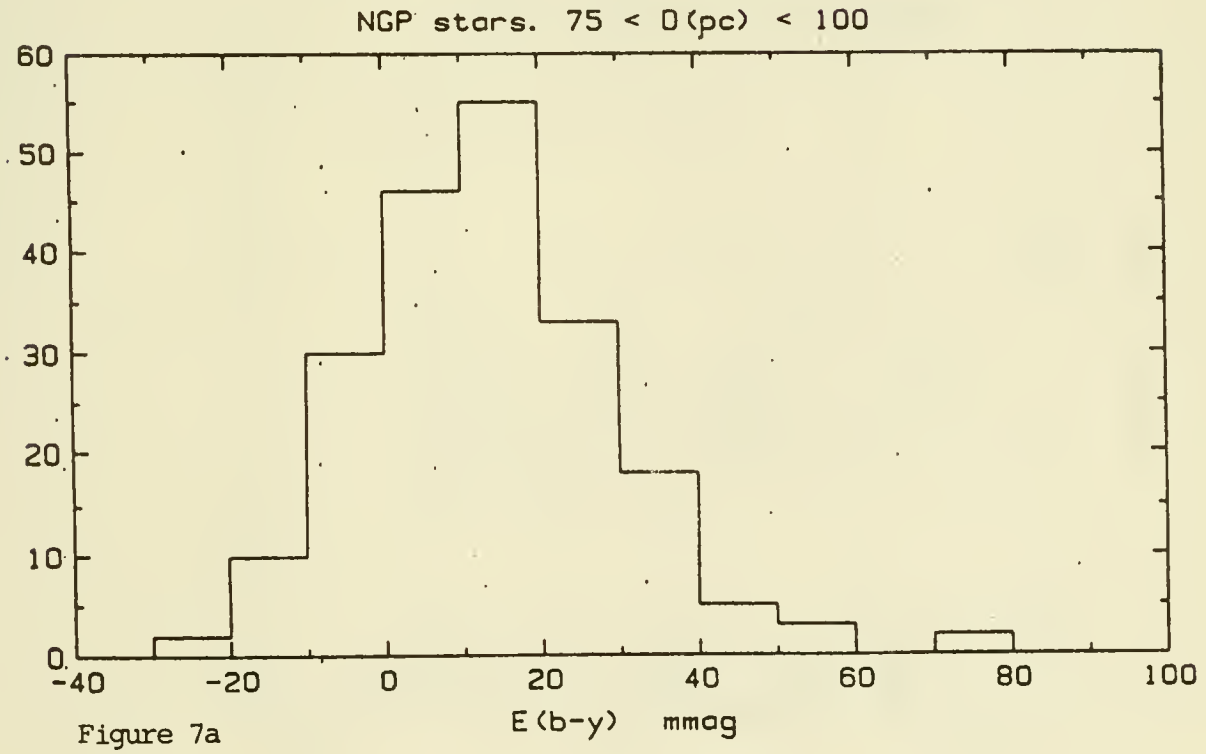

Figure 7a

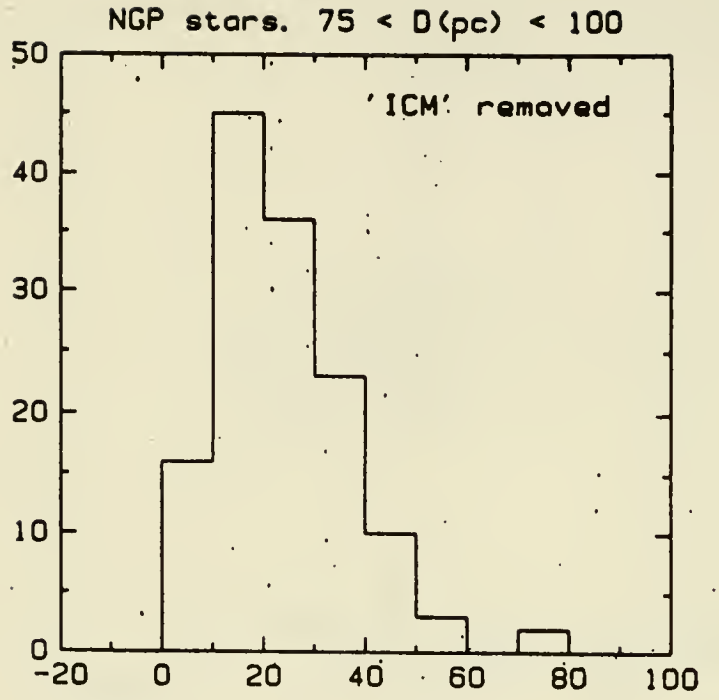

Figure 7b E(b-y) mmag

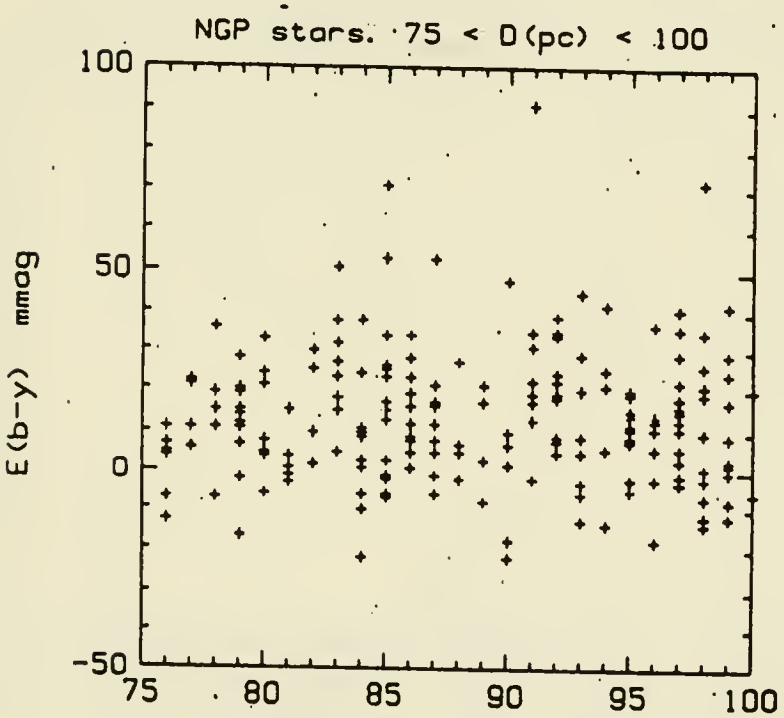

Figure 7c

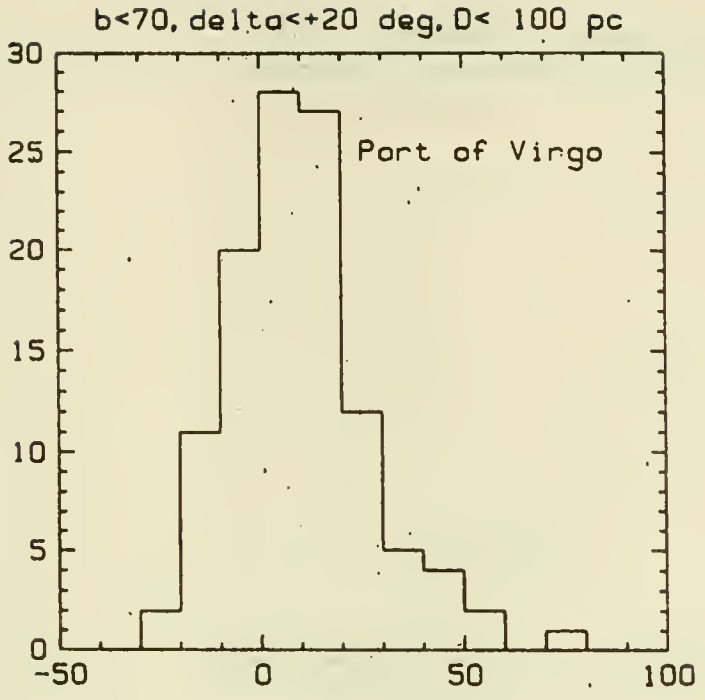

Figure 8

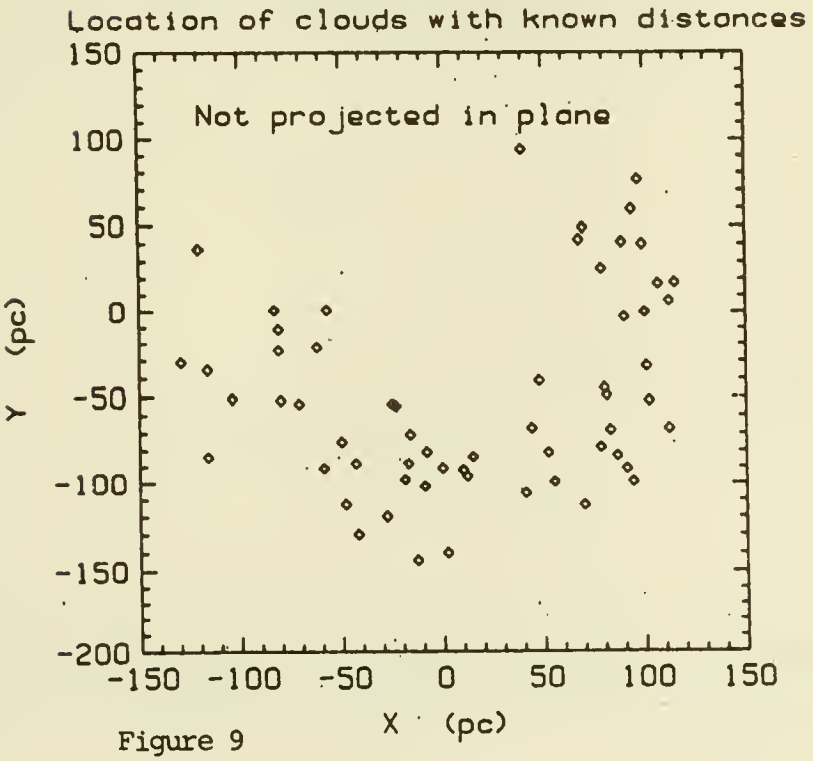

Figure 9

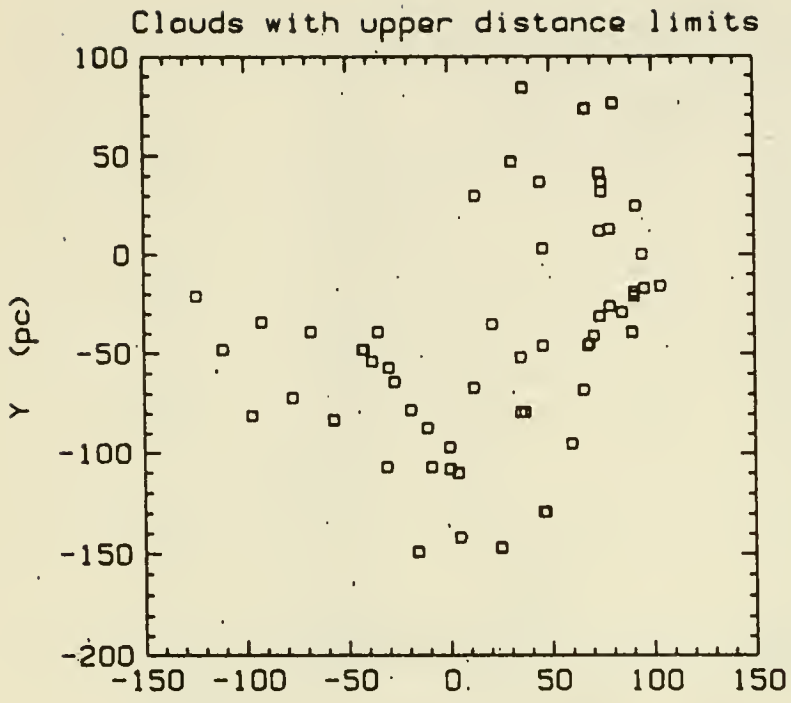

Figure 10

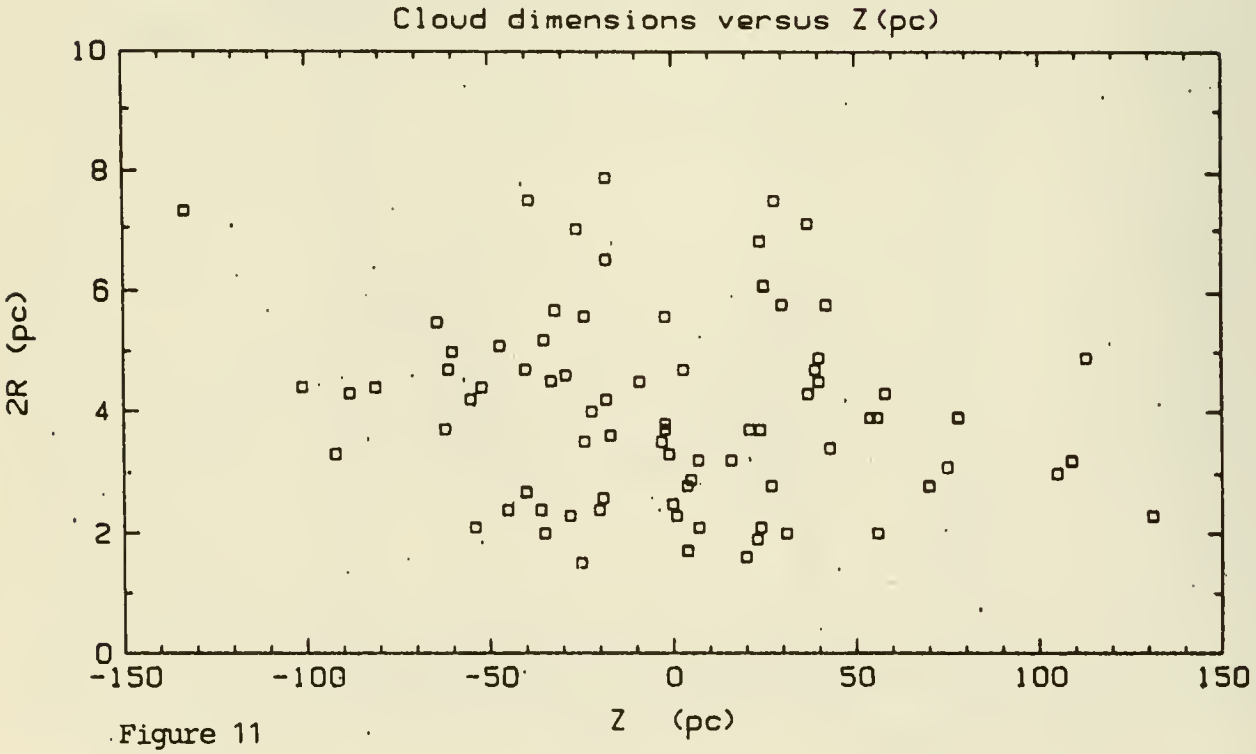

Figure 11

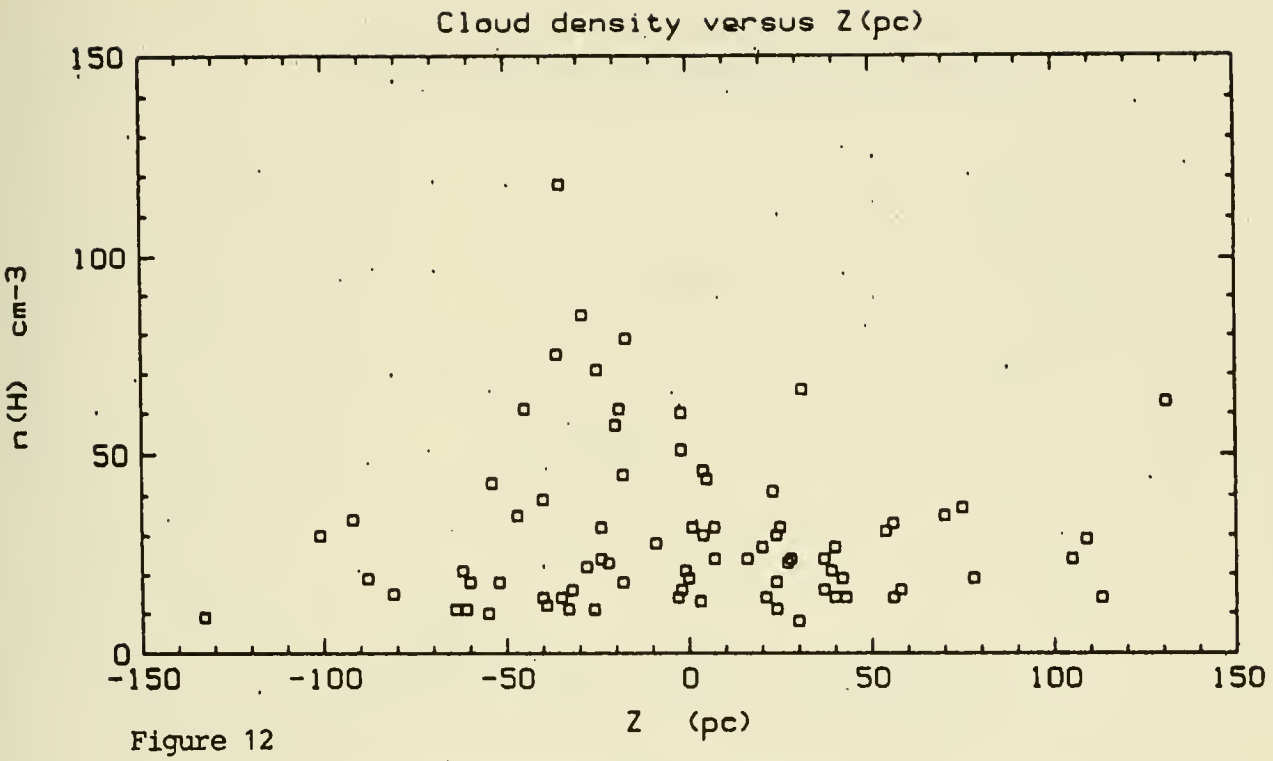

Figure 12

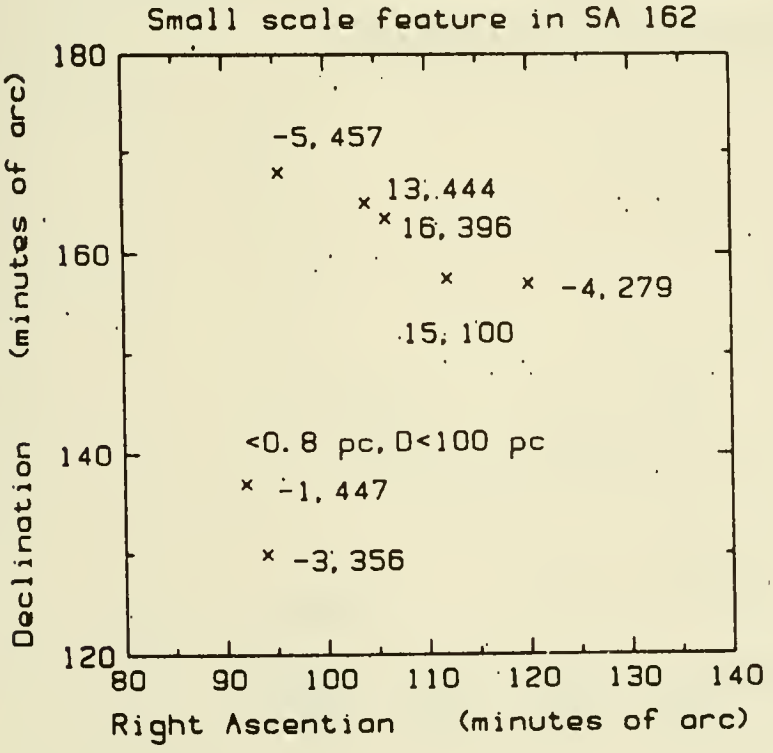

Figure 13

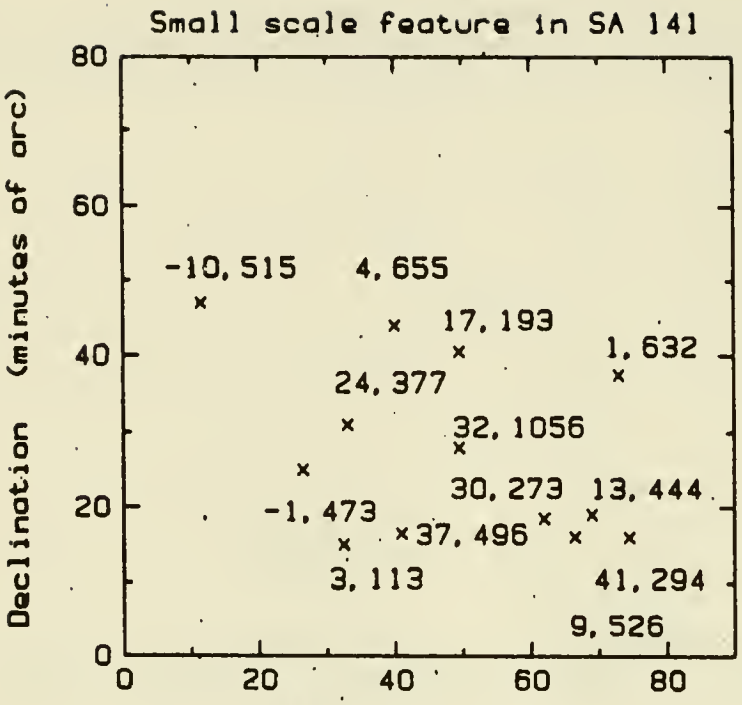

Figure 14

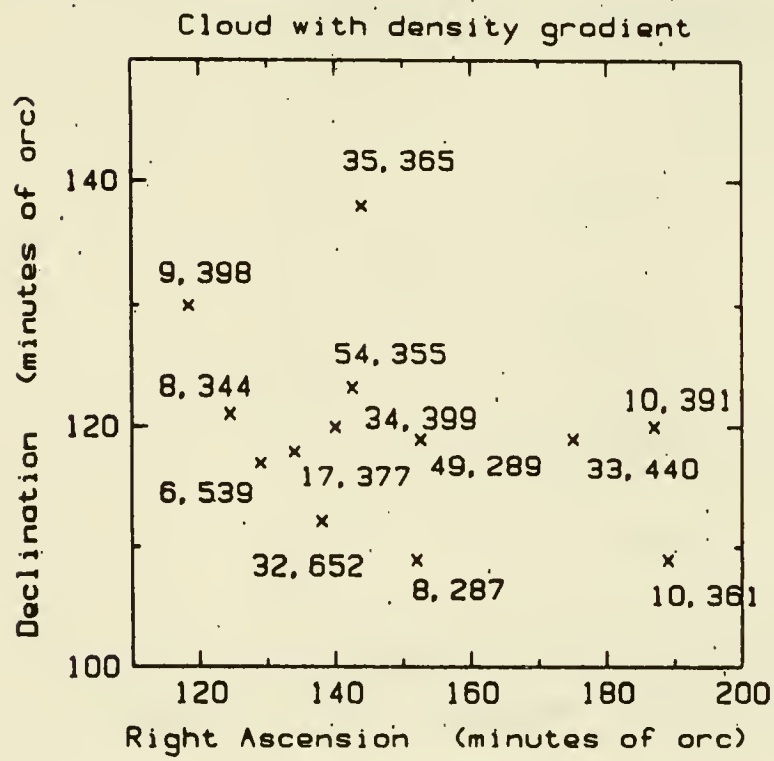

Figure 15a

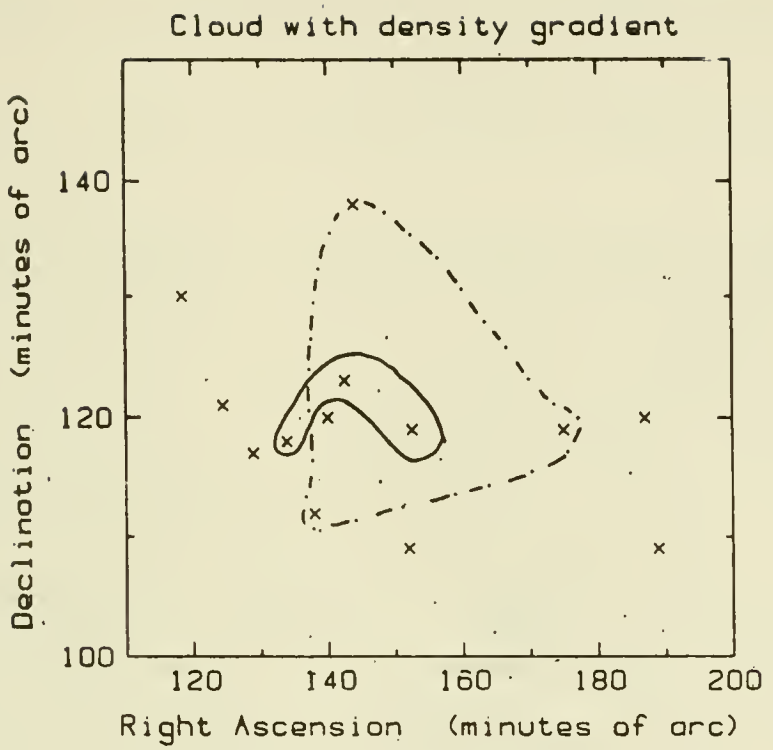

Figure 15b

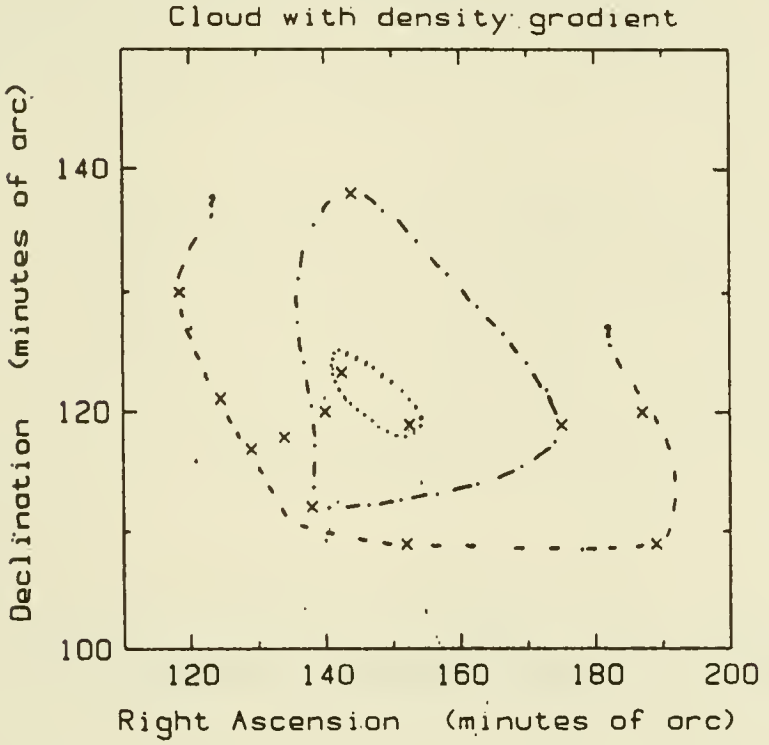

Figure 15c

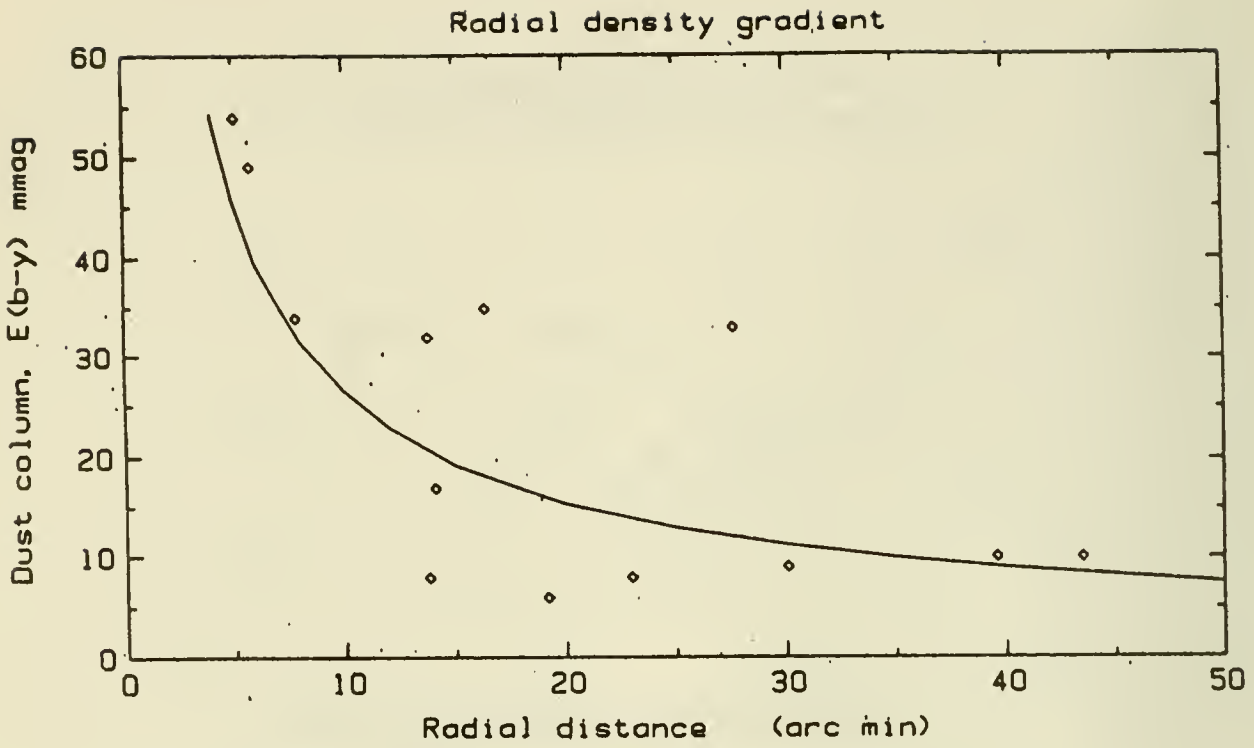

Figure 15 d

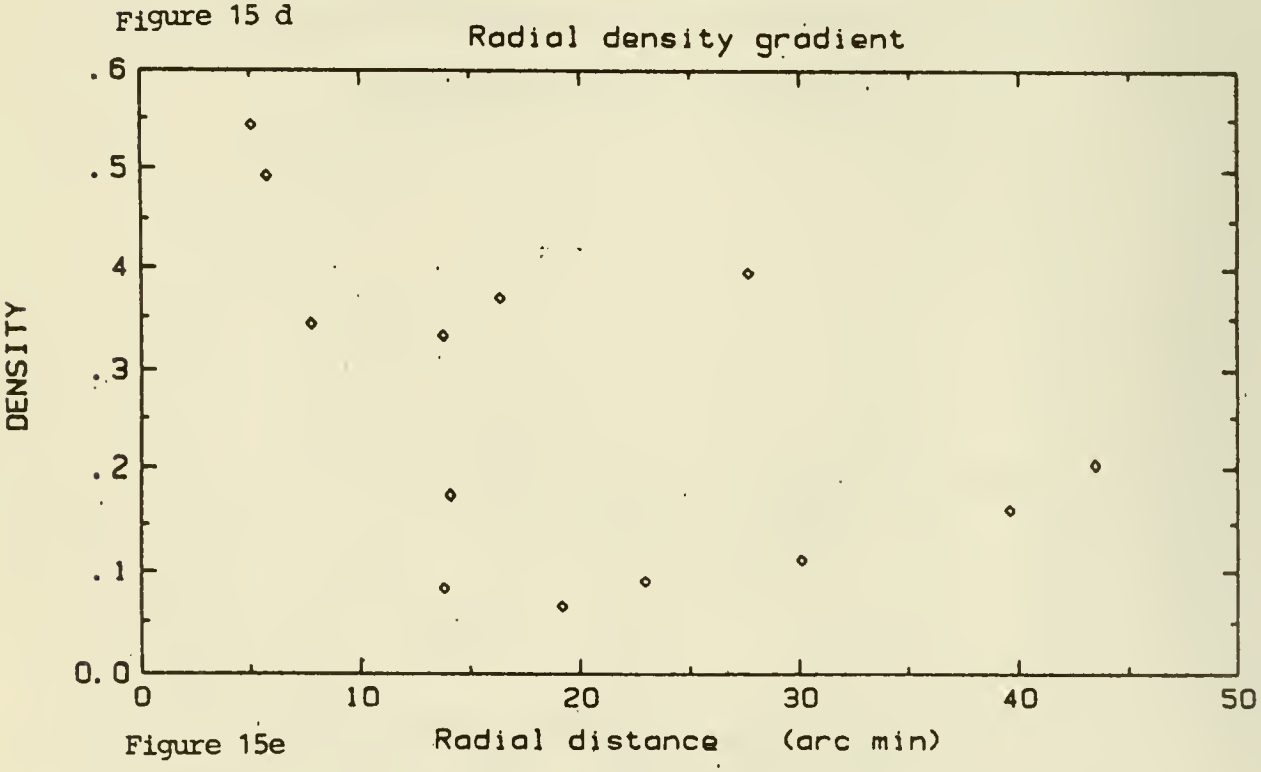

Figure 15e

OPTICAL POLARIZATION AS A PROBE OF THE LOCAL INTERSTELLAR MEDIUM

J. Tinbergen
Sterrewacht, Leiden; Kapteyn Sterrenwacht Werkgroep, Roden (Netherlands)

The use of interstellar polarization as a measurement tool for dust or magnetic field presents practical difficulties (dust and magnetic field configurations inextricably mixed up; limited number of suitable stars). This general rule applies even more in the local environment, for which the polarizations are small and the influence of errors of observation changes in character. Because of this, the use of polarimetry and the design of polarimetric observing programmes for the local interstellar medium must be approached with even greater care than in the general case. I propose in this review to amplify this point, so that the reader can judge for himself to what extent he can use published results and can also, given the opportunity and instrumentation, design an observing programme that will really pay off.
In the immediate solar neighbourhood the average degree of polarization per unit distance is less (possibly much less) than $2.5\ 10^{-6}$ per parsec. At distances between 50 and 100 parsec this figure increases to approximately $3\ 10^{-5}$ per parsec in the Galactic plane and $1\ 10^{-5}$ at the Galactic poles. This information should be taken as very approximate. It is a composite of data from Behr (1959), Walborn (1968), Appenzeller (1974), Piirola (1977) and Markkanen (1979). Table 7 of Tinbergen (1982) provides a summary of this work and relates it to extinction data by Knude (1979) and Neckel and Klare (1980). This sets the astronomical scene. The precision with which polarimetry can nowadays be performed at a number of observatories is about $1\ 10^{-4}$ and this determines the extent to which polarimetry can be used as a local interstellar probe.

The most immediate (<30 pc) local region may be thought of as mostly intercloud medium (the polarization per unit distance, when translated into extinction per unit distance, is consistent with Knude's (1979) intercloud medium). The precision quoted above corresponds to a distance of 40 pc. It is therefore unrealistic to expect to use polarimetry to see detailed structure in this intercloud medium; one may expect to see only local thickenings, which by definition should really not be reckoned part of such a medium, but should perhaps be thought of as the tail of the "cloud" distribution. At larger distances, and particularly in the Galactic plane, the precision quoted corresponds to perhaps 5 pc, so that more spatial detail may be seen. This detail should, however, be interpreted in terms of cloud statistics, rather than a continuous medium.

So far, I have not considered a very practical question: the availability of sufficiently bright stars to obtain the photons required for the precision which we need (and which we can obtain in the way of systematic errors). To obtain a degree of polarization with a precision of 10^{-4} we need approximately $3\ 10^{9}$ incident photons (Q.E.$\simeq$0.1). Using a 300 nm passband and a 10^{4} cm^{2} telescope on a 10th magnitude star, we obtain roughly $3\ 10^{6}$ photons per second and a single observation is going to take 20 minutes of integration

time. One may therefore observe perhaps 20 stars once in a single night and a large programme of n stars each observed 4 times will typically take n/5 nights of dark or grey time on a 1.5-metre telescope. This shows that m_V=10 will always be a rough limit in apparent magnitude for a practicable programme (this does of course depend on the square of the precision one demands). The existing programmes of better than 10^{-4} precision have been limited to the brightest stars (m_V=5), to the first 50 pc, or to special areas like the Galactic poles (see Tinbergen (1982) for references). For extensions to 150 pc denser sky coverage and fainter apparent magnitudes, the potential number of suitable stars is more than 10 000 (extrapolated from 180 with m_V<5 within 35 pc; Tinbergen 1982).

I have mentioned that the influence of observational error has to be examined with care. The reason is that linear polarization is a vector quantity and that we are interested in vectors (either absolute or differential) which are of the same order as the error vectors. It is not a valid approximation to compute the degree of polarization of individual observations and average that. Instead, one must average the Q and U Stokes parameters, but this requires an appropriate frame of reference in which to express them. I have used above a quantity one may loosely refer to as "all-sky average of degree of polarization" as a function of distance. For this the appropriate coordinate frame is not obvious. A quantity which is independent of coordinate frame is the mean square degree of polarization; this can be unambiguously corrected for observational error (Tinbergen 1982, appendix). For use as a probe of dust content this has a slight advantage over the degree of polarization itself. Since linear polarization is proportional to the transverse component of the magnetic field, it is equal to or less than the scaled extinction (e.g. Serkowski et al. fig. 9). The mean square polarization accentuates the higher values, amongst others those where the projection factor is favourable and may therefore be a more reliable dust estimator than the mean polarization itself (it does of course also introduce a bias towards higher values of dust content; it is best to regard the mean square as the prime observable and to compare that with models).
Another kind of error one has to be careful of is that introduced by intrinsic polarization of the stars used as background sources. Criteria for possible intrinsic polarization are:

1) supergiant (extended, anisotropic outer atmosphere);
2) close binary (scattering polarization on companion or gas shell);
3) emission or other spectral peculiarity;
4) CaII K-line activity (solar analogue, but more active);
5) IR excess (circumstellar dust);
6) variable polarization (even when not accompanied by one of the other criteria).

Bearing these many sources of error in mind, we may well ask what we do know of the local interstellar medium from polarization observations. I like to believe that the following statements are approximately correct:

a) on the scale of several hundred parsec, there is a preferential magnetic field direction, as evidenced by observations at the Galactic poles (Appenzeller 1974, Markkanen 1979) and selected longitudes in the Galactic plane (Appenzeller 1974);

b) the local ($r < 50$ pc) region is particular devoid of dust, as evidenced by the mean square degree of polarization as a function of distance (Tinbergen 1982, using also the results by Piirola 1977);

and, less certainly,

c) at a distance of less than 5 pc, there is a patch of dust (Tinbergen 1982) which may be of interest in connection with cloud models.

Lastly, what of the future? When HIPPARCOS flies, reliable distances will become available on a homogeneous system. It would be worthwhile to carry out a polarization programme, extended to the same magnitude limit, at about the same time. For this, the requirements would be:

A) Two telescopes of 10^4 cm^2 aperture, one in the North and the other in the South. 100 to 1 000 nights on each will be needed, depending on the scope of the programme;
B) exclude all stars with possible intrinsic polarization;
C) use a passband from 500 to 700 nm, to discriminate for interstellar and against many types of intrinsic polarization;
D) observe each star at least 4 times and use all possible tricks to randomise error vectors but detect real variability.

Such a programme is time-consuming and requires awareness of all the various pitfalls. It must be carried out by observers and instrumentation dedicated to this for several years. It is only worth doing if the date on local magnetic field, dust content and individual clouds are of sufficient interest and cannot be obtained by more economic means; the present Colloquium should contribute to an informed opinion on this point.

References

Appenzeller I., 1974, Mem. Soc. Astron. Italiana 45, 61.
Behr A., 1959, Veröff. Univ. Sternwarte Göttingen no. 126.
Knude J., 1979, Astron. Astrophys. 77, 198.
Markkanen T., 1979, Astron. Astrophys. 74, 201.
Neckel Th. and Klare G., 1980, Astron. Astrophys. Suppl. 42, 251.
Piirola V., 1977, Astron. Astrophys. Suppl. 30, 213.
Serkowski K., Mathewson D.S., Ford V.L., 1975, Astrophys. J. 196, 261.
Tinbergen J., 1982, Astron. Astrophys. 105, 53.
Walborn N., 1968, Publ. Astron. Soc. Pacific 80, 162.

Postcript to "Optical Polarizaton" - J. Tinbergen

Worried by the expense in telescope time and manpower of the very precise polarimetry required for local interstellar medium investigations, I asked in the general discussion whether it was all worth while, particularly:

-- is the magnetic field of any consequence for local considerations, or is it merely the result of wherever the ionised matter has swept it?
-- if the latter, can the magnetic field configuration tell us something about the history of the gas that drove it into that configuration (cf. SNR radiopolarimetry)?
-- failing this also, can polarization serve some other purpose locally?

Two discussion answers were:

-- magnetic field forces are of importance in supporting hot coronal gas at high z.
-- one may detect that a line of sight passes through a dust cloud from polarimetry of stars at various distances. This technique is 5 to 10 times more sensitive than colour excesses.

I feel this is a somewhat restricted use of hard-to-obtain data. The trouble is that most other techniques applicable to the local interstellar medium are expensive, too.

A point I did not mention explicitly is that in localising clouds in space, one uses differences in colour excess or polarization between 2 stars. Therefore the observing precision required is the same throughout the volume investigated. The problem is not eased as one obtains larger colour excesses and polarizations at increasing distance. This is why I did not mention the older, less precise polarimetry at distances greater than about 50 pc. Such polarimetry is useful for line-of-sight integrals, but is not precise enough to be used differentially as considered during this Colloquium.

If the mismatch between colour excess and polarization precision can be reduced by improved photometry (e.g. by a longer wavelength base and redundant photometry of several absorption lines or spectrophotometry), one may expect to be able to derive approximate magnetic field projection factors from the ratio of (differential) polarization to colour excess (this would assume "uniform" magnetic field strength and dust alignment).

Do the arching HI filaments show in local reddening data ?

Jens Knude

Copenhagen University Observatory

Probable dust counterparts of arching structures are looked for in two cases. (a) the Eridanus expanding shell, Heiles (1976) and (b) the extended Sco-Cen feature, Weaver (1977). Apparently the color excess data may be used to derive distance and dimension estimates of these structures.

(a). Color excesses from two areas SA 121 and SA 144 situated on the position of the 3.2 - 6.3 km/s velocity-slice are applied. Some stratification of the color excesses is noticed for both areas but extreme patchiness typifies particularly the dust in the SA 144 region,Figure 1. This Figure differs from the normal appearence of such diagrams for magnitude limited stellar samples by having an upper reddening limit,constant with distance. This fact alone may indicate the presence of a wall like structure. Three distinct reddening levels E(b-y) are present: 0.012, 0.018 and 0.030 mag. But not over the complete area, only in certain cross sections. If these reddenings are assumed to be due to dust in the HI shell when it is first met, for the second crossing and for lines of sight penetrating the shell twice respectively, the distance to the shells center and its radius may be estimated from the spatial location of the dust. Velocities of interstellar absorption lines for these stars are required to justify this assumption. Figure 2 displays the level E(b-y) = 0.012 mag attributed to the near part of the shell in a 20′by 300′section along the NW-SE diagonal of the area. Stars in this subsample have constant longitude. The distance to the 0.012 mag dust is accurately determined to 110 pc, because the dust is known to be within 115 pc and some unreddened stars are observed in front of it as far out as 100 pc. The 0.018 and 0.03 mag levels are displayed in Figure 3 and 4 respectively. The distance to the 0.018 level is similarly derived to 165 pc whereas only an upper limit,170 pc, for the combination 0.030 mag is deducible. As SA 144 is 14 deg from the shells center a simple calculation results in a distance 137 pc to the shells center and a radius of 46 pc. Only three stars are found to have reddenings above 0.03 mag, indicating the presence of a level at 0.05 mag within 300 pc, about the minimum distance to the H filaments studied by Reynolds and Ogden (1979) at this latitude.Reddenings in SA 121 also display the three levels and their distances result in an estimate 126 pc to the shell center and a ra-

dius of 51 pc. Originaly Heiles (1976) suggested a distance 150 pc to the shells center and a radius 49 pc.

(b). Color excesses in the direction of the proposed Sco-Cen bubble show an organized variation with distance.Most stars more distant than 150 pc have reddenings above 0.02 mag and levels off at 0.07 mag, Figure 5. Such a behaviour may be due to a spatialy confined,non coherent structure with some diffuse matter inside it. Sampling effects can cause biased interpretations. Figure 6 and Figure A = Figure 5 in Knude (Local Interstellar Extinction) go fainter than Figure 5 and more reddened parts of the same volume are picked up. These two figures have a clearly defined lower envelope fitting well to the upper confinement of Figure 5. A sample of B stars beyond 300 pc has also a distinct lower reddening limit. Within the shell concept excesses on the lower envelope of Figure 5 originate either on the front or on the backside; excesses on the upper envelope of Figure 5 are caused by two crossings and a contribution from the matter behind the shells backside. The lower envelopes of Figure 6 and A are populated by reddenings from two encounters, points above in addition by non swept up dust inside. The absence of distant low excess stars may be taken as an indication of a pervasive homogeneous medium.

Shell dimensions are estimated from SA 193,(l,b)= (293,0). Figure 7 shows the excess levels pertaining to the first and combined encounters. From this reddening distribution the shell radius is estimated to 140 pc and the distance to the expansion center to 190 pc. With this dimension and the reddening variation for stars beyond 400 pc in Figure A,which is postulated to be similar to that in the medium before the bubble was blown. The slope of the envelope gives an estimate of a density in a postulated homogeneous medium : 0.22 atoms cm -3. This translates to a swept up gas mass 10**5 solar masses, as a lower limit because the diffuse dust clouds have not been accounted for. The mass of the moving gas has been computed to 10**6 solar masses, Weaver (1977).

References

Heiles,C.,1976,Ap.J.(Letters)208,L137
Reynolds,R.J.,Ogden,P.M.,1979,Ap.J.229,942
Weaver,H.F.,1977,in IAU Symposium 84,ed.W.B.Burton,p.295 .

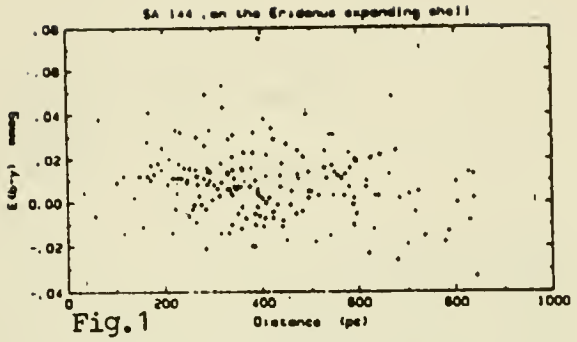

Fig.1

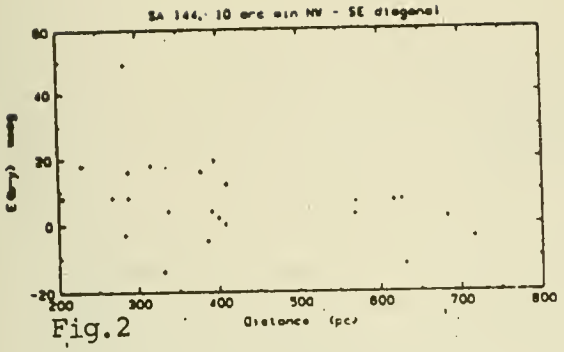

Fig.2

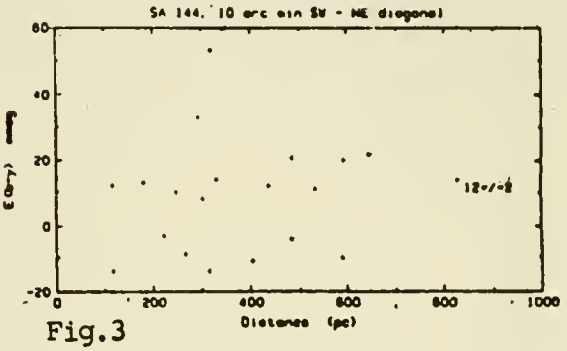

Fig.3

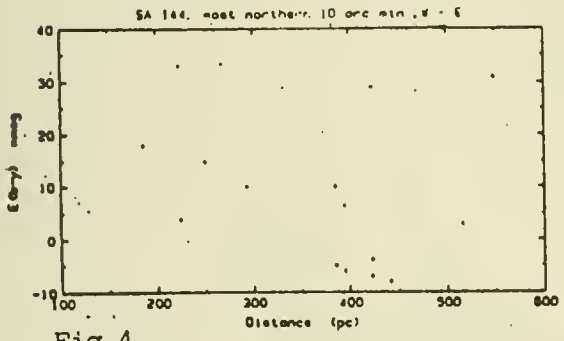

Fig.4

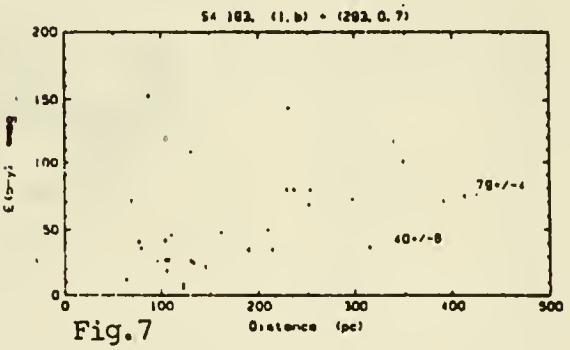

Fig.7

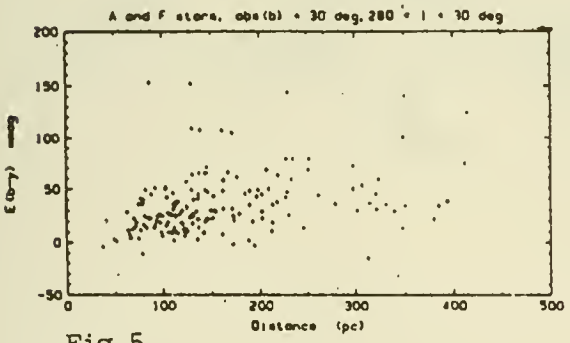

Fig.5

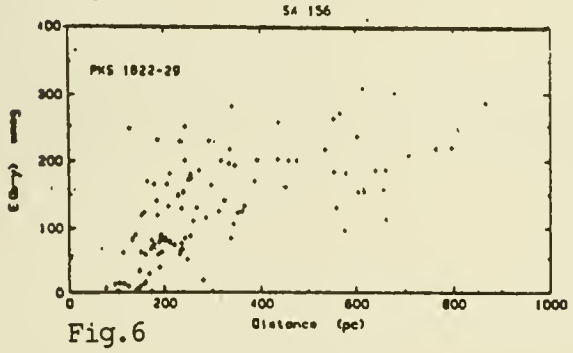

Fig.6

A LARGE-SCALE DARK CLOUD SYSTEM IN THE NORTHERN SKY

Wolfhard Schlosser
Astronomisches Institut, Ruhr-Universität Bochum,
Germany

Wide-angle photographs of the Northern Milky Way reveal a complex system of dark clouds covering the galactic longitudes from $l = 9o^{\circ}$ to about $l = 2oo^{\circ}$ (fig.). This Northern Dark Cloud System is a coherent structure of individual clouds of preferentially cellular appearance. The cloud system has to be assigned to the local spiral arm. This is substantiated by the large extent in galactic latitudes and its proximity to well-established tracers of the local spiral arm.

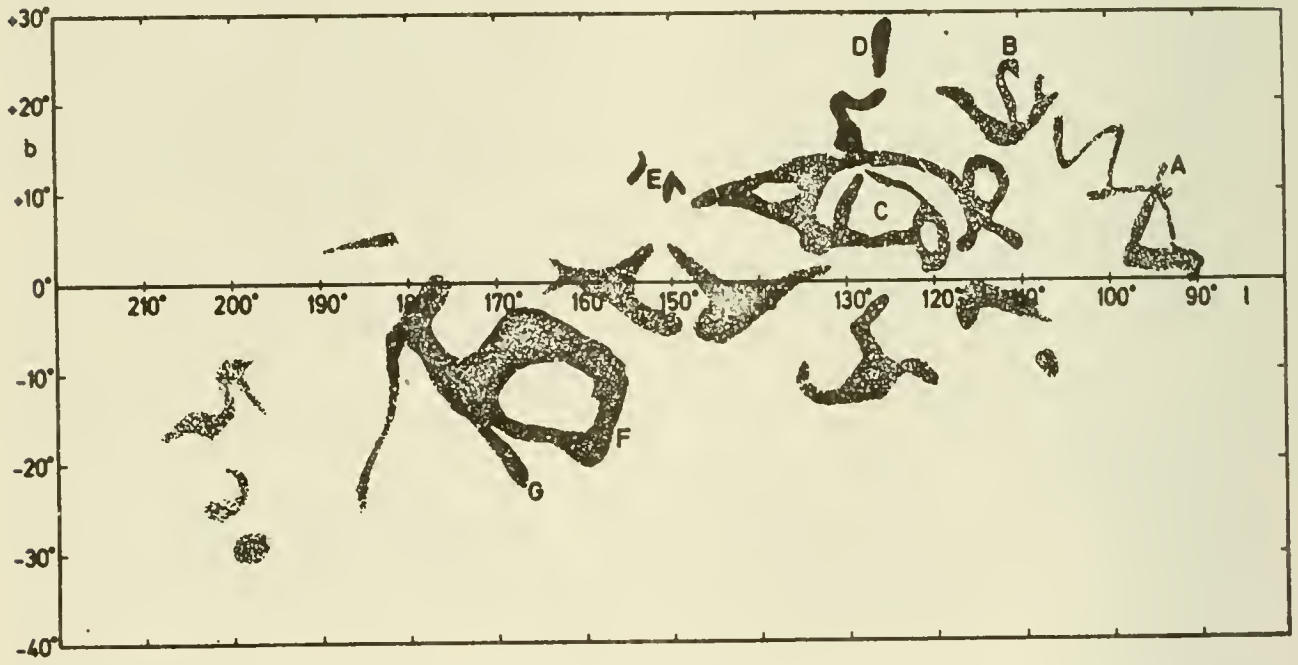

The Northern Dark Cloud System between $l = 9o^{\circ}$ and $l = 2oo^{\circ}$. The letters refer to individual structures discussed in a forthcoming paper (Astronomy and Astrophysics, in print).

HOT GAS IN THE LISM: OPTICAL, UV, AND EUV WAVELENGTHS

OBSERVATIONS OF ABSORPTION LINES FROM HIGHLY IONIZED ATOMS

Edward B. Jenkins

Princeton University Observatory
Princeton, N. J. 08544

ABSTRACT

In the ultraviolet spectra of hot stars, we can see absorption lines from highly ionized species in the interstellar medium. Observations of these features have been very influential in revising our perception of the medium's various physical states and how gases in space are heated and ionized. The pervasiveness of O VI absorption lines, coupled with complementary observations of a diffuse background in soft x-rays and EUV radiation, shows that there is an extensive network of low density gas ($n \approx$ few$\times 10^{-3}$cm^{-3}) existing at "coronal" temperatures, $5.3 \lesssim \log T \lesssim 6.3$. Thus, while we once thought that x-rays and cosmic rays were the dominant sources of excitation and heating of the interstellar gas, we now realize that shocks created by supernova explosions or mass loss from early-type stars can propagate freely through space and eventually transfer a large amount of energy to the medium. To create the coronal temperatures, the shocks must have velocities in excess of 150 km s^{-1}; shocks at somewhat lower velocity ($v \lesssim$ 100 km s^{-1}) can be directly observed in the lines of Si III. Observations of other lines in the ultraviolet, such as Si IV and C IV, may highlight the widespread presence of energetic uv radiation from very hot, dwarf stars. More advanced techniques in visible and x-ray astronomical spectroscopy may open up for inspection selected lines from atoms in much higher stages of ionization.

I. BEGINNINGS

Well before space-borne instruments were launched to observe ultraviolet absorption lines from the interstellar medium, it was suggested that features from highly ionized atoms might provide a valuable insight on the magnitude and character of ionizing and heating processes which were responsible for the observed physical states of gases in space. Early proposals centered on the notion that primarily neutral gas (HI regions) occupied most of the space, and that low energy cosmic ray particles or x-rays were responsible for the observed temperature and small traces of ionization (Pikel'ner 1967, Spitzer 1968, Spitzer and Tomasko 1968, Field, *et al.* 1969, Spitzer and Scott 1969, Goldsmith, *et al.* 1969, Silk and Werner 1969, Dalgarno and McCray 1972). Since low energy cosmic rays are shielded from us by interplanetary magnetic fields and low energy x-rays were difficult to measure with existing experiments, we could not measure the strength of these proposed sources of heating and partial ionization. Instead, it was suggested that the fluxes could be ascertained indirectly by observing the interstellar abundances of some highly ionized forms of particular heavy elements, such as C III, C IV, N III, N

V, Si III, Si IV, S III and S IV, all which had strong resonance lines in the ultraviolet (Silk 1970, Silk and Brown 1971, Weisheit 1973).

A few years after a search for such absorption features in stellar spectra had been initiated by the *Copernicus* satellite, Steigman (1975) cautioned that the highly charged ions could be severely depleted in HI regions if, as seemed likely, the cross section for charge exchange with the neutral atoms were reasonably high. This effect could be much more important than recombinations with free electrons considered earlier. In the years which followed, Steigman's warning was shown to be valid: Blint, *et al.* (1976) calculated $\langle \sigma v \rangle \approx 10^{-9} \mathrm{cm}^3 \mathrm{s}^{-1}$ for charge exchanges between C IV and H for temperatures between 1000 and 20,000 K, and similar conclusions for N IV, the primary reservoir for the observable N V, were derived by Christensen, *et al.* (1977). These calculations using the scattering approximation were valid only for impact energies ~ 1 eV, but Watson, *et al.* (1979) carried out quantal calculations which showed that the large cross sections persisted even to energies which were characteristic of temperatures in ordinary, dense interstellar clouds ($T \sim 100$ K).

While these theoretical conclusions muted one particular incentive for observing highly ionized atoms in the interstellar medium,[1] the *Copernicus* researchers were also interested in the prospect of detecting low density, *thermally ionized* gases which could conceivably inhabit some voids between the clouds of ordinary, cool H I. Their efforts were rewarded by an early indication of absorption near the wavelength of the 1032 Å feature of O VI in the spectra of α Eri and λ Sco, reported by Rogerson, *et al.* (1973). There soon followed definitive studies which showed that both members of the O VI doublet could be seen in many stars, that the absorptions were very likely interstellar, and that the high state of ionization was created by collisions in a hot plasma, instead of cosmic ray or x-ray bombardment in an ordinary cool gas (York 1974, Jenkins and Meloy 1974). From the ubiquity of the O VI lines and their large apparent widths, coupled with a lack of conspicuous features from other ions having a slightly lower ionization potential, these authors concluded that low density gases having a temperature somewhere in the interval 2×10^5 to 2×10^6 K were pervasive.

The O VI findings were published concurrently with an article by Williamson, *et al.* (1974), who suggested that the diffuse, soft x-ray background radiation observed from their sounding-rocket experiments originated from the same very hot medium, although their measurements were mostly sensitive to emissions from gases at the upper end of the temperature range, 1 to several $\times10^6$ K. These two fundamentally different experimental results, the detections of uv absorption features and the emissions at x-ray energies, were important milestones which precipitated a new era of thought on the state of the interstellar medium. In many respects, the widespread existence of hot material was reminiscent of a proposal by Spitzer (1956) that the corona of our galaxy is comprised of a very low density medium in a temperature regime similar to that of the solar corona.[2]

---

[1] Other ways were found to measure indirectly the cosmic ray and x-ray ionization rates in the interstellar medium, using the abundances of HD and OH which are influenced by the proton densities (O'Donnell and Watson 1974, Jura 1974, Black and Dalgarno 1973).

[2] Unfortunately, the *Copernicus* satellite lacked the sensitivity to measure the spectra of sources more than 1 or 2 kpc. from the galactic plane, so the structure of a corona of our galaxy could not be investigated. Recent data from the IUE satellite show evidence for an excess of Si IV and C IV in high latitude sources, indicating the presence of material at "transition layer" type temperatures (Savage and deBoer 1979, 1981, Pettini and West 1982), but the wavelength cover-

II. INVESTIGATION OF THE O VI-BEARING GAS

a) Origins: Stellar, Circumstellar or Interstellar?

The first, and perhaps most critical challenge for those who advocate an interstellar interpretation for certain absorption lines is to convince the skeptics that the stars themselves, or their influences on the environment, are not responsible for the observed features. This problem is not a new one; controversy in this area extends back to the turn of the century when the first interstellar lines, those of Ca II, were identified in the spectra of binary stars (Hartmann 1904, Slipher 1909). For the O VI features, which must arise from material which is subjected to strong heating, a resolution of circumstellar versus interstellar origins is particularly relevant, inasmuch as the O and B type stars which produce enough radiation to show features at 1032 and 1038Å are the very stars which must deliver a large amount of energy to the environment. Plausible theoretical interpretations of the observed O VI column densities were advanced for both viewpoints: The O VI could reside in zones associated with the target stars or whole groups of stars in the association (the "interstellar bubbles" of Castor, *et al.* 1975; also see Weaver, *et al.* 1977) or, alternatively, there could be an interconnected network of regions in space heated, on successive occasions, by supernova blast waves (the "interstellar tunnels" of Cox and Smith 1974).

While the atmospheres of hot stars are responsible for broad O VI absorption features, often with P-Cygni type characteristics, the radial velocities of the narrower features identified as "interstellar" show no correlation with stellar velocities (Jenkins and Meloy 1974, Jenkins 1978b), nor are the O VI lines influenced in any way by the stars' projected rotational velocities, $v \sin i$. In addition, York (1977) studied the O VI feature in the spectrum of the spectroscopic binary λ Sco and found no variation with orbital phase.

The possibility that O VI is circumstellar is a more difficult issue to address. A detailed discussion of the observational clues was presented by Jenkins (1978c), based on a comprehensive survey of O VI lines (Jenkins 1978a) which followed the earlier discoveries. Briefly, Jenkins concluded that *most* of the O VI came from truly interspersed material, but that *some* of the absorptions might be attributable to the evaporation zones within the very hot cavities created by the high velocity mass loss from the stars being observed, as described by Castor, *et al.* (1975) and Weaver, *et al.* (1977).

An interesting outgrowth of Jenkins's (1978c) analysis which is relevant to the local interstellar medium is that the general rate of increase of the O VI column density N(O VI) with distance r, while indicating an average density n(O VI) = 1.7×10^{-8}cm^{-3} but with considerable scatter, favors the existence of a positive intercept with N(O VI) of around 5×10^{12}cm^{-2} at $r=0$.[3] This offset could be

---

age of IUE does not extend down to the O VI lines, so the structure of material at "coronal" temperatures has yet to be determined. This paper will not dwell on the conclusions about gas away from the galactic plane, since the theme of this volume is on the properties of the local interstellar medium.

[3] The few lines of sight with anomalously high column densities (containing Jenkins's [1978b] "second population" regions) were excluded in this study. If one were to include these regions and also insist the intercept is really zero, the average n(O VI) increases to 2.8×10^{-8} cm^{-3}.

interpreted either as an excess resulting from the circumstellar bubbles around many of the stars, or as a contribution from a local concentration of hot gas in our neighborhood which has a disproportionate influence because all of the lines of sight, by necessity, emanate from a single point instead of being randomly scattered about.

b) General Properties

A striking feature of the O VI profiles seen in the survey of 72 stars reported by Jenkins (1978a) is that the dispersion of radial velocities is much smaller than that expected from the shock speeds of $v \sim 150$ km s^{-1} needed to heat the gas to the temperatures $T \sim 3\times10^5$ K for collisionally ionizing oxygen to +5. A composite of all the profiles extending over a total distance of about 50 kpc. to all of the stars had an *rms* spread in radial velocity of 28 km s^{-1}, after applying small corrections to compensate for differential galactic rotation. Moreover, Jenkins (1978b) examined the statistical behavior of the velocity centroids and widths of profiles seen in the individual lines of sight, and he concluded that the distributions were consistent with the notion that individual packets of O VI, each with a column density of about 10^{13}cm^{-2} and internal broadening of 10 km s^{-1}, moved about at random with an *rms* dispersion of radial velocities of only 26 km s^{-1}. Large fluctuations in average O VI densities to different stars independently supported the idea of discrete domains of O VI-bearing gas; such variations were in accord with the expected Poisson statistical fluctuations.

While appreciable concentrations of O VI can exist in collisional equilibrium for temperatures in the range $1.7\times10^5 - 2.0\times10^6$ K (Shull and Van Steenberg 1982), the relative lack of accompanying N V absorptions (York 1977) indicates that most of the material is at $T > 2.5\times10^5$ K, since N V has its peak fractional abundance at $T \sim 1.8\times10^5$ K. The narrowness of many of the individual profiles ($\langle v^2\rangle^{1/2} \lesssim 14$ km s^{-1}), however, puts a restriction on the amount of thermal doppler broadening present, which means $T < 16 m_p \langle v^2\rangle / k = 3.8\times10^5$ K. Actually, the proposition that the hot gas is nearly isothermal is probably overly simplistic and has no compelling theoretical justification.[4] Jenkins (1978b) showed that the effects from the above mentioned observational constraints, when integrated over the peak of the curve for the O^{+5} ionization fraction with temperature, still permitted a power-law distribution in temperature for the electron density n_e, with $d\,n_e / d\ln T = T^{0.5\pm0.5}$ for $4.7 \lesssim \log T \lesssim 6.3$.

The most difficult attribute to measure for the O VI-bearing gas is the average volume filling factor $f \equiv \langle n_e\rangle^2 / \langle n_e^2\rangle$. Contrary to what is seen for the low

[4] Paresce, *et al.* (1983) interpretated the diffuse ultraviolet emission observed by Feldman, *et al.* (1981) to come from gas within a very narrow range of temperatures: $1.6\text{-}2.0\times10^5$ K. Strictly speaking, their conclusions would not permit the existence of any power law distribution over a broad temperature range. However it is quite possible that some of the spectral features have been misidentified; the resolution of the apparatus which observed the emission was only 60Å, and the feature identified as N IV] λ1488 might be something else, such as H_2 fluorescence (Duley and Williams 1980); see, e.g. the emission spectrum shown by Brown *et al.* (1981) which comes from the Lyman bands of vibrationally excited interstellar H_2 exposed to L-α emission. If the N IV identification is indeed incorrect, a power law in temperature would be permitted (and the inferred emission measure could be lower).

energy x-ray background (McCammon, *et al.* 1983), there seems to be no anticorrelation between the excesses or deficiencies of N(O VI) per unit distance and variations of normal (cool) interstellar material, as evidenced by the reddenings to the respective stars. From an upper limit to this anticorrelation, Jenkins (1978b) concluded that $f < 0.2$, provided most of interstellar space is filled with the gas responsible for the reddening and not some other phase at low density. If f were considerably less than this upper limit, we would conclude from the overall average for n(O VI) that the pressure of the coronal gas would exceed a reasonable upper bound for the pressure of most of the interstellar medium, $p/k = 10^4 \mathrm{cm}^{-3}\mathrm{K}$.

c) Comparison with Diffuse Background Emissions

In simplest terms, a measure of N(O VI) can be translated into an integral of the electron density n_e over a well defined path for gases at temperatures near the peak of the curve for the O VI ion fraction. The intensities of the soft x-ray [130 - 850 eV] and EUV [50 - 100 eV] emission backgrounds, which arise chiefly from collisional excitations and radiative decay of the electronic levels of highly ionized atoms, allow us to determine the integral of n_e^2 for the high-temperature phases over paths of somewhat indefinite length, in large part defined by absorption phenomena from intervening or interspersed denser material ("normal" interstellar matter). Thus, the observations of absorption and emission by these atoms are complementary, since they sample the hot material in different ways. We must acknowledge, of course, that the conclusions will have some errors attributable to not only the observations themselves, but also to uncertainties in temperatures of the gas, the relative abundances of key elements, and the calculations of ion fractions (and, for the x-ray and EUV results, the excitation cross sections). Indeed, the ion fractions are probably not governed by an *equilibrium*, since the time scale for heating or cooling of the gas could be substantially shorter than the equilibration time for collisional ionization and recombinations.

It is generally believed that the immediate neighborhood of the Sun contains a gaseous medium which is partially ionized with n(H) ~ 0.1 cm^{-3} and $T \sim 1 - 2\times10^4$ K (Weller and Meier 1981, Dalaudier, *et al.* 1983). In turn, this local complex of warm gas is surrounded by a volume roughly 100 pc in diameter which may be almost completely filled with hot gas (Sanders, *et al.* 1977, Tanaka and Bleeker 1977, Hayakawa, *et al.* 1978, Kraushaar, 1979, Fried, *et al.* 1980, Arnaud and Rothenflug 1984). This conclusion follows from the observation that a good portion of the x-ray background at lower energies is fairly uniform over the whole sky, and this emission seems not to have undergone any (energy dependent) absorption short of reaching known dense clouds which are approximately 100 pc away. A general picture where neutral hydrogen and hot plasmas are intermingling over small scales seems to be disfavored by the steepness of the spectrum of the EUV/soft x-ray emission between 50 and 190 eV (Paresce and Stern 1981). The x-ray results indicate that the emission measure of the hot bubble is generally of order $1 - 3\times10^{-3}\mathrm{cm}^{-6}\mathrm{pc}$ if there is virtually no absorption [$N(\mathrm{H}) << 10^{20}\mathrm{cm}^{-2}$] and $T \sim 10^6$ K (a temperature giving the most emission in the B and C x-ray bands).[5] On

[5] In certain directions, not necessarily associated with identifiable supernova remnants, the emission measure reaches about 10^{-2} cm^{-6} pc. (McCammon, *et al.* 1983, Rocchia, *et al.* 1984)

the basis of the x-ray data alone, one must conclude that the pressure of the gas $p/k \gtrsim 10^4 cm^{-3}K$. While this local pressure seems to exceed by a substantial margin the general value of about $2-3\times10^3 cm^{-3}K$, it is not out of the question that the Sun is inside a supernova remnant 100 pc in diameter having an internal temperature $T \sim 10^6$ K, age $t \sim 1.4\times10^5$ yr and a thermal energy $\sim 3\times10^{50}$ erg (Cox and Anderson, 1982).

When we try to reconcile the O VI data with the x-ray and EUV emission measures, we find that there is too little O VI for the amount of emission seen, if the gas were distributed fairly uniformly. One way to resolve the problem is to say that the hot gas is very patchy (i.e., f is low) and rather dense within the patches, but then the inferred pressure of the medium rises. A discussion of this idea was originally presented by Shapiro and Field (1976) who derived remarkably high pressures, but more recent, refined interpretations seem to indicate that the apparent deficiency of O VI is not too severe.

Burstein, *et al.* (1977) found that the relative strengths of the x-rays in three different energy bands could only be explained by having the emission come from gases at two very different temperatures [also see de Korte, *et al.* 1976. A dissenting view has been presented by Hayakawa (1979) however.] They estimated that the lower temperature regime ($T \lesssim 10^6$ K) was responsible for about half of the emission sensed by their lowest energy [B band: 130 - 190 eV] detector; these temperatures are not too far removed from the range where the O VI is produced. For the power-law temperature distribution defined earlier [§IIb], one can make half of the Wisconsin group's average B-band count rate consistent with $\langle n_e \rangle$ from the O VI data if $p/k = 4\pm1.5\times10^4 cm^{-3}K$, if one assumes for the x-rays that there is very little foreground absorption [$N(H) < 2\times10^{19} cm^{-2}$] and d = 100 pc.(6)

A comparison of the O VI data with EUV emission intensities is less sensitive to uncertainties in temperatures, since the most EUV emission comes from a plasma at T best suited for O VI production. Paresce and Stern (1981) found n(O VI) too low by a factor 5-10 if p/k is set to $10^4 cm^{-3}K$, again assuming the emission is virtually unabsorbed by intervening neutral gases and the existence of a power-law distribution for hot gas temperatures. However they noted that the *local* n(O VI) could be somewhat higher than the overall average (see last para. of § IIa above); by stretching their lower limit for the EUV emission downward by 50% and assuming the local n(O VI) = $1.7\times10^{-7} cm^{-3}$, they could arrive at f = 0.4 and $p/k = 1.5\times10^4 cm^{-3}K$.

d) Interpretation

A principal theme of the theoretical description of the interstellar medium by McKee and Ostriker (1977) is that a very inhomogeneous mixture of gas phases is subjected to shocks from supernova explosions. These shocks propagate rather freely through the intercloud medium and heat it to temperatures of around 5×10^5

(6) This result is obtained by evaluating $p/k = \dfrac{(1.91)25\,\mathrm{counts\,s^{-1}}}{(100\,\mathrm{pc})\,C_e \ln 10 \int_{5.15}^{6.35} T^{\eta-1} R_B d\log T}$, where η = 0.5±0.5 and C_e are as defined by Jenkins (1978b) from the O VI survey, and R_B is the B-band emissivity *vs.* temperature shown in fig. 11a of McCammon, *et al.* (1983).

K. Since the isothermal sound speed in this gas is about 80 km s^{-1} and there is probably considerable turbulence, one might expect that there may be much more O VI in the medium than observed, but that this additional O VI has not been seen because its large velocity dispersion makes the profiles difficult to distinguish from the undulating continua in the spectra of the target stars. Thus the ultraviolet absorption measurements may be badly biased toward only those O VI components which have a low velocity dispersion, and this may explain why there is an apparent deficiency relative to the soft x-ray and EUV backgrounds.

There is some indication that the components which are observed in O VI come only from interfaces undergoing conduction and evaporation between the cool clouds and the hot intercloud medium, which could explain why the profiles appear to be narrow. Cowie, *et al.* (1979) found correlations between the end-point velocities of O VI profiles and those of some N II and Si III components which seem to support this interpretation. It is also interesting to note that the statistical description of Jenkins (1978b) for packets of O VI gas, each with N(O VI) ~ 10^{13}cm^{-2}, implies that roughly 6 of these regions will be intercepted by a random line of sight 1 kpc long. Although possibly coincidental (or attributable to observational effects), this figure is remarkably close to the 7 to 8 clouds kpc^{-1} deduced from surveys of visual interstellar lines and extinction by dust (Spitzer 1968). If the interpretation that we are seeing conductive interfaces is correct, one must employ the theory of such interfaces in concert with models for the clouds and intercloud medium to ascertain the conditions in the medium. It is important to emphasize, however, that we badly need more definitive observations to confirm more directly that the O VI indeed arises from evaporation zones around clouds.

Finally, one might ask whether we should be embarrassed by the apparent mismatch in pressure between the very local, partially ionized medium with $T \approx 1 - 2\times10^4$ K and $n \approx 0.1$cm^{-3}, discussed earlier, and the much hotter, x-ray emitting gas which surrounds it. The answer is, "probably not," or at least, "not yet." When our local cloud was suddenly exposed to a big increase in external pressure as it was overtaken by supernova blast wave, an isothermal shock started to progress toward the cloud's interior. If the ratio of external to internal pressures was, say, a factor of 5, this shock moved at a velocity $5^{\frac{1}{2}}$ times the local sound speed, v_s = 10–20 km s^{-1}. Over the 1.4×10^5yr lifetime for the local supernova remnant calculated by Cox and Anderson (1982), this shock has probably eaten through only the outermost 3 - 6 pc of the perimeter of the local cloud. This length is only comparable to, or possibly much less than, the various estimates for the distance to the cloud's edge, which range from 3 or 4 pc (Bruhweiler and Kondo 1982, Bruhweiler 1982), out to about 50 pc in some directions (Paresce 1984).

III. INTERSTELLAR SHOCKS

Except for the Vela Supernova Remnant and one star (15 Mon) (Jenkins, *et al.* 1976, Jenkins and Meloy 1974), components of O VI at high radial velocity ($v \gtrsim 50$ km s^{-1}) have not been detected. Those which have been seen may be confined within specific regions of enhanced density. The thickness of post-shock, O VI-

bearing gas in the general intercloud medium could be so large that interactions with small clouds may create enough ricochet shocks and turbulence to wash out the profiles of O VI, as discussed above. Slower shocks which produce less energetic ionizations may be more coherent and thus more easily observed.

Cohn and York (1977) have observed high velocity features ($50 \lesssim v \lesssim 100$ km s^{-1}) of C II, C III and Si III, mostly toward stars in active associations (e.g. Orion) or high-latitude stars. The absence of detectable Si II in these components indicates that photoionization is not the primary cause of ionization. Thus, they were not just viewing high speed clumps within ordinary H II regions. Instead, shocks which are strong enough to create temperatures of $3 - 8\times10^4$ K are the most likely explanation, according to the calculations of Shull (1977). More elaborate shock models by Shull and McKee (1979), which include the effects of ionizing radiation on the preshock gas, confirm that Si III should be abundant in the immediate post-shock region for a shock travelling at around 100 km s^{-1}, but that there should be virtually no Si III farther back where appreciable cooling and recombination have occurred, because of the rapid charge exchange with neutral hydrogen.

Cowie and York (1978a) performed additional *Copernicus* observations to look for more high velocity features; this survey extension also emphasized low ionization stages of abundant elements which had intrinsically strong lines in the ultraviolet. They synthesized velocity distribution functions based on the statistics of velocity extrema of the strong lines and concluded that shocks which had reached the isothermal phase were extremely rare (Cowie and York 1978b). Combining their upper limits with estimates for supernova energies and birthrates, they concluded that densities for the intercloud regions with large f, the primary medium for shock propagation, should either be > 0.1 cm^{-3} or $< 7\times10^{-3}cm^{-3}$. The high density alternative is based on the containment of high speed isothermal shocks to small enough radii that they are rarely seen, but this possibility seems pretty unlikely in view of the O VI and EUV/x-ray backgrounds and the theory of McKee and Ostriker (1977). The low density possibility is based on the notion that the shocks never have a chance to become isothermal before they escape from the galactic plane (Chevalier and Oegerle 1979, Cox 1981) or run into other supernova cavities (Cox and Smith 1974, Smith 1977). The upper limit given by Cowie and York (1978b) is consistent with McKee and Ostriker's (1977) estimate of $3.5\times10^{-3}cm^{-3}$ for the typical hot medium.

IV. DIVERGENT CLUES FROM C IV AND SI IV

The spectrometer on the *Copernicus* satellite was not well suited for observing the lines of Si IV and C IV because at these wavelengths it had low sensitivity and uncertain scattered light levels. Hence, in spite of its inferior wavelength resolution, the *International Ultraviolet Explorer (IUE)* has been more productive in exploring the properties of Si IV and C IV absorptions toward a broad selection of sources. Even though results for the narrow features of these ions toward many stars have appeared in the literature, and suitable spectra for hundreds of other stars exist in the archives, several factors have hampered our progress in achieving a clear interpretation on the lines' origins and significance. First, in many instances strong *stellar* (and possibly circumstellar) features have made it very

difficult to achieve a clean differentiation of the narrow, supposedly interstellar components. (Sometimes a fairly drastic overexposure of a spectrum is needed to properly register an interstellar line in trough of a stellar feature: see, for example, fig. 2 of Pettini and West (1982).) Second, and perhaps more important, is that unlike O VI which has a very high ionization potential, we can plausibly attribute the creation of Si IV, C IV, and to some extent even N V to either photoionization from very hot stars (and/or x-ray sources) or, alternatively, to gas which is either part of, similar to, or somehow connected with the hot, coronal phase which is responsible for the O VI, EUV and x-ray results discussed in §II. Finally, for gas at low radial velocities, we usually can not use the presence or absence of species at lower ionization to differentiate between these fundamentally different origins because of the inevitable contamination from H I regions or other H II regions of lower excitation.[7]

So far, the results of many of the standard tests to discriminate between truly interstellar origins and effects from the target stars (or their immediate neighbors) have not been completely satisfactory; the observations are evidently influenced by a complicated interplay of several phenomena, and more definitive investigations may be needed to unravel the picture. A simple relationship to examine is that of column densities versus distance. Column densities toward stars more distant than 1 kpc should not suffer appreciably from fluctuations due to Poisson statistics, if the sizes and separations of discrete interstellar gas complexes are comparable to what has been seen in other studies of the local part of our galaxy. However both N(Si IV) and N(C IV) vary over almost *two orders of magnitude* for any narrow interval of distance beyond 1 kpc (Jenkins 1981, Cowie, *et al.* 1981). A survey of Wolf-Rayet stars by Smith, *et al.* (1980) showed virtually no correlation of the column densities of these ions with distance. Many upper limits for closer stars obtained from the *Copernicus* archives by Jenkins (1981) yield column densities for Si IV and C IV which are lower than 10^{13}cm^{-2}, well below a linear extrapolation of the average N per unit distance from the stars at $d > 1$ kpc. Another classic test, comparing the radial velocities of the features with the expected velocities produced by differential galactic rotation at the positions of the stars, was carried out by Cowie, *et al.* (1981). These results, however, showed too much scatter to indicate whether or not the lines came from the positions of the stars or halfway between.

A very convincing demonstration that *some* Si IV and C IV arises from the general interstellar medium was presented by Savage and deBoer (1979, 1981). In spectra of stars in the Magellanic Clouds, they found features which correspond to velocities in our galaxy, in addition to absorptions from gases attributable to the halo and the Magellanic system. Galactic Si IV features were also seen in the spectrum of 3C273 by York, *et al.* (1983). How much of these low velocity absorptions apply to highly ionized material within the galactic plane, rather than a transition layer below the halo, is unresolved.

[7] On many occasions, discrete features of Si IV and C IV at high velocity have been recorded by *IUE* for sources within or behind special, violently disturbed regions, such as those near O subdwarfs (Bruhweiler and Dean 1983), some binary systems (Bruhweiler, *et al.* 1980), active OB associations (Phillips and Gondhalekar 1981, Cowie, *et al.* 1981, Laurent, *et al.* 1982) or supernova remnants (Jenkins, *et al.* 1984). None have been identified with *generally distributed* material in the local neighborhood, however.

Attempts to correlate the strengths of Si IV and C IV lines with properties of the target stars have not been very fruitful. Black, *et al.* (1980) found that the lines did not seem to correlate with the velocities of stellar winds, and Jenkins (1981) found that N(C IV)/N(Si IV) showed no correspondence with the temperatures of the target stars. In support of the existence of collisionally ionized Si IV and C IV in gases at $T \sim 5\times10^4$ K, Bruhweiler, *et al.* (1979, 1980) called attention to the fairly restricted range in the ratios of N(C IV) to N(Si IV) in their sample, extending between only 0.8 and 3.7 for most cases. This, they contended, was much less than the spread one would expect for photoionization from the widely divergent mix of stellar temperatures. Nearly all of their stars had $T_e < 35{,}000$ K; the calculations of Cowie, *et al.* (1981) indicate that N(C IV) > N(Si IV) in photoionized regions surrounding stars only with $T_e > 50{,}000$ K. While it is possible that these results indicate that photoionization by stellar photons is not the dominant source of ionization, one could equally well propose that the density of ambient material near these stars is low enough that the lines of sight are almost always influenced by the starlight from nearly all of the stars in an association. This may explain why N(C IV)/N(Si IV) does not seem to vary by large amounts and may also account for the hint that observations of different stars within single associations show some coherence (Cowie, *et al.* 1981).

A conclusive way to demonstrate that collisional ionization is not responsible for the production of Si IV and C IV is to find profiles with velocity dispersions lower than that expected for thermal doppler broadening at temperatures needed to produce these ions [at equilibrium, $T \approx 10^5$ K; see Shull and Van Steenberg (1982).] Slightly lower temperatures could be anticipated if the gas is cooling radiatively, because recombination times are slower than cooling times (Shapiro and Moore 1976)]. Since the resolution of *IUE* is only 30 km s^{-1}, the dispersions must be inferred from the b-values derived from doublet ratios. Most of the observations reported in the literature give b-values comparable to or greater than the limiting values of 12 and 8 km s^{-1} for the doppler motions of C IV and Si IV, respectively. A noteworthy exception, however, is Dupree and Raymond's (1983) measurement of C IV absorption in the spectrum of Feige 24.

Some, but not all, white dwarfs observed by *IUE* show prominent features of Si IV, C IV and N V (Bruhweiler and Kondo 1981, Dupree and Raymond 1983, Malina, Basri and Bowyer 1981, Sion and Guinan 1983). The positive measurements to these stars give column densities well above those generally seen within a few hundred pc (Jenkins 1981). However, it is not completely clear whether these enhancements result from the presence of circumstellar material produced by the stars, or alternatively, from the action of these stars on nearby interstellar gas. Calculations by Dupree and Raymond (1983) indicate that hydrogen-rich, hot dwarfs ($t \approx 6\times10^4$ K) should be able to ionize enough Si IV and C IV to be seen with *IUE* if the ambient density is greater than about 0.1 cm^{-3}.[8] If a star has no appreciable helium cutoff at the high energy end of its spectrum, some N V and O VI will also be produced (O VI can not be seen with *IUE* however). More data from local white dwarfs may give us a better insight on what proportion of the medium is filled with gas at moderate densities, as opposed to the very low density

[8] No allowance was made for absorption of the ionizing photons by dust, however, so the actual yields may be somewhat lower than those estimated by Dupree and Raymond (1983); see, e.g. Sarazin (1977).

($n \approx$ few$\times 10^{-3}$cm^{-3}) hot material. As emphasized by Hills (1972, 1973, 1974), white dwarfs may be a very important source of ionizing radiation for the interstellar medium in the galactic plane. Dupree and Raymond's (1983) calculations combined with further results on the distribution of C IV and Si IV from *IUE* may give us more insight on this important topic.

V. FUTURE PROSPECTS

In years ahead, our ability to investigate the ultraviolet absorption lines will improve dramatically. The High Resolution Spectrograph [HRS] (Brandt, *et al.* 1982) aboard the Hubble Space Telescope will have a wavelength resolving power of $\lambda/\Delta\lambda = 8\times10^4$, i.e., $\delta v = 4$ km s^{-1}, in its highest resolution mode (Bottema, *et al.* 1984). The tremendous increase in photometric accuracy and resolution over that obtainable with *IUE* should virtually eliminate the confusion in identifying different parcels of gas at low velocity and allow us to differentiate those which produce the features from highly ionized atoms from those which do not. Information on whether the Si IV and C IV is ionized by uv photons or by collisions in a hot plasma should come from good measurements of the velocity dispersions, provided, of course, that turbulence and/or velocity shears are not too large. Unfortunately, HRS will not be sensitive to wavelengths near the O VI features; to further study O VI we will need a facility such as the Far Ultraviolet Spectroscopic Explorer *Columbus*, now in the planning stages, which will be designed specifically to do spectroscopy at wavelengths below the efficiency cutoff of MgF_2 coated mirrors and conventional uv detector faceplates.

We desperately need absorption line data from ions which have their peak abundances in the range $10^6 \lesssim T \lesssim 10^7$K where most of the x-ray emission occurs. One way to observe them is to use a good crystal or transmission grating spectrometer aboard some reasonably large, orbiting x-ray facility. York and Cowie (1983) have calculated that the continua of brighter x-ray sources (with intensities $\gtrsim$ a few keV cm^{-2}s^{-1}keV^{-1}) should give enough signal-to-noise in a reasonable integration time to permit detection of the strongest lines which might arise over a distance of 1 kpc. These authors have tabulated an assortment of strong transitions to levels $0.2 \lesssim E \lesssim 1.0$ keV above the ground states of appropriate ions.

Another approach for measuring highly ionized species is to record the extremely weak absorption features from some coronal forbidden lines at visible wavelengths, the most promising of which seem to be [Fe X] λ6375 and [Fe XIV] λ5303. Hobbs (1984) and Hobbs and Albert (1984) have already made a bold attempt to detect these ions in the interstellar medium, but except for some tantalizing results for two stars (reported elsewhere in this volume), they were only able to report rather high upper limits because detector instabilities limited their signal-to-noise ratios to about 350. A very important result from these first attempts, however, was an exploration of where one can expect to find interference from telluric absorption lines, diffuse interstellar bands, and stellar features. These unwanted features, while present, do not seem to offer serious problems. Thus in due course, when the practice of obtaining high dispersion spectra using CCDs becomes more highly refined and we can routinely obtain photon-limited accuracies with tens of millions of counts per velocity bin, there is a chance that

the realm of absorption features from highly ionized atoms in space, now the private hunting ground of space astronomers, will soon open up to a much wider community of observers.

The writing of this paper was supported by NASA Grant NAGW-477.

REFERENCES

Arnaud, M. and Rothenflug, R. 1984, preprint.
Black, J. H. and Dalgarno, A. 1973, *Ap. J. (Letters)*, **184**, L101.
Black, J. H., Dupree, A. K., Hartmann, L. W. and Raymond, J. C. 1980, *Ap. J.*, **239**, 502.
Blint, R. J., Watson, W. D., and Christensen, R. B. 1976, *Ap. J.*, **205**, 634.
Bottema, M., Cushman, G. W., Holmes, A. W., and Ebbets, D. 1984, *Proc. SPIE Conf. "Instrumentation in Astronomy V"*, in press.
Brandt, J. C. and the HRS Investigation Definition and Experiment Development Teams 1983, in *The Space Telescope Observatory*, D. N. B. Hall, ed., NASA CP-2244, p. 76.
Brown, A., Jordan, C., Millar, T J., Gondhalekar, P., and Wilson, R. 1981, *Nature*, **290**, 34.
Bruhweiler, F. C. 1982, in *Advances in Ultraviolet Astronomy: Four Years of IUE Research*, Y. Kondo, J. M. Mead, and R. D. Chapman, eds., NASA Conf. Pub. 2238, p. 125.
Bruhweiler, F. C. and Dean, C. A. 1983, *Ap. J. (Letters)*, **274**, L87.
Bruhweiler, F. C. and Kondo, Y. 1981, *Ap. J. (Letters)*, **248**, L123.
_____ 1982, *Ap. J.*, **259**, 232.
Bruhweiler, F. C., Kondo, Y., and McCluskey, G. E. 1979, *Ap. J. (Letters)*, **229**, L39.
_____ 1980, *Ap. J.*, **237**, 19.
Burstein, P., Borken, R. J., Kraushaar, W. L., and Sanders, W. T. 1977, *Ap. J.*, **213**, 405.
Castor, J., McCray, R., and Weaver, R. 1975, *Ap. J. (Letters)*, **200**, L107.
Chevalier, R. A. and Oegerle, W. R. 1979, *Ap. J.*, **227**, 398.
Christensen, R. B., Watson, W. D., and Blint, R. J. 1977, *Ap. J.*, **213**, 712.
Cohn, H. and York, D. G. 1977, *Ap. J.*, **216**, 408.
Cowie, L. L., Jenkins, E. B., Songaila, A., and York, D. G. 1979, *Ap. J.*, **232**, 467.
Cowie, L. L., Taylor, W., and York, D. G. 1981, *Ap. J.*, **248**, 528.
Cowie, L. L. and York, D. G. 1978a, *Ap. J.*, **220**, 129.
_____ 1978b, *Ap. J.*, **223**, 876.
Cox, D. P. 1981, *Ap. J.*, **245**, 534.
Cox, D. P. and Anderson, P. R. 1982, *Ap. J.*, **253**, 268.
Cox, D. P. and Smith, B. W. 1974, *Ap. J. (Letters)*, **189**, L105.
Dalaudier, F., Bertaux, J. L., Kurt, V. G., and Mironova, E. N. 1983, *Astr. Ap.*, in press.
Dalgarno, A. and McCray, R. A. 1972, *Ann. Rev. Astr. Ap.*, **10**, 375.
de Korte, P. A. J., Bleeker, J. A. M., Deerenberg, A. J. M., Hayakawa, S., Yamashita, K., and Tanaka, Y. 1976, *Astr. Ap.*, **48**, 235.
Duley, W. W. and Williams, D. A. 1980, *Ap. J. (Letters)*, **242**, L179.
Dupree, A. K. and Raymond, J. C. 1983, *Ap. J. (Letters)*, **275**, L71.
Feldman, P. D., Brune, W. H., and Henry, R. C. 1981, *Ap. J. (Letters)*, **249**, L51.

Field, G. B., Goldsmith, D. W., and Habing, H. J. 1969, *Ap. J. (Letters)*, **155**, L149.
Fried, P. M., Nousek, J. A., Sanders, W. T., and Kraushaar, W. L. 1980, *Ap. J.*, **242**, 987.
Goldsmith, D. W., Habing, H. J., and Field, G. B. 1969, *Ap. J.*, **158**, 173.
Hartmann, J. 1904, *Ap. J.*, **19**, 268.
Hayakawa, S. 1979, in *X-Ray Astronomy* (COSPAR Symposium), W. A. Baity and L. E. Peterson, eds. (Oxford: Pergammon), p.323.
Hayakawa, S., Kato, T., Nagase, F., Yamashita, K., and Tanaka, Y. 1978, *Astr. Ap.*, **62**, 21.
Hills, J. G. 1972, *Astr. Ap.*, **17**, 155.
_____ 1973, *Astr. Ap.*, **26**, 197.
_____ 1974, *Ap. J.*, **190**, 109.
Hobbs, L. M. 1984, *Ap. J.*, **280**, 132.
Hobbs, L. M. and Albert, C. E. 1984, *Ap. J.*, in press.
Jenkins, E. B. 1978a, *Ap. J.*, **219**, 845.
_____ 1978b, *Ap. J.*, **220**, 107.
_____ 1978c, *Comments Astr.*, **7**, 121.
_____ 1981, in *The Universe at Ultraviolet Wavelengths*, R. D. Chapman, ed., NASA Conf. Pub. 2171, p. 541.
Jenkins, E. B. and Meloy D. A. 1974, *Ap. J. (Letters)*, **193**, L121.
Jenkins, E. B., Silk, J., and Wallerstein, G. 1976, *Ap. J. (Suppl).*, **32**, 681.
Jenkins, E. B., Wallerstein, G., and Silk, J. 1984, *Ap. J.*, **278**, 649.
Jura, M. 1974, *Ap. J.*, **191**, 375.
Kraushaar, W. L. 1979, in *X-Ray Astronomy* (COSPAR Symposium), W. A. Baity and L. E. Peterson, eds. (Oxford: Pergammon), p. 293.
Laurent, C., Paul, J. A., and Pettini, M. 1982, *Ap. J.*, **260**, 163.
Malina, R. F., Basri, G., and Bowyer, S. 1981, *Bull. AAS*, **13**, 873.
McCammon, D., Burrows, D. N., Sanders, W. T., and Kraushaar, W. L. 1983, *Ap. J.*, **269**, 107.
McKee, C. F. and Ostriker, J. P. 1977, *Ap. J.*, **218**, 148.
O'Donnell, E. J. and Watson, W. D. 1974, *Ap. J.*, **191**, 89.
Paresce, F. 1984, *AJ*, in press.
Paresce, F., Monsignori Fossi, B. C., and Landini, M. 1983, *Ap. J. (Letters)*, **266**, L107.
Paresce, F. and Stern, R. 1981, *Ap. J.*, **247**, 89.
Pettini, M. and West, K. A. 1982, *Ap. J.*, **260**, 561.
Phillips, A. P. and Gondhalekar, P. M. 1981, *MNRAS*, **196**, 533.
Pikel'ner, S. B. 1967, *Astr. Zh.*, **44**, 915 (English trans.: *Soviet Astron. A J*, **11**, 737 [1968]).
Rocchia, R., Arnaud, M., Blondel, C., Cheron, C., Christy, J. C., Rothenflug, R., Schnopper, H. W., and Delvaille, J. P. 1984, *Astr. Ap.*, **130**, 53.
Rogerson, J. B., York, D. G., Drake, J. F., Jenkins, E. B., Morton, D. C., and Spitzer, L. 1973, *Ap. J. (Letters)*, **181**, L110.
Sanders, W. T., Kraushaar, W. L., Nousek, J. A., and Fried, P. M. 1977, *Ap. J. (Letters)*, **217**, L87.
Sarazin, C. L. 1977 *Ap. J.*, **211**, 772.
Savage, B. D. and deBoer, K. S. 1979, *Ap. J. (Letters)*, **230**, L77.
_____ 1981, *Ap. J.*, **243**, 460.
Shapiro, P. R. and Field, G. B. 1976, *Ap. J.*, **205**, 762.
Shapiro, P. R. and Moore, R. T. 1976, *Ap. J.*, **207**, 460.

Shull, J. M. 1977, *Ap. J.*, **216**, 414.
Shull, J. M. and McKee, C. F. 1979, *Ap. J.*, **227**, 131.
Shull, J. M. and Van Steenberg, M. 1982, *Ap. J. (Suppl.)*, **48**, 95.
Silk, J. 1970, *Ap. Letters*, **5**, 283.
Silk, J. and Brown, R. L. 1971, *Ap. J.*, **163**, 495.
Silk, J. and Werner M. W. 1969, *Ap. J.*, **158**, 185.
Sion, E. M. and Guinan, E. F. 1983, *Ap. J. (Letters)*, **265**, L87.
Slipher, V. M. 1909, *Lowell Obs. Bull.*, no. 51.
Smith, B. W. 1977, *Ap. J.*, **211**, 404.
Smith, L. J., Willis, A. J., and Wilson, R. 1980, *MNRAS*, **191**, 339.
Spitzer, L. 1956, *Ap. J.*, **124**, 20.
_____ 1968, *Diffuse Matter in Space*, (New York: Wiley Interscience).
Spitzer, L. and Scott, E. H., 1969, *Ap. J.*, **158**, 161.
Spitzer, L. and Tomasko, M. G., 1968, *Ap. J.*, **152**, 971.
Steigman, G. 1975, *Ap. J.*, **199**, 642.
Tanaka, Y. and Bleeker, J. A. M. 1977, *Space Sci. Rev.*, **20**, 815.
Watson, W. D., and Christensen, R. B. 1979, *Ap. J.*, **231**, 627.
Weaver, R., McCray, R., Castor, J., Shapiro, P., and Moore, R. 1977, *Ap. J.*, **218**, 377.
Weisheit, J. C. 1973, *Ap. J.*, **185**, 877.
Weller, C. S. and Meier, R. R. 1981, *Ap. J.*, **246**, 386.
Williamson, F. O., Sanders, W. T., Kraushaar, W. L., McCammon, D., Borken, R., and Bunner, A. N. 1974, *Ap. J. (Letters)*, **193**, L133.
York, D. G. 1974, *Ap. J. (Letters)*, **193**, L127.
_____ 1977, *Ap. J.*, **213**, 43.
York, D. G. and Cowie, L. L. 1983, *Ap. J.*, **264**, 49.
York, D. G., Wu, C. C., Ratcliff, S., Blades, J. C., Cowie, L. L., and Morton, D. C. 1983, *Ap. J.*, **274**, 136.

ABSORPTION AND EMISSION OF EUV RADIATION BY THE LOCAL ISM

Francesco Paresce
Space Telescope Science Institute, Homewood Campus, The Johns Hopkins University, Baltimore, MD 21218, USA and Astrophysics Division, Space Science Department, ESTEC, ESA.

ABSTRACT

The Berkeley EUV telescope flown on the Apollo Soyuz mission in July, 1975 established the existence of a measurable flux of EUV radiation ($100 \leq \lambda \leq 1000$ Å) originating from sources outside the solar system. White dwarfs, flare stars and cataclysmic variables were discovered to be relatively intense compact sources of EUV photons. Moreover, this and other subsequent experiments have strongly suggested the presence of a truly diffuse component of the EUV radiation field possibly due to thermal emission from hot ($T > 10^5$K) interstellar gas located in the general vicinity of the sun ($r \simeq 100$ parsecs.) Closer to the HI, 912 Å edge, the effect of a few hot O and B stars has been shown to be very important in establishing the interstellar flux density. All these results imply that the local ISM is immersed in a non-negligible EUV radiation field which, because of the strong coupling between EUV photons and matter, will play a crucial role in determining its physical structure. Conversely, of course, the local ISM is expected to leave a strong imprint on the EUV field reaching the terrestrial observer.

The objective of this review will be to assemble and critically analyze the available information on the local ISM derived from the limited EUV observations carried out so far. These include measurements of the spectra of bright EUV sources that reveal clear evidence of H photo absorption at $\lambda > 400$ Å and of the He ionization edge at 228 Å. The EUV diffuse background is found to convey interesting information on the density, temperature and possible location of the hot ISM component that can be profitably compared with similar data on far uv absorption lines, principally OVI. The results discussed in this context will be shown to be quite useful in illuminating the path that future EUV sensitive observatories such as EUVE and Columbus might profitably follow in the near future.

INTRODUCTION

The extreme ultraviolet (EUV) band of the electromagnetic spectrum extending approximately from 1000 to 100 Å should, in principle, be perfectly suited to the detailed study of the local interstellar medium (LISM). The high absorptivity of matter in the EUV insures a high probability of light-matter interaction over relatively short, well defined path lengths and the availability of a large number of well studied permitted transitions and spectral features provides the tools required to accurately probe a wide range of ISM materials and configurations. The effective photoionization cross section of the LISM, $\sigma_e = \Sigma n_i \sigma_i / n_H$ where n_i and n_H are the volume densities of

element i and H, respectively for a variety of possible phases has been computed recently by Cruddace et al., 1974. A peak cross section of almost 10^{-17} cm^2 at 912 Å followed by a υ^{-3} decline to shorter wavelengths superimposed more or less prominently on which are the discontinuities due to the ionization edges of heavier elements are the key features of these calculations.

Using these results, the distance at which 90% of the radiation emitted by an EUV source is absorbed in a neutral LISM phase is plotted in Figure 1 as a function of wavelength for n_H varying between 0.2 and 0.03 cm^{-3}, a range consistent with possible scenarios within the first hundred parsecs or so of the sun. This figure clearly shows that for all intents and purposes, the observable EUV source horizon is limited to a few hundred parsecs at the very most at the wavelengths where most of the absorption is occurring. Thus, we can expect to probe accurately the ISM only within this local region by measuring the EUV spectrum of any compact or diffuse sources Nature can provide. This, of course, assumes a decent understanding of the sources' inherent emission spectrum can be obtained independently by some other means. In the following, I describe the progress made so far in this very new and exciting field and discuss some of the possibilities for future work.

COMPACT SOURCES

To move from principles to reality, we need observable EUV sources. Up to 1975 these were mainly gleams in a few scientists' eyes. Since then, thanks mainly to the pioneering observations carried with the EUV grazing incidence telescope on the ASTP, the situation has improved dramatically. The compact sources discovered so far are listed in Table I with their positions in the sky, distance, type, and approximate flux at Earth in the wavelength bands in which they were detected. The reference to the discovery paper for the appropriate source is listed in the last column. A more detailed description of the discovery and characteristics of most of these sources can be found in Paresce, 1980.

Several points about the present source statistics should be emphasized. First, the sources observed so far all fall within 100 parsecs of the sun although distances are somewhat uncertain, possibly up to a factor of two in some cases. Second, only 7 sources in all have been observed so far with, moreover, only four that can be considered bona fide EUV sources. The cataclysmic variables are more aptly described as soft x-ray sources and visible only at ≈100 Å and in outburst (Holberg, 1984). Third, the "true" EUV sources are all DA White Dwarfs. Fourth, only HZ43 has been observed throughout the EUV from ≈800 to 100 Å. Its spectrum between ~200 and 2000 Å is shown in Figure 2, reprinted here by permission from J. Holberg. The solid line represents the expectations of an unblanketed, pure hydrogen, non-LTE model atmosphere with T_e = 55000 K, log g = 8 absorbed by an LISM of density n_H = 0.002 cm^{-3} with the dashed lines quantifying the effects of changing n_H by ±50%.

It is evident from the results displayed in Figure 2 that the 500-800 Å region of the spectrum is the most sensitive to variations in n_H as expected,

Table 1

Catalog of Detected Stellar EUV Sources

Name	RA	Dec	Distance	Flux ergs cm^{-2} s^{-1} 500-780Å	170-620Å	50-150Å	Type	Reference
HZ43	13^h14^m	+29°2'	65±15 pc	$4x10^{-10}$	$4x10^{-9}$	$1.1x10^{-9}$	DA White Dwarf	Lampton et al. 1976
Feige 24	2^h32^m	+3°31'	90±28	-	$3x10^{-9}$	-	DA White Dwarf	Margon et al. 1976b
Proxima Centauri	14^h26^m	-62°28'	1.3	-	-	$7x10^{-10}$	Flare Star	Haisch et al. 1977
SS Cygni	21^h40^m	+43°21'	30-50	-	-	$9x10^{-11}$	Dwarf Nova	Margon et al. 1978
G191-B2B	5^h1^m	+52°46'	48 pc	$4x10^{-10}$	-	-	DA White Dwarf	Holberg et al 1980
VW Hyi	4^h40^m	-71°	-	-	-	$1.3x10^{-9}$	U Gem	Henry et al. 1976b
GD 153	12^h54^m	+22°18'	≈40pc	$8x10^{-11}$			DA White Dwarf	Holberg, 1984

and that the theoretical model fails to account for the detailed structure of the spectrum in this band and for any of the observed data in the region below ≈500 Å. This case well illustrates the difficulties associated with accurate extraction of LISM information from complicated stellar emission patterns. Wesemael et al., 1980, and Wesemael, 1981 have computed the expected EUV emission from hot, high gravity stars with pure H or He atmospheres that can be used to compare with observations. The shape of the unabsorbed inherent stellar spectrum above ≈400 Å for these objects depends critically on the effective temperature T_e, the surface gravity g and the chemical composition of the surface. In order to reproduce a discontinuity of a factor of ≈2 at the He^+ ionization edge at 228 Å, Malina et al., 1982 resorted to pure hydrogen models having a trace amount of helium ($\sim 6 \cdot 10^{-5}$ fractional number density of hydrogen). The Malina et al. model, however, still fails to account for the soft x-ray and far uv spectrum. The large uncertainties in the stellar models clearly influence the determinations of the LISM parameters since the former must be well known before precise inferences can be drawn on the latter. This problem becomes particularly acute when observational upper limits to EUV emission features whose origins are extremely controversial and uncertain are used to draw conclusions on the LISM as has been attempted recently with Capella and the He II, 304 Å line by Bobroff et al., 1984.

Armed with a better appreciation of the difficulties involved with this brief introduction, we can understand the results of the attempts made so far to derive the neutral hydrogen column density towards EUV sources listed in Table 2. The best studied source, HZ43, shows how dramatically this parameter can vary with the sophistication of the stellar model employed and, to some degree, on the quality of the data obtained. Thus, we see the log of the H column dropping from a high of 18.6 when a black body (BB) model at T_e = 110000 K was used to less than 17.3 when the Berkeley rocket experiment was analyzed in terms of a sophisticated mixed chemical composition model. The variation is not trivial since it implies a change of the average hydrogen volume density from $2 \cdot 10^{-2}$ to less than 10^{-3} cm^{-3}. Although it is pretty well established that n_H cannot be larger than ≈0.01 cm^{-3} towards HZ43 without violating observational constraints in the visible (Auer and Shipman, 1977), any stronger statement might not be appropriate at the present time in view of the still large uncertainties in the correct stellar model and even in the observations themselves. Contamination due to contributions from the second order of the Voyager grating have been invoked to explain part of the signals above 500 Å seen in the Voyager data in Figure 2 and the discontinuity at 228 Å has not been confirmed by EXOSAT. These are all troubling questions that need to be securely resolved before more progress can be made.

Nevertheless, the results reported in Table 2 do have important implications for the LISM. As discussed in more detail by Paresce, 1984 most of the EUV determinations of N(HI) except perhaps G191-B2B lie well below the column density expected at their distance from an extrapolation of a very local medium having $n_H \simeq 0.07$ cm^{-3}. This discrepancy is particularly striking in the case of HZ43 at l = 50°, b = 84° where it reaches at least an order of magnitude. Since GD153 is only 8° away from HZ43 and at a similar distance it is comforting that its implied column density is consistent with HZ43. A lower than average density implies that the very local cloud described by

TABLE 2

Source	$T_e \cdot 10^{-3}$	n_{He}/n_H	log N_H	$\bar{n}_H$	REF
HZ43	110 (BB)	-	18.6	$2 \cdot 10^{-2}$	Lampton et al., 1976 Margon et al., 1976a
	125	10^{-1}	18.9	$4 \cdot 10^{-2}$	Durisen et al., 1976
	55-70	10^{-6}-10^{-3}	17.8-18.4	$3 \cdot 10^{-3}$-10^{-2}	Auer & Shipman, 1977
	60	Layered	$\leq$ 18.3	$\leq 10^{-2}$	Heise & Huizenga, 1980
	55	0	17.3-17.8	10^{-3}-$3 \cdot 10^{-3}$	Holberg et al., 1980
	45-64	10^{-5}-$6 \cdot 10^{-5}$	$\leq$ 17.3	$\leq 10^{-3}$	Malina et al., 1982
Feige 24	60	0	18.5	10^{-2}	Margon et al., 1976b
	$\geq$ 55	0	18.7-19	2-$5 \cdot 10^{-2}$	Cash et al., 1979
G191-B2B	$\geq$ 55	0	$\geq$ 18.7	$\geq 3 \cdot 10^{-2}$	Cash et al., 1979
	62.5	0	17.9-18.2	$\leq 10^{-2}$	Holberg et al., 1980
GD 153	50	0	17.7-18.0	$5 \cdot 10^{-3}$	Holberg, 1984
GD 246	55	0	$\geq$ 18.2	$\geq 10^{-2}$	Holberg, 1984

Bruhweiler (1982) can only be a few parsecs in extent outside the galactic plane. If the discrepancy between Cash et al., 1979 and the Voyager results on G191-B2B could be settled, this object might resolve the important issue concerning the extent of the local cloud in the plane itself, since it lies at $l = 156^\circ$, $b = 7^\circ$.

A correlated issue in this context is the extent of the ionization cavity around the very hot white dwarfs used in the survey summarized in Table II. As first pointed out by Hills, 1972 and further developed by Dupree and Raymond, 1983, cavities of many parsecs in extent may be carved out of the ISM if the H density is of order 0.01-0.1 cm^{-3}. Feige 24 shows clear evidence for such an extended H II region. Consequently, if the cavity radius is a fair fraction of its distance, transforming the measured column density into an average volume density over the whole distance might lead to an underestimate of the actual density of the absorbing medium. The effect would be most critical for very nearby objects and probably does not significantly affect the results shown in Table II but might have to be accounted for in the future when more white dwarfs will, hopefully, be detected by ROSAT, EUVE and Columbus/FUSE.

A way out of this problem is to use the EUV emission from hot transition regions and coronae of nearby cool stars. The expected emission from these sources have been computed by Landini et al., 1984 using a self-consistent formulation of a magnetically confined coronal loop model. The effect of even a small amount of absorption is quite dramatic and should be exploited. The crucial advantages of using such sources are their very high space density and their better understood spectrum as it is very similar to the sun's. The advantage of using white dwarfs, on the other hand, is their better defined continuum and relative absence of emission lines which may hamper absorption work. An interstellar He^+ ionization edge, for example, could be separated from a purely stellar one by even moderate resolution ($\lambda/\Delta\lambda \geq 100$) instrumentation as is being presently comtemplated for EUVE and Columbus/FUSE.

THE DIFFUSE COMPONENT

Between ≈2 and 10 keV, the intensity of the x-ray background exhibits a power law dependence with photon energy and appears essentially isotropic to moderate angular resolutions surveys. Possible sources of this emission are discussed by Marshall et al., 1980 and Fabian, 1981. Below 2 keV, however, the diffuse background becomes decidedly anisotropic and deviates sharply from the extrapolation of the higher energy spectrum even in the absence of hydrogen absorption as shown in Figure 3. The spectrum continues to climb well into the EUV, peaking at 4-10 photons cm^{-2} s^{-1} eV^{-1} at ≈ 200 Å before appreciable ISM absorption sets in. The background fluxes plotted in Figure 3 are described in Paresce and Stern, 1981 and represent average intensities in regions of the sky far from the established soft x-ray enhancements due to emission from much higher temperature gas (see McCammon et al., 1983 and Marshall and Clark, 1984 for a review of soft x-ray survey results). Although

there is evidence for a substantial (~20%) contribution due to unresolved point sources above ≈250eV, in the EUV the radiation field is almost certainly truly diffuse in origin (Stern and Bowyer, 1980; Rosner et al., 1981).

The failure of any known non-thermal emission mechanism to account for the observed spatial variations and the average spectrum shown in Figure 3, compelling evidence for the existence of hot ($T > 10^5$K) gas in the ISM from O VI absorption measurements and a supernova blast wave production mechanism at least theoretically identified and understood all together make a strong case for a thermal plasma origin of the EUV background. In this case, the intensity of the radiation field is given by:

$$I(E) = \frac{1}{4\pi} \int_l \int_T \phi(E,T)\, n_{ec}\, \frac{d\, n_{ec}}{d\, \ln T}\, e^{-\tau(E)} dl\, d\ln T \qquad 1)$$

where $\tau(E) = \sigma(E)N(HI)$ is the optical depth of the absorbing medium, $\phi(E,T)n_{ec}^2$ is the volume emissivity of the gas at E and T, n_{ec} the electron density of the emitting cloud of gas and l is the distance parameter along the line of sight. Unfortunately, eq. 1) is not invertible easily unless some simplifying assumptions are introduced. The most common is that the bulk of the emission is due to a single temperature component. Although there is no a-priori theoretical reason to suppose the gas is thermostatted precisely at one temperature, observations are normally made with instruments that are sensitive only to a rather narrow range of photon energies. Moreover, the temperature distribution around a classical evaporating cloud is very sharply peaked around the typical substrate temperature (McKee and Cowie, 1977).

Having thus disposed momentarily of the inhomogeneities in the physical structure of the emitting plasma, its spatial distribution has still to be dealt with. Not having any knowledge of this parameter it is common practice to consider two limiting extreme cases. The first assumes the emitting plasma is homogeneously mixed or finely interspersed with the absorbing medium. In this case, it can be shown that eq. 1 reduces to:

$$I(E) = \frac{1}{4\pi} \phi(E,T) \frac{\langle n_e \rangle^2}{\sigma_e \langle n_H \rangle} (1 - \exp[-\sigma(E)N(HI)]) \qquad 2)$$

where $\langle n_e \rangle = f n_{ec}$ and f is the filling factor of the hot plasma and $\langle n_H \rangle$ is the average neutral hydrogen density in the line of sight. In this scenario, the observations shown in Figure 3 can be fitted by models parameterized by the variables $\langle n_e \rangle^2 / \langle n_H \rangle$, T and N(HI).

In the other extreme we assume that the emission from the hot plasma is absorbed by a single cool slab of material of column density N(HI). Then the intensity I(E) can be expressed simply as:

$$I(E) = \frac{1}{4\pi} \phi(E,T) \langle n_e^2 \rangle R \exp[-\sigma(E)N(HI)] \qquad 3)$$

where R is the physical length of the emitting region. In this case, the theoretical expectations may be parameterized by N(HI), T and the emission measure EM of the gas:

$$EM = \int n_e^2 dr = \langle n_e^2 \rangle R = n_{ec}^2 \, fR = \frac{(p/k)^2}{(1.91\ T)^2} fR \qquad 4)$$

The actual spatial distribution clearly lies somewhere between these extreme cases. For $\tau < 0.5$, in fact, the interspersed plasma model becomes, for all intents and purposes, indistinguishable from the slab absorbed model with N(HI) = 0. Finally, we can relax the isothermal assumption adopted so far by allowing the emitting plasma to have a specified distribution of temperatures for each of the two cases considered above. This effect was first explored by Paresce and Stern (1981) who adopted the power law form suggested by Jenkins (1978b):

$$\frac{d\, n_e}{d\, \ln T} = C_e \, T^{\alpha} \qquad 5)$$

where C_e is an independently determined normalization parameter and α is the power law index. In this more complicated scenario, the theoretical slab absorbed model for example depends on α, N(HI), EM, and the temperature limits of integration in eq. 1, T_1 and T_2.

Computations of the plasma emissivity $\phi(E,T)$ have been carried out by a number of authors in the last few years. Only very recently, however, has the full 1 to 2000 Å range of the spectrum been covered systematically (see Gaetz and Salpeter, 1983, Paresce et al., 1983 and references therein for a more complete discussion). The expected emission spectrum in photons $cm^{-2}\ s^{-1}\ sr^{-1}Å^{-1}$ of a plasma at $T = 2 \cdot 10^5$ K, EM = 0.1 cm^{-6} pc absorbed by a slab of $N(HI) = 2 \cdot 10^{19} cm^{-2}$ is shown in Figure 4 as a function of wavelength. The main assumption that has to be made to generate expected fluxes such as those shown is that the gas is in steady state collisional ionization equilibrium. If the plasma has been recently subjected to shock heating such an assumption may be naive and we should expect substantial deviations for some if not all of the emission features in the EUV and far UV displayed in this figure.

Detailed comparison with observations, however, come so close to self consistency that this desperation move with its huge associated uncertainties may not actually be required at least not with the quality of the data presently available. The situation for the EUV and far UV has been discussed in some detail by Paresce and Stern, 1981; Paresce et al., 1983 and Kimble, 1983. In general, the observations down to 100 Å and perhaps slightly beyond to the C soft x-ray band can be reasonably well explained by emission from a relatively nearby hot ($10^5 \leq T < 10^6$ K) plasma that pervades a fair fraction of space out to ≈100 pc or so. More specifically, if the simple slab absorbed single temperature model comes closest to reality, the range of the three free parameters allowed by the observations is given by the regions bounded by the

solid lines in Figure 5. These curves are the 90% confidence level contours obtained by using a minimum x^2 fitting procedure with three degrees of freedom.

Several conclusions leap out from even a cursory glance at Figure 5. First, the temperature of the hot gas cannot be much higher than $\approx 5 \cdot 10^5$ K. Second, there cannot be much more than $\approx 10^{20}$ absorbing H atoms in the way and, third, the temperature cannot be much lower than $2.5 \cdot 10^5$ K if we impose an upper limit on the gas pressure of $p/k = 10^4$ cm^{-3} K as shown by the dotted line in Figure 5 for a fixed effective path of 100 parsecs. Using the interspersed models reduces these ranges even further. The real problem with isothermal models, however, apart from the absence of a known physical mechanism that would thermostat the plasma in a region of high cooling rates, is that they imply far too much O VI absorbing gas. If we demand, as we should, consistency with the O VI results summarized by Jenkins (1978a, b) we are forced to look for another source of the EUV background or require a significant pressure imbalance in the ISM, evidence for which has yet to surface. Notice that there is no easy escape from this conclusion here as there is in the soft x-rays since the preferred temperatures at which a plasma emits in the EUV is precisely the same as the one at which the O^{+5} ion is most comfortable.

The temperature distribution models represented by eq. 5 go a long way towards easing this dilemma, however. The allowed parameter space for this case and the absorbing slab scenario is shown in Figure 6 for log T_1 = 5.0 and log T_2 = 5.8. Allowing for the customary factor of two uncertainty both in the predictions and the observations, a model of this type having f = 0.4, R = 100 pc, $p/k = 1.5 \cdot 10^4$ cm^{-3} K, α = 1.5 reconciles all the available observations and theory in a self consistent manner. The predicted average O^{+5} ion density is $1.2 \cdot 10^{-7}$ cm^{-3} over this pathlength which, although is $\approx$ a factor of four higher than the average of $3 \cdot 10^{-8}$ cm^{-3} over kpc pathlengths, is quite consistent with the more local lines of sight (Jenkins, 1978a). We note in passing that the EUV background compatible value of $\langle n(O\ VI) \rangle$ is much more consistent with that predicted by the McKee and Ostriker (1977) theory to be present in the conduction interfaces.

As Figure 4 clearly illustrates, if we assume the EUV background is generated by a hot plasma in the $T > 10^5$ K, EM = 10^{-1} cm^{-6} pc range, a substantial part of the total emission has to show up in the 912 to 1600 Å band. The expected fluxes may have been detected towards the north galactic pole by Feldman et al., 1981 but an interpretation of these observations by Paresce et al., 1983 in terms of a hot plasma emission model yields only a marginal compatibility with the EUV emitting plasma. Since the lines in the far UV are all of lower ionization stages, sufficient emissivity is achieved at generally lower temperatures at comparable emission measures. The tail of the best fit EUV power law distribution is insufficient to account for the intensity of the observed EUV lines. In the absence of additional data on this fascinating subject, one must conclude that the present observations may indicate either the presence of a new cooler component of the local ISM or that the assumption of a steady state ionization equilibrium needs to be

revisited. Maneuvering room in the steady state isothermal models is very limited, unfortunately since upper limits on N V place severe constraints on filling factors of any gas at temperatures around $2 \cdot 10^5$ K.

Similarly interesting are the observations in the 900-1200 Å region summarized by Kimble, 1983. In this range, the density of the radiation field is dominated by emission of known normal stars. The observational upper limits to the specific intensity of the radiation field in particular directions available presently are just beginning to constrain the allowed regions of the physical characteristics of a hot plasma. If the upper limits to the 912-1200 Å radiation field intensity obtained recently by the ECOM-721 spectrometer on the STP78-1 satellite that surveyed an appreciable fraction of the sky where the contribution of known sources is negligible are converted by means of equations 1-5 into a limit on emission measure as a function of T, for example, the allowed region of Figure 5 is reduced to the log $T \geq 5.4$, EM ≤ 0.1 region of the plane. More sensitive observations made by Voyager 2 are now becoming available and a closer scrutiny of the implications of the measurements in this range deserves the highest priority. What has been definitely lacking up to now is a systematic study of the global pattern of the diffuse background from the soft x-rays through the EUV and well into the far UV. The theoretical underpinnings should now exist for a thorough study of the local hot gas with a more physically plausible distribution of temperatures and, perhaps, filling factors such as that suggested by eq. 5.

CONCLUSIONS

We have established in this brief overview that the local ISM leaves a clear signature of its presence on the EUV spectra of nearby compact sources, on the spectrum and, probably, on the spatial variations of the diffuse EUV background. Compact objects such as hot white dwarfs and even main sequence stars certainly disturb the surrounding ISM by creating large ionization cavities and by contributing to the general radiation density at any point. The diffuse background whether truly diffuse or not also contributes to the ionization of the local ISM. The most efficient photons in this respect are those in the Lyman continuum. The observational situation in this region is presently very confused, unfortunately. A measurement of the intensity of the radiation field at 750 Å in a particular direction has been claimed by Sandel et al., 1979 to be $2.3 \cdot 10^{-8}$ ergs cm^{-2} s^{-1} sr^{-1} $Å^{-1}$ or approximately 900 photons cm^{-2} s^{-1} sr^{-1} $Å^{-1}$.

It is very instructive to consider what implications this flux averaged over the whole sky would have on our LISM. This problem has been studied by Meier, 1980 and Kimble, 1983. In a steady state situation where recombination just balances photoionization, a local Hydrogen ionization fraction of 0.5 or less is maintained by a Lyman continuum flux of 10 photons cm^{-2} s^{-1} sr^{-1} $Å^{-1}$ or less. Since 0.5 is a reasonable observational upper limit set by solar backscatter observations, the local flux cannot be much greater than this value. Conversely, if the Voyager field were actually as high as quoted, the LISM would have an ionization fraction of at least 0.9. The implication has to be that the Voyager measurement is not of a typical line of sight. A

recent theoretical calculation performed by Grewing (1975) also predicts a radiation field that would ionize the LISM to a degree not observed in practice.

Consequently, it is in the 700-900 Å range that the LISM and the radiation field are most intimately coupled and where observations of one crucially implicate the other. It is safe to conclude that the EUV is one of the most promising and fertile areas of LISM research today and in the immediate future.

REFERENCES

Auer, L. H., and Shipman, H. L., 1977, Ap. J. (Lett), 211, L105.
Bobroff, N., Nousek, J., and Garmire, G., 1984, Ap. J., 277, 678.
Bruhweiler, F., 1982, in "Advances in UV Astronomy: Four Years of IUE Research," NASA CP-2238, p. 125.
Cash, W., Bowyer, S., and Lampton, M., 1979, Astr. Ap., 80, 67.
Cruddace, R., Paresce, F., Bowyer, S., and Lampton, M., 1974, Ap. J., 187, 497.
Dupree, A. K., and Raymond, J. C., 1983, Ap. J. (Lett.), 275, L71.
Durisen, R. H., Savedoff, M. P., and Van Horn, H. M., 1976, Ap. J. (Lett.), 206, 449.
Fabian, A. C., 1981, in "Tenth Texas Symposium on Relativistic Astrophysics," eds. R. Ramaty and F. C. Jones, N.Y. Acad. Sci., 375, 235.
Feldman, P. D., Brune, W. H., and Henry, R. C., 1981, Ap. J., 249, L51.
Gaetz, T. J., and Salpeter, E. E., 1983, Ap. J. Suppl., 52, 155.
Grewing, M., 1975, Astr. Ap., 38, 391.
Haisch, B., Linsky, J., Lampton, M., Paresce, F., Margon, B., and Stern, R., 1977, Ap. J. (Lett.), 213, L119.
Heise, J., and Huizenga, H., 1980, Astr. Ap., 84, 280.
Henry, P., Bowyer, S., Rapley, C. G., and Culhane, J. L., 1976b, Ap. J. (Lett.), 209, L29.
Hills, J. G., 1972, Astr. Ap., 17, 155.
Holberg, J. B., Sandel, B. R., Forrester, W. T., Broadfoot, A. L., Shipman, H. L., and Barry, J. L., 1980, Ap. J. (Lett.), 242, L119.
Holberg, J. B., Forrester, W. T., and Broadfoot, A. L., 1980, Bull. AAS, 12, 872.
Holberg, J., 1984, these proceedings.
Jenkins, E. B., 1978a, Ap. J., 219, 845.
Jenkins, E. B., 1978b, Ap. J., 220, 107.
Kimble, R. A., 1983, Ph.D. Dissertation, University of California, Berkeley.
Lampton, M., Margon, B., Paresce, F., Stern, R., and Bowyer, S., 1976, Ap. J. (Lett.), 203, L71.
Landini, M., Monsignori Fossi, B. C., Paresce, F., and Stern, R., 1984, Ap. J., in press.
Malina, R. F., Bowyer, S., and Basri, G., 1982, Ap. J., 262, 717.
Margon, B., Liebert, J., Gatewood, G., Lampton, M., Spinrad, H., and Bowyer, S., 1976a, Ap. J., 209, 525.
Margon, B., Lampton, M., Bowyer, S., Stern, R., and Paresce, F., 1976b, Ap. J. (Lett.), 210, L79.

Margon, B., Szkody, P., Bowyer, S., Lampton, M., and Paresce, F., 1978, Ap. J., 224, 167.
Marshall, F. E., Boldt, E. A., Holt, S. S., Miller, R. B., Mushotzky, R. F., Rose, L. A., Rothschild, R. E., and Serlemitsos, P. J., 1980, Ap. J., 235, 4.
Marshall, F. J., and Clark, G. W., 1984, Ap. J., in press.
McCammon, D., Burrows, D. N., Sanders, W. T., and Kraushaar, W. L., 1983, Ap. J., 269, 107.
McKee, C. F., and Cowie, L., 1977, Ap. J., 215, 213.
McKee, C. F., and Ostriker, J. P., 1977, Ap. J., 218, 148.
Meier, R. R., 1980, Astr. Ap., 91, 62.
Paresce, F., 1980, in "Astrophysics from Spacelab," eds. P. L. Bernacca and R. Ruffini, Astrophysics and Space Science Library, Reidel, 81, 243.
Paresce, F., and Stern, R., 1981, Ap. J., 247, 89.
Paresce, F., Monsignori Fossi, B. C., and Landini, M., 1983, Ap. J. (Lett.), 266, L107.
Paresce, F., 1984, A. J., 89, (7), July, 1984.
Rosner, R., Avni, Y., Bookbinder, J., Giacconi, R., Golub, L., Harnden, F., Maxson, C. W., Topka, K., and Vaiana, G. S., 1981, Ap. J. (Lett.), 249, L5.
Sandel, B. R., Shemansky, D. E., and Broadfoot, A. L., 1979, Ap. J., 227, 808.
Stern, R., and Bowyer, S., 1980, Astr. Ap., 83, L1.
Wesemael, F., 1981, Ap. J. Suppl., 45, 177.
Wesemael, F., Auer, L. H., Van Horn, H. M., and Savedoff, M. P., 1980, Ap. J. Suppl., 43, 159.

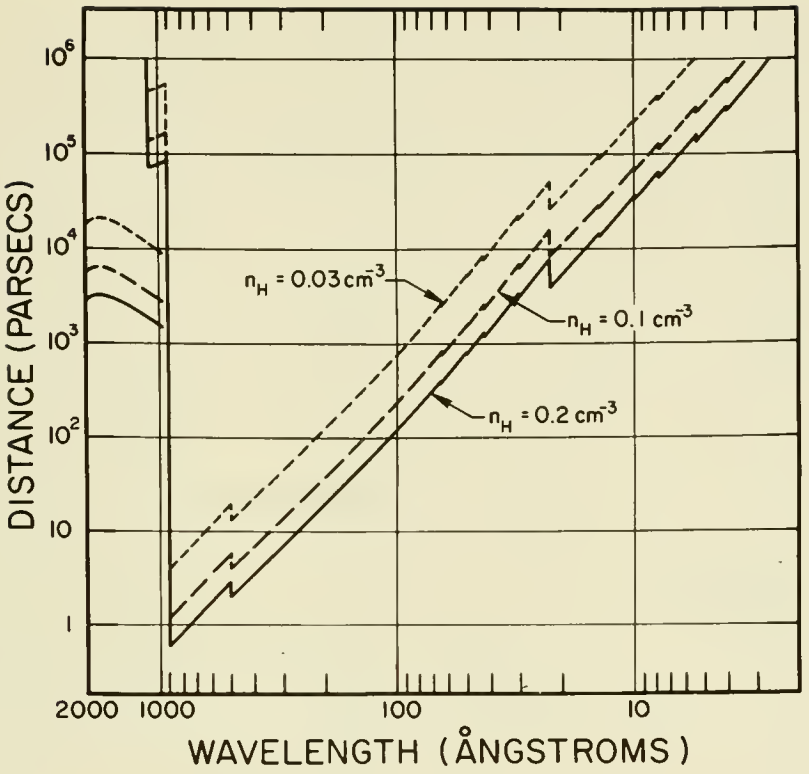

Figure 1

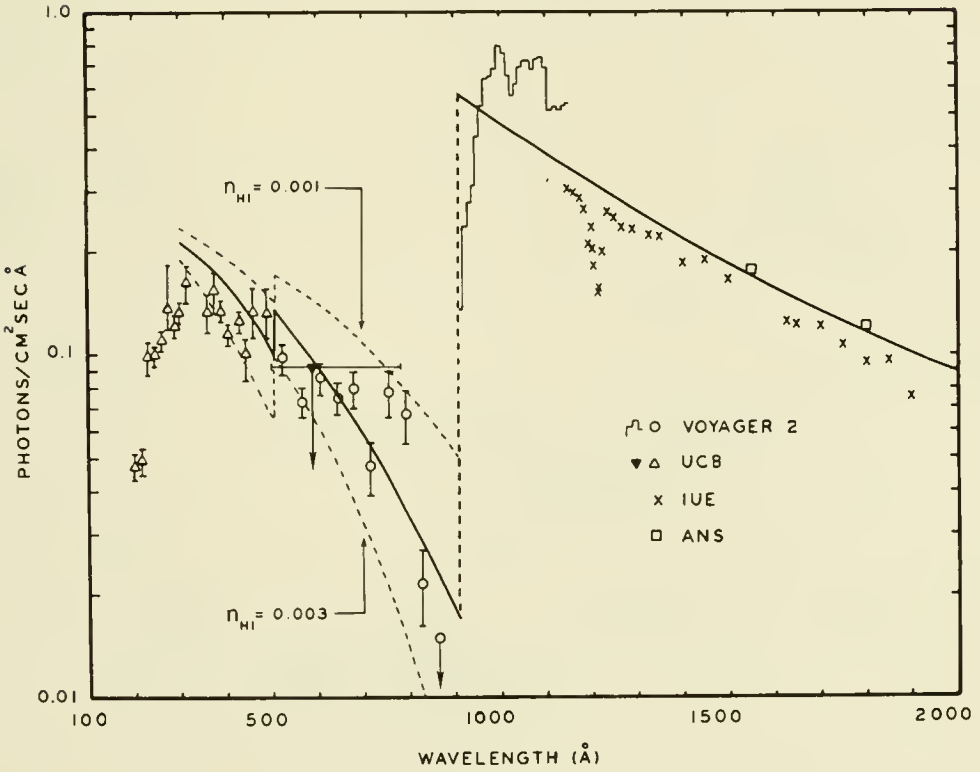

Figure 2

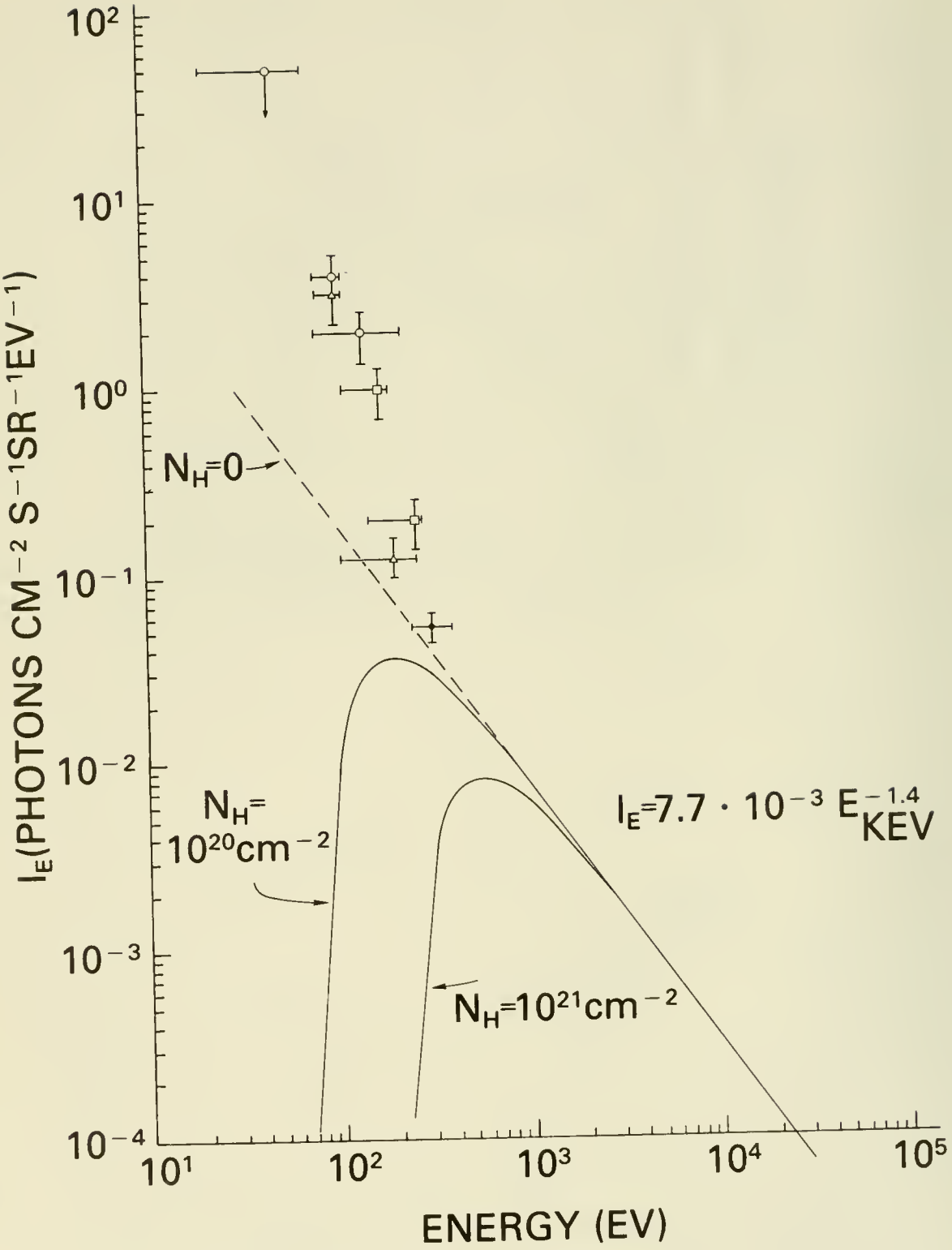
10^2
10^1
10^0
10^{-1}
10^{-2}
10^{-3}
10^{-4}
I_E(PHOTONS CM^{-2} S^{-1}SR^{-1}EV^{-1})
N_H=0
N_H= 10^{20}cm^{-2}
N_H=10^{21}cm^{-2}
I_E=7.7 · 10^{-3} $E_{KEV}^{-1.4}$
10^1
10^2
10^3
10^4
10^5
ENERGY (EV)

Figure 3

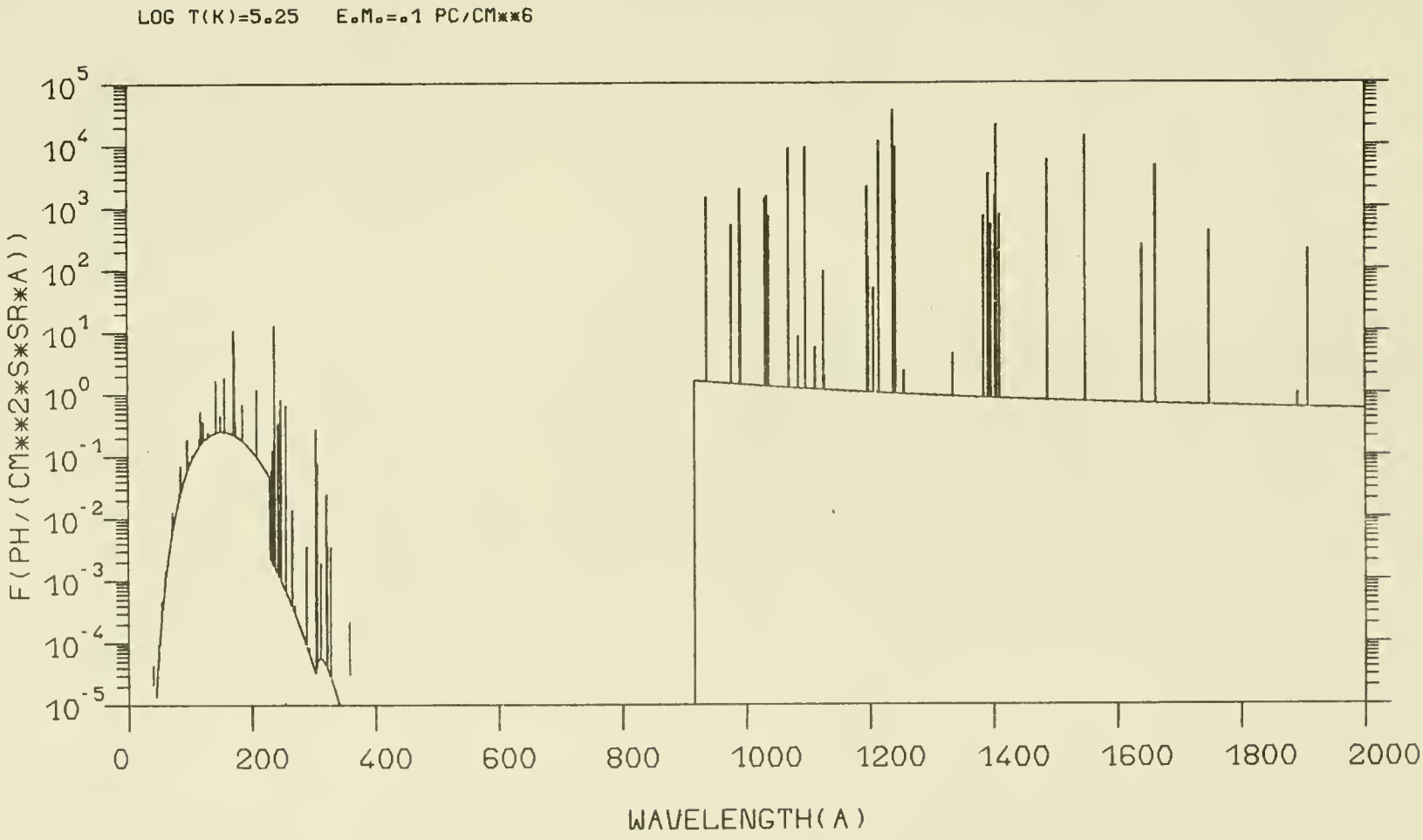
LOG T(K)=5.25 E.M.=.1 PC/CM**6
F(PH/(CM**2*S*SR*A))
10^5
10^4
10^3
10^2
10^1
10^0
10^-1
10^-2
10^-3
10^-4
10^-5
0
200
400
600
800
1000
1200
1400
1600
1800
2000
WAVELENGTH(A)

Figure 4

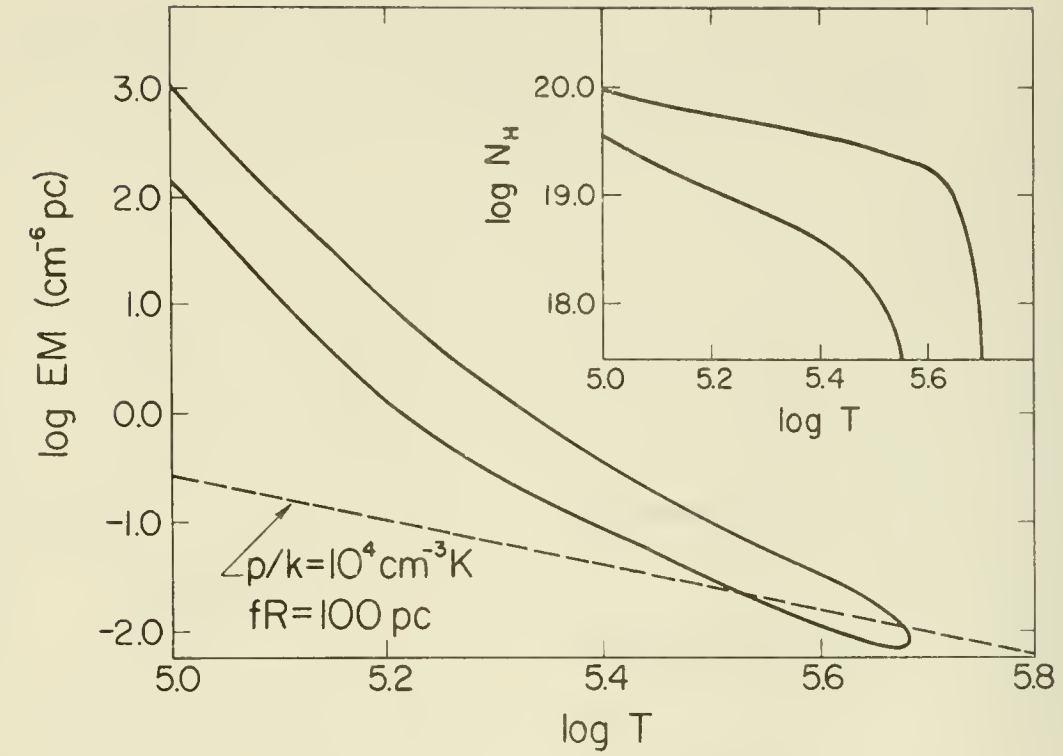

Figure 5

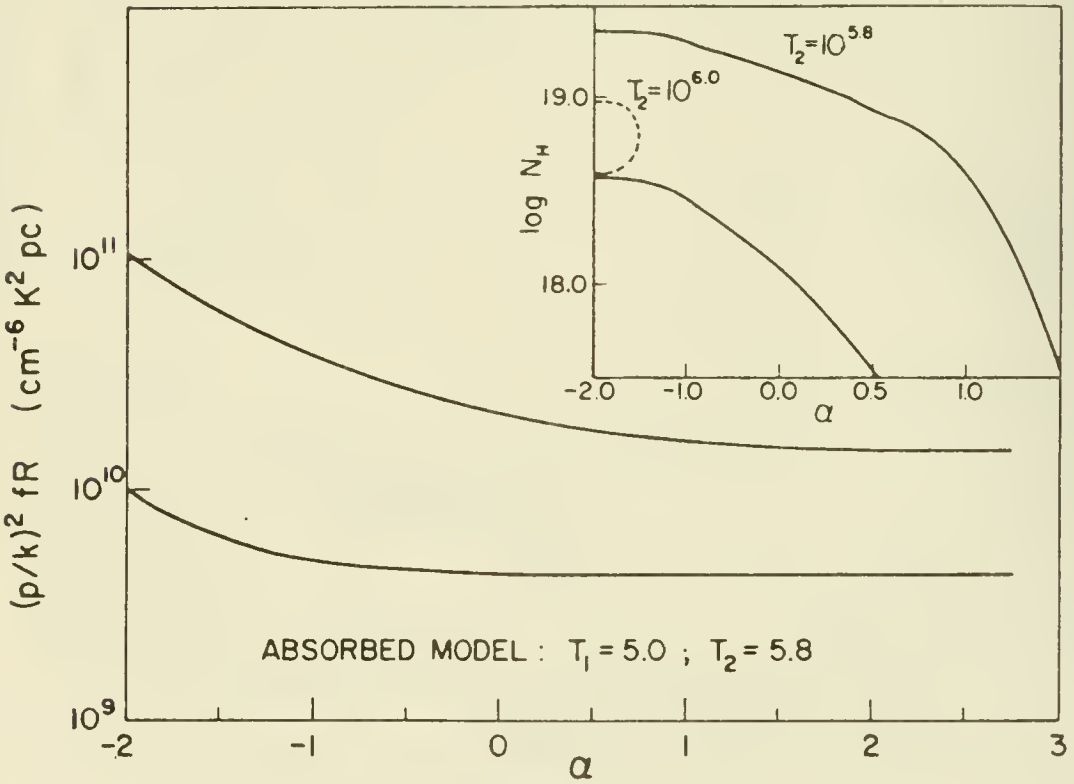

Figure 6

DETECTION OF NARROW C IV AND SI IV ABSORPTION FEATURES IN SPECTRA OF STARS WITHIN 200 PC OF THE SUN

P. Molaro (1,2), J.E. Beckman (3), M. Franco (4), C. Morossi (1) and M. Ramella (1)

1)Astronomical Observatory of Trieste, Italy
2)I.S.A.S. Miramare, Trieste, Italy
3)Queen Mary College, London, England
4)I.A.F.E., Buenos Aires, Argentina

ABSTRACT

Detection of narrow ($\delta\lambda$< 0.5 A) absorption features in C IV at $\lambda\lambda$1548 and 1550 have been made in the spectra of 4 late B dwarfs within 200 pc of the sun; the Si IV doublet at $\lambda\lambda$1393 and 1403 shows up in two of them. We argue that it is difficult to account for the strengths, widths, shapes , and C IV/Si IV ratios in terms consistent with a circumstellar origin except possibly for an asymmetric C IV component in one star (HD 185037). The most probable source is "semi-torrid" gas (cf. Bruhweiler et al. 1980) in the 50,000 K range forming the interfaces between cooler H I clouds and the ambient medium at coronal temperatures. Our technique, using late B rapid rotators, is useful for LISM probing of this kind.

INTRODUCTION

Sharp line detections of Si IV and C IV have been made widely using the SWP spectrograph of IUE in the spectra of O and early B stars (Cowie et al. 1981 , Bruhweiler et al. 1980) and also of Wolf-Rayet stars (Smith et al. 1980, Black et al. 1981). In at least some of these stars the observed C IV and Si IV features can be formed by photoionization in the H II regions around the parent objects, while there is also evidence that C IV and Si IV absorptions can originate in an intermediate phase at temperature between the cool neutral and the hot coronal gas. In order to distinguish circumstellar contributions from true interstellar absorption it is desirable to use cooler stars. Although the strong photospheric absorption spectrum would normally make such detection very difficult, the use of rapid rotators allows us to detect narrow features even when quite faint (W $\gtrsim$ 30 mA). This method also offers the possibility of exploring the intermediate temperature phase in a volume of space significantly closer to the sun than

previous methods have permitted.

OBSERVATIONS

High resolution spectra of 4 late B dwarfs were taken on 4 April 1984 with the SWP spectrograph of IUE as part of a programme for observing stars rotating at close to their break-up velocities. The relevant observational parameters are given in Table 1.

Table 1

Star(HD)	SWP No.	Type	Vsin i	l	b	d(pc)	z(pc)
23383	22664	B9 V	415	146	1	165	3
38831	22666	B8 V	400	154	16	180	50
135734	22669	B8 V	310	327	8	77	11
185037	22665	B8 V	400	71	8	185	25

RESULTS

Figs. 1 and 2 show the C IV and S IV doublet resonance regions respectively. Abscissae are in A and ordinates are linear in relative flux. All the Si IV regions and two of the C IV regions have been smoothed once with a triangular filter to reduce high frequency noise. C IV features are present in all four objects whereas unambiguous detection of Si IV was possible in only two of them (HD 23383 and HD 185037). Table 2 gives equivalent widths (W), widths at half maximum (FWHM) and column densities (N) derived from the lines. Column densities were computed assuming no saturation and should therefore be regarded at this stage as lower limits.

Table 2

Star(HD)	W(mA)				FWHM(A)		Log N		CIV/SiIV
	CIV		SiIV		CIV	SiIV	CIV	SiIV	
23383	172	94	75	40	0.4	0.2	13.2	12.5	5.3
38831	50	50	<30	<30	0.25	-	12.7	<12.2	>3.9
135734	122	116	<30	<30	0.4	-	13.1	<12.2	>9.5
185837	58	26	60	33	0.25	0.2	12.8	12.5	2.2

ARE THE LINES INTERSTELLAR OR CIRCUMSTELLAR?

Because our stars are so cool (Teff ≃ 12,000 K) it is not possible for the C IV or Si IV to be formed by photoionization from stellar UV, nor do these stars have powerful stellar

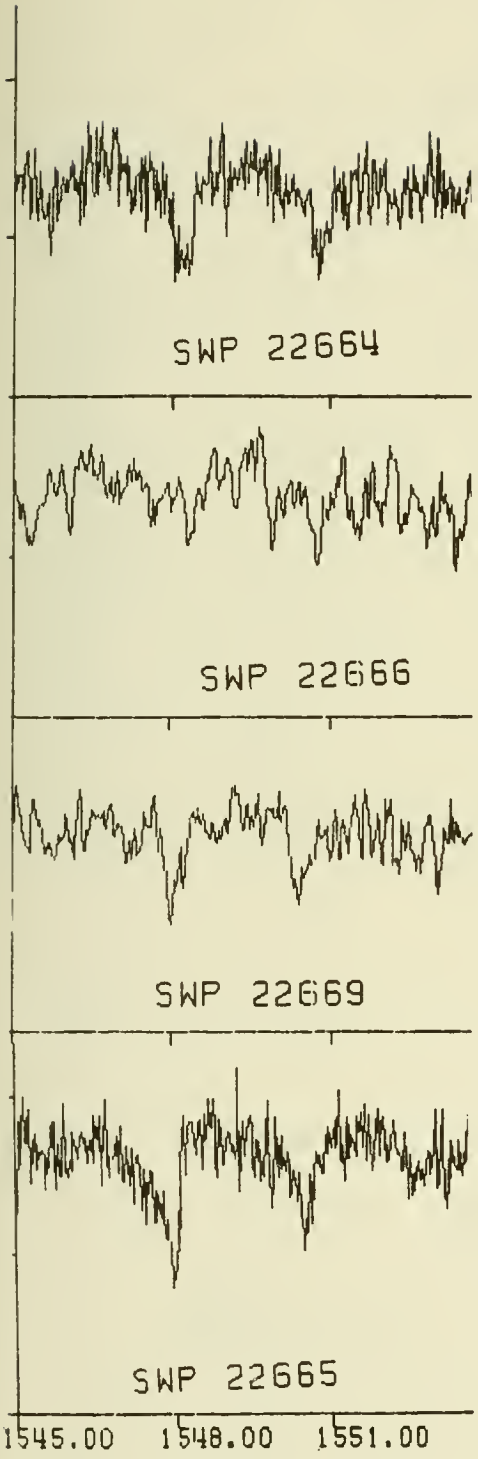

Fig. 1 C IV doublet

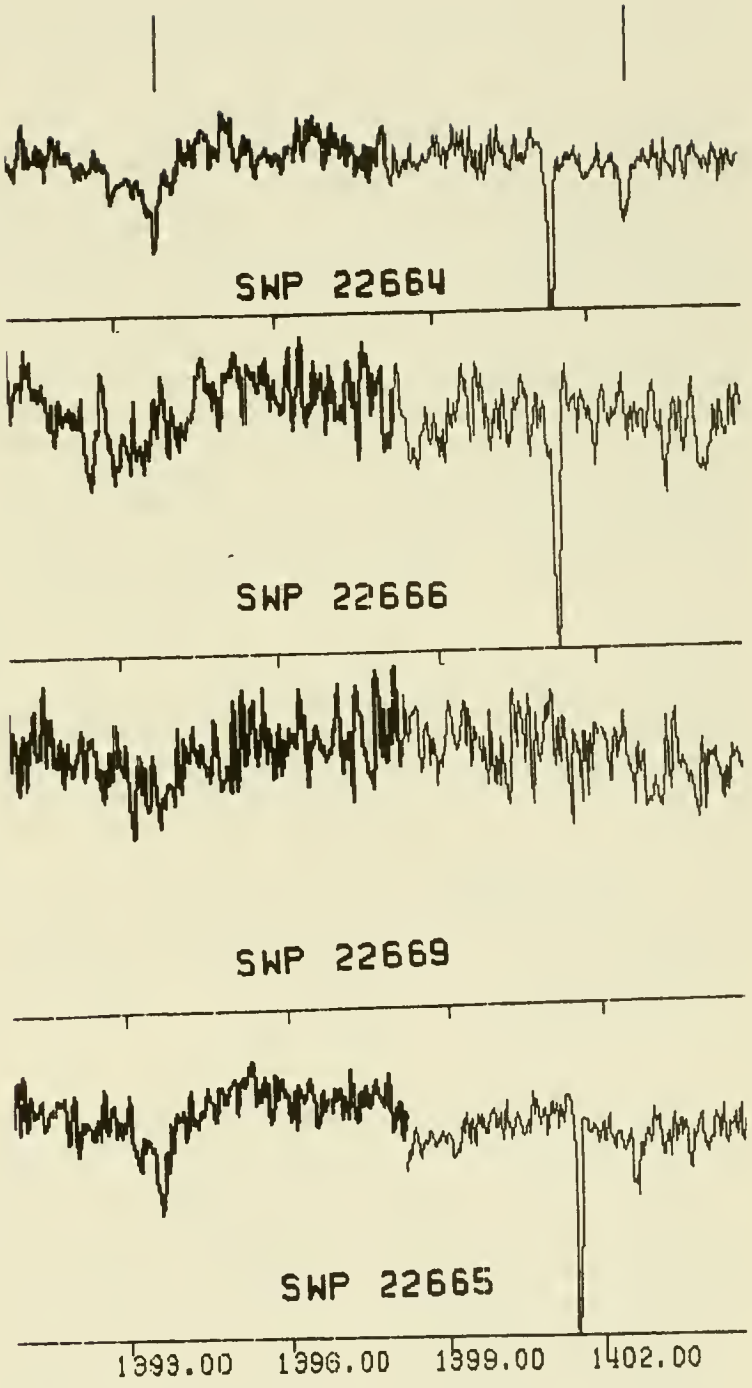

Fig. 2 Si IV doublet

winds which might collisionally produce the lines. Theoretically, values for C IV/S IV of order 0.2 arise from photoionization (Cowie et al. 1981), even in stars with Teff 30,000 K, and of order 16 collisionally in stellar bubbles (Weaver et al 1977). These should be compared with our observed ratios of 2.8 and 5.3 and lower limits of 3.9 and 9.5. We cannot rule out the possibility that our present stars are causing the observed lines by the unknown mechanism that produces observed "superionization" in somewhat hotter stars (Slettebak and Carpenter 1983). However the lines here are considerably narrower. The best agreement with models appears to be with the "semi-torrid" gas scenario of Bruhweiler et al. (1979,1980). Our FWHM's are consistent with collisional ionization in an ambient plasma at around 50,000 K. We cannot apply a radial velocity test for the LISM as we have deliberately chosen rotationally broadened objects. But the weight of the evidence points to an intestellar origin for these lines. If the IS nature of the present detection is confirmed the importance of direct measurements of the nearby 50,000 K plasma is clear. Our column densities are not strongly longitude or latitude dependent implying a general pervasion of the galactic plane by this medium, in addition to its known presence in the galactic corona (Pettini and West 1982). The method of late B rapid rotators offers a new tool for detailed exploration of the intermediate temperature LISM, and for elucidating its geometrical relation to the cool neutral component and to the higher temperature medium characterized by such ions as O VI. The present detections are not co-spatial with local O VI observations (Jenkins 1978).

REFERENCES

Bruhweiler F.C., Kondo Y., and McCluskey G.I.:1980, Astrophys. J. 237, 19.

Bruhweiler F.C., Kondo Y. and McCluskey G.E. : 1979 Astrophys.J. 229, L39.

Black J.H.,Dupree A.K. Hartmann L.W. and J.C. Raymond :1980, Astrophys. J. 239,502.

Cowie L.L.,Taylor W., and York D.G. :1981, Astrophys. J. 248, 528.

Jenkins E.B. :1978, Astrophys. J. 219, 845.

Pettini M. and West K.A.:1982, Astrophys. J. 260,561.

Slettebak A. and Carpenter K. G.: 1983, Astrophys. J. Suppl. 53,869.

Smith L.J., Willis A.J. and Wilson R.:1980 Mon. Not. R.A.S. 191,339.

Weaver R., McCray R., Castor J., Shapiro P. and Moore R.: 1977, Astrophys. J. 218, 377.

OBSERVATIONS OF HIGHLY-IONIZED INTERSTELLAR IRON

L. M. Hobbs

Yerkes Observatory, University of Chicago

ABSTRACT

The spectra of 24 stars, including 5 at distances d < 200 pc, have been observed in the regions of the coronal [Fe X] λ6375 and [Fe XIV] λ5303 lines at detection limits near an equivalent width of 1 mÅ in the best cases. In general agreement with predictions based on a multi-phase model of the interstellar medium, no absorption which can be attributed to Fe X or Fe XIV ions in hot interstellar gas emitting the soft x-ray background is seen in any of these spectra, except for two. Toward λ Cephei an absorption line near λ6375 is measured with an equivalent width of 8.1 ± 2 mÅ, a width corresponding to 20 ± 5 km s^{-1} or a temperature $T \leq (0.5 \pm 0.25) \times 10^6$ °K, and, if it is caused by Fe X ions, a radial velocity of -355 km s^{-1}. On that hypothesis, the hot interstellar gas constitutes at least 63% of the column density of gas along this light path.

INTRODUCTION

The goal of the observations described here is to determine whether the physical properties, such as the space distribution, temperature, and kinematics, of the hot, diffuse, broadly distributed component of the interstellar gas can be observed directly, perhaps over kiloparsec path lengths, by a new method. Direct observations of this gas apparently have been possible hitherto only by virtue of its background emission at soft x-ray and extreme UV wavelengths (McCray and Snow 1979; Cowie et al. 1979). The new method consists of searching for the forbidden coronal [Fe X] λ6375 and [Fe XIV] λ5303 lines as extremely weak interstellar lines toward bright stars (Hobbs 1984; Hobbs and Albert 1984).

The method prospectively offers at least two advantages. (1) The ionization balance of Fe in steady-state collisional equilibrium in the temperature range $0.7 \lesssim T_6 \lesssim 2$, where T_6 is the temperature in units of 10^6 K, is generally favorable for Fe X (Shapiro and Moore 1976), in contrast to the cases of C IV, N V, and Si II, which are present predominantly in the cooler surfaces of and transition regions around embedded cold clouds. The lower part of this temperature range is that expected for the hot gas, as judged from its soft x-ray emission (McCammon et al. 1983). Non-equilibrium effects also could somewhat increase the ionization level of this gas, further enhancing its Fe X fraction. (2) With ground-based telescopes of large aper-

ture at which adequate amounts of observing time can be utilized for the search, very favorable detection limits at equivalent widths $W_\lambda < 1$ mÅ or $W_\lambda/\lambda < 2 \times 10^{-7}$ are routinely achieved. This advantage is further enhanced by the moderate instrumental resolution required, owing to the thermal line broadening $\Delta\lambda \lesssim 0.5$Å or $\Delta v \lesssim 25$ km s^{-1} contributed by the hot gas. A third consideration is that a sensitive study of very weak lines near λλ5303, 6375 in suitable stellar spectra has not previously been reported.

The principal disadvantage of the method is that it relies upon detection of a single, broad, extremely weak line of each ion. The McKee-Ostriker (1977) model can be used to predict typical line strengths $W_\lambda < 0.1$ mÅ; for a line width $\Delta\lambda \lesssim 0.5$, the fractional absorption will not exceed 10^{-4}, so that a detector capable of delivering a signal-to-noise ratio $S/N \gtrsim 10^{-4}$ is required. Practical limits for existing detectors seem to be $S/N \lesssim 500$. Nonetheless, uncertainties about the ionization balance and the column-density fluctuations in the hot gas prompted this study of a potentially powerful diagnostic method for the hot interstellar gas.

RESULTS

The initial results obtained in the period 1979 to 1983 using the 2.7 m reflector of McDonald Observatory have been reported in two current papers (Hobbs 1984; Hobbs and Albert 1984). Observations made with the coudé spectrograph and a dual-array Digicon detector were carried out for 32 stars at the [Fe X] line and for 26 stars at the [Fe XIV] line, with 24 stars in common. Detector limits near $W_\lambda = 1$ mÅ, corresponding to $S/N \gtrsim 400$, were achieved in the best cases. Catalogues of telluric and stellar lines, and of the diffuse interstellar bands at λλ6376 and 6379, were established through observations of bright standard stars, to avoid erroneous identifications of such lines as [Fe X] or [Fe XIV] absorption. The discovery of about a dozen very weak, previously unreported telluric or stellar lines empirically attests to the unprecedented sensitivity, at these two spectral regions, of the search.

With two exceptions, the practical limit of $S/N \gtrsim 400$ yielded negative results for interstellar Fe X and Fe XIV absorption, in general agreement with theoretical predictions. It should be emphasized that present telescopes are entirely adequate to achieve the required $S/N \gtrsim 10^4$ in practical exposure times toward a suitable array of bright target stars, once future improvements in detector stability are achieved.

Uniquely toward λ Cep and ν Cep, which are two high-luminosity members of the Cepheus OB2 association, an absorption

line which can be identified as [Fe X] λ6375 is unmistakably present, with a strength $W_\lambda = 8.1 \pm 2$ (3σ) mÅ, a width $\Delta v = 20 \pm 5$ km s^{-1} or $T_6 \leq 0.5 \pm 0.25$, and a radial velocity $v_r = -355$ km s^{-1}. The presence of the line in two stars separated by $d \geq 50$ pc demonstrates that the inferred hot gas is not locally confined near either star, owing, for example, to the impact of a stellar wind upon the ambient interstellar medium. The absorption apparently arises in an unusually dense, low-latitude concentration of hot interstellar gas. It may be possible to construct a simple, physically consistent model, which consists of a thin sheet of hot gas expanding outward from the plane and seen nearly edge on, which is consistent with other existing x-ray, UV, optical, and radio observational data for the region.

REFERENCES

Cowie, L. L., Jenkins, E. B., Songaila, A., and York, D. G. 1979, Ap. J. 232, 467.

Hobbs, L. M. 1984, Ap. J. 280, 132.

Hobbs, L. M., and Albert, C. E. 1984, Ap. J. 281, 639.

McCammon, D., Burrows, D. N., Sanders, W. T., and Kraushaar, W. L. 1983, Ap. J. 269, 107.

McCray, R., and Snow, T. P. 1979, Ann. Rev. Astr. Ap. 17, 213.

McKee, C. F., and Ostriker, J. P. 1977, Ap. J. 218, 148.

Shapiro, P. R., and Moore, R. T. 1976, Ap. J. 207, 460.

HOT GAS IN THE LISM: SOFT X-RAY OBSERVATIONS

THE SOFT X-RAY DIFFUSE BACKGROUND: IMPLICATIONS FOR THE NATURE OF THE LOCAL INTERSTELLAR MEDIUM

Dan McCammon
Physics Dept., Univ. of Wisconsin, Madison

ABSTRACT

Observations of the diffuse X-ray background in the B and C bands (130-188 eV and 160-284 eV, respectively) provide convincing evidence for the existence of high-temperature interstellar gas. Since the opacity of normal interstellar material is very high, we must assume that the soft X-ray flux observed in the galactic plane originates within a few hundred parsecs of the Sun. The intensity and B/C ratio of this low-latitude flux can be provided by emission from an equilibrium plasma with normal abundances, $T = 10^{6.0}$ K, and 0.0019 cm^{-6} pc emission measure. More sophisticated nonequilibrium models of material heated by a supernova blast wave would reduce the required emission measure somewhat, but not by so much as a factor of two. Arbitrarily limiting the pressure to 10^4 cm^{-3} K gives a maximum density of 0.005 cm^{-3} and a minimum radius for the emitting region of 75 pc. This fits in well with UV interstellar absorption measurements which indicate that the ISM is very deficient in neutral hydrogen out to $\sim$100 pc from the Sun.

The constancy of the observed B/C ratio implies that there are less than 5×10^{19} cm^{-2} variations in any cooler material lying between us and the bulk of the emission. This is consistent with the much smaller column densities of neutral or partially ionized material detected in the solar neighborhood through UV absorption measurements, but the organization of the cooler gas and its interaction with the coronal material require further investigation.

X-ray intensities at high latitudes are larger than those in the plane by as much as a factor of three. The fluctuations show a global anti-correlation with H I column density which suggests that they might be caused by variations in the transmission of X-rays from an extragalactic source, such as a galactic halo or corona. Such models are very difficult to reconcile quantitatively with existing H I measurements, however, and it seems more likely that the bulk of the high-latitude excess is produced by an extension of the unabsorbed interstellar emission in those directions with the remaining fluctuations produced by a combination of absorption and displacement by embedded cooler material, or possibly by transmission of flux from a hot halo.

While it would be most interesting to resolve this point because of its impact on the nature of the galactic halo and the high-latitude H I distribution, it does not greatly affect the amount of hot gas which apparently exists in the solar neighborhood: an isotropic emitting region with only the emission measure required by the average intensity near the galactic plane would account for about two-thirds of the integrated B and C band flux observed at the Earth. The total energy flux is $\sim 1 \times 10^{-6}$ ergs cm^{-2} s^{-1} if we

assume a thermal equilibrium spectrum.

INTRODUCTION

A rather large body of data now exists which pertains to the nature and distribution of interstellar material within ∿100 pc of the Sun. Models are available which satisfactarily explain various subsets of these data, but it is not obvious that they can all be combined in any physically reasonable way.

Rather than giving a model to explain the X-ray data which would contain oversimplifications and misinterpretations making it impossible to reconcile with other kinds of observations, I will try to present the constraints introduced by the X-ray observations which must be satisfied by any general model of the local ISM. Two simplified models illustrating how some of these might be met are given near the end.

OBSERVATIONS

Maps of the diffuse X-ray emission in galactic coordinates are show in Figures 1 and 2 for the B and C bands, respectively. The B band responds from approximately 130 eV up to the boron K-shell absorption edge at 188 eV. The C band extends from about 160 eV to the carbon cutoff at 284 eV. More detailed data can be found in McCammon et al. (1983), but the most important features can be summarized as follows:

1. The B and C band maps appear very similar, with the exception of a northern-hemisphere feature near $\ell=30^0$ that has been identified with the North Polar Spur.
2. There is a finite flux in the galactic plane which is approximately the same at all longitudes.
3. The observed flux is generally higher by a factor of two to three at high latitudes. A large-scale anticorrelation with H I column density exists which becomes quite detailed in certain parts of the sky.

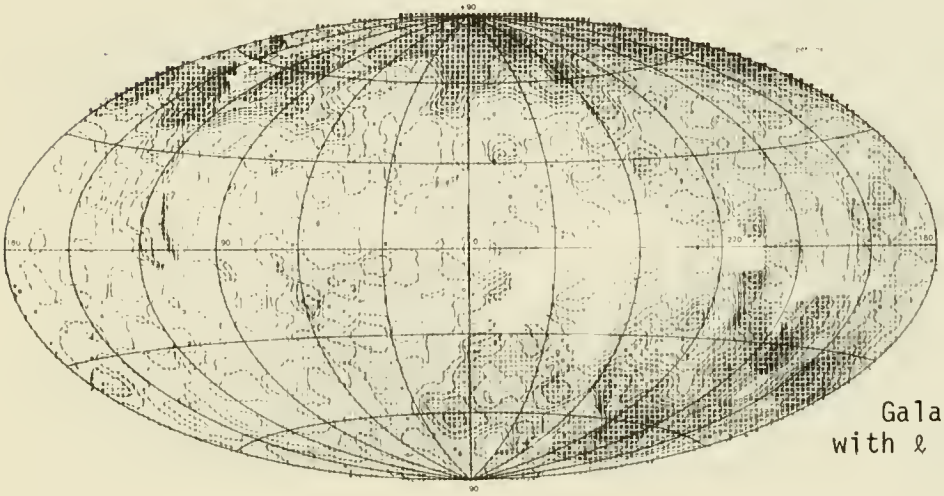

Fig. 1-- B band (130-188 eV) map. Galactic coordinates with $\ell = 0^0$ at center.

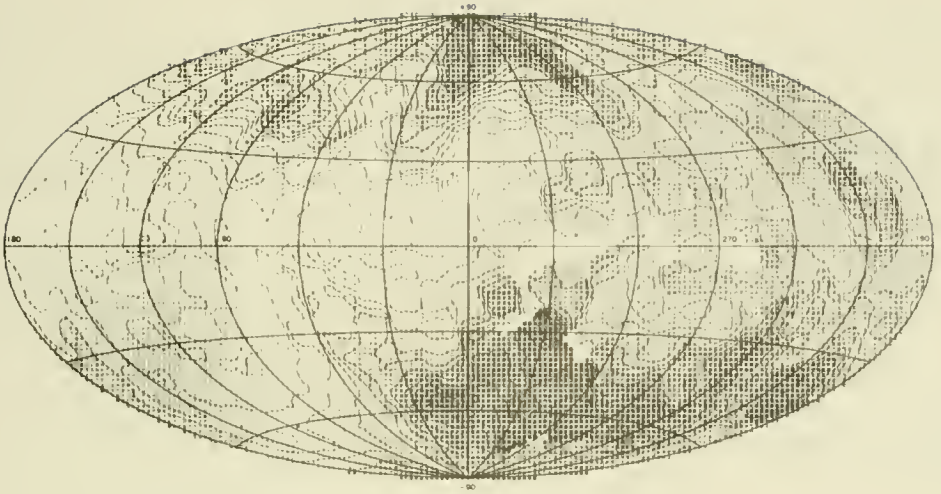

Fig. 2 --C band (160-284 eV) map.

DISCUSSION

The interaction of these X-rays with interstellar material is almost entirely due to photoelectric absorption. The mean free path for B band is about 5.6×10^{19} atoms cm^{-2} and that for C band is about 1.3×10^{20} cm^{-2}. About one third of the absorption is due to hydrogen and almost all of the remainder is due to helium.

The arguments that the X-rays are produced primarily as thermal radiation from a hot component of the interstellar gas near the Sun can be summarized as follows:

1. The rather short mean free paths imply that the X-ray flux observed near the plane, at least, must originate within a few hundred parsecs of the Sun.

2. The small-scale smoothness would require a space density of discrete sources equal at least to that of all stars. Stars provide less than 3% of the flux observed in these bands (Rosner et al., 1981). Therefore the source must be truly diffuse.

3. No non-thermal diffuse emission mechanism has been proposed which is not in serious conflict with other observations. We therefore assume that the source is thermal emission from hot interstellar gas.

4. For emission from a plasma in thermal equilibrium (Raymond and Smith, 1979) the observed B/C ratio implies a temperature near 1×10^6 K. The average intensity in the galactic plane requires an emission measure near 0.002 cm^{-6} pc. With a filling factor of

unity over a 75 pc pathlength, this gives a density ~ 0.005 cm^{-3} and a pressure of $\sim 10^4$ cm^{-3} K. Including non-equilibrium effects reduces the required emission measure, but by less than a factor of two. It also will provide the observed B/C ratio over a wider range of temperature (Cox and Anderson, 1982; Edgar and Cox, 1983).

5. At these temperatures, the emission is almost entirely in lines of the partially ionized heavy elements, even for heavily depleted material. There is strong observational evidence for emission lines from the region within Loop I, and weaker evidence for other parts of the diffuse background (Inoue et al., 1979; Schnopper et al., 1982; Rocchia et al., 1984).

With any diffuse background, it can be difficult to demonstrate that it is indeed coming from where you think it is, rather than, say, the solar wind, the upper atmosphere, or just background in the intrument. We can offer the following arguments:

1. A few features are identifiable with known objects, such as the North Polar Spur. However, these are probably not part of the general emission, and they have somewhat different specta.

2. The lack of parallax in other features requires them to be at a distance greater than 40 pc.

3. The above argument does not apply to the minimum observed flux level. This level accounts for 60% of the total B and C band X-ray flux at the earth if it is assumed to be isotropic, and its removal would greatly alter the apparent connection between the soft X-rays and the local ISN, We have primarily the following evidence for its origin beyond the solar system:

   a. The Wisconsin observations were made from sounding rockets over almost a full solar cycle, with little evidence for variability on scales of minutes, weeks or years.

   b. A map at energies comparable to our C band has been made using data from a quite different instrument on the SAS-C satellite (Marshall and Clark, 1984). It is in excellent agreement with the Wisconsin C band map.

   c. The broad-band spectrum of this component is the same as that of the features (which are known to be at D > 40 pc). This would have to be coincidence if the isotropic component were more local.

The true location of the X-ray emitting material could most readily be determined by looking for absorption by objects with known distances. The few such objects tried so far are at distances $\gtrsim 150$ pc, and none has showed any absorption. Column densities observed in UV absorption within 75 pc of

the Sun are for the most part less than 1×10^{19} cm^{-2}, and would be difficult to observe, even in the B band. If X-rays at still lower energies can be shown to be coming from the same material as the B and C band X-rays, they would make a more sensitive probe for these small column densities, and should enable us to pin down the location of the emitting material much more precisely. Meanwhile, if molecular clouds or other such objects with $N_H \sim 5 \times 10^{19}$ or greater can be identified and located within the solar neighborhood, they could be looked for on the existing C and B band maps.

CONSTRAINTS

A more detailed examination of the B and C band maps leads to the following conclusions:

1. The close tracking of the intensities in these two energy bands implies that the majority of the B band emission is either from the same material emitting the C band X-rays or from material closely associated with it in space.

2. There is a general anticorrelation of X-ray intensity and H I column density as measured by its 21 cm emission. In some parts of the sky a rather good fit is obtained to a partially absorbed model of the form $I = I_o + I_1 \exp(\sigma_{eff} \times N_{HI})$ while in other parts of the sky there is a very large scatter (Marshall and Clark, 1984).

3. The apparent cross section, σ_{eff}, required to fit the above model is smaller than the expected cross section of interstellar material by a factor of $\sim$0.65 in C band and $\sim$0.35 for the B band. This makes the apparent cross sections almost the same for the two bands, where a factor of two difference is expected because of the E^{-3} dependence of photoelectric cross sections.

4. An exception to (3) is found for the B and C band X-ray emission supposed to be associated with the North Polar Spur. The spatial variation of this is consistent with its being absorbed with normal interstellar cross sections by the large concentration of gas extending north from the galactic plane at these longitudes which has been located a distance of 75 - 120 pc. We therefore assume that we are looking at a bright portion of the limb of Loop I which lies somewhat beyond this gas.

Point (2) above causes the greatest difficulties in interpreting the soft X-ray background. A simple way of handling it is to assume that essentially all of the interstellar gas at intermediate and high latitudes is clumped into randomly distributed clouds with average thickness $\sim 2 \times 10^{20}$ cm^{-2}. Such clouds would be optically thick to both B and C band X-rays, but still thin to 21 cm radiation. This would reduce the apparent cross sections in both bands to approximately the derived values. One can then identify I_o with an isotropic local component produced by 10^6 K gas in a spherical cavity surrounding the Sun and providing the X-ray flux

observed in the plane, and I_1 with an extensive galactic corona or other source at approximately the same temperature which lies beyond the galactic H I distribution.

This model is simple and attractive, and it is not very difficult to explain the parts of the sky where the correlation is poor as being due to random variations in I_o or I_1. The major problem is that 21 cm observations measure rather directly those properties of the H I distribution which are important to its apparent X-ray absorption, and existing data seem inconsistent with the existence of the required clumping on any angular scale (Jahoda et al., 1984, and references therein). This two-component model seems viable only if some other way of reducing the apparent cross sections can be found.

Another scenario has the local cavity spatially extended at high latitudes where the ambient gas density is lower. In directions where the extent of the hot gas is greatest, there is the least room left for neutral gas beyond it, and this displacement effect could be the source of most of the anticorrelation.

In this case, it is somewhat troubling that the detailed anticorrelation is as good as it is observed to be in some areas. However, these areas tend to be ones where the total H I column density is very low, and it is possible that a hot corona or other extragalactic source exists, and that transmission of some of this flux by the galactic gas with normal cross sections provides the more detailed anticorrelation, but only a small fraction of the observed X-ray flux.

A theoretical difficulty with the displacement explanation for anticorrelation is that models of supernova blast waves in existing cavities show most of the X-ray emission coming from a thin shell at the boundary of the cavity (Cox and Anderson, 1982; Edgar and Cox, 1983). This tends to make the intensity observed from inside the cavity simply a surface-brightness effect, independent of the extent. It should be possible to produce an anticorrelation of X-ray intensity with the density of the material the blast wave finds at the cavity boundary if the age is properly chosen, but it would be surprising to find the space density so closely related to total column density as the X-rays appear to be in some directions.

We note that both of the above models require the majority of the observed X-rays to be produced in a region surrounding the Sun which contains little cooler material. Either of the models also at least allows the existence of a hot galactic corona of approximately the same intrinsic luminosity.

THE DIFFUSE BACKGROUND AT HIGHER ENERGIES

The M band (440-1100 eV) may or may not be at all related to the local interstellar medium. As can be seen in Fig. 3, the spatial distribution

is entirely different from that of the B and C bands. This is not surprising, since the mean free path in the interstellar medium is now a kiloparsec or so. What is surprising is that aside from the large feature in the direction of the galactic center, the flux is very nearly isotropic. In particular, it shows little tendency to either go up in the plane, as would be expected for a source associated with the galactic disk, or down in the plane, as would be expected from absorption of a source lying outside the disk.

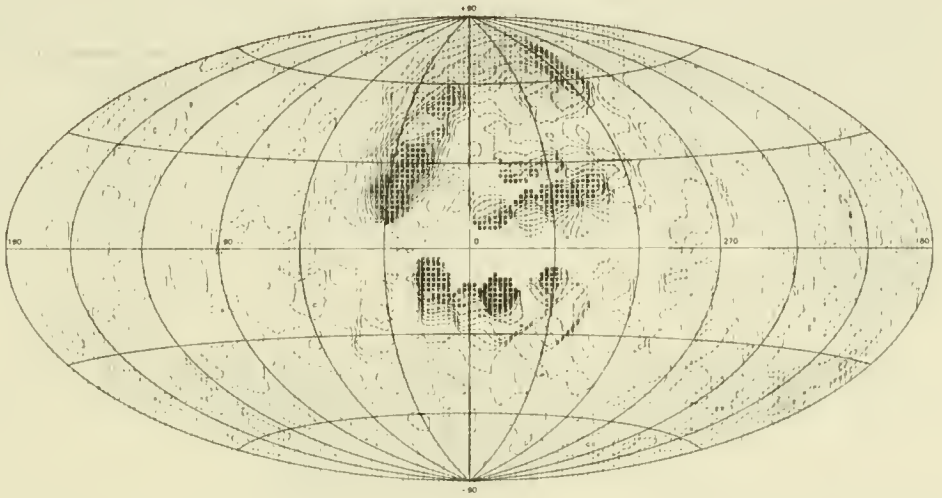

Fig. 3-- M band (440-1100 eV) map.
Galactic coordinates with $\ell=0^0$ at center.

The bright area on the M band map corresponds fairly well with the interior of Loop I, and most of this emission may be associated with it. Possible sources of the remainder include an extrapolation of the extragalactic power-law spectrum observed above 2 keV, which provide about half the high latitude M band X-rays, and dM stars, which could provide up to 25% of the flux seen near the plane (Rosner et al., 1981), and help fill in the absorption dip in the extragalactic contribution. Additional flux at high latitudes could be provided by either a hot component of the halo, or by emission from the local hot cavity. A distribution of structures similar to Loop I could provide additional flux in the plane.

A very reasonable model can be constructed which balances contributions from these four anisotropic sources to produce an isotropic total (Sanders et al., 1982), and this may turn out to be correct. One would be more comfortable of course, with obtaining an isotropic flux from an inherently isotropic source, which would have to be local to the solar neighborhood. The interior of the local cavity is a candidate, but current blast wave models do not easily make very many M band X-rays. It would also probably require that the extragalactic power law spectrum turn over somewhere between 1 and 2 keV.

SUMMARY

We can briefly summarize the constraints introduced by diffuse X-ray observations for models of the local ISM and make suggestions for further observations:

1. Gas with a temperature near $10^{6.0}$K and an emission measure near 2×10^{-3} cm^{-6} pc must exist in all directions near the Sun. The tracking of the B and C band intensities seems to rule out any concentrations of cool material between us and the bulk of this emission with spatial extents greater than $\sim 6^0$ and column densities greater than $\sim 4 \times 10^{19}$ cm^{-2}.

2. The H I concentration extending northward from the galactic plane near $\ell = 20^0$ with a distance believed to be 75 - 120 pc must lie beyond most of the local emitting region, but appears to lie between us and the North Polar Spur which is assumed to be the limb of Loop 1.

3. A mechanism must be provided to supply the observed anticorrelation of the soft X-ray intensity and H I column density which can explain its apparent lack of energy dependence.

4. It would be most useful to locate and observe optically thick targets within $\sim$100 pc of the Sun to determine the extent of the local X-ray emission in various directions.

5. Similar shadowing experiments should help resolve the very interesting question of the origin of the M band X-rays. Much larger column densities are required for the absorbers, but they could be fairly small; ROSAT should be capable of making such measurements reliably on features from 1 arcmin up to about a degree.

The Wisconsin diffuse X-ray observations have depended on the work of a large number of people over an extended time period, and while I can acknowledge all of them anonymously, I should name in particular D. N. Burrows, W. L. Kraushaar, and W. T. Sanders. This work was supported in part by NASA grant GL 50-002-004.

REFERENCES

Cox, D. P., and Anderson, P. R. 1982, Ap. J., 253, 268.
Edgar, R. J., and Cox, D. P. 1983, Ap. J., submitted.
Inoue, H., Koyama, K., Matsuoka, M., Ohashi, T., Tanaka, Y., and Tsunemi, H. 1979, Ap. J. (Letters), 227, L85.
Jahoda, K., McCammon, D., Dickey, J. M., and Lockman, F. J. 1984, Ap. J., submitted.
Marshall, F. J., and Clark, G. W. 1984, Ap. J., in press.
McCammon, D., Burrows, D. N., Sanders, W. T., and Kraushaar, W. L. 1983,

Ap. J., 269, 107.
Raymond, J. C., and Smith, B. W. 1977, Ap. J. Suppl., 35, 419.
_____. 1979, private communication (update to Raymond and Smith 1977).
Rocchia, R., Arnaud, M., Blondel, C., Cheron, C., Christy, J. C., Rothenflug, R., Schnopper, H. W., and Delvaille, J. P. 1984, Astr. Ap., 130, 53.
Rosner, R., Avni, Y., Bookbinder, J., Giaconni, R., Golub, L., Harnden, F. R. Jr., Maxson, C. W., Topka, K., and Vaiana, G. S. 1981, Ap. J. (Letters), 249, L5.
Sanders, W. T., Burrows, D. N., Kraushaar, W. L., and McCammon, D. 1982, in IAU Symposium 101, Supernova Remnants and their X-ray Emission, ed. J. Danziger and P. Gorenstein (Dordrecht: Reidel).
Schnopper, H. W., Delvaille, J. P., Rocchia, R., Blondel, C., Cheron, C., Christy, J. C., Ducros, R., Koch, L., and Rothenflug, R. 1982, Ap. J., 253, 131.

NON-LOCAL ORIGIN OF A SUBSTANTIAL PORTION OF THE SOFT X-RAY BACKGROUND

George W. Clark
Center for Space Research and Department of Physics
Massachusetts Institute of Technology
Cambridge, Massachusetts 02139

Comparison of the SAS-3 soft X-ray sky survey (F. Marshall and G. Clark 1984) with the 21-cm neutral hydrogen survey of Stark et al. (1984) confirms the well-known anticorrelation between the counting rates in the C-band (0.10-0.28 keV) and the column density of neutral hydrogen, and demonstrates that this anticorrelation is significant on all angular scales ranging from that of the general trend from the galactic equator to the poles down to the angular resolution of the detector ($2^{\circ}.7$ FWHM). Included in this general anticorrelation are numerous instances of what appear to be soft X-ray "shadows" of nearby (100-300 pc) 21-cm features, and several bright X-ray regions coincident with "holes" in the ISM.

The final set of selected data has an exposure of 2.2×10^4 cm^2 s sr, a sky coverage of 80%, and is free of spurious effects due to charged particles and solar radiations. It affords an improved opportunity to examine the validity of the two-component model of the X-ray background, introduced by Davidsen et al. (1977), whereby the C-band intensity in a given direction is represented as a sum of a constant term, I_1, due to unattenuated emission from a local "hot bubble" in which the solar system is immersed, and a term, $I_2 \exp[-(N_H/N_{th})]$, due to emission from a diffuse source beyond the neutral hydrogen (e.g., the galactic corona). In this latter term N_H is the column density of neutral hydrogen and N_{th} is the theoretical attenuation column density due to photoelectric absorption in interstellar matter. When this model is used to predict the counting rates of a soft X-ray detector with a field of view that encompasses substantial variations in column density due to the clumping of interstellar matter in clouds with optical depths of the order of 1 or more, it implies a counting rate given by the formula

$$c' = C_1 + C_2 \exp\left[-N_i/N_{ap}\right] \qquad (1)$$

where c'_i is the predicted counting rate and N_i the average column density in the ith field of view. Clumping, which causes the apparent attenuation length, N_{ap}, to be greater than N_{th} (Bowyer and Field 1967, Bunner et al. 1967) must also cause spatial fluctuations in the C-band counting rates. The question therefore arises as to whether a two-component model can be constructed which fits both the anticorrelation and fluctuation properties of the survey data with clumping parameters that are consistent with other information about the ISM.

The C-band survey is displayed in Figure 1 in the form of an Aitoff-projection map, smoothed to an effective angular resolution of $4.^{\circ}5$ (FWHM). Figure 2 is a similar map of the neutral hydrogen column density data, most of which was measured with the Bell Telephone Laboratory Horn Antenna on 2° centers over most of the sky. The BTL survey has comparatively little sidelobe contamination and is well matched in angular resolution to our X-ray survey. The numerical analysis of correlations and fluctuations in the X-ray and radio data were carried out with unsmoothed data stored in arrays of elements corresponding to equal solid angles of $1.^{\circ}8 \times 1.^{\circ}8$.

For analysis of the fit to the two-component model the data were divided into eight sets corresponding to octants of the sky running from the galactic equator to pole between meredia of longitude separated by 90°. Figure 3 shows semilog correlation plots of the counting rates versus column densities after removal of data contaminated by identified discrete sources like the Cygnus Loop, Capella, and HZ 43. The curves are the least-squares fits of equation (1). The best fit is in the "second" octant defined by $0^{\circ}<b<90^{\circ}$, $90^{\circ}<l<180^{\circ}$ where:

$$C_1 = 0.16\ s^{-1}$$
$$C_2 = 0.43\ s^{-1}$$
$$N_{ap} = 2.7 \times 10^{20}\ \text{H-atoms cm}^{-2}$$

The rms residual deviation between the model values and observed values of the counting rates in this octant is 13%, after allowance for Poisson fluctuations in the counting rates and estimates of baseline errors ($\pm 1 \times 10^{19}$ cm^{-2}) and measurement errors ($\pm 5\%$) in N_i. Since fluctuations in systematic errors of the X-ray measurements can account for a good portion of the 13%, it is clear that the two-component model fits the data in the second octant very well indeed. For the SAS-3 soft X-ray detectors the value of N_{th} for thermal X rays from a 10^6K plasma after attenuation by passage through 2×10^{20} H-atoms cm^{-2} of the ISM is 1.4×10^{20} cm^{-2}. Thus the fact that N_{ap} is substantially larger than N_{th}, first brought to light by Bowyer, Field, and Mack (1968), is confirmed here with particular clarity.

To evaluate the small-scale spatial fluctuations in the C-band rates that might be caused by clumping of the ISM, the difference between each counting rate and the mean rate in the immediate neighbor (8) elements of the counting rate map was evaluated. After allowance for Poisson fluctuations, the residual rms fluctuation in the second octant is 10%.

Monte Carlo simulations of the X-ray attenuation by the clumpy interstellar medium were carried out to explore the range of model parameters that yield results consistent with the above findings, namely that N_{ap} is about $2xN_{th}$ and C-band fluctuations on a scale of 2° are about 10%. Figure 3 illustrates the model. Figure 4 summarizes the results of many runs which yield mean values and standard deviations of N_{ap} and the rms fluctuation, F_x, for each set of model parameters. A parameter set which yields values close

to those found for the second octant is as follows:

Distance to edge of local hot bubble = 104 pc

Mean density of HI outside bubble =
$0.75 \exp[-(z/h)^2]$ cm^{-3}, h = 190 pc

Distribution in radius of spherical clouds
$dm \sim R^{-4} dr$, 0.4 pc<R<10 pc

Density of H1 in clouds n_c = 80 cm^{-3}

Fraction of H1 in clouds g = 0.75

The results for this set and others in which one parameter is changed are shown in Figure 4 as ellipses centered on the means with radii equal to the standard deviations. Also shown are the results obtained for a model with parameters derived from the estimates of McKee and Ostriker (1977).

Clouds with approximately the above distribution of linear sizes and optical depths have been observed in radio and optical studies. However, detailed evaluations of the depression of mean transmission factors by clumping in mid-latitude fields of view where high-resolution 21-cm data are available consistently fail to yield values that can account for the high values of N_{ap}. The value of g (0.75) used in our model is probably unrealistically large. Moreover, the Wisconsin survey (McCammon et al. 1983) shows that the ratio of B-band to C-band counting rates is approximately independent of N_H, contrary to the expectation of an attenuation model with a substantial fraction of the absorbing gas not concentrated in clouds. Thus some mechanism or combination of mechanisms other than simple clumping must be found to increase the apparent attenuation column density of counting rates if the two-component model with absorption of a distant component is to be sustained.

If one accepts the view that C_2 does, indeed, represent the rate due to a galactic corona before attenuation, then one can estimate the soft X-ray luminosity of the galaxy from these data. Assuming a uniform corona in the form of a disc of radius 14 kpc, a density scale height of 10 kpc, and a temperature of 10^6 K, we find a coronal luminosity of 5×10^{39} ergs s^{-1}, which can easily be supplied by halo supernovae.

ACKNOWLEDGEMENT

This research was sponsored in part by a grant from the National Aeronautics and Space Administration under Contract NAS5-24441.

REFERENCES

Bowyer, C. S. and Field, G. B. 1969, Nature, 223, 573.

Bowyer, C. S., Field, G. B., and Mack, J. E. 1968, Nature, 217, 32.

Bunner, A. N., Coleman, P. L., Kraushaar, W. L., McCammon, D., Palmieri, T.M., Shilepsky, A., and Ulmer, M. 1969, Nature, 223 1222.

Davidsen, A., Shulman, S., Fritz, G., Meekins, J. F., Henry, R. C., and Friedman, H. 1972, Ap. J., 177, 629.

Marshall, F. J. and Clark, G. W. 1984, Ap.J., in press.

Stark, A. A., Bally, J., Linke, R., and Heiles, C. 1984, (in preparation).

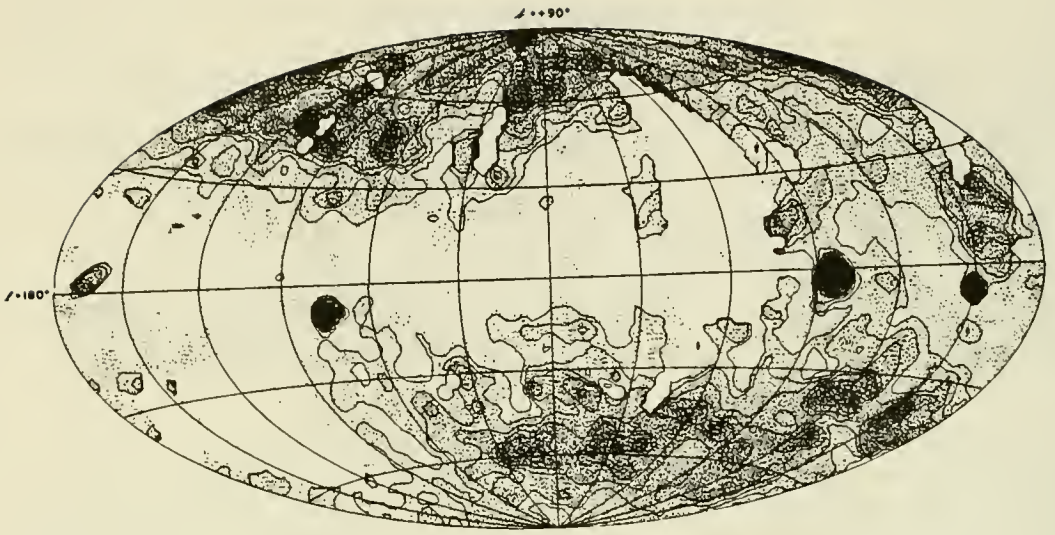

Figure 1: SAS-3 C-band (0.10-0.28 keV) survey map in Aitoff projection. Contours are at intervals of 0.05 cts s^{-1} from 0.20 to 0.45 cts s^{-1}.

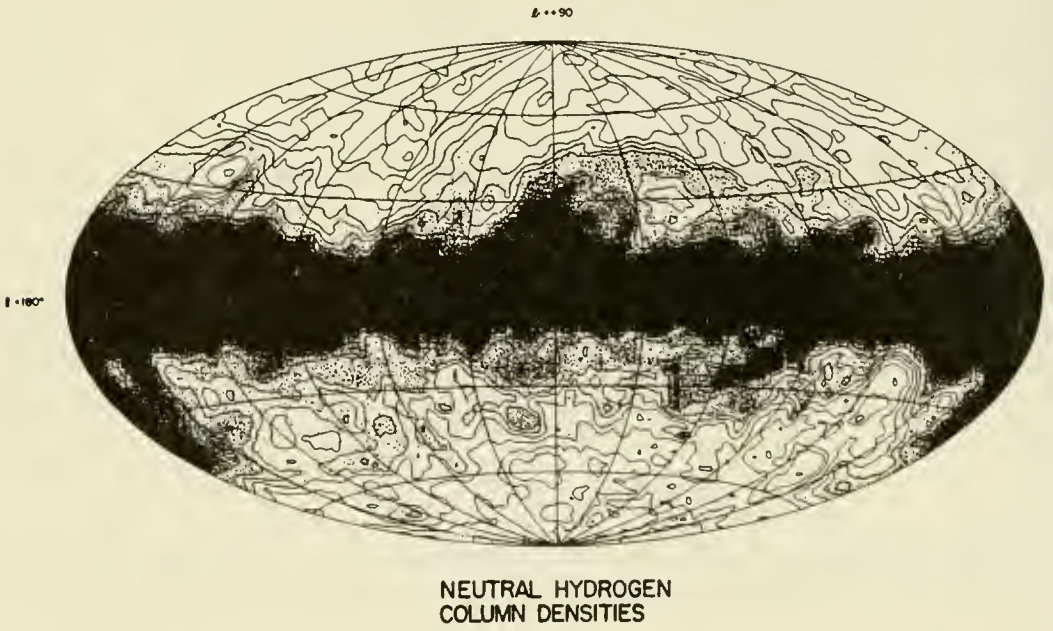

Figure 2: Aitoff projection map of 21-cm survey data of Stark et al. (1984).

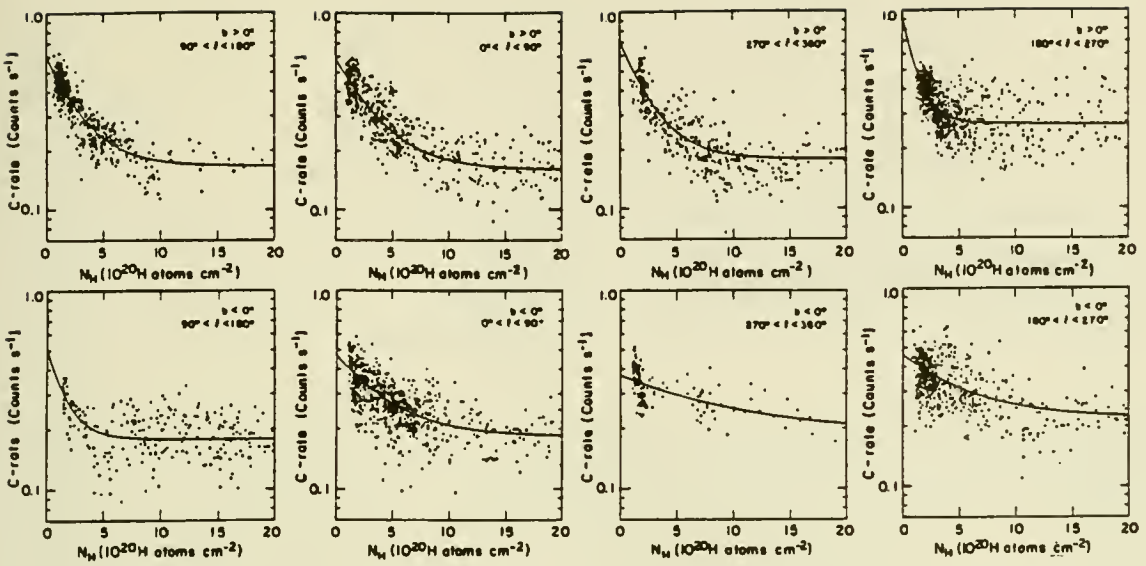

Figure 3: Semilog correlation distributions of C-band counting rates versus neutral hydrogen column densities, with best-fit two-component model curves.

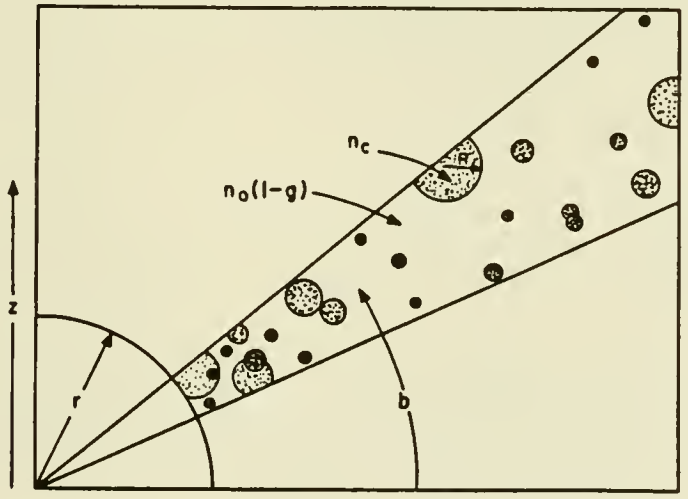

Figure 4: Schematic diagram of the model used in Monte Carlo simulations of attenation and spatial fluctuation of the C-band rate with a clumpy

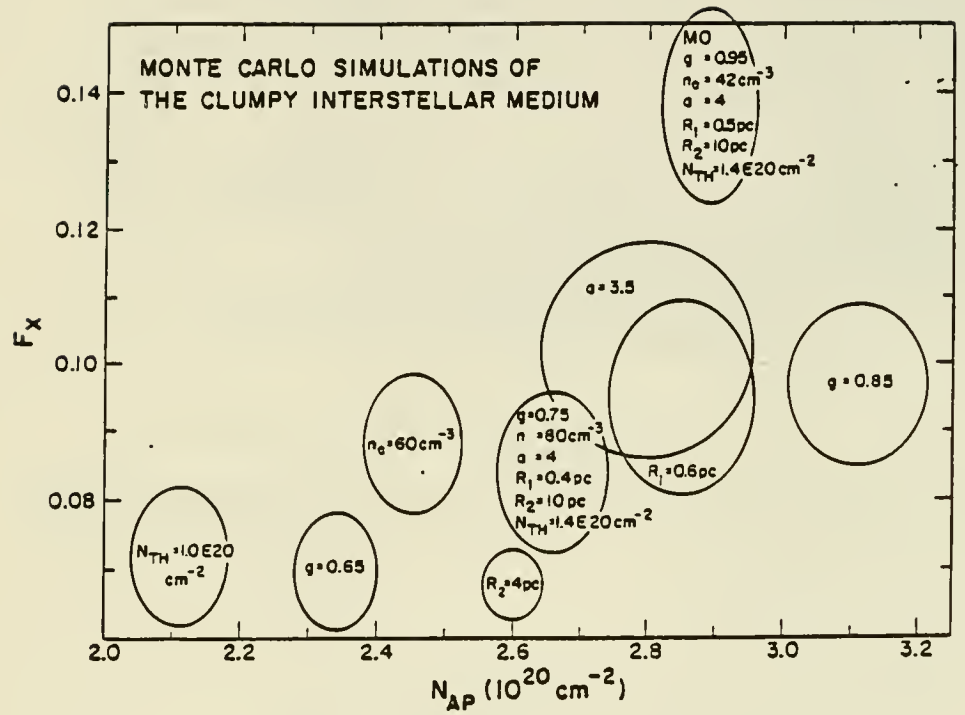

Figure 5: Results of Monte Carlo runs to determine mean values (ellipse centers) and standard deviations (ellipse radii) of N_{ap} and F_x for many trials with each of the sets of parameters indicated in the ellipses. Where only a single parameter is specified the others are assumed to have the values in the ellipse centered at $F_x = .08$ and $N_{ap} = 2.7 \times 10^{20}$ cm^{-2}.

THE NATURE OF THE SOFT X-RAY EMITTING REGION IN THE DIRECTION OF THE NORTH POLAR SPUR

James P. Morrison* and Wilton T. Sanders

Space Physics Laboratory, Department of Physics
University of Wisconsin Madison

*presently with Jet Propulsion Laboratory,
California Institute of Technology, Pasadena, California.

The spatial structure of the X-ray sky in the direction of the North Polar Spur was examined in two energy bands, the B band (0.10 - 0.18 keV) and the C band (0.15 - 0.28 keV). A model with two emitting regions, one local with unabsorbed emission, and the other more distant with emission partially absorbed by spatially varying amounts was investigated.

Using the distribution of atomic hydrogen as a measure of absorbing material, this model was used to predict the flux in the direction of the North Polar Spur. The predicted flux was compared to the data obtained from several sounding rocket flights. The derived flux was found to correlate well with the observed data.

If the model is valid, several conclusion can be drawn from this analysis. The B band flux is almost entirely local in origin. While the local emitting region provides a substantial portion of the observed C band diffuse background, the majority of the C band X-ray originate in a more distant region. The contribution of the local region is relatively constant while the emission from the more distant region, partially absorbed by varying amounts of material, dominates the spatial structure of the X-ray sky in this direction.

This paper discusses one possible cause for the spatial structure observed in the soft X-ray sky as observed in the direction of the North Polar Spur. The data are from a series of sounding rocket flights. The detectors are two gas-filled proportional counters whose seven degree field of view is determined with honeycomb collimators.

Figure 1 shows the relative efficiency of the counters at various energies. Energy resolution is provided at lower energies by carbon and boron filters and at higher energies by pulse height discrimination. The minima which follow the K-edges very effectively define a boron band (B band) from 130 to 188 eV and a carbon band (C band) from 160 to 284 eV. Pulse height discrimination allows a third band (M band) to be defined from 0.45 to 1.0 keV.

The North Polar Spur refers to a region of enhanced radio emission along a longitude of 30°. That this region is also associated with enhanced soft X-ray emission was shown by Bunner et al. (1972) and is apparent in the M and C band maps and to a lesser extent in the B band map (Figure 2).

For the purposes of this discussion we will assume that the source of the X-rays is thermal in nature and consists of a mixture of bremsstrahlung and

lines from recombination and collisionally excited ions. By convolving the emission spectrum of such a hot gas with the detector response functions, one can predict the count rates as seen by the detectors within the various bands. The relevant parameters are temperature, relative elemental aboundances, the extent of the emitting region, and absorption. In this discussion, absorption is an important effect.

Figure 3 shows the relative intensity for each band for a one million degree emitting region with varying amounts of absorption. The absorber is described in terms of the column density of neutral hydrogen with the relative amounts of heavier elements given by a specific set of relative abundances. For B and C band X-rays, helium and hydrogen are the dominant absorbers with oxygen becoming effective in the M band. It is important to note that, while the count rates depend on the extent of the emitting region, the ratios of the count rates do not. Figures 4 and 5 illustrate the C/B and M/C ratios as a function of temperture for various amounts of absorbing material.

The M/C and C/B ratios for a series of points along the spur were determined. Figure 6 indicates the temperatures implied by the two sets of ratios. It is immediately apparent that the C/B ratio implies increasing temperature with latitude while the M/C ratio implies decreasing temperature. This behavior persists for increasing amounts of absorption. Clearly, the data cannot be made consistant with emission from a single temperature region for any varying amounts of absorption. In an analysis of data from a single point of the spur, John Nousek (1978) demonstrated that, for the observations to be fit by a model of thermal emission, the data required two emitting regions, one local and unabsorbed at about one million degrees and another at a temperature of about 3 million degrees behind an absorbing layer.

Savage et al. (1977) have determined the column densities of molecular and atomic hydrogen towards a number of nearby stars which include the general direction of the galactic center and the NPS (Figure 7). Although the data here tend to be for stars at less than twenty degrees latitude, the distribution of the data suggests several important points. (1) There appears to be little neutral material in the direction of the NPS out to about 135 pc. (2) There is a dramatic increase in material at 135 pc. (3) The fact that the column densities do not continue to increase beyond 135 pc suggests that much of the neutral gas may be concentrated at about 135 pc.

This suggests a model in which the soft X-ray flux from the direction of the North Polar Spur originates in two regions, one local and unabsorbed and the other, more distant and partially absorbed by varying amounts of material. The model is illustrated in Figure 8. The two equations state that the observed C and B band fluxes originate in a local unabsorbed region, the first terms, and a more distant partially absorbed region, the second terms. The respective C and B ratios are determined by the assumed temperatures. Since B band X-rays are strongly absorbed by even small amounts of material, the observed B band flux in this model acts primarily as a measure of the local region. By using the observed B band flux and the neutral hydrogen column density as obtained from 21-cm measurements (Heiles et al. 1976) we can make the model predict a C band flux and then compare it to observations.

To improve statistics, data were averaed over six by six degrees for a number of pixels which are indicated in Figure 9. The model was then used to pre-

dict C band rates which were then compared to observed rates. The NH used was the total NH from -20 to +20 km/sec.

Figure 10 compares the predicted C band flux with the observed rates. The predicted and observed fluxes appear to agree well. The error bars reflect the uncertainty in the measured B and C band count rates. The correlation coefficient for this plot is 0.89.

Figure 11 is a plot of the local and distant contributions to the C band flux as predicted by the model. If the model is valid, it implies that, at least in the direction of the NPS, much of the flux originates in the more distant region (in this case slightly more than half). Also, as evidenced by the large intensity variations in the upper part of the figure, the bulk of the spatial structure is caused by absorption effects. That almost all of the B band flux is local is implicit in the model.

Bunner, A. N. et al. 1972, Ap. J. (Letters), 172, L67.
Nousek, J. A. 1978, Ph.D. Thesis, University of Wisconsin.
Savage, B. D. et al. 1977, Ap. J., 216, 291.
Heiles, C. et al. 1976, Astr. Ap., 46, 333.

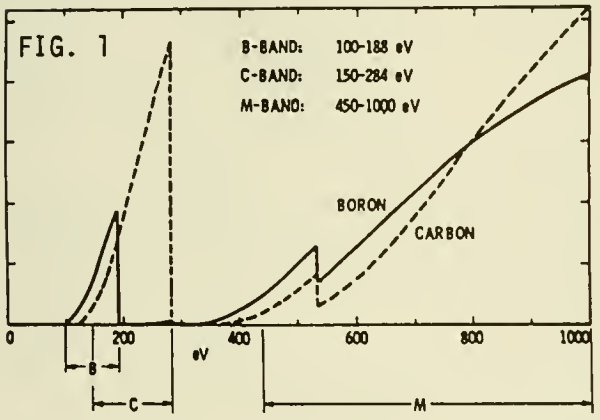

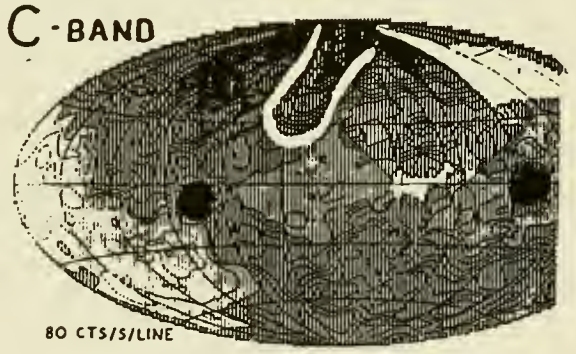

FIG. 2

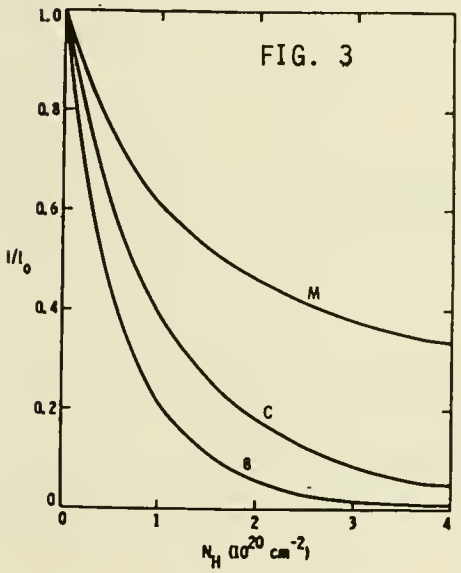

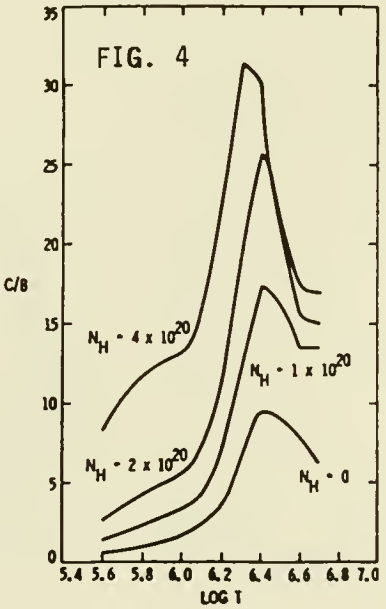

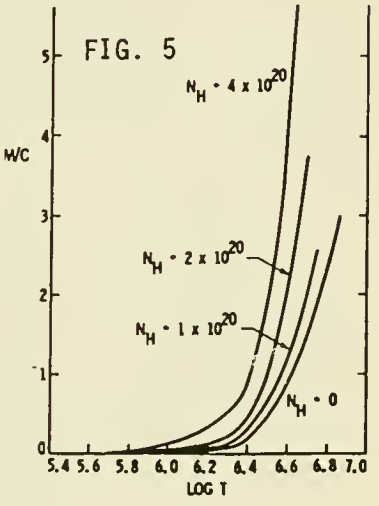

FIG. 6

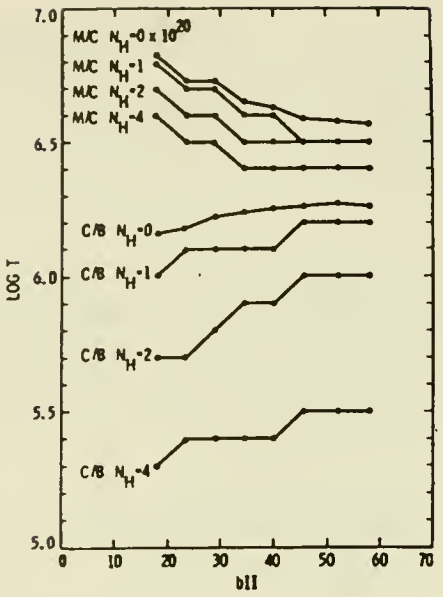

FIG. 7

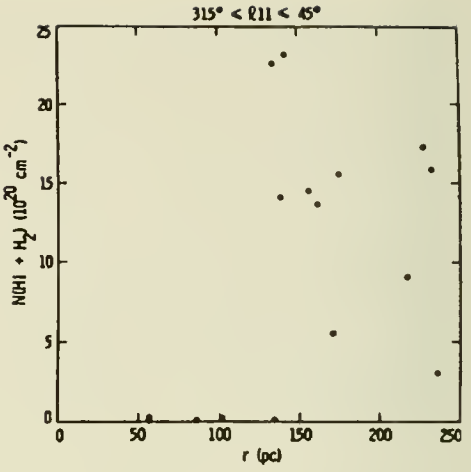

FIG. 8

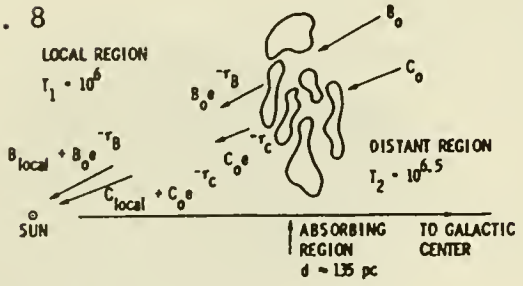

C-BAND FLUX OBSERVED = $C_{Local} + C_o e^{-\sigma_C N_H}$

B-BAND FLUX OBSERVED = $B_{Local} + B_o e^{-\sigma_B N_H}$

$\frac{C_{Local}}{B_{Local}}$ (T = $10^{6.0}$ K) = 2.1

$\frac{C_o}{B_o}$ (T = $10^{6.5}$ K) = 10.4

+

N_H (|V| < 20 Km/sec, Heiles and Jenkins (1975))

CALCULATE C-BAND FLUX

FIG. 9

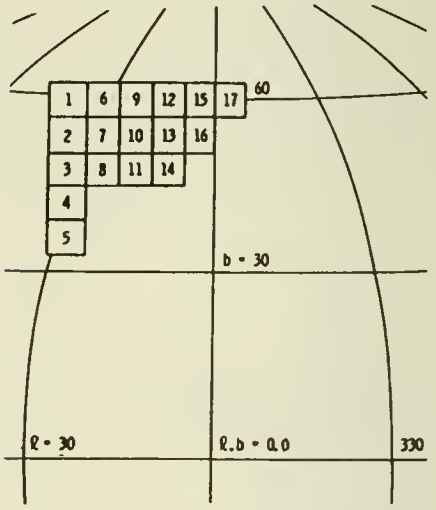

FIG. 10

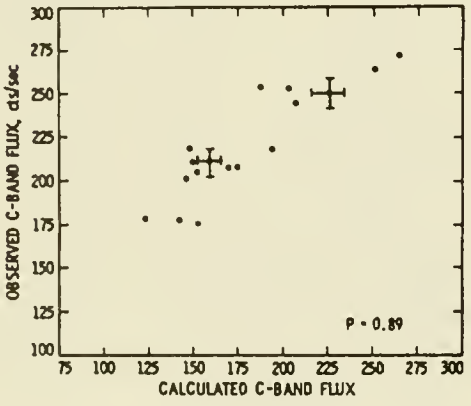

FIG. 11

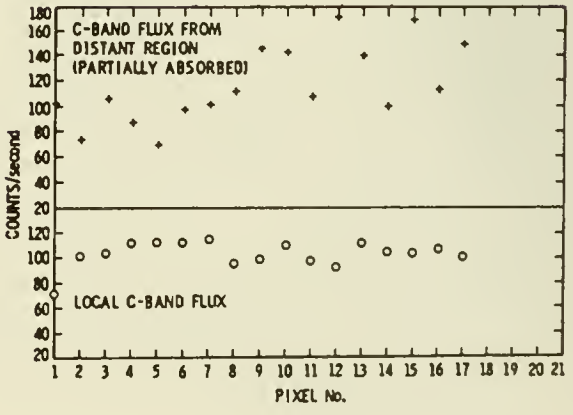

LOCAL CONTRIBUTIONS TO THE 0.6 KEV DIFFUSE X-RAY BACKGROUND

David N. Burrows
Astronomy Department, The Pennsylvania State University

ABSTRACT

The intensity of the X-ray background between 0.5 and 1.0 keV has surprisingly little dependence on galactic latitude. Possible mechanisms for the production of these X-rays include extragalactic emission and emission from dM stars, both of which should be strongly dependent on galactic latitude, and diffuse emission from hot gas ($T \sim 3 \times 10^6$ K) surrounding the Sun. These mechanisms can be distinguished by the presence or absence of absorption by gas within a few hundred parsecs of the Sun. We use X-ray data from the HEAO-1 LED detectors and HI data from the recent Crawford Hill 21 cm survey to place limits on the 0.6 keV intensity originating within 300 pc of the Sun in the general direction of $(\ell,b) = (150°, -30°)$.

INTRODUCTION

The morphology of the X-ray diffuse background (XRB) varies greatly with energy. At energies above 2 keV, where the galactic plane is optically thin, the XRB is nearly isotropic, which implies that it is extragalactic in origin. At energies below 0.28 keV, where the mean free path is of order 100 pc, the XRB becomes highly anisotropic, and is generally thought to be primarily local in origin.

In the interval 0.5-1.0 keV, the source of the XRB is probably less well understood than in any other energy range. With the exception of several well-defined features produced by supernova remnants and hot cavities created by stellar winds or supernovae (e.g. the North Polar Spur and interior of Loop I, the Eridanus enhancement, the Cygnus Loop and Cygnus superbubble), the intensity of the XRB in this energy band is independent of galactic latitude (Nousek et al. 1982, Sanders et al. 1982). This is remarkable, because a mean free path for X-rays in this band is roughly a kiloparsec, so any non-local source mechanism (such as an extragalactic diffuse background, a hot halo, or emission from dM stars) should result in latitude-dependent intensity due to either emission or absorption in the galactic disk.

A model of the .6 keV XRB can be constructed that reproduces the latitude-independence of the data by balancing components from the three likely sources of emission: extragalactic flux, dM stars in the galactic plane, and local emission from hot gas (Burrows 1982, Sanders et al. 1982). This model requires a substantial contribution from the local region, suggesting the presence of gas with $T \sim 3 \times 10^6$ K within a few hundred parsecs of the Sun. An independent test for the presence of such gas in desirable.

Local and non-local sources of diffuse X-rays can be distinguished observationally by the presence or absence of absorption by gas at a known distance. Such a test was performed by Bunner, Sanders, and Nousek (1979), using the SMC as an absorbing N_H feature. The results suggested that the X-rays originated on the near side of the SMC. (However, Seward and Mitchell (1981) found that this result could be influenced by unresolved X-ray sources in the SMC.) We use the same technique to look for evidence of the 0.6 keV absorption in nearby HI features.

DATA

The HEAO-1 A-2 LED experiment surveyed the sky in the energy range 0.18-3.0 keV. A map of a region centered on $(\ell,b) = (150°, -30°)$ was made for this analysis for an energy band with peak response at 0.62 keV. The angular resolution of the map is about 3° x 4°. The data used are from layer 1 of the LED detectors. Several stripes on the map parallel to the scan direction indicate that some of the data are contaminated by electrons or non-cosmic X-rays; these pixels were discarded. The response of the 0.6 keV band is shown in Figure 1. The absorption cross section for this energy band is about 6.7×10^{-22} cm^2 at unit optical depth, for the $E^{-1.4}$ power law spectrum of the 2-10 keV diffuse background.

We performed the analysis for two regions parallel to the galactic plane which include a wide range of N_H values. Region 1 is roughly bounded by $(142° < \ell < 165°)$, $(-27° < b < -15°)$. The Crawford Hill 21 cm survey (Stark et al. 1984) shows an N_H feature in region 1 with column densities of about 1.5×10^{21} cm^{-2}. Comparison of the 21 cm data with UV absorption data (Bohlin, Savage, and Drake 1978) and reddening data (FitzGerald 1968) suggests that the bulk of this gas is within 200-300 pc of the Sun. Region 2 is roughly bounded by $(140° < \ell < 175°)$, $(-46° < b < -38°)$. No UV absorption data and little reddening data are available for region 2, but the data available suggest that this gas may also be relatively close to the Sun.

In order to place limits on the fraction of the 0.6 keV intensity produced on the near side of this gas, a simple model was assumed for the 0.6 keV intensity. We assume that there are two emission components: an unabsorbed isotropic component, and an absorbed isotropic component. The model is given by

$$I(\ell,b) = I_L + I_D \exp(-\sigma N_H(\ell,b)),$$

where I_L is the local component, I_D is the distant component, σ is the cross section, and N_H is the measured HI column density.

RESULTS

The results of the model fitting in region 1 are shown in Figure 2. The solid line is the best-fit model ($I_L = 1.3$, $I_D = 6.5$, $\chi^2_\nu = 5.3$), while the dashed and dotted lines represent the cases of purely local ($I_L = 4.3$, $I_D =$

0.0, χ^2_ν = 8.7) and purely distant (I_L = 0.0, I_D = 9.2, χ^2_ν = 5.52) emission, respectively. Clearly, none of the fits are very good, but the fits with substantial fractions of the X-rays coming from beyond the gas are significantly better than that in which all of the X-rays originate locally. The poor fits may be due to small-scale structure in the emission region or to residual contamination in the data. Unfortunately, the quality of the fits does not permit the model parameters to be constrained in a statistically valid way. However, it is probably fair to conclude that the evidence favors a distant, rather than local, origin of these X-rays.

The opposite conclusion is reached from the data in region 2. The results are shown in Figure 3. Again, the solid line is the best-fit model (I_L = 3.6, I_D = 1.5, χ^2_ν = 1.9), the dashed line is local (I_L = 4.4, I_D = 0.0, χ^2_ν = 2.1), and the dotted line is distant (I_L = 0.0, I_D = 7.6, χ^2_ν = 5.4). These fits indicate that most or all of the X-rays come from the near side of the gas. This result suggests that the extragalactic power law observed at high energies does not continue below 1 keV. It is not completely clear whether it implies a truly local source of 0.6 keV X-rays, however, because the location of the absorbing gas in region 2 is not well established. If this gas is as much as a kiloparsec away, the results from region 2 may be consistent with those from region 1, where the gas is known to be close, if the X-rays are coming from fairly distant regions rather than from the local cavity that produces the 1/4 keV XRB in these regions.

ACKNOWLEDGEMENTS

George Weaver was responsible for producing the maps. John Nousek provided advice on processing the data. Carl Heiles kindly provided the Crawford Hill 21 cm data before publication. This work was supported by NASA grant NAS5-26809.

REFERENCES

Burrows, D.N. 1982, Ph.D. Thesis, University of Wisconsin-Madison.
Bohlin, R.C., Savage, B.D., and Drake, J.F. 1978, Ap.J., 224, 132.
FitzGerald, M.P. 1968, Astron. J., 73, 983.
Nousek, J.N., Fried, P.M. Sanders, W.T., and Kraushaar, W.L. 1982, Ap.J., 258, 83.
Sanders, W.T., Burrows, D.N., Kraushaar, W.L., and McCammon, D. 1982, in IAU Symposium #101, Supernova Remnants and their X-ray Emission, ed. P. Gorenstein and J. Danziger (Dortrecht:Reidel).
Seward, F.D., and Mitchell, M. 1981, Ap. J., 243, 736.
Stark, A.A., Heiles, C., Bally, J., and Linke, R. 1984, in preparation.

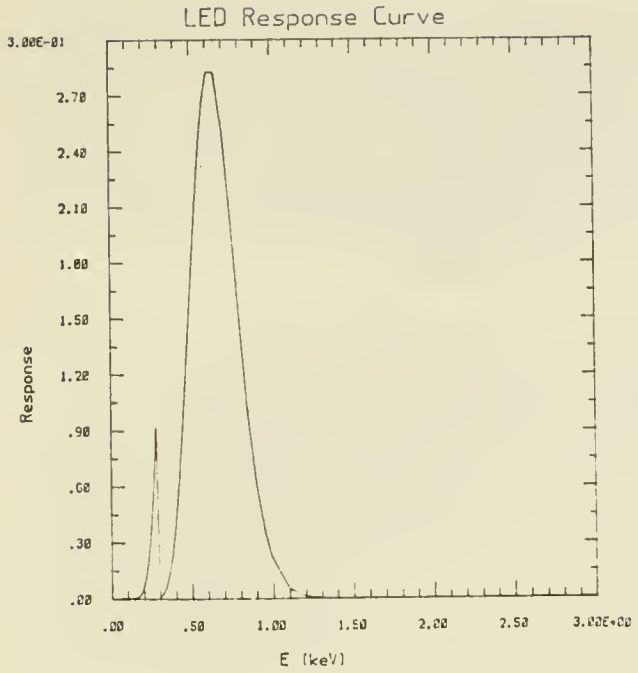

Fig. 1

Fig. 1 - Response curve for the 0.6 keV band used for this analysis.

Fig. 2 - Data and models for region 1. Details given in text.

Fig. 3 - Data and models for region 2. Details given in text.

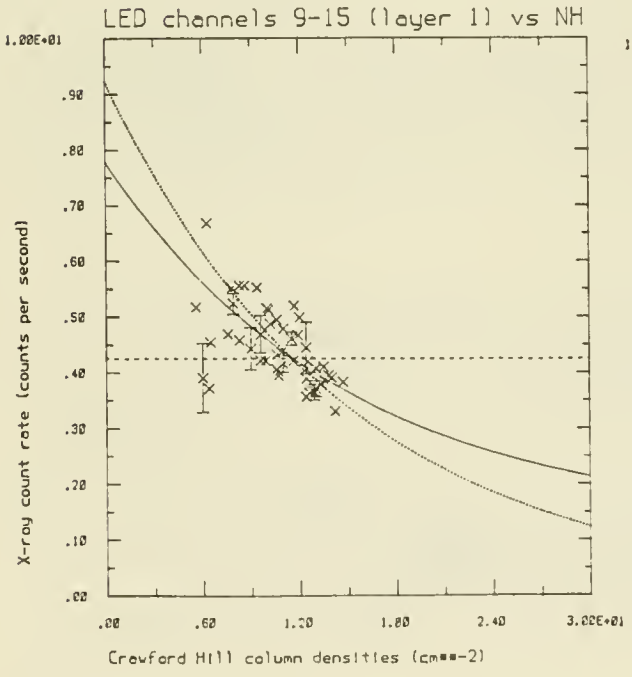

Fig. 2

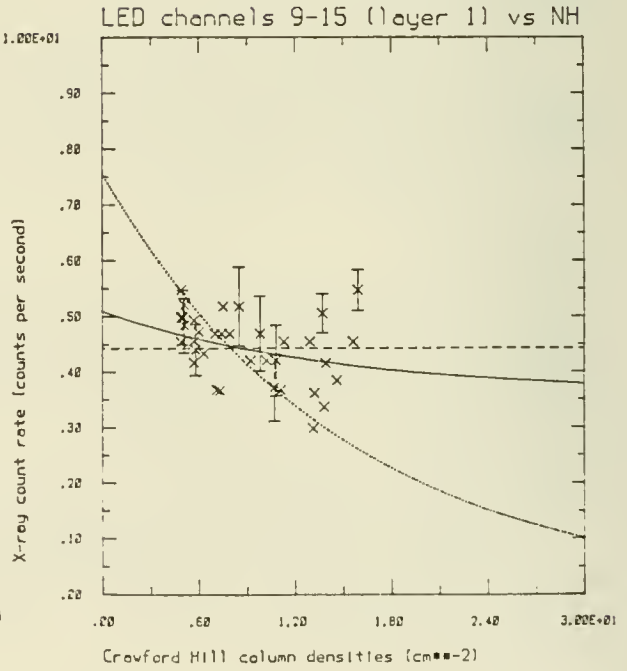

Fig. 3

HEAO-1 DIFFUSE SOFT X-RAY SKY MAPS

John A. Nousek, Gordon P. Garmire, and George Weaver
Department of Astronomy, The Pennsylvania State University

ABSTRACT

Maps of the diffuse soft X-ray background intensity are presented, spanning four energy intervals. The lowest energy interval (0.18-0.56 keV) is dominated by local emission, while the next two intervals (0.56-1.0 keV and 1.0-1.4 keV) reveal more distant and more sharply defined structures. Enlarged maps of several of these structures are presented, including the North Polar Spur, the Galactic Center region and the Eridanus Loop.

INTRODUCTION

The HEAO-1 Satellite A-2 LED (Low Energy Detectors) experiment surveyed the sky at soft X-ray energies using thin window proportional counters. Despite a premature end of the survey due to depletion of the counting gas more than 95% of the sky was observed during its nine months of operation.

Although many point sources of soft X-rays were studied with the LED (cf. the source catalog, Nugent et al 1983), its combination of respectable collecting area ($\sim$400 cm^2), moderate solid angle ($\sim$2.2 msr), long integration time ($\sim$100 hours) and broad sky coverage make the LED data an important source for study of the diffuse soft X-ray background.

A serious problem with all efforts to study the diffuse sky X-ray background with proportional counters is the presence of low energy particles able to penetrate the thin window and mimic X-ray events in the detector. Evidence of such contamination can be seen in the LED data, despite the presence of magnetic brooms designed to prevent charged particles from entering the detector. The contamination appears in our data as long streaks at constant ecliptic longitude. Fortunately most of the charged particle background can be rejected by employing data taken from the central detector volume. Charged particles with energies low enough to mimic soft X-rays are stopped before they enter this volume.

Such residual non-X-ray background as remains in the current maps is not easily explained by charged particles. In some cases every indication points to a true X-ray origin of these events. A speculation, unpalatable because of the high electron flux required, is that some of these non-celestial X-rays are produced by fluorescence of the residual atmosphere near the satellite.

Regardless of the nature of the contamination, the residual in these maps is no more than 20% of the diffuse sky intensity, as infered from the fluctuations.

MAPS

The LED data were collected in one detector having two separate mechanically collimated fields of view. The response of each is approximately triangular in orthogonal directions, being 1.55° x 2.95° FWHM for one (L), and 2.80° x 2.55° in the other (R). The collecting areas are 176.5 cm^2 for L, and 205 cm^2 for R.

The collecting volume is surrounded on front, back and sides by active veto volumes, rejecting charged particles. Data have also been excluded from geographical regions of high background.

The data are grouped into pulse height bins prior to display. The response of the four intervals is shown in Fig. 1. Note that the absorption due to the front layer causes the sensitivity of the intervals to be less at low energy than the nominal pulse height labelling would imply. Thus the 0.56-1.0 keV band, for example, has half response points at 0.75 and 1.2 keV.

DISCUSSION

The higher resolution and longer exposure of the HEAO-1 LED provide a better glimpse of the intricate structure of the soft X-ray background. At 1/4 keV the features are largely diffuse. A reasonable explanation for the origin of this radiation is in local emission from a hot plasma. Near 1 keV the features are better defined, hinting at a more distant origin.

The true test for the origin of this radiation must come from detailed comparison, at comparable resolution, of the X-ray intensity with other aspects of the interstellar medium, for example 21-cm radio data, interstellar extinction, and ultraviolet absorption.

ACKNOWLEDGEMENT

David Burrows provided Fig. 1. Ryland Truax assisted with the image processing computer. This work was sponsored by NAS contract NAS 5-52049.

REFERENCE

Nugent, J.J. *et al.* 1983, Ap.J. Suppl. *51*, 1.

FIGURE CAPTION

Efficiency of each pulse height interval to a mono-energetic flux as a function of energy. A-0.18-0.56 keV band. B-0.56-1.0 keV band. C-1.0-1.4 keV band. D-1.4-2.8 keV band.

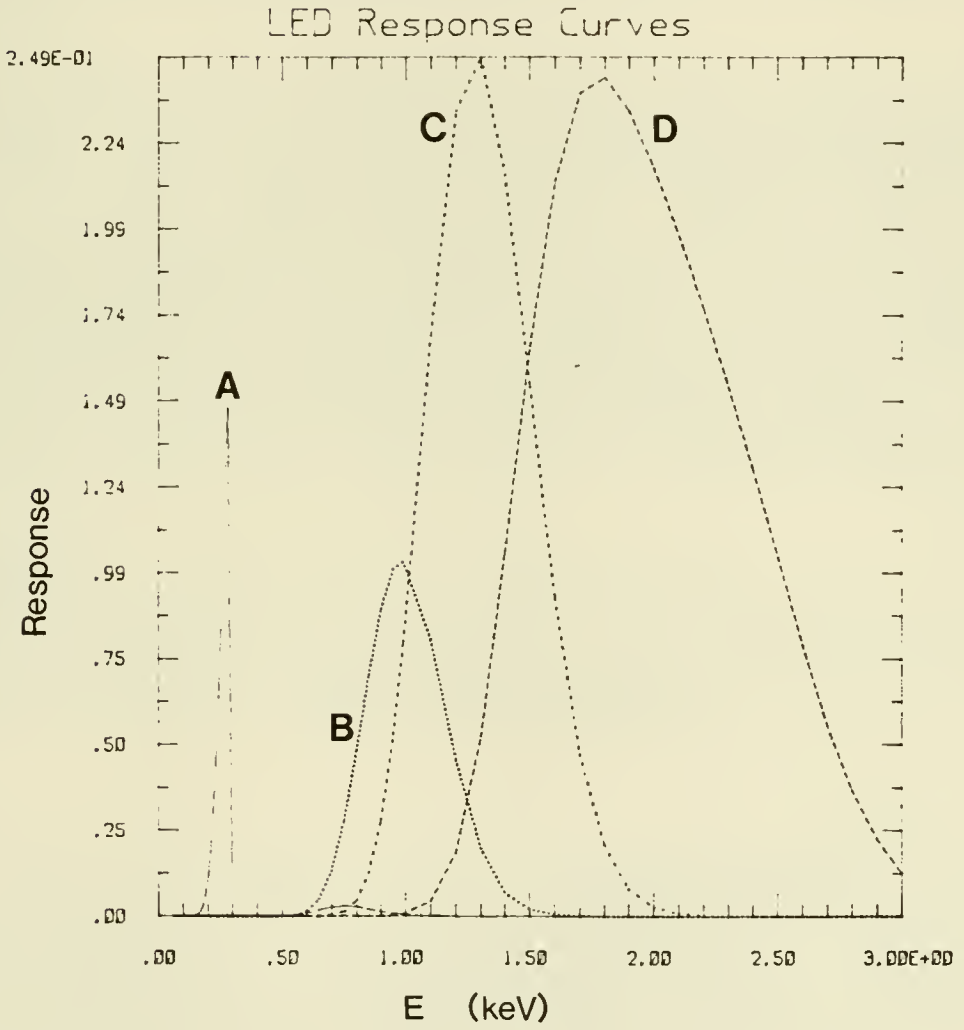

ULTRASOFT X-RAY BACKGROUND OBSERVATIONS OF THE LOCAL INTERSTELLAR MEDIUM

W. T. Sanders, S. L. Snowden, J. J. Bloch
M. Juda, K. M. Jahoda, and D. McCammon

Department of Physics, Univeraity of Wisconsin - Madison

ABSTRACT

Preliminary results from a May 8, 1984 sounding rocket survey of the soft X-ray background are presented. The X-ray detectors are sensitive to X-rays in three soft X-ray bandpasses: 80-110 eV, 90-188 eV, and 284-532 eV (at 20% of peak response). The lowest energy X-rays in this range have a mean free path of order 10^{19} cm^{-2} and provide information about the local interstellar medium. The count rate in the 80-110 eV energy band (the Be band) tracks the 90-188 eV band (the B band) very well, indicating that the same ~1 million degree gas that is responsible for the B band emission may be responsible for the bulk of the Be band X-rays as well. We estimate for the flux in the Be band ~1 photon $cm^{-2}s^{-1}sr^{-1}eV^{-1}$, about a factor of four lower than that found by Stern and Bowyer (1979) and Paresce and Stern (1981) over a similar energy band.

INTRODUCTION

The soft X-ray background appears in all directions of the sky and is thought to be emitted by hot (~1 million degree) interstellar gas surrounding the Sun (e.g., see Edgar and Cox, this colloquium). The mean free path for Be band X-rays against interstellar absorption is $10^{19}cm^{-2}$. Thus the bulk of the X-rays detected in the 80-110 eV band originate closer to the Sun than the closest few times 10^{19} cm^{-2} of neutral material.

EXPERIMENTAL DETAILS

Figure 1 shows the scan path of the experiment superimposed on a map of the soft X-ray B band (130-188 eV) intensity (McCammon et al. 1983). The instrument covered a swath of sky, ~ 15° x 140° degrees, stretching from the inside of Loop I, across the northern extreme of the North Polar Spur, passing within 15° of the North Galactic Pole, skirting the edge of the Hercules soft X-ray enhancement, heading towards the galactic plane along $l = 150^{\circ}$. The detectors were proportional counters filled with 100 torr of methane, 1 cm thick, collimated to a 14° circular field of view. Detector "Y" had a 24 microgram cm^{-2} Formvar window behind a 5500 Angstrom beryllium filter, thus defining the Be band, 80-110 eV. Detector "Z" had a 30 microgram cm^{-2} Formvar window with a ~200 microgram cm^{-2} boron coating, defining a soft B band, 90-188 eV. The area-solid angle curves as a function of energy are shown in Figure 2.

SPATIAL STRUCTURE

Figure 3 shows the count rate in both the Be band (circles) and B band (squares) as a function of angle along the scan path. They clearly are highly correlated as shown in Figure 4. This suggests that the source of the Be band X-rays is the same 1 million degree gas that is thought to produce the B band X-rays (and most of the C band X-rays, 160-284 eV). Because the Be band X-rays must originate closer than the closest $\sim 2 \times 10^{19}$ cm^{-2} of neutral material, the implication is that the B band and C band X-rays also originate in the local interstellar medium.

SPECTRAL FITS

Figure 5 shows the pulse height distribution from both the Be band and B band detectors accumulated over the times when the experiment scanned angles 0 to +25 degrees (see Figure 1). The solid line shows the calculated detector response to a three-component model of the soft X-ray background (McCammon et al. 1983). It assumes an $11E^{-1.4}$ extragalactic spectrum absorbed by $N_H = 2 \times 10^{20}$, an equilibrium hot plasma of T = 3 million degrees absorbed by 2×10^{20}, and an equilibrium hot plasma of 1 million degrees with no absorption. We find no need for an additional softer component. The 80-110 eV flux that we measure is ~1 photon $cm^{-2} s^{-1} sr^{-1} eV^{-1}$, which is a factor of 4 lower than that found by Stern and Bowyer (1979) over a similar energy band. Figure 5 also shows the pulse height distribution that we would expect in our detectors for a thermal emission component of log T = 5.6, $n_e^2 d$ = 0.01 and N_H = 0 (Paresce and Stern 1981).

REFERENCES

McCammon, D., Burrows, D. N., Sanders, W. T., and Kraushaar, W. L. 1983, Ap. J., 269, 107.

Paresce, F., and Stern, R. 1981, Ap. J., 247, 89.

Stern, R., and Bowyer, S. 1979, Ap. J., 239, 755.

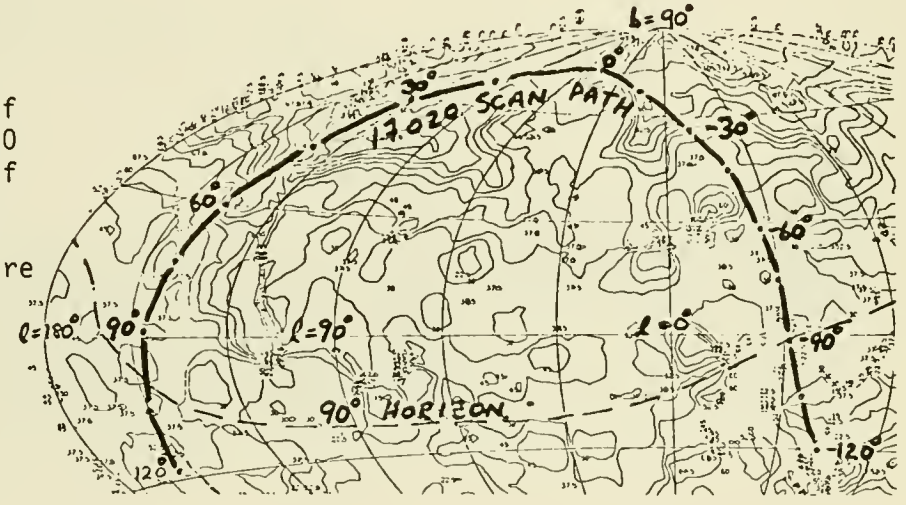

FIG. 1 - Scan path of sounding rocket 17.020 superposed on a map of the soft X-ray B-band intensity. Degrees along the scan path are indicated.

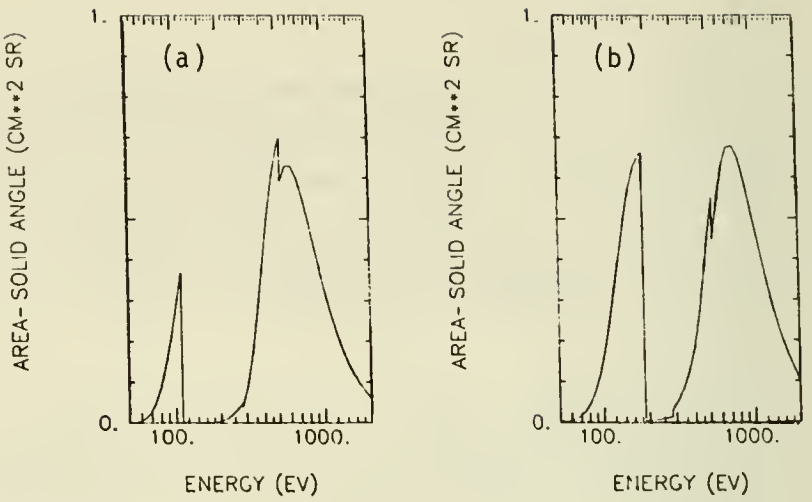

FIG. 2 - Area-solid angle product as a function of energy
a) for the beryllium filter detector (Y), and
b) for the boron window detector (Z).

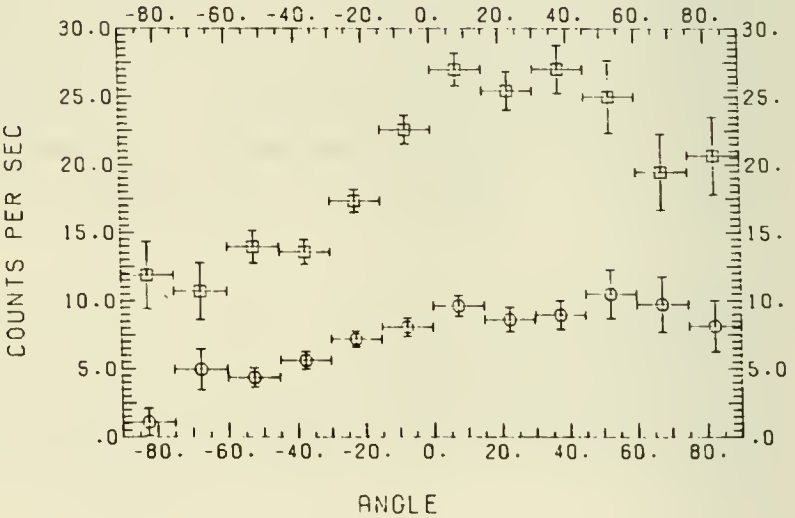

FIG. 3 - Count rate in the Be band (circles) and in the B band (squares) as a function of angle along the scan path (see Fig. 1) of flight 17.020.

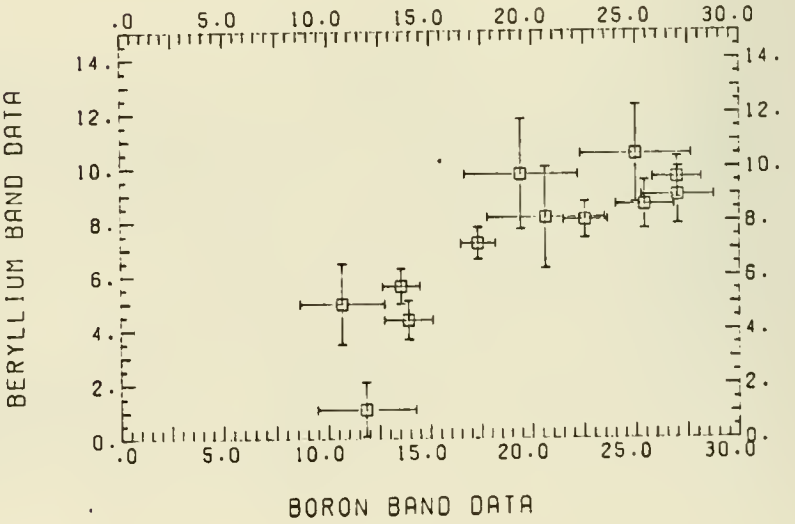

FIG. 4 - Be band count rate (counts s^{-1}) plotted versus B band count rate (counts s^{-1}) for the data of Fig. 3.

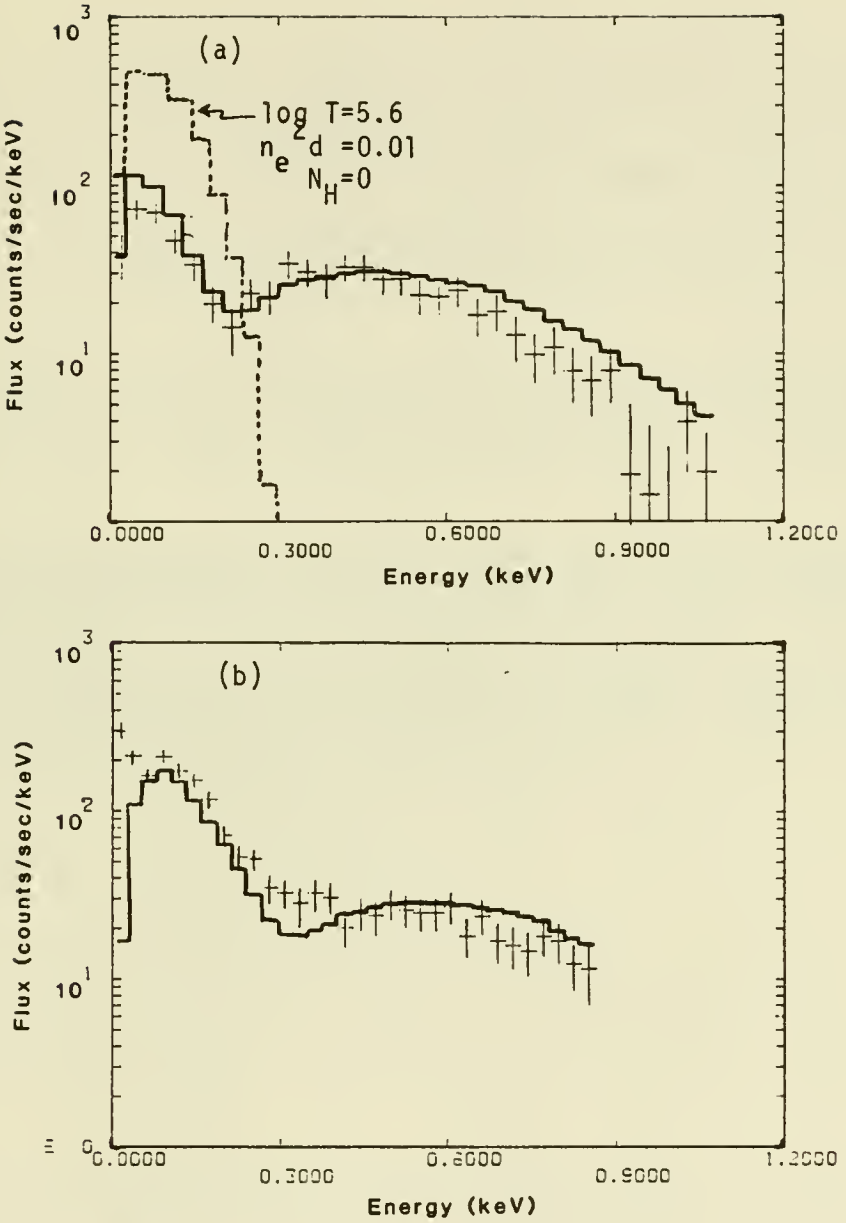

FIG. 5 - Pulse height distributions measured when experiment scanned from 0° to +25° along the scan path (see Fig. 1). The solid line shows the flux expected from a "typical" spectrum that fits (on the average) the B and C band pulse height distributions. The dashed line shows the flux expected from the log T = 5.6 spectrum of Paresce and Stern (1981), a) for the beryllium filter detector, and b) for the boron window detector.

Inverse relations between 0.25 keV counts and local interstellar dust

J.Knude P.Jakobsen
Copenhagen University Observatory

S.Labov S.Bowyer
Space Sciences Laboratory,Berkeley

A preliminary comparison of color excesses and HEAO-1, A2 0.25 keV counts have been performed on two angular levels in order to search for indications of local photoelectric absorption.

a. Color excesses and background counts are smoothed to a common 1.5 1.5 sq.deg. beam. Although distance information on the color excesses are available it is not used in this first attempt. The lines of sight to which the excesses pertain have however a length comparable to the expected viewing distance at these energies in the local medium. Figure 1 displays the resulting average counts/pixel versus average excess/pixel for the five areas investigated. A general decrease of the counts with excess is apparent. The wide scatter in the individual regions is probably due to excess variations on scales smaller than the collimated beam. The minimum counts on the diagram come from a region where an almost coherent sheet of dust is present within a distance ~200 pc. The constancy of the minimum counts in this particular direction indicates that the soft X-ray emission probably originate exclusively in front of the matter observed to be present. Note that the SGP counts show a shallow inverse dependence on excess. The latitude distribution of the five areas assures that the general inverse relation of the 0.25 keV counts on color excesses is not a latitude effect.

b. What may appear more exciting is the existence of an inverse relation between 0.25 keV counts and color execesses on angular scales 0.001 sr, corresponding to the projected size of individual diffuse clouds. For this purpose SA 162,(l,b)=(21,-59) data are presented . The counts and color excesses are now compared on a 0.5×0.5 sq.deg scale.Given a measured number of counts/pixel the excesses do show quite a range of values. The absorbing material varies however on scales ~30'. All excesses pertain to the nearest few hundred pc. Most of the excess variation is due to the small scale angular variation and nct to any radial variation. The main problem is to decide which measure of the amount of absorbing matter to compare to the counts. In order to have a representation of absorbing matter present as typical as posibel, and selected in an unbiased way,the comparison is restricted to the

pixels where the excess has been measured along at least two different lines of sight. Figure 2 is a display of the upper and lower excess limits versus counts/pixel for the subsample where such a detailed comparison was possible. The 0.25 keV counts/pixel do decrease with both the lower and upper excess limit. Part of this variation is undoubtedly due to photoelectric absorption but depends also on the fraction of the beam coevered by absorbing material. The lower envelope may be due to the largest clouds and accordingly be the best representation of the dependence of counts on excess. To have an idea of the relative distribution of local and remote contributions to the counts an exponential is fitted to the average excess for a given count:

$$N(\text{counts}) = 5 \exp(-\sigma(0.25\ \text{keV}) \times N(H)/E(b-y) \times \langle E(b-y) \rangle) + 11$$

This expression indicates that 2/3 of the background originates in front of the absorption but that the remote contribution has about the same importance in the directions where there is little obscuration.

It remains to be investigated whether the HEAO-1,A2 soft X-ray data are sufficiently accurate to support a variation of only 10 - 20 %. The discussion also tacitly assumed a constant ratio between gas and dust in the diffuse medium.

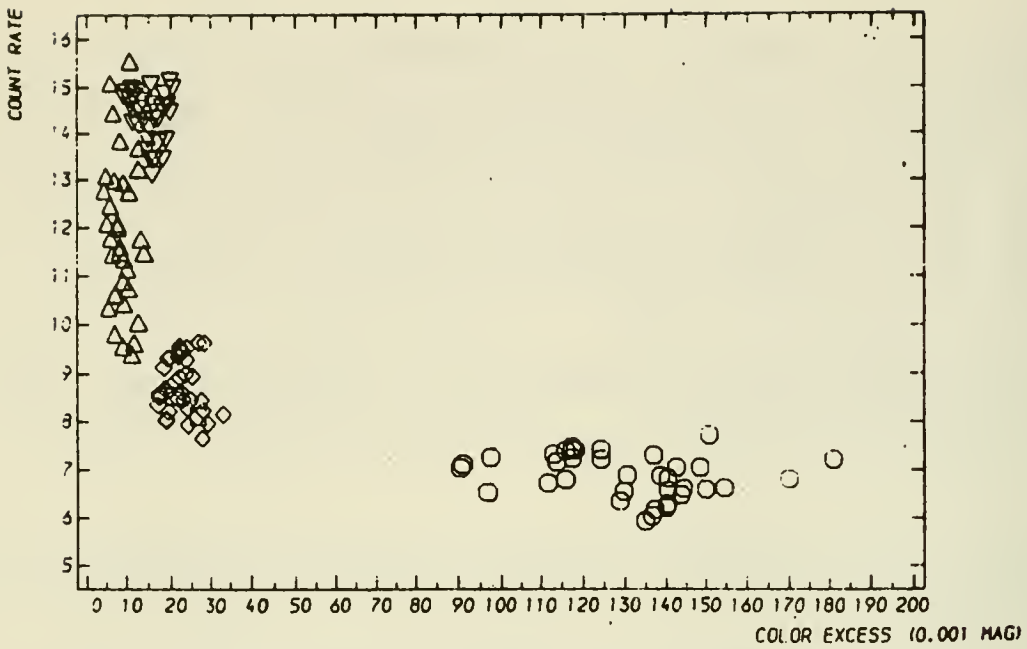

Fig. 1. 0.25 keV counts versus color excess for five Selected Areas: □ SA 128, ◇ 141, △144, ○156, ▽162. Averaged over 4 sq.deg beams.

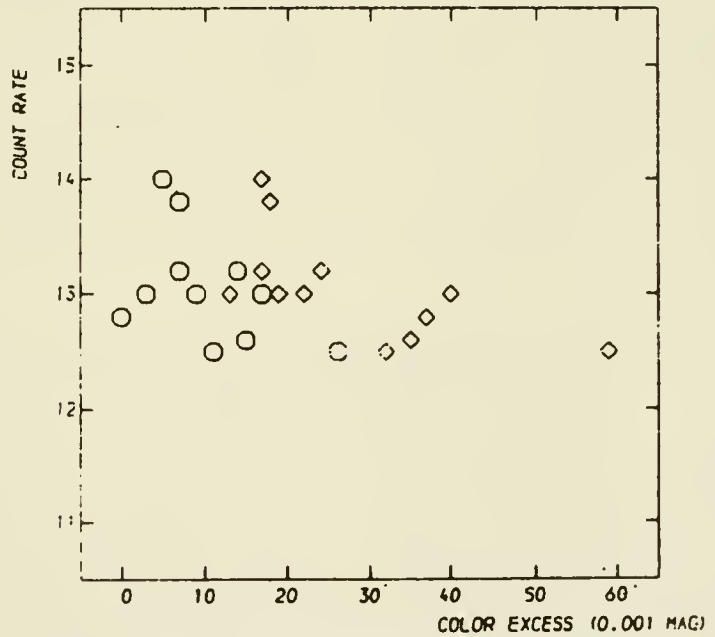

Fig.2. 0.5 0.5 sq.deg counts versus upper and lower excess limit. Only pixels with more than two extinctions observations.

THE LISM AT INFRARED AND MILLIMETER WAVELENGTHS

MOLECULAR CLOUDS WITHIN 100 PC

Leo Blitz and Loris Magnani
Astronomy Program, University of Maryland

Lee Mundy
Astronomy Department, University of Texas

ABSTRACT

Observations at the 2.6 mm line of CO reveal the presence of a large number of molecular clouds at high galactic latitude. If the velocity dispersion of the clouds is a measure of their scale height, the mean distance of the ensemble we have detected is 100 pc. The clouds are unusual in that either they are not gravitationally bound or they are very deficient in CO relative to molecular hydrogen. These clouds represent a heretofore unrecognized component of the local interstellar medium. If they are pervasive in the Milky Way, they probably represent the small molecular cloud component of the interstellar medium.

OBSERVATIONS

The observations were based on a careful search of the Palomar Sky Survey prints for regions of apparent obscuration. All of the prints at $|b|>20^{o}$ were examined and 457 candidate regions were identified. Of these, 439 were observed in the J = 1-0 transition of CO using the 5m dish at the Millimeter Wave Observatory near Fort Davis, Texas. CO was detected from 105 (24%) of the sources, a number in complexes of large angular extent. More than half of the clouds at $|b|>30^{o}$ have been mapped, and there are a limited number of observations at the J = 2-1 transition of CO and at the J = 1-0 transition of ^{13}CO.

CO observations were also made of two regions which show ultraviolet excesses (Paresce, Jakobsen and Bowyer 1983, Paresce private communication) and of Cloud X, identified by Low et al. (1984) as a region of diffuse, cold infrared emission detected by IRAS. We did not detect CO from any of these.

RESULTS

The clouds are generally well distributed on the sky, but a number of them are clustered together in complexes. The richest of these appear to be high latitude extensions of complexes which occur predominantly at $b<20^{o}$, such

as the ρ Oph complex. The only empty region extends from $180^{\circ}<\ell<315^{\circ}$ at positive latitudes (a large fraction of this range at negative latitudes is not accessible from the northern hemisphere).

Of the clouds at $|b|>30^{\circ}$, CO was detected from 37 directions; these appear to be in 29 distinct clouds. The CO lines tend to be relatively strong, indicating that the observations are not sensitivity limited. Sixteen of the clouds have been mapped, including 5 clouds previously mapped by Montani and Morris (unpublished). Some have large angular extents (up to 5.4 square degrees) indicating that the high latitude molecular clouds may be responsible for at least some of the 'infrared cirrus' detected by IRAS (Low et al. 1984).

The observed and derived properties of the clouds are given in Table 1. The internal velocity dispersion of a cloud, σ_v(internal) is determined from the velocity at the emission peak of each observed position within a given map. The quantity σ_v(c-c) is the velocity dispersion of the ensemble; the ensemble mean is 1.3 ± 0.2 (km s^{-1}) relative to the LSR.

The derived properties are based on a mean distance to the clouds at $|b|>30^{\circ}$ of 100 pc. This number is based on the scale height the clouds would have with the measured velocity dispersion and the surface density of stars in the solar neighborhood (van der Kruit and Shostak 1984). A longitude velocity plot of the clouds indicates, however, that the velocity dispersion may not be random and that the derived distance may be in error. The H_2 column density $N(H_2)$ is based on the conversion $N(H_2) = 2.5\times10^{20}\int T_A^*(CO)dv$ cm^{-2} derived from X-ray, CO and HI observations of the inner Galaxy (Lebrun et al. 1983; Bloemen, et al. 1984). Our ^{13}CO observations indicate, however, that $N(H_2)$ may be overestimated by a factor of 3 using this conversion. N(HI) is determined from the survey of Heiles and Habing (1974), and A_v is based on the gas-to-extinction ratio of Savage and Mathis (1979). The quantity ε is the fractional completeness of the survey.

If the clouds are virialized, the velocity dispersion is given by $\sigma_v(\text{internal}) = 0.0657(M/R)^{0.5}$ km s^{-1} if M is in $M_\odot$ and R is in pc. Table 2 gives the measured velocity dispersion of ten clouds we mapped and the expected velocity dispersion based on the derived mass and radius for each cloud. The table shows that six of the ten clouds have measured dispersions which exceed the expected dispersions by a factor of 2.3 to 6.9. Since the expected value of the velocity dispersion varies only as the square root of the distance to a cloud, and since the masses may be overestimated, it appears that the discrepancy between the expected and measured velocity dispersion is real. The clouds are not gravitationally bound unless the masses or distances (or a combination of the two) of the first six clouds in Table 2 is underestimated by a factor of 20 on average. If the clouds are indeed expanding, their ages are less than the crossing time of a gas clump within a cloud: $\lesssim10^6$ y! These clouds appear to be extraordinarily young and may represent the earliest stages of molecular clouds condensing from the interstellar medium.

In any event, the high latitude molecular clouds are a heretofore unrecognized and uncatalogued component of the local interstellar medium. If the solar vicinity is representative of the galactic disk, the clouds probably represent the small molecular cloud component of the interstellar medium.

References

Bloemen, J.B.G.M. et al., 1984, Astron. Ap., in press.
Heiles, C., and Habing, H. J., 1974, Astron. Ap. Suppl., 14, 1.
Lebrun, F., et al., 1983, Ap. J. 274, 231.
Low, F. J., et al., 1984, Ap. J. (Letters), 278, L19.
Paresce, F., Jakobsen, P., and Bowyer, S., 1983, Astron. Ap. 124, 300.
Savage, B. D., and Mathis, J. S., 1979, Ann. Rev. Astron. Ap., 17, 73.

Table 1

Properties of the High Latitude CO Clouds

Observed Properties

quantity		range or value	mean
$T_A^*(CO)$	(^oK)	0.6-6.8	2.6
$\int T_A^*(CO)dv / \int T_A^*(^{13}CO)dv$		2.3-18	10.5
$\Delta V(CO)$(FWHM)	(km s^{-1})	1.0-5.7	1.9
σ_v(internal)	(km s^{-1})	0.2-2.2	0.73 (median)
σ_v(c-c)	(km s^{-1})	5.7±1.2	
Projected area	(sq deg.)	0.1-5.4	1.3
Number detected		29	

Derived Properties

Distance	(pc)	100 (mean of ensemble)	
Size	(pc)	2.0 (mean of ensemble)	
Mass	($M_\odot$)	2.0-260	66
H_2 density	(cm^{-3})	46-250	170
$N(H_2)/N(HI)$		0.2-30	5
$A_v(H_2)$	(mag)	0.3-1.4	0.7
Age	(yr)	$\lesssim 10^6$y	
Number within 100 pc		$64/\varepsilon$	
Surface filling fraction within 100 pc		$2.5\times10^{-3}/\varepsilon$	
$\sigma(H_2)$	$M_\odot$ pc^{-2}	$0.1/\varepsilon$	

Table 2

cloud	σ_v[1](expected)	σ_v (observed)
30	0.48	2.18
2	0.15	1.04
18	0.27	0.95
16	0.20	0.87
8	0.35	0.82
24	0.20	0.64
	Stable Clouds	
12	0.34	0.43
23	0.19	0.25
25	0.10	0.17
27	(0.15)	(0.10)

[1] $\sigma_v(\text{expected}) = 0.0657(M/R)^{1/2}$ km s^{-1}

A WIDE LATITIUDE CO SURVEY OF MOLECULAR CLOUDS

IN THE NORTHERN MILKY WAY

T.M. Dame and P. Thaddeus
Goddard Institute for Space Studies and Columbia University

INTRODUCTION

It is now well established that molecular clouds are an important part of the interstellar medium, containing much or most of the dense, cold component of the gas, and producing the massive stars and supernovae responsible for the diffuse, hot component. It would therefore appear essential in formulating a complete picture of the local interstellar medium to have some knowledge of the distribution and properties of nearby molecular clouds. To this end we have used the Goddard-Columbia 1.2-meter telescope to carry out a wide latitude, low angular resolution survey of CO along most of the first galactic quadrant and a small part of the second. The survey is uniform and fully sampled in galactic longitude from 12° to 100°, and in latitude from -5° to +6°, with extensions to as high as +11° to include specific dark clouds; the total area surveyed, 1128 deg^2, is much larger than any region previously studied in CO or any other interstellar molecule. In order to fully sample such a large area in a reasonable amount of time, angular resolution has been sacrificed to coverage and speed; an angular resolution of 1° was obtained synthetically by simply scanning a square 8 x 8 raster of points separated by 1/8°, the size of the primary beam, and summing the resulting 64 spectra at the end of an observation.

DISCUSSION

Figure 1 is the plane-of-the-sky map which results from numerically integrating the survey over radial velocity. The velocity range of the spectrometer was adequate to include all material in the longitude range of the survey within ~11 kpc of the galactic center for $\ell < 60°$, and within ~19 kpc of the galactic center for $\ell > 60°$. This map is the most direct way to compare CO molecular clouds with continuum radio, IR, and γ-ray surveys, and has been used to study the relation of molecular clouds in the first quadrant to high-energy γ-rays observed by COS-B (Lebrun et al. 1983).

A striking aspect of Figure 1 is the large filling factor of the CO emission - roughly 50% of the total area observed. About half this emission comes from quite local clouds within ~1 kpc; most of the rest is confined to the intense central ridge of emission about 2° thick at $\ell < 45°$. This is the dense concentration of clouds in the distant Scutum and 4-kpc spiral arms that has been called the molecular ring on the assumption that it represents an axisymmetric distribution of clouds with respect to the galactic center. These distant clouds are so heavily obscured by the foreground Rift material

that the associated H II regions and young stars are almost entirely invisible from the solar system; we can remove them to study the local clouds by restricting the range of the velocity integration.

Figure 2 has been integrated over the range -10 to 34 km s^{-1}, the upper limit chosen to include in the map all major clouds which contribute to the obscuration of the Great Rift. On the same scale we show a wide-angle photograph of the Milky Way with the lowest CO contour overlaid. It is obvious from this comparison that there exists a remarkably good correlation between the low-velocity CO emission and the optical obscuration of the Great Rift. Nearly every dark nebula is a CO molecular cloud and vice versa.

The nature of the Great Rift is a very longstanding problem. In recent times, there have been various attempts to divide the Rift into regions of roughly uniform obscuration, on the assumption that each region corresponds to an individual dust cloud at some fixed distance. With the aid of our CO survey, it is a simple matter to resolve the Rift into discrete molecular clouds, since even clouds which overlap in direction can be distinguished from one another by their radial velocities. The Rift is decomposed into its individual molecular clouds in Figure 3. Distances were determined either kinematically (for some of the more distant clouds), or with the aid of associated Population-I objects, or with graphs of visual absorption vs. distance for stars within the cloud boundaries (Neckel and Klare 1980). The entire Rift system is seen to be composed of a small number of fairly well-defined clouds at distances ranging from 150 pc to more than 2 kpc.

Of particular interest to the study of local matter is the Aquila Rift, the large lane of obscuration between ℓ = 20° and 40° apparently produced by a single cloud containing several 10^4 $M_\odot$ of molecular gas at a distance of about 150 pc. This cloud is probably related to the very extended, cold HI cloud observed by Riegel and Crutcher (1972) (see Crutcher, this volume), seen as an HI self-absorption feature in the region from ℓ = 345° through the galactic center to ℓ = 25°, at $|b| < 10°$. The CO and HI clouds are comparable in angular size, are similarly displaced to postive latitude, have similar narrow linewidths and quite constant velocities; they are estimated to be at nearly the same distance, and partially overlap spatially in the region ℓ = 20° to 25°. The Aquila Rift molecular cloud and the Riegel-Crutcher HI cloud may therefore comprise a single large lane of cold gas extending over 55° of galactic longitude, corresponding to a linear size of 140 pc. Why this object is molecular at one end, and apparently deficient in dust and molecules at the other, as Riegel and Crutcher find, is a puzzle.

REFERENCES

Lebrun, F. et al. 1983, Ap. J., 274, 231.
Neckel, Th. and Klare, G. 1980, Astr. and Ap. Suppl., 42, 251.
Riegel, K.W., and Crutcher, R.M. 1972, Astr. and Ap., 18, 55.

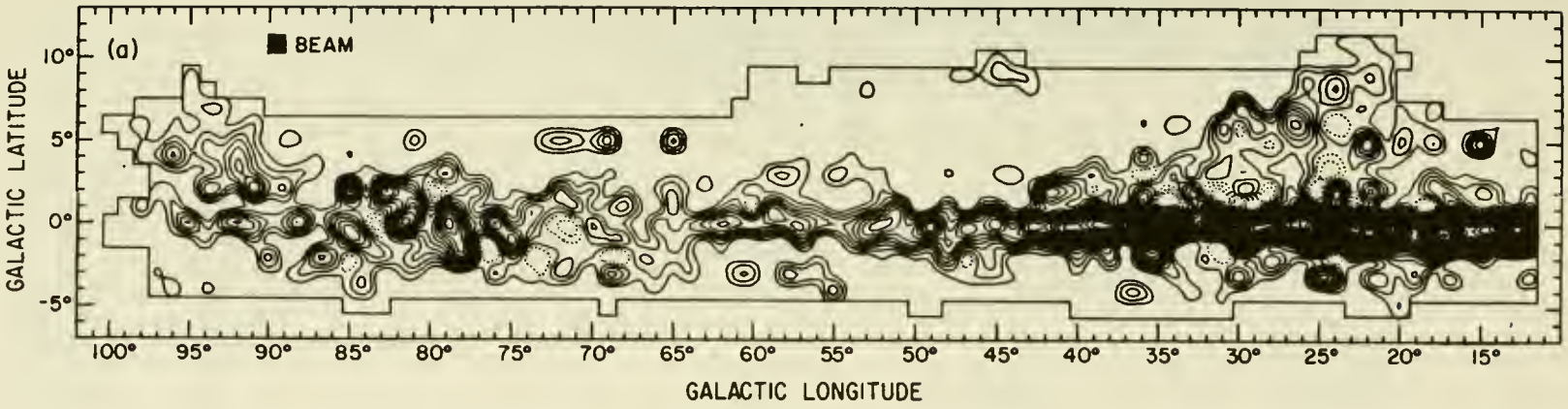

Figure 1. Contour map of the survey integrated over the full velocity range observed. For $|b| \geq 3°$ the velocity range is -83 to 83 km s^{-1}, while for $|b| < 3°$ the range is -13 to 153 km s^{-1} at $\ell \leq 60°$, and -113 to 53 km s^{-1} at $\ell > 60°$. The contour interval is 4 K km s^{-1}.

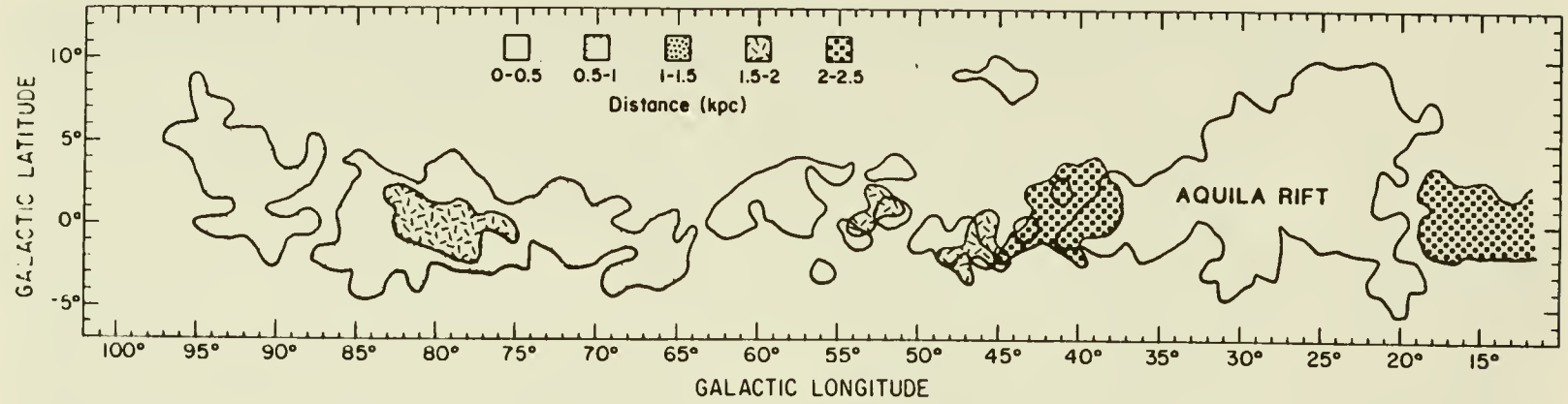

Figure 3. Schematic map of the individual molecular clouds which comprise the Great Rift. The clouds are outlined by their 4 K km s^{-1} CO emission contours. Distances are indicated by the shading.

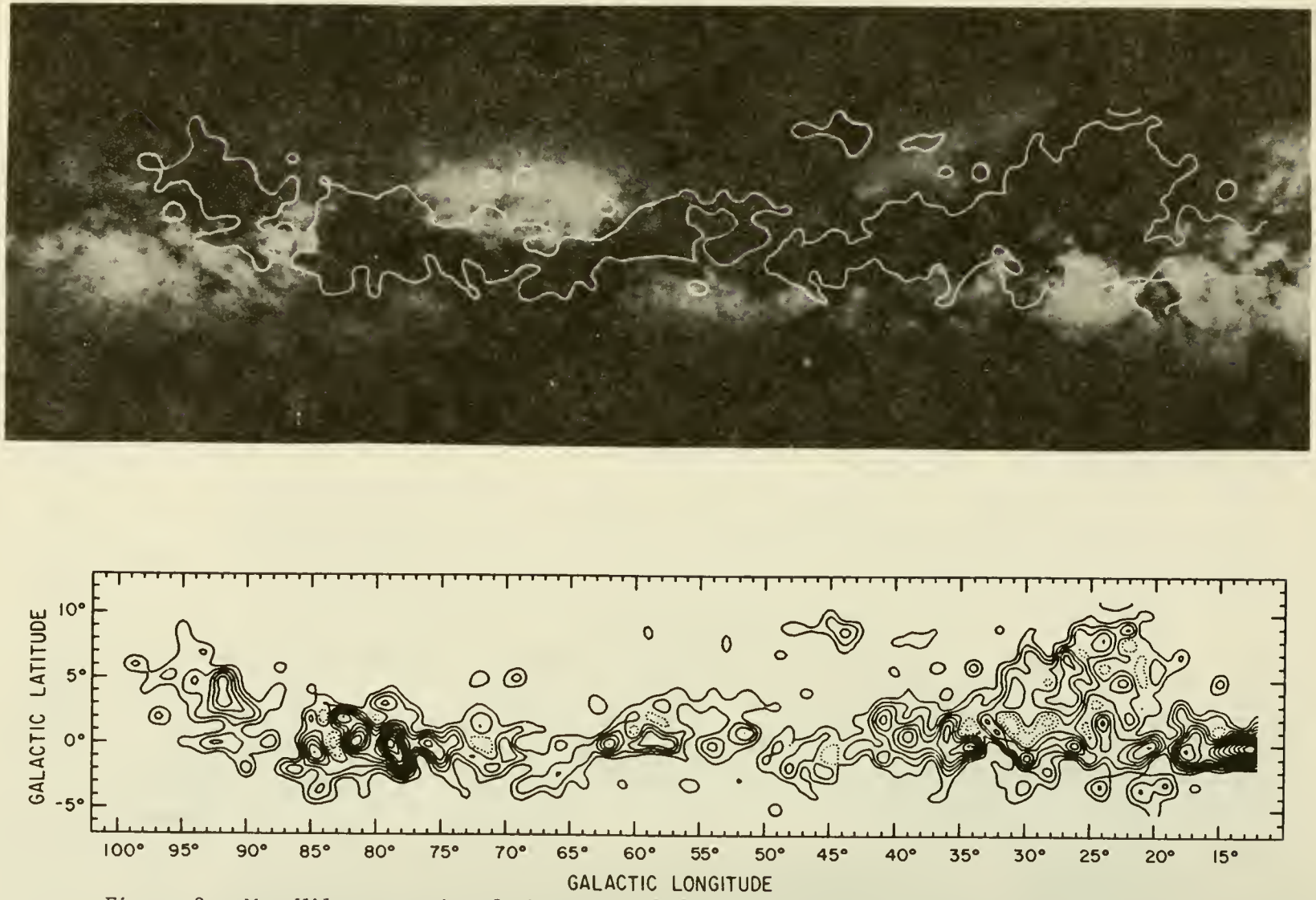

Figure 2. Mt. Wilson mosaic of the Milky Way, with a contour map on the same scale of the CO emission integrated between -10 and 34 km s^{-1}. The contour interval is 4 K km s^{-1}; the lowest contour is overlaid on the photo.

DARK CLOUD AND GLOBULE DISTRIBUTION FOR GALACTIC LONGITUDES 23o TO 36o DEGREES

J.V. Feitzinger and J.A. Stuewe
Astronomical Institut, Ruhr-University, Bochum, FRG

ABSTRACT

A catalogue of dark nebulae and globules has been compiled from a study of the ESO-B and SRC-J sky atlas for galactic longitudes $23^o < l < 36^o$. This catalogue closes the great southern gap open since the work of Lynds (1962). We have listed 489 dark nebulae and 311 globules. The catalogue contains positions, sizes, opacities and the van den Bergh classification (1972) on the filamentary morphology of dark clouds. We present statistics concerning the northern and southern distributions and sizes of the nebulae.

THE CATALOGUE

The 606 fields of the southern atlas were examined for the presence of dark clouds; for $|b| > 3^o$ no dark clouds are found, although our search extended up to $|b| = 9^o$. The overlapping regions between the POSS-Lynds survey and our work were used to calibrate our opacity classes. This linkage secures the equality of the opacity classes in both surveys, inspite the differing limiting magnitudes. The distribution of the dark clouds (> 0.01 sqdeg) in galactic coordinates is shown in Fig.1. The map of this survey exists in a machine readable, digitized form as a 500 x 1400 pixel image (1 pixel = $0^o.1$). In Fig.2 we present the distribution of the globules defined as ≤ 0.01 sqdeg. The numbers count globules almost at the same position. Besides their different opacities interstellar clouds show a bewildering variety of shapes and sizes. To take this fact into account we supplemented the catalogue by descriptive categories (for example: worm track, cometary globule) and the classification scheme of van den Bergh (1972)(for example: amorphous cloud, very fuzzy).

STATISTICS AND COMPARISONS

The percentage of the sky obscured by dark clouds is 4.98% for the northern ($0^o < l < 24^o$) and 1.92% for the southern part ($24^o \leq l < 36^o$). The absolute numbers are: N=1273 clouds, area= 1396 sqdeg, north and N=437 clouds, area=264 sqdeg, south. This reflects the well known fact that the visible Milky Way band

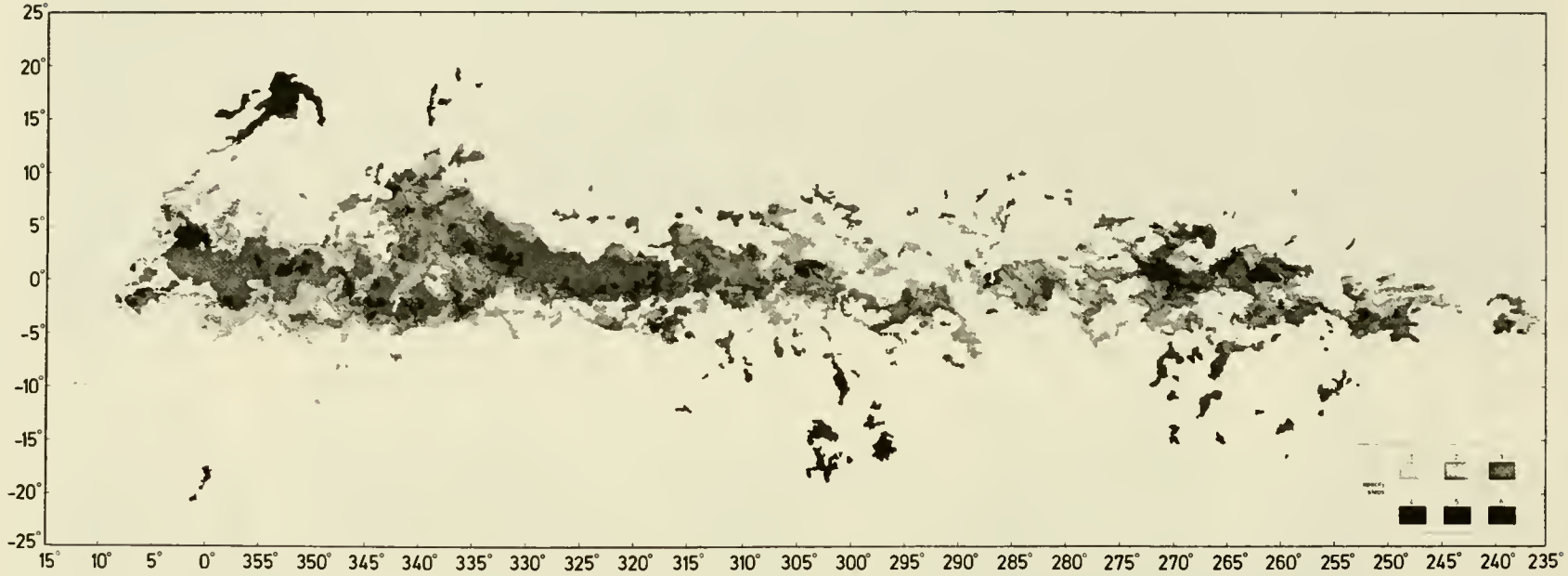

Fig.1 Distribution of dark clouds (> o.o1 sqdeg)

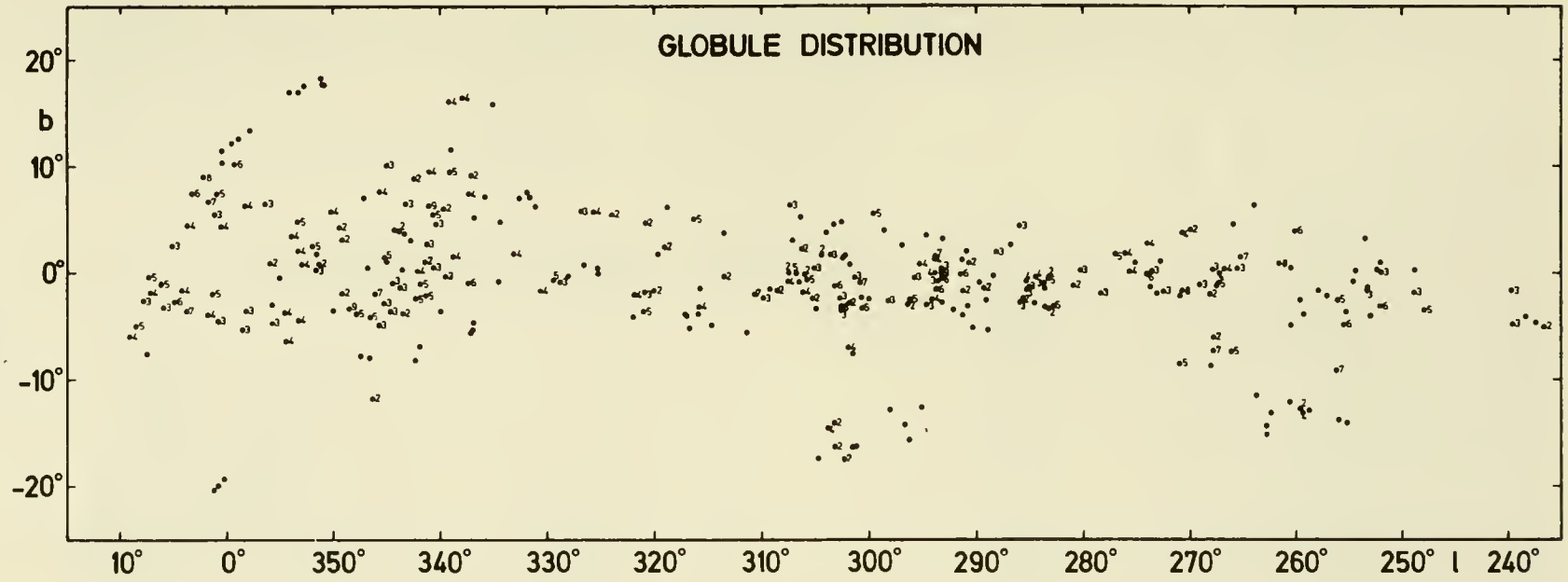

Fig.2 Distribution of globules (o.o1 sqdeg). The numbers count globules almost at the same position.

changes its morphological appearance from north to south. In Fig.3 we discriminate between the northern, southern and the anticenter regions. The percentage of area covered by the different opacity classes for the northern and southern regions are nearly the same. The percentage of obscured area as a function of |b| in Fig.4 reveals that the southern distribution is much more smoother as the northern distribution. This is a consequence of the absence of the Great Northern Rift in the southern Milky Way and results in fewer clouds of high opacity, which are responsible for the ruggedness. Furthermore the southern part is much brighter also a reason for greater homogenity of the Milky Way band.

An extended version of this paper will be published elsewhere.

REFERENCES

Lynds B.T., 1962, Ap.J. Supp. 7, 1
van den Bergh S., 1972, Vistas 13, 265

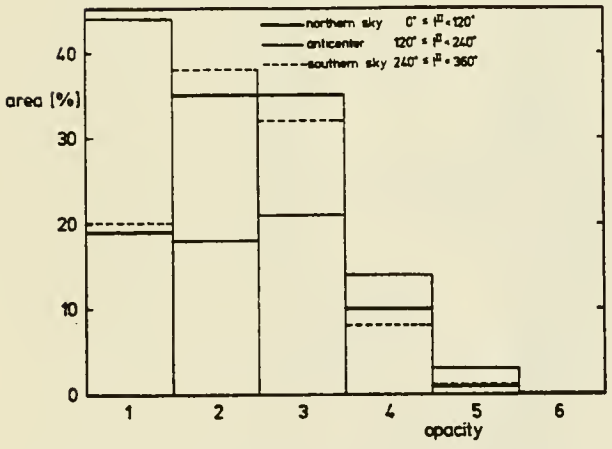

Fig.3 Percentage of obscured area as function of the opacity classes

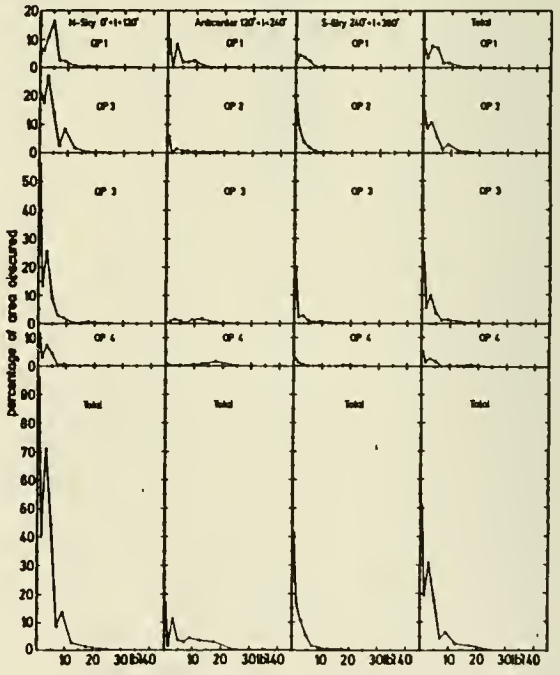

Fig.4 Percentage of obscured area as function of the galactic latitude |b| and the opacity classes

A Neutral Gas Jet in a Low Velocity Shock Front at the Boundary of the Draco Nebula

P.W.M. Kalberla, U. Herbstmeier and U. Mebold
Radioastronomisches Institut der Universität Bonn,
Auf dem Hügel 71, 5300 Bonn 1, Fed. Rep. Germany

Abstract

21-cm line observations with the Westerbork Synthesis Radio Telescope of a dust and molecular filament at the boundary of the Draco Nebula ($\ell \approx 91^{\circ}$, $b \approx 38^{\circ}$) reveal a jet-like neutral hydrogen feature funneling through an outlet in the low velocity shock front at the interface between the Draco Nebula and the surrounding gas. The jet-like feature is apparently connected with a high velocity filament at VLSR = -180 km s^{-1}. We suggest that the soft x-ray emission observed in the area is thermal bremsstrahlung produced by the deceleration of high velocity gas in galactic gas.

Introduction

Dracula, a faint bright nebula (Lynds, 1965) located at $\ell \approx 93^{\circ}$, $b \approx 38^{\circ}$ in the constellation Draco exhibits HI λ21-cm and CO λ2.6 - and λ2.7-mm line emission with a radial velocity of VLSR $\approx$ -22 km s^{-1} in detailed positional agreement (Goerigk et al., 1983) with the faint patches visible at the Palomar Observatory Sky Survey (POSS) red and blue prints (cf. paper I, "The Draco Nebula, a Molecular Cloud Associated with a High Velocity Cloud" by Mebold et.al., in the present volume). One of the most striking aspects of Dracula is the filamentary structure of its boundary facing the direction of decreasing galactic longitude, ℓ, and decreasing galactic latitude, b, i.e. more precisely galactic position angle GPA $\approx 240^{\circ}$. HI- line observations with 9 arc min angular resolution show the presence of a positive velocity gradient towards that position angle of about 5 km s^{-1} per 9 arc min for a strech of $\sim 1^{\circ}.5$ along this boundary (cf. Goerigk et al., 1983). This indicates that Dracula which is approaching us at a velocity of VLSR $\approx$ -22 km s^{-1} is beeing decelerated at this interface.

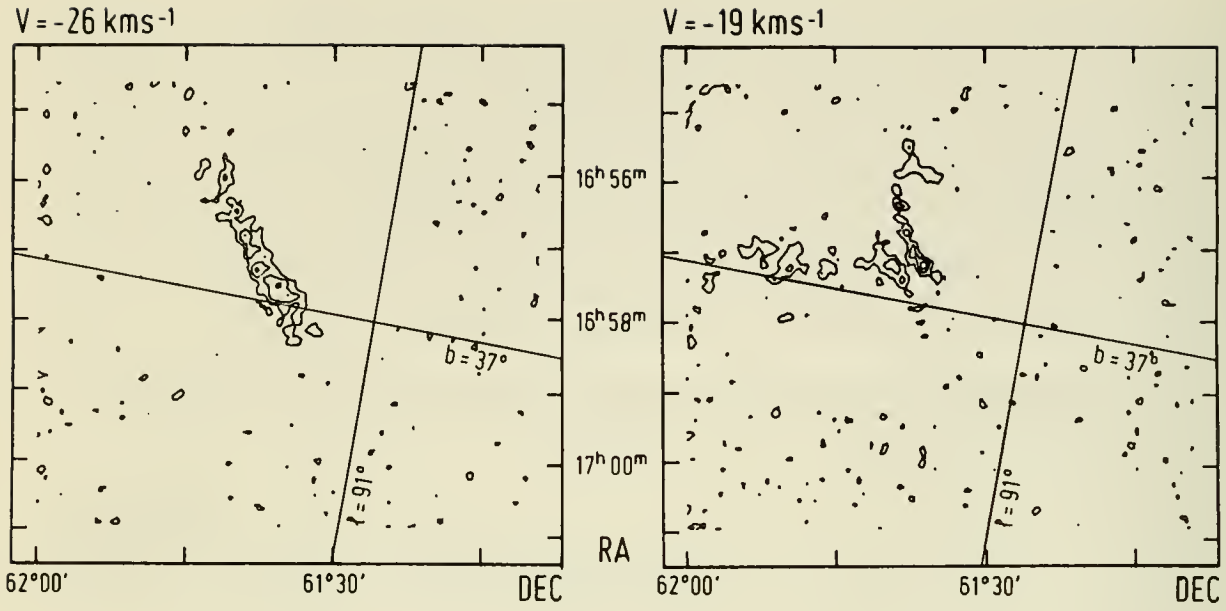

Fig. 1 WSRT channel maps of 21-cm line emission associated with a dust and molecular filament. The contours are at 4,8 and 12 K. Note that the jet-like feature at V= -26 km s^{-1} is centered at the gap which is visible in the map at V= -19 km s^{-1}. The maps which are observed in equatorial coordinates have been rotated by 90^{o} to allow an approximate orientation in galactic coordinates(see Fig. 3).

Results and Discussion

The most prominent filament at this boundary which can be identified at the POSS and in the HI- and the CO lines and which is called Drac 1 in paper I has been observed with the Westerbork Synthesis Radio Telescope (WSRT) in the 21-cm line. The angular resolution is 48 arc sec in right ascension and 55 arc sec in declination. The velocity resolution is 0.5 km s^{-1}. Only a small fraction of the results of three observations can be presented here. In Fig. 1 we present isophotes of 21-cm line brightness temperatures in velocity intervals of 0.5 km s^{-1} width centered at VLSR= -26.2 km s^{-1} (left hand side) and VLSR= -18.9 km s^{-1} (right hand side). This so-called channel maps were chosen to be typical for a velocity intervall of

-28 to -25.5 km s^{-1} and -19.5 to -17 km s^{-1}, respectively. At the more negative velocities we see a jet-like feature of about 20 arc min length and a width of 2 to 3 arc min at the position where an outlet - like feature at the more positive velocities has its narrow-most opening. We get the impression that the negative velocity gas (VLSR $\approx$ -26.5 km s^{-1}) is funnelled through an outlet in the boundary of Dracula which is formed by gas at a velocity of VLSR $\approx$ -18 km s^{-1}. Adopting the view point that Dracula is moving towards us with VLSR $\approx$ -22 km s^{-1}, it appears that the jet-like feature is accelerated towards us by about 4 km s^{-1} and the outlet is decellerated towards us by about 4 km s^{-1} in the boundary region of Dracula.

The channel maps at the other velocities ($-10 \leq VLSR \leq -35$ km s^{-1}) confirm the notion of a deceleration of the boundary region of Dracula with respect to its interior. The velocity gradient is about +5 km s^{-1} per 5 arc min GPA $\approx 225^{o}$. This is however not so for the notion that the jet-like feature is accelerated towards us. We propose that the jet is decelerated material coming from a high negative velocity cloud filament at VLSR $\approx$ -180 km s^{-1} located about 15 arc min outside the frames in Fig. 1 along the axis of the jet-like feature.

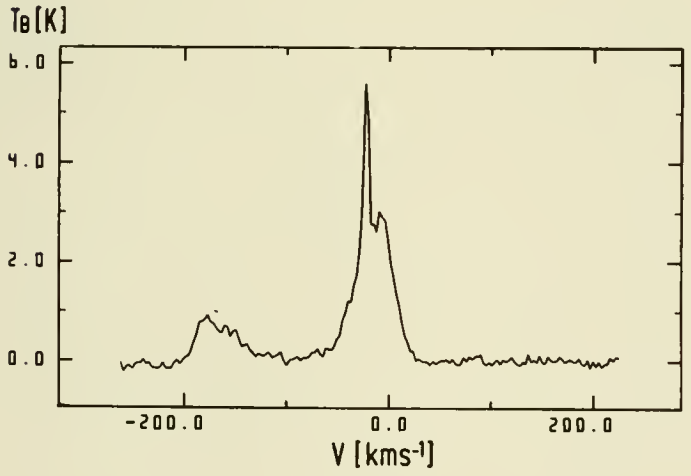

Fig. 2 21-cm emission line from a high velocity filament at V= -180 km s^{-1} located close to the jet-like feature in Fig. 1.
See Fig. 3 for the orientation of the high velocity filament relative to the WSRT field and the jet-like feature.

Fig. 2 shows the 21-cm line spectrum averaged over the spectra observed with the Effelsberg 100-m Telescope at the position indicated by five small crosses (x) next to the frames of Fig. 1 scetched into Fig. 3. In Fig. 2 the high velocity gas is seen with a peak intensity at VLSR $\approx$ -180 km s^{-1} and a tail towards more positive velocieties. This tail indicates that the high negative

velocity gas is beeing decelerated. The peak at VLSR= -22 km s^{-1} corresponds to the emission of Dracula.

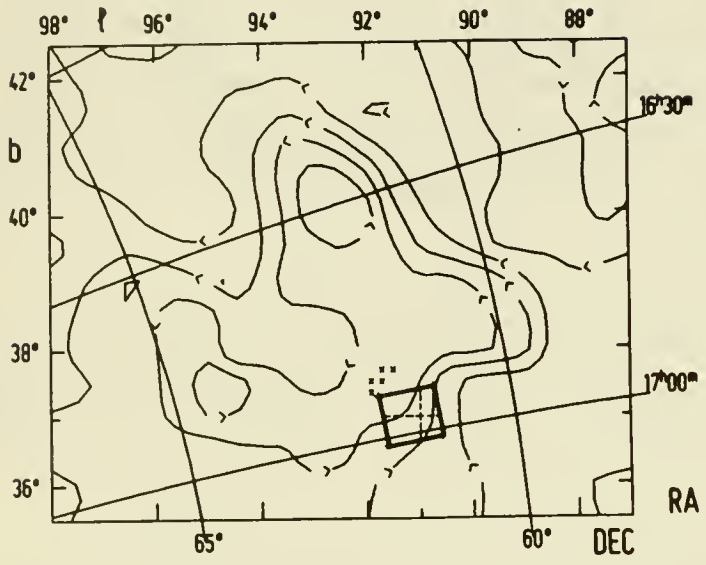

Fig. 3 Large scale distribution of 21-cm line emission at V= -21 km s^{-1} associated with the Draco Nebula. The contours are at 0,2,4,6 and 8 K. Both, galactic and equatorial coordinates are given. The WSRT field-located at the low latitude border of this nebula- is sketched in. The crosses give the positions where the peak emission of the V= -180 km s^{-1} HVC (Fig.2) was observed with the Effelsberg 100-m telescope.

In Fig. 3 the total extent of the VLSR= -22 km s^{-1} emission feature of Dracula is shown in an isophotal representation of 21-cm line brightness temperatures averaged from VLSR= -22 to -20 km s^{-1}. The data are from the Heiles and Habing (1974) survey. We see that Dracula is horse-shoe-shaped with an axis of symmetry roughly in-line with the axis of the jet-like feature in Fig. 1. It is probably more than accidental that this axis is paralled to the direction of the stream of negative high velocity gas extending from $\ell = 120^{o}$, $b = 55^{o}$ to $\ell = 30^{o}$, $b = 20^{o}$ (Giovanelli, 1980). Finally we point out that the Darcula complex itself as well as the stream of high velocity gas just mentioned are in a fair positional coincidence with soft x-ray features in the B-, C- and M-Band sky maps of McCammon et al. (1982).

It is therefore very suggestive that the jet-like feature in Fig. 1 and possibly even the whole Dracula complex are related to the high velocity cloud phenomenon and that the soft x-ray emission is thermal bremsstrahlung produced by the interaction of the high velocity gas with the galactic gas. An important link that is missing here could be the discovery of soft x-ray emission between the high velocity filament at VLSR= -180 km s^{-1} and the jet-like

feature at VLSR= -26 km s^{-1}.

Acknowledgements

The Westerbork Synthesis Radio Telescope is operated by the Netherlands Foundation for Radio Astronomy with the financial support of the Netherlands Organisation for Advancement or Pure Research (Z.W.O.). The project was supported by the Deutsche Forschungsgemeinschaft (DFG, SFB 131, Radioastronomie).

References

Giovanelli, R.: 1980, Astron. J. 85, 1155

Goerigk, W., Mebold U., Reif, K., Kalberla, P.W.M., Velden, L.: 1983, Astron. Astrophys. 120, 63

Heiles, G., Habing, H.J.: 1974, Astron. Astrophys. Suppl. 14, 1

Lynds, B.T.: 1965, Astrophys. J. Suppl. 12, 163

McCammon, D., Burrows, D.N., Sanders, W.T., Kraushaar, W.L.: 1982, Astrophys. J. 269, 107

The Draco Nebula, a Molecular Cloud Associated with a High Velocity Cloud?

U. Mebold and P.W.M. Kalberla

Radioastronomisches Institut der Universität Bonn,
Auf dem Hügel 71, 5300 Bonn 1, Fed. Rep. Germany

Extended and very faint bright nebulae are found in high ($b \gtrsim 30^{\circ}$) galactic latitudes at the Palomar Observatory Sky Survey (POSS) (Lynds, 1965) and even more pronounced at a very sensitive photographic survey of the galactic polar caps by Sandage (1976). Such a nebula, located in the constellation Draco and called "Draco Nebula" or "Dracula", was found to be in detailed positional coincidence with a 21-cm emission line feature at a LSR velocity of VLSR $\approx$ -22 km s^{-1} by Goerigk et al. (1983). Estimates of the minimum visual extinction, AV $\gtrsim$ 1 mag, from star counts ON and OFF Dracula (Goerigk et al., 1983) and an estimated visual surface brightness of

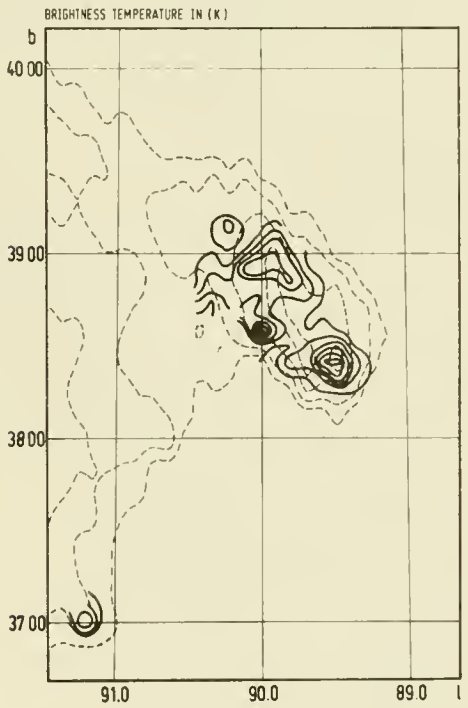

Fig. 1
Isophotes of integrated ^{12}CO brightness temperatures (full lines) superimposed on the distribution of the maximum 21-cm line brightness temperature (broken lines) for the Draco cloud. ^{12}CO-contours are at intervals of 1.5 K·km s^{-1} starting at 1.5 K km s^{-1}, HI contours at 1.5, 5, 10, 15 and 20 K.

SBV $\simeq$ 24 mag (arc sec)$^{-2}$ (Lynds 1965) indicate that Dracula fits the relation

$$SBV = 24.2 - 2.5 \log AV$$

for dust clouds located above the galactic plane and reflecting the integrated starlight of the galactic disk (Sandage 1976). Hence Dracula is probably a reflection nebula. The quoted observations gave a ratio NHI/E(B-V) of atomic neutral hydrogen column density and colour excess that is about a factor of 10 smaller than the standard ratio NH/E(B-V) of hydrogen nuclei and colour excess.

This lead us to search for indicators of molecular hydrogen, H2, like the CO molecule. We used the 2.5-m mm-Telescope of the University of Bordeaux (Baudry et al., 1980) for observations of the λ 2.6-mm and λ 2.7-mm transitions of the ^{12}CO and the ^{13}CO molecule. The ^{12}CO results are presented in Fig. 1 as isophotes of integrated brightness temperature (full lines) superimposed on the distribution of the maximum 21-cm line brightness temperature (broken lines). We see at Fig. 1 and by inspection of the POSS that ^{12}CO is brightest where HI and - even more pronounced - where the dust is brightest. ^{13}CO-lines were measured only at the positions of the peaks of the two CO-clumps with lowest latitudes, called Drac 1 and Drac 2.

The results of the CO observations at these positions are summarized in Table 1. From the top to the bottom we give for these clumps the galactic longitude, ℓ, and latitude, b, of the centre of the clumps, the amplitudes, T_L, the half power line widths, ΔV, and the LSR centre velocities of the ^{12}CO and ^{13}CO lines, VLSR, the LTE excitation temperature of the CO molecules, T_{EX}, the optical depth, τ^{13}, and the column density, N^{13}CO, (cf. Dickman 1978) of the ^{13}CO molecules.

We have estimated molecular hydrogen column densities, NH2, first from a direct observational correlation of CO column densities, NCO, with NH2 (Federman et al., 1980) adopting a CO- isotopic ratio of $N^{12}CO/N^{13}CO = 50$, and second from observational correlations of N^{13}CO and AV and the "standard" ratio NH2/AV = $0.94 \cdot 10^{21}$ molecules cm^{-2} mag^{-1} (Frerking et al., 1982).

These two estimates of NH2 called NH2(UV) and NH2(AV), the total column density of hydrogen nuclei,

$$NT = NHI + 2\ NH2,$$

derived from the average of NH2(UV) and NH2(AV) and the 21 cm lines, and the extinction, AV, derived from the "standard" ratio of NH2/AV are also listed in Table 1.

In order to be able to study the dynamics of our CO-clumps we have attempted to determine the distance of Dracula in two ways: First we have conducted a UBV photo electric photometry with the 1 m telescope of the Calar Alto Observatory in Spain of about 60 stars in the brightest part of Dracula. With some uncertainty due to the unknown metallicity of possible halo stars we found only unreddened stars up to a distance of about 800 pc. Also from the extinction given in Table 1, from a relative star count defizit of 11 percent ON and OFF Dracula and from models of the stellar distribution perpendicular to the galactic plane (Scheffler, 1982) we derive a distance of about 800 pc. Adopting a distance of 800 pc and the apparent sizes of our CO-clumps we estimate the densities, n, and total masses, M, given in Table 1. The virial theorem was applied to test whether or not the CO- clumps are gravitationally bound systems. From the velocity dispersions $\sigma = \Delta V/2.355$ of the ^{13}CO lines, the total masses M and the linear diameters, d, we have (κ = gravitational constant)

$$\sigma^2 < 2\kappa\ M/d,$$

i.e. both clumps appear to be gravitationally bound systems.

Finally we like to point out that Dracula has a close positional and possibly even astrophysical relationship to the high velocity cloud (HVC) phenomenon. Dracula is located at the low latitude end of Hulsbosch's (1979) HVC complex CI; indeed high negative velocity HI-gas is observed over most of the region covered by Dracula. Further, Dracula is positionally coincident with a C-band x-ray emission feature in the SAS- satellite sky maps (Clark, private communication, see also the C-, M- and J-band maps of McCammon

et al., 1982). It is therefore suggestive that the x-ray emission is thermal bremsstrahlung produced by electrons and ions in HVC CI and the galactic gas and that Dracula is a part of a decelerated high velocity cloud.

Summary

An extended and faint bright nebula at $\ell \approx 91^{\circ}$, $b \approx 38^{\circ}$ exhibits HI λ21-cm, ^{12}CO λ2.6-mm and ^{13}CO λ2.7-mm emission lines in detailed positional agreement with the brightness distribution at the Palomar Observatory Sky Survey. Three colour UBV photometry of $\sim$ 60 stars in the field of the bright nebula indicates a distance of $\sim$ 800 pc. With this distance the total mass of two molecular clumps in the nebula is 27 and 219 $M_{\odot}$ and they appear to be gravitationally bound systems. A possible astrophysical relation to the high velocity HI- cloud phenomenon is pointed out.

References

Baudry, A., Brillet, J., Desbats, J.M., Lacroix, J., Montignac, G., Encrenaz, P., Lucas, R., Beaudin, G., Dierich, P., Germont, A., Landry, P., Rerat, G.: 1980, J. Astron. Astrophys. 1, 193

Dickman, R.L.: 1978, Astrophys. J. Suppl. 37, 407

Federman, S.R., Glassgold, A.E., Jenkins, E.B., Shaya, E.J.: 1980, Astrophys. J. 242, 545

Frerking, M.A., Langer, W.D., Wilson, R.W.: 1982, Astrophys. J. 262, 590

Goerigk, W., Mebold, U., Reif, K., Kalberla, P.M.W., Velden, L.: 1983, Astron. Astrophys. 120, 63

Hulsbosch, A.: 1979, in IAU Symp. 84, 525

Lynds, B.T.: 1965, Astrophys. J. Suppl. 12, 163

McCammon, D., Burrows, D.N., Sanders, W.T., Kraushaar, W.L.: 1982, Astrophys. J. 269 No 1, 107

Sandage, A.: 1976, Astron. J. 81, 954

Scheffler, H.: 1982, in Landolt-Börnstein, Vol. 2, Astron. Astrophys., Subvol. c, p. 175

Table 1

	Drac 1		Drac 2	
gal. long	91^{o} 11'		89^{o} 32'	
gal. lat.	36^{o} 59'		38^{o} 24'	
	^{12}CO	^{13}CO	^{12}CO	^{13}CO
T_L/K	4.2	0.5	5.5	0.7
ΔV/km s^{-1}	1.3	0.8	2.0	1.4
V_{LSR}/km s^{-1}	-25.2	-25.1	-23.7	-23.3
T_{EX}/K	7.4		8.8	
τ^{13}	0.12		0.13	
$N^{13}CO/cm^{-2}$	$3.4\ 10^{14}$		$8.6\ 10^{14}$	
$NH2(UV)/cm^{-2}$	$1.6\ 10^{21}$		$2.6\ 10^{21}$	
$NH2(AV)/cm^{-2}$	$1.2\ 10^{21}$		$1.6\ 10^{21}$	
NT/cm^{-2}	$2.9\ 10^{21}$		$4.3\ 10^{21}$	
AV/mg	1.6		2.3	
n/cm^{-3}	620		400	
$M/M_{\odot}$	27		219	
$\sigma^2(2\kappa M/d)^{-1}$	0.74		0.69	

"IRAS OBSERVATIONS OF SMALL SCALE DUST STRUCTURE IN THE GALAXY"

N. Gautier, M. Hauser, and I. Low

(No Abstract or Text Available)

THE LISM AT RADIO WAVELENGTHS

"Structures in the H I in the Local Solar Neighborhood"

H. Weaver

(No Abstract or Manuscript Received)

THE SMALLEST SIZES OF DIFFUSE INTERSTELLAR CLOUDS

John M. Dickey, J. Crovisier and I. Kazes
University of Minnesota, Obs. Paris

ABSTRACT

By observing the difference in optical depths between absorption spectra toward the two components of double sources we have measured the variations in opacity over lengths of less than 0.1 up to 10 pc inside diffuse interstellar clouds. Significant variations are detected on scales larger than about 0.2 pc, but not less. This may represent the minimum size for diffuse cloud structure. By comparing the variations of Gaussian fitted line parameters we find that variations in the internal velocity field of diffuse clouds explain the data rather better than tiny independent "cloudlets."

INTRODUCTION

Interstellar diffuse clouds are difficult to map. In 21 cm emission it is possible to trace the broad outlines of clouds and cloud complexes (e.g., Verschuur 1974); and with large telescopes it is possible to measure the fluctuations of emission on smaller scales (10' to 1°, e.g., Jahoda et al. 1984), but these fluctuations cannot be interpreted directly as cloud structure because of spatial confusion, self-absorption, and line of sight blending of various regions overlapping in velocity. The ambiguity of higher resolution interferometer emission studies is even greater (e.g., Crovisier and Dickey 1983). Absorption studies at 21 cm have the drawback that they can only be done in the directions of strong background continuum sources, which are sparse, but they have the great advantage that only the cool gas appears in the spectrum. Since linewidths are narrow for the cool gas there is less velocity blending, and kinematic distance estimates are more accurate than for emission features. Warm gas, which may be associated with the cool cloud (Liszt 1983) does not appear in absorption.

There are two ways to use 21 cm absorption to study the smaller scale structure of diffuse clouds and cloud complexes. The first is to map the absorption across the face of an extended continuum source. This was first done toward Cas A, Cyg A, and Vir A (Greisen 1973a,b), and it has been improved by many other groups (e.g., Schwarz et al. 1980, Bregman et al. 1983, Lockhart and Goss 1978, Landeker et al. 1981, Liszt et al. 1982). In many cases small scale structure is found, but interpretation is difficult because the noise level in absorption usually varies drastically from point to point, and even with the highest resolution interferometers there are seldom more than five to ten independent pixels in either dimension across the source. Gradients in optical depth have been unambiguously identified, and in some cases higher order fluctuations are apparent, but a full statistical characterization of the small scale structure, e.g., the cloud size spectrum or the turbulence spectrum, is not tractable from these isolated regions. The other strategy is to use double sources for the background continuum; if the two components are unresolved such a double gives simply two spectra separated by angle θ. Surveys of absorption toward many such sources are possible with modest telescope and reduction time; the results provide a measure of the average change of optical depth over small angles in diffuse H I clouds.

A preliminary survey was performed with the NRAO Green Bank interferometer (Dickey 1979); in the present work we have extended this using the WSRT to higher sensitivities and more sources at lower galactic latitudes. Many cases of significant optical depth changes over angles of about 1' or less have been detected, these correspond to appreciable variations in the column density of cold gas over distances of 0.1 to 10 pc. Several clouds are sampled at points separated by less than this distance, but none of them show significant optical depth variations. As discussed below, this is strong evidence that the smallest structures ("cloudlets") in diffuse clouds are at least this large.

OBSERVATIONS

For background sources for this experiment we have selected extragalactic doubles whose continuum structure was well known, which were at low galactic latitude, with component separations of about 2' to about 30". At low latitudes we can use a rotation curve to get kinematic distance estimates for the various spectral features ("clouds") detected. These distances are particularly important for this experiment because they tell us the linear separation between the two lines of sight toward the two components as measured in the absorbing interstellar cloud. If we call the kinematic distance D, then this separation is $D\Theta$, where Θ is the angular separation of the two components. For our sample, $D\Theta$ varies from a bit less than 0.1 pc to about 10 pc, with most values between 0.2 and 3 pc.

The observations were taken at the WSRT in 1981. The velocity channel separation was 1.25 km s^{-1}, which we Hanning smoothed to 2.5 km s^{-1} to minimize overlap between adjacent channels. About three hours of integration were spent on each source, the shortest baselines were rejected to eliminate 21 cm emission which could pollute the absorption spectra. For each velocity channel showing absorption toward both components we computed the difference between the two, and construct a difference spectrum $\Delta t(v)$ for each background source. In this experiment every source shows significant differences in one or more absorption lines. We have also fitted Gaussians to the absorption features toward each component. Data and results in more detail are given by Crovisier et al. (1984).

DISCUSSION

The structure of an interstellar diffuse cloud may be as complex as a Rorshach figure, and studying maps, no matter how detailed, may be of little value beyond the psychological. The important astrophysical questions relate to the range of sizes of clouds present, the ordered motions and turbulence, and the density, temperature, ionization, and thermodynamic balance. Our results can be used to derive statistics for the small scale structure of clouds in two different ways. These two approaches differ in their assumptions about the way the observed absorption spectra sample the clouds. The first assumes each velocity channel (after Hanning smoothing and resampling) to be a different statistical sample corresponding to a different location inside the cloud. Comparing the corresponding channels of the two spectra gives a sample of the variation of the medium over the distance $D\Theta$. This approach gives the distribution shown in the figure, which plots $D\Theta$, the linear separation of the two points, vs. the magnitude of the difference in optical depths at the two points. There is a dramatic change in the distribution of the points on the figure between $D\Theta$ less than about 0.2 pc and $D\Theta$

greater than 0.2 pc. This change is pronounced even if one deletes several of the highest points, or if one deletes certain background source directions. The implication of the figure is that there is very little variation in optical depth over distances DΘ of less than about 0.2 pc, but that for larger distances the rms change in optical depth quickly increases. We may interpret this as evidence that structures with sizes greater than 0.2 pc are common in interstellar diffuse clouds, but that smaller "cloudlets" are rare.

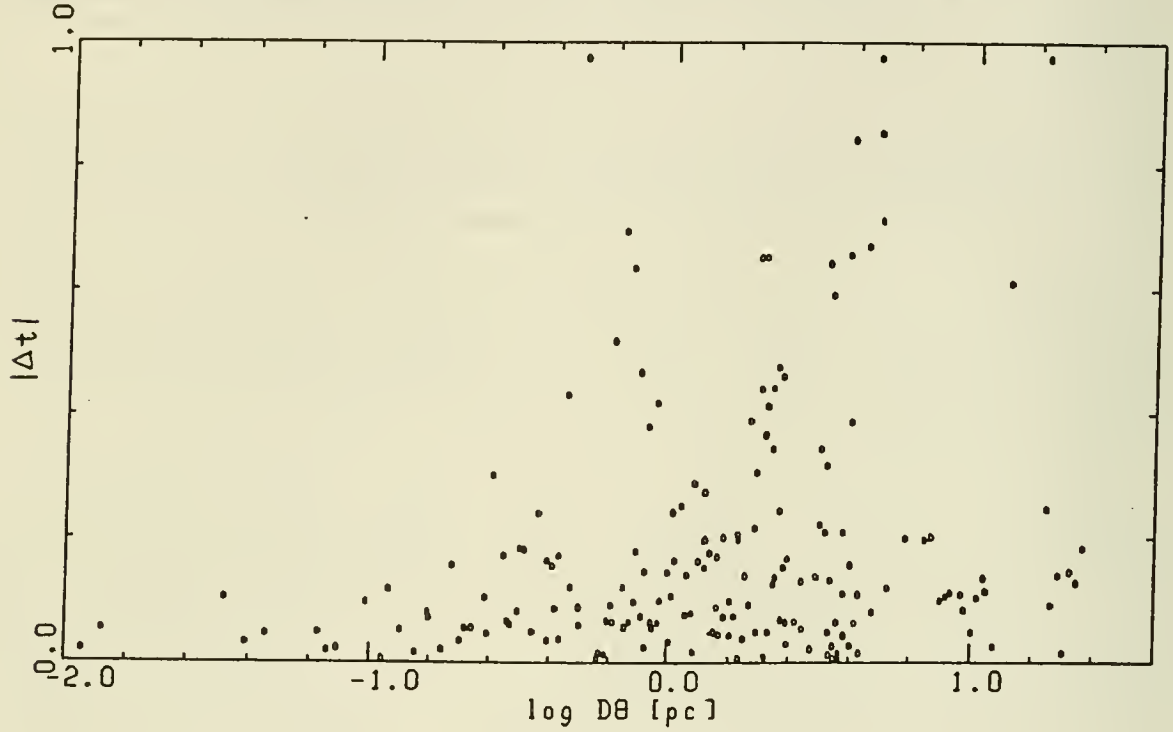

Fig. 1. The distribution of variations in absorption (absolute scale) vs. the linear separation of the two samples (DΘ). Each point represents one velocity channel for which two optical depths were detected. The abcissa is the difference in relative absorption.

The figure is somewhat deceiving because the points are not necessarily independent. This is not simply because of the velocity resolution, whose effects have been minimized by the Hanning smoothing and resampling, but because of the velocity correlation inherent in the interstellar clouds. It is not correct to assume that each velocity channel is a separate measurement of the fluctuation of optical depth, since the lines are generally Gaussians with widths of several channels. An alternative approach is to look at the variation in the Gaussian fit parameters (line depth, center velocity, and velocity width) between the two lines of sight. Each difference gives a measure of the variation of that quantity over the distance DΘ. We can then study separately the increase in variation of line depth with DΘ, line center velocity with DΘ, etc. The increase in variation with DΘ is still apparent, but the sudden jump at 0.2 pc is no longer so abrupt. In general the increase of variation with DΘ is more pronounced for the line center and line width than for the line depth, at least for DΘ less than about 1 pc. This result is highly suggestive that the variations we detect are not due to individual,

distinct structures with overall sizes of less than one parsec ("cloudlets"), but rather to velocity variations inside larger structures. Whether these variations are due to ordered motion such as rotation, expansion, or collapse (e.g., Goldsmith 1984), or due to random turbulent motion might be tractable if we could measure whether the variation of line center is greater than the variation of line width. This is not yet clear from the data.

If the variations in Gaussian parameters are due to turbulence inside the clouds a parameter of great interest is the turbulence spectrum (Armstrong et al. 1981, Larson 1980, Myers 1983, Dickey 1984). Looking only at the variation in line center velocities between the two lines of sight we find an rms velocity difference of about 1.5 km s^{-1} at DΘ of 1 to 10 pc, vs. 0.5 km s^{-1} at DΘ of 0.1 to 1 pc. These numbers agree roughly with Myers and Benson's (1984) results for turbulent velocities on the same scales inside molecular clouds, although their measurement used line width observations rather than direct differential absorption observations such as these.

On the other hand if the optical depth variations observed are due to tiny independent cloudlets it is hard to understand why the velocity centers and widths vary more strongly on small scales than the line peaks. It is also difficult to understand how such small clouds could be thermodynamically stable in the interstellar environment. As Cowie and McKee (1977) show, a cloud embedded in the hot phase must be at least a few parsecs in radius to resist evaporation. Smaller clouds might be stable if they were embedded in a classical "inter-cloud medium" of warm H I (Field et al. 1969), but the passage of the shock from a young supernova remnant would soon destroy them in a McKee-Ostriker (1977) interstellar medium. One possibility is that they are debris from recent cloud collisions (Cowie 1980), and therefore have relatively short ages. But altogether the data at this point seem to suggest a velocity field origin for the small scale structure rather than a cloudlet explanation.

REFERENCES

Armstrong, J.W., Condes, J.M., and Rickett, B.J., 1981, Nature 291, 561.
Bregman, J.D., Troland, T.H., Forster, J.R., Schwarz, U.J., Goss, W.M., and Heiles, C., 1983, Astron. Astrophys. 118, 157.
Cowie, L.L. and McKee, C.F., 1977, Ap.J. 211, 135.
Cowie, L.L., 1980, Ap.J. 236, 868.
Crovisier, J. and Dickey, J.M., 1983, Astron. Astrophys. 122, 282.
Crovisier, J., Dickey, J.M. and Kazès, I., 1984, Astron. Astrophys., in preparation.
Dickey, J.M., 1979, Astrophys. J. 233, 558.
Dickey, J.M., 1984, in IAU Symposium No. 106, The Milky Way, ed. H. van Woerden (Dordrecht: Reidel).
Field, G.B., Goldsmith, D.W., and Habing, H.J., 1969, Ap.J. Lett. 155, L149.
Goldsmith, P.F., 1984, Icarus, in press.
Greisen, E.W., 1973, Astrophys. J. 184, 363 and 379.
Jahoda, K., Dickey, J.M., Lockman, F.J., and McCammon, D., 1984, Astrophys. J. submitted.
Landecker, T.L., Roger, R.S., and Higgs, L.A., Astron. Astrophys. Suppl. 39, 133 (1980).
Larson, R.B., 1981, M.N.R.A.S. 194, 809.
Liszt, H.S., Dickey, J.M., and Greisen, E.W., 1982, Ap.J. 261, 102.

Liszt, H.S., 1983, Ap.J. 275, 163.
Lockhart, I.A. and Goss, W.M., 1978, Astron. Astrophys. 67, 355.
McKee, C.F. and Ostriker, J.P., 1977, Astrophys. J. 218, 148.
Myers, P.C., 1983, Astrophys. J. 270, 105.
Schwarz, U.J., Arnal, E.M., and Goss, W.M., 1980, M.N.R.A.S. 192, 678.
Verschuur, G.L., 1974, Astrophys. J. Suppl. 27, 65.

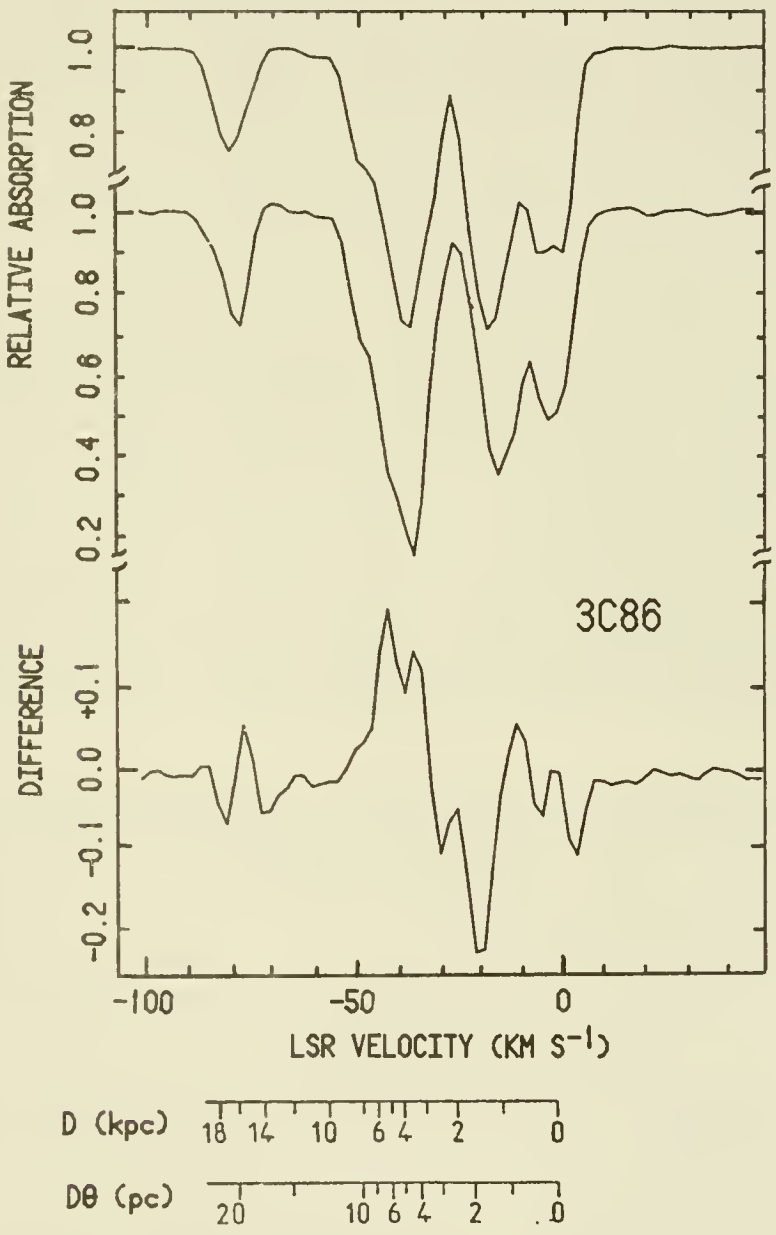

Figure 2. Typical absorption spectra toward 3C86 (ℓ = 143.9, b = -1.0). The difference spectrum, $\Delta t(v)$ is below.

A WARM MAGNETOACTIVE PLASMA IN A LARGE VOLUME OF SPACE

Carl Heiles

Astronomy Department

University of California, Berkeley

1. INTRODUCTION

This paper will show that a diffuse ionized warm gas fills a large volume of space in the general direction of Radio Loop II. There are three types of observational evidence: Faraday rotation measures (RM's) of extragalactic sources; emission measures (EM's) derived from the Hα emission line in the diffuse interstellar medium; and magnetic field strengths in HI clouds derived from Zeeman splitting observations.

2. OBSERVED CHARACTERISTICS

The region of interest, 'Region A' of Simard-Normandin and Kronberg (1980), occupies 80°to 130°in Galactic longitude and about -40°to +10°in latitude. This is a very large solid angle, a bit more than one steradian. All extragalactic radio sources within this region have large negative RM's and none have small RM's. This implies that the region contains a magnetoactive plasma smooth in the large-scale, without small-scale structure. RM's in the opposite direction of the sky tend to be positive, instead of negative, which might imply that Region A lies immediately adjacent to the Sun. However, the RM's are much smaller in magnitude than in Region A, which might mean simply that the gas is less highly ionized than that in Region A, or alternatively that Region A lies some distance from the Sun. Typical RM's in Region A are about 200 rad m^{-2}. This constrains the product

$$n(e)BL = 1.23E\text{-}3\ RM$$

where n(e) is the electron density in cm^{-3}, B is the line-of-sight component of the magnetic field in μG, and L is the extent of the plasma along the line of sight in kpc.

Some marginally interesting additional information is available from one pulsar that lies at a high enough latitude to help constrain the picture, although only weakly. PSR 2154+40, at (l,b)=(91°,-11°), has RM=-44 rad m^{-2} and DM=71 cm^{-3} pc (Taylor and Manchester, 1975). This corresponds to a magnetic field strength, computed in the usual naive manner from the ratio RM/DM, of 0.7 μG. However, with an RM of -44 rad m^{-2}, this pulsar samples only about 25% of the total RM of region A. Thus the derived field strength need not characterize the full extent of Region A. Furthermore, its

DM implies a distance of about 2 kpc if the electron density is equal to its usual value of 0.03 cm^{-3}. However, this distance might well be misleading, because at the relatively low latitude of 11° there might be an intervening HII region along the line of sight--and, indeed, from the map of diffuse Hα of Reynolds, Roesler, and Scherb (1974), there does appear to be enhanced Hαemission in this direction. It is more likely that the pulsar lies closer than 2 kpc and that the true magnetic field strength in Region A is higher than 0.7 μG.

Diffuse Hα emission has been surveyed with very high sensitivity on a rough grid of 5 or 10 degrees by Reynolds et al (1974). The intensity of Hα emission increases towards the Galactic plane, where ordinary HII regions exist in abundance. Further from the plane, at latitudes below -20°, the Hα emission is weak, corresponding to EM's smaller than about 7 cm^{-6} pc except for one position near longitude 120°; and at latitudes below -30°, the EM is smaller than 4 cm^{-6} pc. These EM's assume a temperature of 6000 K. A somewhat lower upper limit, for that temperature, of 1.8 cm^{-6} pc is derived by Simard-Normandin and Kronberg from the low-frequency radio data of Novaco and Brown (1978). Upper limits for Hαemission scale roughly $T^{-0.75}$, while upper limits for low-frequency free-free absorption of radio emission scales as $T^{-1.35}$. We will be interested in gas at higher temperatures than 6000 K, so we should use the EM limit derived from Hα Thus, the EM of 4 or somewhat less constrains the product

$$n(e)^2 \, (T/10000 \text{ K})^{-0.75} \, L = 1.47E\text{-}3 \text{ EM}$$

Measurements of Zeeman splitting of the 21-cm line in emission (Heiles, 1984), made in the directions of many of the same extragalactic sources used in the RM study, show very weak fields in the HI gas, typically no more than a few μG. All of the detected fields point in the same direction as the field that produces the RM's. Nevertheless, the magnetoactive plasma cannot reside in the HI clouds, because then the EM would far exceed the above limit. Thus the HI measurements provide no directly relevant information about the magnetic field in the plasma. However, it seems reasonable to assume that the magnetic field strength in the less dense plasma is no larger than that in the denser HI clouds.

3. DERIVED CHARACTERISTICS

Given the above observational constraints, together with an assumption concerning the ratio of magnetic energy to thermal energy, we can derive the properties of the plasma as a function of a single parameter, which we choose to be L. We assume that the energy ratio is equal to R. It is presumably difficult to obtain R>1, because then the magnetic field would be dominant. However, it is difficult to obtain large RM's unless R is large. So it seems likely that R is roughly equal to unity.

Putting all of the above together with a little algebra, we derive the following:

$$n=1.08E-2\ RM^{6/17}\ EM^{4/17}\ R^{-3/17}\ L^{-10/17}$$

$$B=1.14E-1\ RM^{11/17}\ EM^{-4}\text{Å}^{17}\ R^{3/17}\ L^{-7/17}$$

$$T=3.44E+2\ RM^{16/17}\ EM^{-12/17}\ R^{-8/17}\ L^{-4/17}$$

For the observed values, which we take as RM=200 rad m^{-2} and EM=4 cm^{-6} pc, for an assumed value R=1, and L=1 kpc, we obtain the following:

$$n=0.097\ cm^{-3}$$

$$B=2.5\ \mu G$$

$$T=19000\ K$$

Since the adopted EM might be larger than that characterizing the magnetoactive region alone, the true density might be lower, and the magnetic field and temperature higher, than the values quoted above.

These values don't seem particularly unreasonable from an a priori standpoint. They are quite reasonable in that the pressure nT is about 2000 cm^{-3} K, which is close to the standard interstellar pressure. Over a region 1 kpc in diameter, one expects this criterion to be satisfied.

However, they are unreasonable in an important way. The cooling time scale for such gas is only 5000 years. Such a short cooling time for a diffuse gas occuping such a large volume is unacceptable. Instead, there would need to be an efficient heating source to keep the gas so hot. It is interesting to note that this temperature is just below that where collisional excitation of heavy elements, not just hydrogen, starts to become effective (see, e.g., Dalgarno and McCray, 1972), so it could be an equilibrium temperature if a suitable heating source were available.

It would be more comfortable, however, for the gas to a bit cooler than 10000 K, where the cooling rate rises suddenly with temperature by a factor of about 40 for a fully ionized gas having a normal heavy element content. However, this requires a very large region, because the derived temperature varies slowly with L. A temperature of 10000 K requires that the product R^2L = 15 kpc. Presumably, $R < 1$, which means $L > 15$ kpc! This size is reminiscent of a Galactic halo, which hardly falls within the domain of this conference! Nevertheless, we pursue this possibility briefly. The density and magnetic field strength would be 0.020 cm^{-3} and 0.83 μG, respectively. The recombination time scale would be very short, about 4E6 yr, and a source

of ionization would be required. It would be surprising for such a region to lie near the outer periphery of the Galaxy unless its primary association was not with our Galaxy. In this context, it is curious that the general direction of this region is the same as that of the most of the galaxies in the local group, including M31 (!). None of all this is totally impossible, we supppose, but in the absence of compelling reasons we prefer to drop this possibility.

Alternatively, if we consider smaller values of L, then the density, magnetic field strength, and temperature all increase. The cooling time scale decreases, both because of the increased density and temperature, and the requirement for a heating mechanism is accentuated. Roughly speaking, the cooling time varies a $L^{0.65}$. Furthermore, the temperature increases above the possible natural equilibrium value caused by heavy element excitation. These factors require a powerful heating mechanism, and it seems preferable for such a heating mechanism to occupy a small, rather than a large, volume of space. A small value of L, e.g. 10 pc, gives n=1.5 cm^{-3}, B=17 μG, and T=56000 K. This field strength is much stronger than that observed in HI clouds in this region. Furthermore, such a strong field strength is encountered only rarely in interstellar space, and then only in relatively dense clouds near regions of star formation. It would be remarkable for such a region to extend over a steradian of sky. Finally, we note that PSR2154+40, mentioned above, has an RM just 25% that of region A. If L were small, it would be improbable for this pulsar to be located within the magnetoactive region.

In the absence of further information it is impossible to make definitive statements about the physical conditions in this region. However, we believe that our arguments above are reasonable, and that without further information we should accept them.

4. DISCUSSION

We conclude that the magnetoactive plasma in Region A probably occupies a very large volume of space and that its properties are roughly as given above for the L = 1 kpc case. The main problem with this possibility is the short cooling time scale for the gas. A pervasive heating mechanism is required to keep the gas at its temperature of about 20000 K.

Two possibilities suggest themselves. One is heating by cosmic rays. Region A lies within the nonthermal radio continuum feature known as Loop II (Berkhuijsen, Haslam, and Salter, 1971). The origin of Radio Loop II is unknown. However, a similar feature, Loop I (also known as the North Polar Spur), was caused by stellar winds and superovae and is filled with hot gas and, probably, cosmic rays (see Heiles et al, 1980). It is reasonable that Loop II and Loop I have similar origins, although Loop II is probably older because it is weaker. Energetically, this picture is attractive because Region A contains about 3E51 erg in thermal energy, close to that expected

inside an old shell formed by a collection of supernova and stellar winds. Thus an excess of cosmic rays might well exist inside Loop II, and this could be the heating agent for the gas. Alternatively, but very improbably because of time scale considerations, the gas could be cooling from the original very hot temperature that it had when the Loop was younger.

A less likely possibility is that the plasma is produced and heated by infalling very high velocity gas. The tip of the Magellanic Stream descends into the Galaxy near (l,b) = (90°,-40°) and seems to break up into a multitude of very high negative velocity clouds (Giovanelli, 1981; Mirabel, 1981; Cohen, 1982a,b). It seems quite likely that this disturbance could produce heating of a diffuse ionized gas, perhaps by generating magnetoacousic disurbances. In this case we would expect abnormal velocities of HI clouds because recombination and cooling times are short, However, these are not observed, which seems to be a strong argument against this possibility.

It is a pleasure to acknowledge stimulating discussions of this material with Dr. Shri Kulkarni.

REFERENCES

Berkhuijsen, E.M., Haslam, C.G.T., and Salter, C.J. 1971, Astron Ap 14, 252.

Cohen, R.J. 1982a, MNRAS 199, 281.

Cohen, R.J. 1982b, MNRAS 200, 391.

Dalgarno, A. and McCray, R.A. 1972, Ann Rev Astron Ap 10, 375.

Giovanelli, R. 1981, Astron J 86, 1468.

Heiles, C., Chu, Y-H, Reynolds, R.J., Yegingil, I., and Troland, T. 1980, Ap J, 242, 533.

Heiles, C. 1984, in preparation.

Mirabel, I.F. 1981, Ap J 250, 528.

Novaco, J.C. and Brown, L.W. 1978, Ap J 221, 114.

Reynolds, R.J., Roesler, F.L., and Scherb, F. 1974, Ap J 192, L53.

Simard-Normandin, M., and Kronberg, P.P. 1980, Ap J 242, 74.

Taylor, J.H. and Manchester, R.N. 1975, A.J. 80, 794.

An Investigation of Small Scale H I Structure at High Galactic Latitude

K. Jahoda, J. M. Dickey, F. J. Lockman, D. McCammon

We present results of a search for small scale H I structure at high galactic latitudes using the NRAO 140 foot telescope, which has a 21' beam at 21 cm. We examined randomly selected 4° x 5° regions, as well as regions of particularly low total column density. The amount of apparent structure is small in directions with total column densities of a few times 10^{20} cm^{-2}.

The z-dependence of the Spin Temperature of HI

Shrinivas R. Kulkarni and Carl Heiles, U. C. Berkeley
and
J. Van Gorkom, NRAO, Socorro
and
John M. Dickey, Univ. of Minnesota, Minneapolis

I. INTRODUCTION

In 1981 we conducted an extensive, low-latitutde, HI 21-cm absorption survey from the VLA. The goal of the survey was to answer the following questions:

(a) What is the vertical distribution of the cold HI clouds?
(b) Do HI clouds get systematically warmer at high $|z|$?
(c) Does the fraction of warm intercloud medium HI increase with high $|z|$?
(d) How much HI has been missed in previous HI emission surveys because of optical depth effects?
(e) What is the galactic distribution of cool HI clouds?

In order to answer these questions a low-latitude survey is needed because studies of local HI (i.e. distance < 1 kpc) are severely hampered by our lack of knowledge of distances to the HI clouds and hence their $|z|$ values. This problem is circumvented in low-latitude studies wherein a rotation curve can be used to determine distances to the HI absorption features. The HI emission/absorption data has already been reported (Dickey et al. 1983). Here, we present preliminary results which shed some light on the first four questions (§III).

II. INTEGRATED MEASURES

a) Spin Temperature of HI

The 21-cm emission spectrum is described by

$$T_B(v) = T_s[1 - e^{-\tau(v)}] \quad (1)$$

where

$$\tau(v) = N_H(v)\ C^{-1}\ T_s^{-1} \quad (2)$$

Here $C = 1.823 \times 10^{18}$ cm^{-2} K^{-1} (km s^{-1})$^{-1}$, $N_H(v)$ is the column-density of HI with velocity v, and T_s is the spin temperature of the gas. Thus if $\tau(v) << 1$ then

$$T_B(v) = N_H(v)\ C^{-1}. \quad (3)$$

The 21-cm absorption spectrum is simply $\tau(v)$. From (2) and (3) it should be clear that absorption is biased towards cold clouds whereas emission is unbiased. T_s', the deduced spin temperature, is given by

$$T_s' = T_B(v)[1 - e^{-\tau(v)}]^{-1}. \quad (4)$$

T_s' is equal to T_k, the kinetic temperature only when the HI along the entire line-of-sight is isothermal. In general, as can be seen from (2), (3) and (4), T_s' is the column-density weighted harmonic-mean temperature of HI. It is important to appreciate this point when interpreting the results given below.

b) Definition of Integrated Measures

The integrated emission brightness, V_B is defined by $V_B = \int T_B(v)dv$ and the integrated optical depth, V_τ, is similarly given by $V_\tau = \int \tau(v)dv$. Here the integration is over the observed velocity range. Due to optical depth effects, V_B does not increase with N_H, the total line-of-sight column density of HI. However V_τ samples all HI along the line of sight and is not beset with any problems arising out of the relative location of the clouds with respect to each other. Another interesting parameter is F': $F' \equiv F_{local}/(V_B/V_\tau)$ where $F_{local} = V_B(Poles)/V_\tau(Poles)$ and is the mean ratio of the integrated emission brightness to the integrated optical depth towards the North and the South Galactic poles. The column density of HI towards the poles is small enough that $V_B(Poles)$ is not affected by optical depth effects. F_{local} has been measured to be 200 ± 20 K (Kulkarni 1983).

The use of integrated measures may appear to throw away a lot of velocity information in the data. However because of the small number of assumptions made, the analysis of integrated measures leads to model independent results. In particular, two broad class of problems are avoided by the use of integrated measures:
(1) Since there is no attempt to finely bin the data by z or R, all the problems connected with the determination of distance are avoided. The distance ambiguity problem in the inner galaxy is also avoided.
(2) Since there is no attempt to do a detailed comparision of the emission and the absorption spectrum, the problems arising from small-scale angular-structure in the HI features are avoided. Structures in HI on an angular-scale smaller than the emission beamwidth lead to systematic biases in analysis involving velocity information. In contrast, integrated measures are not statistically biased.

III. RESULTS

We have divided the galaxy into three regions:
(a) inner galaxy ($R < R_o$ and $|l| < 90°$; R_o has been assumed to be 10 kpc)
(b) outer galaxy in the second and third quadrants ($R > R_o$; $90° < l < 270°$)
(c) outer galaxy in the first and fourth quadrants ($R > R_o$; $|l| < 90°$).
Now consider a line-of-sight with $90° < l < 270°$. This line-of-sight has a minimum $|z|$, z_{min} of 0 pc at the position of the sun and a maximum $|z|$, z_{max} when the line-of-sight crosses a circle with R = 20 kpc; this radius corresponds to the assumed edge of the HI disk (Kulkarni, Blitz and Heiles 1982). For lines-of-sight with $|l| < 90°$, there is an additional complication due to the fact that the line-of-sight will traverse both the inner and the outer galaxy regions (i.e. regions (a) and (c)). For such lines-of-sight we compute F' separately for region (a) and (c). For region (a), z_{min} is clearly 0 pc and z_{max} is the $|z|$ of the line-of-sight when it crosses the circle $R = R_o$. For region (c), z_{min} and z_{max} are simply the $|z|$ value of the

line-of-sight when it crosses a circle of radius R_o and 20 kpc respectively.

In Figs. (1) and (3) we show F' as a function of the z-extent of the line-of-sight for regions (a), (b) and (c) respectively. The z-extent is shown by means of the vertical "error-bar"; thus the tips of this "error-bar" correspond to z_{min} and z_{max} of the line-of-sight. The square in the center of the "error-bar" is simply the arithmetic mean of z_{max} and z_{min} i.e. $\langle z \rangle = 1/2(z_{min}+z_{max})$. In Fig. (2) we show F' as a function of $\langle z \rangle$ to avoid a clutter of lines.

In all the three regions of the galaxy we find that the points with the smallest z-extent have $F' > 1$. This is understandable since at low $|b|$, V_B saturates due to large optical depths whereas V_τ is unaffected. Another striking correlation is the increase of F' with $\langle z \rangle$, or in other words, F' values which average over higher-$|z|$ HI seem to be systematically smaller than F' values which represent smaller-$|z|$ HI. This is most clearly seen and is statistically extremely significant in region (c) (Fig. 3) and somewhat evident in region (b) (Fig. 2) and not seen at all in region (a) (Fig. 1). We attribute this correlation to an increase of Not-Strongly-Absorbing HI with $|z|$.

Stray radiation can produce the correlation seen in Figs. (2) and (3). We believe that this is not an important effect quantitatively since a) stray radiation is important at high latitudes where the signal is weak and the sidelobes lie in the galactic plane and b) all the points shown in Figs. (2) and (3) have V_B in excess of 10^3 K km s^{-1} and V_τ, in all but two lines-of-sight, is not dominated by measurement noise. Thus neither measurement errors nor stray radiation vitiate our conclusion.

IV. DISCUSSION

Concentrating on Fig. 3, where the variation of F' with the z-extent is best seen, we note that at high $|z|$, F' decreases to at least a sixth of the local value of unity. Now a decrease in F' could be either due to (i) an increase in the temperature of HI clouds or (ii) an increase in the fraction of the warm intercloud medium HI or both. In an attempt to determine the variation of the spin temperature of clouds with $|z|$ we estimated the spin temperatures corresponding to the absorption features through the use of eqn. (4). Binning T_s' in $|z|$ shows a weak correlation of increasing T_s' with $|z|$ - T_s' at most increases by a factor of 2 from low-$|z|$ to high-$|z|$. If this is true then the intercloud medium HI increases by a factor of 3 from low-$|z|$ to high-$|z|$. There is a problem with such a naive determination of T_s' because at low-$|z|$, the plethora of absorption components makes determination of emission brightness of each absorption component uncertain. Correspondingly, at high-$|z|$ the increased background of the intercloud medium HI increases T_s'.

We would like to point out that studies of local HI show that the velocity-dispersion of clouds with $\tau < 0.1$ is twice as much as that of clouds with $\tau > 0.1$ (Dickey 1977). Statistically low-τ clouds have larger T_s (this

is the so called T_s-τ relation; e.g. Liszt 1983). Thus there is an indication of a z-dependence of of the temperature of HI clouds. For this reason we are in the process of doing a detailed gaussian-component analysis to quantitatively assess the importance of (1) above.

We have also derived average correction factors to account for the underestimation of the density of HI at z = 0 pc as derived from HI emission studies. The underestimation arises because the 21-cm line is optically thick. We find that the HI mid-plane densities have to be revised upwards by ~2 (inner galaxy) and ~1.6 (outer galaxy). The details of the procedure adopted in obtaining these results can be found in Kulkarni (1983).

REFERENCES

Dickey, J. M.: 1977, Ph. D. Thesis, Cornell Univ.

Dickey, J. M., Kulkarni, S. R., Van Gorkom, J. and Heiles, C.: 1983, Astrophys. J. Suppl. Ser. 53, 591

Kulkarni, S. R.: 1983, Ph. D. Thesis, U. C. Berkeley.

Kulkarni, S. R., Blitz, L. and Heiles, C.: 1982, Astrophys. J. 253, L63

Liszt, H. E.: 1983, Astrophys. J. 275, 163

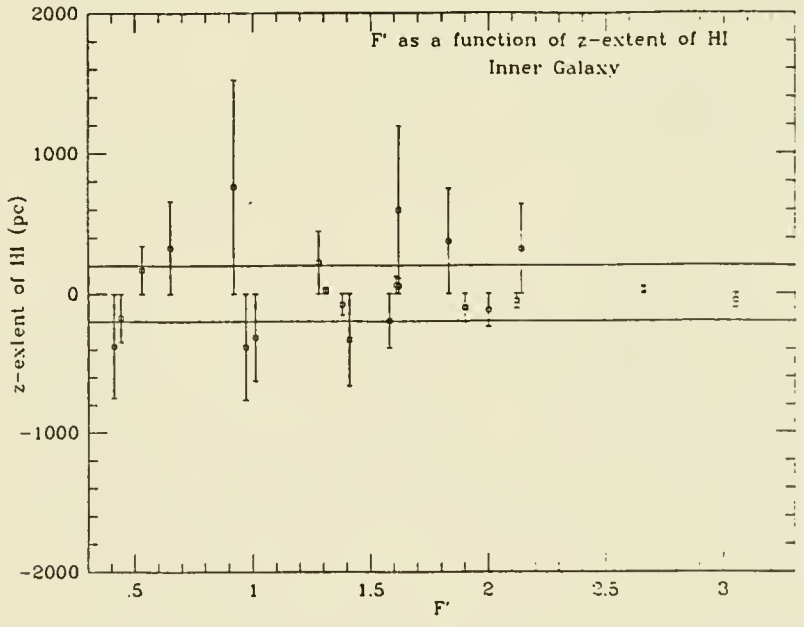

FIG. 1

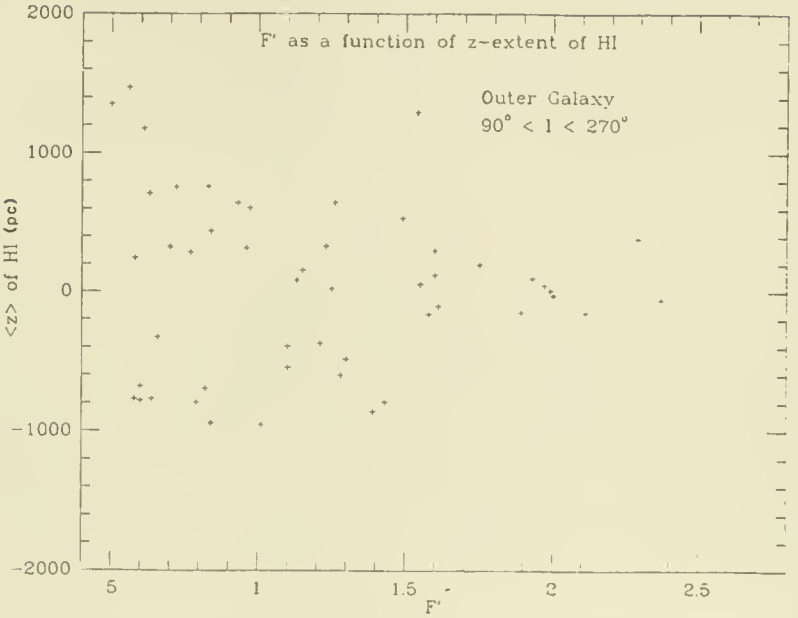
F' as a function of z-extent of HI
Outer Galaxy
90° < l < 270°
<z> of HI (pc)
2000
1000
0
-1000
-2000
.5
1
1.5
2
2.5
F'

FIG. 2

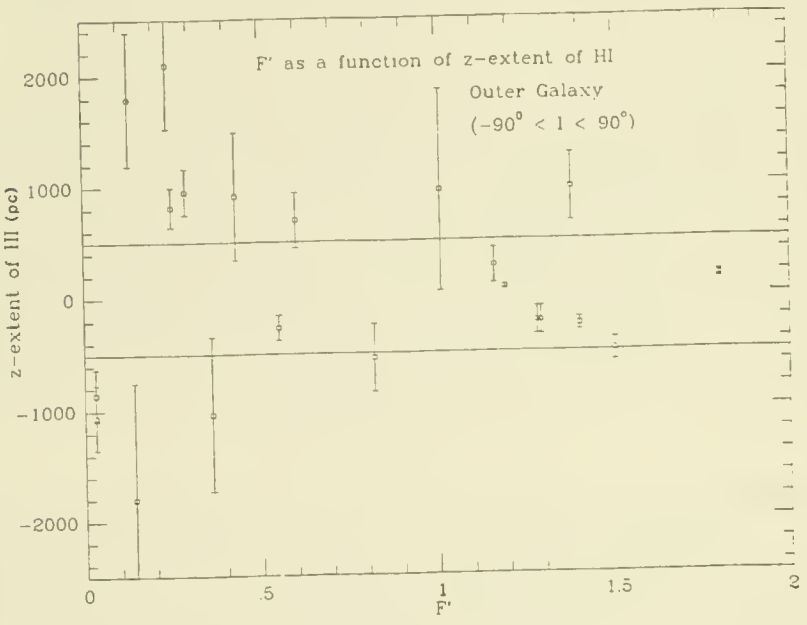
F' as a function of z-extent of HI
Outer Galaxy
(-90° < l < 90°)
z-extent of HI (pc)
2000
1000
0
-1000
-2000
0
.5
1
1.5
2
F'

FIG. 3

POLARIZATION OF RADIO MOLECUAR LINES

AND MAPPING OF MAGNETIC FIELD DIRECTION

Shuji Deguchi and William D. Watson
University of Illinois at Urbana-Champaign

ABSTRACT

Two level calculations by others for the linear polarizations expected for molecular emission lines from interstellar clouds are extended by considering a number of coupled rotational states of a diatomic molecule. Higher transitions commonly have strengths comparable with that of the J=1-0 transition so that depolarization due to coupling between the various J-states might be expected to reduce the predicted linear polarization. The significance of the null observational results obtained recently by Wannier, Scoville and Barvainis is assessed. The inclusion of additional states tends to decrease the maximum polarizations, though the calculated polarization is increased under conditions for which "superthermal" excitation occurs.

INTRODUCTION

Linear polarization of the emitted radiation is likely to occur when the radiation field within the emitting region is not isotropic. Anisotropy of the radiation in gas clouds can occur because of the optical depths for the escape of line radiation are not the same in all direction. Goldreich and Kylafis (1981, 1982) have examined the influence of anisotropy caused by velocity gradients in producing linear polarization of thermal radio emission lines from molecular clouds. At radio frequencies, the Zeeman splitting of molecular rotational lines is normally much greater than the natural line width. Then, the direction of the net linear polarization can be utilized as an observational diagnostic for the direction of magnetic field. For their idealized model, they find that linear polarization up to 10-20 % does occur. Wannier, Scoville and Barvainis (1983) performed an extensive search for linear polarization in CO, HCN and CS emission lines, but no linear polarization has been detected. An approximation in the Goldreich and Kylafis calculation is to include only two levels and obtain explicit results for only the J=1-0 transition of CO. Coupling of the J=1 state to the J=2 and higher states by radiation and by collision would be expected to scramble the populations of the magnetic substates and to reduce the predicted linear polarization.

NUMERICAL RESULTS

The treatment for the J=1-0 transition of diatomic molecule by Goldreich and Kylafis can be readily extended to multilevel problems. The equations of radiative transfer for the intensities having two polarizations are solved with the large-velocity-gradient approximation. All of our results are obtained for either (a) the one dimensional case in which the velocity gradient is only along the magnetic field or (b) the two dimensional case in which the

velocity gradient is present only in the plane prependicular to the magnetic field. The two dimensional case is that of a cloud expanding with constant velocity and may be a more realistic simulation of a molecular cloud. Results are given for various ratios of the collision rate to the radiative decay rate C/A for the J=1-0 transition.

We have compared the multilevel (J up to 4) calculations for the CO molecule with those including only the J=1 and 0 levels. The peak polarization in the J=1-0 transition is decreased by about a factor of two as a result of including the higher J-levels. Cascading from the higher levels increases the intensity (the superthermal effect), however. For C/A=0.1, the multilevel calculation actually gives higher values for Q^2+U^2 . The higher transitions exhibit less polarization. For the J=1-0 transition, the fractional polarization is largest for the smallest C/A considered (about 7% for C/A=0.01). However, the critical quantity for detecting the linear polarization is Q^2+U^2 and this decreases at low C/A because of the intensity decrease. For the two dimensional geometry, Q^2+U^2 does not exceed about 0.25 K for CO and CS molecules.

In the one dimensional geometry, the velocity gradient is along the magnetic field so that the photons escape along the field. We consider line-of-sight to the observer that is perpendicular to the magnetic field. The optical depth is infinite and the observed intensity (temperature unit) is equal to the excitation temperature. The polarizations computed for this geometry may be unrealistic because the superthermal excitation strongly influences the result and such excitation apparently has not been observed for CO. The maximum fractional polarization (approximately 12-14%) is similar to that found by Goldreich and Kylafis. The temperature of linear component can go up to about 3.5 K for C/A=1.

CONCLUSIONS

Though noise levels of about 0.1-0.2 K (one standard deviation) were achieved in a few cases in the search by Wannier et al. (1983), no definite polarization was detected. If three standard deviations or more is accepted as the detectable limit, this level of sensitivity would be marginal for detecting polarization of CO and CS as is expected from our calculations unless the one dimensional case is applicable. Our explicit treatment of polarization for the J=2-1 transition shows that it tends to be somewhat less than predicted for J=1-0, and the latter is the preferable transition with which the linear polarization is seeked.

REFERENCES

Goldreich, P. and Kylafis, N. D., 1981, Ap. J. (Letters), 243, L75
Goldreich, P. and Kylafis, N. D., 1982, Ap. J., 253, 606
Wannier, P. G., Scoville, N. Z., and Barvainis, R., Ap. J., 267, 126

NEARBY MOLECULAR HYDROGEN

F. Lebrun

Service d'Astrophysique, C.E.N. Saclay, France

Abstract

If the gas-to-dust ratio is sufficiently uniform throughout the local interstellar medium, galaxy counts may provide a useful probe of the large scale structure of the interstellar gas. This idea substantiated by gamma-ray observations has led to the discovery of nearby molecular cloud complexes. The reddening studies indicate that one of them lies between 80 and 140 pc from the sun. From CO observations, its molecular mass is estimated to be a few 10^3 $M_\odot$.

1 INTRODUCTION

The observations of the U-V absorption lines by the Copernicus satellite have shown that even in the solar neighborhood, molecular hydrogen (H_2) is an important component of the ISM. This type of observations can put useful constraints on the gas distribution but cannot reveal its detailed structure. 21 cm radio surveys on large angular scales (e.g. Heiles and Habing 1974) have determined precisely the atomic hydrogen (HI) distribution but that of H_2 is still lacking. Three independent ways of assessing the large scale distribution of the nearby molecular hydrogen will be discussed in this paper: i) galaxy counts ii) gamma-ray obervations iii) CO line observations. Galaxy counts (Shane and Wirtanen 1967) provide a uniform survey of the interstellar extinction over the entire northern celestial hemisphere ($\delta > -25°$). If the gas-to-dust ratio is sufficiently uniform in the nearby interstellar medium, this survey may provide one of the best current estimate of the total gas (HI + H_2) distribution. Diffuse gamma rays (E>50 MeV) are produced by the interactions of cosmic rays in the interstellar gas. Collisions of cosmic-ray protons with gas nuclei produce π° mesons which decay in two gamma-rays. High energy bremsstrahlung radiation is emitted by cosmic-ray electrons in the electric field of the interstellar-gas nuclei. If the cosmic-ray density is uniform within a few hunded parsecs, gamma-ray emission may be considered a total gas column density tracer. After H_2, CO is the most abundant molecule in the interstellar medium. Its 1→0 rotational transition is easily observable at 2.6 mm by standard radioastronomical

techniques. If the velocity-integrated intensity of that line is closely related to the H_2 column density ($N(H_2)$), CO would be the best tracer of H_2.

Heiles (1976) and Burstein and Heiles (1978) studied the relationship between galaxy counts, interstellar reddening and atomic hydrogen column density (N(HI)). They found that the ratio between N(HI) and the interstellar absorption (Apg) - as traced by galaxy counts - is non uniform over the sky. Some regions where this ratio is low correspond to well-known molecular complexes, namely Orion, Taurus, Perseus and ρ Ophiuchi, where with a constant gas-to-dust ratio, the HI deficiency can be well accounted for by molecular hydrogen formation (Strong and Lebrun 1982). The lowest values of N(HI)/Apg are located inside the Ophiuchus-Sagittarius region. Lebrun and Paul (1983) noted that in the same region, HI is also deficient compared to the gamma-ray intensity observed by *SAS-2* and concluded that there exists gamma-ray-emitting material linked to the dust, this material being most likely molecular hydrogen. This conclusion is also supported by the *COS-B* gamma-ray observations (Strong et al.1982).

2 THE CO OBSERVATIONS

We have undertaken an extended survey (370 square degrees) in the CO (1→0) line of the northern part of Ophiucus and Sagittarius. The observations were performed in frequency switching mode with the 1.2 m millimeter-wave telescope at Columbia University with an angular resolution degraded to 0.5 ° and a velocity resolution of 0.65 km s^{-1}. Further details concerning the observational procedure and the data processing can be found elsewhere (Lebrun and Huang 1984). The results in the form of a map of the integrated CO line intensity ($Wco = \int Ta^* dv$) are presented in figure 1.

3 RESULTS AND DISCUSSION

The molecular clouds found here (see fig. 1) appear as an extension towards higher latitudes of the very extended CO complex associated with the Aquila Rift (Dame and Thaddeus 1984). The eastern clouds have the same velocity as this complex (6 – 7 km s^{-1}), while the western ones have the same velocity (~ 3 km s^{-1}) as the ρ Oph cloud complex which is 15° away. These clouds are located in or near the plane of the Gould Belt and the average velocity of these clouds matches that of the HI feature A of Linblad et al. (1973).

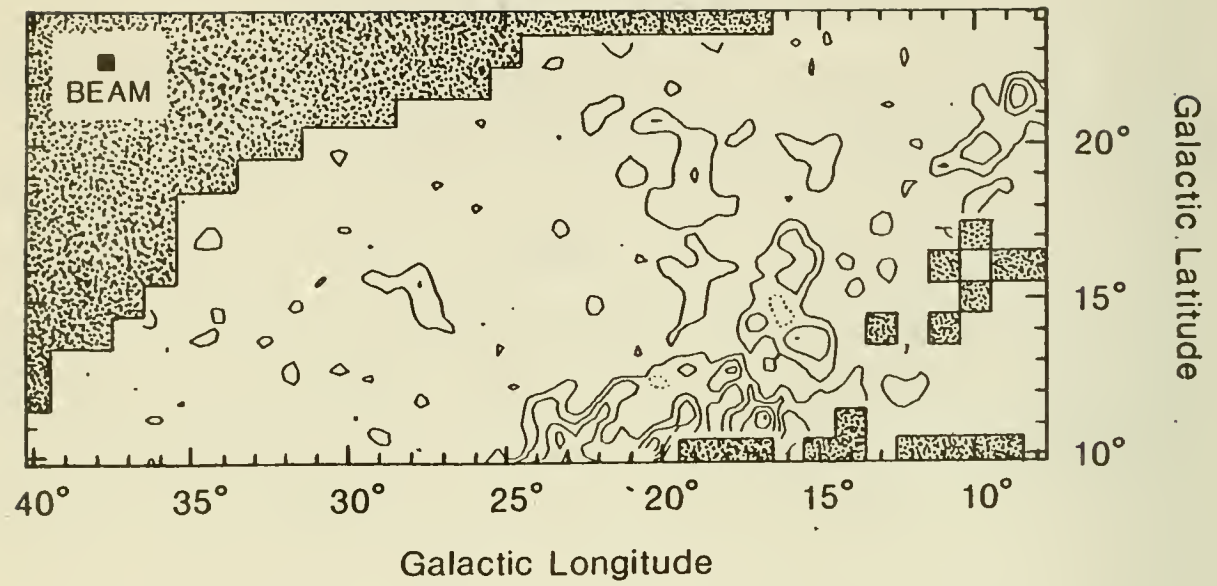

Figure 1. Contour map of the integrated CO line intensity, Wco. The contour interval is 2.5 K km s^{-1}. The shaded areas indicate unobserved regions.

Although this dicovery confirms qualitatively the predictions based on galaxy counts and gamma-ray observations, a quantitative study is necessary. Lebrun and Huang (1984) studied the relations between CO,HI and Apg (traced by star counts) in the upper part (b>16°) of this region. They found that the gas to dust ratio is normal and proposed a calibration of NH_2 estimates from CO measurements: $NH_2/Wco = 10^{20} cm^{-2} K^{-1} km^{-1} s$. However, the column densities predicted with this calibration, based on star counts, are at least 50% lower than those based on galaxy counts and HI. The origin of this discrepancy must lie in the calibration of the absorption measurements. It could be either an underestimate of the absorption by the star counts or an overestimate of the absorption by the galaxy counts.

Another interesting effect is that the observed gamma-ray intensity (70-5000 MeV) appears higher (~40%) than that predicted from galaxy counts (Strong et al. 1982). An underestimate of the absorption by the galaxy counts is hard to believe since it would imply an unrealistic underestimate of the absorption by the star counts. It seems more reasonable to consider this region as having a gamma-ray emissivity higher than the local average. This could be either the result of an

additional gamma-ray component (inverse Compton emission, unresolved weak point sources) or the result of an enhanced cosmic-ray density throughout the complex.

The distance of these clouds can be estimated from the distribution of the interstellar reddening material along the line of sight. In the study of OB stars in the solar neighborhood by Lucke (1978), this region stands out as having the highest reddening per unit distance of the entire sky. The reddening distribution suggests that the complex lies between 50 and 375 pc from the sun. On the basis of the study by Knude (1978) of the reddening of A and F stars, Arnaud et al.(1980) derived a distance consistent with Lucke's estimate: 80-150 pc. Therefore this cloud complex seems to be one of the closest to the sun. The fact that at these latitudes it is unlikely that a line of sight intercepts any other cloud, makes it a good candidate for detailed study. If we adopt the calibration proposed by Lebrun and Huang (1984) and a distance of 100 pc the H_2 mass of the complex is a few $10^3 M_\odot$. Although this mass may be considered a lower limit, the total mass of the complex is probably dominated by that of HI.

REFERENCES

Arnaud, M., Rocchia, R., Rothenflug, R., and Soutoul, A. 1980 ,Proc.17th Int.Cosmic Ray Conf. (Paris), **1**, *131.*

Burstein, D., and Heiles, C. 1978, ApJ., **225**, *40.*

Dame, T.M., and Thaddeus, P. 1984, these proceedings.

Heiles, C. 1976, ApJ., **204**, *379.*

Heiles, C., and Habing, H.J. 1974, Astr.Ap.Suppl., **14**, *1.*

Knude, J. 1978, Astr.Ap.Suppl., **33**, *347.*

Lebrun, F., and Huang, Y.-L. 1984, ApJ., scheduled for the june 1st issue

Lebrun, F., and Paul, J.A. 1983, ApJ., **266**, *276.*

Linblad, P.O., Grape, K., Sandquist, Aa, and Schober, J. 1973 , Astr.Ap., **24**, *309.*

Lucke, P.B. 1978, Astr.Ap., **64**, *367.*

Shane, C.D., and Wirtanen, C.A. 1967, Pub. Lick Obs., **22**, *1.*

Strong, A.W., and Lebrun, F. 1982, Astr.Ap., **105**, *159.*

Strong, A.W., et al. 1982, Astr.Ap., **115**, *404.*

Radio and UV Observations of High Latitude HI

Felix J. Lockman, National Radio Astronomy Observatory,
L. M. Hobbs, Yerkes Observatory, University of Chicago,
and J. Michael Shull, Joint Institute for Laboratory
Astrophysics, University of Colorado.

Interstellar Lyman-α observations toward high latitude stars, which give the column density of HI between us and the star, and 21 cm radio observations, which give the total HI column density to and beyond the star, can be combined to map out the amount of neutral gas as a function of distance from the sun. We present recent observations of the 21 cm and Lyman-α lines made toward ~50 high latitude OB stars, and use these data to discuss the distribution of HI in the solar neighborhood.

THE PARALLAX OF PULSAR 0950+08 AND THE LOCAL FREE ELECTRON DENSITY

C. R. Gwinn[1], J. H. Taylor, J. M. Weisberg and L. A. Rawley
Physics Department, Princeton University

ABSTRACT

We report a parallax of 7.9±0.8 mas for PSR 0950+08, corresponding to a distance of 130±15 pc. The measured pulse dispersion of this pulsar implies an average free electron density of 0.023±0.002 cm^{-3} along the line of sight. This parallax measurement is subject to systematic errors and questions of interpretation which have not yet been fully explored.

INTRODUCTION

Annual parallaxes of nearby radio pulsars, in combination with their pulse dispersions, provide determinations of the local free electron density which are independent of other astrophysical models. The pulse dispersion is proportional to the dispersion measure, $DM=\int n_e \, dl$, where n_e is the free electron density and dl the line element along the line of sight (Manchester and Taylor 1977). The pulsar's parallax π is the inverse of its distance, so the average free electron density is along the line of sight is $\langle n_e \rangle = DM \cdot \pi$. PSR 0950+08 has the lowest dispersion measure of any known pulsar, so its parallax is of particular importance to studies of the local interstellar medium.

TECHNIQUES

Very Long Baseline Interferometry (VLBI) offers extremely high resolution at radio frequencies, allowing correspondingly precise measurements of radio source positions. In practice this precision is difficult to exploit, due to VLBI's sensitivity to minute variations in interferometer baseline length and orientation, and to changes in the radio signal's propagation medium. A particular difficulty in astrometric VLBI observations of pulsars is that pulsar spectra fall off steeply for frequencies f>100 MHz, while the ionosphere introduces a phase error which varies as f^{-2}, and which can change by an order of magnitude each day. With suitable ionospheric corrections, observations near 1.5 GHz represent the best compromise between these effects.

We observed at 1.66 GHz, measuring pulsar positions relative to nearby reference quasars with a phase-referencing technique similar to that used by Shapiro et al. (1979) for astrometric observations of quasars. We referenced the position of PSR 0950+08 to that of 0938+119, a quasar 4.8 degrees away. We recorded data with the Mark II VLBI system at radio telescopes at Arecibo, PR; Green Bank, WV; and Owens Valley, CA.

The tapes were cross-correlated to produce interference fringes at the Mark II processor in Charlottesville, VA. The cross-correlation functions were

1 Present address: Center for Astrophysics, Cambridge MA

corrected for the effects of clock errors, precession and nutation, and the free motions of the earth. We also corrected for the ionosphere, the atmosphere, and the gravitational deflection of light by the sun. The ionospheric correction was made with data on the Faraday rotation of satellite signals, as observed at stations near the telescopes. The Faraday rotation data were related to ionospheric phase errors within a framework devised for correction of ionospheric effects on navigation satellite signals (Klobuchar 1975). The accuracy of this correction falls off rapidly with increasing separation, at ionospheric altitude, of the lines of sight from the telescope to the radio source and from the satellite antenna to the satellite. We observed at separations of up to 9 degrees in longitude. Comparisons of relative source positions as measured on different days indicate that our corrections reduce the systematic errors to an rms level of 0.03 turns of fringe phase per degree of program-reference source separation (Gwinn 1984). These comparisons are not complete due to lack of knowledge of the Mark II processor model.

Though enormously sensitive, the Arecibo telescope can observe only within 20 degrees of zenith. One can therefore obtain only a narrow range of orientations of interferometer baselines relative to a source, corresponding to a narrow range of interferometer fringe spacings on the sky. Information from our two more sensitive baselines, Arecibo-Green Bank and Arecibo-Owens Valley, yields a lattice of possible positions separated by integral numbers of turns of fringe phase. Additional assumptions are necessary to decide which combination of possible positions at each epoch represent the pulsar's motions between observations.

RESULTS

We have eight positions at four epochs for PSR 0950+08. To resolve fringe ambiguities, we took the pulsar's motion to agree as closely as possible with the proper motion as measured by Lyne, Anderson and Salter (1982). These positions yield, as a solution for parallax and proper motion,

$$\mu_\alpha = 17.9 \pm 3.0$$
$$\mu_\delta = 35.8 \pm 4.0 \qquad C(\mu_\alpha, \mu_\delta) = 0.79$$
$$\pi = 7.9 \pm 0.8 \qquad C(\mu_\alpha, \pi) = -0.34 \qquad C(\mu_\delta, \pi) = -0.11$$

where μ_α and μ_δ are the components of the pulsar's proper motion and π is its parallax. The C's are the normalized covariances, and the reduced chi-squared is 0.86. The proper motion agrees with Lyne, Anderson and Salter at the 1σ level. The solution differs from that reported by Taylor et al. (1984) only in the correction for the gravitational deflection of light by the sun. Deleting the positions from any one epoch leaves the parallax unchanged to within 0.8 mas, as does deleting positions from two epochs and solving for parallax with the proper motion fixed at the value of Lyne, Anderson and Salter. We searched for alternative solutions by shifting positions from each epoch by one or two fringe ambiguities. All solutions with a reduced chi-squared of 2.5 or less yielded a parallax within 0.8 mas of the above result; these solutions resulted from moving a single position by one fringe ambiguity, and are not fundamentally different. Significantly different solutions have greater reduced chi-squared and proper motions agreeing poorly with that of Lyne, Anderson and Salter.

CONCLUSIONS

PSR 0950+08's parallax of 7.9±0.8 mas corresponds to a distance of 130±15 pc. Its dispersion measure is 2.969 cm^{-3} pc, so we conclude that the average free electron density along the line of sight to this pulsar is 0.023±0.002 cm^{-3}.

This result is in good agreement with free electron densities measured along longer lines of sight by other techniques, which are consistent with an average free electron density of 0.03 cm^{-3} over kiloparsec scales (Weisberg, Rankin and Boriakoff 1984).

Previous attempts to measure pulsar parallax have used radio-linked interferometers, with much shorter baselines and about a factor of 30 lower resolution. Salter, Lyne and Anderson (1979) obtained nine results, only one of which was significantly nonzero: they obtained a parallax of 21.5±8.0 mas for PSR 1929+10, corresponding to an average free electron density of 0.069±0.026 cm^{-3} along the line of sight. They combined all nine of their results to find an average free electron density of 0.029±0.014 cm^{-3} in the solar neighborhood, in good agreement with our result for PSR 0950+08 above. Backer and Sramek (1982) reported an upper limit of 4 mas for the parallax of PSR 1929+10; this controversy has not yet been resolved.

REFERENCES

Backer, D. C., and R. A. Sramek: 1982, Ap. J. **260**, 512

Gwinn, C. R.: 1984, PhD. Thesis, Princeton University

Klobuchar, J. A.: 1975, Air Force Cambridge Research Laboratories Report AFGL-TR-75-0502 (NTIS ADA 018862)

Lyne, A. G., B. Anderson and M. J. Salter: 1982, Mon. Not. Roy. Astron. Soc. **201**, 503

Manchester, R. N. and J. H. Taylor: 1977, Pulsars (San Francisco: W. H. Freeman and Company)

Salter, M. J., A. G. Lyne, and B. Anderson: 1979, Nature **280**, 477

Shapiro, I. I., J. J. Wittels, C. C. Counselman, D. S. Robertson, A. R. Whitney, H. F. Hinteregger, C. A. Knight, A. E. E. Rogers, T. A. Clark, L. K. Hutton and A. E. Neill: 1979, A. J. **84**, 1459

Taylor, J. H., C. R. Gwinn, J. M. Weisberg and L. A. Rawley: 1984, Proceedings of I. A. U. Symposium 110: VLBI and Compact Radio Sources, ed. R. Fanti, K. Kellerman and G. Setti (Dordrecht: Reidel), to be published

Weisberg, J. M., J. Rankin and V. Boriakoff: 1984, to be published

THEORETICAL MODELS

Modelling the Local Interstellar Medium As A Supernova Remnant In A Multiphase Gas

Lennox L. Cowie[+]

Space Telescope Science Institute

Physics Department, M.I.T.

and

Physics Department, J.H.U.

INTRODUCTION

Trying to understand the local interstellar gas in detail may be a hopeless task for a theorist. In the interstellar medium as a whole, we can at least address global properties and perhaps come to some reasonable "time averaged" conclusions such as those of Cox and his collaborators (e.g. Cox and Smith 1974, Cox 1979) or McKee and Ostriker (1977). Even this is quite uncertain of course, both because the ISM gas has structure on scales from at least 1 Pc (and probably much smaller) all the way up to the size of the galaxy, and because none of us are quite sure which physical processes (such as thermal evaporation or heating of cooler gas by magnetohydrodynamic processes) are really important. However, in the local ISM things are significantly worse in that we no longer have even the ergodic hypothesis available to us - rather we have to try and deal with individual events and structures. On the other hand, we do have more detailed observations and hence a laboratory to try to decide on the importance of the various physical processes.

More specifically, it now seems highly likely from the X-ray measurements that locally we live within a "middle aged" supernova remnant with a radius of about 100 Pc (e.g. Cox and Anderson 1982 and references therein) and that the local ISM was reheated about 10^5 years ago. The question I would like to answer here is whether we can construct a model of this remnant which is consistent in detail with the observations and what it tells us about the theory. It is clear at once that this is far too complex and I will indeed concentrate on certain of the observations. However, I shall argue that thermal evaporation and local inhomogeneity are crucial elements which are essential to any satisfactory description.

Inhomogeneity

The optical and UV absorption line studies would seem to unequivocally demonstrate the presence of high column density cold gas in some regions within the local hot bubble. From Paresce's (1984) recent compilation one sees that eight of the stars (αOph, δ Cyg, σ Sgr, o And, o Per, κ Vel, η Cen and α Crucis) within 100 Pcs could have hydrogen column densities in excess of $10^{19.5}$. In the cases of α Oph, κ Vel and η Cen, such material is certainly present. The total sampled line of sight distance of all observed stars is 1300 Pc and the average line of sight distance to high column density cold gas is then between 150 Pc and 430 Pc compared to typical ISM values of around 100 Pc (e.g. Spitzer 1977). This may suggest a local deficiency of high column density cold gas by a factor of up to 4, but there is no doubt that such material does exist locally. It should be emphasized of course, that the number of objects expected (12 or so) is so small that the deficiency has little significance. Similar conclusions arise from the Na optical absorbtion line studies (see the discussions of Frisch and Ardeberg in the present colloquium).

All this of course says nothing about whether the material is in sheets or clouds but we can leave this for the moment because in modelling the hot gas in the supernova remnants this type of material is actually of minor importance. It has too high a space density and too high a column density to much affect (or be affected by) the hot gas. (A corollary is, of course, that it would have been surprising if it had been locally absent and it is just as well it isn't). The material which can provide a mass source and energy sink to the hot gas is the 10^4 ^oK material (hereafter the WM) which, as MO pointed out, must form given the presence of the cold gas. Given a typical UV flux, standard interstellar pressures and the presence of the cold gas, ionized warm material will rapidly occupy a significant fraction of interstellar medium. While we have no good heating mechanisms available except perhaps magnetohydrodynamic waves (e.g. Spitzer 1982), presumably a substantial fraction of warm neutral material forms too.

EVAPORATIVE SUPERNOVA REMNANTS

The importance of the WM lies in its potential to contribute mass to the hot gas by thermal evaporation (MO, Cowie McKee and Ostriker, 1981 hereafter CMO). The importance of thermal evaporation is the major controversial question in describing the hot gas in the local supernova remnant (and indeed in supernova remnants in general). Supernova remnant evolution with thermal evaporation from embedded material (such as described by MO and CMO) has a radically different appearance from the classical Sedov solution. (The Sedov solution is an approximately valid description of the gas when evaporation is not present even if there is a population of embedded cold gas, provided only this gas does not occupy too large a fraction of the volume or cover too large a fraction of the surface area.)

Since many people may not be familiar with the evaporative remnant theory let me run at least briefly through the principal features. In figure 1, I have shown the density profiles for the hot component of the gas obtained by CMO for a 3×10^{50} ergs fully evaporative supernova remnant (their model 1). Before I even start describing it, I should say that the salient features of the WM in this numerical model is that it had a filling factor of 27%, an assumed cylindrical shape, and a size of 2.7 Pc. It would have made very little difference if the WM had initially been in sheets since, because of the low column densities in WM structures, dynamical effects would fragment them very rapidly anyway. The density distribution inside the remnant is very flat compared to Sedov solutions which are sharply peaked towards the outside edge. It should also be noted that once the WM properties are specified, the density of the hot gas is predicted.

Specifically, we can make an approximate calculation of the average density of the hot gas as follows. If,

n = average hot gas proton density, T = average hot gas temperature
R = remnant radius, E_{51} = supernova energy in units of 10^{51} ergs (70% thermal, 30% kinetic)
c = isothermal sound speed at T, m = average mass per proton
$R = \alpha c$ (defines α), a_{pc} = cloud radius in parsecs
M = mass of hot gas in remnant, n_{clouds} = number density clouds/Pc^3
$m = 2.8 \times 10^4 \, T^{5/2} \, a_{pc} \, \Phi$ g/s (Φ = efficiency)
= thermal evaporation rate from single cloud,

then

$$T = \frac{0.7 \, \bar{m} \, E}{3 \, Mk} = 1.7 \times 10^9 \, E_{51} \left\{ \frac{M}{M_\odot} \right\}^{-1} {}^\circ K$$

and $$M = \frac{4 \, \Pi}{3} \, R_{pc}^{\,3} \, n_{clouds} \, m$$

This can be integrated to give

$$M = 16 \, R_{pc}^{\,4/3} \, E_{51}^{\,2/3} \left\{ \frac{n_{clouds} \, \Phi \, a_{pc}}{\alpha} \right\}^{1/3} M_\odot$$

or $$n = 130 \, R_{pc}^{\,-5/3} \, E_{51}^{\,2/3} \left(\frac{\sigma}{\alpha} \right)^{1/3} cm^{-3}$$

where $\sigma = n_{clouds} \, \Phi \, a_{pc}$

α is an indeterminate parameter of order unity which is best determined by comparison with the numerical solutions. Setting standard parameters of $f_{wm} = 0.23$, $a_{pc} = 2.3$ and $\Phi = 1$ (or $n_{clouds} = 6 \times 10^{-3}$ Pc^3 to σ define standard $= 1.2 \times 10^{-2}$ gives:

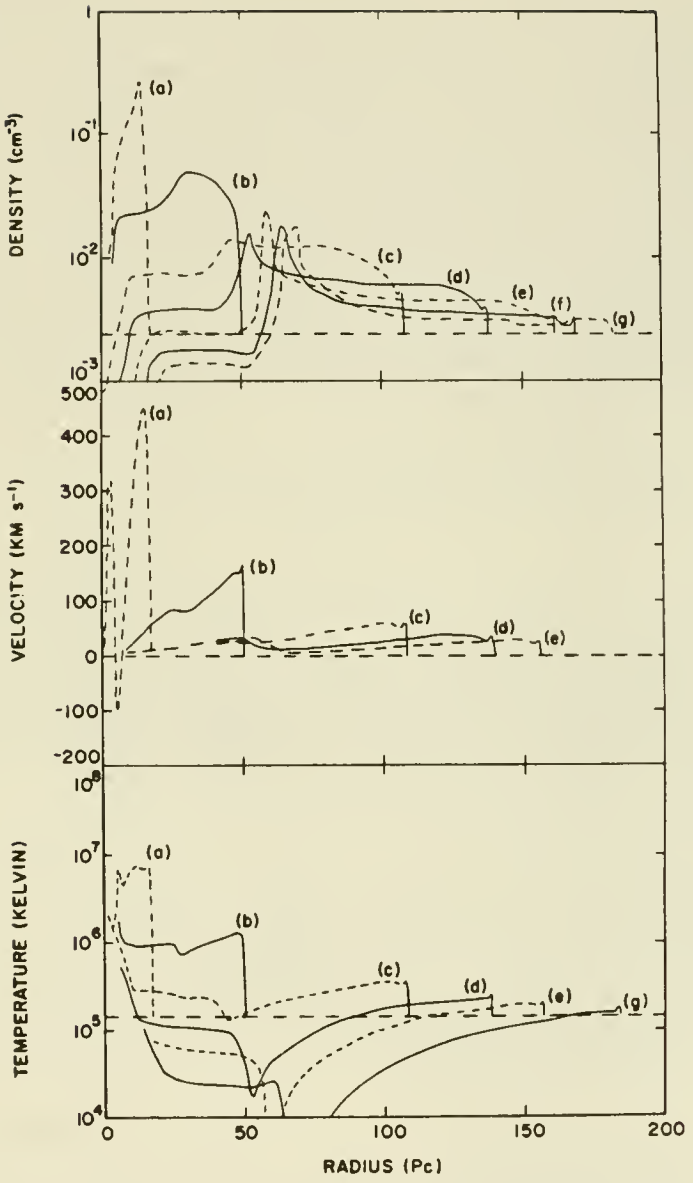

Figure 1 Density, velocity and temperature of hot gas within an evaporative supernova remnant at various timesteps. (From Cowie, McKee and Ostriker 1981). The parameters of the remnant (model 1 of CMO) are discussed in the text. Ages are a = 1.01×10^4 yrs., b = 9.9×10^4 yrs, c = 4.6×10^5 yrs, d = 7.7×10^5 yrs., e = 9.8×10^5 yrs., f = 1.21×10^6 yrs., g = 1.36×10^6 yrs. Stage (b) corresponds most closely to the radius, age and density of the local region, but for the assumed model parameters the density of the hot gas is too high.

$$n = 40\ R_{pc}^{-5/3}\ E_{51}^{2/3} \left\{ \frac{\sigma}{\sigma_{\text{standard}}} \right\}^{1/3}\ cm^{-3}$$

The rapid fall-off in interior density radius and age is another striking difference between evaporative and Sedov models. The final striking difference of the evaporative solutions (and the one I like best) is that they go radiative in the interiors rather than at the edge (c,f, Fig. 1). This is just a consequence of the constant density and temperature profiles, but it is extremely useful because cooling occurs at low velocities. As Ed Jenkins discussed in his presentation, observationally we cannot let cooling occur at high velocities (Cowie and York 1978) because low column density material in ionization stages such as Si III and N II is relatively scarce at velocities much greater than about 50 km S^{-1}. This means in turn that evaporative models can achieve radiation balance in the disk and non evaporative models cannot.

Looking out from the interior of the evaporative supernova remnant, one sees ony a slightly lower emission measure than one would see in a Sedov solution with an ambient density equal to the average interior density. This means that we can draw on the results of Cox and Anderson for example (at least to the degree of some uncertainty in the ionization balance) and that we should have temperatures of about 10^6 °K, a radius of about 100 Pc, and an average interior density of about 5×10^{-3} cm^{-3}. (We adopt a slightly higher value for the density than Cox and Anderson because the interior density is more uniform.)

This means in turn that we need a σ which is about 15% of my so- called standard value. This is probably mainly caused by inefficiency in the evaporative process (MO suggest = 1/3) but could also correspond in part to the possible local deficiency of material by factors of 2 or 3. The accuracy of the prediction is actually remarkably good however, (and it should be emphasized that it is a prediction).

THE DISTRIBUTION OF WARM MATERIAL

A substantial fraction of the interior of the remnant is cleaned of WM by the supernova remnant. There are three contributory processes:

1) WM sweep out
2) WM evaporation

} dominate in earlier stages

3) WM compression — later stages

The numerical solutions show that the last mechanism is probably dominant by radii of 100 Pc. The rise in pressure by about a factor of four or five reduces the volume of the WM by a corresponding amount given a fixed heating source. However, it does take a finite time to compress, and after entering the remnant, WM "clouds" will remain through a region of approximately

$$R = \left\{ \frac{n_{WM}}{n_{Hot}} \right\}^{1/2} a \quad \approx 10 \text{ a or rougly 20-25 Pc}$$

The sun probably should lie in this region because the local heliospheric hydrogen and helium measurements suggest pressure of less than 2000 $^{o}K\ cm^{-3}$ which is almost an order of magnitude lower than the remnant pressure. (As Ed Jenkins pointed out during the conference, searching for surface motions of this very local WM driven by the remnant pressure might provide a very interesting test of this point. However, as Don Cox pointed out, magnetic field pressure might allow us to avoid it.)

I've illustrated this schematically in figure 2 and initially looking at this one might worry about isoptropy. However, in the Sedov, and to a lesser extent, the evaporative models the outer regions dominate and as long as one is interior to most of the emission, it will appear rougly isotropic.

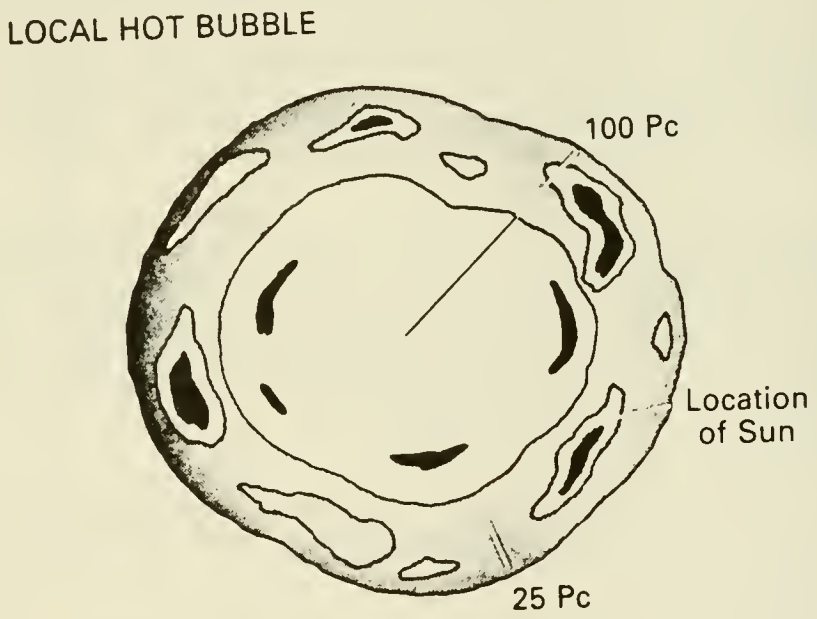

Figure 2 A schematic illustration of the local hot bubble. Cold dense material is shown by the darkest shading and is spread throughout the region. Regions of warm material only survive in the outer regions where they may not yet have come to pressure equilibrium with the hot gas. (The sun is shown as lying in such a region). The density of the hot gas is slightly lower to the center and higher towards the outside edge as illustrated by the uniform shading. The dimensions indicated are quite approximate.

O VI AS A DIAGNOSTIC OF THERMAL EVAPORATION

Apart from the theoretical considerations about energy balance there is little to choose between the models to this point and to my mind the key diagnostic between evaporative and non evaporative models is the local O VI (Jenkins 1978). Of the eight stars observed by Jenkins, within 100 Pc and tabulated in Table I, three have been detected in O VI with column densities around 10^{13} cm^{-2}; the remaining stars are undetected. (In one or two cases at significantly lower levels.)

TABLE I

LOCAL OVI OBSERVATIONS OF STARS WITHIN 100 PC

	DISTANCE (Pc)	LOG N(OVI) (cm^{-2})	(l,b)
αLEO	25	$\leq$13.4	226,49
αGRU	25	$\leq$12.9	350,-52
ηU Ma	30	$\leq$12.4	100,65
αER3	40	13.1	291,-59
σSGR	65	$\leq$12.9	10,-12
δPER	80	$\leq$13.7	150,-6
αVIR	85	13.4	316,51
ζCEN	100	13.1	314,14

The evaporative model finds it easy to interpret these results. With substantial WM destruction, the O VI arises on the evaporative surfaces of cold clouds or on residual WM clouds. From Cowie, Jenkins, Songaila and York (1980) (CJSY) each cloud has a column density (both surfaces included) of

$$N_{O\ VI} = 6 \times 10^{12} \left\{ \frac{\beta}{3} \right\} T_6^{-3/2}\ a_{pc}\ n_{-2}\ cm^{-2}$$

where the β factor allows for time dependent ionization effects. For $a_{pc} = 2.1$ $n_{-2} = 0.6$, $N_{OVI} = 7 \times 10^{-12}$ cm^{-2} and intersection of a single cloud can give the positive detections. Sheets with longer dimensions would give a somewhat larger value (Cowie and Songaila 1977) since the OVI column density depends roughly linear on the longest dimension. The measured mean free path to individual O VI regions is roughly 120 Pc, which again suggests some deficiency of cold local material. Apart from accounting for the discrete nature of the detections, this mechanism also nicely accounts for the velocity width and velocity structure of the O VI and its correlation with lower ionization stages (CJSY), as Ed Jenkins has emphasized in his talk. In the final figure (3), I've illustrated this with some examples including the nearby α Vir.

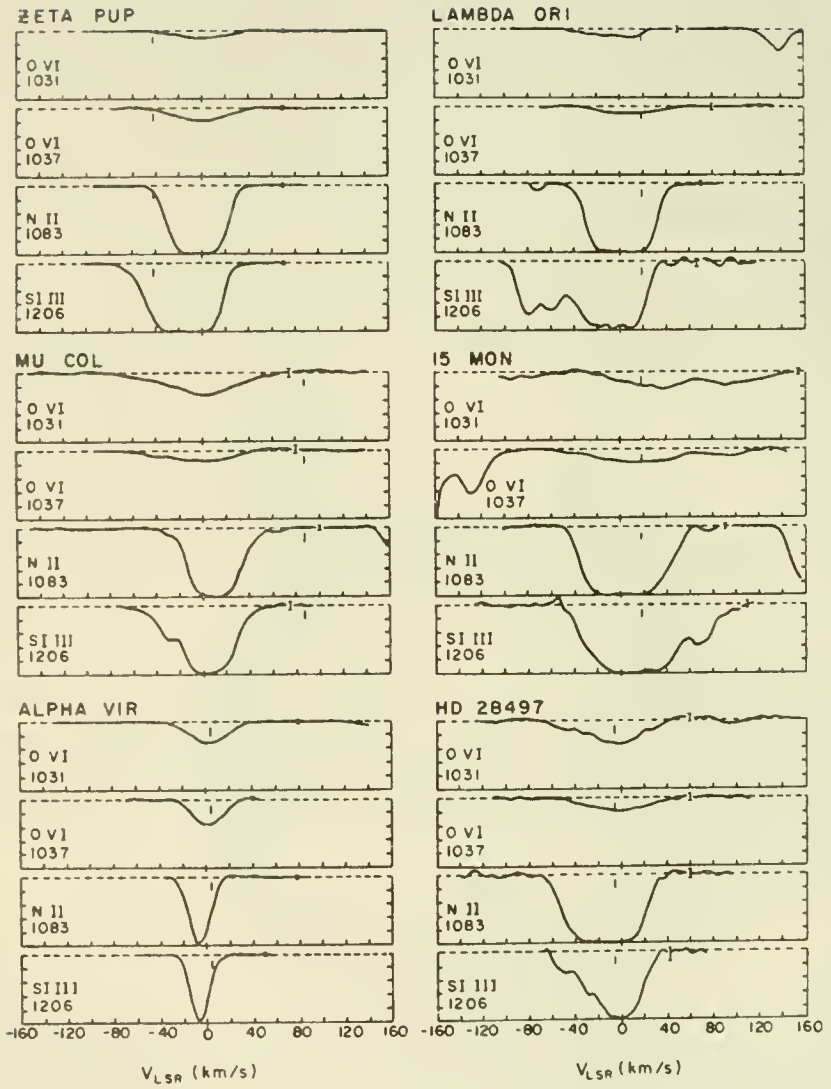

Figure 3 Profiles of OVI lines are shown in comparison with the lower ionization stages (from Cowie, Jenkins, Songaila and York (1980)). All the profiles have been normalized to second order polynomial continua and plotted against LSR velocity. (Wider OVI components could be hidden by this procedure) α VIR lying at 85 Pc has the simplest and narrowest profiles.

The Sedov models get into severe trouble with the OVI, however. There is little OVI production in the interior of the remnant which is too hot and too difuse. If the preshock material is in low ionization stages, one can get enormous amount of OVI in the shock front (C.F. Cox and Anderson 1982), but this would be at velocities of several hundred km s^{-1}. Therefore, stars with observed OVI must lie outside the blast wave and in the ambient material. Fortunately, all the stars with observed OVI do lie to one side so that this interpretation is at least possible, particularly since I have argued above that we may be close to the edge of the remnant. However, there still seems no way to account for the near zero velocity, narrow velocity character of the OVI nor for its correlation with lower ionization stages.

CONCLUSIONS

The conclusions from all of this would seem to be

1. A Multiphase SNR does seem to provide a plausible description of the local ISM.

2. The local region could quite likely have been deficient (by about a factor of 2-3) in cool gas prior to the supernova both on theoretical and observational grounds. However, there are no totally compelling arguments for this as yet.

3. The sun may lie in a region towards the outside of the supernova remnant which hasn't yet come into pressure equilibrium with the hot gas.

4. Evaporative models give a much more satisfactory description of the OVI observations than Sedov Solutions.

ACKNOWLEDGEMENTS

This work was supported in part by NASA grant NAGW464 and by a Fellowship from the Alfred P. Sloan Foundation.

References

Cowie, L.L., Jenkins, E.B., Songaila A., and York, D.G. 1980, Ap. J. 232, 467.

Cowie, L.L., McKee, C.F., and Ostriker, J.P. 1981, Ap. J. 247, 908.

Cowie, L.L. and Songaila, A. 1977 Nature 266, 501.

Cowie, L.L. and York, D.G., 1978 Ap. J., 223, 876.

Cox, D.P. 1979, Ap. J. 234, 863.

Cox, D.P. and Anderson, P.R., 1982 Ap. J. 253, 268.

Cox, D.P. and Smith, B.W. 1974 Ap. J. (letters) 189, L105.

Jenkins, E.B. 1978 Ap. J. 219, 845.

McKee, C.F. and Ostriker, J.P. 1977 Ap. J. 218, 148.

Paresce, F. 1984 submitted to Astronomy and Astrophysics.

Spitzer, L. 1977 "Physical Processes in the Interstellar Medium" (New York: Interscience).

Spitzer, L. 1982 Ap. J. 262, 315.

A Model of the Soft X-Ray Background as a Blast Wave Viewed from Inside

Richard J. Edgar and Donald P. Cox[1]
Space Physics Laboratory, Department of Physics
University of Wisconsin-Madison

ABSTRACT

The suggestion that the soft x-ray background arises in part from the Sun being inside a large (R ~ 100 pc) supernova blastwave is examined by producing models of spherical blastwaves. Such models can produce quantitative fits to both surface brightnesses and energy band ratios (for the lowest energy bands) when $t \sim 10^5$ yr, $E_o = 5 \times 10^{50}$ ergs, and $n_o \approx 0.004$ cm^{-3}.

Such models can be generalized by varying the relative importance of such factors as thermal conduction, Coulomb heating of electrons, and external pressure; by allowing the explosions to occur in pre-existing cavities with steep density gradients, or by examining the effects of large obstructions or other anisotropies in the ambient medium.

I. INTRODUCTION

One suggestion that has been advanced (e. g. McKee and Ostriker 1977) to explain the soft x-ray background ($0.1 \lesssim E \lesssim 1.0$ keV) is that the solar system lies within a blast wave of present radius ~100 pc which was caused by a sypernova.

Cox and Anderson (1982, CA) examined this idea quantitatively by producing spherical blast wave models in a uniform ambient medium (with finite pressure). By following the ionization history of each gas parcel as it is shocked and moves into the interior of the supernova remnant (SNR), it was possible to calculate x-ray spectra despite the fact that the ionization state of the gas is far from equilibrium in the x-ray emitting region. It was found that essentially all of the emission comes from quite near the shock, so that the location of the observer within the bubble is unimportant.

The CA models produced qualitative agreement with the all-sky average count rates measured by the Wisconsin group (McCammon et al 1983 and references therein) in the lowest energy bands. Both surface brightness and the band ratio B/C (analogous to B-V colors in the optical) could be fit for the boron (B) and carbon (C) bands. These fits constrained the ambient density closely to $n_o = 0.004$ cm^{-3}, and

[1] Also, Department of Space Physics and Astronomy, Rice University

suggested that the age of the SNR is roughly 10^5 yr, for explosion energy $E_o = 5 \times 10^{50}$ ergs.

Current efforts are directed to answering questions such as the following, representative of those suggested by the CA study.

(1) CA produced a set of SNR parameters (n_o, shock radius R_s, age t) that fit the B and C band data for $E_o = 5 \times 10^{50}$ ergs. What ranges can these parameters take on without substantially impacting on the quality of the fit?

(2) How would these ranges change if E_o is allowed to vary?

(3) Is it possible (for example, by setting off the explosion in a pre-existing cavity) to make models that will produce a more significant fraction of the M-band (medium energy) flux that is observed?

(4) Are there parameter choices for which the x-rays could be produced without at the same time generating a large local O VI component?

(5) Is it possible that the soft x-ray background arises from a much older (and hence larger) cavity than those studied by CA? If so, the solar system need not be situated in quite such a special place for the models to apply.

(6) Can the observed variations in the B and C bands over the sky be explained as the result of moderate variations in the pre-shock ambient density? For example, if large clouds were present in some directions (and not in others) prior to the explosion, would the resulting non-spherical blast wave exhibit variations in surface brightness correlated (or anti-correlated) to the H I column densities?

II. BLAST WAVES IN CAVITIES

Cox and Franco (1981), Cox and Edgar (1983) and Edgar and Cox (1984, in press) have produced dynamical models of blast waves in cavities in an attempt to address these questions. Such a cavities might have been produced by the previous supernovae of members of an OB association so that the present explosion finds the ambient density rising steeply with R. In particular, we have explored the cases with $n_o \propto R^0$, R^2, and R^4 (uniform density and two steepnesses of cavities) with models which include non-Coulomb shock heating of electrons and the consequent significant (and partially saturated) thermal conduction flux. Representative structures are shown in Figure 1 for the R^4 case. Figure 1a shows pressure profiles of five snapshots at various radii as the SNR expands. Figure 1b shows electron (dashed lines) and average (solid lines) temperature profiles, and figure 1c shows density structures, as well as the ambient and post-shock densities (lower and

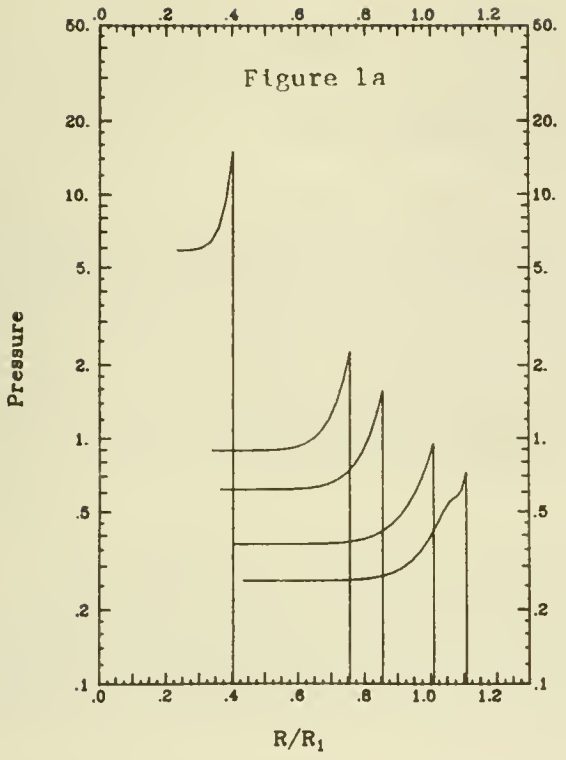
Figure 1a
Pressure
R/R1

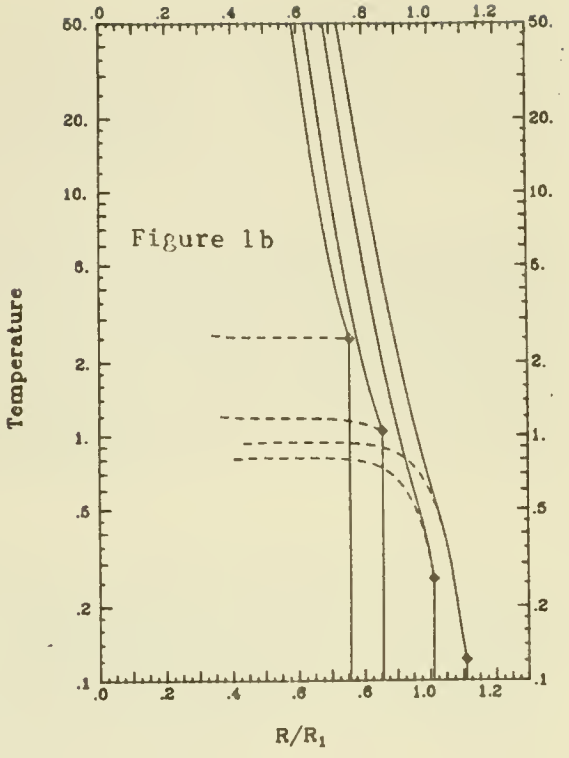
Figure 1b
Temperature
R/R1

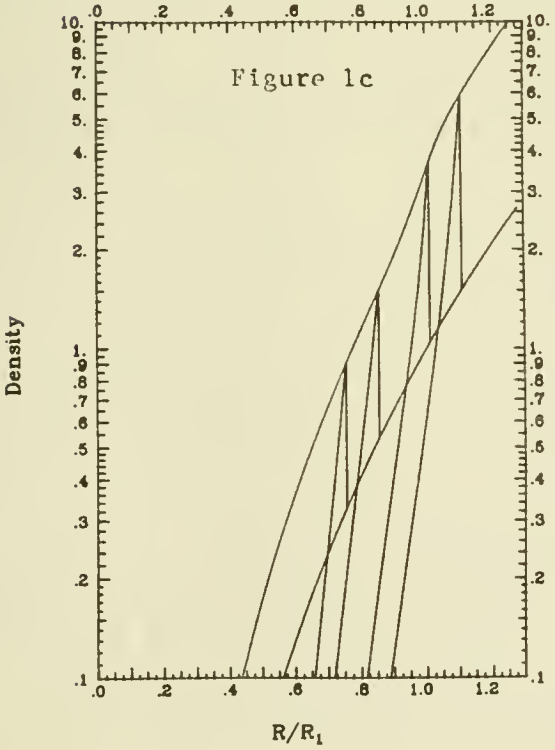
Figure 1c
Density
R/R1

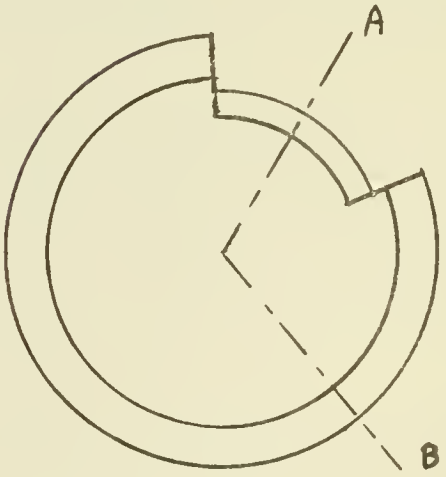
A
B

Figure 2

upper envelopes, respectively). Present work includes producing model spectra for a class of such cavity models. Models produced to date for the R^4 case show comparable spectral results to those of CA, but with thinner emission regions and hence higher present-day ambient densities ($n_o \sim 6\text{-}10 \times 10^{-3}$ cm^{-3}) for similar counting rates.

III. LARGE OBSTRUCTIONS IN THE AMBIENT MEDIUM

As a first approximation, we are modelling such things as large clouds protruding into the pre-existing cavity as follows. Let the ambient density $n_o \propto R^4$, but pick the constants of proportionality to be larger in some directions (toward the cloud, A), producing an ambient density contour plot like Figure 2. We then use two carefully selected spherically symmetric blast wave models to compare the two regions A and B. Clearly, with this crude level of approximation, nothing can be said reliably about the edges of the "cloud".

The two spherical blast wave models are selected to have equal ages and the same central pressure history (since the interiors of the two remnants clearly communicate). They need not have the same (or even simply related) explosion energies E_o; indeed, we adjust E_o to satisfy the above constraints. It can be shown that the smaller remnant A reaches maturity faster than the larger remnant B, because it processes more material in a given period of time.

One such pair of models has been generated, and suggests that in fact the cloud (direction A) is somewhat brighter in the B and C bands. Further work is needed in this area, especially as a general anticorrelation between soft x-ray brightness and H I column density is observed (e. g. McCammon et al 1983). Our present result, that directions with higher densities will be brighter rather than dimmer, was anticipated from scaling CA results. However, this scaling should fail as the blast waves in the clouds slow to very low velocities, and it is our expectation that the observed anticorrelation can be accommodated by modelling the hot central regions of blast wave pairs older than those studied by CA. We expect to succeed in suppressing the O VI column density as well, though again only in the more mature remnants.

REFERENCES

Cox, D. P. and Anderson, P. R. 1982, Ap. J., 253, 268.
Cox, D. P. and Edgar, R. J. 1983, Ap. J., 265, 443.
Cox, D. P. and Franco, J. 1981, Ap. J., 251, 687.
Edgar, R. J. and Cox, D. P. 1984, Ap. J., 283, in press.
Jenkins, E. B. 1978a, Ap. J., 219, 845.
Jenkins, E. B. 1978b, Ap. J., 220, 107.
McCammon, D., Burrows, D. N., Sanders, W. T., and Kraushaar, W. L. 1983, Ap. J., 269, 107.
McKee, C. F., and Ostriker, J. P. 1977, Ap. J., 218, 148.

NON EQUILIBRIUM IONIZATION IN THE LOCAL HOT BUBBLE

M. Arnaud, R. Rothenflug, R. Rocchia
Service d'Astrophysique - CEN Saclay -

ABSTRACT. Soft X-ray surveys proved the existence of a local hot bubble surrounding the solar system (Mc Cammon et al 1983). Recently two experiments measured the spectrum of this hot interstellar medium with solid state detectors during rocket flights between 300 and 1000 eV (Rocchia et al 1984). The good resolution of the experiment permitted to measure CV, CVI and OVII line emissivities with good accuracy. We use these data to put some constraints on a model where the emission comes from a supernova remnant expanding in a finite pressure medium (Cox and Anderson 1982). We show the importance of non equilibrium ionization phenomena.

1. INTRODUCTION

In a recent paper, Rocchia et al (1984) reported spectral observations of the soft X-ray background between 0.3 and 1 keV with solid state detectors. One of their spectra is characteristic of the local hot bubble, and concerns a part of the North Galactic hemisphere including the Hercules Hole and the North Galactic pole. This spectrum exhibits features identified with lines of CV-CVI around 300 eV and OVII around 530 eV.

In this paper, we use these data to put some constraints on a model where the emission of the soft X-ray background comes from a supernova remnant surrounding the solar system. Such a model was previously developed by Cox and Anderson (1982) in order to reproduce the X flux in the so-called B band (130-188eV) and C band (160-284 eV).

2. HYDRODYNAMICAL MODEL AND METHOD FOR COMPUTING THE IONIZATION STRUCTURE

Gaffet (1978) proposed a simple analytical approximation for the hydrodynamical evolution and the structure of a supernova in the case where the external medium pressure is not negligeable with respect to the shock pressure. The model parameters are E_o , the explosion energy and n_o , T_o the external electronic density and temperature. In this first approach, we fix the dimension of the remnant to R_S=80pc which is equivalent, for a given set of parameters, to settle the age of the remnant. This dimension corresponds to the maximum radius we established for the local hot bubble from studies of soft X-ray absorption by an interstellar cloud (Arnaud, Rothenflug 1984a). We also settle the external temperature to $T_o = 5.10^5$ K (see Mc Kee, Ostriker 1977).

In order to calculate the X-ray spectrum of such a remnant, the ionization structure must be determined in following the history of each shell from the time it is shocked until the time to be considered. The method we follow is very similar to the method described by Cox and Anderson (1982). The derivatives of each ionization stage of each element were integrated numerically by an implicit method of the Runge-Kutta type. Fifty shells were followed, divided in such a way to obtain a great number of shells near the shock where the conditions vary very quickly. The ionization and recombination rates we used are taken from an up-to dated evaluation we recently made (Arnaud, Rothenflug, 1984b).

3. THE SOFT X-RAY SPECTRUM

We reproduce in figure 1 the soft X-ray spectrum of the local hot bubble discussed in Rocchia et al (1984). The contribution of the various components to the total spectrum is depicted in the figure. Instead of calculating the total spectrum with our model, we extracted from the data the intensities of lines corresponding to the (CV + CVI) blend and to the OVII ion. To do so, we assumed that the continuum in our non equilibrium model will have about the same low intensity than that of figure 1. Moreover, we do not use N VI intensity as a constraint, since its intensity is about the same as the continuum intensity.

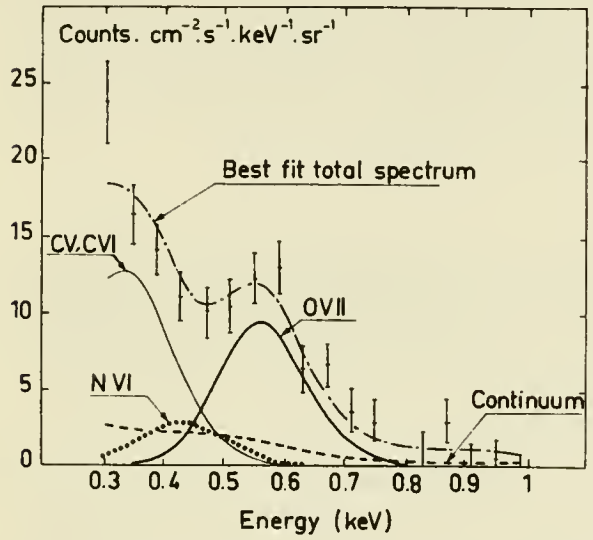

Fig.1 : Contribution of the various ion species to the local hot bubble spectrum (Rocchia et al 1984). The dot-dashed curve is the total spectrum. The dashed curve shows the contribution of the continuum (bremsstrahlung + recombination radiation). Small contributions of several species of S,Si,Fe, are not depicted.

To obtain the statistical uncertainties on each line, we followed the method described by Inoue et al (1980). We corrected for the detector sensitivity and for an interstellar absorption of $\sim 6.10^{19}$ H atoms/cm^2 (Inoue et al (1979). We obtained the following figures :

CV + CVI 45 ± 9 photons/cm^2.s.ster.

O VII : 4 ± 0.9 photons/cm^2.s.ster. (error at the 99% confidence level).

4. CONSTRAINTS ON THE MODEL

Once fixed the supernova remnant radius R_S and the external temperature T_o , two parameters, E_o and n_o remain free. It is more convenient to use the couple E_o and T_S , where T_S is the temperature just behind the shock. Indeed, one can show, from the work of Gaffet, that for a given set of R_S , T_S and T_o , both the temperature profile and the reduced density $(n(r)/n_o)$profile do not depend on E_o. The ionic fraction profiles do not vary in a so simple way on E_o, because the collisionnal ionization and recombination times are proportional to the true value of the density. However in the emissive region, i.e just behind the shock, ionic fractions of CV, CVI and O VII do not strongly depend on n_o (and E_o), for a given set of R_S ,T_S and T_o .

This explains why both the intensities of (CV + CVI) lines and O VII lines are proportional to n_o (for R_S , T_S ,T_o fixed) and that the intensities of both set of lines

are proportional. This is illustrated in figure 2 where we plotted the variation of the CV + CVI line intensity in function of the OVII line intensity, for different values of E_o and T_s (with fixed values of R_s = 80pc, $T_o = 5.10^5$ K). The dashed contour delimits the constraints given by our observational data on the line intensities. The constraints on (E_o, T_s) can be transformed in constraints on (E_o, n_o) as shown in figure 3 : our data lead to relatively tight constraints on the values of E_o and n_o. A good agreement with the data is reached for $E_o = 6.\ 10^{50}$ ergs, $n_o = 1.8\ 10^{-2}$ cm^{-3} ($T_s = 1.1\ 10^6$ K).

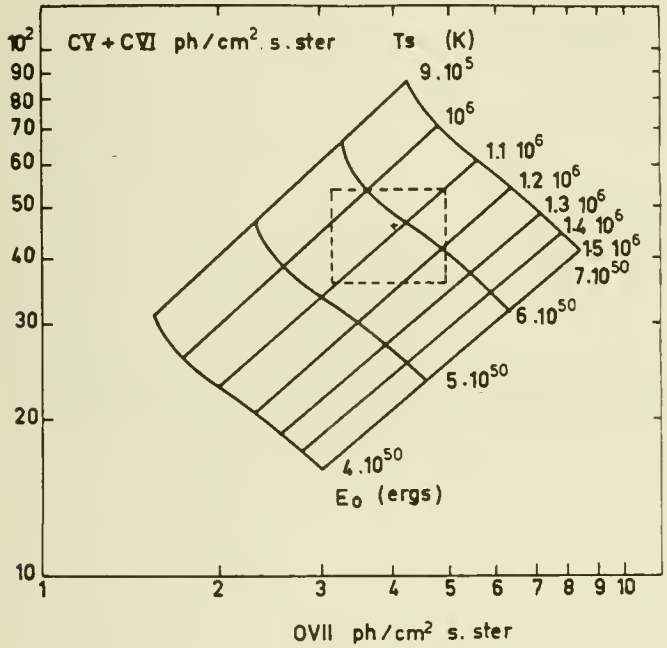

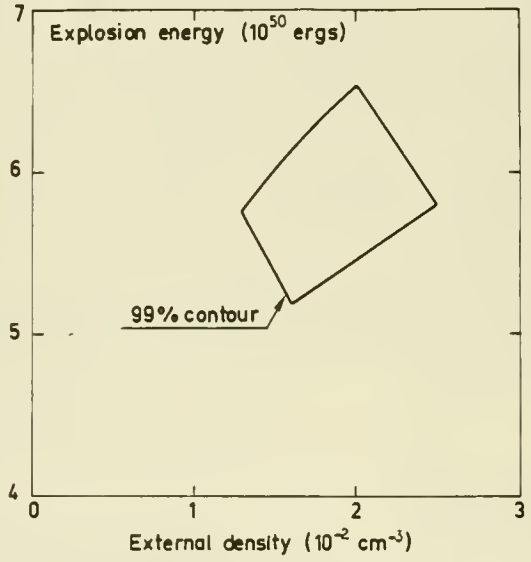

Fig.2 : Full lines: (CV + CVI) and OVII line intensities computed in our model for different values of E_o and T_s. Dashed line : intensity range allowed by observations.

Fig.3 : 99% confidence contour on the parameters.

For this set of parameters, the ionic fraction profiles of C and O ions are depicted in figure 4, in comparison with their values in ionization equilibrium. If the O VII (helium-like) ion pratically keeps its equilibrium value in the most emissive region, just behind the shock, carbon ions present a strong ionization delay.

In addition, for the range of parameters determined from the X-ray spectroscopic measurements by Rocchia et al (1984), we deduced an OVI volumn density N OVI = 2 - 7 10^{12} ions cm^{-2}, quite coherent with the values deduced from UV spectroscopy in the direction of nearby stars (Jenkins 1978).

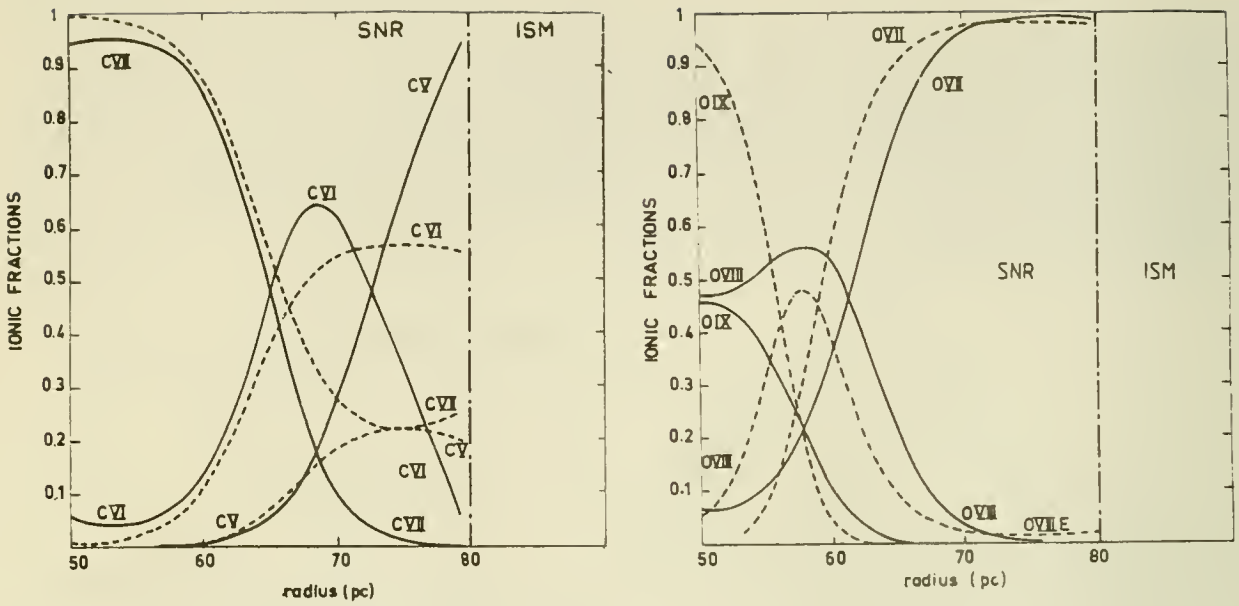

Fig.4 : Ionic profiles behind the shock for the set of parameters corresponding to the best fit. Full curve: non-equilibrium values. Dashed curve: equilibrium values

REFERENCES

Arnaud M., Rothenflug R. 1984a A.A. (in press)
1984b A.A. (in press).
Cox D.P., Anderson P.R.1982, Ap.J. 253, 268.
Gaffet B. 1978, Ap.J. 225, 442.
Inoue H., et al 1979, Ap.J.(Lett) 227, L85.
Inoue H., et al 1980, Ap.J. 238, 886.
Jenkins E.B., 1978, Ap.J. 219, 845.
Mc Cammon D., et al 1983, Ap.J. 269, 107.
Mc Kee C.F., Ostriker J.P., 1977, Ap.J. 218, 148.
Rocchia R., et al 1984, A.A. 130, 53.

LARGE-SCALE BUBBLE STRUCTURE OF THE INTERSTELLER MEDIUM (ISM) AND PROPERTIES OF THE LOCAL SPIRAL ARM (LSA)

Nikolay G. Bochkarev
Sternberg State Astronomical Institute, Moscow, USSR

ABSTRACT

Bubbles are very common structure units in the Galaxy and galaxies. Collection of radio, optical, infrared and x-ray observations of the Cyg superbubble (CSB) region of the sky show that the CSB is not a single bubble object. Between 50 to 75 percent of its x-ray emission can be ascribed to discrete sources. The other 25 to 50% x-ray emission, probably originates from bubbles around 8 OB associations of the region. All bubbles located within the spiral structure of Galaxy, M31 and M33 have diameter $\lesssim$ 300pc.

The large distance of stellar association from the galactic plane (GP) combined with picture of the gas distribution within the LSA shows that a Reyleigh-Taylor instability in the LSA can develop and give use to the formation of compact steller clusters, such as the Cyg OB2 association. Development stages of the Reyleigh-Taylor instability, some peculiarities of the dust distribution and departures of the local structure from the galactic grand design suggest the absence of a spiral shockwave in the LSA.

I. Giant and Supergiant Ring Structure in the Intersteller Medium

Numerous HII shells about 100-200pc in size and several HII shells up to about 1 kpc in size have been found in the Magellanic Clouds (Goudis and Meaburn, 1978; Meaburn 1980). Some spiral galaxies have been found to contain HII bubble regions inside of the spiral structure up to about 300pc in diameter (see summary of Sharov's Data [1982] on M31 and M33).

In Galaxy large-scale shells are usually distinguished not from optical but from other ranges of radiation. Heiles (1979, 1984) found about 100 HI supershells in the Galaxy, while Georgelin et al. (1979) observed there 13 giant HII shells. Also described were two large bubbles showing soft x-ray radiation, one in the Orion and Eridanus, associated with the star formation complex in Orion (Reynolds and Ogden, 1980; Goudis, 1982) and others associated with Seo-Cen association and the North Polar Spur (Weaver, 1979, 1984). Nevertheless the very large (75°) Gum nebulae is not apparently a single object, because it does show x-ray radiation (e.g., Reynolds, 1976).

II. Cygnus Superbubble (CSB)

In connection with the data of section I, special attention was put to a giant (13°x18°) horseshoe shaped source emitting soft x-rays. This is the Cyg Superbubble discovered by Cash et al (1980). They suggested that the CSB corresponded to a ring of optical filaments (15°x13°) noted by Ikhsanov (1960), Dickel et al. (1969) and Brand and Zealey (1975) and to the Cyg OB2 association, located on the distance 2 kpc from the sun. In this case, sizes of the CSB equal 450 x 600pc, that is it could be the largest shell inside the spiral structure of our Galaxy.

Bochkarev and Sitnik (1983, 1984) showed that the CSB is a projection on the sky of many sources, located at different distances from the sun within

the LSA, along which we are looking in the Cygnus direction. The main arguments against the singular nature of the CSB are: (1) Greater elongation of the CSB along the GP (18°) than across it (13°). For a quasipoint source of energy, as suggested by Cash et al. (1980), Higdon (1981), Abbott et al. (1981), Blinnikov et al. (1982), and a bubble size that exceeds the thickness of the gas disk (200-300pc), the CSB must show greater elongation across the GP, as found for the Ori-Eri region. (2) Comparison of the surface brightness of the ring of filaments in optical and radio radiation showed that the ring is not a single structure (Kapp-herr and Wendker, 1972). (3) Multicompnent radio source Cyg X which covers ~ 1/4 the CSB region is also a projection on the sky of objects located over 1-4 kpc from the sun (Dickel et al. 1969, Dickel and Wendker, 1978). (4) CSB radioradiation does not show any large-scale envelopes of thermal or nonthermal originations. (5) Comparison of the x-ray spectrum of the CSB (according to Cash et al., 1980) and individual parts of it, Cyg X-6 and Cyg X-7 (Davidsen et al., 1977) and also SS Cyg (Cordova, 1981) show that in spite of the statement by Cash et al., the CSB spectrum is, apparently, inhomogenious (Bochkarev and Sitnik, 1984). (6) According to Bochkarev and Sitnik (1983, 1984) 50-75% of the x-ray emission of the CSB originates from ~ 20 faint x-ray sources included mainly to Amnuel et al. (1982) catalogue. In particular, Higgs et al. (1982) discovered that in spite of Cash et al's. (1980) opinion the brightest part the CSB Cyg X-7 is the SNR DR4, as was suggested by Davidsen et al. (1977). The region of interest includes many other active objects capable of radiating x-rays: among them 8 OB-associations, 110 stars of superhigh luminosity (Hamphreys, 1978), about 15% galactic Of stars from Losinskaya's (1982) list and about 15% of the galactic WR stars from the list of Hucht et al. (1981).

Bochkarev and Sitnik (1983, 1984) concluded that 25-50% of the CSB x-ray emission which is not radiated by known x-ray sources is emitted by giant envelopes blown by the 8 steller association of the CSB region. Good correspondence of position on the sky with maximum of x-ray emission and the associations and gas and dust ring structures recognized by Brand and Zealey (1975) around the associations suggest this conclusion. Strong interstellar absorption and the low temperature of sources contribution to x-radiation of the CSB result in the similarity of the spectra of all components of the CSB (Bochkarev, 1984, Bochkarev and Sitnik, 1984).

III. On the Nature of the Giant Envelope around Stellar Associations

The quantative analysis by Bochkarev and Sitnik (1984) shows that for producing of caverns with observed radiation each amoung 8 OB association in the CSB region must have blown $3 \cdot 10^4 - 3 \cdot 10^5$ $M_\odot$ of ISM. It is a typical mass for giant molecular clouds from which associations can be formed. A similar result was found by Dopita et al. (1981) for shell N70 (diameter ≈ 120pc) in the LMC.

Stellar winds of average total power $\langle L_w \rangle \gtrsim (3-5) \cdot 10^{35}$ erg/s are necessary for the formation of such gas caverns. But such L_w is very great for a typical OB association averaged over $(2-10) \cdot 10^6$ years, because only during short supergiant evolutionary stages of massive stars have $L_w \sim 10^{35}$ erg/s. Important contributions to $\langle L_w \rangle$ can come from WR and Of stars which produce strong winds of $\sim 10^{37}$ erg/s (Abbott, 1982; Bochkarev and Sitnik, 1984).

Large contributions to cavern formation can be produced by SN explosions in stellar associations (Bruhwailer et al., 1980). Total contribution of SNR

to support of peculiar movements of the ISM is ≈ 90% (Salpeter, 1979). But inside of OB associations the contribution must be lower as a result of (1) absence of SNI in the associations; (2) presence of a large quantity of high luminosity stars with strong stellar winds. Therefore within bubbles surrounding young OB associations appoximately equal contibution can be expected from L_w and impulse from SN explosions, WR stars and other stars.

To estimate exactly the corresponding contributions to cavern energy is not possible in view of indeterminate and, probably, nonuniversality of the initial mass function (Freeman, 1977; Zasov and Demin, 1979) and also the small number of stars in individual association and consequently large statistical deviations from an average value. Frequency of SN explosions in association and kinetic energy ejected by the most massive stars are also very uncertain (see Bochkarev and Sitnik, 1984).

Thus, the diffuse component of the CSB x-ray emission is, probably, traceable to ≈ 8 caverns surrounding associations located on 0.5 -2 kpc from the sun in the LSA. It may be that 30-40% of the CSB is occupied by a cavern around unusual Cyg OB2 association (Bochkarev and Sitnik, 1984).

According to the calculations of Castor et al. (1975) and Weaver et al. (1977), the gas caverns must be surrounded by cold gas envelopes. For parameters typical for the caverns (R ~ 50pc, $t=(2-10)\cdot10^6$ yrs) the cold envelope must have column density ~ $10^{21}cm^{-2}$ and, therefore show important interstellar extinction (~ $0.^m5$). That means that around OB associations dust envelopes can be present. Such envelopes were discovered by Brandt and Zealey (1975).

IV. A Rayleigh-Taylor(RT) Instability and a Structure of the Local Spiral Arm

Stellar associations in the western part of the CSB located near tops of sinous-like system of gas filaments (Bochkarev and Sitnik, 1983) correspond to Pikel'ner's (1970) scenario of association formation by RT instability. Some of the association in the CSB region are distant from the GP. These assiciations have distances < 2 kpc from the sun, where curvature of the GP is not important. Therefore large distances from the galactic equator correspond to locations of the association out of the GP. Two other caverns found in the LSA (Ori-Eri region and cavern connected with Sco-Cen association discussed by Weaver, 1979, 1984) are also formed by associations on large distances (≈100 pc) from the GP.

Formation of associations at large distances from the GP are a difficult point for any mechanisms except the RT instability. However inside of spiral structures of S-galaxies, star formations by slow developing RT instability must be prevented by spiral shockwaves, which stimulate star formation inside the inner parts of spiral arms on shorter time scales than the RT instability. As a result, the RT instability can split the matter in gas-dust complexes, which are converted into a star formation region by spiral shocks before then RT instability forms massive stellar clusters. Thus, the presence of spiral shockwaves prevents the formation of objects similar to young globular clusters of Magellanic Clouds, as was suggested, e.g., by Efremov (1979).

But very compact (0.1 degree on the sky or 17 x 28pc) and massive ($(3-6)\cdot10^4$ $M_\odot$) stellar association Cyg OB2, which was studies in detail by Reddish et al. (1966), is very similar to young glubular clusters of the Magellanic Clouds. This fact can be very easily understood assuming that the LSA has no spiral shockwave. Such an assumption agrees with reconstructions of the galactic grand design by Georgelin and Georgelin (1976), Mishurov et al. (1979) and others, which shows that the sun is located almost exactly in

the middle between spiral arms.

Distribution of the ISM extiction across the LSA also shows peculiarity of the LSA. Uranova (1984) discovered that the distribution has a cut off near the outer side of the LSA and smoothly decreasing to the inner side. Such distribution is difficult to understand in terms of blast wave theory.

The probable reason for the absence of a spiral shockwave in the LSA is close its position to galactic corotation radius. As a result the gas enters into the LSA with undersound speed and does not form a spiral shock-wave.

Thus, it is possible to think that in the LSA absence of the spiral shockwave results in the full development of a RT instability with subsequent formation of stellar associations far from the GP and also very dense ones, such as Cyg OB2. They have formed hot gas caverns, which we can see from the ~ 2 kpc distance because of the caverns located above the obscuring matter.

Typical sized of the caverns are probably ≈ 100-150pc. Such sizes are also typical for other spiral galaxies (Sharov, 1982). These are few examples of supergiant shells with diameters up to 3 kpc in spiral galaxies as given by Heiles (1979b, 1984) in the Galaxy and by Zasov and Kyasumov(1981) in NGC 157. Supergiant rings with diameters of 0.5-3 kpc can originate by Elmegreen and Lada (1977) mechanism where synchronizing action of spiral shockwaves is absent namely in irregular galaxies and outer parts of spiral galaxies.

V. Conclusions

1. Ring structures with diameters 100-300pc are typical kind of large-scale structures of the ISM of spiral and irregular galaxies. Inside of the spiral structure sizes of the rings are probably ≤ 300pc (giant shells) and in IR galaxies and outer parts of S-galaxies together with giant shells are present supergiant shells with diameter >0.5kpc.

2. Observed picture of the x-ray Cygnus Superbubble is a result of projection on the sky of a large quantity of discrete sources and giant envelopes around 8 OB associations in the SCB region. These sources are located at different distances (mainly 0.5-2.5kpc) in the LSA, along which sight lines go to 4 kpc in the Cygnus direction.

3. Giant shells (as emissional as dust) can be produced by winds of stars of stellar association. Approximately equal contributions to shell formation apparently provided by SN explosions, WR stellar winds, and stellar winds of other stars in associations.

4. Positions of a number of stellar association of the LSA far from the GP and presence of the extremely compact and massive Cyg OB2 association suggests good conditions for a full developed RT instability in the LSA.

5. Galactic grand design, distribution of absorption matter in the LSA and evidences of full developing RT instability in the LSA suggests probably the absence of a spiral shockwave in the LSA.

References

Abbott, D.C. 1982, Ap. J., 263, 723.
Abbott, D.C., Bieging, J.H., Churchwell, E. 1981, Ap. J., 250, 645.
Amnuel, P.R., Guseinov, O.H., Rakhamimov, Sh.Yu. 1982, Ap. Space Sci., 82, 3.
Blinnikov, S.I., Imshennik, V.S., Utrobin, V.P. 1982, Pis'ma Astr. Zh., 8, 671, (Sov. Astr. Lett., 8, 361).
Bochkarev, N.G. 1984, Astron. Zh., in press.
Bochkarev, N.G., Sitnik, T.G. 1983, Astr. Tzircular USSR, No. 1261, 1.
Bochkarev, N.G., Sitnik, T.G. 1984, Ap. Space Sci., in press.
Brand, P.W.J.L., Zealey, W.J. 1975, Astr. Ap., 38, 363.
Bruhweiler, F.C., Gull, T.R., Kafatos, M., Sofia, S. 1980, Ap. J., 238, L27.
Cash, W., Charles, P., Boywer, S., Walter, F., Garmire, G., Riegler, G. 1980, Ap. J., 238, L71.
Castor, J., McCray, R., Weaver, R. 1975, Ap. J. (Letters), 200, L107.
Cordova, F.A. Jensen, K.A., Nugent, J.J. 1981, M.N.R.A.S., 196, 1.
Davidsen, A.F., Henry, R.C., Snyder, W.A., Friedman, H., Fritz, G., Naranan, S., Shulman, S., Yentis, D. 1977, Ap. J., 215, 541.
Dickel, H.R., Wendker, H.J. 1978, Astr. Ap., 66, 289.
Dickel, H.R., Wendker, H., Bieritz, J.H. 1969, Astr. Ap., 1, 270.
Dopita, M.A., Ford, V.L., McGregor, P.J., Mathewson, D.S., Wilson, I.R. 1981, Ap. J., 250, 103.
Efremov, Yu. N. 1979, Pis'ma Astr. Zh., 5, 21 (Sov. Astr. Lett., 5),
Elmegreen, B.G., Lada, C.J. 1977, Ap. J., 214, 725.
Freeman, K.C. 1977, in Eds. B.M. Tinsley, R.B. Larson, The evolution of Galaxies and stellar population, (New Haven: Yale Univ. Obs.) p. 133.
Georgelin, J.M., Georgelin, J.P. 1976, Astr. Ap., 49, 57.
Georgelin, J.M., Georgelin, J.P., Sivan,J.-P. 1979 in Ed W.B. Burton Large-scale characteristics of the Galaxy,IAU Symp No.84,(Dordrecht:Reidel),p.65.
Goudis, C. 1982, The Orion Complex: a case study of interstellar matter (Dordrecht: Reidel).
Goudis, C., Meaburn, J. 1978, Astr. Ap., 68, 189.
Heiles, C. 1979a, Ap. J., 229, 533.
Heiles, C. 1979b, in Ed. W.B. Burton, Large-scale characteristics of the Galaxy, IAU Symp. No. 84 (Dordrecht: Reidel), p. 301.
Heiles, C. 1984, Ap. J., in press.
Higdon, J.C. 1981, Ap. J., 244, 88.
Higgs, L.A., Landecker, T.L., Seward, F.D. 1983 in Eds. J. Danziger, P. Gorenstein, Supernova remnants and their x-ray emission,IAU Symp. No. 101, p. 281.
Hutch, K. van der, Conti, P., Lundstrom, I., Stenholm, B. 1981, Space Sci. Rev., 3, 227.
Humphreys, R.M. 1978, Astrophys. J. Suppl., 38, 309.
Ikhsanov, R.N. 1960, Astr. Zh., 37, 988 (Sov. Astr., 4, 923).
Kapp-herr, A.v., Wendker, H.J. 1972, Astr. Ap., 20, 313.
Lozinskaya, T.A. 1982, Ap. Space Sci., 87, 313.
Meaburn, J. 1980, M.N.R.A.S., 192, 365.

Mishurov, Yu.N., Panlovskaya E.D., Suchkov, A.A. 1979, Astr. Zh., 56, 268, (Sov. Astr. 23, 147).
Pikel'ner, S.B. 1970, Astr. Zh., 47, 254 (Sov. Astr., 14, 208).
Reddish, V.C., Lawrence, L.C., Pratt, N.M. 1966, Publ.Roy.Obs.Edinburg,5,111.
Reynolds, R.J. 1976, Ap. J., 206, 679.
Reynolds, R.J. Ogden, P.M. 1979, Ap. J., 229, 942.
Salpeter, E.E. 1979, in Ed. W.B. Burton, The large scale characteristics of the Galaxy, IAU Symp. No. 84, p. 245.
Sharov, A.S. 1982, The Andromeda Nebula (Moscow: Nauka).
Uranova, T.A. 1984, Astr. Zh., in press.
Weaver, H. 1979, in Ed. W.B. Burton, Large-scale characteristics of the Galaxy, IAU Symp. No. 84 (Dordrecht: Reidel), p. 295.
Weaver, H. 1984 in this volume.
Weaver R., McCray,R., Castor,J., Shapiro,P., Moore,R. 1977, Ap. J., 218, 377.
Zasov, A.V., Demin, V.V. 1979, Astr. Zh., 56, 941 (Sov. Astr., 23, 941).
Zasov, A.V., Kyazumov,G.A. 1981, Pis'ma Astr.Zh.,7,131 (Sov.Astr.Lett,7,73).

STROMGREN TRAILS OF HOT WHITE DWARFS

John C. Raymond

Harvard-Smithsonian Center for Astrophysics

ABSTRACT

High resolution IUE spectra of Feige 24 reveal sharp C IV absorption features at both the stellar velocity and the velocity of the interstellar lines. Dupree and Raymond have shown that the ionization zone created by Feige 24 itself accounts for the interstellar components of C IV and Si IV, and that the density of hot white dwarfs in the galaxy implies that similar ionized zones around hot white dwarfs make a significant contribution to the C IV column densities observed toward distant O and B stars. Typical white dwarf velocities of around 30 km/s and C IV ionization zone diameters less than 1 pc imply that the crossing time is comparable to the ionization time, so that non-equilibrium ionization models are required. Models of the resulting elongated trails are presented.

MODELS

Most techniques for studying interstellar gas average along the line of sight. O stars and supernovae light up specific regions for study, but they tend to occur in abnormal regions of space, and they strongly perturb the illuminated gas. By measuring the C IV, Si IV and N V column densities associated with a hot white dwarf, we can determine the ambient density of the gas near the white dwarf. Space Telescope may make it possible to observe enough hot white dwarfs to determine the filling factor of the warm component of the ISM in the neighborhood of the Sun.

The major difficulty in such a determination in confusion of narrow stellar absorption lines of C IV, Si IV and N V (e.g. Sion, Guinan and Wesemael 1982; Bruhweiler and Kondo 1981) with interstellar lines. Feige 24 is a convenient object for study in that the stellar features are redshifted and their velocity varies with the 4.2 day orbital period, while the interstellar features stay fixed near zero velocity (Dupree and Raymond 1982). While the interstellar C IV and Si IV might be unassociated with Feige 24, these lines are not present in spectra of a star 1^{o} from Feige 24 but only 20 pc away or of a more distant star 3^{o} from Feige 24. The column densities of C IV and Si IV and the upper limit on N V agree with predictions of a simple static H II region model provided that the density near Feige 24 is at least 0.1 cm^{-3} (Dupree and Raymond 1983). The model of a static photoionized region is only approximate, however, since typical white dwarf velocities (30 km/s) are large enough that the ionization time is comparable to the time in which the white dwarf crosses the zone of high ionization. Thus non-equilibrium ionization models are required.

A computer code designed to model radiative interstellar shock waves

(Raymond 1979) has been modified to compute the structure of the ionized trail left by a hot white dwarf moving through the interstellar gas. Many improvements to the atomic rates in the code have also been made, of which the relevant ones are Reilman and Manson (1979) photoionization cross sections, low temperature dielectronic recombination (Nussbaumer and Storey 1983) and charge transfer (as described in Butler and Raymond 1980). Figure 1 shows the 1%, 3%, 10% and 30% contours of the C IV, Si IV and N V ionization fractions for a model specific to Feige 24. A radius of 0.2 $R_\odot$, a temperature of 70,000 K and a velocity of 60 km/s were used. The stellar flux distribution was taken from the log g = 8 pure hydrogen model of Wesemael et al (1980). The density was held constant at 0.1 cm^{-3}, and a background ionization rate sufficient to maintain 95% ionization of hydrogen and 5000 K was assumed to approximate the 'warm ionized' component of the interstellar medium. Figure 2 shows the 3% contours of C IV for different assumed density, white dwarf radius, and ambient ionization state. The models having neutral and ionized ambient gas differ in that the neutral gas is heated to 20,000 K when it is ionized, while the ionized ambient gas is heated only to about 8,000 K. Thus if the ambient gas is neutral, the heating will result in expansion, and the high pressure will drive a weak shock ahead of the white dwarf.

The predicted column density can vary by an order of magnitude depending on whether the white dwarf is approaching or receding. Since Feige 24 is moving away at 34° to the line of sight, its interstellar lines are unusually strong. Column densities for the model shown in Figure 1 and solar abundances are listed in Table 1.

This work has been supported by NASA contract NAG 5-87 to the Smithsonian Astrophysical Observatory.

REFERENCES

Bruhweiler, F.C., and Kondo, Y. 1981, Ap. J., 248, L123.
Butler, S., and Raymond, J.C. 1980, Ap. J., 240, 680.
Dupree, A.K., and Raymond, J.C. 1982, Ap. J., 263, L63.
Dupree, A.K., and Raymond, J.C. 1983, Ap. J., 275, L71.
Nussbaumer, H., and Storey, P.J. 1983, Astr. Ap. Suppl., in press.
Raymond, J.C. 1979, Ap. J. Suppl., 39, 1.
Reilman, R.F., and Manson, S.T. 1979, Ap. J. Suppl., 40, 819.
Sion, E.M., Guinan, E.F., and Wesemael, F. 1982, Ap. J., 255, 232.
Wesemael, F., Auer, L.H., Van Horn, H.M., and Savedoff, M.P. 1980, Ap. J. Suppl., 228, 127.

TABLE 1

ion	approaching	perpendicular	34°	receding
C IV	13.08	13.26	13.50	13.59
Si IV	12.30	12.43	12.72	13.22
N V	12.46	12.62	12.95	13.64

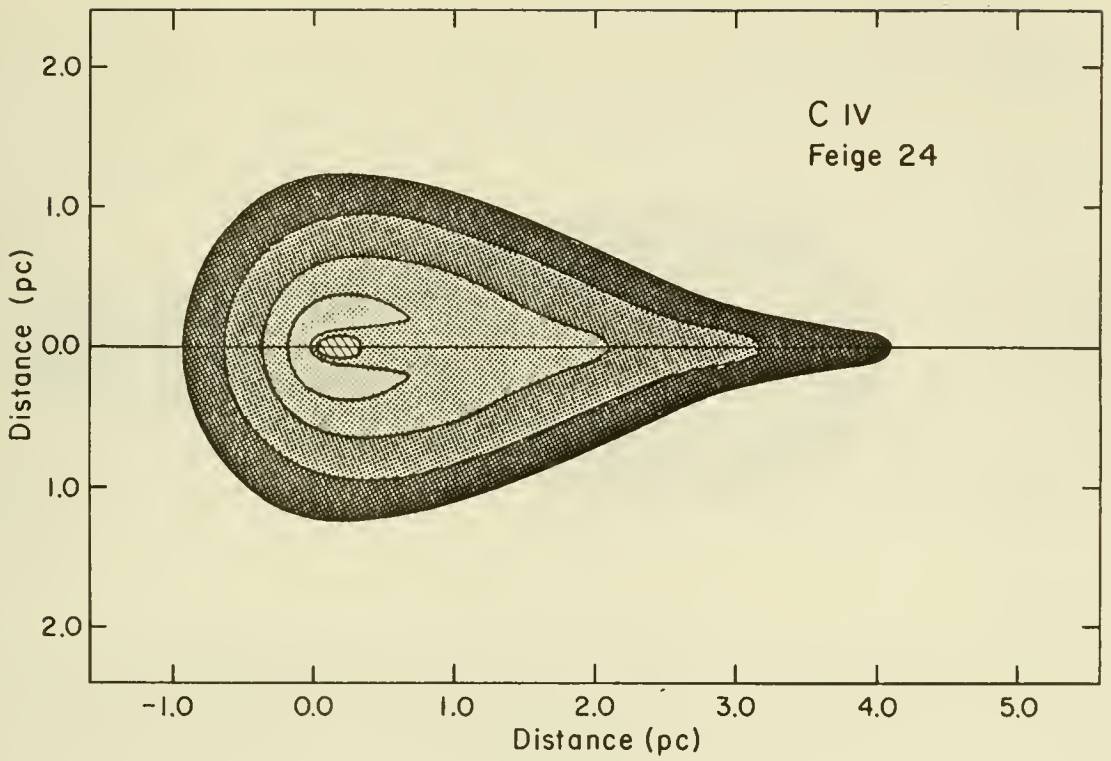

Figure 1a.

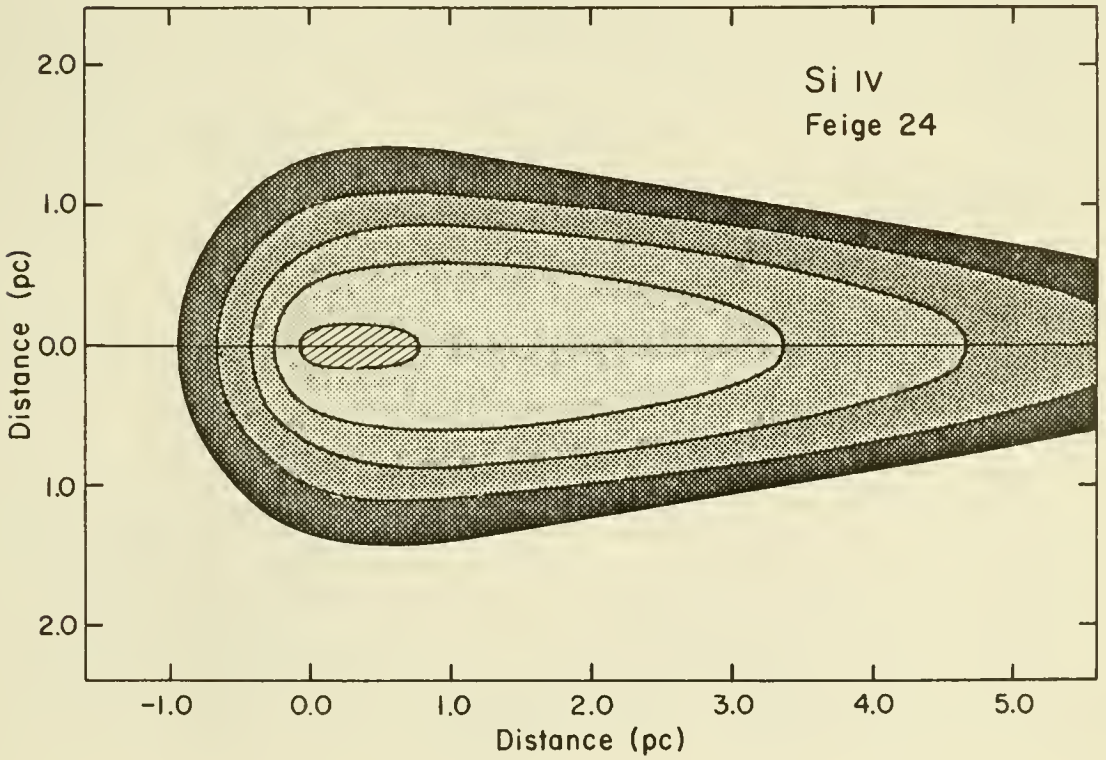

Figure 1b.

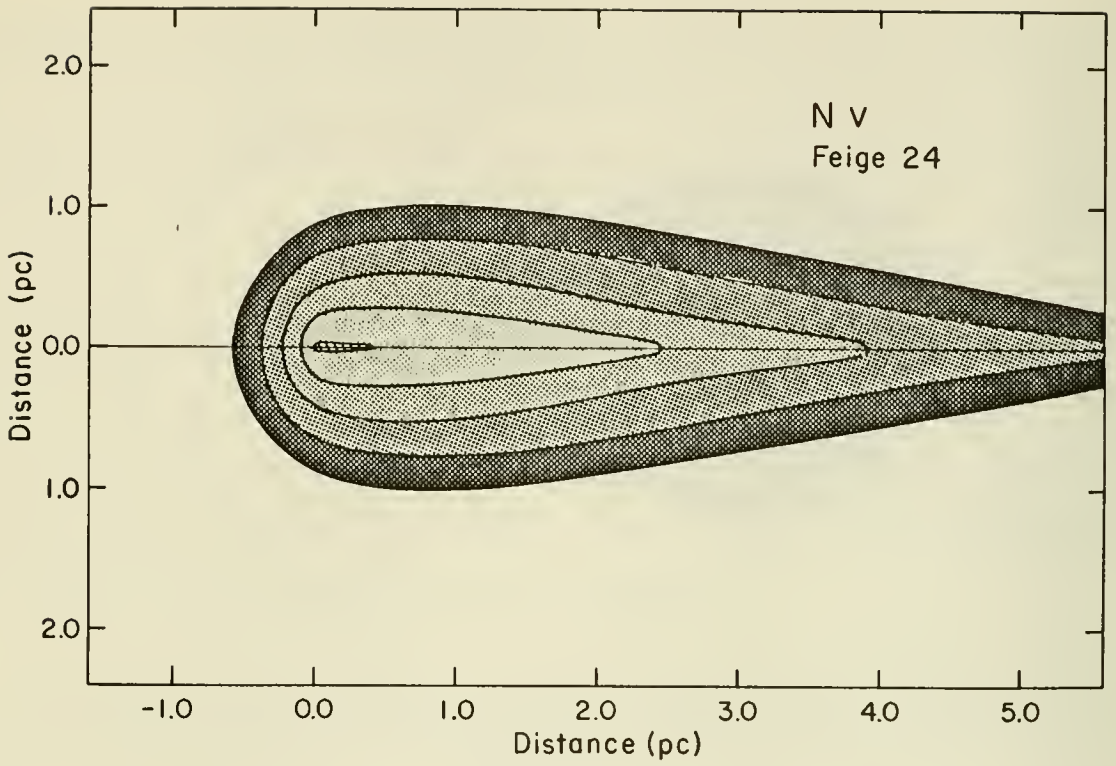

Figure 1c.

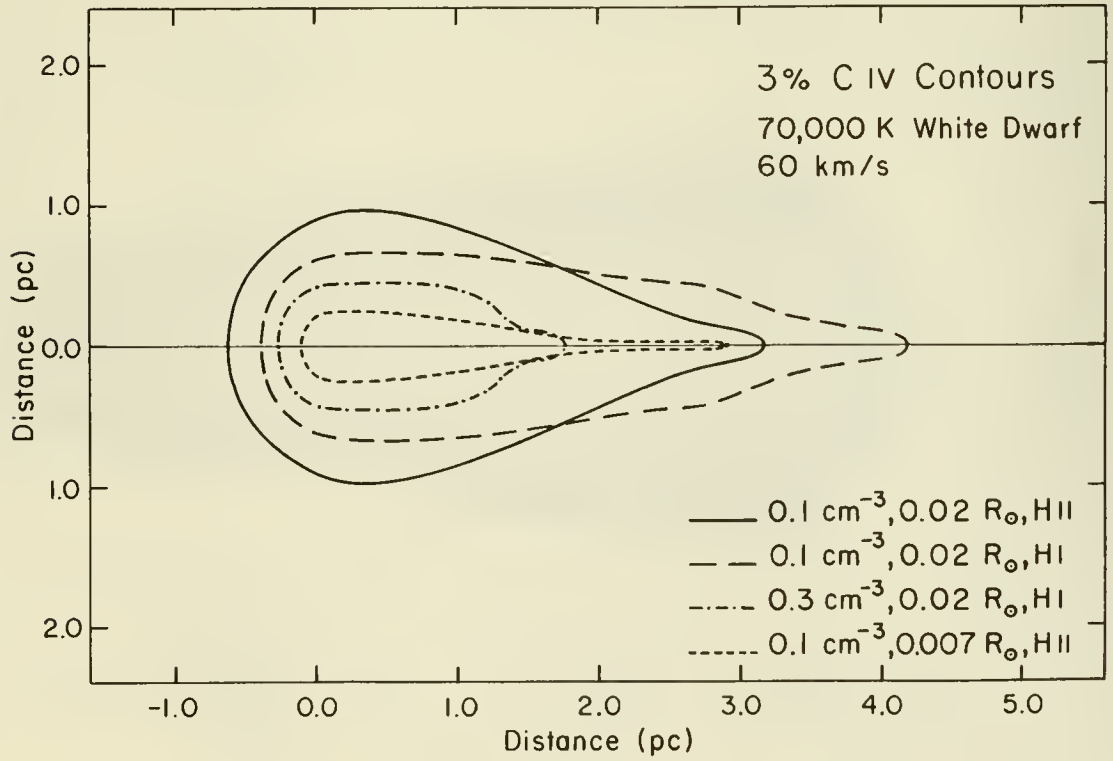

Figure 2.

MAGNETIC ALIGNMENT THEORY AND THE INTERPRETATION OF POLARIZATION

Pierre Cugnon
Observatoire Royal de Belgique

ABSTRACT

This paper presents some reflexions about the theory of magnetic spinning alignment. It is shown that a classical enhanced thermal Davis and Greenstein mechanism may be considered as a limiting case of Purcell's suprathermal spinning alignment theory when the number of active sites on a given grain becomes very important and/or for very short-lived suprathermal sites.

This result is applied to the interstellar medium and some problems in which it may be important are briefly discussed, with special attention to local implications.

INTRODUCTION

It has been shown by some authors (see for example Purcell and Spitzer 1971; Cugnon 1971, 1983; Greenberg 1978) that Davis and Greenstein thermal alignment mechanism (TSA) failed by about one order of magnitude to explain the required degree of alignment when "standard" interstellar conditions were assumed.

That is the reason why Purcell (1975, 1979) proposed an alternative D-G mechanism, in which the grains, driven to "suprathermal" rotational velocities by some constant torque, were thus much more easily aligned by paramagnetic relaxation. This theory appears now to account correctly for the polarization observations (Johnson, 1982; Aannestad and Greenberg, 1983), although there remain some uncertainties in the formulation of the theory and in the values of the parameters (effect of dissipative torques, re-surfacing time, number of active sites). Spitzer and McGlynn (1979) made a very detailed analysis of the problem of disalignment due to grain re-surfacing and concluded that "long-lived" spin-up was necessary to account for grain alignment in Purcell's mechanism.

In his paper of 1979, Purcell pointed out that the rotational temperature of the grain could be quite different from the gas temperature, and should in fact be calculated taking into account all the possible excitation mechanisms acting on a grain provided that excitation occurs randomly with a characteristic time shorter than the collisional damping time. This leads to a rotational temperature T_{eff} which can be quite higher than the commonly used gas temperature, and induces a somewhat more efficient alignment mechanism, we shall call "enhanced thermal alignment" mechanism (ETSA). On the other hand, if the excitation is not random and takes place systematically at a few peculiar sites of long duration, we are in the case of Purcell's suprathermal spinning alignment (SSA).

It appears then that ETSA and SSA respectively refer to extreme opposite cases of rotational excitation. The theoretical analysis which follows briefly developes this point and examines the role of some parameters in the transition from SSA to ETSA. The third section will then be devoted to some interstellar implications of the obtained results.

THEORETICAL DISCUSSION

The starting idea of this analysis was to apply Purcell's theory to spheroidal particles. The impossibility of inducing any suprathermal torque along the symmetry axis for such grains (an essential condition for SSA) was avoided assuming that each active site had a preferential direction of molecular ejection, allowing then for a tangential impulsive force. The point is subject to discussion, but this is out of the frame of this short paper.

The grain surface of a 2:1 prolate spheroid was then divided into 10000 equivalent elements among which a fixed number (s) of active sites with their ejection direction were randomly selected. We then computed the mean and mean square of the impulsive angular momentum variation corresponding to a great number (50000 and 100000) of such configurations with the same s, also randomly generated. The histogram of fig. 1 shows, for s=40, the deduced distribution of the grains with respect to $\langle \delta J_z \rangle$ in units of $a(E_m\, m_H)^{1/2}/20$, where a is the transverse radius, E_m the part of the recombination energy converted to kinetic energy. This distribution is fairly well described by a gaussian curve; this is confirmed by 7 other runs, with $1<s<160$, for which only the adjusted curve is plotted.

Two quantities are then derived from each distribution (the outer brackets denoting the average on the configurations) : the dispersion $\sigma=(2\langle\langle \delta J_z\rangle^2\rangle)^{1/2}$ of the gaussian approximately equal to $.7\, a\, s^{-1/2}(E_m m_H)^{1/2}$ (fig 2), and the mean fluctuation $\Delta=(\langle\langle \delta J_z^2\rangle-\langle\delta J_z\rangle^2\rangle)^{1/2}$ (fig 3), fast increasing from zero (s=1) to an asymptotic value of $.4883a\{2(E_m m_H)^{1/2}\}$, which is derived from an analytical expression.

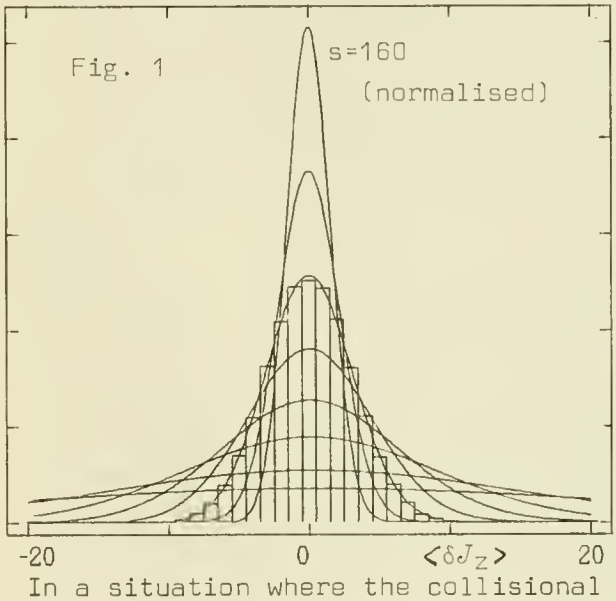

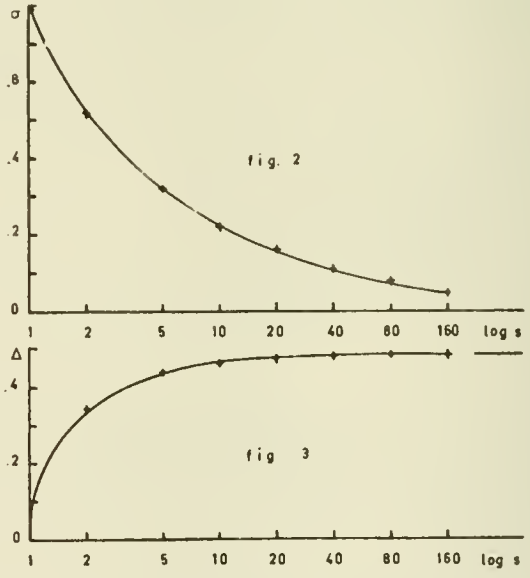

In a situation where the collisional damping time t_c is short with respect to the re-surfacing time t_s (ideal suprathermal case), the acceleration produced by the mean resulting torque $n_m \langle \delta J_z \rangle$, where n_m is the number of hydrogen molecules leaving the grain surface per time unit, will be damped after a time of the order of t_c and will induce a stationary mean angular momentum of $n_m\, t_c \langle \delta J_z \rangle$ around which the grains will be gaussian distributed (micro-distribution), because of the different thermal excitation processes (Purcell, 1979), among which the most important one is generally related to the fluctuation Δ defined above. We shall also define a "macro-distribution" which is the gaussian distribution of the stationary values of $\langle J_z \rangle$, whose dispersion is equal to $n_m\, t_c\, \sigma$. It must be emphasized that if a temperature can be associated with the micro-distribu-

tion, this is not the case with the macro-distribution as long as exchanges of grains between "cells" of the angular momenta space are impossible. It may be confirmed, using a simple one-dimentional F-P equation, that the stationary situation is well the state described above whith the dispersion of the micro-distribution equal to $(n_m t_c)^{1/2} \Delta$. The comparison between both dispersions provides in our "ideal" case a way of measuring the efficiency of SSA versus ETSA. We then define $g = n_m t_c \sigma / \{(n_m t_c)^{1/2} \Delta\} = (n_m t_c)^{1/2} (\sigma/\Delta)$. With the above expressions for σ and Δ and using Cugnon's formulation, we obtain, for a 2:1 prolate spheroid, $g \cong 2 \{(f M)/(s m_H)\}^{1/2}$ where M is the mass of the grain and f the fraction of incoming hydrogen atoms which leaves the grain as molecules. When assuming realistic intervals of variation for the parameters, i.e. $10^8 \lesssim M/m_H \lesssim 10^{10}$, $10 \lesssim s \lesssim 1000$, $1 \lesssim f \lesssim 1$, we obtain $10^2 \lesssim g \lesssim 10^5$, so that if we associate a "pseudo-temperature" with the macro-dispersion, it will be generally quite higher than the rotational temperature T_{eff} defined by Purcell. This makes ETSA generally impossible under our ideal assumption. However, re-surfacing can occur much more frequently. The other extreme limit corresponds to $t_s \ll t_c$, at which a grain then suffers a great number of mean impulsive torques gaussian distributed (fig 1). The resulting net torque vanishes, allowing then for ETSA. For intermediate cases, this torque will not vanish, but will be statiscally reduced compared with the torque computed for the ideal case, the amplitude of this reduction depending on the number q of complete re-surfacing. The resulting macro-dispersion for $\langle J_z \rangle$ will also decrease with increasing q. A very rough approach consists of saying that q re-surfacing correspond to multiply the number of emitting sites by a factor q, so that g becomes $2\{(f M)/(q s m_H)\}^{1/2}$. If this is not too bad, the conditions in which ETSA becomes operative ($g \sim 1$) are certainly peculiar but not too exotic. The next section will examine some consequences of this provisional conclusion.

POLARIZATION AND INTERSTELLAR PHYSICAL PARAMETERS

It is well-known that for thermal D-G mechanism the magnetic field intensity can be calculated using a theoretical expression of the degree of alignment, this quantity being itself deduced from the observed ratio of polarization to extinction. A formula has been proposed for this purpose by Cugnon (1983), which takes into account asymptotical calculation combined with the main results obtained in this domain (Purcell and Spitzer 1971; Cugnon 1971; Greenberg 1978). Unfortunately the formulation of SSA is not so firmly established because of uncertainties in the role of some parameters; furthermore, it is still difficult to predict the final state of orientation for prolate grains. The situation naturally appears still more complicated for intermediate cases between SSA and ETSA. Consequently, very few can be said about the field strenght when SSA is working except that it is lower than the field required to achieve ETSA.

It has been shown above that SSA overcomes ETSA in most interstellar situation so that estimating the magnetic field using formulations of classical D-G alignment appears now subject to criticism. From this point of view, we shall now examine rapidly the case of two nearby regions which have been studied in details by Coyne et al. (1979)(I) and Vrba et al. (1981)(II). It appears that in case (I), the observed densities and temperatures are not far from the diffuse ISM values. The λ_{max} distribution is also similar to-, though broader than the general ISM curve. Because of this similitude, we assume, like Johnson (1982), that long-lived active sites make SSA efficient in this region, so that the magnetic field may be quite smaller than the value of 200 μG proposed by the authors. On the other hand, in the dark cloud of R Coronae Australis (II), the distribution of grain sizes seems to permit local situations where frequent re-

surfacing by accretion may occur. It is then possible that in certain regions of this cloud, the ETSA formulation can be used in order to obtain the magnetic field intensity. Using Cugnon's expression of Rayleigh reduction factor and the values of the physical parameters taken from Vrba et al., we obtained, for the same elongation of .2, a value of the field of about 100 μG, thus very close to the value found by the authors (classical TSA, $T_{rot} = T_{gas}$). However, if ETSA is assumed with $300 < T_{eff} < 500$ K (this is not critical), and elongations around .4, the field is reduced by a factor 2. Furthermore, under slightly thus reasonable different assumptions on gas and grain temperatures and densities, grain size and elongation, a factor 3 between extreme estimations of the field may exist, i.e. from 40 to 120 μG in this particular case. However, such a situation would be present quite generally in the few regions where ETSA may be supposed to act, despite the fact of a well-established theoretical formulation.

Let us now have a look on the temperatures and densities which can play a role in the different spinning alignment processes. In classical TSA, the ratio of two temperatures $\xi = T_{gra}/T_{rot}$, where $(T_{gas}+T_{gra})/2 \leq T_{rot} \leq T_{gas}$, depending on the type of collisions, plays a fundamental role; $\xi=1$ implies no polarization and one could expect for $\xi>1$ an inversion of the polarization. This point is important in clouds where T_{gra} is approaching T_{gas} (Johnson 1982). The role of the gas density is also fundamental, for the collisional damping time increases with decreasing gas densities; this could made the alignment easier in regions poor in gas where the occasional presence of important quantities of dust is expected. This conclusion also holds for ETSA. In this case, however, the temperature ratio $\xi = T_{gra}/T_{eff}$ is much smaller than for TSA so that it can be put equal to zero in most cases. For SSA also, the grain temperature appears not to be a relevant parameter. In this late case, one should also expect that higher gas densities could make the alignment more difficult. However, the ratio of the re-surfacing time by accretion to t_c appears to be quite independant of gas densities and temperatures, but very sensitive to depletion (Greenberg 1978, 1983).

This rapid survey shows the importance of collected results from independant sources, and how this collection can help to decide between one or another mode of magnetic alignment. However, a point to point comparison appears to be necessary, implying a relatively important number of stars behind the dusty region studied, a good angular resolution of the measurements, and a rather unimportant column density of dust in front of it. These conditions are best fulfilled in the local ISM; the two regions quoted above are good examples of this conclusion.

REFERENCES.

Aannestad P.A., Greenberg J.M. 1983, Ap. J. 272, 551.
Coyne G.V., Tapia S., Vrba F.J., 1979, Astr. J. 84, 356.
Cugnon P., 1971, Astr. Ap. 12, 398.
Cugnon P., 1983, Astr. Ap. 120, 156.
Greenberg J.M., 1978, in *Cosmic Dust* ed. J.A.M. McDonnell, (New-York, Wiley), p. 187.
Johnson P.E., 1982, Nature 295, 371.
Purcell E.M., 1975, in *The Dusty Universe* ed. G.B. Field & A.G.W. Cameron, (New-York, Neal Watson), p. 155
Purcell E.M., 1979, Ap. J. 231, 404.
Purcell E.M., Spitzer L., 1971, Ap. J. 167, 31.
Spitzer L., McGlynn T.A., 1979, Ap. J. 231, 417.
Vrba F.J., Coyne G.V., Tapia S., 1981, Ap. J. 243, 489.

KINEMATICS OF NEARBY GAS AND STARS

Thomas Goulet and William L.H. Shuter

Department of Physics, University of British Columbia

ABSTRACT

The kinematic properties of gas and stars in the Solar neighborhood are described in terms of the line-of-sight component of a three-dimensional first order Taylor series expansion of the local velocity field. The types of object analysed are (1) 21 cm absorbing clouds (2) intercloud medium (3) main sequence B stars closer than 200 pc (4) B stars of luminosity class ranging from I to IV (5) main sequence A stars (6) K-giant stars. The least squares fitting procedure used to derive the 10 coefficients describing each of the six velocity fields was essentially the same, so that a valid comparison could be made. Marked departures from circular motion are found in most cases, but the only systematic trend is a correlation between $\partial u/\partial x$ (u being the velocity component along the x-axis directed towards the Galactic center) and stellar spectral type, where the gas behaves like a medium 'younger' than the early type stars. Our analysis of the gas indicated that the standard plane-parallel model provided a good description for the intercloud medium, but was inadequate for the absorbing clouds. A velocity ellipsoid description of the residuals is presented for each type of object. The influence of the Gould belt on local kinematics is discussed.

INTRODUCTION

When the velocity field around the Sun is represented by a three-dimensional first order Taylor series, as was done by Helfer (1961), the line-of-sight component, V_ℓ, takes the form:

$$V_\ell = K(1) + K(2)\cos b \cos \ell + K(3)\cos b \sin \ell + K(4)\sin b$$
$$+ K(5)d \cos^2 b \cos^2 \ell + K(6)d \cos^2 b \sin^2 \ell + K(7)d \sin^2 b$$
$$+ K(8)d \cos^2 b \sin 2\ell + K(9)d \sin 2b \sin \ell + K(10)d \sin 2b \cos \ell$$

where d is the distance from the Sun.

In this expression K(1) is the usual 'K term', K(2)-K(4) give the reflex of the 3 components $(u_\odot, v_\odot, w_\odot)$ of the Solar motion with respect to the LSR, and the remaining coefficients represent velocity gradients as follows:

$$K(5) = (\partial u/\partial x)_{d=0} \quad : \quad K(6) = (\partial v/\partial y)_{d=0} \quad : \quad K(7) = (\partial w/\partial z)_{d=0}$$
$$K(8) = \tfrac{1}{2}(\partial u/\partial y + \partial v/\partial x)_{d=0}$$
$$K(9) = \tfrac{1}{2}(\partial v/\partial z + \partial w/\partial y)_{d=0}$$
$$K(10) = \tfrac{1}{2}(\partial w/\partial x + \partial u/\partial z)_{d=0}$$

where x & u are directed towards the Galactic center, y & v towards $\ell = 90°$, and z & w towards the Galactic North pole.

The coefficients K(5) - K(7) represent velocity gradients as indicated, and K(8) - K(10) are velocity shear terms. In the case of pure differential circular motion about the Galactic center all these coefficients are zero except K(8) which represents the usual Oort A constant.

ANALYSIS

The 21 cm absorption data analysed were from the Nancay 21 cm Absorption Survey of Crovisier et al. (1978), and the 21 cm emission data representing the intercloud medium were from Henderson (1973), and were restricted to intermediate Galactic latitudes ($10° \leq |b| \leq 30°$).

In analysing the 21 cm absorption data we found that the usual plane-parallel model did not properly describe the distribution of clouds. Their average distance, $< d >$, was given much better by a relation of the form

$$< d > = C(d_{min} + Z_o \text{ cosec } |b|)$$

in which d_{min} represents a minimum distance to the clouds, and Z_o is a scale height. C is a constant equal to 15/A which is unity if one assumes, as we did, that the Oort constant A = 15 km s^{-1} kpc^{-1}. We restricted our analysis to Galactic latitudes with magnitude greater than 10°, and for this sample we found d_{min} = 234 pc and Z_o = 74 pc. In this and all subsequent cases we rejected data which in an initial trial fit gave residuals greater than 3σ. The values of the coefficients for all velocity fields are listed in Table I, and plots of each field in the Galactic midplane are shown in Figures 1 and 2.

In the case of the 21 cm emission data we found d_{min} = 0, Z_o = 113 pc, and therefore used the standard model.

The data for all stellar groups were obtained from Sky Catalogue 2000.0. We selected stars with measured distances and line-of-sight velocities, and all stars with noted peculiarities were rejected. In contrast to the case for the gas, our analysis leads to a determination of the Oort constant A for each group.

The nodal deviation, ℓ_o, obtained when the terms K(5) - K(10) are replaced by a single term of the form A'd $\cos^2 b \sin 2(\ell-\ell_o)$ is also given in Table I for each field.

The average residual, σ, was determined for each group. We attempted a velocity ellipsoid analysis on the residuals for each group, in which we made a standard assumption that one of the axes of the ellipsoid was perpendicular to the Galactic plane. Values of σ, the ellipsoid axes $\langle u^2 \rangle^{1/2}$, $\langle v^2 \rangle^{1/2}$ and $\langle w^2 \rangle^{1/2}$, and the vertex deviation, ℓ_v, are listed in Table I. In the case of both 21 cm absorption and emission, we found $\langle w^2 \rangle$ to be negative, and thus the ellipsoids could not be determined.

DISCUSSION

Here we elaborate on the numerical results presented in Table I.

The coefficient K(1) - the 'K term' - was not determined for the gas because it was highly correlated with some of the other coefficients - see e.g. Takakubo (1967). For the stellar groups it was generally not significant except for the BI-IV stars, for which it takes a positive value

as found in several previous studies.

The coefficients K(2) - K(4) giving the Solar motion are generally similar for all groups with the exception of $v_{\odot}$ = 11.7 km s^{-1} for AV stars which, although in agreement with other studies, is significantly smaller than the value found for the rest of our objects.

Of the coefficients K(5) - K(7) which represent velocity gradients, K(5) = $\partial u/\partial x$ shows a clear systematic decrease with increasing 'age' of the studied objects. It ranges from positive values for the gas to a large negative value for the K-giants. K(6) = $\partial v/\partial y$ is not generally significantly different from zero, and the same applies to K(7) = $\partial w/\partial z$ in the case of the stars. In the case of the gas, K(7) takes a negative value for the absorbing clouds suggesting an inflow from both Galactic poles which is consistent with the picture given by McGee and Murray (1961) based on 21 cm emission studies. Figure 3(a) shows that this inflow is matched by an outflow in the Galactic plane, and this is kinematically consistent with the suggestion made by Weaver (1974). Figure 3(b) shows the corresponding situation for BI-IV stars, and in this case an inflow is seen from latitudes $\sim \pm 60°$ but there is no outflow. We do not regard the positive value of K(7) derived from 21 cm emission data as being astronomically significant, because Henderson did not observe polar latitudes.

K(8) - K(10) represent velocity shears. Of these only K(8), which corresponds to the Oort constant A, takes significant values. In all cases we find a value smaller than the standard one of 15 km s^{-1} kpc^{-1}.

The nodal deviation, ℓ_0, which depends on K(5) and K(6), shows a systematic tendency to increase with increasing 'age' of the studied objects. This is related to the change of K(5) with age. The anomalous value for the BV stars may be attributed to the large positive value of K(6) determined for this group.

We now consider the velocity residuals obtained from our fits, and their description in terms of velocity ellipsoids.

The average residual, σ, shows the well studied increase with age. The low value noted for the 21 cm emission data may be ascribed to the fact that Henderson presented a single velocity, representing an average weighted by brightness temperature, for each spectrum in his catalog. This method of averaging gives low weight to the individual peaks representative of clouds. For this reason we believe that our analysis of Henderson's data described the intercloud medium, which is known to be kinematically 'smooth'.

Our values for the velocity ellipsoid dispersion parameters obtained from stellar data generally are in good agreement with those presented by Mihalas and Binney (1981), except in the case of BI-IV stars where our value of $\langle w^2 \rangle^{\frac{1}{2}}$ is larger than the standard one. This discrepancy is resolved when the velocity ellipsoid is determined, as is usually done, from residuals after only Solar motion terms have been subtracted.

For both sets of 21 cm data we were unable to determine velocity ellipsoids because, as previously mentioned, we found $\langle w^2 \rangle$ to be negative. However, we were able to derive a velocity ellipsoid for a subset of the absorption data in which we selected only those spectra that showed a single absorption line. This subset, for which the average distance was independent of b and best described by a constant equal to 250 pc, had an average velocity residual σ = 3.6 km s^{-1} which is approximately half the

value for the complete set. The values of the velocity ellipsoid parameters were $\langle u^2 \rangle^{\frac{1}{2}} = 3.0$ km s^{-1}, $\langle v^2 \rangle^{\frac{1}{2}} = 3.6$ km s^{-1} and $\langle w^2 \rangle^{\frac{1}{2}} = 4.0$ km s^{-1}. It appears that our inability to determine an ellipsoid for the complete set can be attributed to the absorption spectra with multiple features. These spectra give large velocity residuals and tend to be concentrated at low Galactic latitudes. Taken together these two factors create an artificial variation of σ with b which interferes with the determination of the velocity ellipsoid parameters. Although we were unable to treat the 21 cm emission data in the same way, we suspect that a similar mechanism prevented the determination of the velocity ellipsoid.

Since many previous studies have suggested that the Gould belt plays an important role in the kinematics of the Solar neighborhood, we attempted to investigate its influence on our velocity field determinations. Referring to the work of Olano (1982) we rejected all data within his planar description of the belt between Galactic latitudes ±20°. We then redetermined velocity field coefficients for all groups and found no significant differences. This does not preclude the possibility that the internal kinematics of the Gould belt is atypical, but does indicate that the motions within the Gould belt do not perturb in any significant way the description of Solar neighborhood kinematics in terms of velocity fields.

CONCLUDING REMARKS

The most significant results of this work appear to be the following :

(1) Although in individual cases there exist significant departures from circular motion, these are not uniform for all groups but vary either randomly or show trends as a function of 'age'.

(2) The most noteworthy trend is for the velocity gradient $K(5) = \partial u/\partial x$ to decrease with increasing age. This is accompanied by a corresponding increase in the related parameter, the nodal deviation ℓ_o.

(3) Our analysis of 21 cm absorption data shows that the plane-parallel model does not provide an adequate description of their spatial distribution, since there appears to be a deficit of absorbing clouds within 200 pc of the Sun. On the other hand the 21 cm intercloud medium does have a stratified distribution.

(4) We find that 21 cm absorbing clouds appear to move towards the Sun from the Galactic poles, and away from it in the Galactic plane. Because of the larger statistical errors in the stellar data, velocity gradients of comparable magnitude would have been difficult to detect.

(5) We have not studied the internal kinematics of the Gould belt. However, we can assert that possible anomalous kinematics within the Gould belt does not appear to affect the velocity fields we determined.

A more detailed discussion of all topics introduced here will be presented by Goulet (1984).

ACKNOWLEDGMENTS

We would like to thank Jacques Crovisier for providing us with information regarding the Nancay 21 cm Absorption Survey. We thank NSERC for financial support.

REFERENCES

Crovisier, J., Kazes, J., and Aubry, D. 1978, Astronomy and Astrophysics Suppl., 32, 205.
Goulet, T., 1984, M.Sc. Thesis, University of British Columbia, (in preparation).
Helfer, H.L. 1961, Astronomical Journal, 66, 160.
Henderson, A.P. 1973, Astronomical Journal, 78, 381.
Hirshfeld, A., and Sinnott, R. 1982, Sky Catalogue 2000.0, Volume 1, Cambridge University Press and Sky Publishing Corporation.
McGee, R.X., and Murray, J.D. 1961, Australian Journal of Physics, 14, 260.
Mihalas, D., and Binney, J. 1981, Galactic Astronomy, Structure and Kinematics, W.H. Freeman, San Francisco.
Olano, C.A. 1982, Astronomy and Astrophysics, 112, 195.
Takakubo, K. 1967, Bull. Astr. Inst. Neth., 19, 125.
Weaver, H. 1974, in Highlights of Astronomy, Vol. 3, G. Contopoulos (ed.), D. Reidel Publishing Co., Dordrecht.

TABLE I

Velocity Field Coefficients and Velocity Ellipsoid Parameters

	21 cm absorption	21 cm intercloud	BV d<200pc	BI-IV	AV	K-Giants
Total No. Analyzed	281	406	330	451	1061	981
<d> pc	395	418	133	692	109	167
Taylor Series Coefficients						
K(1) km s^{-1}	-	-	0.7±1.8	3.4±0.8	- 0.2±1.0	2.5±1.6
K(2)= $-u_\odot$ "	-11.0±0.8	-10.1±0.3	-9.1±0.9	-8.2±0.9	-11.6±1.0	-10.5±1.5
K(3)= $-v_\odot$ "	-16.3±1.1	-16.2±0.3	-18.2±1.0	-17.4±0.8	-11.7±1.3	-18.6±1.7
K(4)= $-w_\odot$ "	- 9.5±1.2	-11.7±0.5	- 7.0±1.5	- 6.7±2.0	- 6.8±1.1	-10.2±1.7
K(5)=$\partial u/\partial x$ km s^{-1} kpc^{-1}	8.1±2.4	4.2±0.6	- 2 ±14	- 2.8±1.1	-15 ±11	-29 ±13
K(6)=$\partial v/\partial y$ "	- 0.2±3.8	- 0.1±0.9	30 ±14	- 4.0±1.2	4 ±12	- 9 ±13
K(7)=$\partial w/\partial z$ "	-11.5±5.9	20.3±5.4	24 ±25	- 6.9±5.6	8 ±15	6 ±15
K(8)= 'A' "	(15.0±2.6)	(15.0±0.6)	12.7±6.8	11.2±0.8	11.0±7.4	4.9±7.8
K(9) "	6.9±4.0	3.3±1.1	-29 ±12	- 9.8±3.4	1.8±8.5	16.8±9.3
K(10) "	3.1±2.7	2.3±0.9	15 ±11	5.4±2.4	2.7±8.1	0.2±9.2
ℓ_o	-26°	- 8°	28°	- 2°	23°	36°
Velocity Ellipsoid Parameters						
σ km s^{-1}	6.8	2.7	10.3	11.2	13.2	23.3
$\langle u^2 \rangle^{\frac{1}{2}}$ "	-	-	11.6	10.6	17.4	27.2
$\langle v^2 \rangle^{\frac{1}{2}}$ "	-	-	9.4	10.9	11.2	20.8
$\langle w^2 \rangle^{\frac{1}{2}}$ "	-	-	7.7	14.1	9.9	19.9
ℓ_v	-	-	20°	-	17°	23°

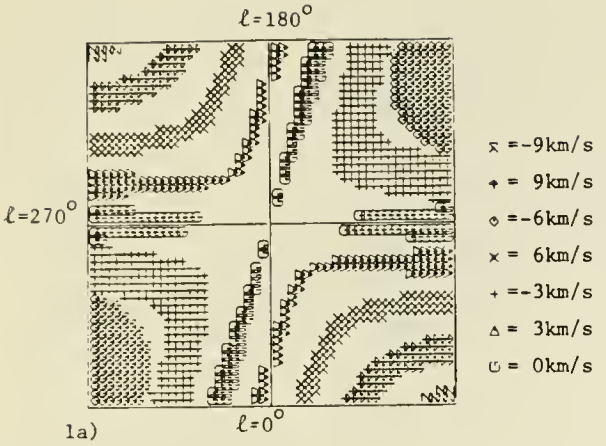

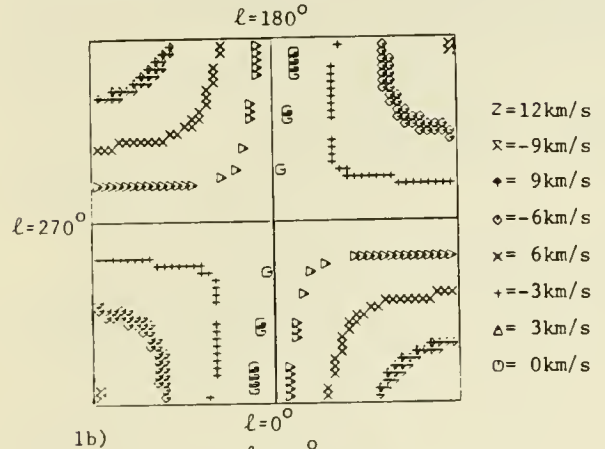

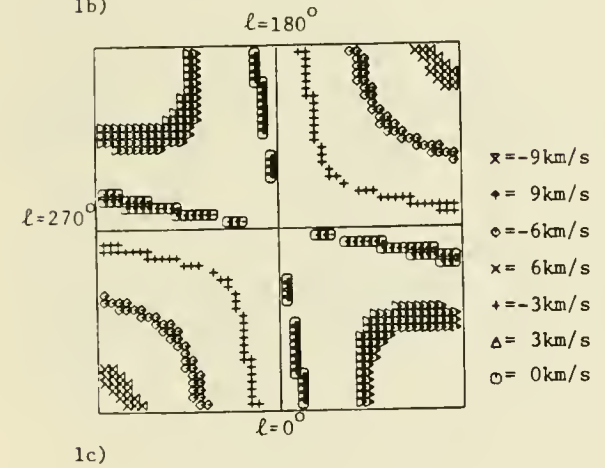

Figure 1. - Velocity fields in the Galactic midplane (x-y plane) for (a) 21 cm absorption, (b) 21 cm intercloud and (c) BI-IV. Each box has a half-width of 500 pc.

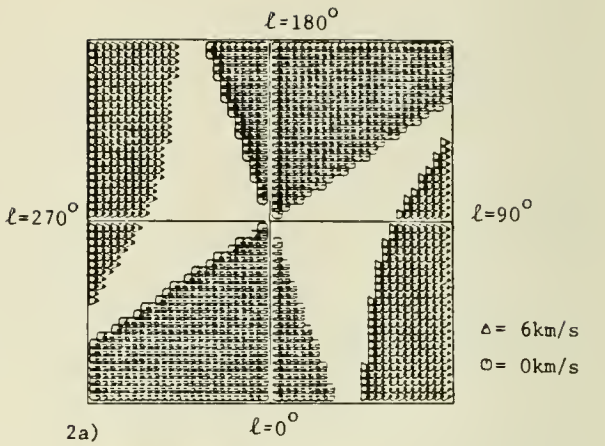

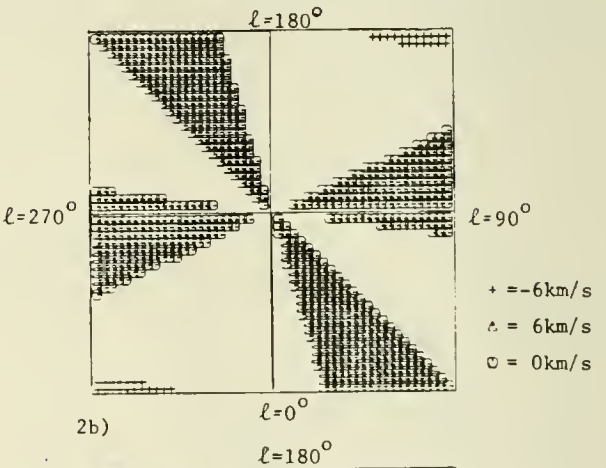

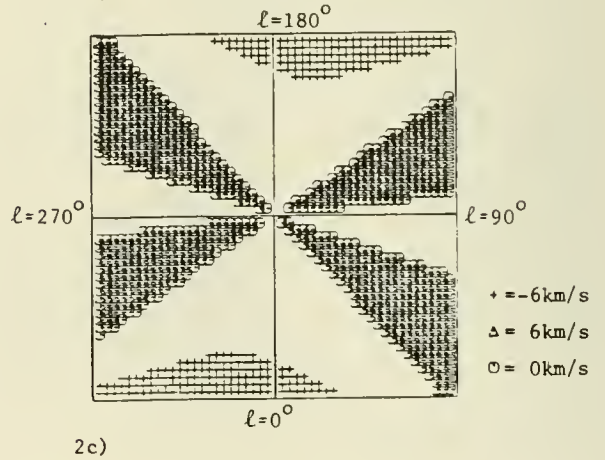

Figure 2. - Velocity fields in the Galactic midplane (x-y plane) for (a) BV d<200 pc, (b) AV and (c) KIII Each box has a half-width of 200 pc.

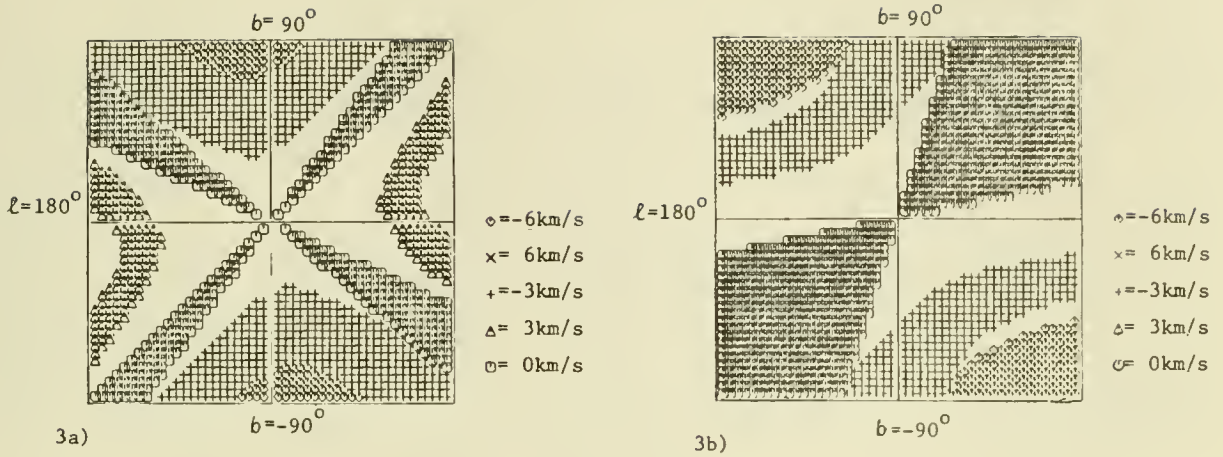

Figure 3. - Velocity fields perpendicular to the Galactic midplane (in the x-z plane) for (a) 21 cm absorption and (b) BI-IV. Each box has a half-width of 500 pc.

Dark Matter near the Sun: Simulated Star Counts and the Oort Limit

David Gilden and John N. Bahcall
The Institute for Advanced Study, Princeton, New Jersey 08540

ABSTRACT

An ensemble of orbits passing through the solar position have been generated for a specific mass model of the galaxy. These orbits are randomly sampled to form simulated density distributions of tracer stars perpendicular to the galactic disk. The simulated distributions are analyzed in order to determine the sampling errors in a self-consistent derivation of the total amount of matter near the sun (the Oort limit).

The total amount of matter in the vicinity of the Sun can be determined by studying the velocity dispersions and distribution with height above the plane of a population of tracer stars. This problem has a long history (see Oort 1965 and Bahcall 1984a,b for references) and the Oort limits that have been computed over a 50 year period are in fair agreement with each other, ranging from about 0.14 to 0.21 $M_{\odot}\,pc^{-3}$. Very recently, Bahcall (1984a,b) has improved the theoretical basis for this analysis by using more realistic Galaxy models and by solving the equations self-consistently. He has also estimated the errors in the theoretical analysis from uncertainties in input parameters and from theoretical approximations.

The various techniques and approximations used in translating the observations into a density of tracer stars have not been previously modeled. One wants to have answers to questions like: How many stars must be studied in order to give an accurate determination of the total matter density? How accurate are the estimates based on existing data for F dwarfs and K giants? Does the fact that the tracer stars are located in a cone (and not a cylinder) centered on the Sun affect the answer? We estimate the probable sampling error in the Oort limit by simulating a determination in a model galaxy where the total mass density is known in advance. We have integrated stellar orbits in a model disk galaxy, sampled these orbits in a way that mimics actual observations, formed model density distributions, and then computed the Oort limit using the self-consistent technique of Bahcall (1984a,b). The derived Oort limits were compared with the known value in the input model. We found that samples of about 890 stars have an (unbiased) error of about 10 - 15%. The sampling error arises in two ways; in determining the density profile from star counts, and in measuring the velocity dispersion of the tracer stars. The peculiar shape of the observing region (see below) does not lead to significant errors for parameters similar to those used in constructing the actual observed samples.

In deriving the Oort limit, Bahcall (1984a,b) fit the observed tracer star density distribution with theoretical models, choosing the best-fit model to have the smallest (least-squares) discrepancies. The mass density and scale height of the dark matter were allowed to vary until a best fit was obtained. The tracer stars were usually assumed to be isothermal, although specific departures from isothermality consistent with the observations were considered and found not to be important.

The galaxy model that provided the gravitational potential in our simulation is described in Bahcall, Schmidt, and Soneira (1983). It consists of a single component disk, a central (nuclear) component, a spheroid, and a halo. All four components are needed to reproduce the Galaxy rotation curve, but for the vertical oscillations, only the disk and halo are important. In this model the halo density is about 5% of the disk density at the solar position. The potential was numerically determined and was accessed by the orbit integrator through spline interpolation of tabulated values.

The initial conditions for the orbits were prescribed by random sampling from the disk density distribution and the velocity ellipsoid. First the disk component of the density distribution was sampled to yield random values of z and R. The axisymmetry of the potential did not require a choice of ϑ. The peculiar velocities v_z, v_R, and v_ϑ were chosen from the ellipsoid that was presumed to exist at (z,R). The velocity ellipsoids were constructed to have the same axial ratios as observed at the solar position, but with magnitudes that varied as $\sigma \sim \exp(-R/2h)$. Orbits were computed for those stars that energy and angular momentum conservation permitted, in principle, to reach to the solar position. The radial density gradient in the disk shifted the mean launching position 300 pc inward of the sun to 7.7 kpc.

The sampling procedure for launching tracer stars does not yield an exact solution to the Vlasov equation for our mass model. Numerical integration of individual orbits is necessary in order to form a phase mixed ensemble. Each star was allowed a random number of passages through the disk (with a mean of 5) before its orbit was sampled for use in the simulated star catalogue. Following this initial relaxation period, the stars were allowed about 15 passages through the disk with orbital data being recorded at 100 representative times. An ensemble of 3000 stars formed the catalogue from which random star count distributions were drawn.

We constructed simulated star counts that resemble as much as possible the F star sample described in Hill, Hilditch, and Barnes (1979) (hereafter HHB). The HHB sample consists of two parts. For apparent magnitudes $m > 6$, the F stars were drawn from a North Galactic Pole (NGP) survey (see Upgren 1962, hereafter UP). The plate area of this survey was 396 square degrees. For $m \leq 6$, the Yale *Catalogue of Bright Stars* (Hoffleit 1964) was used. This latter catalogue covers roughly 4π solid angle in the sky and the star count distribution that one obtains from it has an implicit spherical averaging. It can only be used for setting the asymptotic stellar density at the galactic midplane. The star counts from these two catalogues were divided into ½ magnitude bins and the density distribution determined by a simple application of the $m - \log \pi$ method. The total number of stars used in determining the F star density distribution was about 890. The velocity dispersions were determined from a smaller set of about 200 stars.

HHB analyzed the isothermality of their F stars and concluded that for $z > 200$ pc, the F stars are probably not isothermal. Only 15 stars were available for determining the F star velocity dispersion for $200 < z < 300$ pc, and the conclusions regarding non-isothermality are not firm. For the F stars, 200 pc represents about 1.5 density scale heights. We have computed the Oort limits for our simulated stars for truncations of the density profile at 1.5 and at 2.5 density scale heights in order to determine the penalty suffered for not using more of the available star count data. For most of Bahcall's (1984a) calculations, only stars with $z \leq 200$ pc were used.

In our simulated star count distributions we included only as many stars as were available to HHB in defining their F star densities. Stars were randomly selected at random times in their orbit and included in the sample if they would have been included in the *Bright Star Catalogue* or in the UP compilation. Stars were separated according to their apparent magnitudes, assuming that they had the visual absolute magnitude of an F5 star (3.6; see HHB). If $m \leq 6$, then a star in any direction would have appeared in the *Bright Star Catalogue*. Stars with $6 < m \leq 13$ were included in the sample if they lay within

a cone of opening angle 11.3° centered on the NGP. The solid angle subtended by 11.3° equals the plate area used in the actual observations, 396 square degrees. The galactic potential we use does not distinguish between up or down relative to the midplane. The UP observations do make this distinction in practice by being confined to the NGP.

In order that the simulated star counts have the same statistical properties as the observed sample of stars, we have randomly sampled in angle about the solar position to give our effective observing volume the desired three dimensional shape. The overall shape is that of a sphere (to $m = 6$, $D = 30$ pc) surmounted by a cone with opening angle 11.3°. The sphere represents the observing volume of the *Bright Star Catalogue*, and the cone the volume used by UP. The observed discontinuity at $m = 6$ is simulated as well as the overall shape of the star count distribution (see Table 3 and Fig. 4 of HHB, Table IV of UP, and Fig.2 below). We did not distinguish between F5 and F8 stars; grouped together, they total about 350 stars for $m \leq 6$ and about 500 stars for $6 < m \leq 13$. The stars were, as in UP and HHB, divided in ½ magnitude bins prior to determining the density distribution.

Poisson noise complicates the determination of the density distribution. For the observed F stars, there are never more than 100 stars within a ½ magnitude bin in the UP sample. If we confine our attention to $z < 200$ pc, this number decreases to about 40. (One could bin the data more coarsely to minimize the counting noise, but any poorer resolution of the distribution would make it unsuitable for deriving the Oort limit). It is both conventional and necessary to smooth the star count distribution in order to derive a density profile. There are a variety of smooth curves that acceptably fit the star count data, leading to similar but not identical density distributions. In Figure 1A we show a typical simulation of the star counts scaled to 1 square degree, and three smooth curves that are representative of the fits that one might attempt in deriving the density distribution. In Figure 1B the corresponding density distributions are shown. The flatness of these profiles at $z = 0$ is a result of the assumption used by HHB that the density is constant withing the volume surveyed by the *Bright Star Catalogue*. These density distributions, and those from other independent simulations, form the basis for our study of the Oort limit.

In Figures 2A, 2B, and 2C we show the isothermal fits to the three representative density profiles shown in Fig. 1B. These fits were constructed in the least squares sense using that part of the density profile with $z \leq 1.5 z_0$. The derived Oort limits for the three density profiles are 0.160, 0.171, and 0.184 $M_\odot$ pc $^{-3}$, where the input Oort limit was 0.176 $M_\odot$ pc $^{-3}$. If the density data up to $z = 2.5 z_0$ are utilized in fitting the density profiles, then the derived limits are respectively 0.161, 0.164, and 0.174 $M_\odot$ pc $^{-3}$. From a series of star count realizations we have a preliminary estimate of the expected variance of about 14% for limits derived from data truncated at $z = 1.5 z_0$, and of about 10% for limits derived from data truncated at $z = 2.5 z_0$. The largest errors scale inversely as the square root of the number of stars included in the sample. This research was supported by NSF grant PHY-82-17352.

References

Bahcall, J. N. 1984a, *Ap. J.*, **276**, 169.
_____ 1984b, submitted to *Ap. J.*
Bahcall, J. N., Schmidt, M., and Soneira, R. M. 1983, *Ap. J.*, **265**, 265.
Hill, G., Hilditch, R. W., and Barnes, J.V. 1979, *M.N.R.A.S.*, **186**, 813.
Hoffleit, D. 1964, *Catalogue of Bright Stars* (New Haven: Yale University Observatory).
Oort, J. H. 1965, in *Galactic Structure*, ed. A. Blaauw and M. Schmidt
(Chicago: University of Chicago Press).
Upgren, A. R. 1962, *A. J.*, **67**, 37.

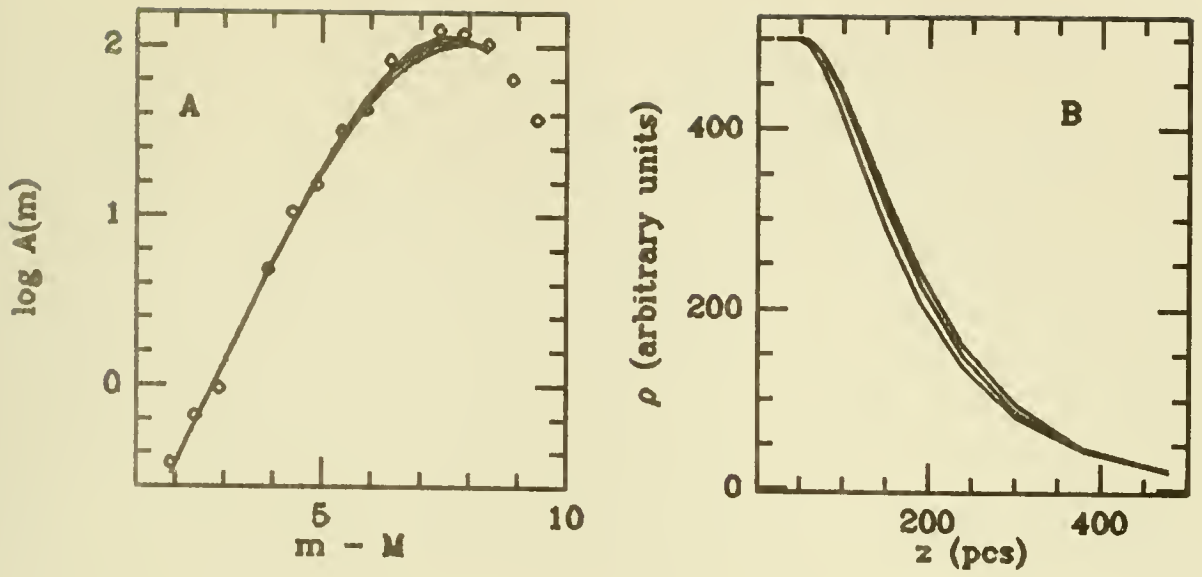

Figure 1: (A) - Star counts per square degree with three trial smooth fits.
(B) - Density distributions resulting from the three trial fits in (A).

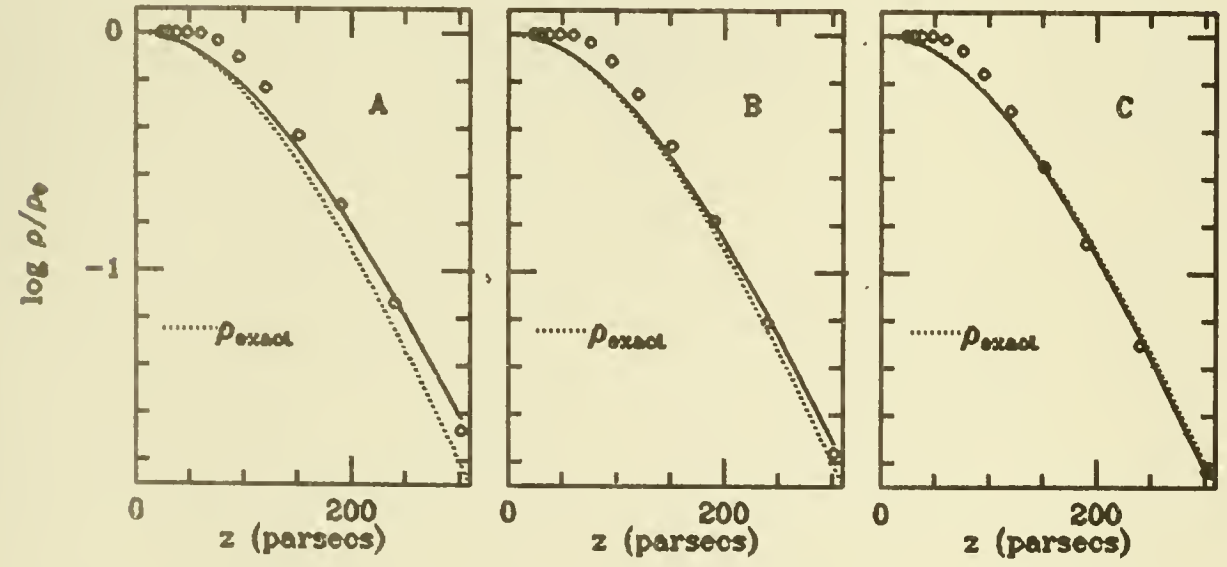

Figure 2: Best isothermal fits for the three density profiles illustrated in Fig. 1B. The open circles define the simulated density distribution, the solid line gives the isothermal fit that minimizes the variance, and the dotted line shows the input density profile.

THINGS TO COME

FUTURE STUDIES OF THE LOCAL INTERSTELLAR MEDIUM WITH SPACE TELESCOPE AND COLUMBUS

Blair D. Savage
Washburn Observatory, University of Wisconsin-Madison

ABSTRACT

The spectrographs aboard Space Telescope and Columbus will provide important new information about the interstellar medium in the immediate vicinity of the sun. The Space Telescope high resolution spectrograph (HRS) will produce resolutions, $\lambda/\Delta\lambda$, of about 18,000 and 70,000 with high sensitivity between 1200 and 3200 A and greatly reduced sensitivity between 1060 and 1200 A. The highest resolution is adequate to define the multi-component nature of interstellar absorption lines and to measure thermal line widths exceeding 3 km s^{-1}. The Columbus mission is in the planning stages. However, it is likely that the spacecraft will contain spectrographs capable of resolutions of 3×10^4 between 912 and 1200 A and 500 between 100 and 900 A. In the longer wavelength region, the very important lines of O VI, S VI, H_2, H I, and D I are available for study. In the short wavelength region, lines of He I and II, are observable. If the 3×10^4 resolution spectrograph can provide extended wavelength coverage to 770 A, lines of Ne VIII which are expected from 8×10^5 K gas are accessible. Astronomers using the ST HRS and Columbus spectrographs will be able to study a wide range of problems relating to cold, warm, and hot gas in the local ISM. Some of the most important observing projects are described.

INTRODUCTION

We have heard from the many papers presented at this meeting that instruments in space are providing important new insights about the nature of the local ISM. The results from IRAS, Copernicus, IUE, Voyager, and the various EUV and soft X-ray programs have revealed a region of our galaxy containing warm and hot gas with embedded clouds of cooler gas and dust. This local region has been studied through its emission and/or absorption characteristics in all parts of the electromagnetic spectrum. Advanced space facilities in the future will help answer many current questions about our local interstellar environment and will undoubtedly raise many new questions.

Table 1 lists missions that are either being built or are in the planning stages that might provide new information about the local ISM. This list does not include the many small instruments that are being designed for Shuttle sortie missions. For example, one such instrument is discussed by C. Martin and S. Bowyer in these proceedings. Another is the ASTRO mission to be flown on the Shuttle starting in 1986 with a complement of three UV telescopes. The major facilities from Table 1 for local ISM studies will likely be the Space Telescope High Resolution Spectrograph (HRS) and the Columbus mission. Most of my discussion will concern these two instruments. However, many of the other instruments listed in Table 1 may provide important new data about the

local ISM. Some of these possibilities are briefly described in the notes to Table 1. For missions such as Columbus, Starlab, AXAF, and SIRTF, the complement of local plane instruments has only been discussed in the broadest terms. I would hope that the final instrument configuration for each of these missions would contain an instrument suitable for studying our local interstellar environment.

TABLE 1: FUTURE MISSIONS

Mission	Aperture	Spectroscopic Capability Wavelength Range (A)	Resolution ($\lambda/\Delta\lambda$)	Approximate Launch Date
ST-HRS	2.4^m	1175-3200	7×10^4	1986
		1175-3200	2×10^4	
		1175-1800	2×10^3	
EUVE	0.4^m	100-900	3	1987
		100-900	1×10^2	
COLUMBUS	$\lesssim1^m$	900-1200	3×10^4	1990's
		1200-2000	1×10^4	
		100-900	5×10^2	
		900-2000	2×10^3	
STARLAB	1^m	1150-3200	1×10^5	1990's
AXAF	1.2^m	$\lesssim$ 100	not determined	1990's
SIRTF	1^m	$\gtrsim$30,000	not determined	1990's

EUVE (Extreme UV Explorer) - This instrument will obtain broad band photometry for a large number of sources between 100 and 1000 A. For the hotter stars detected, it may be possible to estimate the strength of the continuous H I absorption and thereby further delineate the 3 dimensional structure of local neutral hydrogen. The EUVE spectrometer will have a resolution of 10^2. This instrument will provide interstellar He I and He II absorption line information for the hotter white dwarfs.

STARLAB - Although primarily intended for high resolution imaging, Starlab may have spectroscopic modes. An echelle spectrograph operating at $\lambda>1150$ A with $\lambda/\Delta\lambda\sim10^5$ has been considered. With a large area detector, spectra with nearly complete wavelength coverage could be obtained in two integrations. At the highest resolution the ST-HRS Digicons can only record ~5 to 10 A of the spectrum per integration. With Starlab most of the programs considered for the ST-HRS could be pursued, but with greater efficiency.

AXAF (Advanced X-Ray Astronomy Facility) - This 1.2 m facility will very likely have spectroscopic capabilities at wavelengths up to 100 or 200 A. If the resolution is adequate ($\lambda/\Delta\lambda\sim3\times10^3$) interstellar lines produced by the highly ionized atoms of the hot local ISM should be detectable toward sources with adequate continuum fluxes near 100 A. It would be very important to make sure AXAF and Columbus overlap in their wavelength coverage.

SIRTF (Space Infrared Telescope Facility) - This instrument will operate in the IR at $\lambda>30,000$ A. It will likely have a variety of spectroscopic modes and could be used to probe absorption and/or emission from molecules in very local clouds. Of particular importance would be the ability to study H_2 emission near 28 μm.

THE SPACE TELESCOPE HIGH RESOLUTION SPECTROGRAPH

The High Resolution Spectrograph (HRS) is a pulse-counting multichannel ultraviolet spectrograph developed for flight on the Space Telescope. Its design and operation are described by Brandt et al. (1979, 1981, 1982). The HRS was developed by the NASA Goddard Space Flight Center with Ball Aerospace systems Division as the prime contractor and scientific direction by the Principal Investigator (John C. Brandt) and members of the HRS Investigation Definition Team (see Brandt et al. 1979).

The HRS optical system is illustrated in Figure 1. The instrument consists of seven grating spectrometer modes and 4 imaging acquisition modes within a package 0.9 x 0.9 x 2.2 meters and with a weight of 700 pounds. The grating and acquisition modes are divided into two groups, side 1 and side 2, each with its own photon counting diode array (Digicon). Side one is designed to work from 1050 to 1700 A and side two from 1150 to 3200 A. The gratings are mounted on a rotating carrousel.

The HRS has three spectral resolution modes, sometimes characterized by nominal values R = wavelength/(line width) = 100,000, 20,000, and 2,000. They are referred to here as the high, medium, and low resolution modes, respectively. Measurements of the widths (FWHM) of emission lines in the spectrum of the internal Pt-Ne lamp indicate actual resolving powers as given in Table 2. Some of these numbers should increase as the result of instrumental modifications being made during the spring and summer of 1984.

TABLE 2: SPECTRAL RANGE AND RESOLVING POWER OF THE HRS

Resolution Mode	Grating Number	Spectral Range	R = λ/FWHM
Low	G5	1060-1800 A	1,500-2,500
Medium	G1	1060-1800	15,000-26,000
"	G2	1160-2100	15,000-31,000
"	G3	1600-2300	18,000-28,000
"	G4	2200 3200	13,000-21,000
High	G6	1060-1750	60,000-90,000
"	G7	1700-3200	70,000-100,000

Figure 2 illustrates the sensitivity of the various modes. The detector on side 1 has a LiF window which will permit observations down to approximately 1060 A. However, the sensitivity between 1060 and 1200 A will be very low since all the reflecting optical components have MgF overcoats.

The HRS has two entrance apertures. One subtends a 2 arcsec square, the other a 0.25 arcsec square. The larger slit will normally be used for target acquisition, while the smaller slit will be used for observations that require high spectral purity or high spatial resolution (e.g., isolating one star in a group).

The HRS has two redundant platinum-neon hollow cathode lamps which provide a reference spectrum for wavelength calibration. In the high resolution mode, wavelength calibrations with a precision of about 1 km s^{-1} should be possible.

In orbit the primary sources for photometric calibration will be standard stars. However, internal Xenon lamps are used for "flat field" calibrations to map irregularities in the photocathode response and to locate the edges of

the photocathode mask for geometric calibrations. With special observing techniques to reduce the effects of photocathode nonuniformities, it should be possible to detect interstellar spectral features less than one percent in depth.

Two major reasons for selecting the digicon as the HRS detector were its pulse-counting capability and its wide dynamic range. During laboratory calibration, it was found that input count rates as high as 150,000 counts/sec/diode can be accurately measured. With a measured dark count of 0.001 counts/sec/diode, this yields a dynamic range of 150 million. The digicon detector should make it possible to obtain very accurate line profiles of interstellar absorption lines.

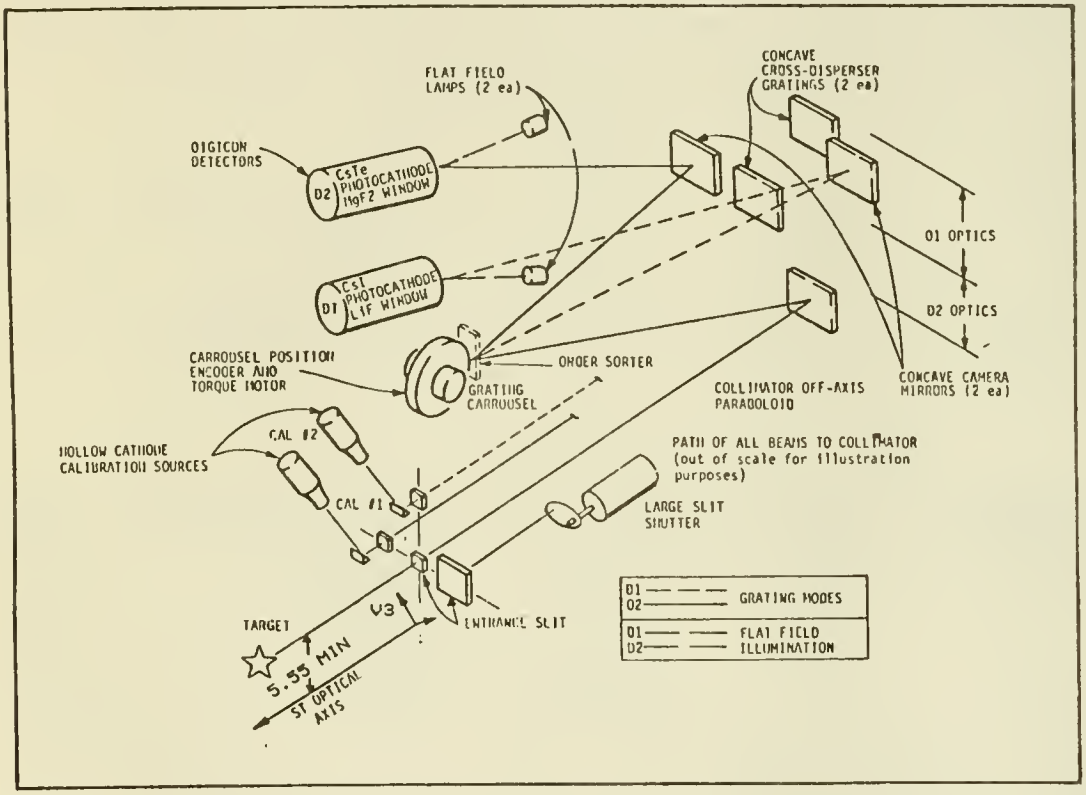

Fig. 1
HRS
Optical
System

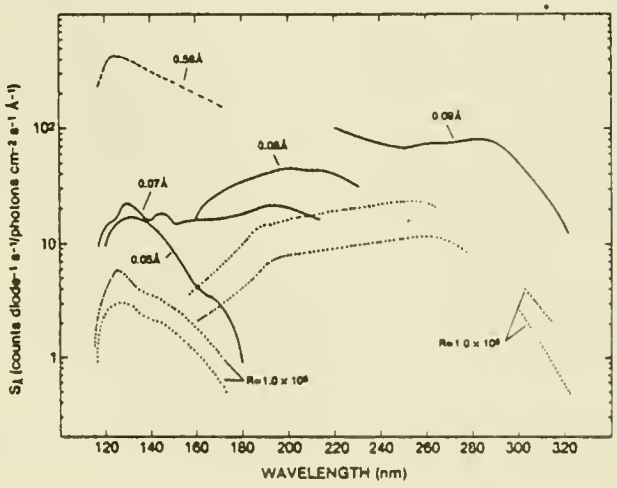

Fig. 2
Combined
HRS
and
Telescope
Sensitivity

THE COLUMBUS MISSION

In July 1983 the European Space Agency (ESA) and the National Aeronautics and Space Administration (NASA) co-sponsored a workshop at Annapolis, Maryland on a possible joint ultraviolet astronomical mission. In setting up this workshop the two agencies recognized that several proposals and studies for such a mission were in circulation. These included the April 1983 report of a NASA working group for the Far Ultraviolet Spectroscopic Explorer (FUSE), a proposal to the UK Science Research and Engineering Council for an Ultraviolet Space Observatory, and a proposal to ESA for the Magellan mission. All three of these proposals or studies involved an instrument optimized for high resolution spectroscopy in the 900 to 1200 A region. However, the various proposed missions had different secondary goals in terms of wavelength regions and resolutions. Furthermore, the various instrument concepts for the primary science goals were very different. The intent of the July 1983 workshhop was to bring together European and American scientists and engineers to discuss the characteristics of a satellite that could be jointly funded. To avoid confusion, it was decided by the conference participants to call the possible joint mission "Columbus". As a result of the success of the first international Columbus workshop, a second workshop was held in Rome, Italy in May 1984. the Columbus mission as described below represents the outcome of the 1983 and 1984 workshops.

The scientific objectives of Columbus require a primary telescope feeding two or more spectrographs. For the primary telescope a one meter class grazing incidence design seems best able to support the science goals. High throughput for $\lambda \simeq 100$ A is possible with grazing incidence angles of about 10 degrees. Such a grazing incidence telescope is easier to build than one with the smaller graze angles required for the X-ray region. The actual telescope aperture will depend on cost constraints and whether the orbit is a low orbit or a geosynchronous orbit. The complex cost trade offs between a larger telescope operating less efficiently in a low orbit versus a smaller telescope operating efficiently in a geosynchronous orbit has not been performed. The issue of repairability must also be considered in this analysis.

Table 3 lists the spectroscopic capabilities the workshop participants thought desirable and practical for the Columbus mission. Of highest priority is the high resolution ($\lambda/\Delta\lambda \simeq 3 \times 10^4$) high throughput capability in the 912 to 1200 A region. Note that Space Telescope will have no capability below 1050 A and only an exceedingly restricted capability between 1060 and 1200 A. The other spectroscopic capabilities include medium resolution ($\lambda/\Delta\lambda \simeq 10^4$) spectroscopy between 1200 and 2000 A, and low resolution spectroscopy ($\lambda/\Delta\lambda \simeq 500$) for $\lambda < 900$ A and ($\lambda/\Delta\lambda \simeq 2000$) for $\lambda > 900$ A. The mode or modes operating below 900 A may extend the spectral coverage to 100 A.

The final complement of spectrographs can only be determined after a thorough study of the various packaging possibilities. For example, with clever design choices it may be possible to extend the high resolution ($\lambda/\Delta\lambda \simeq 3 \times 10^4$) capability well below 900 A. Some of the spectrograph designs being considered are rather new. For example see McClintock and Cash (1982), Cash (1982), Hettrick and Bowyer (1983), and Hettrick (1984).

For the discussions to follow on the science concerning the local ISM that could be accomplished with the Columbus mission, I will assume the wishes listed in Table 3 are indeed achieveable. In addition I will assume the spectrograph operating between 900 and 1200 A at a resolution of 3×10^4 also has the ability to record spectra of bright sources down to 600 A.

TABLE 3: COLUMBUS DESIGN SPECIFICATIONS

EUV and UV Capability	Far UV Capability*	UV Capability
λ = 100-2000 A	λ = 900-1200 A	λ = 1200-2000 A
$\lambda/\Delta\lambda$ = 500 λ<900	$\lambda/\Delta\lambda = 3 \times 10^4$	$\lambda/\Delta\lambda = 1 \times 10^4$
$\lambda/\Delta\lambda$ = 2000 λ>900		
Highest throughput posible.	For Exp = 10^5 sec want S/N = 30 on 18 mag blue object.	For Exp = 10^5 sec want S/N = 30 on 18 Mag blue object.
Imaging capability required.	Imaging capability desirable.	Imaging capability desirable.

*The far UV capability is the prime mission of Columbus.

SPECTROSCOPIC OVERVIEW OF SPACE TELESCOPE AND COLUMBUS SCIENCE

The spectral region extending from the atmospheric cutoff near 3100 A down to 100 A has been divided into three regions in the following discussions; region 1 from 1200 to 3200 A, region 2 from 912 to 1200 A and region 3 from 100 to 912 A. Space Telescope will mostly operate in region 1. The Columbus mission will likely emphasize observations in regions 2 and 3. All three of these regions contain resonance lines of many important interstellar species.

1. The Region 1200 to 3200 A

A partial listing of the many important lines in this region can be found in the various papers involving IUE studies of interstellar gas (e.g., Savage and de Boer 1982). More extensive lists are provided by Morton and Smith (1973). The latter list is relevant to Space Telescope planning because the HRS will likely be able to detect interstellar absorption lines about 200 times weaker than those that are routinely studied with IUE. In addition to the lines of such highly ionized species as N V, C IV, and Si IV, the region contains a multitude of lines of lower ionization. Of particular significance are the many lines of Si II, Fe II, and C I which permit an accessment of the degree of saturation of the absorption lines through curve of growth studies. Several of the very abundant atoms have low f value lines in this region. These include O I λ1355, C II λ2325, C III λ1909 and Si III λ1892. These transitions should produce lines on the linear part of the curve of growth and permit the derivation of accurate column densities.

A number of important molecules have their resonance transitions in the region 1200 to 3200 A. These include CO, C_2, H_2O, HCl, CH_2, OH, O_2, N_2, CS, and SiO. Although one does not normally associate molecules with

the very nearby ISM, the detection of IR cirrus clouds (Low et al. 1984) and high latitude CO clouds (see Blitz, Magnani and Mundy, these proceedings) may force us to change our biased views.

2. The Region 912 to 1200 A

Table 4 lists the more important lines in the rich 912 to 1200 A region. Some of the most important transitions include:

a) The resonance lines of atomic H and D occur at 1025 A (Lyβ), 972 A (Lyγ), 950 A (Lyδ), with higher members extending to the Lyman continuum limit at 912 A.

b) The important electronic bands of molecular hydrogen (H_2) are the Lyman bands located at $\lambda < 1120$ A and the Werner bands at $\lambda^2 < 1008$ A. The molecule HD has its band systems slightly displaced in wavelength from those of H_2.

c) The lines of O VI and S VI . These ions are formed at 3×10^5 K, a higher temperature than any interstellar ion observable in absorption with Space Telescope or IUE.

d) The lines of N I, II and III; P II, III, IV and V; S III, IV and VI; and Cl I, II, III and IV. The ability to probe multiple ionization stages is important for studying the thermal and nonthermal ionization processes in the local interstellar gas.

TABLE 4: SOME IMPORTANT LINES IN THE 912-1216 Å SPECTRAL RANGE

Species	Important Lines (Å)
H I, D I	1216, 1026, 973, 950, ..., 912
H_2, HD	hundreds of lines between 912 and 1120
C III	977, 1175
N I	951, 964, 1133, 1200
N II	916, 1084, 1085
N III	991
O VI	1032, 1038
A I	1048, 1066
P IV	951
P V	1118, 1128
S III	1012, 1190
S IV	1062
S VI	933, 944

3. The Region 100 to 912 A

Below 912 A the most important features are the lines of highly ionized plasma indicative of temperatures between 10^5 and 2×10^7 K. Figure 3 shows the wavelengths of many of these lines together with the temperatures corresponding to the maximum abundance of the various ions. Particularly noteworthy are the lines of Ne VII and VIII, Mg VIII, IX and X, and Fe IX, X, XII, XV, XVI, etc.

All of the strong resonance lines of He I and He II lie in this region. The He I lines (584, 537, 522 A...) lie in a series extending to the continuum edge at 504 A and the He II lines (304, 256, 243 A...) lie in another series extending to their edge at 228 A.

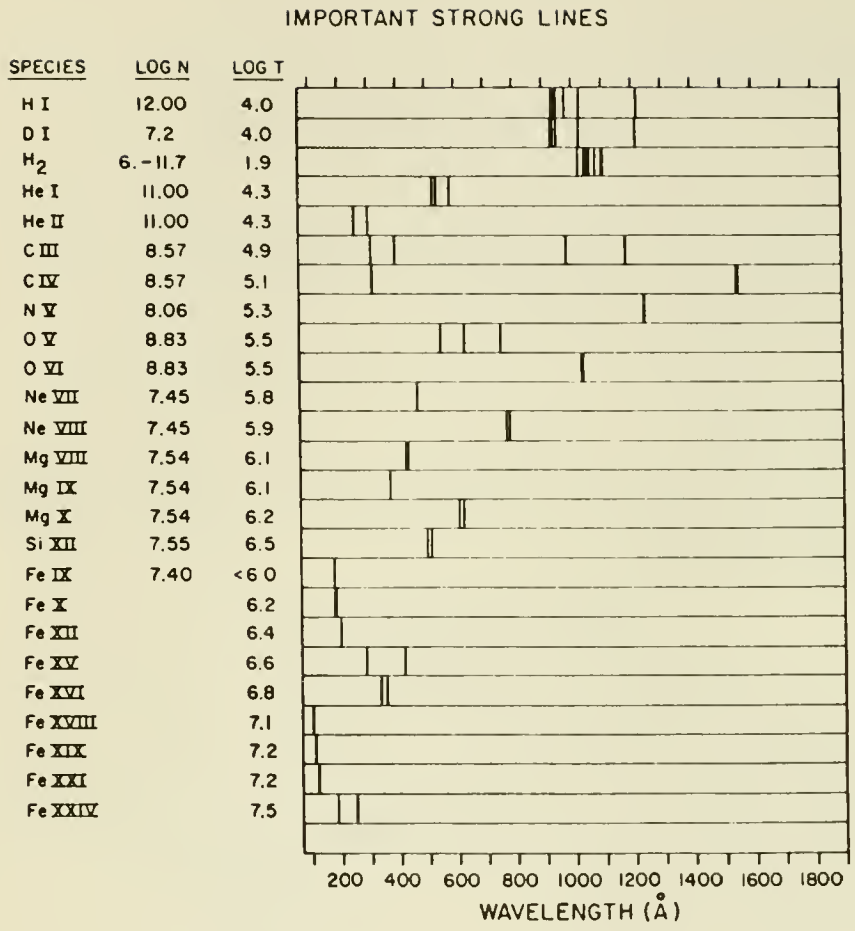

FIGURE 3
Wavelengths of important spectral lines of abundant elements and molecular hydrogen (H_2). Also indicated are the typical element abundances on a logarithmic scale where hydrogen is 12.00, and the temperatures of maximum fractional amount of each ion assuming collisional ionization equilibrium.

LOCAL ISM INVESTIGATIONS WITH THE ST HRS AND COLUMBUS INSTRUMENTS

The following section discusses a few of the many studies of the local ISM that might be undertaken with the ST HRS and Columbus spacecraft. No attempt has been made to indicate which instrument is the most appropriate for each investigation. Some brief comments can provide an overall summary; Columbus will be optimized for measurements of features with $\lambda < 1200$ A. The ST HRS will be most efficient for $\lambda > 1200$ A. However, the HRS will have very limited capability to 1060 A. The highest resolution mode of the HRS will have a resolution 2 to 3 times higher than that of Columbus.

1. Accurate Local Abundances

Both the HRS and Columbus will be able to provide resolutions and photometric accuracies significantly higher than previously available in the UV. These two important gains will lead to much more reliable estimates of absorption line column densities than now exist. For example, the 3 to 4 km s^{-1} resolution of the HRS combined with the ability to measure absorption lines less than 1% deep will almost certainly allow a reliable accessment of curve of growth problems. With accurate column densities and the ability to probe more than a 100 different ionic species a nearly unlimited range of scientific investigations is possible. Some examples include:

a) Depletion studies in local diffuse clouds and in the intercloud medium will provide new insights about the interplay between gas and dust.
b) Studies of the ionization structure of local gas using species having lines for a wide range of ion types, such as Si II, III, IV and S II, III, IV and VI.
c) Estimates of interstellar densities from the population of fine structure levels in such species as C II, Si II, Fe II, O I, N II, etc.
d) Direct temperature estimates for warm and hot gas from measures of thermal line widths.

2. Local Abundances of Cosmological Significance

Various light elements found in the ISM were likely created during the very early evolution of the universe. High precision measures of elemental abundances of these species in a variety of interstellar environments is of fundamental importance. The ST HRS and in particular Columbus will be able to accurately measure D/H in a number of local clouds through an analysis of the Lyman absorption lines. There is a small possibility that Columbus will have the resolution and sensitivity to also probe the He^3 to He^4 ratio from measures of the He I resonance line series starting at 584 A.

3. Local Gas Kinematics

The wavelength calibration of the HRS should allow absolute velocity measurements with an accuracy of about 0.5 km s^{-1}. With this velocity precision, it may be possible to investigate not only cloud motions but also the flow of matter into or out of clouds.

Accurate velocity measurements are important because the most powerful technique for confirming the spatial coexistence of two interstellar species is from a careful intercomparison of their absorption line profiles.

The large f value lines of the abundant ions of C II, Si III, N II, and C III can provide information on high velocity interstellar gas. With the high signal to noise data possible from the HRS and Columbus space craft, it should be possible to use these ions to search for very nearby but low column density, high velocity gas. Detecting this gas phase locally would provide important clues about shock heating in the local ISM.

4. The 3-Dimensional Structure of Local Gas

From studies with Copernicus and IUE we now have a better understanding of the 3 dimensional distribution of gas in the local ISM. Our knowledge of the local gas structure will continue to expand as instruments with greater sensitivity and resolution become available. The HRS will be able to more clearly separate interstellar Lyman α absorption from stellar Lyman α emission

for nearby cool stars. Interstellar Lyman α will be accessible for very faint white dwarfs with the HRS at a resolution of 2000 in relatively short integration times. This ability to probe fainter targets relatively rapidly should eventually lead to a large increase in the number of local targets for which accurate H I column densities are available.

With Columbus the local H I distribution could be inferred from the Lyman lines or the Lyman discontinuity. However, a more exciting prospect is that of determining the local distribution of He I and He II from observations of hot white dwarfs at $\lambda < 600$ A.

5. Local Hot Gas

One of the most important species accessible between 912 and 1200 A is O VI. In collisional equilibrium the abundance of O VI peaks near 3×10^5 K. It is now thought that the O VI absorption seen by the Copernicus satellite is procuced at the boundaries of cooler clouds imbedded in a hot (10^6 K) medium. High S/N spectra of selected species including O VI over simple lines of sight will provide a test of the interface origin idea for O VI.

Copernicus studies of interstellar O VI were limited to O and B stars as the background targets. With Columbus, white dwarfs could be used to probe the local O VI distribution. If the white dwarfs provide a suitably smooth continuum it is possible that very broad O VI absorption associated with gas at 10^6 K could be detected.

The most exciting prospect for the direct detection of gas at 10^6 K or hotter from the Columbus mission will be provided with measurements at $\lambda < 912$ A. If the short wavelength spectrographs finally selected for Columbus have adequate resolution, then many of the species illustrated in Figure 3 may be detected over 100 pc paths. In the case of the lines of Fe this would yield data on ions spanning a temperature range from $\sim 10^6$ to $\sim 3 \times 10^7$ K. At this stage it appears doubtful that the Columbus spectrograph operating between 100 and 900 A will have adequate resolution. A more likely possibility is that the spectrograph designed to operate between 900 and 1200 A at a resolution of 3×10^4 will have coverage to shorter wavelengths with reduced but adequate resolution. If this instrument had spectroscopic coverage to 600 A, which seems reasonable, then the important Mg X and Ne VIII ions should be observable toward targets like HZ 43. Both these ions peak in abundance at temperatures near 10^6 K. The direct spectroscopic detection in absorption of local gas at 10^6 K would provide major insights about the nature of the local hot gas seen in emission at X-ray wavelengths.

6. Molecules in the Local ISM

Because of its great abundance and importance to interstellar chemistry, careful searches should be made for local interstellar H_2. In the H_2 survey of Savage et al. (1977), H_2 detections were reported for 8 stars with distances less than 100 pc. Studies of local H_2 with Columbus could yield new information on the local CO clouds recently discovered by Blitz, Magnani, and Mundy (1984).

REFERENCES

Brandt et al. 1979, Proc. SPIE, 172, 254.
Brandt et al. 1981, Proc. SPIE, 279, 183.
Brandt et al. 1982, in The Space Telescope Observatory (ed. D. Hall) NASA CP-2244, p. 76.
Blitz, L., Magnani, L. and Mundy, L. 1984, (this symposium)
Cash, W. 1982, Appl. Optics, 21, 710.
Hettrick, M. C. and Bowyer, S. 1983, Appl. Optics, 22, 3927.
Low, F. J. et al. 1984, Ap. J. (Letters), 278, L19.
McClintock, W. E. and Cash, W. 1982, Proc. SPIE, 331, 321.
Morton, D. C. and Smith, W. H. 1973, Ap. J. Suppl., 26, 333.
Savage, B. D., Bohlin, R. C., Drake, J. F. and Budich, W. 1977, Ap. J., 216, 291.
Savage, B. D. and de Boer, K. S. 1982, Ap. J., 243, 460.

Observations of Local ISM Emission with the Berkeley EUV/FUV Shuttle Telescope

Christopher Martin and Stuart Bowyer

Space Science Laboratory, University of California, Berkeley

ABSTRACT

The Berkeley Extreme Ultraviolet/Far Ultraviolet Shuttle Telescope (BEST) will be launched on the Space Shuttle in November, 1984, as part of the NASA UVX project. The Berkeley spectrometer will make observations of the cosmic diffuse background in the 600-1900 Å band, with a spectral resolution of 10 Å. The sensitivity and spectral resolution of the instrument make it ideal for the study of components of the interstellar medium in the 10^4 - 10^6K range.

Introduction

A number of observations have been made of the diffuse ultraviolet background, but have been subject to the adverse effects of stellar contamination, airglow and geocoronal emission, and high internal background, as well as generally marginal sensitivity. Combined with significant differences in observation platforms and instrument design, these problems have caused serious discrepancies to appear between different observers (cf. review by *Paresce and Jakobsen*, 1980), even when observing identical parts of the sky (*Paresce, McKee, and Bowyer*, 1980). A primary objective of the first mission is to perform coobservations with the Johns Hopkins Ultraviolet Spectrometer, and attempt to resolve these differences. Beyond this goal, detailed and sensitive measurements of the diffuse background, free of systematic errors, should hold considerable information about a variety of processes originating in the interstellar medium.

Instrument Design

The Berkeley spectrometer has been designed primarily as a nebular spectrophotometer, which is optimized by a high geometric area-field of view product, and encorporates a fast (f/2.0) off-axis paraboloid/Rowland spectrograph combination. Figure 1 shows a schematic view of the instrument, and Table 1 summarizes the instrument characteristics. The use of photon counting microchannel plate detectors with a wedge-and-strip readout (*Martin et al.* 1981) and a high yield CsI photocathode (*Martin and Bowyer*, 1982) maximizes the throughput and minimizes the detector dark background. The two-dimensional imaging of the detectors allows complete spectral multiplexing over the 600-1900 Å range.

Stellar contamination is avoided by imaging along the long axis of the spectrometer entrance slit, which is accomplished with a toroidal grating and the 2-D detectors. In addition, a superpolished mirror and holographically ruled grating eliminate scattering into the entrance slit or within the spectrometer. A star camera is used to reconstruct the true aspect post-mission to determine the positions of all stars, and the CsI photocathode efficiency drops rapidly longward of 1900 Å eliminating more ubiquitous F stars from scattering and effecting the spectrum.

Scattering from geocoronal and airglow lines that would otherwise be imaged into 10 Å of the spectrum has been minimized by using a holographic grating. Filters are placed at the detectors to eliminate the residual scattered Lyman α 1216, OI 1304 and 1356 Å emission. A test filter is periodically interposed at the entrance slit which permits a measurement of the residual Lyman α in the EUV (600-1150 Å) band.

The effect of detector internal background is minimized by using a fast optical system, and the level is measured regularly on orbit using a rotating shutter mechanism. Background inducing particle ingress is minimized by using a gas tight spectrometer box and ion-repeller grid at the entrance slit. All operations will be performed outside of areas of high energetic particle flux.

Shuttle glow phenomena could interfere with the measurements, but the spectral resolution, time resolution, photon counting nature of the detectors, and the use of filters against OI lines should reduce the impact of such emission.

The instrument sensitivity to continuum and line emission are shown in Figure 2, along with the sensitivity of a number of other instruments, including IUE and the Voyager UVS. The FUV continuum sensitivity (expressed as a minimum detectable flux for one orbital night integration) is a factor of 30-50 lower than the lowest level detected (~300 ph cm^{-2} s^{-1} A^{-1} sr^{-1}) (*Paresce, McKee, and Bowyer*, 1980; *Jakobsen et al.*, 1984). The EUV continuum sensitivity is ~300-1000 ph cm^{-2} s^{-1} A^{-1} sr^{-1}, for an integration of 10^4 seconds, which will be achieved by summing the data from ten single orbit observations. The FUV line sensitivity is limited by the level of the FUV continuum, and is ~500 ph cm^{-2} s^{-1} sr^{-1} (0.004 Ry) for a 1000 sec integration.

Observations of ISM Emission

The high sensitivity and moderate spectral resolution of the Berkeley spectrometer should permit the separation of a variety of interstellar emission processes which have unique spectral signatures. In general, observations of ISM emission will give information about spatial extension, morphology, and emission measures which lead to filling factors when compared with measurements that make a linear average of line of sight densities.

Dust is detectable via scattered starlight (*Paresce and Jakobsen*, 1980), and the spectrum will include effects of wavelength dependent albedo and dust size spectra. Targets in directions of anomalous gas-to-dust ratios may reveal clues about the origin of these anomalies, including varying dust properties and the presence of molecular hydrogen.

Molecular hydrogen should produce FUV fluorescence as a natural byproduct of its formation/destruction cycle (*Jakobsen*, 1982). Observable fluorescence should be produced in clouds of density greater than $n_H \sim 10(10^{20}/N_H)$, so that typical diffuse clouds should exhibit detectable emission. Since this process is density sensitive, the levels detected are indicative of the density, morphology and filling factor of diffuse clouds.

Warm ionized gas at 10^4K will produce 2-photon continuum emission, which can be directly correlated with observations of recombinant Hα emission (*Deharveng et al.*, 1982). Gas at "semi-torrid" temperatures ~$10^{4.8-5.8}$ should exhibit collisionally excited line emission from a variety of metal resonance transitions (*Jakobsen and Paresce*, 1981). *Feldman et al* (1981) subsequently made tentative identification of this type of line emission from Si IV 1398 Å, N IV 1487 Å, C IV 1549 Å, and O III 1663 Å, in the direction of the north galactic pole. *Paresce et al* (1983) have interpreted this emission as arising from the same

$10^{5.2}$K gas that could account for observed EUV emission. The derived constraints on the EM vs. temperature are shown in Figure 3, along with the EM required to produce detectable lines for the Berkeley spectrometer. A variety of lines should be detectable in more than one ionization state, allowing the determination of temperature (or temperature distribution), filling factors (when compared to absorption line measurements), spatial distribution, and possibly the effects of non-equilibrium ionization.

References

Deharveng, J.M., Joubert, M., Barge, P. 1982, *Astron. Astrop.* **109,** 179.

Feldman P.D., Brune, W.H. and Henry, R.C. 1981, *Ap. J. Lett.* **249,** L51.

Jakobsen, P., and Paresce, F. 1981, *Astron. Astrop.* **96,** 23.

Jakobsen, P. 1982, *Astron. Astrop.* **80,** 67.

Jakobsen, P., Bowyer, S., Kimble, R., Jelinsky, P., Grewing, M., Kramer, G. 1984, *Astron. Astrop.*, Submitted

Martin, C., Jelinsky, P., Lampton, M., Malina, R.F., and Anger, H.O. 1981, *Rev. Sci. Instrum.* **52,** 1067.

Martin, C. and Bowyer, S. 1982, *Applied Optics* **21,** 4206.

Paresce, F. and Jakobsen, P. 1980, *Nature* **286,** 119.

Paresce, F., McKee, C., and Bowyer, S. 1980, *Ap. J.* **240,** 387.

Paresce, F. and Stern, R. 1981, *Ap. J.* **247,** 89.

Paresce, F., Monsignori Fossi, B.C., Landini, M. 1983., *Ap. J. Lett.* **266,** L107.

Table I
BEST Instrument Summary

Objective	15 cm f/2 off-axis paraboloid
Grating	Toroidal holographic
Grating radius	30 cm × 28.9 cm
Groove density	2000 l/mm
Dispersion	16.7 Å/mm
Mirror/Grating Coating	Al + 150 Å MgF
Field of View	0.1 × 4.0 degrees
Bandpass	600 - 1140 Å 1350 - 1930 Å
Resolution	10 Å
Detectors	2 microchannel plate
Detector readout	wedge & strip anode
Photocathode	6000 Å CsI
Filters	Tin (1500 Å) 600-750 Å Indium (1600 Å) 750-1150 BaF (2mm) 1350-1930 Å
Sensitivity	
Continuum	EUV 1000-2000 ph cm^{-2} s^{-1}Å^{-1} sr^{-1} FUV 4-10 ph cm^{-2} s^{-1}Å^{-1} sr^{-1}
Line	EUV 10^4 ph cm^{-2} s^{-1} sr^{-1} FUV 400-600 ph cm^{-2} s^{-1} sr^{-1}

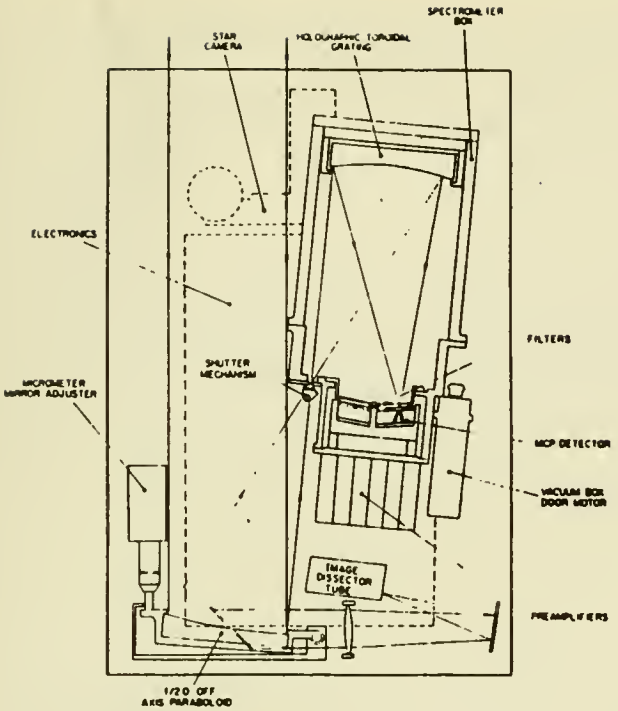

Figure 1.

Schematic of Berkeley Spectrometer

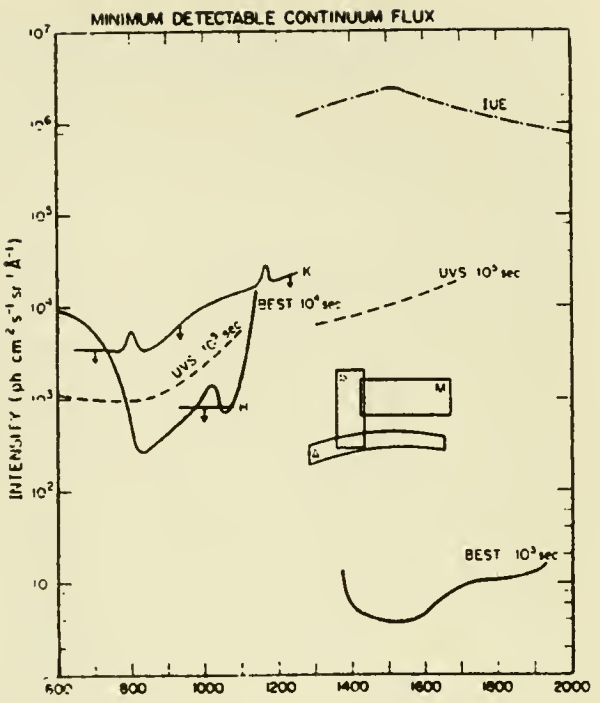

Figure 2. Sensitivity (minimum detectable flux) for 10^3sec (EUV) are 10^4 sec (EUV), with Voyager UVS and IUE sensitivities.

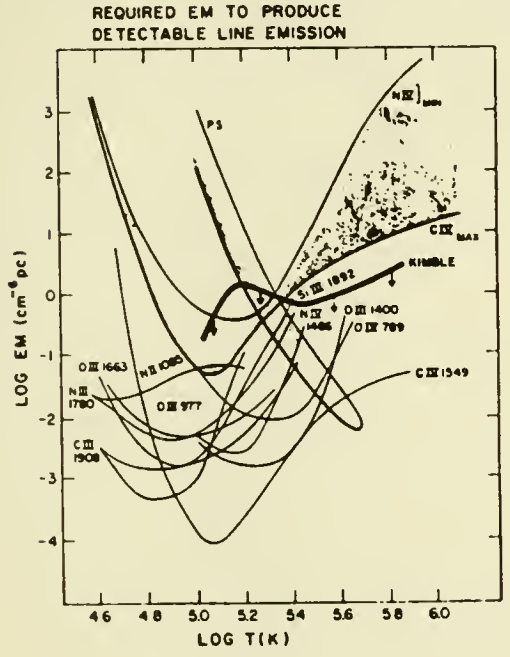

Figure 3. Plasma constraints derived by Paresce, et al 1983 from EUV line detections by Feldman et al 1983 and Paresce and Stern, 1981, and Kimble, 1983 (U.C. Berkeley PhD), along with detectable line emission.

Measuring EUV Line Emission from the Hot Interstellar Medium

Simon Labov, Christopher Martin, and Stuart Bowyer

Space Sciences Laboratory, University of California, Berkeley

ABSTRACT

In the local interstellar medium, the presence of hot gas (log T ~ 5 to 6) has been inferred from measurements of oxygen VI absorption in the ultraviolet, and from diffuse emission in the extreme ultraviolet (EUV) and soft X-ray regions. Here we describe a spectrometer that is very sensitive to gas in this temperature range. The spectrometer uses an array of plane-ruled gratings at grazing incidence in the extreme off plane mount. A set of Kirkpatrick-Baez mirrors focuses the conically diffracted light on to one of two microchannel plate detectors. The field of view of the instrument is 0.2° by 12°. The predicted sensitivity ranges from 50 to 200 ph/(cm^2 sec str) with a resolving power ($\lambda/\Delta\lambda$) of 15 to 50 over the 50 to 700Å wavelength band. The instrument is currently under construction for a sounding rocket flight.

As indicated by soft X-ray and EUV emission, EUV stellar observations and far ultraviolet absorption line studies, much of the space within 100 parsecs of the sun contains hot tenuous gas. We describe here a new instrument to explore this phase of the interstellar medium by observing diffuse line emission in the EUV.

In the past, a variety of techniques have been used to measure diffuse emission at wavelengths below 1200Å. These measurements are summarized in Figure 1. Soft X-ray measurements show emission lines from highly ionized species (*Inoue et al*, 1979). The gas scintillation proportional counter produced

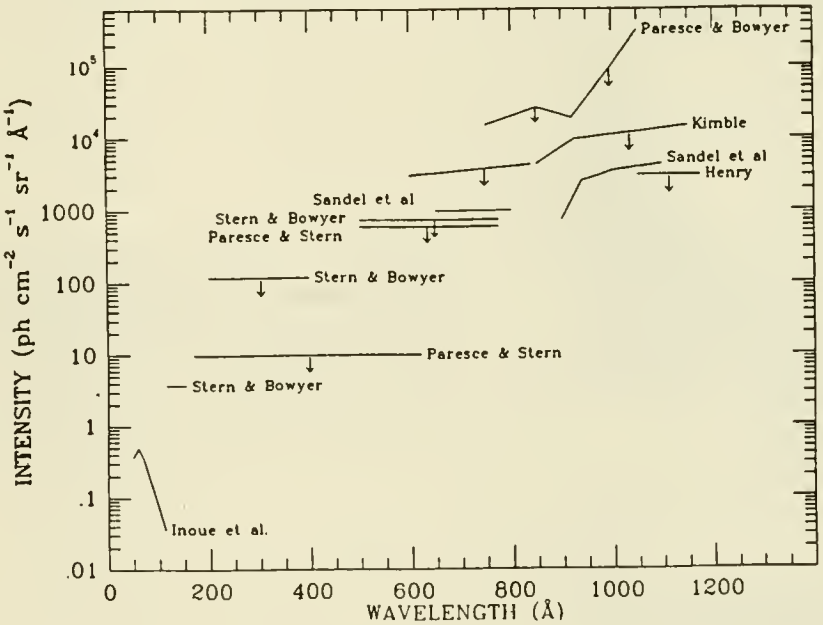

Figure 1. Existing measurements of diffuse radiation between 50 and 1200Å.

low resolution spectra at higher energies, but only photometric measurements at lower energies. In the EUV, diffuse emission was first detected by a Berkeley sounding rocket instrument (*Cash, Malina and Stern*, 1976), and later confirmed with the Berkeley Apollo Soyuz Test Project EUV telescope (*Stern and Bowyer*, 1979). These results are shown in Figure 1, along with further reductions of the same data with additional assumptions by *Paresce and Stern* (1981). The Voyager spectrometer results (*Sandel, Shemansky, and Broadfoot*, 1979) are shown near 750Å and above the Lyman limit at 912Å out to the far ultraviolet. Also shown in this range are the measurements made by *Kimble* (1983), using an airglow spectrometer flown on a rotating satellite. Kimble used the "up looking" data to derive upper limits. A sounding rocket spectrometer (*Paresce and Bowyer*, 1976) and a sounding rocket photometer (*Henry*, 1973) also produced upper limits in this region.

Notice that only upper limits to the diffuse radiation exist between 130 and 700Å. Furthermore, no spectral measurements of the diffuse flux have been made between 50 and 700Å. Conventional spectrometers cannot observe line emission in this region lack the high sensitivity and spectral resolution necessary to observe line emission in this region. To surmount the problem, we are developing a novel type of spectrometer that operates between 50 and 700Å with high sensitivity and moderate resolution. The purpose of the instrument is to detect line emission from a hot coronal component of the ISM.

Figure 2 shows the light path through the optical system. Diffuse radiation enters the instrument through a wire grid collimator that restricts the field of view to 0.2° by 12° (not shown). The light is then diffracted by an array of objective gratings at grazing incidence in the extreme off plane mount. The gratings are mechanically ruled with high line density at the appropriate blaze angle to improve efficiency. The diffracted light is focused by a Kirkpatrick-Baez array of mirrors orthogonal to the gratings. To construct these mirrors

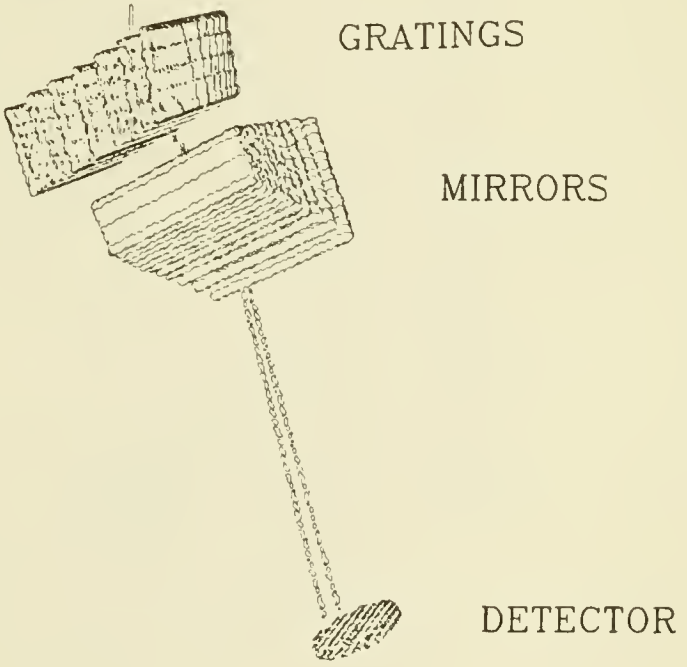

Figure 2. The optical configuration of the EUV diffuse background spectrometer.

we heat float glass, a naturally smooth and flat substate, and allowed it to settle on a properly shaped steal mandrel. Using this technique we will inexpensively fabricate mirrors with adequate resolution.

Notice that each grating is tilted at a slightly different angle with respect to the axis of the system. This simulates a second Kirkpatrick-Bacz array, focusing in the non-spectral direction (i.e., along the 12° field of view). As shown by numerical ray tracing shows that the gratings produce spatial resolution of 1.2' even though they are flat, rather than parabolic. This focusing will help insure that no point sources are contaminating the diffuse spectra. In addition, it allows a large geometric area to be concentrated on a reasonably sized detector.

Once the light has been focused, it passes through thin filters and is imaged by one of two microchannel plate type detectors. The filters reduce scattered light and also isolate the detectors from any residual pressure or particle contamination. The detectors use wedge and strip type anodes (*Martin et al*, 1981) to achieve high resolution imaging in two dimensions with low background noise. A cesium iodide photocathode (*Martin and Bowyer* 1982) deposited on the front microchannel plate gives it high photon counting quantum effciency.

Many features contribute to the instruments high sensitivity. It uses most of the geometric area available within the diameter of a Black Brant type sounding rocket. It subtends a large solid angle and has only two optical elements, both at grazing incidence. High grating efficiency is obtained by blazing the gratings and mounting them off plane, and the detectors have high quantum efficiency and add little background noise. The system shown in Figure 2 is actually only one of four systems employed in the spectrometer to cover the bandpass from 50 to 700Å with resolving power ranging from 15 near 150Å to 50 near 550Å. The four systems are arranged in two pairs, with each pair focusing on one detector. The two pairs are set side by side in a square configuration.

One way to examine the usefulness of this instrument is to show how well it can constrain a model. Figure 3 shows such results for an isothermal model in which all the absorbing material is between the instrument and the emitting material. The dark line at the bottom of this emission measure vs. temperature plot indicates the minimum emission measure necessary to detect two lines during a 400 second rocket flight. The lines considered are all resolvable from each other and from any nearby airglow, geocoronal or interplanetary lines. Also shown are the constraints on this model from the broad band detection with the Apollo-Soyuz telescope as analyzed by *Paresce and Stern* (1981), the constraints implied by the upper limits of *Kimble* (1983), and by a tentative detection of several emission lines in the far ultraviolet by *Feldman, Brune, and Henry* (1981) as analyzed by *Paresce, Monsignori Fossi, and Landini* (1983). By exploring new parameter space, this instrument will vastly improve the constraints on any model of this hot phase of the ISM.

The sensitivity of the instrument can be described by the minimum detectable line flux. For a 400 second sounding rocket flight, this varies from 50 to 200 photons/(cm^2 sec str) across the bandpass, and is shown by the dark line in Figure 4. Also plotted in Figure 4 is a range of predicted line intensities from a hot coronal medium. To make these predictions we used two isothermal models, the "slab absorption" type described above, and a model in which the absorbing material is interspersed with the emitting material. The steady state plasma codes of *Stern, Wang and Bowyer* (1978) and *Raymond and Smith* (1977), were applied to these models with the constraints imposed by the broad

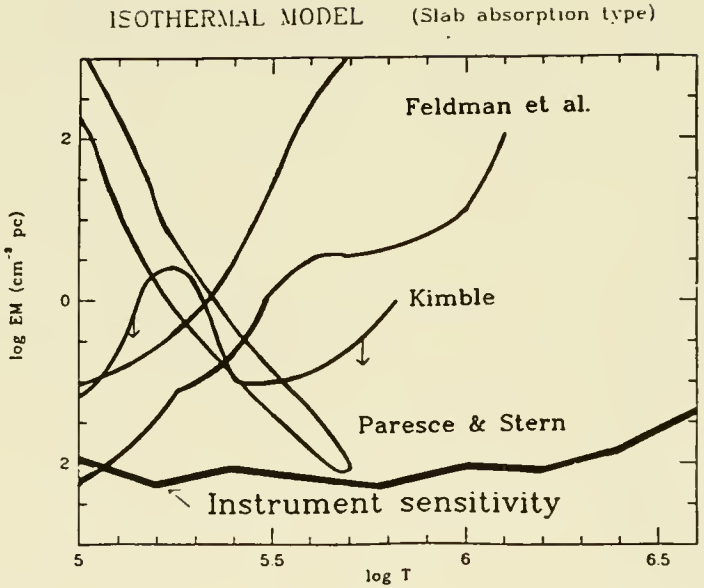

Figure 3. The constraints imposed on an isothermal model by previous observations is shown with the minimum emission measure necessary to detect two emission lines.

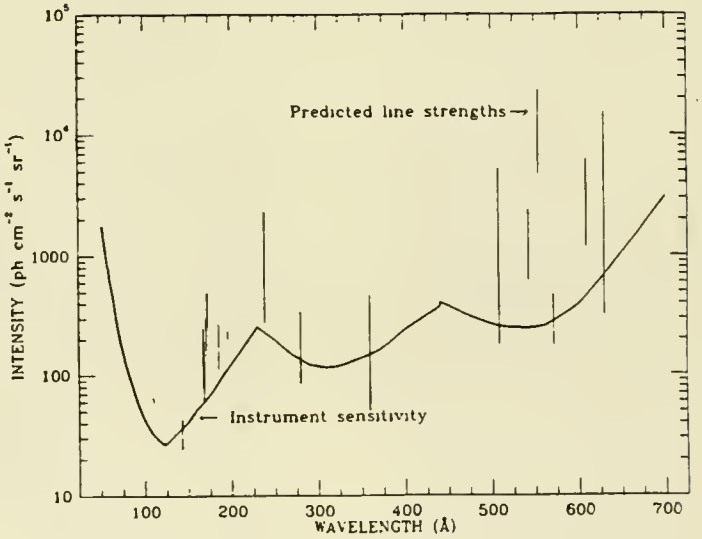

Figure 4. The minimum detectable line flux and a range of predicted line strengths.

band measurements. The large range in strengths reflects the different models and parameters used. After the initial rocket flight, the spectrometer will be suitable for flight in a type container attached to the Space Shuttle With the longer exposures allowed on Shuttle, different regions of the sky can be examined to determine the spatial distribution of the emitting material.

To summarize, we have designed a new type of spectrometer that will be capable of making make the first spectral measurements of the diffuse emission between 50 and 700Å. It will be 1 to 2 orders of magnitude more sensitive to diffuse line emission than any of the current broad band measurements. Attached to the Shuttle in a GAS type container, it will also be able to explore the spatial distribution of the emission with even higher sensitivity. We expect that this instrument will aid our understanding of the hot coronal component of the interstellar medium.

References

Cash, W., Malina, R., and Stern, R. 1976, *Ap. J. (Letters)*,**204**, L7.

Feldman, P. D., Brune, W. H., and Henry, R. C. 1981, *Ap. J. (Letters)*,**249**, L51.

Inoue, H., Koyama, K., Matsuoka, M., Onashi, ..., and Tanaka, Y 1979, *Ap. J. (Letters)*, **227**, L85

Kimble, Randy 1983,*PhD. Thesis*, "Observations of the EUV/FUV Radiation fields," University of California, Berkeley.

Martin, C., Jelinsky, P., Lampton, M., Malina, R.F., and Anger, H.O. 1981. *Rev. Sci. Instrum.*, **52**, 1067.

Martin, C. and Bowyer, S. 1982, *Applied Optics* **21**, 4206.

Paresce, R. and Bowyer, S. 1976, *Ap. J.*,**207**, 432.

Paresce, F., Monsignori Fossi, B. C., and Landini, M. 1983, *Ap. J. (Letters)*, **266**, L107.

Paresce, F. and Stern, R. 1981, *Ap. J.*, **247**, 89.

Raymond, John C. and Smith, Barham W. 1977, *Ap. J. Suppl.*,**35**,419.

Sandel, B. R., Shemansky, D. E., and Broadfoot, A. L. 1979, *Ap. J.*,**227**, 608.

Stern, R. and Bowyer, S. 1979, *Ap. J.*, **230**, 755.

Stern, R., Wang, E., and Bowyer, S. 1978, *Ap. J. Suppl.*,**37** 195

INDEX TO AUTHORS

INDEX TO AUTHORS

INDEX TO AUTHORS (Continued)

The Editors wish to extend special thanks to Teresa L. Evans of the Department of Physics at Catholic University of America for her invaluable assistance in preparing these proceedings.

1. Rep... NA	...ion No. / 3. Recipient's Catalog No.
4. Titl... LOCAL... ASTRO...	5. Report Date November 1984
	6. Performing Organization Code 684
7. Aut... Y. Ko...	...age / 8. Performing Organization Report No.
9. Perf... NASA (... Greenl...	10. Work Unit No.
	11. Contract or Grant No.
12. Spc... Nation... Washin...	...ion / 13. Type of Report and Period Covered Conference Publication
	14. Sponsoring Agency Code

15. Sup...

Y. Kon... ...eenbelt, Maryland.
F. C. ... ...of America, Washington, D.C.
B. D. ... ...Madison, Wisconsin.

16. Abst...

This book contains the proceedings of the International Astronomical Union Colloquium Number 81 "Local Interstellar Medium", which was held on June 4 through 6, 1984 at the University of Wisconsin, Madison, Wisconsin. The primary theme of the conference was the physical conditions of the interstellar matter within about 150 parsecs of the Sun. Observational and theoretical papers presented at the meeting are included in this volume.

17. Key Words (Selected by Author(s)) Local Interstellar Medium	18. Distribution Statement Unclassified - Unlimited Subject Category 90

19. Security Classif. (of this report)	20. Security Classif. (of this page)	21. No. of Pages	22. Price
Unclassified	Unclassified	373	A16

As* qQB 790 .I573 1984

International Astronomical Union. Colloquium 1984 :

Local interstellar medium

Wellesley College
Dept. of Astronomy
Wellesley, MA 02181

NASA